

AN INVESTIGATION INTO THE FEASIBILITY OF
THE STRUCTURAL USE OF GLASS REINFORCED PLASTICS
IN LONG SPAN LIGHTLY LOADED STRUCTURES

KEITH WINSTON MOLYNEUX

A THESIS SUBMITTED FOR THE DEGREE OF
DOCTOR OF PHILOSOPHY

624.01178 MOL
204630 18 MAR 1977

DEPARTMENT OF CIVIL ENGINEERING
UNIVERSITY OF ASTON IN BIRMINGHAM

OCTOBER 1976

SYNOPSIS

The problem of feasibility is approached by first reviewing the general properties of grp. In Chapter three, the more relevant properties are discussed in greater depth. Experimentally determined data is presented for both long and short term strength and stiffness characteristics. Results show that elastic properties can be predicted reasonably well by theory, and that empirical creep data can be represented by power laws.

In Chapter four, analyses are presented to determine the effect of fibre volume fraction and the relative cost of fibres and resin on the cost-effectiveness of laminates under various loading conditions. Also, various production processes and their associated costs are analysed at various production levels to assist in making design and manufacturing decisions.

On the basis of the properties of grp, a roof structure is chosen as a suitable structure to investigate, in order to establish economical and structural feasibility of long span lightly loaded grp structures in general. The structural feasibility is tested by the design of a 60 m span roof, and the building and testing of a 10 m span model roof. The economic feasibility is investigated by

comparing the estimated cost of grp roofs with the cost of conventional roof structures.

It is concluded that 60 m grp roofs, and, therefore, long span lightly loaded grp structures are structurely and economically feasible. Grp roofs are competitive with conventional roof structures at a span of 20 - 30 m and their position improves with increasing span. It is estimated that the annual British market for glass fibres in this application is 5600 Tonnes.

ACKNOWLEDGEMENTS

The author would like to thank his supervisors, Prof. M. Holmes, Mr. J. Huddart, Prof. Pick and Prof. Scott for their assistance and advice during the course of this investigation.

The author is also most grateful to Mess. Pilkington Bros. Ltd. for their financial support and permission to carry out the investigation.

Further thanks are also extended to: Mr. W. Parsons, the Civil Engineering Departmental Superintendent and his staff for their willing assistance, Miss N. A. Byrne for her excellent typing of the script, and the author's wife for her help, patience and encouragement.

CHAPTER 2 (Contd)

Page No.

2.10.8	Hot Press Moulding	2.21
2.10.9	Filament Winding	2.22
2.10.10	Pultrusion	2.22
2.10.11	Continuous Laminating	2.23
2.10.12	Preforming	2.23
2.11	Fire	2.24
2.12	Cost	2.25

CHAPTER 3

THEORETICALLY & EXPERIMENTALLY
DETERMINED PROPERTIES OF GRP

3.1	Introduction	3.1
3.2	Elastic Properties of Orthotropic Laminates	3.2
3.2.1	Introduction	3.2
3.2.2	Prediction of Elastic Constants of the Basic Mono-Layer (Fig. 3.2)	3.3
3.2.2.1	Law of Mixtures	3.3
3.2.2.2	Tasi Approach	3.5
3.2.2.3	Halpin-Tsai Approach	3.6
3.2.3	Stress-Strain Relationships Referred to Natural Axes	3.7
3.2.4	Stress-Strain Relationships Referred to Arbitrary Axes	3.10
3.2.5	Elastic Constants of Laminated Grp	3.13
3.3	Strength Properties of Laminated Grp	3.16
3.3.1	Introduction	3.16
3.3.2	Prediction of the Strength of the Basic Mono-Layer	3.17

3.3.2.1	Longitudinal Tensile Strength	3.18
3.3.2.2	Longitudinal Compressive Strength	3.18
3.3.2.3	Transverse Strengths	3.19
3.3.2.4	Interlamina Shear Strength	3.19
3.3.2.5	Flexural Strength	3.20
3.3.3	Strength Properties of Laminated Grp	3.20
3.3.3.1	Laminate Behaviour Under Load	3.21
3.4	Theoretically & Experimentally Determined Elastic & Strength Properties of Selected Grp Laminates	3.23
3.4.1	Introduction	3.23
3.4.2	Design of Specimens	3.23
3.4.3	Experimentally Determined Properties	3.25
3.4.3.1	Properties of the Basic Lamina & Selected Laminates	3.25
3.4.4	Conclusions	3.28
3.5	Time-Dependent Properties of Grp	3.29
3.5.1	Introduction	3.29
3.5.2	Creep Mechanism	3.29
3.5.3	Nature of Strength Reduction	3.32
3.5.4	Prediction of the Loss of Stiffness with Time	3.32
3.5.4.1	Extrapolation Techniques	3.33
3.5.4.2	The Larson-Miller Parameter	3.35
3.5.5	Prediction of the Loss of Strength with Time	3.37
3.5.5.1	Larson-Miller Parameter	3.37
3.5.5.2	Wohler Method	3.37
3.5.5.3	The Monkman and Grant Relationship	3.38

3.5.5.4 Charles' Equation	3.40
3.5.6 Experimentally Determined Time- Dependent Properties of Grp	3.41
3.5.6.1 Introduction	3.41
3.5.6.2 Design of Test Specimens	3.42
3.5.6.3 Design of Test Equipment	3.43
3.5.6.4 Test Procedure	3.45
3.5.6.5 Results & Discussion of Results	3.46
3.5.6.6 Conclusions	3.51

CHAPTER 4

STRUCTURAL ENGINEERING DESIGN WITH GRP

4.1 Introduction	4.1
4.2 The Design Process in Grp	4.2
4.3 Material Cost-Effectiveness	4.4
4.3.1 Axial Stiffness	4.5
4.3.2 Flexural Stiffness	4.6
4.3.3 Shear Stiffness	4.7
4.3.4 Plate Buckling	4.8
4.3.5 Cylinder Buckling	4.9
4.4 Process Economics	4.10
4.4.1 The Hand Lay-up Process	4.12
4.4.2 The Basic Spray-up Process	4.17
4.4.3 The Robot Spray-up Process	4.20
4.4.4 The Continuous Spray-up Process	4.21
4.4.5 The Resin Injection Process	4.22
4.4.6 The Hot Press Process	4.23
4.4.7 Discussion of Process Analysis	4.25

<u>CHAPTER 4</u> (Contd)	<u>Page No.</u>
4.5 Preferential Fibre Orientation	4.27
4.6 Joint Design	4.28
4.6.1 Adhesive Joints	4.28
4.6.2 Mechanical Joints	4.31
4.6.3 Combination Joints	4.32
4.7 Safety Factors	4.33
<u>CHAPTER 5</u>	DISCUSSION AND PRELIMINARY DESIGN OF A STRUCTURAL SYSTEM
5.1 Introduction	5.1
5.2 Suitable Structural Function	5.2
5.3 The Preliminary Design of a Long-Span Grp Roof	5.3
5.4 5.3.1 Introduction	5.3
5.3.2 Roof Loading	5.3
5.3.3 Macroscopic Design	5.4
5.3.4 Analysis of Roof Structure	5.7
5.3.4.1 Proposed Design of Roof Surface Element Cross-Section	5.7
5.3.4.2 Verification of the Proposed Roof Design	5.9
5.3.5 Discussion & Assessment of Roof Design	5.19
<u>CHAPTER 6</u>	DESIGN, MANUFACTURE & TESTING OF A MODEL SPAN ROOF
6.1 Introduction	6.1
6.2 Scale of Model Roof	6.2
6.3 Design of Model Roof	6.3

6.3.1	Surface Unit Design	6.3
6.3.2	Cross-bracing Design	6.3
6.3.3	Joint Design	6.4
6.3.4	End Fixing Design	6.5
6.3.5	Materials Summary	6.5
6.3.6	Analysis of Model	6.6
6.3.6.1	Theoretical Elastic Analysis	6.6
6.3.6.2	Empirical Elastic Analysis	6.7
6.3.6.3	Visco-elastic Analysis	6.12
6.4	Preliminary Tests	6.13
6.4.1	Surface Unit Compression Test	6.13
6.4.1.1	Introduction	6.13
6.4.1.2	Description of Test	6.14
6.4.1.3	Results of Test	6.15
6.4.1.4	Conclusions	6.17
6.4.2	Tensile Joint Tests	6.18
6.4.2.1	Introduction	6.18
6.4.2.2	Description of Tests	6.18
6.4.2.3	Results of Tests	6.19
6.4.2.4	Discussion of Results	6.19
6.4.2.5	Conclusions	6.20
6.5	Model Roof Manufacture	6.20
6.6	Model Roof Testing	6.21
6.6.1	Introduction	6.21
6.6.2	Loading Details	6.22
6.6.3	Gauging	6.23

	<u>Page No.</u>
<u>CHAPTER 7</u>	DISCUSSION BETWEEN THEORY & EXPERIMENTAL MODEL TEST RESULTS
7.1	Introduction 7.1
7.2	Presentation & Comparison of Results 7.2
	7.2.1 Deflection 7.2
	7.2.2 Member Loads, Strains & Buckling 7.4
7.3	Discussion of Results 7.6
	7.3.1 Deflection 7.6
	7.3.2 Member Forces, Strains & Buckling 7.8
7.4	Conclusions 7.11
<u>CHAPTER 8</u>	ECONOMIC ASPECTS
8.1	Introduction 8.1
8.2	The Cost of Long Span Grp Roofs 8.2
	8.2.1 Selection of a Grp Production Process 8.2
	8.2.2 Calculation of Roof Cost 8.3
	8.2.3 Additional Costs 8.5
	8.2.4 Possible Developments & Modifi- cations 8.6
8.3	The Long Span Grp Roof Market Potential 8.8
<u>CHAPTER 9</u>	CONCLUSIONS & RECOMMENDATIONS FOR FURTHER WORK 9.1
APPENDIX A	A1
APPENDIX B	B1
REFERENCES	R1

NOMENCLATURE

A

- A - Area
- APM - Factory area per mould.
- A_{ij} - Orthotropic cylinder stiffness elements or inplane stiffness matrix.
- A'_{ij} - Inplane compliance matrix.
- a - Cylinder radius.

B

- B - Material Stiffness.
- B_{ij} - Coupling Matrix.
- b - Plate width.

C

- C - Contiguity factor.
- CPMM - Cost of patterns and master moulds.
- CYCRN - Cylinder buckling cost-effectiveness.
- CYT - Cycle Time.
- CF - Fibre cost to resin cost ratio.
- CT - Cure Time.

- C_f - Cost of fibres.
- C_{ij} - Stiffness matrix.
- \bar{c}_{ij} - Transformed stiffness matrix.
- C_m - Cost of resin.

D

- D_f - Density of fibres.
- D_{ij} - Flexural stiffness matrix.
- D_m - Density of resin.
- d - Maximum depth of roof.

E

- E - Modulus of elasticity.
- EEAN - Axial stiffness cost-effectiveness.
- E_f - Fibre elastic modulus.
- E_l - Longitudinal modulus of elasticity.
- E_m - Matrix modulus of elasticity.
- E_t - Transverse modulus of elasticity.
- \bar{E} - Apparent modulus of elasticity.
- E_1 - Apparent modulus after 1 hour of creep.

F

- F, F_1, F_2 - Force in roof surface.
- FC - Factory costs.
- FLEXN - Flexural stiffness cost-effectiveness

$F_{1(T)}, F_{1(C)}$ - Longitudinal tensile strength and compressive strength respectively.

F_t - Transverse strength.

G

G_f - Shear modulus of the fibres.

G_{lt} - Composite shear modulus.

G_m - Shear modulus of the matrix.

H

H - Laminate thickness.

h - Cylinder wall thickness.

I

I - Second moment of area.

IT - Resin injection time.

K

K - Fibre misalignment factor.

k - Stress intensification factor.

k_x, k_y, k_{xy} - Midplane curvatures.

L

LUR - Laminate lay-up rate.

LUT - Laminate lay-up time.

- l - Crack length, roof span.
- l_c - Ineffective fibre strength.

M

- MPT - Material preparation time.
- MT - Mould Committed time.
- M_x, M_y, M_{xy} - Laminate moment resultants.

N

- N - Buckling load per unit width.
- NOMR - Number of moulds required.
- N_x, N_y - Midplane stress resultants in the x or y direction respectively.
- N_{xy} - Midplane shear stress resultant.

P

- PA - Plan area.
- PCRN - Plate buckling cost-effectiveness
- P_E - Euler buckling load.
- PEL - Product edge length.
- PRPD - Production rate per day.

R

- R - Radius of crack tip.
- RDT - Material consolidation time.
- r - Cylinder radius.

S

- SA - Surface Area.
- SUT - Spray-up time.
- S_A - Fatigue stress amplitude.
- S_C - Stress rupture strength.
- S_E - Fatigue strength at stated life.
- S_M - Mean Stress
- S_U - Ultimate strength of material.
- S_{ij} - Compliance matrix.
- \bar{S}_{ij} - Transformed compliance matrix.

T

- T - Absolute temperature.
- TC - Hot press mould cost.
- TK - Thickness.
- T_{ij} - Transformation matrix.
- t - Time.
- t_r - Time to rupture.

U

- ULT - Unskilled labour time.

V

- V_f - Fibre volume fraction.
- V_m - Matrix volume fraction.

W

- W - Weight.
- WT - Mould preparation time.
- w - Load intensity.

GREEK SYMBOLS

α	- Fibre angle or wind angle
γ_{12}	- Shear strain
δ	- Roof deflection
σ	- Normal stress
σ_{ij}	- Stress component
σ_0	- Stress rupture constant
σ_r	- Rupture stress
ϵ	- Normal strain
ϵ_{ij}	- Strain component
ϵ_w	- Allowable strain
ϵ_r	- Resin percentage elongation at failure
ϵ_t	- Strain at time t.
$\epsilon_x^0, \epsilon_y^0, \epsilon_{xy}^0$	- Midplane strains
ϵ_0	- Constant depending upon material stress and environment
ϵ'_0	- Constant depending upon material environment
τ	- Shear stress
μ_f	- Poisson's ratio of the fibres
μ_m	- Poisson's ratio of the matrix
μ_{lt}	- Major or longitudinal Poisson's ratio
μ_{tl}	- Minor or transverse Poisson's ratio

SUFFIXES

f	- Glass fibre
m	- Resin
csm	- Chopped strand mat
UD	- Uni-directional roving
t	- Time, transverse direction
l	- Longitudinal direction
EB	- Edge-beam
r	- Stiffening ring property
S	- Denoting property per unit width
st	- Stringer property
s	- Skin property
v	- Visco-elastic term
EP	- Empirical elastic term

CHAPTER 1

INTRODUCTION

CHAPTER ONE

Introduction

Glass reinforced plastic (grp) has now been available as a structural material for several decades. However, its use as a major load-bearing material has been very limited in civil and structural engineering. In the main, its structural use has been restricted to roofs of moderate span such as the 17 m span roof over the Morpeth Secondary School in London.

The concern of this project is to investigate the feasibility of long span lightly loaded structures where grp is used as the major structural material. Many forms of glass reinforced laminates have exceptionally good strength to weight ratios. Structures in which this property may be used to advantage, and yet are not rendered unsatisfactory by grp's relatively low modulus of elasticity, may be well suited to this material. Long span lightly loaded structures are potentially of this type.

The problem of feasibility will be approached by making a general survey of the properties of glass reinforced plastics, and then investigating in greater depth, theoretically and in some cases experimentally, the more relevant structural properties. With the knowledge gained, general design philosophies will be discussed and the cost effective design of laminates under various loading systems investigated. Also the financial aspects of several production techniques will be studied. Having examined the material and its application, suitable long span structures are discussed and a particular structural function chosen for further investigation. A design study will then be carried out and analysed on a structural and financial basis. The design will be verified by the manufacture and testing of a model structure. Attention will be paid to the potential market of the structure and hence the associated consumption of glass fibres, since the Pilkington Group, who manufacture glass fibres, sponsored this project.

CHAPTER 2

DISCUSSION OF THE PROPERTIES OF GRP
RELEVANT TO STRUCTURAL ENGINEERING

CHAPTER TWO

Discussion of the Properties of Grp Relevant to Structural Engineering.

2.1

Introduction

Grp has been used for some years in structural engineering, although in comparatively small quantities. By far the most common constituent materials used have been 'E' glass fibres, as reinforcement, and polyester resin, as the matrix. The reason for this is that these two materials possess the best combination of economic and structural properties relevant to the construction industry. Consequently, most attention has been directed towards these materials in preparation of this thesis. It should, however, be realised that these materials are available in many forms and thus may have a wide range of properties. Figure 2.1 shows several forms of glass reinforcement.

The following chapter is a brief description of grp's important and relevant properties together with the role played by the constituents.

2.2

Ultimate Strength

As mentioned above, glass reinforcement, the main strength - giving constituent, can be incorporated in grp in many different forms and as a result the material may possess either general anisotropic properties, special cases of anisotropy, or isotropic properties. The materials are never microscopically homogeneous but are often considered to be macroscopically homogeneous. The strongest forms of grp are those with orientated reinforcement. In this case, high strengths are only found in particular directions and the composite is of the anisotropic type. Figure 2.2 demonstrates the strength anisotropy of various designs of laminates in tension. A similar diagram could be drawn for compressive strengths which in general are lower. The difference in these strengths can be explained in terms of the micromechanics of fibre-reinforced plastics.

Composite tensile strength in the direction of the fibres depends upon a strong, stiff bond, either frictional or chemical, between the glass fibres and the resin. This is necessary so that the applied force can be transferred through the resin into the fibres by a shear mechanism. Thus a finite length of fibre is required before the maximum stress in the fibre is reached. This is particularly important for short fibre reinforcements such as chopped strand mat. Fig. 2.3 shows a simple model of a fibre in a matrix and how the load varies in the fibre and matrix. Solutions for this model have been

obtained by Cox [2.1], Dow [2.2], and Rosen [2.3]. Due to the ineffective length of fibre l_c , the longer the fibre then the greater the proportion of the fibre that is used efficiently, and the stronger the composite. Continuous fibres are the ideal, but in practice, although such fibres may have been used in the manufacture of the laminate, fibres will only be continuous at low stress levels. The strength of fibres reduces with increase in length [2.4, 2.5] due to a statistical distribution of flaws.

Resin structural properties have little effect on the longitudinal tensile properties, provided that elongation of the resin at failure is greater than the ultimate strain of the glass fibres [2.6.]

The tensile strength of aligned grp increases approximately linearly with fibre volume fraction within practical limits determined by the type of reinforcement used. Outside these limits, resin - rich or starved regions have a deleterious effect.

The transverse tensile strength of a unidirectional laminate is resin-dominated according to Hashin [2.7] and is of the same order as the strength of the matrix but lower [2.8]. The void content of the resin has a significant adverse effect on the strength; as much as 50% of the unvoided strength can be lost with a 2% voidage [2.9]. Increasing fibre volume fraction also has a deleterious effect.

Since the modulus of elasticity of the glass fibres is far greater than that of the resin the average stress is much greater in the fibres than in the resin. Notwithstanding this, the resin plays a major part in the longitudinal compressive strength of grp. The fibres act as columns supported in a continuous elastic or elastic/plastic medium; the resin. Ultimate failure occurs on fibre

buckling or debonding between the resin and glass [2.10]. Figure 2.4 shows schematically two modes of fibre buckling and the expected compressive strengths on this basis according to Rosen [2.3] for a glass-epoxy laminate. Predicted strengths have never been achieved in practice. The maximum strength is obtained when the fibre volume fraction is about 60 - 65% [2.8, 2.11]. At higher volume fractions the fibres are not adequately supported, and the strength reduces. In general, anything which gives additional support to the fibres improves the compressive strength, particularly high resin yield strengths and stiffnesses [2.11].

Voids again play an important role in decreasing the strength both in the longitudinal and transverse directions [2.9, 2.12].

The transverse compressive strength is largely governed by the compressive strength of the matrix which is an upper bound [2.7].

Flexural strength has been found commonly to lie between the compressive and tensile strengths of the material. Usually failure occurs in the outermost fibres in compression, but with compressive stresses higher than the simple compressive strength. This may be due to fibres closer to the neutral axis, under lower stress, providing the outer fibres with more support than they would receive if all fibres were equally stressed.

Glass fibres, within laminated composites, are rarely found in directions other than in the plane of the composite. This produces the possibility of interlaminar shear (ILS); a phenomenon peculiar to fibre-reinforced composites. The ILS strength may be an order of magnitude lower than the longitudinal tensile or compressive

strengths and must be considered an important weakness of the material. ILS occurs along resin-rich planes where there are very few or no transverse fibres to halt the progression of cracks.

This strength is largely dependent on the resin shear strength and the resin-glass interfacial bond strength. The fibre content has a small but adverse effect on the interlaminar shear strength [2.8].

Voids tend to accumulate in resin-rich areas particularly between layers of cloth or mat, and greatly reduce the ILS strength [2.12, 2.13].

Voids in laminates clearly have an important effect on their strength. The quantity of voids depends upon many factors, particularly the type of glass fibre, mat or fabric used and the laminate manufacturing process. For many commercial laminates the volume of voids can be expected to lie between 1 and 2.5% [2.14]. Reductions in strength of upto 10% to 40% can be expected on the void-free strength.

Figure 2.5 shows a range of tensile and compressive strengths which are found in commercially available grp laminates and sections compared to other structural materials. Steel is grp's strongest competitor but even this material compares poorly with many types of grp on a specific strength basis.

In general, for maximum efficiency, the fibres should be parallel to the direction of the major stresses. Where these stresses occur in more than one direction, fibre reinforced composites become

less efficient. Proctor [2.15] illustrates the reason for this (Figure 2.6); not only is the fibre reduced in the principal directions but also the total fibre volume fraction is reduced.

2.3

Stress Rupture

Stressed grp in normal environments exhibits a loss of strength with time (Figure 2.7). The magnitude of the loss may be significant and should be considered when choosing design stresses. Both the major constituents of the composite, the resin and fibres, together with the interface, contribute to the loss. Water is well accepted as a major cause of the phenomenon. Temperature also greatly affects the rate of reduction in strength.

Figure 2.7 shows the results of several workers in this field [2.16, 2.17, 2.18, 2.19]. Although they all worked with apparently similar material there is clearly a great difference in the results. Consequently the designer must make conservative estimates of strength, which leads to inefficiency unless tests are carried out on the design material.

This topic will be treated more fully both theoretically and experimentally in the following chapter.

Figure 2.8 compares the absolute and specific flexural modulus of commercially available laminates and sections in grp with other structural materials. Grp compares poorly on both bases although better from the specific point of view. As stated previously, laminated grp exhibits in-plane anisotropy unless specially orientated or random reinforcement is used. Figure 2.9 illustrates the stiffness anisotropy for several fibre systems. A derivation of these curves may be found in Chapter 3.

Moduli in the direction of fibres are governed principally by the fibres and increases linearly with increase in fibre volume fraction. Shear and transverse stiffness in unidirectional laminates are similar to the resin moduli. They are increased slightly with fibre volume fraction and the compressive transverse modulus tends to be greater than the tensile. Voids in general have a considerably smaller effect on laminate moduli than strength, but are significant in the case of transverse and shear moduli [2.9].

In the short term, grp is generally accepted as being linearly elastic to failure even though this is only approximately true.

Grp is visco-elastic; that is, its extension under stress is a function of time. Hence, where grp is to be stressed for other than very short periods, which could be as short as a few minutes at relatively high stress levels, the consideration of only the short term modulus of elasticity is insufficient. Examples of the work of Kabelka [2.16] and Boller [2.17] are shown in Figure 2.10 in this respect. The characteristic creep curve, as suggested by Steel [2.18], consists of three stages: initial rapid increase in strain; a comparatively long period of time at a minimum rate of creep; and finally a second period of rapid extension to failure (Figure 2.11). Steel's work was endorsed by Diggwa and Norman [2.19]. However, these workers based their conclusions on flexural creep results. Boller [2.17] and Kabelka [2.18] who were concerned with tensile or compressive creep failed to observe the tertiary stage. This may be explained in that progressive failure in flexure may be extended due to the non-uniform stress distribution; highly stressed outer fibres failing first, causing a loss in flexural rigidity and an increased deflection. Inner fibres having been previously under lower stress would not have lost as much strength and may be expected to resist the increased load for some time. Diggwa and Norman's characteristic curve may be further held in doubt since their equipment design would cause an increase in applied bending moment with increasing strain. Thus it is possible that the creep curve is different under direct stress from that in flexure. There may be a tertiary stage under direct stress but spanning a much shorter

period of time in relation to the secondary stage, than suggested by Steel.

Both the resin and the fibres contribute to the creep but the greater contribution is made by the resin. Consequently, short fibre grp is most prone to creep. Unidirectional continuous fibre grp is the most resistant to creep. The creep mechanism will be considered in greater depth in Chapter 3.

2.6

Dynamic Fatigue

As is the case with other structural materials, repeated loading of grp can cause failure at stresses below the short term ultimate stress. Unlike ferrous metals, however, grp does not have an endurance limit whereby the material can withstand unlimited cycles provided the stress is below this limit.

Owen et al [2.20, 2.21] have observed that failure in chopped strand mat (CSM) occurs in three stages; debonding, cracking and finally separation. After 10^6 cycles CSM was found to endure approximately $4 \times 10^4 \text{ KN/M}^2$ reversed stress before separation and approximately $1.2 \times 10^4 \text{ KN/M}^2$ before debonding and cracking. Boller [2.22], using epoxy resin and 181 fabric reported a reversed stress fatigue strength of $8 \times 10^4 \text{ KN/M}^2$ after 10^6 cycles. After 10^7 cycles polyester laminates can be expected to have a strength of between 18% and 37% of their short term strength [2.23].

In general the order of superiority for reinforcements under uni-axial stress is the same as for other properties; orientated reinforcement is better than random, unidirectional material being best; and unwoven fabric is preferable to woven.

Grp is relatively sensitive to mean stress, and as a consequence the Goodman law:

$$\frac{S_A}{S_E} = 1 - \frac{S_M}{S_U} \quad 2.1$$

where S_A = stress amplitude

S_E = fatigue strength at stated life

S_M = mean stress

S_U = ultimate strength of the material

has been found inadequate [2.22, 2.21]. Boller has suggested a modified law:

$$\frac{S_A}{S_E} = 1 - \frac{S_M}{S_C} \quad 2.2$$

where S_C = stress rupture strength

A further adjustment has been proposed by Owen and Smith [2.21] where the mean stress is tensile:

$$\frac{S_A}{S_E} = \frac{1 - \frac{S_M}{S_C}}{1 + \frac{S_M}{S_C}} \quad 2.3$$

Little work has been done on the anisotropy of fatigue, multi-axial stress and random stress cycles. Water appears to have

little effect on grp when there is a long life span [2.24].

2.7

Ductility and Fracture Toughness

Glass and polyester resin are both brittle materials and their combination produces a brittle composite; that is, the large plastic deformation mild steel and other metals experience before ultimate failure does not occur. This has two important structural implications. Grp cannot stress-relieve as effectively as mild steel at points of stress concentration. Hence mechanical jointing requires more care, and stress redistribution due to plastic deformation cannot be relied upon in statically indeterminate structures. Steel structures exhibit large deformations before catastrophic failure, which may serve as a warning to people in their locality. Such warning signs would not be automatically inherent in a grp structure.

Although grp is brittle it does have fracture toughness. A crack in the resin, which may be caused by a broken or transverse fibre, a void, a pre-existing crack or a surface irregularity, does not necessarily cause failure as it may do in a brittle homogeneous material. Cracks in brittle materials propagate easily because the average field stress is magnified by a factor k where

$$k \doteq 1 + 2\sqrt{l/R} \quad 2.4$$

and l = length of crack

R = radius of crack tip.

Thus sharp cracks are more dangerous than blunt ones.

If the resin-glass interface strength is less than approximately $\frac{1}{3}$ of the cohesive strength of the matrix then an advancing crack encountering a fibre behaves as shown in Figure 2.12. The fibre-resin interface breaks down and the crack spreads along the fibre. In effect, the radius of the crack tip has been increased and the stress concentration factor, k , reduced. It should be noted that there is a conflict of interests between fracture toughness, requiring low interface strengths, and composite strength requiring high interface strength. Normally, a satisfactory compromise is obtained if the interface strength lies between $1/5$ and $1/3$ of the matrix cohesive strength [2.6].

2.8

Durability

It is known that grp may suffer a reduction in strength, modulus and appearance and an increase in brittleness on exposure to the elements. Water and ultra-violet light are the main agents of degradation [2.25]. Hence, resins with low water absorption and which are stabilised against ultra-violet light give better weathering characteristics. Heat can also permanently affect the properties of the composite.

Manufacturing technique and quality control are important if the laminate is to be durable. Resin-rich and resin starved areas, which are crack prone, can lead to rapid deterioration due to the resulting ingress of moisture. However, high resin contents are desirable.

Resin rich surfaces, known as gel coats, have been beneficial to the durability of grp laminates. In addition, when the gel coat is reinforced with a surface tissue its good appearance is prolonged, and where relevant, transparency maintained [2.25, 2.26].

The magnitude of the reduction in mechanical properties has not been satisfactorily established. A loss in strength of 10 and 20% is common after exposure for 3 years [2.27]. Algra and von der Beck [2.28] tested various laminates under several conditions for upto 10 years. They found that bi-phenol A polyester resin was superior to iso-phthalic resin, with phthalic acid anhydride polyester enduring least well. Laminates with the bi-phenol resin showed no deterioration in flexural strength or stiffness after exposure for 5 years. A similar laminate of phthalic acid anhydride resin reduced in strength by under 25% and in stiffness by less than 10%. Fire retardant resins generally have poorer strength retention than other resins, and Rugger [2.29] estimates that a factor of 2 applies.

The degree of degradation depends on the climate of the location of the composite, whether the location is urban or rural; if urban the level of atmospheric pollution is important. Even when these variables are known, one side of a pitched roof may weather differently from the other depending upon the amounts of sunlight each receive.

Weathering under stress has not been widely studied. However, tests in Florida, USA, [2.30] with a chrome finish glass fabric and polyester resin composite unstressed, and stressed in flexure at about 25% of the ultimate strength, showed that upto 40% of the strength was lost over 3 years. The difference between the

stressed and unstressed results was small.

Storage in water at 20^oc was found to be more severe than outdoor exposure in Holland [2.28]. A considerable amount of work has been carried out on creep and stress rupture in water, which could be used as a conservative estimate of durability in northern European climates.

In the past, grp has been marketed as maintenance-free. This is not so if its initial properties are to be retained for as long as possible. Estimates as to the required frequency of maintenance are varied and will depend upon the exposure conditions. Hosing down regularly and refinishing every 7 or 15 years if a special gel coat or pvf film is used, is more than adequate, according to grp manufacturers [2.25].

Grp is a relatively new material, and consequently manufacturers are not yet prepared to give guarantees on the life of products. However, grp boats have been in use for over 20 years, and as this period extends, manufacturers will become more confident. Scott and Metthan [2.17] expect guarantees of 60 years soon to become commonplace.

2.9

Thermal Properties

As with other properties, the thermal properties of grp vary with the form and quantities of the constituents. Polyester resin has a larger coefficient of expansion and is a better thermal insulator

than glass. Grp is a considerably better insulator than either steel or aluminium, and has a lower coefficient of expansion than aluminium. Thermal properties are summarised in Figure 2.13.

Grp is readily combined with low density plastic foams to form sandwich panels which can have exceptionally good insulating properties [2.31].

Since glass and polyester have differing coefficients of expansion, when laminating takes place at temperatures above ambient, residual stresses result. These stresses may reduce the composite strength and cause warping [2.32].

2.10

Mouldability

Grp has often been said to give the designer a new degree of freedom in that he can now design the material as well as the shape of the component. The extent to which he can do this is limited by the economic moulding techniques available to him for producing a particular form of reinforcement. The reinforced plastics industry has developed many moulding techniques, some of which are listed below:

- 1) Contact Moulding
- 2) Spray-up
- 3) Robot-spray
- 4) Pressure bag
- 5) Vacuum bag
- 6) Autoclave

- 7) Cold press moulding and resin injection
- 8) Hot press moulding
- 9) Filament winding
- 10) Pultrusion
- 11) Continuous laminating
- 12) Preform

Basic aspects of these processes are outlined below.

2.10.1 Contact Moulding

Contact moulding, otherwise known as hand lay-up, is the original, most basic and common manufacturing technique. Its widespread adoption is mainly due to the low capital cost involved in setting up production. Only one male or female mould is required. The mould is relatively cheaply made from polyester, or, for longer life, epoxy resin. Ancillary equipment may be limited to brushes, ringed rollers, mixing equipment, trimming knives, and safety equipment, all of which can be bought for tens rather than hundreds of pounds. As the process requires little capital it is most suitable for low production rates.

This process is particularly appropriate to the construction industry since there are no size limitations. Complex shapes and changes in thickness are readily accommodated.

All types of reinforcement can be used, with the exception of continuous filament mat. Unwoven rovings are not often used. Low density plastic foams are frequently incorporated to increase

flexural rigidity.

Since only one mould is used, only one smooth surface is possible. The other surface is rough and shows fibre patterns. The thickness of the composite is difficult to control accurately and depends upon the skill of the laminator. Generally laminate quality is very variable and can lead to high void contents and resin-rich areas.

Although little capital equipment is involved the process is labour intensive. The main operations involved are outlined below, assuming the mould is already in use:

- 1) The mould is treated with release agent to facilitate removal of the product.
- 2) A gel coat and surface tissue are applied if required.
- 3) If only a gel coat is applied this must be allowed to gel.
- 4) Catalysed resin and tailored glass reinforcements are layed-up.
- 5) The laminate is stippled with a brush and rolled to ensure good wet-out and minimum voidage.
- 6) The laminate is allowed to gel. This may take place at room temperature, or heated, quickening the reaction.
- 7) Preliminary trimming may take place once the resin has reached a leathery hardness.
- 8) Full curing.
- 9) Removal from the mould and finishing.

A common time-saving modification to this process is to spray the resin onto the fibreglass.

2.10.2 Spray-up

In spray-up, as the title suggests, the glass and resin are sprayed together from a gun onto a mould. This results in considerable labour saving on contact moulding and, provided the spray-up machine is fully utilised, can result in corresponding cost reductions. The initial investment is higher than in the previous process but is still low compared with other industries.

This process is most applicable where large simple mouldings are required, and strength and accuracy of thickness are not a major requirement. In pure spray-up only one reinforcement is used, i.e. chopped rovings. However, other reinforcements can be hand-layed in position in addition to the sprayed material.

The same moulds may be used for spray-up as for contact moulding and the laminating procedure is similar. Stippling and material tailoring is not necessary but rolling is required.

2.10.3 Robot Spray

Robot spray is a further step towards mechanisation beyond spray-up. In this case the spray gun operator is replaced by a numerically controlled machine. In other respects the process is similar to spray-up.

The removal of the spray gun operator leaves a requirement for only unskilled labour.

2.10.4 Pressure Bag

This process is again similar to contact moulding except that consolidation is achieved with the use of a tailored flexible membrane. The mould is sealed using a pressure plate, and compressed air is pumped between the plate and the membrane.

2.10.5 Vacuum Bag

In this case, rather than applying a pressure as in the preceding process, air is drawn out from between the membrane and the mould surface. Thus atmospheric pressure is used in consolidation.

2.10.6 Autoclave

This system is an adaptation of the previous two processes and can operate in two ways. In one case a positive pressure is applied to the flexible membrane using steam, and in effect the autoclave replaces the pressure plate. Alternatively, steam is used in addition to a vacuum between the membrane and mould. The size of moulds is restricted by the capacity of the autoclave.

2.10.7 Cold Press Moulding & Resin Injection

These processes involve both male and female moulds which are brought together to enclose the product. Both moulding surfaces can thus be of high quality if desired and close thickness tolerances are obtainable. Relatively few voids obtained with these processes lead to high strength laminates. All types of reinforcement may be used, but if chopped strand mat is used it must incorporate an insoluble binder.

The two processes differ primarily in the timing of resin introduction. In cold press moulding resin is poured into position before closure of the moulds. This forces the resin through the reinforcement, pushing air out before it. When the resin is to be injected the moulds are closed before introduction of catalysed resin under pressure.

Size limitations for cold press techniques depend upon the size of the press. There are no size limitations associated with resin injection, but more than one injection point may be required.

Capital outlay is higher for these processes compared with hand lay-up and spray-up. The moulds are between $2\frac{1}{2}$ and 5 times more expensive than simple contact moulds [2.33]. Presses and resin injection equipment also have to be procured. Injection equipment can often be considerably cheaper than a press, but when large mouldings are required, mould-opening equipment is necessary.

2.10.8 Hot Press Moulding

The title "Hot Press Moulding" is normally reserved for processes using sheet-moulding compound or dough-moulding compound, both of which are plasticine-like materials comprising of short glass fibres, resin, and filler. Both types of compound are highly viscous and require high pressure for moulding. They also require heat to cure. Consequently, the cost of presses and moulds leads to much higher capital investment than for other processes.

The main advantage of hot press techniques is that they greatly increase production rates; a factor of 30 or 40 applies when compared to hand lay-up [2.33].

2.10.9 Filament Winding

After passing through a reservoir of resin, continuous reinforcement is wound onto a mandrel-like mould. This process is capable of producing grp of the highest strengths and stiffnesses. However, production rates are normally slow and its use has been mainly in the aero-space industry.

Modifications to the process have been made for the production of pipes where reinforcement is sprayed onto a rotating mould [2.34].

2.10.10 Pultrusion

Pultrusion is a continuous process mainly for producing rod stock. However, any straight section which has a constant thickness along the length is suitable.

Continuous reinforcement is fed through a resin bath, formed in dies and then oven-cured. Production rates of upto 5 or 6 ft. per minute are possible [2.31].

2.10.11 Continuous Laminating

In continuous laminating, reinforcement may be either sprayed or unrolled onto a conveyor belt between two sheets of cellophane. Resin may be either sprayed or applied using a resin dip. Curing takes place as the laminate passes through a heated zone.

This process is the most economical way of producing large quantities of long flat or corrugated sheets which are used typically for cladding purposes.

2.10.12 Preforming

Chopped fibres are drawn onto a preform screen by air suction, together with a binder to hold the fibres in position. The shape of the screen matches the final product, so that material tailoring is eliminated. The preform is transferred to a press where the resin is added and the product finished.

This process is readily automated and is very economical for large numbers of small and medium sized products.

These processes may be studied in greater depth by referring to "SPI Handbook of Technology and Engineering of Reinforced Plastics/Composites" 2nd ed., by Mohr, J.G., Van Nostrand Reinhold, 1973.

Polyester resins inherently have a low resistance to fire compared with other structural materials such as steel and concrete. Grp's fire resistance can be improved, however, by the use of additives such as paraffin wax, chlorinated paraffin [2.35] and Halogen [2.36].

Resins are commercially available which meet standard Class 1 in BS 476 part 7, 1972, for surface spread of flame. The requirements of BS 476, part 3, 1958, Ext FAA and Ext SAA can also be met.

With the use of additional materials, grp cladding panels have achieved Class '0' surface spread of flame standard, which is the most demanding classification. The conventional gel coat, in this case, was replaced by a urethane lacquer [2.36]. Comparatively long fire penetration times have been achieved using phenolic foam, manufactured by SRL. Ltd., Liverpool, in conjunction with grp.

The type of reinforcement used can effect the performance of grp in fires. Woven rovings have been found to act as a fire barrier after the resin has been burnt off. Discontinuous fibres would fall away once the resin was lost.

A major obstacle to the widespread acceptance of grp in the construction industry is its cost. Weight for weight, grp can be 4 or more times as expensive as structural steel. Due to grp's relatively low density it is much more competitive on a volume basis.

In many circumstances it is possible to overcome the cost disadvantages with careful design. The designer must utilise the material to the full by taking into consideration its durability, aesthetic potential, mouldability and strength-to-weight ratio. Normally, economics will lead the designer to use light, thin-walled sections rather than solid ones as may be found in concrete.

FIG. 2.1 TYPES OF GLASS REINFORCEMENT

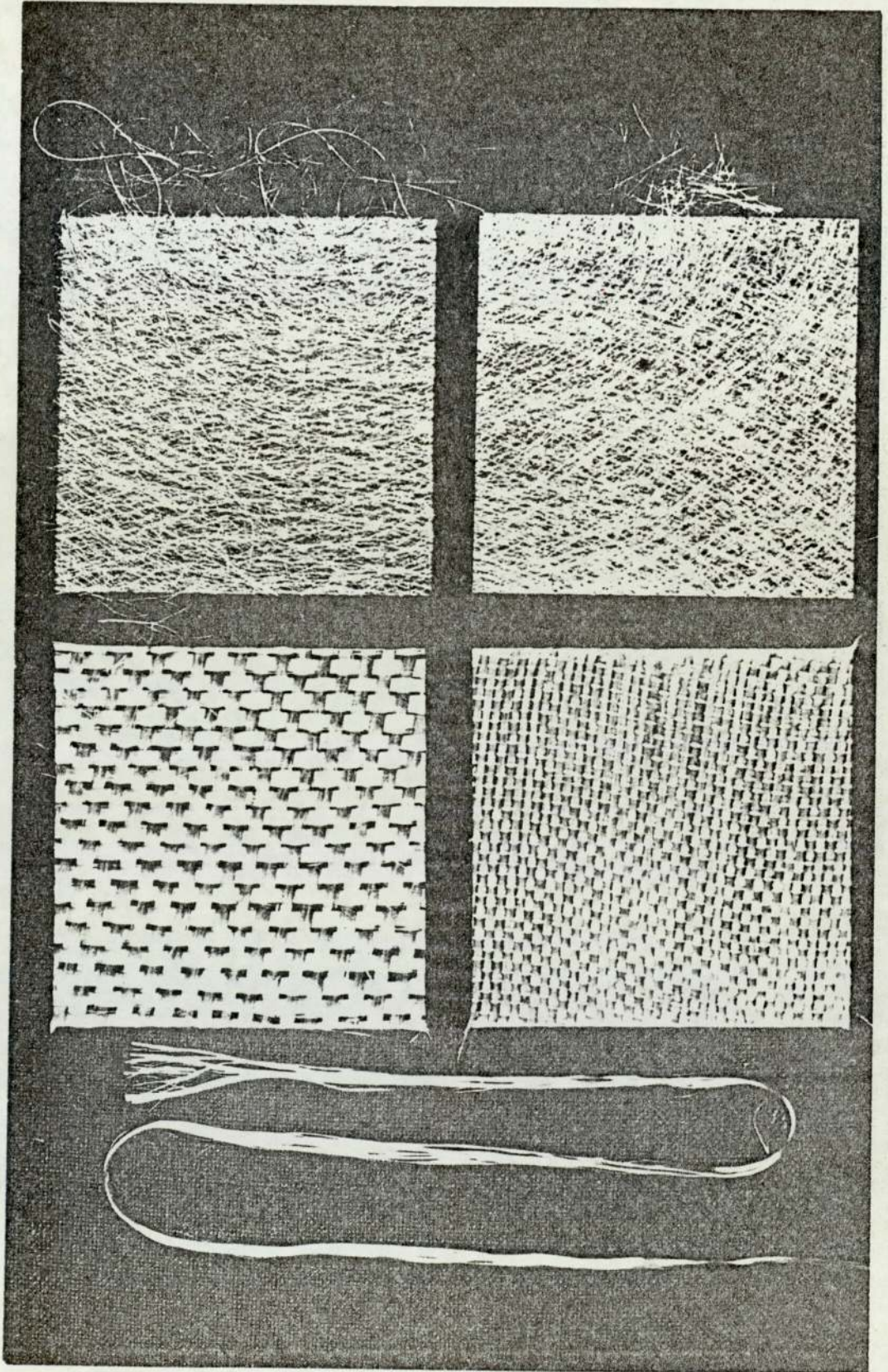


FIG. 2.2 STRENGTH ANISOTROPY

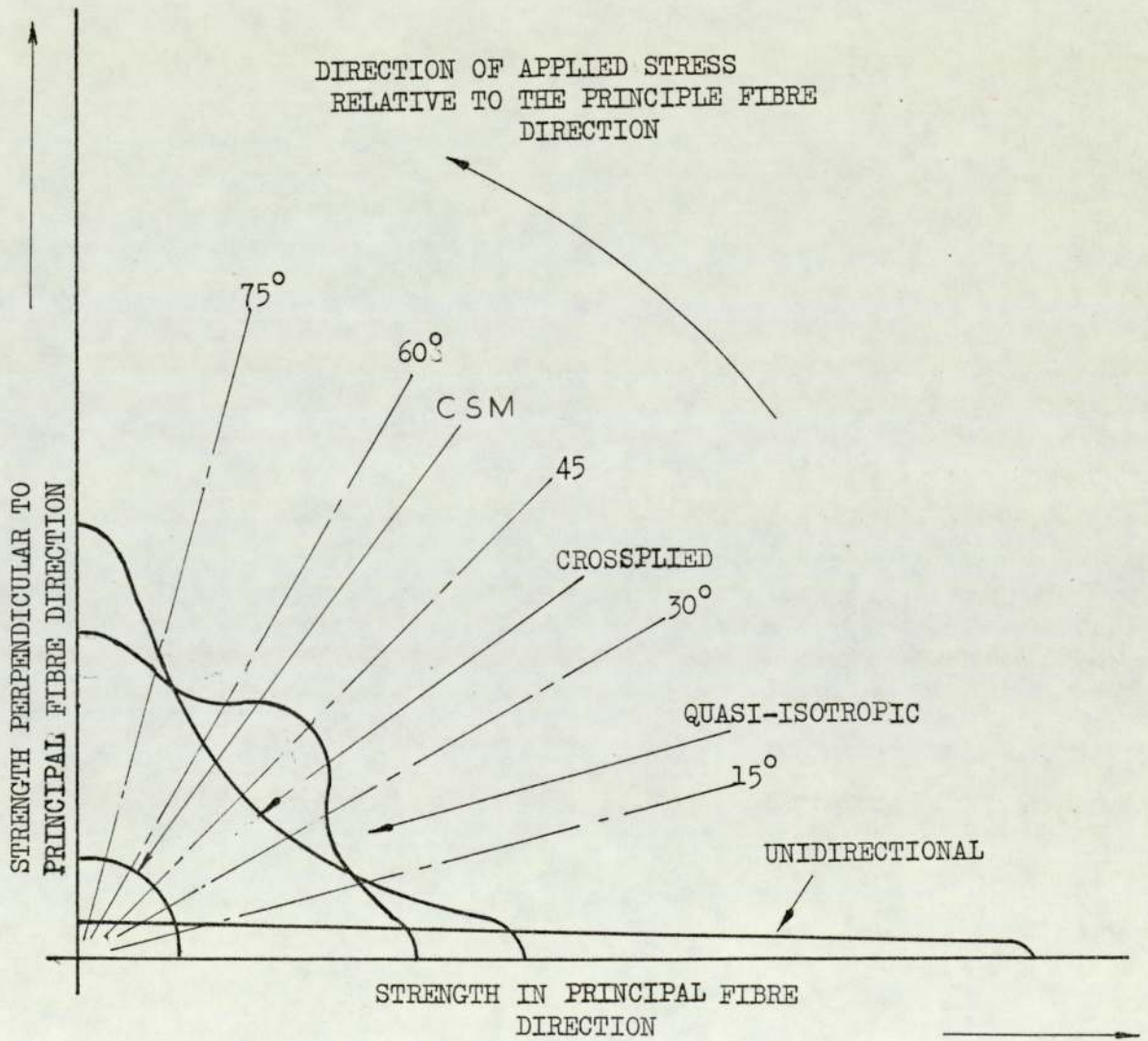
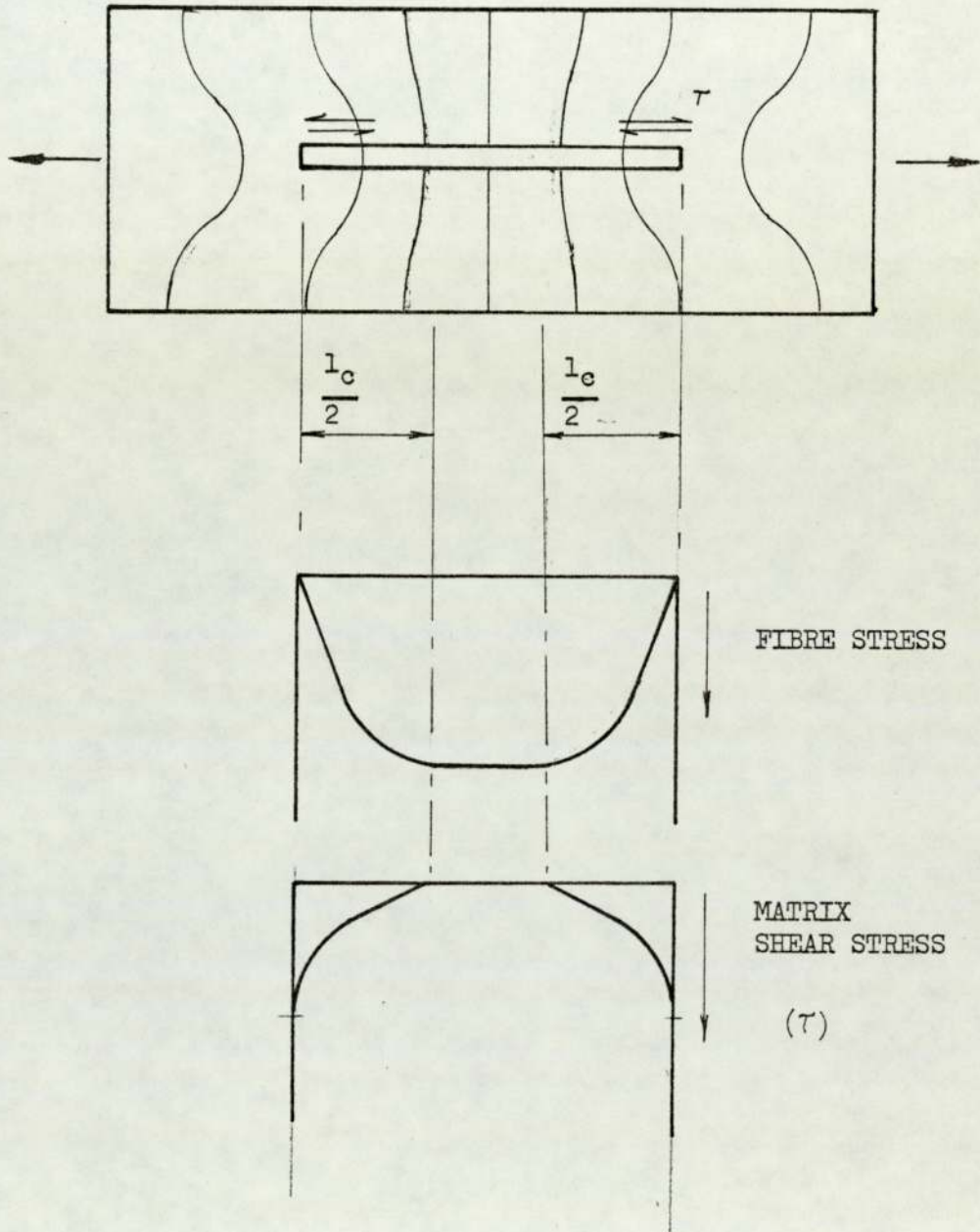


FIG. 2.3 STRENGTHENING MECHANISM



$l_c =$ INEFFECTIVE FIBRE LENGTH

FIG. 2.4 COMPRESSION STRENGTH

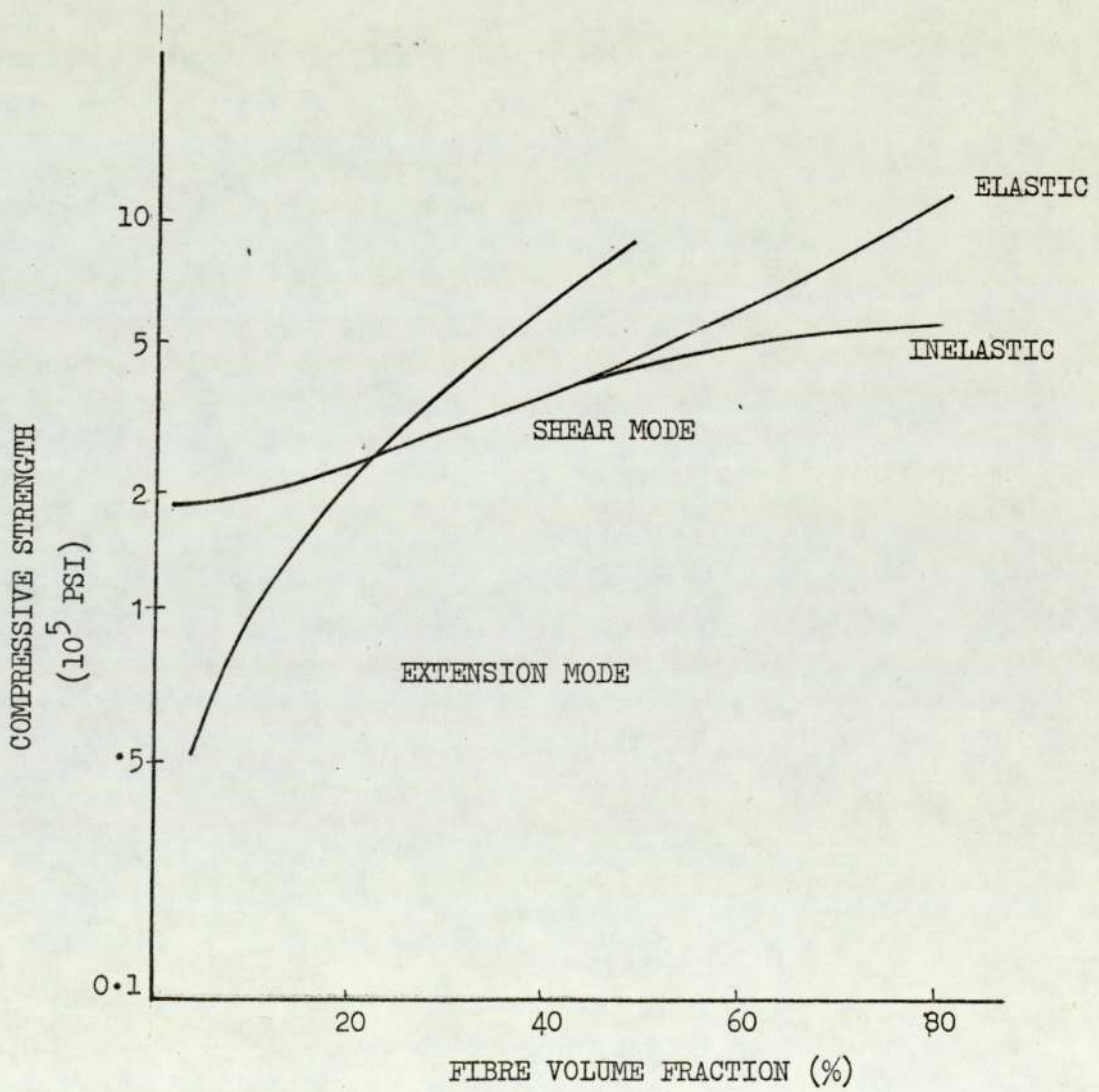
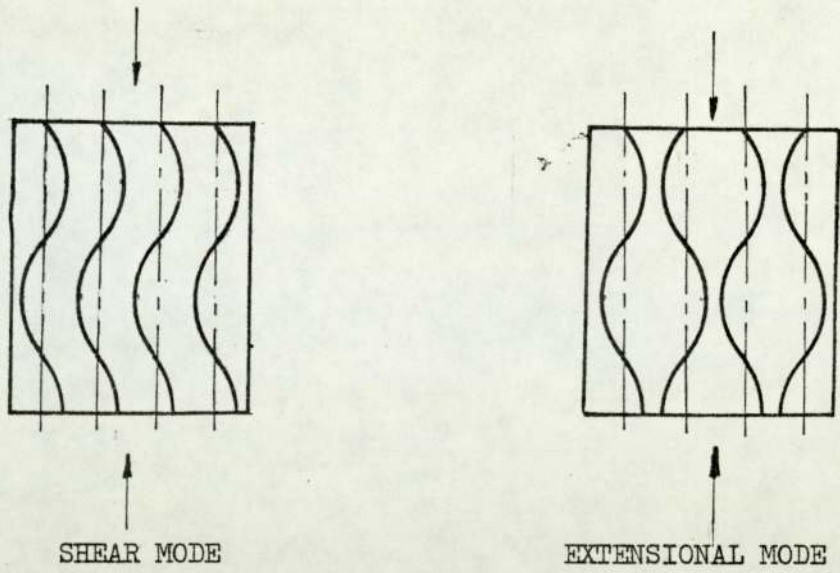
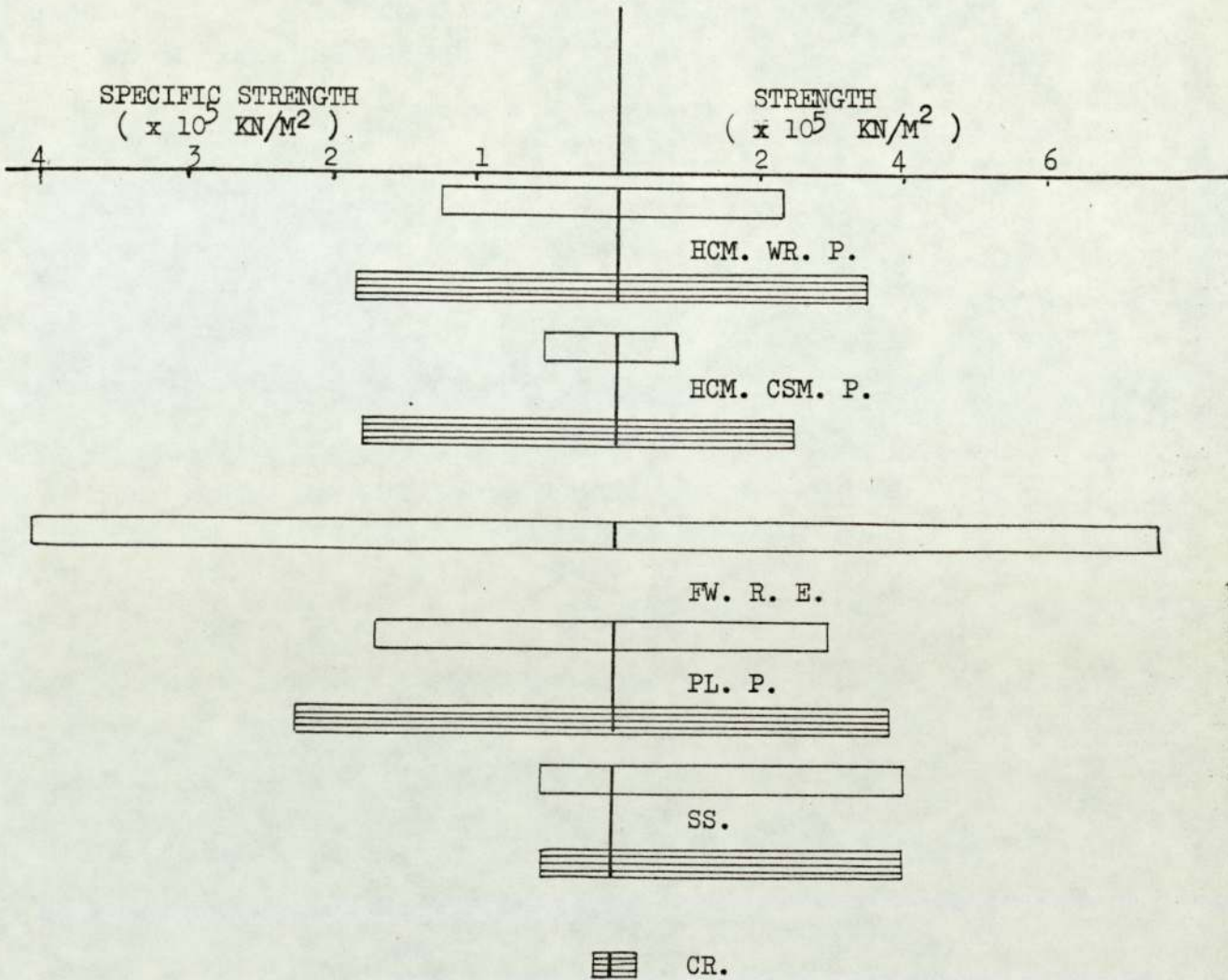


FIG. 2.5 STRENGTH OF STRUCTURAL MATERIALS



KEY

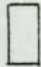



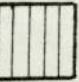
-  - TENSILE STRENGTHS
-  - COMPRESSIVE STRENGTHS
- HCM - HOT COMPRESSION MOULDING
- FW - FILAMENT WINDING
- PL - PULTRUSION
- CSM - CHOPPED STRAND MAT
- WR - WOVEN ROVINGS
- SS - STRUCTURAL STEEL
- CR - CONCRETE
- R - ROVINGS
- P - POLYESTER
- E - EPOXY

FIG. 2.6 FIBRE PACKING DENSITIES & COMPOSITE STRENGTHS

-  - THEORETICAL MAX. FIBRE VOLUME FRACTION
-  - PRACTICAL MAX. VOLUME FRACTION
-  - COMPOSITE PROPERTIES AS A FRACTION OF FIBRE PROPERTIES

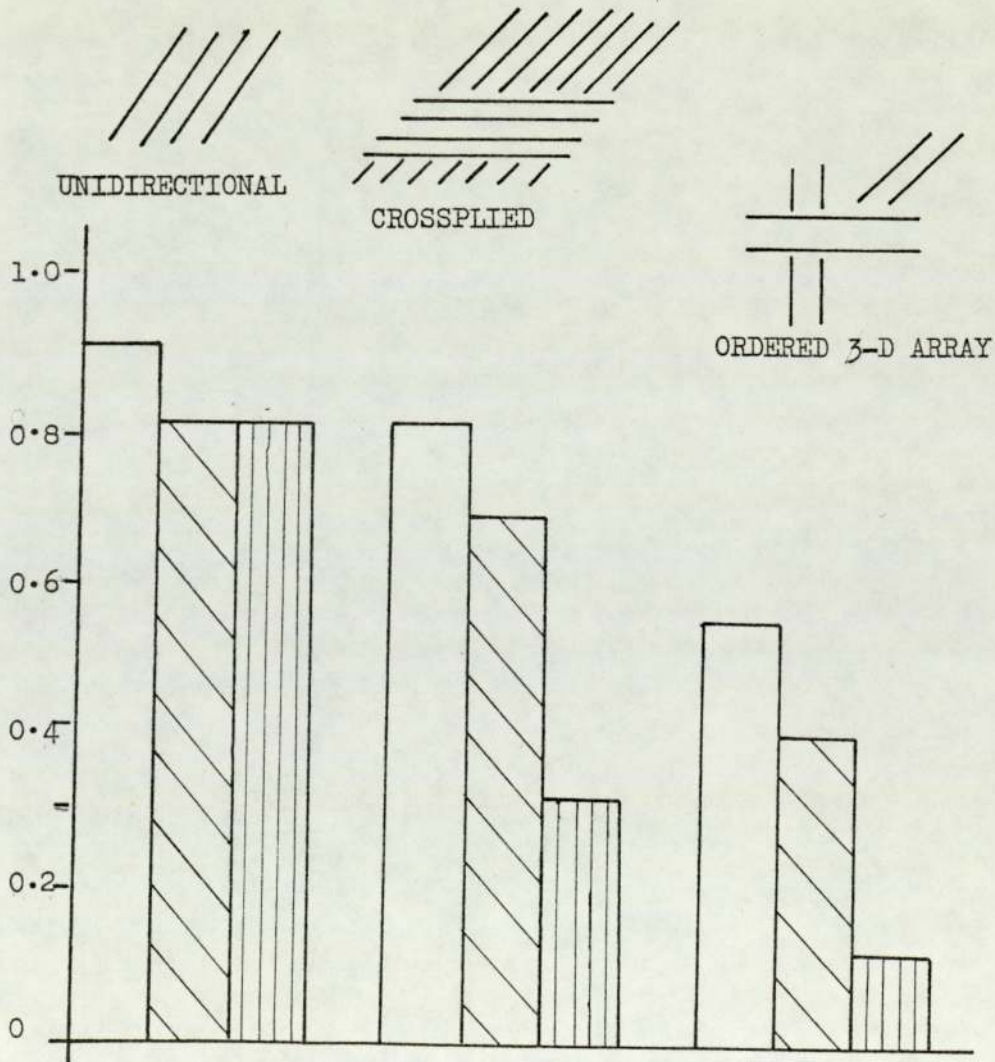


FIG. 2.7 LOSS STRENGTH WITH TIME

1	BOLLER	IN AIR	TENSION	[2.17]
2	BOLLER	IN WATER	TENSION	
3	BENJAMIN	IN WATER	TENSION	[2.31]
4	STEEL	IN AIR	FLEXURAL	[2.18]
5	STEEL	IN AIR	FLEXURAL	
6	KABELKA	IN AIR	COMPRESSION	[2.16]
7	KABELKA	IN AIR	TENSION	

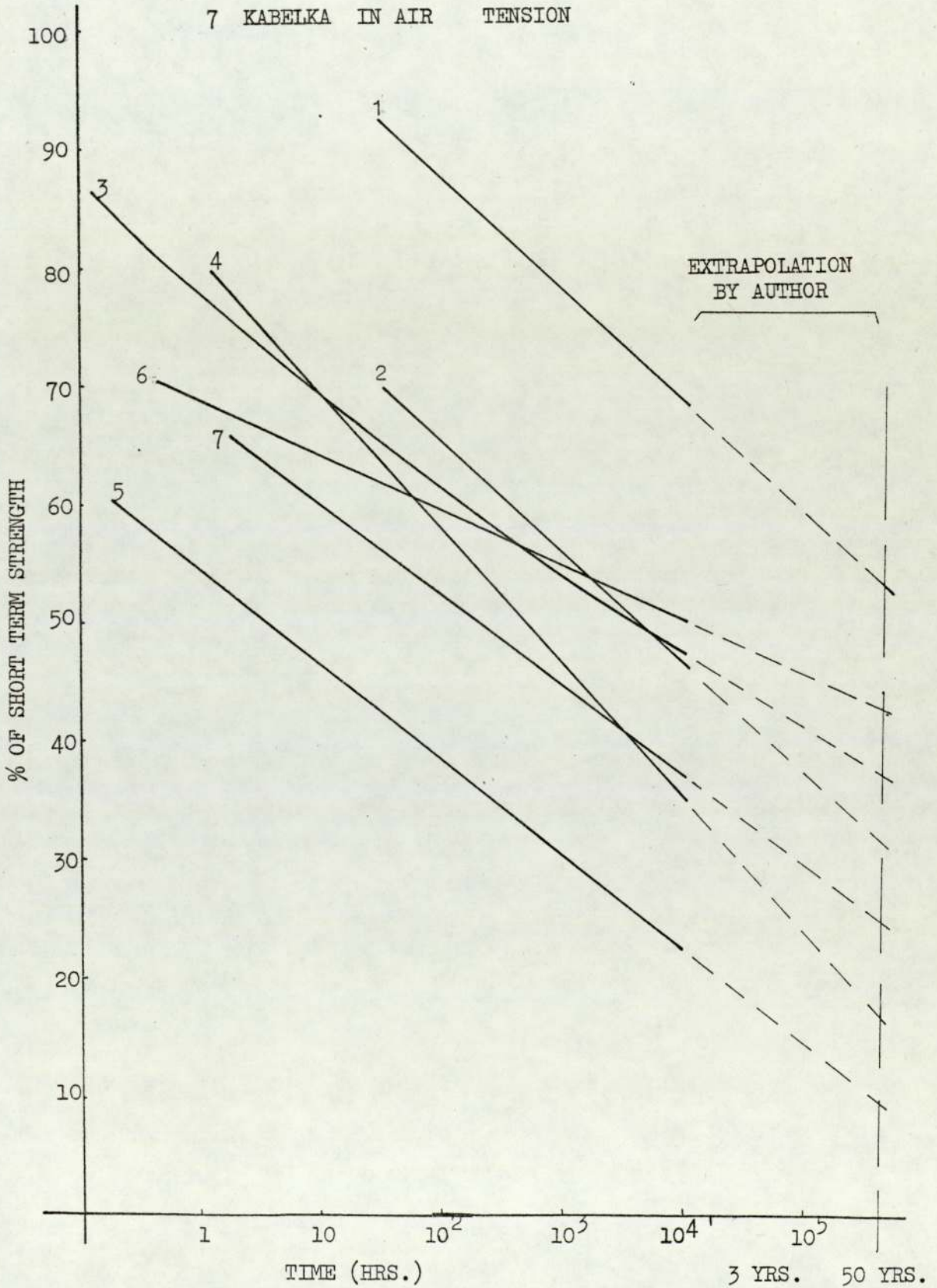
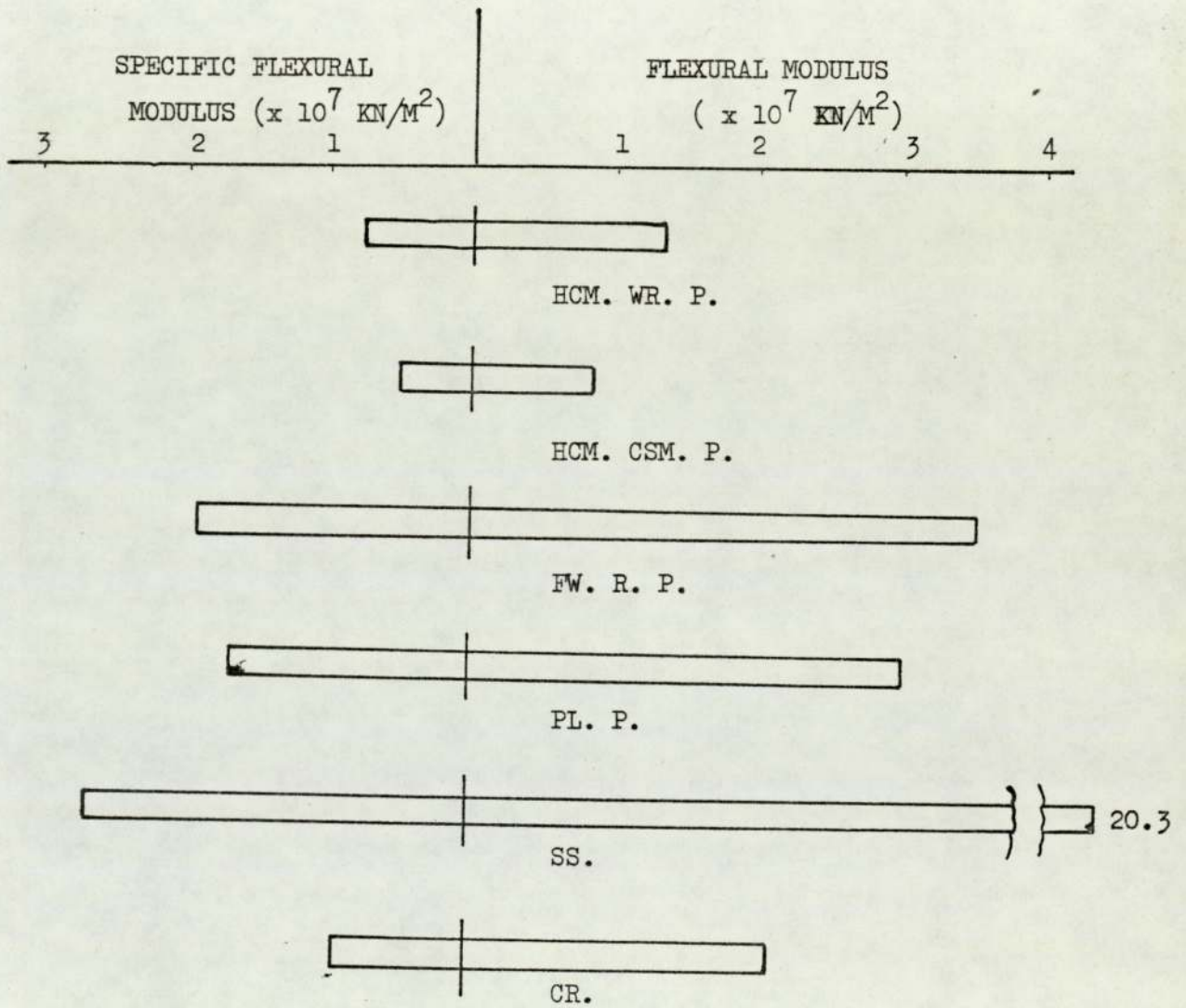
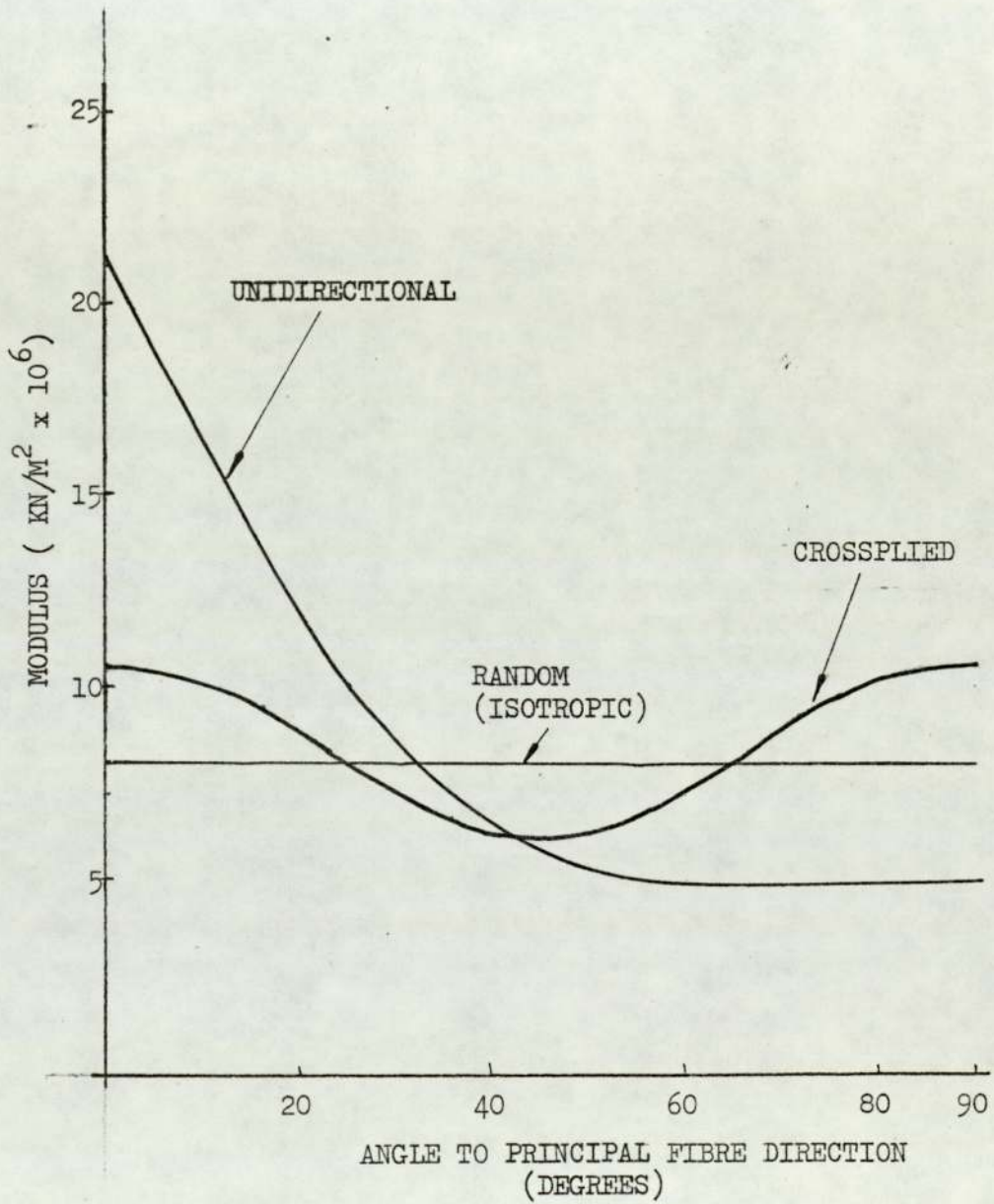


FIG. 2.8 FLEXURAL MODULUS OF STRUCTURAL MATERIALS



FOR ABBREVIATIONS SEE FIG. 2.5

FIG. 2.9 STIFFNESS ANISOTROPY



KABELKA - WOVEN FABRIC, 50% GLASS BY WEIGHT, 18°C, 20,000 KN/M².

BOLLER - WOVEN ROVING, 23°C, 20,000 KN/M².

POLYESTER RESIN WAS USED IN BOTH CASES

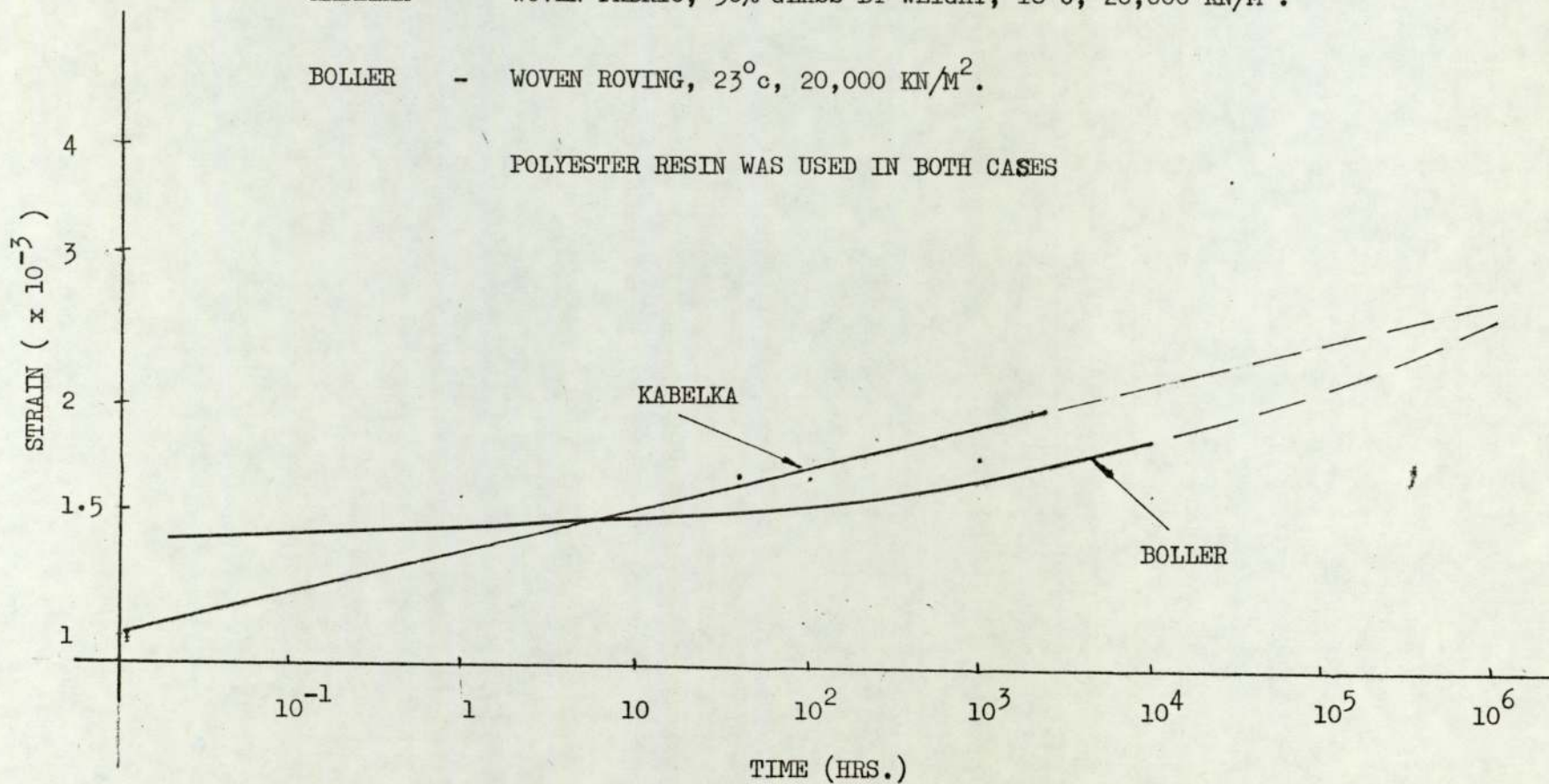


FIG. 2.10 CREEP OF GFRP

FIG. 2.11 CHARACTERISTIC CREEP CURVE
ACCORDING TO STEEL [2.18]
(SCHEMATIC)

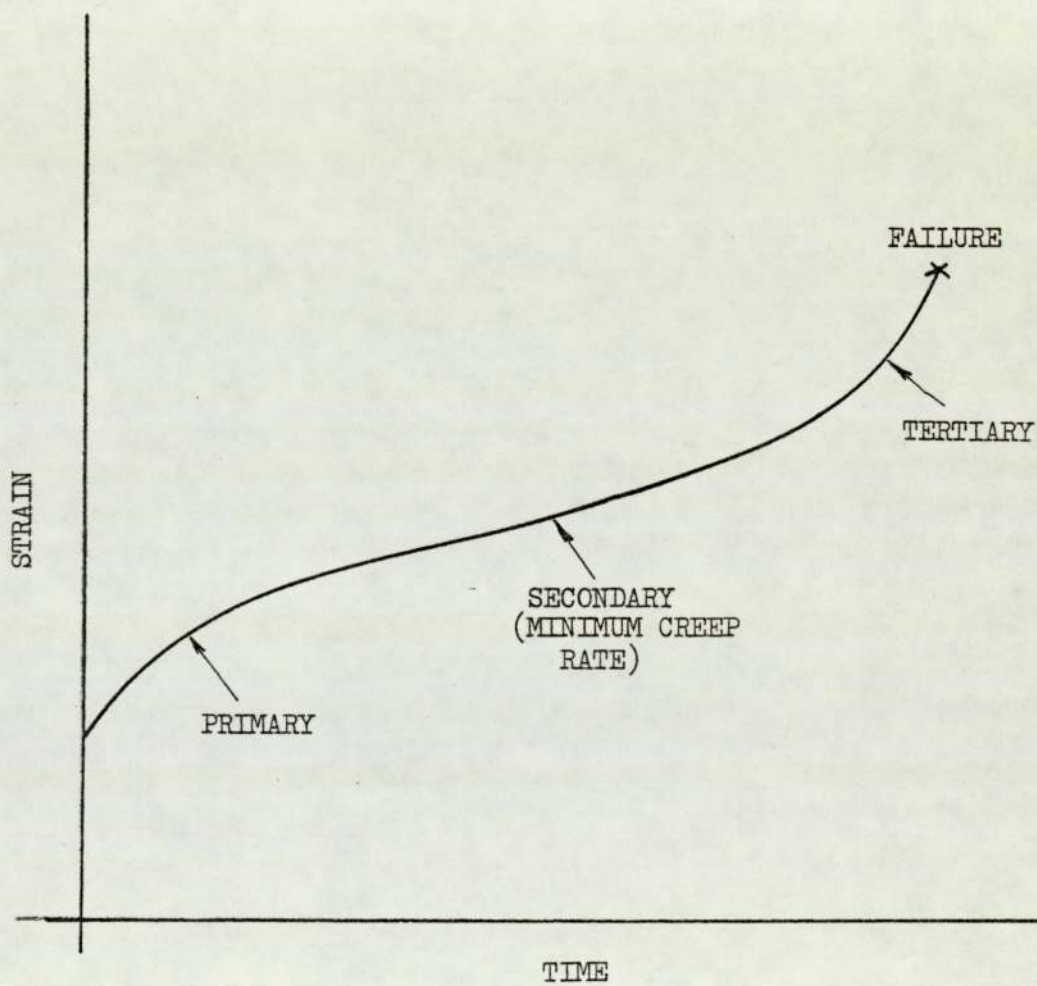


FIG. 2.12 CRACK STOPPING

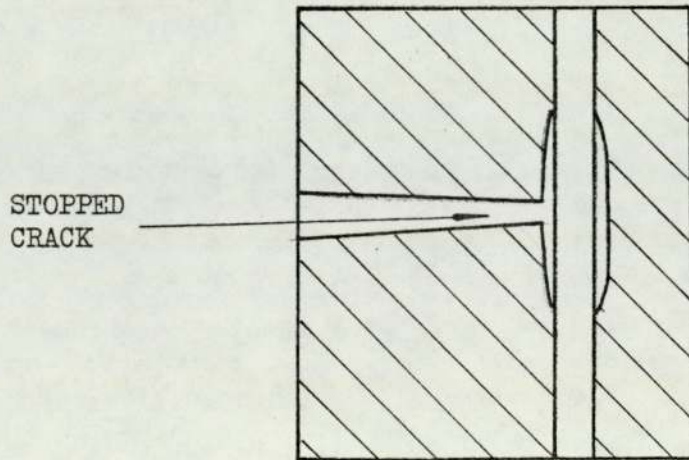
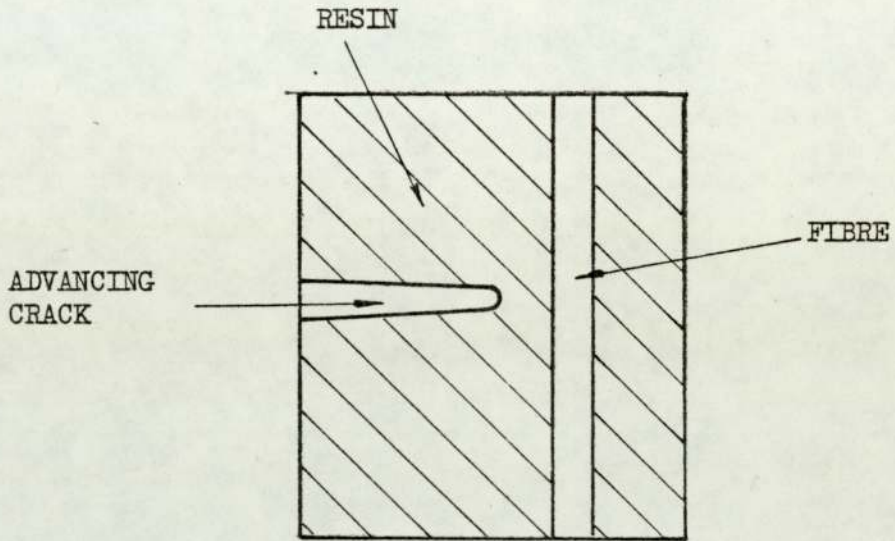


FIG. 2.13 THERMAL PROPERTIES

	COEFF. OF EXPANSION deg. C x 10 ⁻⁶	CONDUCTIVITY W/M deg. C
POLYESTER	9.9 - 18	0.21
GLASS	4.9	1.04
GRP	5 - 18	0.25 - 1
MILD STEEL	11 - 14	46
ALUMINIUM	22 - 23	140 - 190

CHAPTER 3

THEORETICALLY & EXPERIMENTALLY

DETERMINED PROPERTIES OF GRP

CHAPTER THREE

Theoretically and Experimentally Determined

Properties of Grp

3.1

Introduction

The preceding chapter discussed various properties of grp in a qualitative manner, and where relevant in relation to other structural materials. This chapter will deal specifically with grp in a quantitative fashion.

The chapter is in two main parts; that concerning short term properties, and that related to time-dependent properties. A further general division can be made between experimentally and theoretically determined properties.

3.2.1 Introduction

Hooke's law in its most general form is:

$$\sigma_i = C_{ij} \epsilon_j \quad i, j = 1, 2, 3, 4, 5, 6 \quad 3.1$$

where: σ_i are stress components,

C_{ij} is the stiffness matrix,

and ϵ_j are the strain components.

A material requiring this general form of Hooke's law to describe its elastic behaviour is known as a three dimensional anisotropic material. It can be shown that 21 independent elastic constants are required to form the stiffness matrix [3.1]. Such a material has no natural axes of symmetry.

Grp is not commonly used as a three dimensional material because of its relatively high cost, but frequently in laminate form. The number of independent elastic constants required to describe an anisotropic lamina is reduced to six (Figure 3.1a). When such laminas are layed together, to form a laminate, coupling may take place and eighteen elastic coefficients are required (Figure 3.1b).

A special case of the anisotropic lamina exists when the natural axes of the lamina coincide with the principal stress directions.

Such a lamina is known as orthotropic. In this case four elastic constants fully describe the material (Figure 3.1c).

Isotropic materials require only two constants for elastic characterisation (Figure 3.1d). These materials are symmetric about all axes.

It is possible to form laminated composites from anisotropic laminas that behave orthotropically under axial loading. These are known as specially orthotropic laminates. Six elastic constants are sufficient to describe such materials. This will be clarified in section 3.2.5.

Equations, in the following sections, will be presented so that if the basic properties of glass fibres and resin are known, the constitutive equations of a specially orthotropic laminate can be formed, and hence elastic problems solved.

3.2.2 Prediction of Elastic Constants of the Mono-layer (Figure 3.2)

3.2.2.1 Law of Mixtures

This theory is often known as the "mechanics of materials approach". The assumptions in this case are very general and greatly simplify the problem.

a Prediction of the longitudinal modulus of elasticity (E_1)

The main assumption made here is that the strain in the fibres and matrix is equal. Calcote [3.2] derives the following expression:

$$E_1 = V_f E_f + V_m E_m \quad 3.2$$

Where: E_f = Modulus of elasticity of the fibre.

E_m = Modulus of elasticity of the matrix.

V_f = Fibre volume fraction.

V_m = Matrix volume fraction.

b Prediction of the transverse modulus of elasticity (E_t)

In this case it is assumed that the fibres and the matrix experience equal stress [3.2] and the following equation results:

$$E_t = \frac{E_f E_m}{V_f E_m + V_m E_f} \quad 3.3$$

c Prediction of the major Poisson's ratio (μ_{1t})

Again the strain is assumed to be uniform in the fibres and matrix [2] .

$$\mu_{1t} = \mu_f V_f + \mu_m V_m \quad 3.4$$

d Prediction of the shear modulus (G_{1t})

The derivation here is similar to that of the transverse modulus.

$$G_{1t} = \frac{G_f G_m}{V_f G_m + V_m G_f} \quad 3.5$$

where G_m = Shear modulus of the matrix and fibre respectively.

a Prediction of E_1

Tsai bases his prediction of E_1 on the "mechanics of materials" approach but modifies it to allow for poor alignment of the fibres.

$$E_1 = K (E_f V_f + E_m V_m) \quad 3.6$$

where K = fibre misalignment factor ≤ 1 .

b Prediction of E_t

The approach here is based upon variational methods, where classical elasticity is used. Using the concept of fibre contiguity, Tsai obtains:

$$E_t = 2 \left[1 - \mu_f + (\mu_f - \mu_m) V_m \right] \left[\frac{(1 - C) K_f (2K_m + G_m) - G_m (K_f - K_m) V_m}{(2K_m + G_m) + 2(K_f - K_m) V_m} \right. \\ \left. + C \frac{K_f (2K_m + G_f) + G_f (K_m - K_f) V_m}{(2K_m + G_f) - 2(K_m - K_f) V_m} \right] \quad 3.7$$

where C = Contiguity factor, $0 \leq C \leq 1$

$$K_f = E_f / 2(1 - \mu_f)$$

$$K_m = E_m / 2(1 - \mu_m)$$

$$G_f = E_f / 2(1 + \mu_f)$$

$$G_m = E_m / 2(1 + \mu_m)$$

c Prediction of μ_{1t}

Using the same approach as before, the following equation is obtained:

$$\begin{aligned} \mu_{1t} = & \frac{(1 - C K_f \mu_f (2 K_m + G_m) V_m + K_m \mu_m (2 K_m + G_f) V_m)}{K_f (2 K_m + G_m) - G_m (K_f - K_m) V_m} \\ & + \frac{C K_m \mu_m (2 K_f + G_f) V_m + K_f \mu_f (2 K_m + G_f) V_f}{K_f (2 K_m + G_f) + G_f (K_m - K_f) V_m} \end{aligned} \quad 3.8$$

d Prediction of G_{1t}

Again in a similar way, the following equation is given:

$$\begin{aligned} G_{1t} = & \frac{(1 - C) \cdot G_m 2 G_f - (G_f - G_m) V_m}{2 G_m + (G_f - G_m) V_m} \\ & + \frac{C G_f (G_f + G_m) - (G_f - G_m) V_m}{(G_f + G_m) + (G_f - G_m) V_m} \end{aligned} \quad 3.9$$

Although contiguity has a significant effect on the values of E_t and G_{1t} Tsai does not give a method of theoretically determining C . He does present results from an E-glass epoxy resin composite, the majority of which lie within the range of $0 \leq C \leq 0.4$, $C = 0.2$ giving a reasonable mean. For the same composite K was found to lie between 0.9 and 1.0. Al-Khyatt [3.4] using polyester resin found that a value of K between 0.8 and 0.9 and $C = 0$ was more appropriate. However, Al-Khyatt used a very low percentage of catalyst (0.01%) which may have presented full polymerisation of the resin and reduced the quality of the bond between the resin and the glass. Tsai's analysis assumes perfect bonding between fibres and matrix. Other fully polymerised polyester systems may give results closer to Tsai's predictions.

3.2.2.3 Halpin-Tsai Approach [3.5]

Halpin and Tsai formulated simple equations based upon more exact elastic solutions. Their equations for E_1 and μ_{1t} are the

same as those for the mechanics of materials approach, equations 3.2 and 3.4.

$$E_t = \frac{E_m (1 + \nu \eta V_f)}{(1 - \eta V_f)} \quad 3.9$$

$$G_{lt} = \frac{G_m (1 + \nu \eta V_f)}{(1 - \eta V_f)} \quad 3.10$$

where $\nu = 1$ for G_t

$\nu = 2$ for E_t

$$\eta = \frac{\frac{G_f}{G_m} - 1}{\frac{G_f}{G_m} + 1} \quad \text{for } G_{lt}$$

$$\eta = \frac{\frac{E_f}{E_m} - 1}{\frac{E_f}{E_m} + 2} \quad \text{for } E_t$$

Micro-Mechanical Methods Closure

The values of the elastic constants of the basic mono-layer can vary widely, depending upon which theory is applied. This is particularly true for E_t and G_{lt} . However, it is possible to predict properties with sufficient accuracy to be of value in the design of composite structures.

3.2.3 Stress-Strain Relationships Referred to Natural Axes

As described in Section 3.2.1 an orthotropic laminate may be characterised by four elastic constants and it can be shown [3.2]

that they are related by the following equation:

$$\begin{bmatrix} \epsilon_1 \\ \epsilon_t \\ \gamma_{1t} \end{bmatrix} = \begin{bmatrix} s_{11} & s_{12} & 0 \\ s_{12} & s_{22} & 0 \\ 0 & 0 & s_{33} \end{bmatrix} \begin{bmatrix} \sigma_1 \\ \sigma_t \\ \tau_{1t} \end{bmatrix} \quad 3.11$$

Equation 3.11 may be inverted to give:

$$\begin{bmatrix} \sigma_1 \\ \sigma_t \\ \tau_{1t} \end{bmatrix} = \begin{bmatrix} c_{11} & c_{12} & 0 \\ c_{12} & c_{22} & 0 \\ 0 & 0 & c_{33} \end{bmatrix} \begin{bmatrix} \epsilon_1 \\ \epsilon_t \\ \gamma_{1t} \end{bmatrix} \quad 3.12$$

$$\text{where } c_{11} = \frac{s_{22}}{\Delta}$$

$$c_{12} = \frac{s_{12}}{\Delta}$$

$$c_{22} = \frac{s_{11}}{\Delta}$$

$$c_{33} = \frac{1}{s_{33}}$$

$$\Delta = s_{11} s_{22} - s_{12}^2$$

The normal engineering constants may be related to the independent constants in the following way: in equation 3.12, if we let σ_1 be the only non zero stress the equation becomes:

$$\sigma_1 = c_{11} \epsilon_1 + c_{12} \epsilon_t$$

$$0 = c_{12} \epsilon_1 + c_{22} \epsilon_t$$

Solving for ϵ_1 and ϵ_t using Cramer's Rule:

$$\epsilon_1 = \frac{\sigma_1 c_{22}}{c_{11} c_{22} - c_{12}^2} \quad 3.13$$

$$\epsilon_t = -\frac{\sigma_1 c_{12}}{c_{11} c_{22} - c_{12}^2}$$

If the modulus E_1 is defined as:

$$E_1 \equiv \frac{\sigma_1}{\epsilon_1}$$

then from 3.13,

$$E_1 = C_{11} - \frac{C_{12}^2}{C_{22}} \quad 3.14$$

Defining μ_{1t} as

$$\mu_{1t} \equiv \frac{-\epsilon_t}{\epsilon_1}$$

yields from equation 3.13

$$\mu_{1t} = \frac{C_{12}}{C_{22}} \quad 3.15$$

If a similar operation is performed with σ_t being the only applied stress then

$$E_t \equiv \frac{\sigma_t}{\epsilon_t} = C_{22} - \frac{C_{12}^2}{C_{11}} \quad 3.16$$

$$\mu_{1t} \equiv \frac{-\epsilon_1}{\epsilon_t} = \frac{C_{12}}{C_{11}} \quad 3.17$$

If only τ_{1t} is non-zero and G_{1t} is defined as

$$G_{1t} \equiv \frac{\tau_{1t}}{\gamma_{1t}} \quad 3.18$$

then similarly it is found that

$$G_{1t} = C_{33}$$

If equations 3.13 and 3.15 are divided and the expressions for μ_{t1} and μ_{1t} are similarly divided it is found that:

$$\frac{E_1}{E_t} = \frac{\mu_{1t}}{\mu_{t1}} = \frac{C_{11}}{C_{22}} \quad 3.20$$

If equations 3.13 to 3.20 are rearranged, the following equations may be derived:

$$\begin{aligned}
C_{11} &= \frac{E_1}{1 - \mu_{1t} \mu_{t1}} \\
C_{12} &= \frac{E_t \mu_{1t}}{1 - \mu_{1t} \mu_{t1}} = \frac{E_1 \mu_{t1}}{1 - \mu_{1t} \mu_{t1}} \\
C_{22} &= \frac{E_t}{1 - \mu_{1t} \mu_{t1}} \\
C_{33} &= G_{1t}
\end{aligned}
\tag{3.21}$$

Substituting equations 3.21 into equations 3.11 and 3.12

yields:

$$\begin{aligned}
S_{11} &= \frac{1}{E_1} \\
S_{12} &= -\frac{\mu_{1t}}{E_1} = -\frac{\mu_{t1}}{E_t} \\
S_{22} &= \frac{1}{E_t} \\
S_{33} &= \frac{1}{G_{1t}}
\end{aligned}
\tag{3.22}$$

3.2.4 Stress-Strain Relationships Referred to Arbitrary Axes

It can be shown [3.5] that stresses and strains on arbitrary axes, 1, 2, (see Figure 3.2) transform to stresses and strains on the natural axes, l, t, as follows:

$$\begin{bmatrix} \sigma_1 \\ \sigma_t \\ \tau_{1t} \end{bmatrix} = T \begin{bmatrix} \sigma_1 \\ \sigma_2 \\ \tau_{12} \end{bmatrix}
\tag{3.23}$$

$$\begin{bmatrix} \epsilon_1 \\ \epsilon_t \\ \frac{1}{2}\gamma_{1t} \end{bmatrix} = T \begin{bmatrix} \epsilon_1 \\ \epsilon_2 \\ \frac{1}{2}\gamma_{12} \end{bmatrix}$$

$$\text{where } T = \begin{bmatrix} \cos^2 \alpha & \sin^2 \alpha & (2 \sin \alpha \cos \alpha) \\ \sin^2 \alpha & \cos^2 \alpha & (-2 \sin \alpha \cos \alpha) \\ -2 \sin \alpha \cos \alpha & \sin \alpha \cos \alpha & (\cos^2 \alpha - \sin^2 \alpha) \end{bmatrix}$$

and tensorial strains are used rather than engineering strains.

Applying equations 3.23 to equation 3.12, with tensorial strains replacing engineering strains:

$$\begin{bmatrix} \sigma_1 \\ \sigma_t \\ \tau_{1t} \end{bmatrix} = [T] \begin{bmatrix} \sigma_1 \\ \sigma_2 \\ \tau_{12} \end{bmatrix} = [C] [T] \begin{bmatrix} \epsilon_1 \\ \epsilon_2 \\ \frac{1}{2}\gamma_{12} \end{bmatrix} \quad 3.24$$

and

$$\begin{bmatrix} \sigma_1 \\ \sigma_2 \\ \tau_{12} \end{bmatrix} = [T]^{-1} [C] [T] \begin{bmatrix} \epsilon_1 \\ \epsilon_2 \\ \frac{1}{2}\gamma_{12} \end{bmatrix} \quad 3.25$$

$$\text{Let } [\bar{C}] = [T]^{-1} [C] [T]$$

then, carrying out the algebra:

$$\bar{C}_{11} = C_{11} \cos^4 \alpha + 2(C_{12} + 2 C_{33}) \sin^2 \alpha \cos^2 \alpha + C_{22} \sin^4 \alpha$$

$$\bar{C}_{12} = (C_{11} + C_{22} - 4 C_{33}) \sin^2 \alpha \cos^2 \alpha + C_{12} (\sin^4 \alpha + \cos^4 \alpha)$$

$$\begin{aligned}
\bar{c}_{13} &= (c_{11} - c_{12} - 2 c_{33}) \sin \alpha \cos^3 \alpha \\
&\quad + (c_{12} - c_{22} + 2 c_{33}) \sin^3 \alpha \cos \alpha \\
\bar{c}_{22} &= c_{11} \sin^4 \alpha + 2 (c_{12} + 2 c_{33}) \sin^2 \alpha \cos^2 \alpha \\
&\quad + c_{22} \cos^4 \alpha \\
\bar{c}_{23} &= (c_{11} - c_{12} - 2 c_{33}) \sin^3 \alpha \cos \alpha \\
&\quad + (c_{12} - c_{22} + 2 c_{33}) \sin \alpha \cos^3 \alpha \\
\bar{c}_{33} &= (c_{11} + c_{22} - 2 c_{12} - 2 c_{33}) \sin^2 \alpha \cos^2 \alpha \\
&\quad + c_{33} (\sin^4 \alpha + \cos^4 \alpha)
\end{aligned} \tag{3.26}$$

In a like manner the compliance matrix \bar{S} can be formed

where:

$$\begin{aligned}
\bar{s}_{11} &= s_{11} \cos^4 \alpha + (2 s_{12} + s_{33}) \sin^2 \alpha \cos^2 \alpha \\
&\quad + s_{22} \sin^4 \alpha \\
\bar{s}_{12} &= s_{12} (\sin^4 \alpha + \cos^4 \alpha) + (s_{11} + s_{22}) \sin^2 \alpha \cos^2 \alpha \\
\bar{s}_{13} &= 2(2 s_{11} - 2 s_{12} - s_{44}) \sin \alpha \cos^3 \alpha \\
&\quad - 2 (2 s_{22} - 2 s_{12} - s_{33}) \sin^3 \alpha \cos \alpha \\
\bar{s}_{22} &= s_{11} \sin^4 \alpha + (2 s_{12} + s_{33}) \sin^2 \alpha \cos^2 \alpha \\
&\quad + s_{22} \cos^4 \alpha \\
\bar{s}_{23} &= 2 (2 s_{11} - 2 s_{12} - s_{33}) \sin^3 \alpha \cos \alpha \\
&\quad - 2 (2 s_{22} - 2 s_{12} - s_{33}) \sin \alpha \cos^3 \alpha \\
\bar{s}_{33} &= 2 (2 s_{11} + 2 s_{22} - 4 s_{12} - s_{33}) \sin^2 \alpha \cos^2 \alpha \\
&\quad + s_{33} (\sin^4 \alpha + \cos^4 \alpha)
\end{aligned} \tag{3.27}$$

Tsai [3.6] has developed relationships between stress and moment resultants at the laminate midplane and the strains and curvatures of the laminate when the working temperature is different from the laminating temperature. This temperature difference depends on the production technique used and is difficult to quantify accurately. Often, where low temperature processes are used, such as hand lay-up, spray-up or cold press, the temperature difference will have little effect. This is particularly so in the case of specially orthotropic laminates, since much of the coupling between constituent laminae is removed. For these reasons the effect of the temperature difference will be neglected in this thesis and Tsai's relationship becomes:

$$\begin{bmatrix} N_x \\ N_y \\ N_{xy} \\ M_x \\ M_y \\ M_{xy} \end{bmatrix} = \begin{bmatrix} A_{11} & A_{12} & A_{13} & B_{11} & B_{12} & B_{13} \\ A_{12} & A_{22} & A_{23} & B_{12} & B_{22} & B_{23} \\ A_{13} & A_{23} & A_{33} & B_{13} & B_{23} & B_{33} \\ B_{11} & B_{12} & B_{13} & D_{11} & D_{12} & D_{13} \\ B_{12} & B_{22} & B_{23} & D_{12} & D_{22} & D_{23} \\ B_{13} & B_{23} & B_{33} & D_{13} & D_{23} & D_{33} \end{bmatrix} \begin{bmatrix} \epsilon_x^0 \\ \epsilon_y^0 \\ \gamma_{xy}^0 \\ k_x \\ k_y \\ k_{xy} \end{bmatrix}$$

3.28

$$\text{or } \begin{bmatrix} N \\ M \end{bmatrix} = \begin{bmatrix} A & B \\ B & D \end{bmatrix} \begin{bmatrix} \epsilon^0 \\ k \end{bmatrix}$$

where N = Midplane stress resultants.

M = Laminate moment resultants

ϵ^0 = Midplane strains

k = Laminate curvatures

$$A_{ij} = \sum_{K=1}^n (\bar{C}_{ij})_K (h_K - h_{K-1}) \quad 3.28a$$

K relates to the layer number.

$$B_{ij} = 0.5 \sum_{K=1}^n (\bar{C}_{ij})_K (h_K^2 - h_{K-1}^2) \quad 3.28b$$

$$D_{ij} = 0.333 \sum_{K=1}^n (\bar{C}_{ij})_K (h_K^3 - h_{K-1}^3) \quad 3.28c$$

Equation 3.28 may be inverted to give:

$$\begin{bmatrix} \epsilon^0 \\ K \end{bmatrix} = \begin{bmatrix} A' & B' \\ C' & D' \end{bmatrix} \begin{bmatrix} N \\ M \end{bmatrix} \quad 3.29$$

where

$$\begin{aligned} \begin{bmatrix} A' \end{bmatrix} &= \begin{bmatrix} A^* \end{bmatrix} - \begin{bmatrix} B^* \end{bmatrix} \begin{bmatrix} D^{*-1} \end{bmatrix} \begin{bmatrix} C^* \end{bmatrix} \\ \begin{bmatrix} B' \end{bmatrix} &= \begin{bmatrix} B^* \end{bmatrix} \begin{bmatrix} D^{*-1} \end{bmatrix} \\ \begin{bmatrix} C' \end{bmatrix} &= - \begin{bmatrix} D^{*-1} \end{bmatrix} \begin{bmatrix} C^* \end{bmatrix} \\ \begin{bmatrix} D' \end{bmatrix} &= \begin{bmatrix} D^{*-1} \end{bmatrix} \\ \begin{bmatrix} A^* \end{bmatrix} &= \begin{bmatrix} A^{-1} \end{bmatrix} \\ \begin{bmatrix} B^* \end{bmatrix} &= - \begin{bmatrix} A^{-1} \end{bmatrix} \begin{bmatrix} B \end{bmatrix} \\ \begin{bmatrix} C^* \end{bmatrix} &= \begin{bmatrix} B \end{bmatrix} \begin{bmatrix} A^{-1} \end{bmatrix} \\ \begin{bmatrix} D^* \end{bmatrix} &= \begin{bmatrix} D \end{bmatrix} - \begin{bmatrix} B \end{bmatrix} \begin{bmatrix} A^{-1} \end{bmatrix} \begin{bmatrix} B \end{bmatrix} \end{aligned}$$

The complexity of the general anisotropic laminate can be seen from equations 3.28 and 3.29. The normal stress resultants N_x and N_y are developed in part by shearing of the midplane and by twisting of the plate. The shear stress resultant is a ramification of normal strains in the midplane, and bending of the plate. Also, bending and twisting can be induced by normal straining of the midplane as well as bending moments.

From equation 3.28b it is evident that laminates having identical laminae above and below the midplane (that is identical in thickness, distance from the midplane and fibre orientation) have a coupling matrix $[B]$ equal to zero. Such a laminate is known as specially orthotropic and was mentioned earlier. Further simplification can be made if the laminate is symmetrical about its natural axes on both sides of the midplane. That is to say, for each lamina at $+\alpha$ to the x axis there is an adjacent lamina at $-\alpha$ both above and below the midplane. For this type of laminate:

$$\begin{pmatrix} A_{13} \\ A_{23} \end{pmatrix} = \begin{pmatrix} A_{23} \\ A_{13} \end{pmatrix} = 0$$

That is, there is no inplane shear deformation, and four elastic constants describe the inplane behaviour, as is the case with the orthotropic laminae. However, unlike orthotropic laminae the bending behaviour is coupled due to the existence of the coefficients (D_{13}) and (D_{23}) (Equation 3.28c). The use of orthotropic theory in the bending and stability of plates where (D_{13}) and (D_{23}) are not zero leads to non-conservative results [3.7]. There are certain circumstances, however, where (D_{13}) and (D_{23}) are zero, that is, when angle α is 0° or 90° since (\bar{C}_{13}) and (\bar{C}_{23}) (Equation 3.26), are equal to zero. (D_{13}) and (D_{23}) are also equal to zero when $\alpha = \pm 45^\circ$ and balanced woven fabric is used. Furthermore, when the number of pairs of laminates at $\pm \alpha$ becomes large (say ≥ 3) (D_{13}) and (D_{23}) become small [3.7] and their effect may be neglected.

In the remainder of this thesis only specially orthotropic laminates where:

$$(A_{13}) = (A_{23}) = 0 \quad \text{and}$$

$$(D_{13}) = (D_{23}) = 0 \quad \text{or where they are negligible,}$$

will be considered. These laminates are the most commonly used in

industry, and other laminates experience undesirable stresses and strains as previously described. The constitutive equations may now be simplified to:

$$\begin{aligned}
 [N] &= \begin{bmatrix} A_{11} & A_{12} & 0 \\ A_{12} & A_{22} & 0 \\ 0 & 0 & A_{33} \end{bmatrix} [\epsilon^0] \\
 [M] &= \begin{bmatrix} D_{11} & D_{12} & 0 \\ D_{12} & D_{22} & 0 \\ 0 & 0 & D_{33} \end{bmatrix} [K]
 \end{aligned}
 \tag{3.30}$$

Laminates described by equation (3.30) behave as the orthotropic laminas from which they are constituted, but generally, will have coefficients of different values.

3.3

Strength Properties of Laminated Grp

3.3.1 Introduction

Theories have been developed for strength in a similar way to those for stiffness. Knowing the strengths of the constituents, the strengths of the basic composite mono-layer can be predicted, and from this the strengths of laminates can be developed.

Unfortunately, the theories for predicting the strength of the mono-layer give estimates which are very much higher than the actual strength with the possible exception of the longitudinal tensile

strength [3.4, 3.8]. Consequently these theories will only be described briefly. If empirically determined mono-layer strengths are used in conjunction with laminate theory, predictions of adequate accuracy for design purposes can be made.

3.3.2 Prediction of the Strength of the Basic Mono-layer

The important strengths of a grp lamina are:

- a) longitudinal tensile strength
- b) longitudinal compressive strength
- c) transverse tensile strength
- d) transverse compressive strength
- e) interlamina shear (ILS) strength
- f) flexural strength

Broadly, two approaches have been made to predict the various strengths; netting analysis, and continuum analysis. Netting analysis [3.9] assumes that the fibres take all the load and the resin serves only to hold the fibres in position in the longitudinal direction. In shear and transverse directions only the matrix is effective. Continuum analysis is a more rigorous approach, and considers the elastic and strength properties of both constituents [3.10, 3.11]. Results of the latter approach will be outlined briefly here.

3.3.2.1 Longitudinal Tensile Strength ($F_{1(T)}$)

Rosin [3.11] developed the following:

$$F_{1(T)} = V_f (\alpha \beta \delta \rho)^{-1/\beta} \quad 3.31$$

α and β are factors depending upon the relationship between fibre strength and length. δ is the ineffective fibre length (see Fig. 2.3) and ρ is the base of natural logarithms. The equation is applicable when fibre strains are large and Poisson's ratio for the fibres and resin is similar.

Harris [3.12] found that the law of mixtures generally gave adequate accuracy.

$$F_{1(T)} = \sigma_f V_f + \sigma'_m (1 - V_f) \quad 3.32$$

where σ_f = fibre failure stress

σ'_m = resin stress at composite failure strain.

3.3.2.2. Longitudinal Compressive

Strength ($F_{1(c)}$)

In compression, glass fibres are considered to behave as columns supported by a surrounding elastic medium or plastic medium at higher strains. As described in Chapter 2, failure occurs when fibres buckle in one of two modes; shear or extensional. Considerable

effort has been exerted on this basis, to predict the compressive strength [3.11, 3.13], but theories have been found inaccurate and non-conservative. The following factors will contribute to the inaccuracy:

- 1) Misalignment of fibres.
- 2) Crooked fibres.
- 3) Inaccurate knowledge of the resin properties when in the composite.
- 4) The presence of voids in the matrix causing reductions in strength and stiffness.
- 5) Poor bonding between the resin and fibres.

3.3.2.3 Transverse Strengths

Several workers have attempted to model the tensile and compressive transverse strengths [3.14 - 17] but results were inaccurate. Hashin [3.16] concluded that the matrix was the dominant phase in determining strengths.

3.3.2.4 Interlamina Shear (ILS) Strength

No reliable model exists for the prediction of this strength. ILS strength is often assumed to be equal to the shear strength of the resin.

3.3.2.5 Flexural Strength

The flexural strength lies between the tensile and compressive strengths, and the mean will normally give a conservative estimate of sufficient accuracy for design purposes.

3.3.3 Strength Properties of Laminated Grp

The model used for analysing the elastic behaviour may also be used for predicting material failure. It is assumed that the behaviour of an arbitrary lamina within an arbitrary laminate, for given stresses and strains in that lamina natural axis system, is the same as the behaviour measured in the natural axis system when the lamina is part of any other laminate under the same stresses and strains. Plane stress is assumed, and in bending, plane sections remain plane.

$$\text{i.e. } \begin{bmatrix} \epsilon \\ \epsilon \\ \gamma_{xy} \end{bmatrix} = \begin{bmatrix} \epsilon_x \\ \epsilon_y \\ \gamma_{xy} \end{bmatrix} = \begin{bmatrix} \epsilon^0 \end{bmatrix} + Z \begin{bmatrix} k \end{bmatrix} \quad 3.33$$

and from equations (3.30)

$$\begin{bmatrix} \epsilon \end{bmatrix} = \begin{bmatrix} A \end{bmatrix}^{-1} \begin{bmatrix} N \end{bmatrix} + Z \begin{bmatrix} D \end{bmatrix}^{-1} \begin{bmatrix} M \end{bmatrix} \quad 3.34$$

The stresses and strains can now be found for each lamina in the laminate axis system and then transformed to stresses and strains in the lamina natural axis system using equations (3.25 - 3.27)

for which the strengths are known. At this stage failure criteria may be applied to each pair of laminas to test for fracture.

3.3.3.1 Laminate Behaviour Under Load

For design purposes, laminates behave linearly upto initial failure. This initial failure may or may not be ultimate failure, depending upon fibre orientation, and the nature of the stress causing failure. In the case where a tensile load is the cause of lamina failure, e.g. when the laminate is subjected to uniaxial tension, the remaining laminas may be capable of sustaining the load. The remaining laminas must be reappraised by forming a new constitutive equation (3.30) ignoring the failed laminas and retesting for failure. This process may be repeated until all laminas have been found to fail, at which point the ultimate strength has been reached or exceeded. If after initial failure the remaining laminates proved strong enough to take all the load, then the stress-strain relationship would not be linear but would have a "knee" representing the point of initial failure. Fig. 3.3 shows a typical progressive failure curve for a 3 fibre system, 0° , $\pm 45^\circ$, 90° .

Where compressive loads are the cause of failure, initial failure is also considered ultimate. Compressive failure being mainly dependent on the matrix, failure of the matrix in one lamina will cause failure in the other laminas [3.4].

Initial failure in flexure will also be ultimate since it will be precipitated by compressive failure of the outermost fibres.

Behaviour of laminates under complex stress systems is not as yet well defined, and care should be taken if initial failure is not also assumed to be ultimate.

To test a lamina for failure under complex stress the Hill criterion, modified for use with grp by Tsai [3.6] has, generally been accepted as the most applicable.

$$\left[\frac{\sigma_l}{F_l} \right]^2 - \frac{\sigma_l \sigma_t}{F_l^2} + \left[\frac{\sigma_t}{F_t} \right]^2 + \left[\frac{\tau_{lt}}{S} \right]^2 = 1 \quad 3.35$$

where σ = axial stress

F = axial strength

τ = shear stress

S = shear strength

l = longitudinal direction

t = transverse direction

If the axial and shear strengths of the laminate are known then this theory may be applied directly to the laminate.

Other failure theories have been reviewed by Al-Khayatt [3.4].

Theoretically and Experimentally
Determined Elastic and Strength
Properties of Selected Grp Laminates

3.4.1 Introduction

The properties of grp have been shown to be dependent upon the properties of the constituents. The constituents will generally be chosen according to the end use. For example, in a chemical plant a chemically-resistant resin would be chosen, in buildings a fire-resistant resin would frequently be necessary. Since the end use at this stage in the project is not precisely defined, a general-purpose resin will be adopted. Such a resin has been used recently by Al-Khayatt in the characterisation of the basic lamina and several laminates, in the University Department where this project was carried out [3.4]. Hence the work reported here is designed partly as a quality control programme and partly to provide relevant data not provided by Al-Khayatt. In the latter case, where possible, other sources of data have been used for comparison.

3.4.2 Design of Specimens

The design of specimens for the characterisation of fibre-reinforced plastics has been the object of a great deal of work. The traditional designs of test specimens in metal have been found inadequate because they do not allow for the brittle and anisotropic

nature of these materials. The specimen designs adopted in this project are shown in Figs. 3.4 and 3.5. The designs are similar to those adopted by Al-Khayatt, who reviewed the design of test specimens. The necked specimens Fig. 3.4a) were used to determine the tensile strength and modulus for all materials other than chopped strand mat (CSM) reinforced laminates. In the latter case the parallel-sided specimens, Fig. 3.4b) were used. Fig. 3.4c) shows the design of the compression specimens adopted for all materials. In both tensile and compressive tests the elastic properties were obtained with the use of electrical resistance strain gauges.

The materials used in the experimental programme were as follows:

Resin : BIP, Beetle Polyester Resin 836 plus approx.
3% BIP Accelerator B and 1.5% MEKP. catalyst.
The exact proportion of the accelerator and catalyst used was dependent upon the ambient temperature.

Reinforcements : Fothergill and Harvey Limited, uni-directional cloth type Y-996 and bidirectional woven roving Y-023, Fibreglass Limited, "Eque mat".

The preparation of the samples was designed to give a laminate whose properties would be similar to those which could be expected from a good-class hand lay-up laminator. Thus no special techniques were employed to reduce voidage. Laminates were layed-up on a flat steel surface treated with wax release agent. To obtain

smooth, uniform laminates, after lay-up a second steel surface was positioned and pressed on top of the laminate. Spacers were used to control the laminate thickness. Before testing all specimens were post-cured for 3 hrs. at 80°C.

3.4.3 Experimentally Determined Properties

The specimen designs discussed above are such that both elastic and strength properties may be obtained simultaneously. The use of parallel-sided compression specimens may result in slightly lower strengths than if necked specimens were used [3.4] but the difference is not considered significant in this project. The loading rate of both tensile and compressive specimens was such that failure occurred within 1.5 - 2.5 mins.

3.4.3.1 Properties of the Basic Lamina and Selected Laminates

In this section both strength and elastic properties of various laminates will be presented as determined experimentally, and, in the case of elastic properties, compared with theory. Experimental results will be drawn from previous work by Al-Khayatt and work associated with this project. Theories used for comparison will be those of Tsai and Halpin-Tsai, equations 3.6 - 3.9 and 3.9 & 10 respectively.

Fig. 3.6 shows unidirectional material's longitudinal elastic modulus as a function of the fibre volume fraction. Results obtained by Al-Khayatt and the author are in close agreement, as would be expected since similar materials and moulding techniques were employed. However, experimental results were only 80 - 85% of the theoretically predicted modulus. The stress-strain relationship was found to be approximately linear (see Fig. 3.7) as expected for the materials tested.

Fig. 3.8 compares tensile and compressive strengths obtained by the author and Al-Khayatt. Tensile strengths are shown to be 50 - 100% greater than compressive strengths. The greatest difference was at higher glass proportions where the compressive strength begins to reduce.

The axial strengths of several laminates are shown in Fig. 3.9. In tension, cross-ply is shown to be superior to CSM which in turn is stronger than $\pm 45^\circ$ angle-ply. In compression the position of CSM and cross-ply is reversed. In all cases strengths were found to be below those obtained for unidirectional laminates.

Fig. 3.10 compares theoretical and experimental values for the longitudinal and transverse modulus of laminates. The order of superiority is: cross-ply, CSM and $\pm 45^\circ$ angle-ply. In general, theoretical values were marginally higher than empirical ones.

Experimental results obtained by the author were similar to those obtained by Al-Khayatt. The greatest discrepancies occurred

when testing axial strengths of the basic lamina. Al-Khayatt's tensile strengths were greater than those obtained by the author, but in compression the reverse was the case. The proposed reason for this is that the author post-cured specimens before testing, whereas Al-Khayatt did not. Post-curing can be expected to lead to a polymer with more cross-links which give it greater stiffness. Thus fibres would receive greater support against buckling, giving the lamina higher compressive strengths. Post-curing also causes greater resin shrinkage than otherwise would be expected. The high temperature of post-curing induces thermal strains on cooling. These strains then cause premature tensile failure.

Figs. 3.11a & b show photographs of typical tensile and compression failure modes.

Figs. 3.12 and 3.13 compare theoretically determined lamina properties as predicted by Tsai and Halpin-Tsai and empirical properties according to Al-Khayatt. The transverse elastic modulus determined by Al-Khayatt is shown to lie between those predicted theoretically. The Tsai theory, with contiguity factor $C = 0$, gives the most conservative values. With the same value of contiguity factor the Tsai formula for predicting the basic lamina shear modulus is the same as that of Halpin and Tsai. Theoretically and experimentally determined values of the shear modulus agree reasonably well, but the theory is only shown to be conservative at low glass proportions.

The Halpin-Tsai approach, Section 3.2.2.3, adopts the "mechanics of materials" or "law of mixtures" equation for predicting the longitudinal Poisson's ratio. Consequently this equation and

Tsai's theory have been compared to Al-Khayatt's results for the principal Poisson's ratio. Except at high fibre contents, Al-Khayatt's values are marginally lower than those predicted by theory. Again, Tsai's theory is the more conservative.

In Figs. 3.14 and 3.15 three of the more common orthotropic laminates have been treated theoretically. The great effect of fibre orientation on the value of Poisson's ratio is shown in Fig. 3.14. The angle-ply laminate has the largest values, followed by the random fibre laminate and the cross-ply laminate respectively. The same laminate order of superiority is found in the case of the shear modulus; Fig. 3.15.

3.4.4. Conclusions

Experimentally determined property values in this project are, in general, similar to those obtained by Al-Khayatt. Data obtained by Al-Khayatt and the author, therefore, are sufficiently repeatable for design use.

The Halpin-Tsai theory, not reviewed by Al-Khayatt, is shown to be a useful method of predicting the basic lamina elastic properties, but not as accurate as the Tsai approach. However, the Halpin-Tsai equations are simpler and are therefore recommended for preliminary design work.

3.5.1 Introduction

In Chapter 2, the creep and stress rupture properties of grp were outlined. The results of various investigators show that the loss of strength and stiffness is important and must be considered in any structure that is under load, for anything other than very short periods. Further, the results of different workers with similar materials and under similar conditions differ significantly, particularly in the case of stress rupture. In this section the relevant mechanisms will be described in greater depth, and methods of prediction discussed.

3.5.2. Creep Mechanism

Creep is a time-dependent strain in a material, resulting from constant stress. Each phase of the composite contributes to the increase in strain. In grp the resin plays the major role and there is evidence to suggest that for practical purposes creep does not occur in glass [3.18]. However, glass fibres in most composites are buckled or bent due to handling during lamination and/or shrinkage of the resin on cure. Under tension these fibres will tend to straighten, and under compression buckling would advance, thus contributing to creep strain.

The effect of continued stress on polymers, such as polyester resin, is the straining of molecular bonds, and in some cases their rupture. It has been shown that the thermal energy associated with a molecular bond is a function of time [3.19]. Hence, the total amount of energy available to break the bond is not constant. Therefore, under constant stress, bonds near their ultimate strength are not stable, and this results in relative movements between neighbouring segments within molecules and between molecules themselves. Not surprisingly, temperature has been found to play an important role in the creep rate [3.20].

In general, increasing stress and temperature leads to greater mobility of molecules and increased creep rates. Reduction of the creep rate will be achieved by reducing molecular mobility. Thus, highly cross-linked polymers, full curing of the resin and strong resin/fibre bonds are desirable.

Creep has been observed to be less in compression than in tension for some polymers and laminates [3.20, 3.21]. This has been explained with reference to shear stress components and the associated direct stress (Fig. 3.16). If the normal stress, ' σ ', is tensile then a lower value of shear stress, τ , is required for slippage of the molecules than if σ is compressive. Mechanical bonding between molecules will be increased by compression and molecular mobility reduced.

At low loadings it has been observed that about 95% of the creep strain is recoverable after unloading for a period of about

4 times the loaded period [3.18]. This could only occur if strain energy had been stored. Thus at low loads over the time of testing, little failure of the glass fibres and molecular bonds could have occurred. Slippage between unbonded molecules resulting in larger stresses in the fibres could be the mechanism for energy storage provided that the bonds between the glass fibres and the resin remained undamaged.

Water has been commonly observed to increase greatly the rate of creep. This can be explained in terms of the resin, the resin-glass interface, and the glass itself. Water plasticises polyester resin and aids its deformation. In addition, resin has been observed to swell in aqueous environments [3.22] which may lead to strength reduction or failure of the interface bond. A redistribution of stress and an increase in strain would result.

Material construction is an important creep consideration. CSM has been found to be the least creep resistant type of reinforcement, since the resin plays a greater part in load bearing. The resin has to continually transfer the stress from one fibre to another. In addition, the fibre volume fraction is relatively low. Woven fabric has improved creep resistance, provided the warp or weft is parallel to the applied load, since the fibres are continuous, but initially they will not be straight since where perpendicular fibres intersect they have to bend round one another. As mentioned previously, this will contribute to creep. Unidirectional unwoven reinforcement has been found to have the best time-dependent characteristics.

Little work has been carried out on creep and anisotropy. However, Weidmann and Ogorkiewicz [3.23] found that the anisotropy of a unidirectional laminate increases with time under creep conditions.

3.5.3 Nature of Strength Reduction

As pointed out in Chapter 2, grp under stress below its short term strength will eventually fail. The mechanism of failure is closely related to the creep mechanism. Weak bonds in the resin and weak fibres will fail first, causing higher stresses in the remaining material which may lead to further failures. This, associated with a phenomenon known as stress corrosion where the fibres weaken under load with time, eventually causes failure. Loss of fibre strength has been found to accelerate in the presence of water and is associated with crack growth [3.24].

The strain at which failure occurs has been observed to be higher than the short term ultimate strain, particularly when failure occurs after relatively short periods [3.25 & 3.26].

3.5.4 Prediction of the Loss of Stiffness with Time

Interest in the prediction of creep in grp has centred on various empirical methods. These include basic creep modelling,

where a sample of the material is tested in the laboratory under simulated working conditions, and tests in which the environment is modified to accelerate creep.

3.5.4.1 Extrapolation Techniques

a) Findley's Equation [3.21, 27 & 28].

Findley found that the following empirical power function closely described the creep behaviour of several plastics:

$$\epsilon_t = \epsilon_0 + m t^n \quad 3.36$$

where ϵ_t = strain at time t

t = time

ϵ_0 , m , = constants dependent upon the material stress and environment

n = constant depending upon the material and environment.

Using chemical rate theory, Findley modified this equation to take account of the effect of stress on constants ϵ_0 and m .

$$\epsilon_t = \epsilon'_0 \sinh \frac{\sigma}{\sigma_e} + m' t^n \sinh \frac{\sigma}{\sigma_m} \quad 3.37$$

Boller [3.26] in subsequent work found that the equation described the performance of five different forms of grp in both wet and dry conditions. Rawe [3.29] also obtained satisfactory results from the equation for glass-epoxy laminates in several environments.

Finally, Findley [3.19] generalised his equation to take account of multi-axial stress as follows:

$$\begin{aligned} \epsilon_{t1} = \epsilon'_0 & \left[\sinh \frac{\sigma_1}{\sigma_m} - \mu (\sinh \frac{\sigma_2}{\sigma_m} + \sinh \frac{\sigma_3}{\sigma_m}) \right] \\ & + m' \left[\sinh \frac{\sigma_1}{\sigma_m} - 1/2 (\sinh \frac{\sigma_2}{\sigma_m} + \sinh \frac{\sigma_3}{\sigma_m}) \right] t^n \quad 3.38 \end{aligned}$$

where: $\sigma_1, \sigma_2, \sigma_3$ are orthogonal stresses and $\epsilon_{t1}, \epsilon_{t2}, \epsilon_{t3}$ are the corresponding strains.

In the derivation of the above equation it is assumed that the volume of material remains constant, creep in tension and compression is equal, and most importantly that the material is homogeneous and isotropic. The general equation will not, therefore, be applicable to many grp material designs. Further, results have not yet been published verifying the equation, although Findley indicated that work was under way.

b) McLaughlin's Equation [3.30]

McLaughlin proposes an exponential function:

$$-\frac{d \log E_t}{d \log t} = C K \log t$$

where E_t = apparent modulus of elasticity at time t , $= \frac{\sigma}{\epsilon_t}$

C, K = constants,

to describe the creep behaviour of a rigid thermoplastic. McLaughlin demonstrated that his equation could be written:

$$\text{Log} (\text{Log} \epsilon_t - \epsilon_0) = \log m + n \log t \quad 3.39$$

which differs from Findley's equation only in the use of $\log \epsilon_t$ instead of ϵ_t .

McLaughlin claims better accuracy describing polymethyl methacrylate's creep using his equation, than when Findley's is used,

especially when extrapolating from 100 to 10^6 hours. The equation is also used to describe several reinforced plastics in flexural creep for upto 1000 hrs. with good accuracy.

McLaughlin has not extended his equation to accommodate changes in stress as did Findley. However, because of the similarity between the two equations, the hyperbolic relationship used by Findley may be directly applied to McLaughlin's equation thus:

$$\text{Log } \epsilon_t = \epsilon'_0 \sinh \frac{\sigma}{\sigma_\epsilon} + m' t^n \sinh \frac{\sigma}{\sigma_m} \quad 3.40$$

Although Findley's and McLaughlin's equations have been classified as being mainly useful for extrapolation, by testing at higher stresses than the proposed working stresses considerable time may be saved.

3.5.4.2 The Larson-Miller Parameter

Using activation energy theory based upon the Arrhenius equation it can be shown that:

$$K = T (23.78 + \log t)$$

where $K = \text{constant}$

$T = \text{absolute temperature deg. Rankine for materials where the zero strength temperature is much higher than the applied temperature } (T).$ Larson and Miller [3.31] derived empirically the equation:

$$K = T (20 + \log t) \quad 3.41$$

which has been found to work equally well for several materials. Although not derived from work on grp the Larson-Miller parameter has given useful results with this material [3.32, 3.33].

The parameter can be used by testing material at the required stress and at a temperature above the proposed working temperature. The apparent modulus of elasticity is then plotted against parameter K over a period of time as illustrated in Fig. 3.16a. The information may then be used in the following way: suppose a laminate were tested at 150°F and after 100 hours the apparent modulus reduced to 6×10^6 KW/M², which was the minimum allowable stiffness, the period of time the material could sustain the test stress before exceeding the creep limit at 75°F would be given by:

$$K = (460 + 150) (20 + \log 100) = (460 + 75) (20 + \log t) \\ t \approx 10^5 \text{ hours.}$$

Hence a considerable amount of time can be saved.

Alternatively, the testing time may be kept constant but the temperature varied. A similar plot and calculations can then be made.

The accuracy of predictions depends heavily upon the accuracy of the test temperature. For instance, in the example given, if the actual test temperature was 1° in error at 149°F the creep limit would have been approximately 10% in error.

3.5.5 Prediction of the Loss of Strength with Time

3.5.5.51 Larson-Miller Parameter

In a similar way to creep behaviour, the stress rupture properties of grp have been predicted by the Larson-Miller parameter with useful accuracy [3.32 - 34]. Master curves of K against rupture stress can be drawn, and results at elevated temperatures can be used to calculate strengths at working temperatures over longer periods of time (Fig. 3.17).

3.5.5.52 Wohler Method

In this method specimens are tested in an environment similar to the expected working conditions at various stress levels below their short term ultimate strength. The failure times are then plotted against the testing stress on a semi-log graph.

The relationship between log-time to failure and stress has been found by several investigations [3.20, 25 & 26] to be linear, and Boller proposes the equation:

$$\sigma_R = \sigma_0 - M \log t_R \quad 3.42$$

where σ_R = stress causing rupture

σ_0 = stress causing failure after 1 hour

M = constant

t_r = rupture time

This equation was found to apply over testing periods upto 3×10^4 hrs. Data over longer periods is not available.

3.5.5.3 The Monkman and Grant Relationship

Monkman and Grant discovered empirically that the following equation was applicable to a wide range of alloyed metals.

$$\log t_R = C - b \log (\text{mcr}) \quad 3.43$$

where c, b = constants

mcr = minimum creep rate

'c' and 'b' were found to be almost constant for a wide range of materials and temperatures.

In the discussion following Monkman and Grant's paper, Underwood pointed out that the relationship could be derived from the Arrhenius equation. Thus, although the relationship was derived from work on other materials, useful results may be expected from work on grp since the Larson-Miller parameter may also be derived from the Arrhenius equation. Unfortunately, if the Findley or McLaughlin equation is accepted then there is no minimum creep rate. However, in applying the Arrhenius equation any rate may be used so that the minimum creep rate could be replaced, conveniently, by the creep rate at 1 hour. The Monkman and Grant equation then becomes:

$$\log t_R = c - b \log (\dot{\epsilon}_1)$$

3.44

where $\dot{\epsilon}_1$ = creep rate at $t = 1$ hour

Using the relationship for creep and stress rupture proposed by Findley and Boller, the following calculation can be made:

$$\epsilon = \epsilon_0 + m t^n$$

differentiating $\dot{\epsilon} = m n t^{n-1}$

but $m = m' \sinh \frac{\sigma}{\sigma_m}$

$$\therefore \dot{\epsilon} = n m' \sinh \frac{\sigma}{\sigma_m} t^{n-1}$$

when $t = 1$ hr.

$$\dot{\epsilon}_1 = n m' \sinh \frac{\sigma}{\sigma_m}$$

and $\sigma = \sigma_m \sinh^{-1} \left(\frac{\dot{\epsilon}_1}{n m'} \right)$

$$\sigma_R = \sigma_0 - M \log t_R$$

if $\sigma = \sigma_R$

$$\sigma_m \sinh^{-1} \left(\frac{\dot{\epsilon}_1}{n m'} \right) = \sigma_0 - M \log t_R$$

rearranging the constants gives

$$\sinh^{-1} \left(\frac{\dot{\epsilon}_1}{A} \right) = B - C \log t_R$$

$$\sinh \left(\frac{\dot{\epsilon}_1}{A} \right) = \log \left(\frac{\dot{\epsilon}_1}{A} + \sqrt{\left(\frac{\dot{\epsilon}_1}{A} \right)^2 + 1} \right)$$

$$\therefore \log \left(\frac{\dot{\epsilon}_1}{A} + \sqrt{\left(\frac{\dot{\epsilon}_1}{A} \right)^2 + 1} \right) = B - C \log t_R$$

3.45

This formula is similar in form to that of Monkman and Grant.

At low stresses, i.e. when $\sigma_R < \sigma_m$ the above equation simplifies since $\sinh \frac{\sigma}{\sigma_m} \rightarrow \frac{\sigma}{\sigma_m}$ and it follows that

$$\dot{\epsilon}_1 = B - C \log t_R \quad 3.46$$

3.5.5.4 Charles' Equation [3.36]

Using theories of crack propagation and process rates, Charles developed the following formula for stress rupture of glass fibres

$$\log t_R \approx A \log \frac{1}{\sigma_R} - B \quad 3.47$$

Cameron [3.37] applied this relationship to results of other workers and stated that the agreement was much closer than when the simpler equation $\sigma_R = \sigma_0 - M \log t_R$ was used, but did not demonstrate this statistically.

If the above procedure is repeated using Charles' formula and assuming low stresses it can be shown that

$$\log \dot{\epsilon}_1 = A - B \log t_R \quad 3.48$$

This relationship is similar to the one observed by Monkman and Grant.

3.5.6 Experimentally Determined Time- Dependent Properties of Grp

3.5.6.1 Introduction

As pointed out in Section 3.4.1 the selection of laminate constituents depends upon the end use. However, the choice of resin and the form of the reinforcement have possibly an even greater effect on laminate properties in the long term compared with those in the short term. It is impossible, in a project of this type, to fully characterise all materials and their combinations. Neither sufficient resources nor time are available. Thus, only a limited number of laminates will be tested and will correspond to those used in the short term tests. Also, reliance has to be made upon previous work for data, particularly in the case of stress rupture due to the time involved in testing.

Boller, Steel and Kabelka [3.20, 3.25 & 3.26] have each produced considerable quantities of long-term data from tests in air. Boller and Steel have also presented results from tests in water. Steel's work was concerned with flexural stress. Kabelka's work was with a modified form of flexural stress where the laminates formed part of a composite beam. One side of the beam's neutral axis was grp and the other side, steel. Thus, initially an approximately linear stress distribution would be expected across the thickness of grp. However, since steel does not creep, the stress distribution would be expected to change with time. Boller's work was concerned solely with uniform tensile stresses. Boller's tests covered periods of

time of upto 3 years and examined a wider variety of laminates than did Kabelka and Steel. Consequently, Boller's work is considered the most useful for design data and will be used for comparison with work in this project.

As was the case with Boller's work, only tensile creep will be studied in this project. It will be necessary, therefore, to assume, in design, that the tensile and compressive properties of grp are the same. However, to the best of existing knowledge this assumption is conservative, since as pointed out in Section 3.5.2, lower rates of creep and loss of strength have been observed in compression.

Stress rupture tests at two temperatures will be presented, i.e. at 70°C and at 20°C. Results from the tests at the higher temperature are for use with the Larson-Miller parameter so that rupture may be accelerated as described in Section 3.5.5.1. Creep and stress rupture tests were carried out at 20°C. In both cases tests were carried out at a relative humidity of 100%. This level of humidity was chosen for ease of control.

3.5.6.2 Design of Test Specimens

As is the case in short-term testing, in order to obtain extension and failures in the required mode, anisotropy and the lack of ductility has to be allowed for. Indeed, locally high-stressed areas are not only more prone to short-term failure but can be expected to creep and lose strength more rapidly under extended loading

periods. As a result, loading points require reinforcement, and changes in cross-section have to be gradual.

The measurement of strain must be such that readings can be taken upto the failure strain, where relevant, and the sensitivity should be of the order 0.00001 strain [3.36]. Figure 3.17 shows a typical tensile test specimen. The long parallel section accommodates the strain measurement. The strain measuring technique chosen was that which uses a "Demec" gauge. In this system a dial test indicator is used which is sensitive to 0.0001 ins. and the gauge length can be 2", 4", 6" or 8" depending upon the strain range required. The minimum and maximum strain measurement ranges are 0 - 0.02 strain and 0 - 0.08 strain respectively. The corresponding sensitivities are 0.00005 and 0.0000125 units of strain. The aluminium end-pieces were adhered in position using Araldite epoxy resin. For the 70°C tests high temperature adhesive was used: Araldite HT972/AY105, and for the lower temperature tests Araldite HY951/AY103 was used.

3.5.6.3 Design of Test Equipment

A fundamental requirement of a tensile creep testing machine is that the load should be applied axially to the specimen, and the possibility of moments being applied to the specimen reduced to a minimum. In the machine used for creep testing in this project, moment transmission to the specimen was prevented by the use of orthogonal pin joints in the loading mechanism. The possibility of axial torsion being applied was prevented visually. Assuming that an angle of twist of 10° could be detected visually, and then

corrected, shear stresses of less than 1 KN/M^2 would be prevented. In general, the length of the test specimens greatly reduced the possibility of any significant unwanted stresses.

For accurate results it is important that friction in the loading mechanism be reduced to a minimum. Friction in this situation would lead to a non-constant stress being applied to the specimen. As the specimen extends the loading mechanism should move correspondingly. However, the effect of friction would be to resist and reduce this movement and hence reduce the load applied to the specimen. Where appropriate, knife edges were used to reduce friction.

In order to keep dead weights manageable and still be able to apply satisfactorily high loads, a lever arm of approximately 20:1 was used. No provision was adopted to control the rate of application of load to the specimen, except manual control. Theory, however, assumes instantaneous application of load. The effect of this is to cause the theory to be invalid for periods of time of the order of 10 times the loading period [3.36].

The test environment was controlled by testing the specimens just above the surface of water, the temperature of which was thermostatically controlled. During tests at 70°C , temperature could be controlled to within $\pm 2^{\circ}\text{C}$ and during tests at 20°C , $\pm 4^{\circ}\text{C}$. Stabilisation of the environment was achieved by enclosing with covers positioned just above the specimens. Figure 3.18 shows the design of the loading mechanism.

3.5.6.4 Test Procedure

Although the test equipment was designed to give a loading mechanical advantage of 20:1 it was necessary to calibrate each loading station. This was done using a proving ring (Clockhouse Eng. Ltd. proving ring No. 2998) with attachments made especially to fit the creep machine.

Before testing, specimens were kept in the test environment for 1 hr. before tests at 70°C and 24 hrs. before tests at 20°C.

With the specimens in position, the load was applied in stages but completed within 1 minute. Readings were then taken with a Demec gauge. Demec gauges used in the tests were:

- a) Demec gauge No. 1130 with dial No. 281272 and
- b) Demec gauge No. 876 with dial No. 252253.

The first reading was taken after 0.1 hrs. of creep, being the shortest possible time for meaningful results. Thereafter, intervals between readings were initially 0.1 hrs. and then steadily increased as the test duration increased.

It was necessary to take considerable care not to bend the specimens when taking readings, particularly with low specimen loadings. However, with practice sufficient skill was developed to avoid bending.

Due to the limited time available, tests were, on occasions, terminated before failure of the specimens. This action was taken

when failure appeared to be some considerable time away and sufficient data for creep analysis had been obtained.

3.5.6.5 Results and Discussion of Results

The stress rupture results are as tabulated in Figs. 3.19 and 3.21 for tests at 70°C and 20°C respectively. These results are also shown graphically in Figs. 3.20 and 3.22.

Figure 3.20 shows that CSM at stresses below 10 N/MM² could be expected to last 50 years or more by use of the Larson-Miller parameter. However, when these results are shown together with results from tests at 20°C in Fig. 3.22 they appear rather conservative. CSM tested at 20°C is shown to be superior to Boller's CSM upto approximately 10³ hrs. Results calculated using the Larson-Miller parameter shows Boller's CSM to be far superior from approximately 10³ hrs. onwards. It would appear from these results that the temperature increase resulted in a material modification in addition to the predicted increase in static fatigue rate. The resin manufacturers, however, state that no fundamental chemical changes would be expected at this temperature other than those associated with ageing. It is known that water causes swelling and plasticisation of the resin and this may be exaggerated at higher temperatures. In addition, changes in temperature from the laminating temperature are known to cause internal stresses because of the different thermal expansion coefficients of the constituents. Thus although the applied loads at the two test temperatures were equivalent, the internal

stresses would not be equal. Cracks may have been formed in the resin and at the interface, leading to a change in the physical structure of the laminate. It may be observed that the rate of loss of strength at the two test temperatures does not appear dissimilar. A similar rate would be expected if thermal internal stresses were additive to the applied mechanical stresses. The gradients are also similar to those obtained by Boller for CSM. Discrepancies would also be expected between the results at different temperatures due to the accuracy of the temperature control. It was shown in Section 3.5.4.2 that creep acceleration rates were very sensitive to temperature.

The change in glass volume fraction did not significantly change the stress rupture properties of the CSM laminates. However, the creep properties of the high volume fraction laminate showed a slight improvement (Fig. 3.21).

Results at both temperatures indicate that the cross-ply woven roving tested in this project was superior in strength retention to that tested by Boller.

Unfortunately, there was not sufficient time available in this project to cause failure of the unidirectional material tested. Boller did not test this type of laminate. Results obtained however, show the unidirectional material to sustain higher stresses for longer periods than either the woven roving or the CSM laminates.

The creep results tabulated in Fig. 3.21 show that the order of material superiority in resisting creep is the same as that

in resisting stress rupture. This is in line with expectations, since creep rates and time for rupture have been related earlier in this chapter.

The table, Fig. 3.21, shows that Findley's equation:

$$\epsilon = \epsilon_0 + m t^n$$

can be fitted satisfactorily to individual specimen results since the standard errors, when a regression analysis is performed, are small. The equation used for this analysis is:

$$\log (\epsilon - \epsilon_0) = \log m + n \log t$$

The constant " ϵ_0 " is determined by an iterative procedure which minimises the standard error. The computer programme written to perform this analysis is shown in Appendix A. Fig. 3.23 shows typical results of a creep test together with the curve fitted to the results, using Findley's equation, on a linear scale. Further results are shown on logarithmic scales in Figs. 3.24 to 3.28. Confidence limits are also given in these figures showing the accuracy of fit between theory and experiment.

From the above graphs and the table - Fig. 3.21, constant "n", which according to Findley should be dependent only upon the material and environment, is shown to vary more than can be explained by small variations in material. Thus, it appears that some variation in the test conditions occurred. However, these variations were small compared with the differences in the value of "n" caused by changes in reinforcement type.

In all cases the value of constant ϵ_0 was found to be very small ($< 1 \times 10^{-4}$) and negligible when considering practical

structures. On this basis Findley's equation may be simplified to:

$$\epsilon = mt^n$$

The graph of Fig. 3.29 shows that within the stress range tested, for random and bidirectional laminates, the constant "m" varies approximately linearly with stress. Findley, however, predicts the variation of "m" with stress " σ " as follows:

$$m = m' \sinh \frac{\sigma}{\sigma_m}$$

where m' and σ_m are constants independent of stress. If σ/σ_m is small the above equation simplifies to:

$$m = \frac{m' \sigma}{\sigma_m}$$

Thus Findley's equation extended to account for variations in stress is consistent with the results obtained. Findley's equation for the results obtained may now be written:

$$\epsilon = \frac{m' \sigma t^n}{\sigma_m} \tag{3.49}$$

At time $t = 1$ hr.

$$\epsilon_1 = \frac{m' \sigma}{\sigma_m}$$

Rearranging

$$\frac{\sigma}{\epsilon_1} = \frac{\sigma_m}{m'}$$

Since σ_m and m' are constants which are dependent upon material and environment only, $\frac{\sigma_m}{m'}$ may be considered as the apparent modulus of elasticity after 1 hr. of creep (E_1) which is independent

of stress. Finally, Findley's equation may be amended to:

$$\epsilon = \frac{\sigma t^n}{E_1} \quad 3.50$$

Thus, within the range of stresses used in testing, the creep characteristics of the laminates tested may be determined from tests at one stress only.

In Section 3.5.2 it was stated that creep strain was largely recoverable after a period of 4 times the creep period after unloading. The effect of partial unloading of CSM is shown in Fig. 3.30. In this case the stress was reduced by 50% after a loading period of 468 hrs. After a total time of 2000 hrs. recovery was incomplete. Recovery is considered complete when the two curves at equal stresses meet. That is to say, that the amount of creep is that which would be expected if the stress had been constant at the lower value. It is not possible to state whether total recovery would ever be achieved. The experimentally determined curve shows a constant strain over approximately 1000 hrs. This may continue until the constant stress creep curve, reaches the strain of the partially unloaded creep curve in which case the curves would thereafter coincide. Alternatively, the partially-unloaded creep curve may start to show an increased strain before coincidence of the two curves, and recovery would never be complete. This second alternative is the case if the Boltzmann superposition principle is applied to viscoelastic theory [3.37]. Fig. 3.30 shows that strain begins to increase again after approximately 900 hrs., using this theory and equation 3.50.

Figs. 3.31-33 show creep specimens before and after testing. Fig. 3.31 shows CSM specimens, Fig. 3.32 bidirectional specimens, with

cross-ply and $\pm 45^\circ$ angle-ply reinforcement, and Fig. 3.33 uni-directional reinforcement. A marked change in colour is apparent in the specimens after testing which appear on the right of the photographs. The whitening effect is considered to be due to chemical ageing of the resin, to cracking of the resin, debonding of the resin/glass interface and the ingress of water to the interface. The whitening occurred at both test temperatures but was more marked at the higher temperature as shown in the extreme right hand specimen of Fig. 3.33. At the higher temperature the cause of the colour change appeared to be mainly ageing and the ingress of water. At the lower temperature cracking appeared to be the major cause of colour change. This view is supported by the fact that colour change occurred more in narrow high stress areas than in the broad low stress areas of the specimens.

Failure modes may be seen in Figs. 3.31 & 32 and are similar to the short-term failure modes.

3.5.6.6. Conclusions

Results from tests at 70°C when transformed to 20°C using the Larson-Miller parameter were found to be conservative with respect to data from tests at 20°C .

Laminates with continuous fibres in the direction of the principal stress were shown to be superior in creep and stress rupture resistance than other laminates. The $\pm 45^\circ$ angle-ply laminates

exhibited the greatest propensity for creep.

The results obtained by the author for CSM and bidirectional woven roving at 20°C showed these laminates to be superior to the corresponding laminates tested by Boller.

The following equations may be used to predict the creep behaviour of the laminates tested under the test conditions. Where more than one value of a constant has been obtained the mean value is given:

$$\text{CSM } (V_f = 16.5\%): \epsilon_t = \sigma \cdot t^{0.091} \cdot 4,149^{-1}$$

(Units of stress = N/MM²)

$$\text{CSM } (V_f = 21.5\%): \epsilon_t = \sigma \cdot t^{0.076} \cdot 4,367^{-1}$$

$$\text{CROSS-PLY } (V_f = 24\%): \epsilon_t = \sigma \cdot t^{0.037} \cdot 10,015^{-1}$$

$$\pm 45^\circ \text{ ANGLE-PLY } (V_f = 24\%): \epsilon_t = \sigma \cdot t^{0.237} \cdot 1,729^{-1}$$

UNIDIRECTIONAL WOVEN

$$\text{ROVING } (V_f = 45.5\%): \epsilon_t = \sigma \cdot t^{0.008} \cdot 18,140^{-1}$$

UNIDIRECTIONAL WOVEN

$$\text{ROVING } (V_f = 54\%): \epsilon_t = \sigma \cdot t^{0.010} \cdot 20,823^{-1}$$

Creep recovery for CSM after partial unloading is largely recoverable; total recovery, however, may take a considerable period, if indeed total recovery occurs. The Boltzmann superposition principle gave a reasonable approximation to the recovery curve for CSM but over-estimated the recovery. If this theory is assumed to apply, total recovery is never achieved.

FIG. 3.1 ELASTIC MATERIALS - IN TENSION

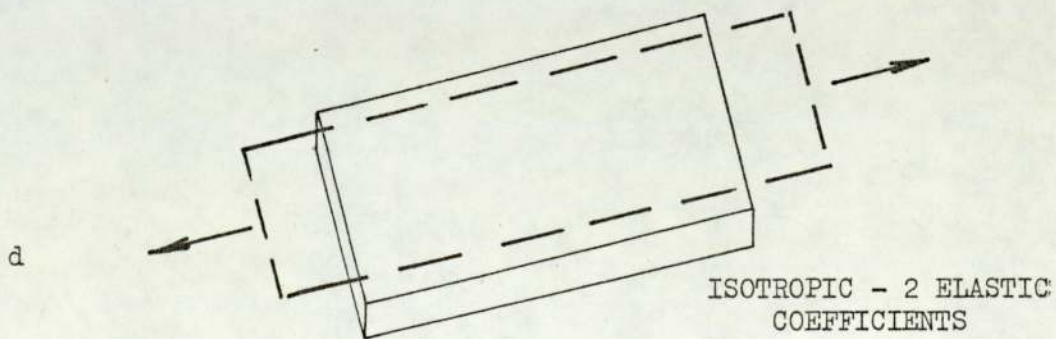
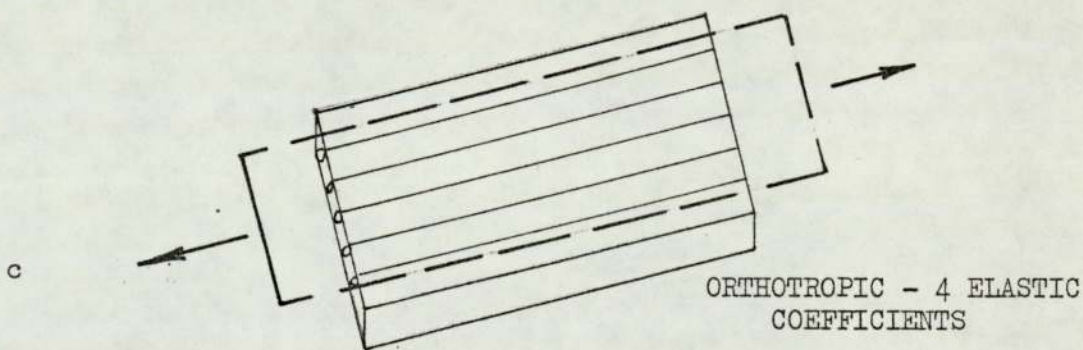
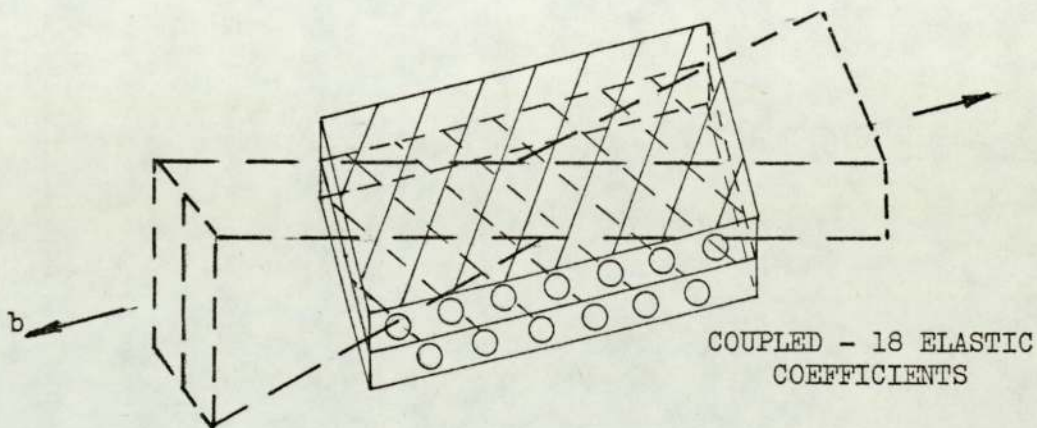
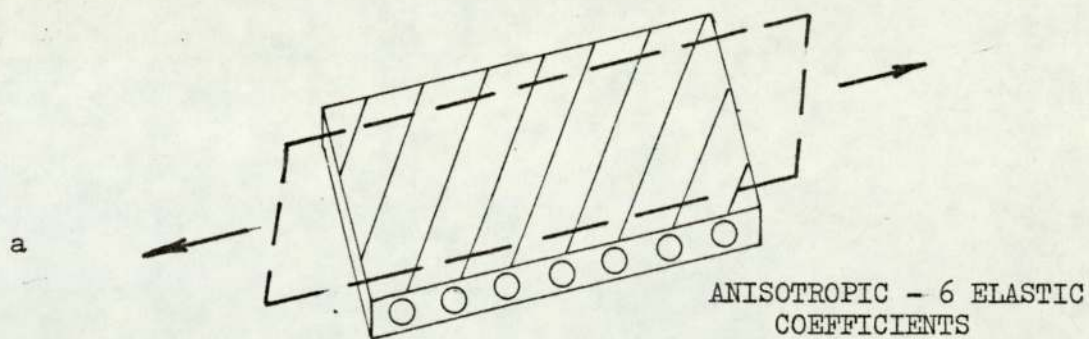
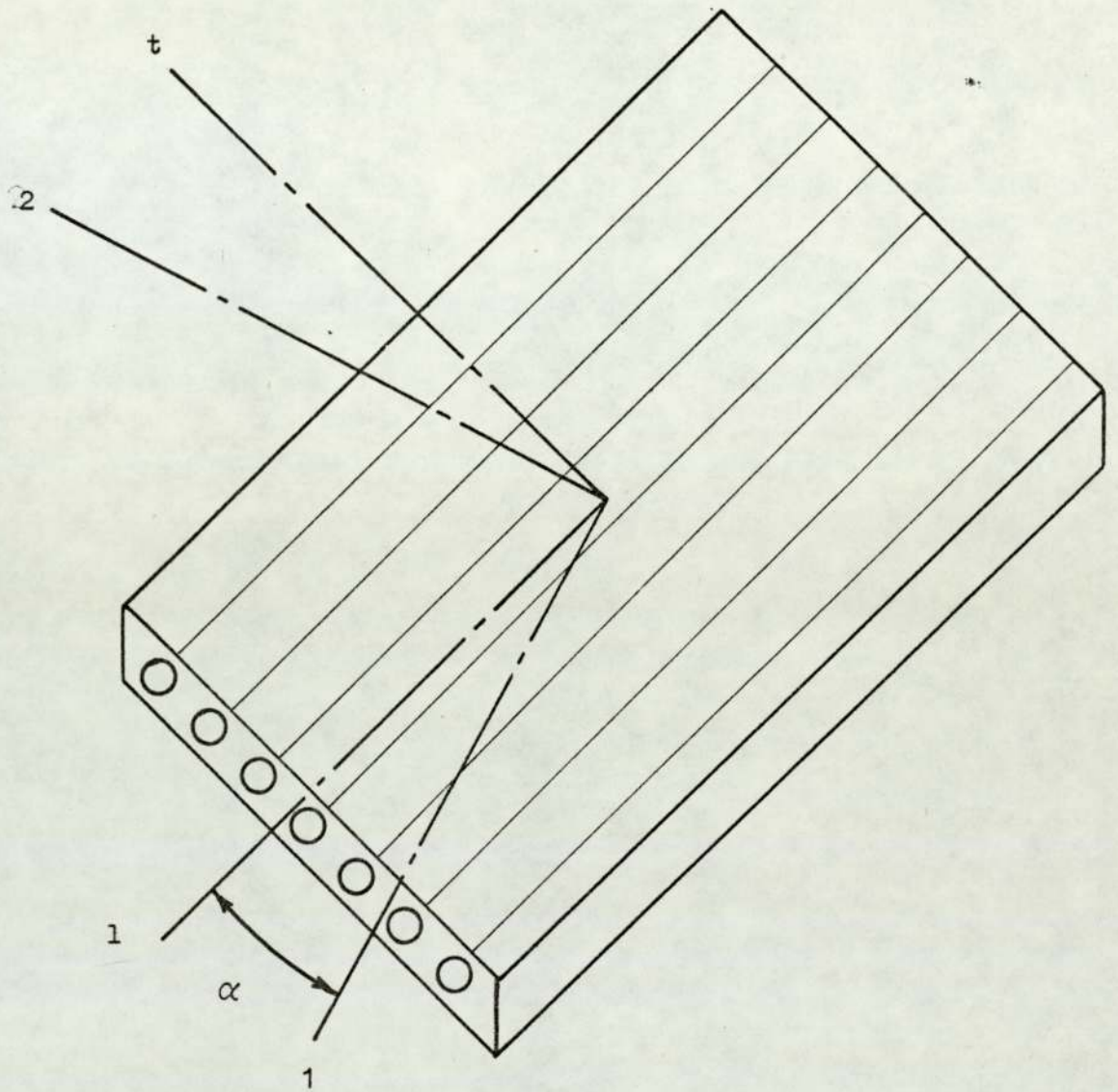


FIG. 3.2 THE BASIC LAMINA



LAMINA PRINCIPLE AXES 1-t
LAMINA ARBITRARY AXES 1-2

FIG. 3.3 FAILURE CURVE FOR A 3-FIBRE SYSTEM

$$\alpha = 0, 45^\circ + 90^\circ$$

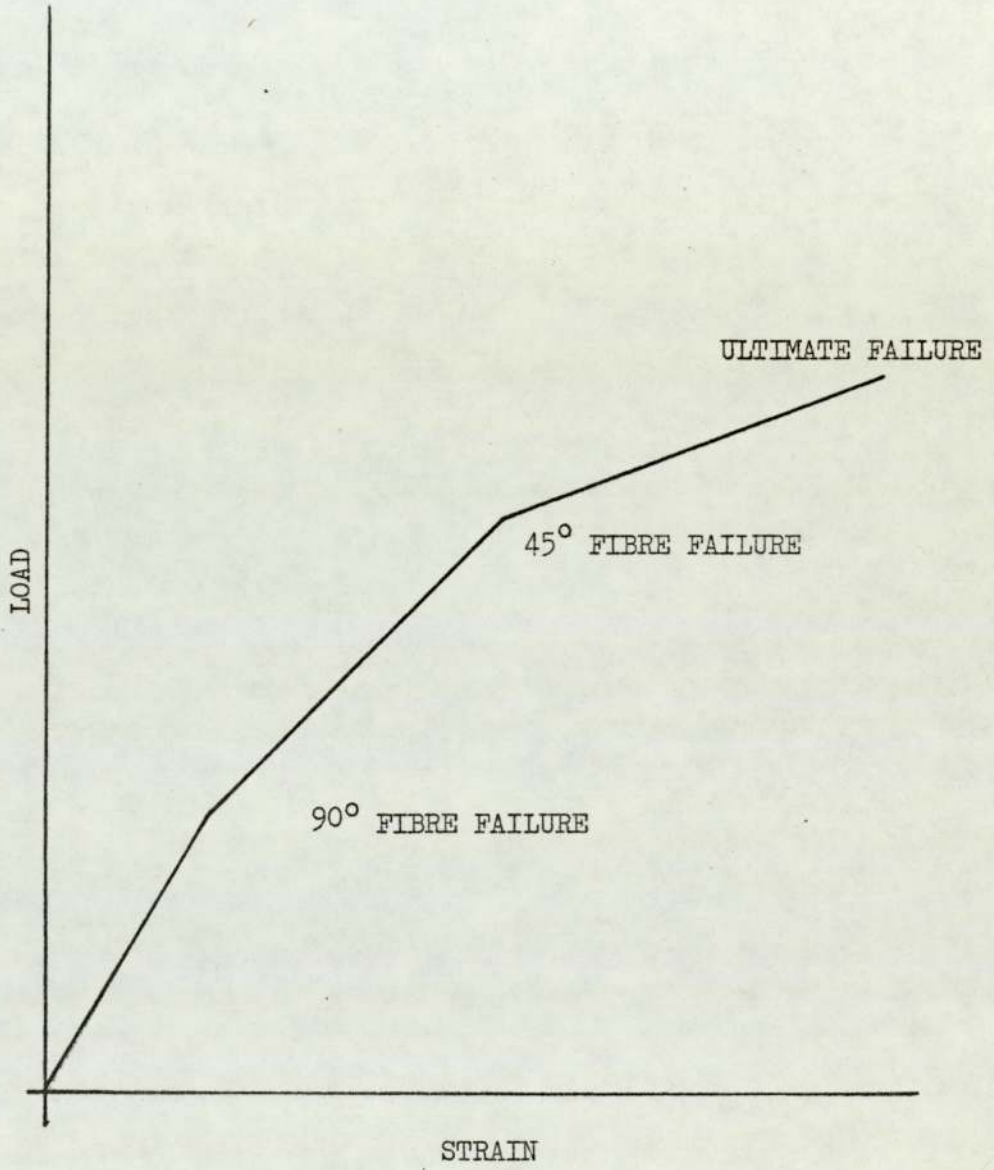
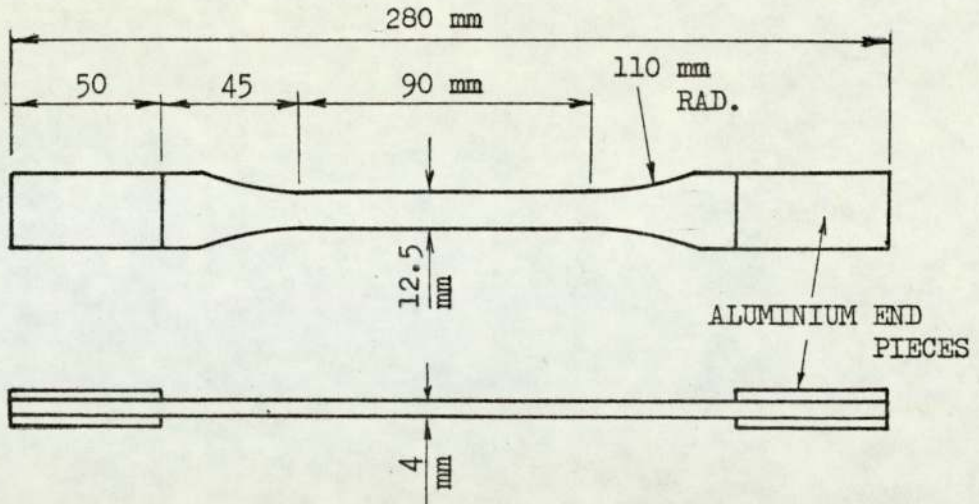
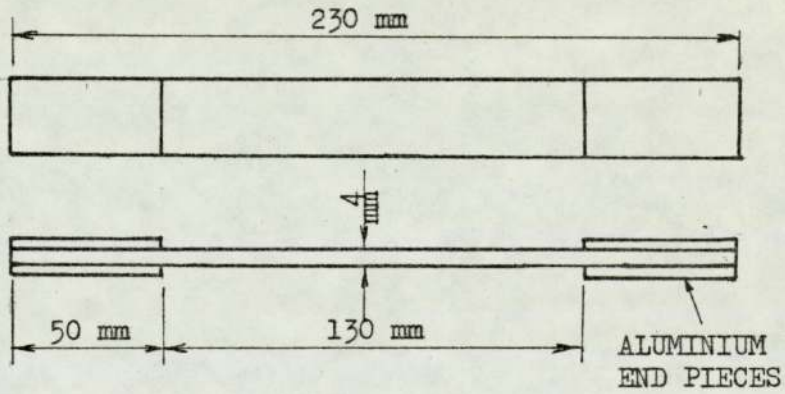


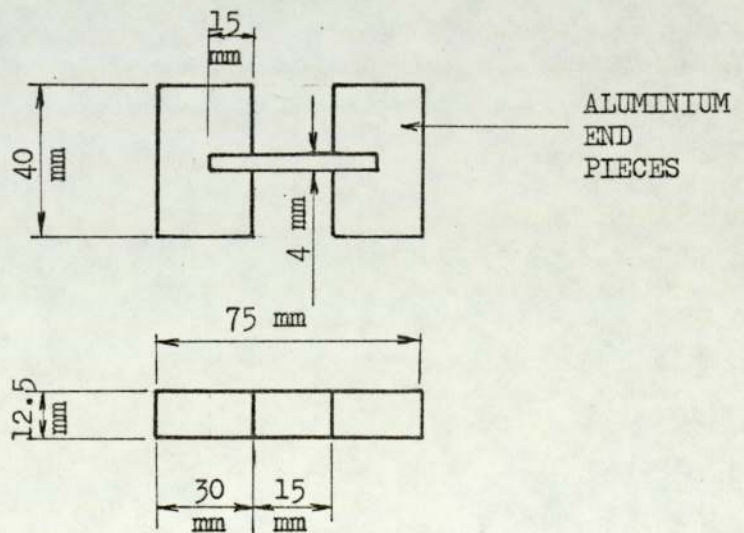
FIG. 3.4 DESIGN OF SHORT TERM TEST SPECIMENS



a) TENSILE SPECIMEN : UNIDIRECTIONAL,
BIDIRECTIONAL & ANGLE-PLY MATERIALS



b) TENSILE SPECIMEN : CSM



c) COMPRESSION SPECIMENS

FIG. 3.5 PHOTOGRAPH OF TYPICAL SHORT TERM SPECIMENS

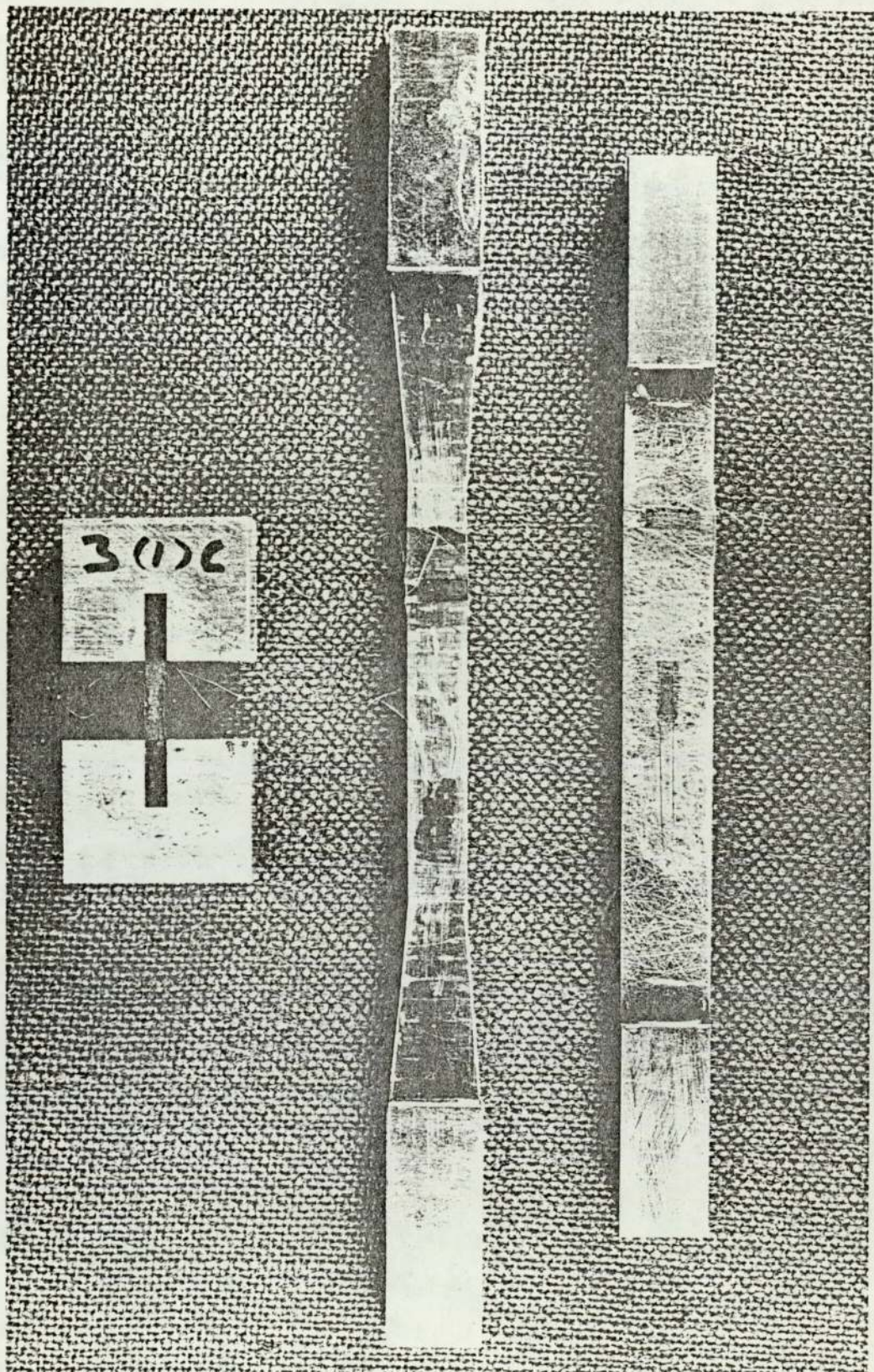


FIG. 3.6 AXIAL ELASTIC MODULUS OF LAMINA

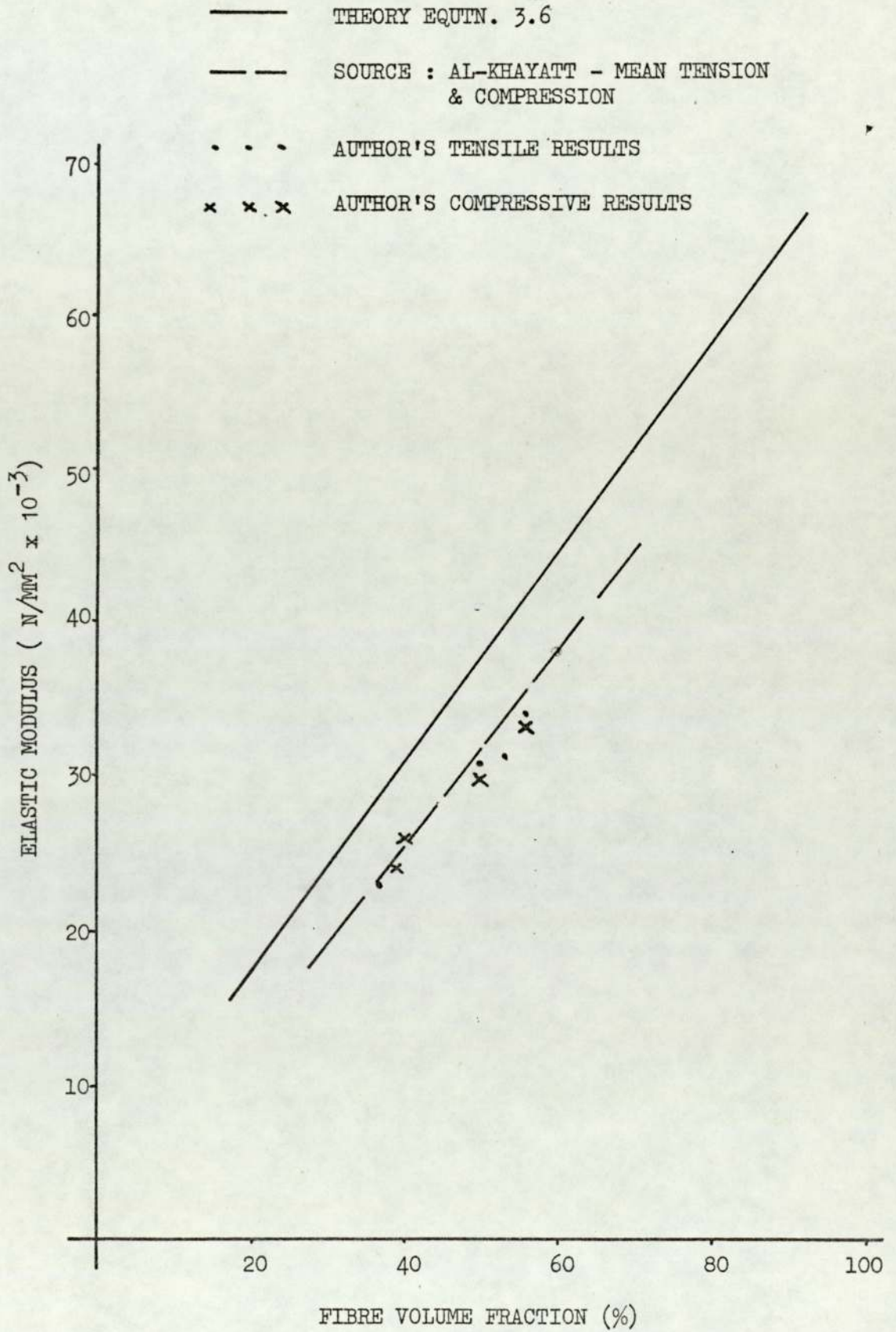


FIG. 3.7 TENSILE STRESS-STRAIN CHARACTERISTICS

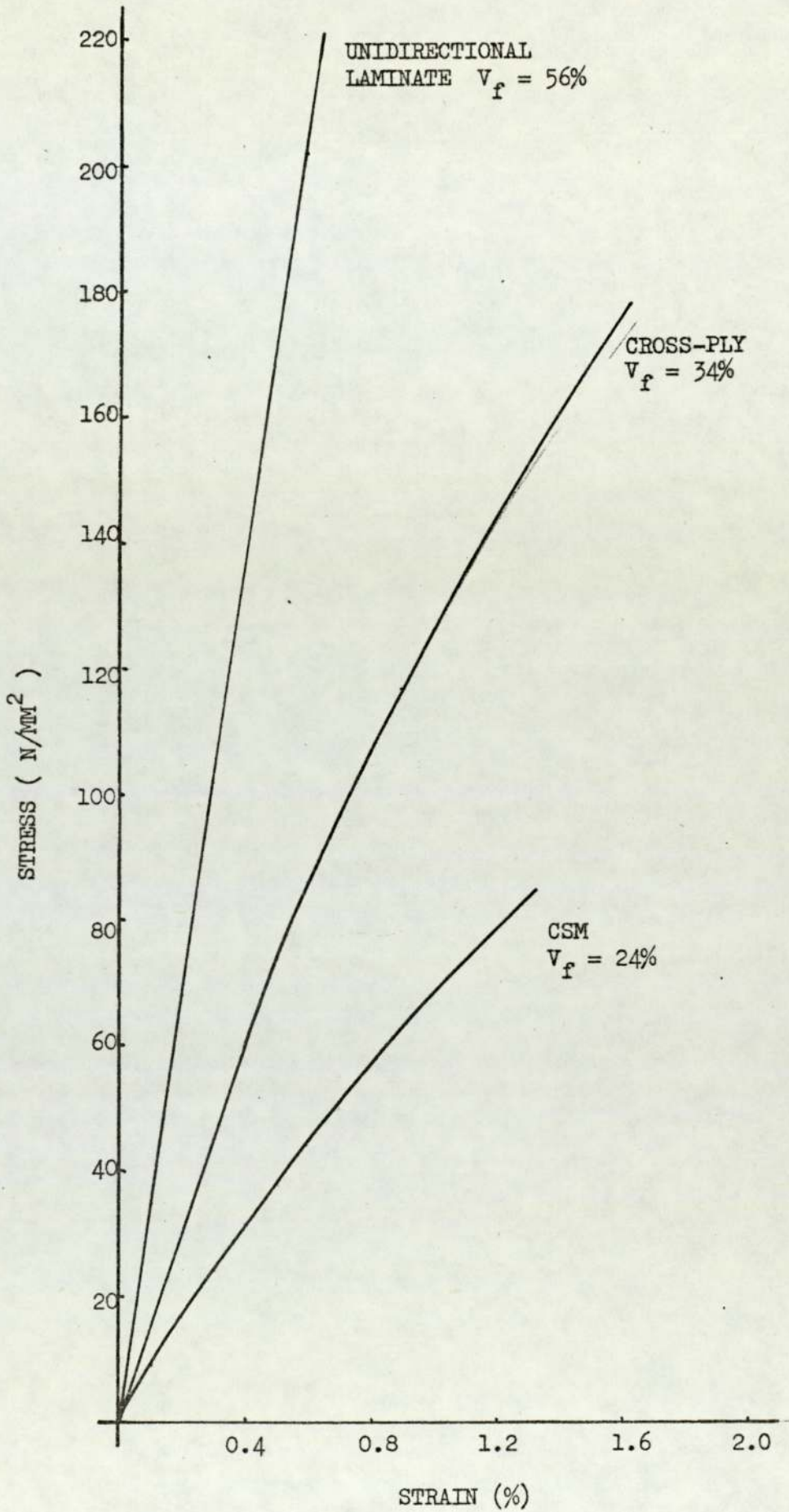


FIG. 3.8 AXIAL STRENGTH OF LAMINA

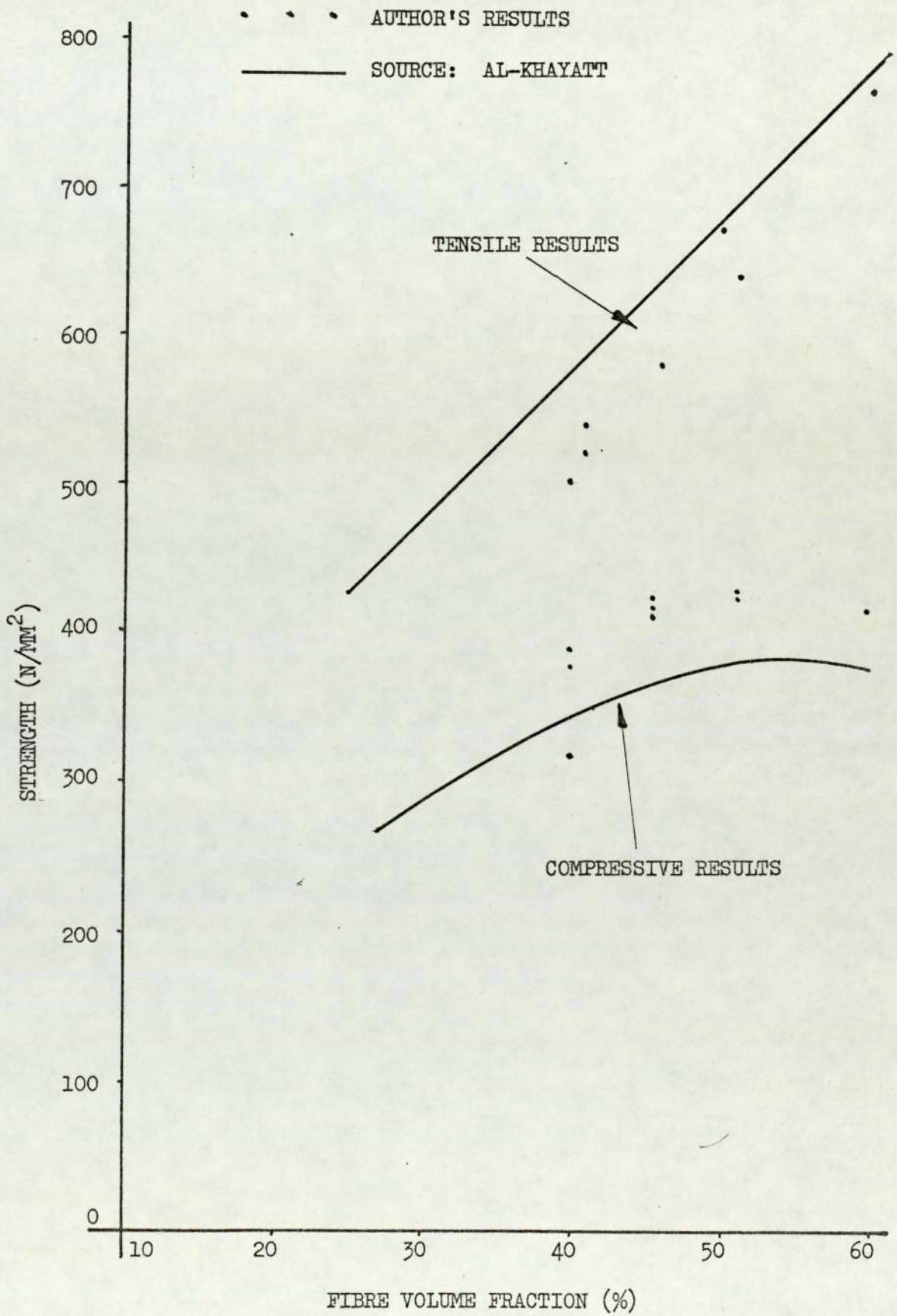


FIG. 3.9 TENSILE & COMPRESSIVE STRENGTHS OF SEVERAL LAMINATES

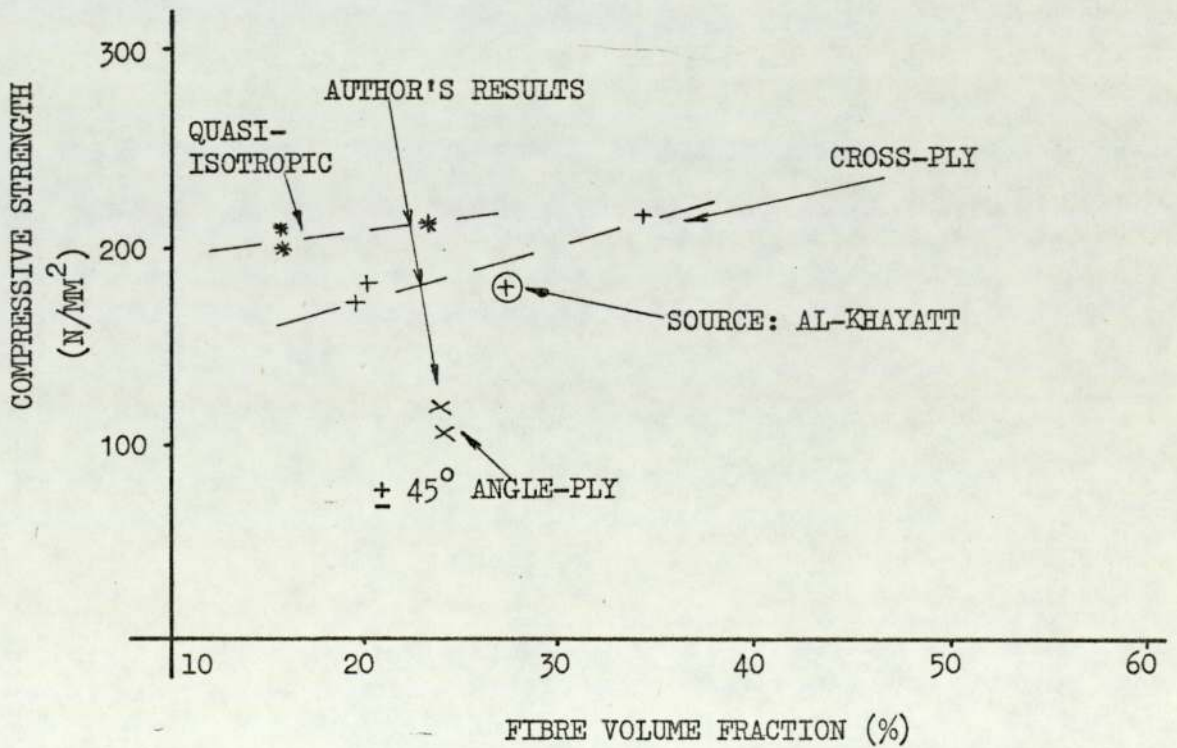
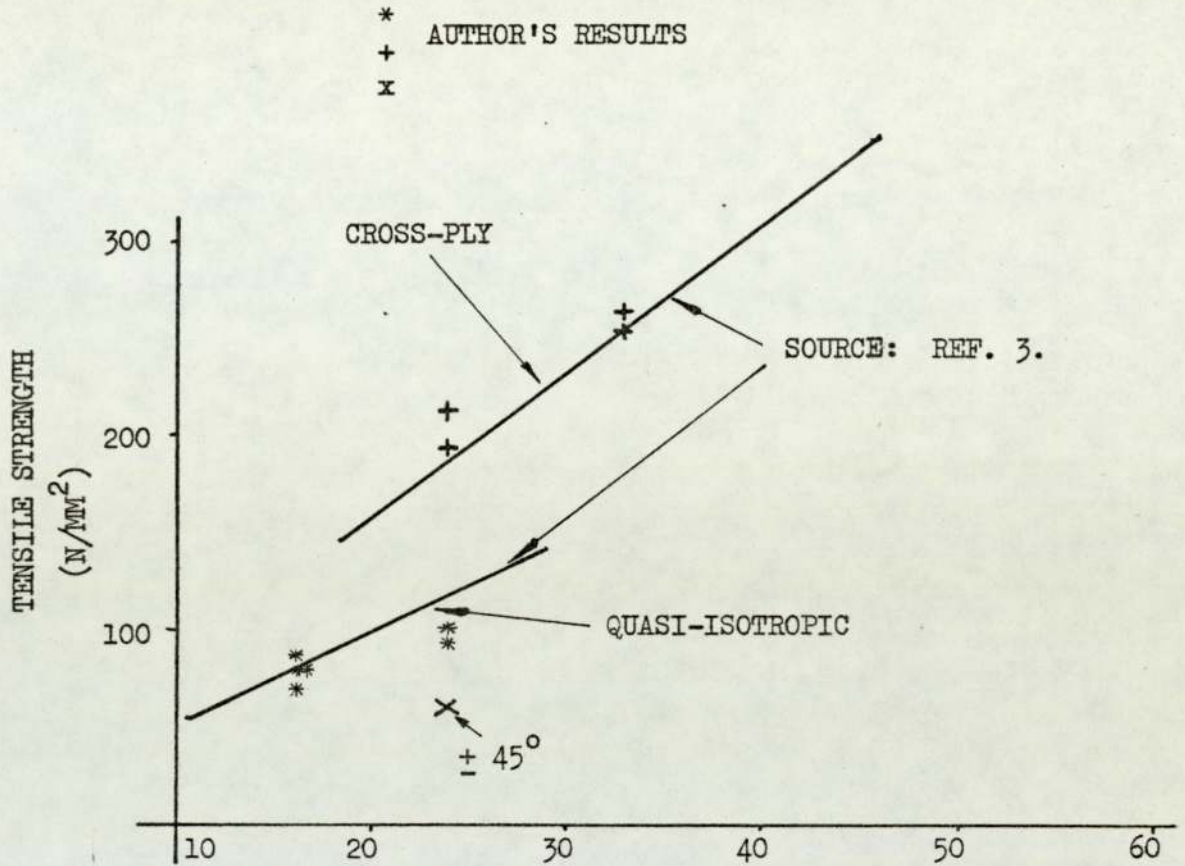


FIG. 3.10 LONGITUDINAL AND TRANSVERSE ELASTIC MODULUS

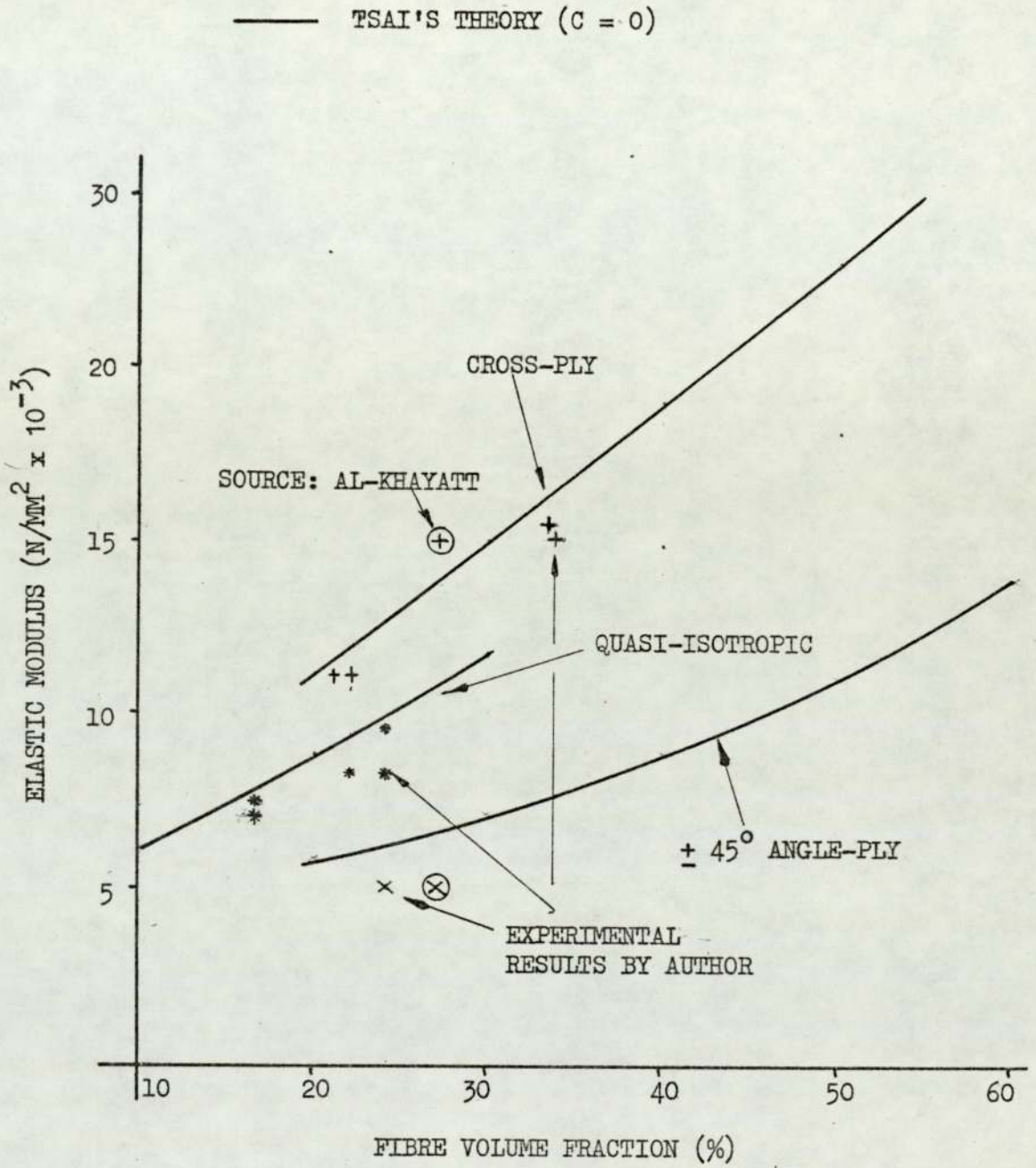
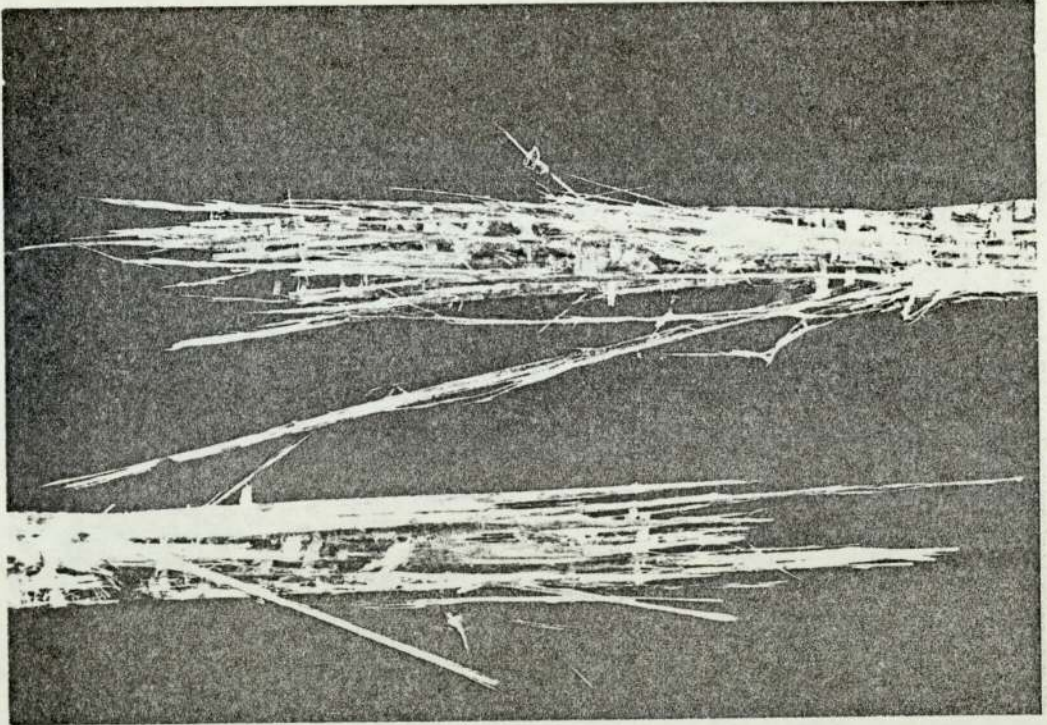
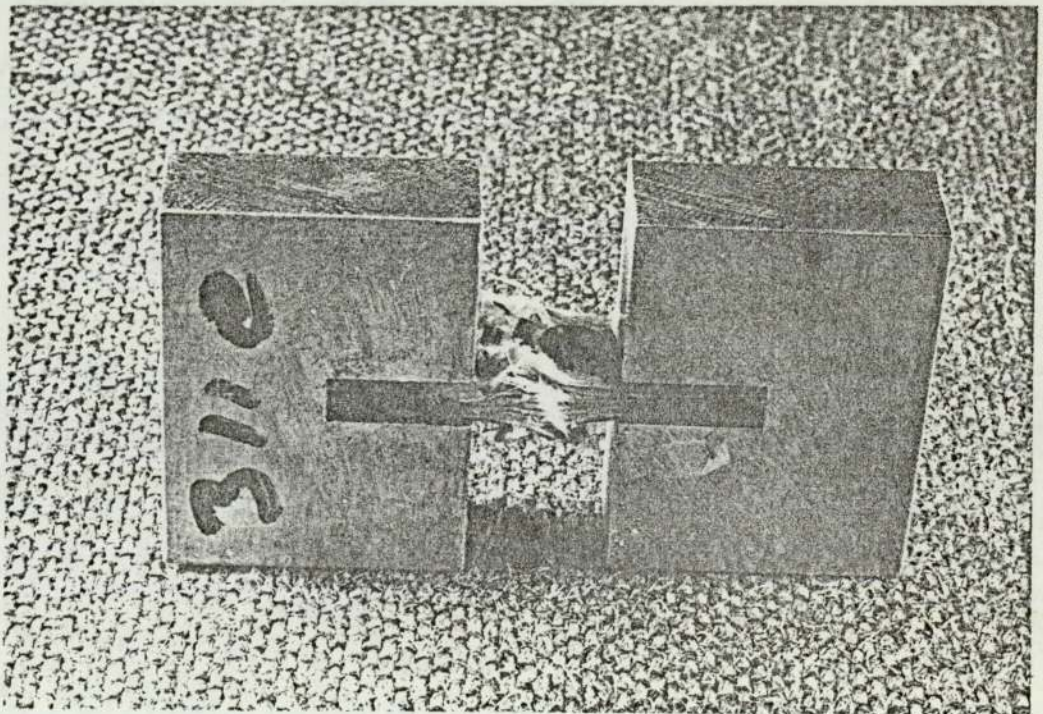


FIG. 3.11 TYPICAL FAILURE MODES

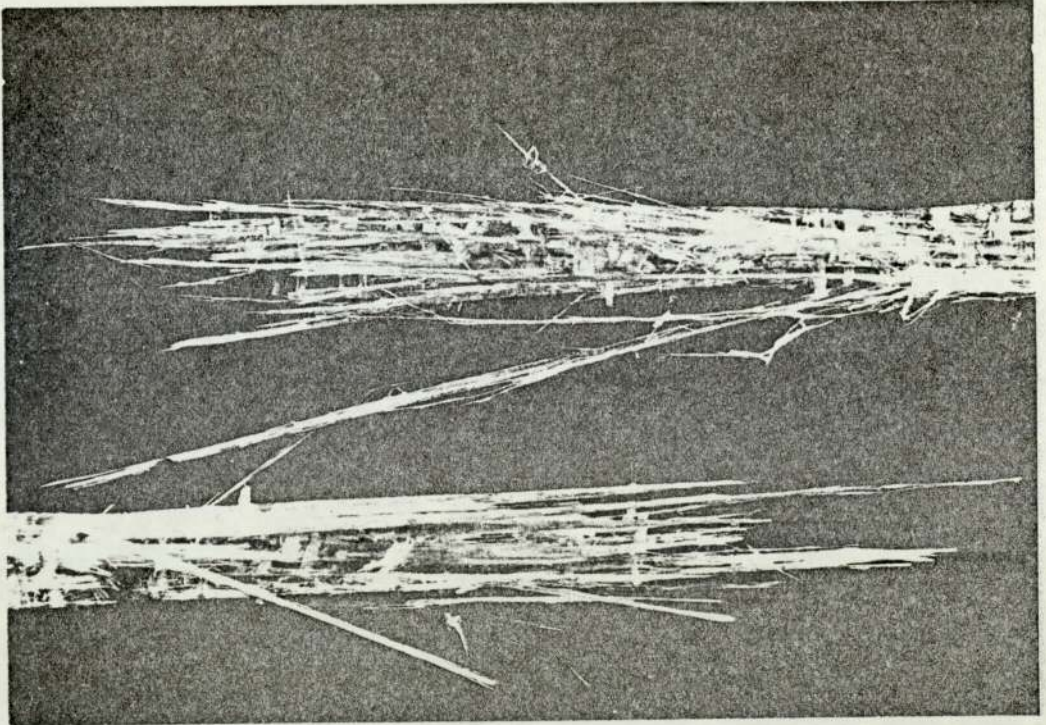


a) TENSILE FAILURE

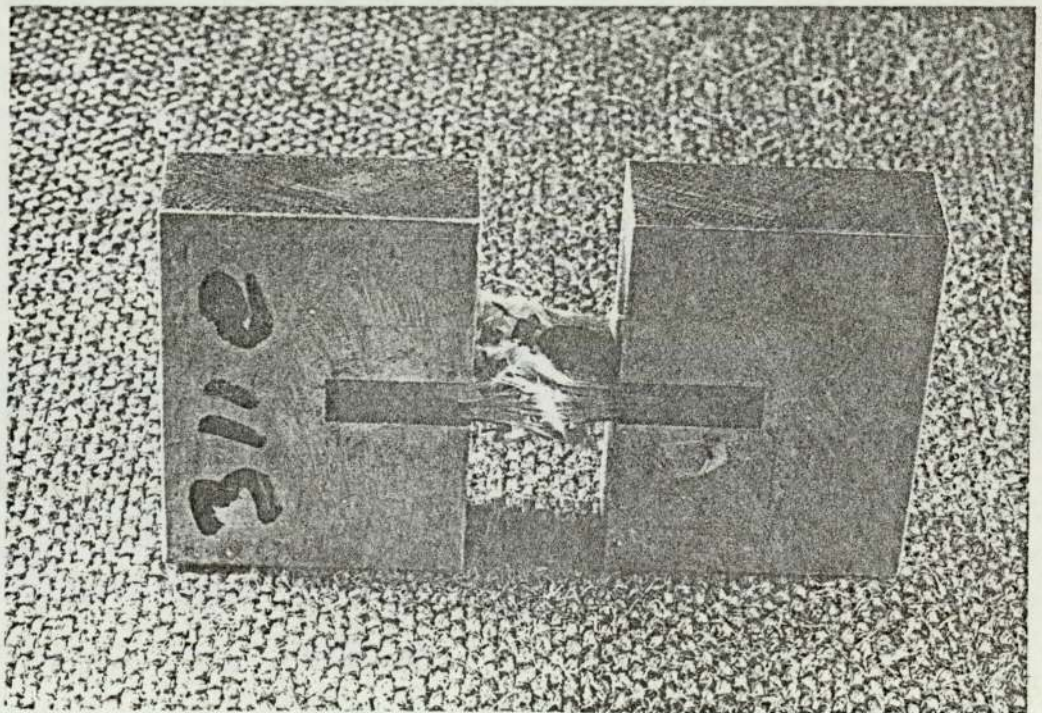


b) COMPRESSION FAILURE

FIG. 3.11 TYPICAL FAILURE MODES



a) TENSILE FAILURE



b) COMPRESSION FAILURE

FIG. 3.12 TRANSVERSE AND SHEAR MODULUS

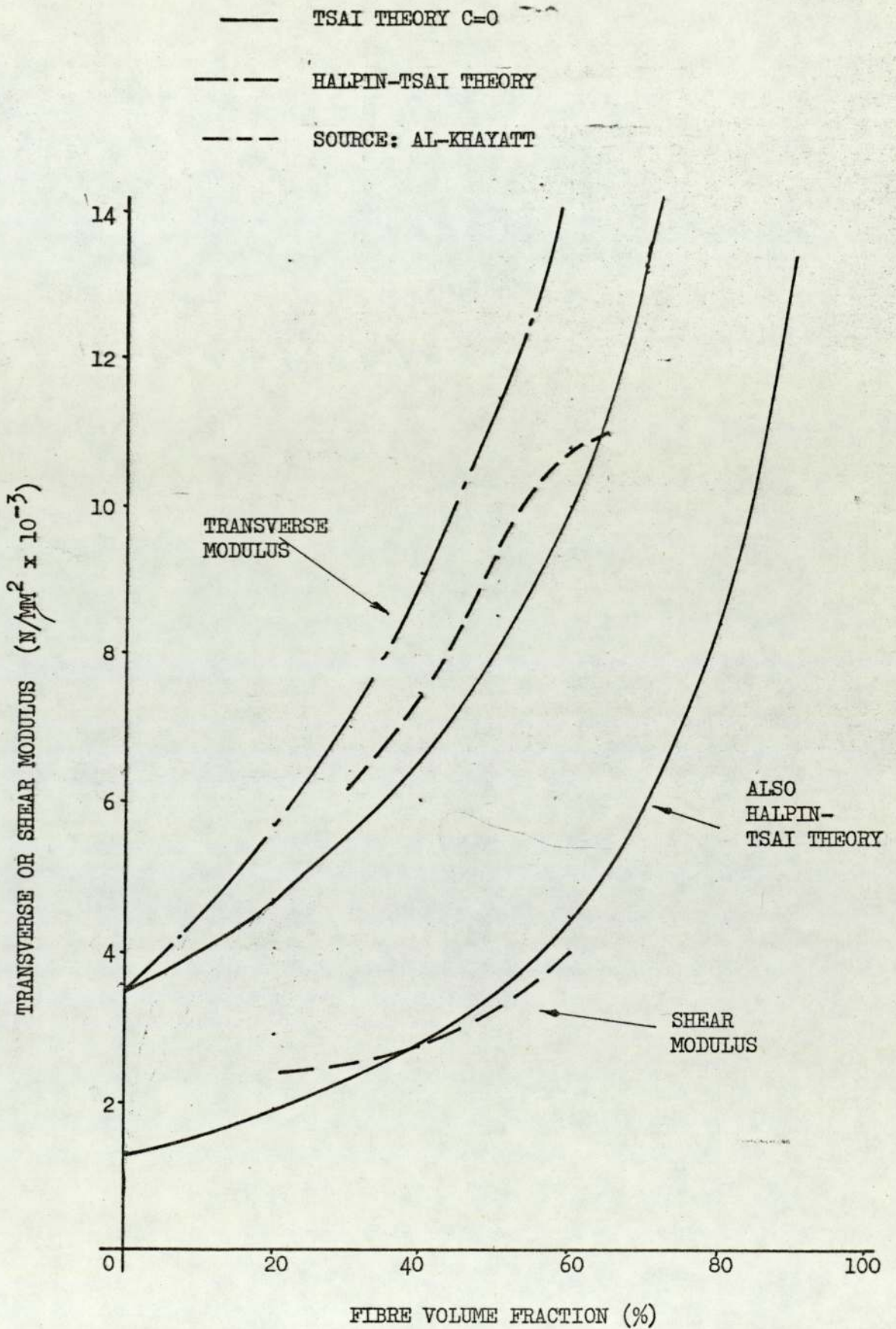


FIG. 3.13 LONGITUDINAL POISSON'S RATIO

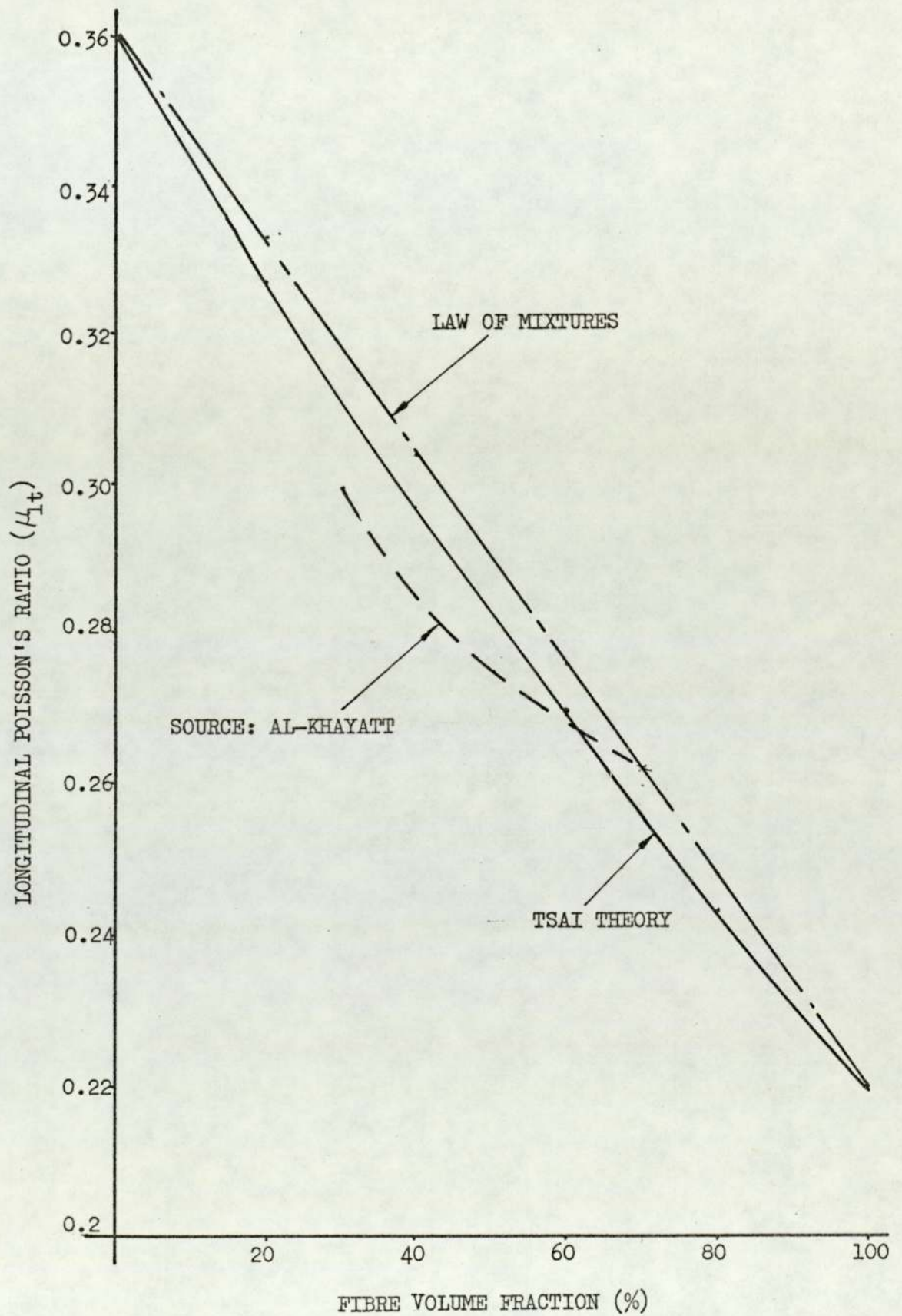


FIG. 3.14 LONGITUDINAL AND TRANSVERSE POISSON'S
RATIO FOR SELECTED LAMINATES

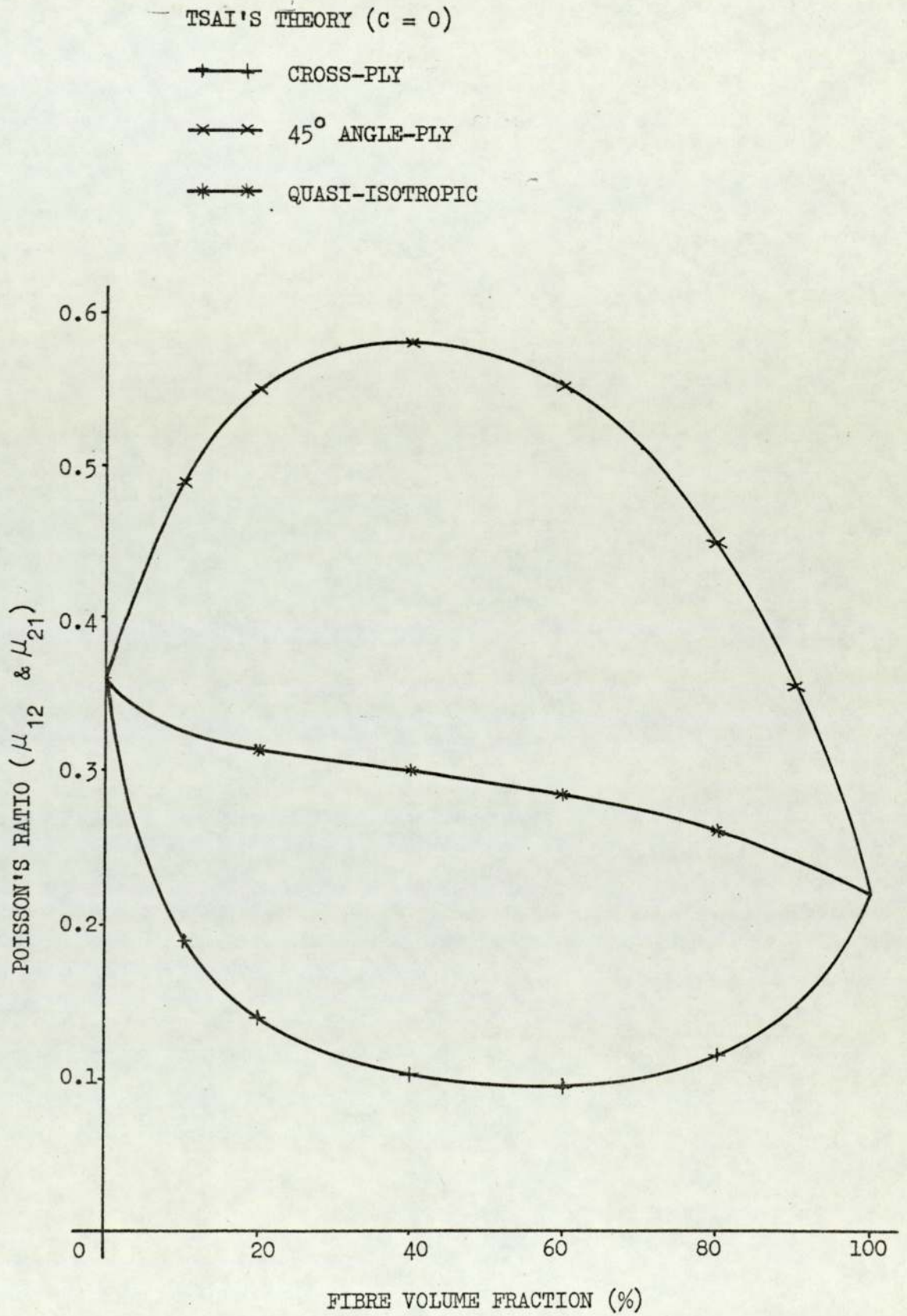


FIG. 3.15 THEORETICAL SHEAR MODULUS FOR
SELECTED LAMINATES

TSAI'S THEORY ($c = 0$)

- + — + CROSS-PLY
- × — × 45° ANGLE-PLY
- * — * QUASI-ISOTROPIC

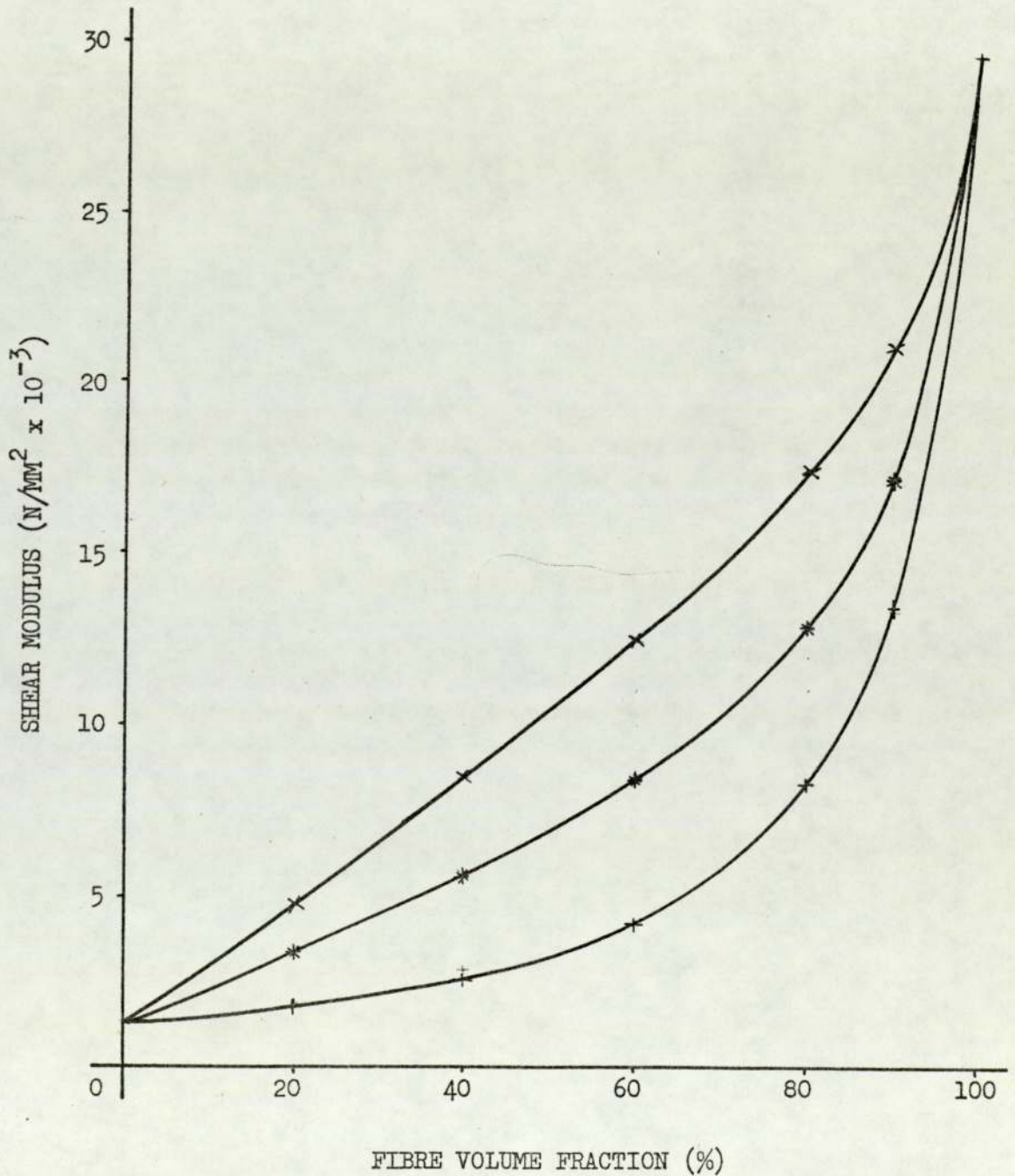


FIG. 3.16

CREEP ACTIVATION STRESS

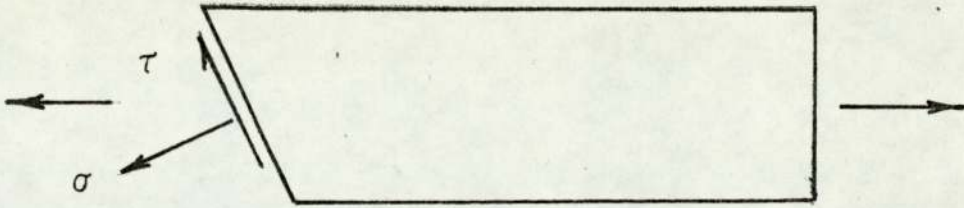


FIG. 3.16a

LARSON-MILLER PARAMETER

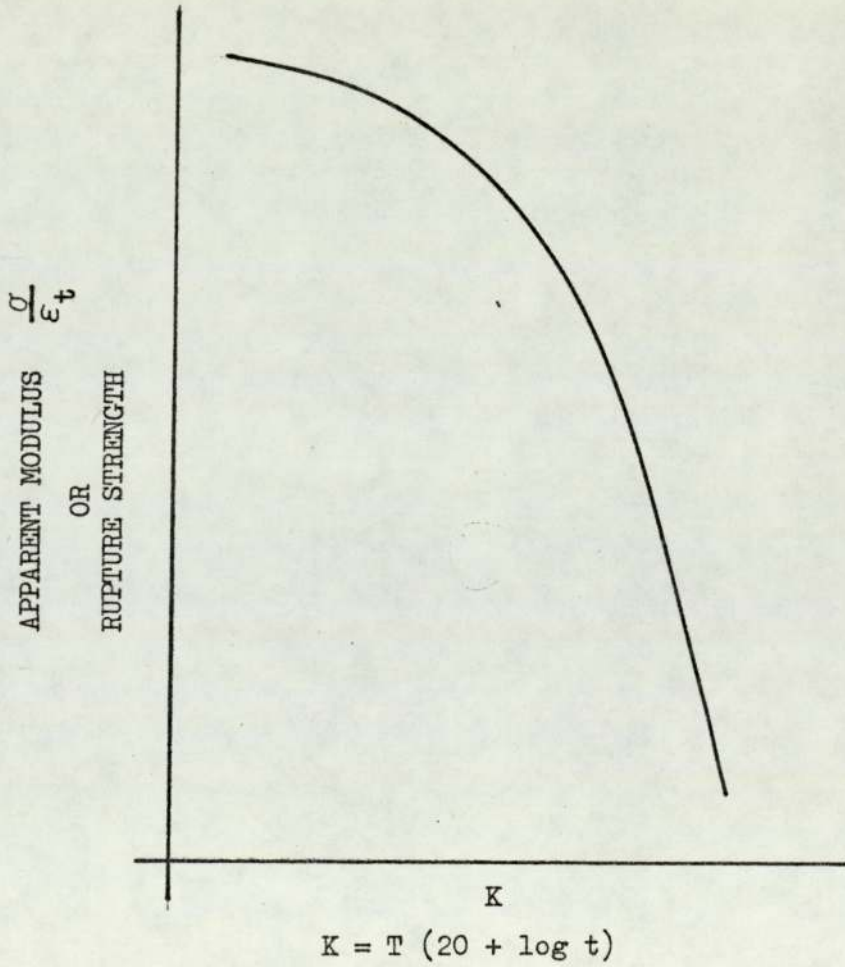
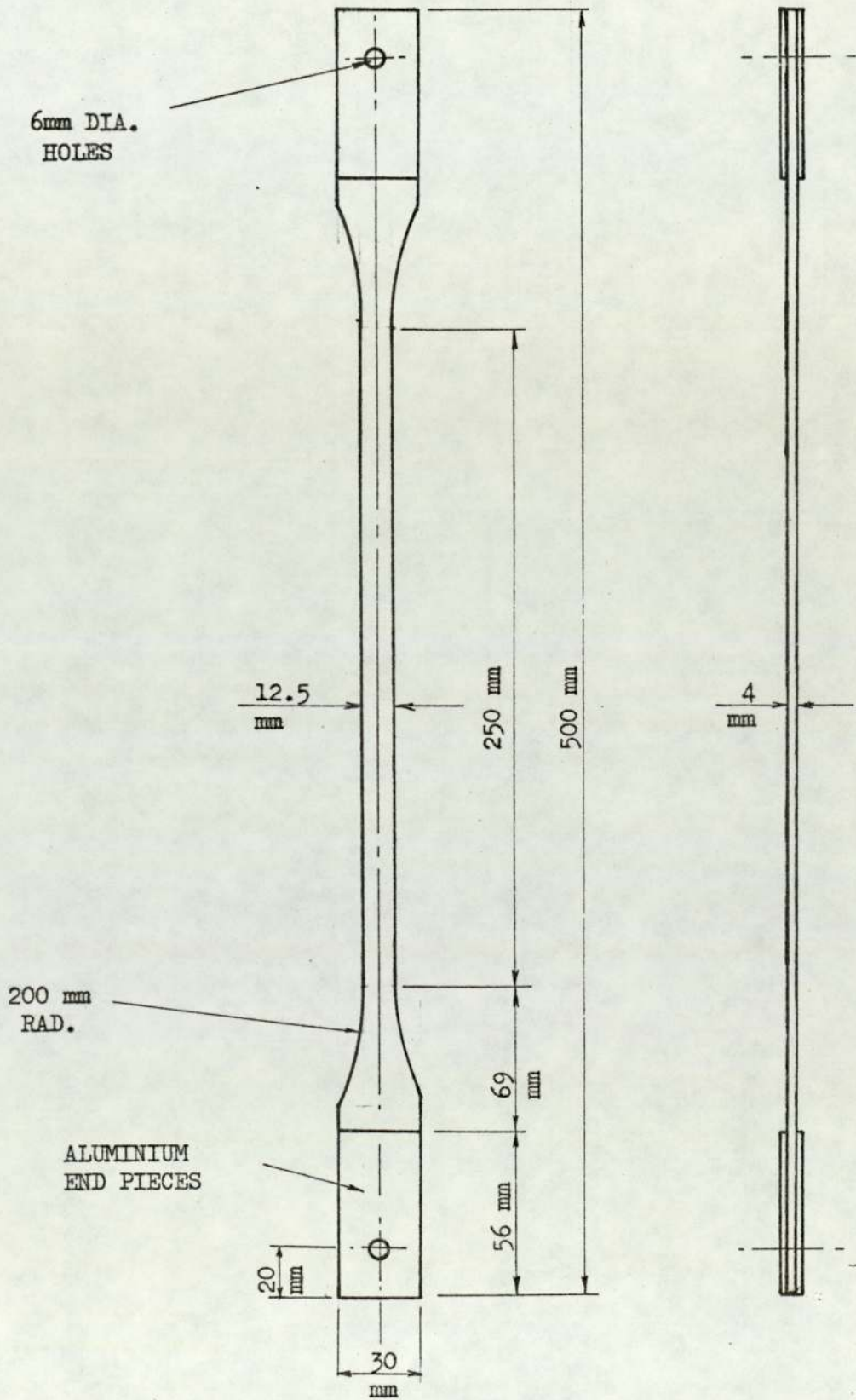


FIG. 3.17 CREEP AND STRESS RUPTURE

SPECIMEN



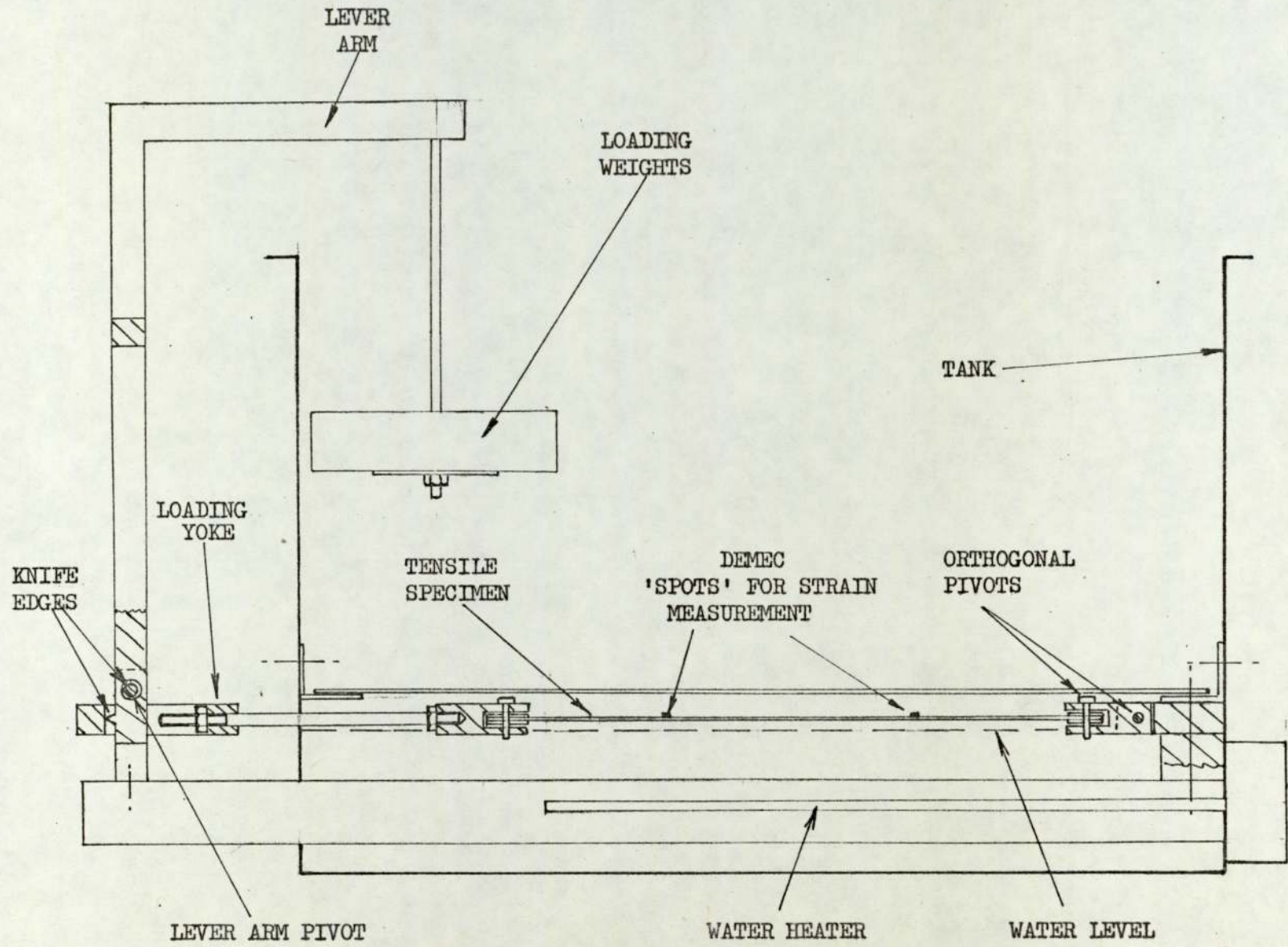


FIG. 3.18 CREEP TEST EQUIPMENT

FIG. 3.19 TABLE OF LONG TERM LOADING RESULTS

AT 70°C & 100% RH.

REINFORCEMENT	VOL. FRAC-TION (V_f) %	STRESS (N/MM ²)	TEST DURA-TION (HRS.)	EQUIVALENT TIME AT 20°C (HRS.)	MAX. STRAIN (%)
CHOPPED STRAND MAT (CSM)	16.5	7	700*	5.5 x 10 ⁶	0.8%
	16.5	10.5	3	9.3 x 10 ³	1.6%
	16.5	10.5	6.75	2.4 x 10 ⁴	2.0%
	16.5	10.5	23	1.0 x 10 ⁵	2.1%
	16.5	10.5	9.25	3.5 x 10 ⁴	2.2%
	16.5	10.5	6.0	2.1 x 10 ⁴	1.8%
	16.5	10.5	12.0	4.7 x 10 ⁴	1.6%
	16.5	10.5	15.0	6.1 x 10 ⁴	1.8%
	16.5	12.25	2.5	7.5 x 10 ³	2.1%
	16.5	12.25	4.0	1.3 x 10 ⁴	1.7%
	16.5	12.25	9.8	3.7 x 10 ⁴	1.7%
	16.5	17.0	0.5	1.1 x 10 ³	-
	BIDIRECTIONAL WOVEN ROVING	24	9	1,104*	9.3 x 10 ⁶
24		15	90*	5.0 x 10 ⁵	
24		42	522*	3.89 x 10 ⁶	0.5%
24		42	90*	5.0 x 10 ⁵	
24		42	96*	5.4 x 10 ⁵	
24		72	25.2	1.1 x 10 ⁵	1.9%
24		72	66	3.5 x 10 ⁵	2.2%
UNIDIRECTIONAL WOVEN ROVING	45.5	9	1,400*	1.27 x 10 ⁷	0.5%
	45.5	60	96*	5.4 x 10 ⁵	
	54	9	1,400*	1.27 x 10 ⁷	0.4%
	54	60	96*	5.4 x 10 ⁵	
		72	96*	5.4 x 10 ⁵	

* SIGNIFIES TEST TERMINATED BEFORE MATERIAL FAILURE

KEY :

* CSM $V_f = 16.5\%$

+ BIDIRECTIONAL WOVEN ROVING $V_f = 24\%$

Δ UNIDIRECTIONAL WOVEN ROVING $V_f = 54\%$

\square UNIDIRECTIONAL WOVEN ROVING $V_f = 45.5$

\rightarrow INDICATES TEST DISCONTINUED BEFORE FAILURE

EQUIVALENT TIME AT 20°C

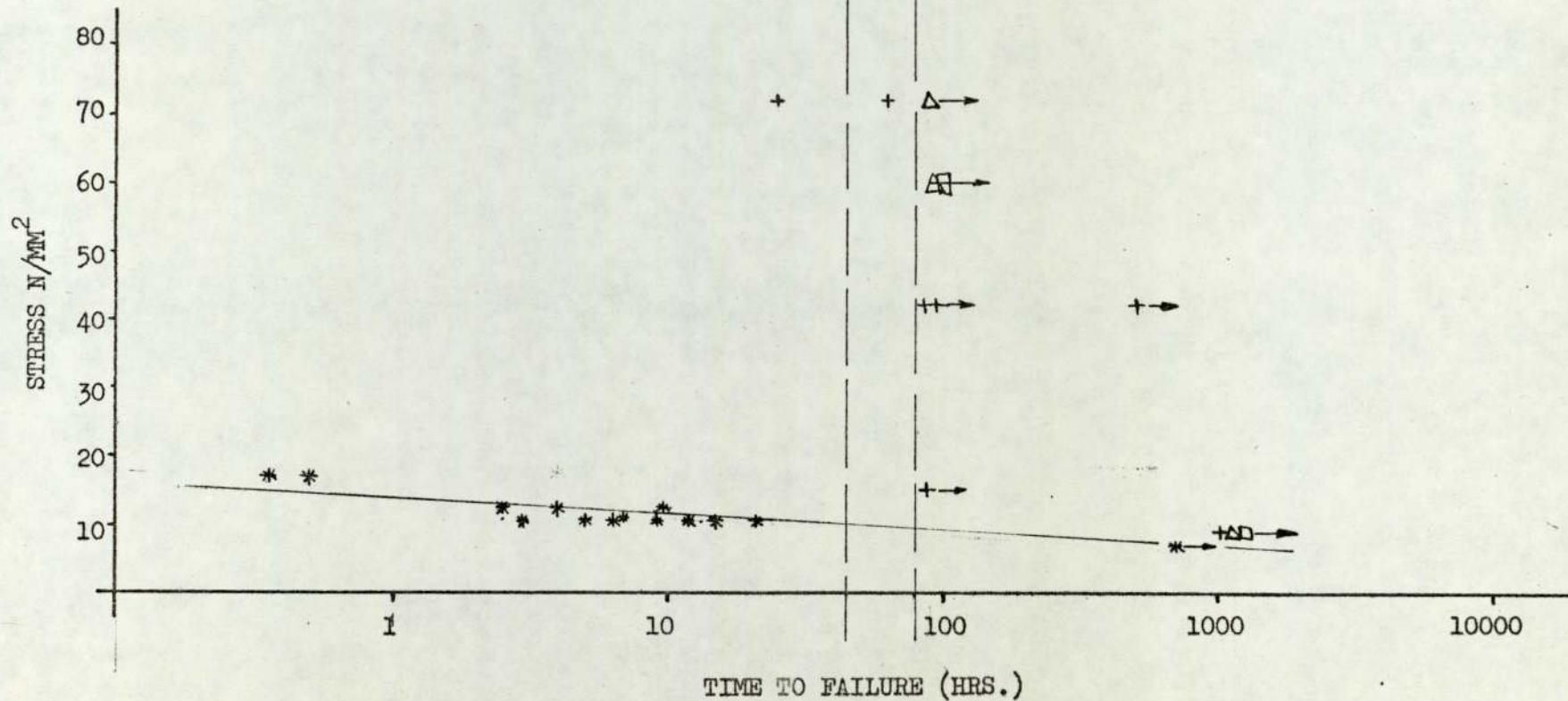


FIG. 3.20 LONG TERM LOADING RESULTS
AT 70°C

FIG. 3.21 TABLE OF LONG TERM PROPERTY RESULTS

AT 20°C & 100% RH.

REINFORCEMENT	VOL. FRAC-TION (V _f) %	STRESS (N/MM ²)	TEST DURA-TION (HRS.)	CREEP CONSTANTS			MAX STRAIN (%)	STD. ERROR lg (t _o)	
				o (M/M)	m (M/M) 10 ⁻²	n			
CHOPPED STRAND MAT (CSM)	16.5	28	468*	0.63x10 ⁻⁵	0.655	0.088	1.13	0.13x10 ⁻¹	
	16.5	37	1430*	0.95x10 ⁻⁵	0.812	0.089	1.55	0.16x10 ⁻¹	
	16.5	44	69	0.39x10 ⁻⁵	1.037	0.111	1.66	0.25x10 ⁻¹	
	16.5	45	45.5	0.55x10 ⁻⁴	1.142	0.086	1.59	0.26x10 ⁻¹	
	16.5	49	78	0.22x10 ⁻⁴	1.214	0.072	1.66	0.15x10 ⁻¹	
	16.5	48	43.5	0.31x10 ⁻⁴	1.13	0.09	1.59	0.23x10 ⁻¹	
	16.5	54	19.5	0.12x10 ⁻⁵	1.36	0.10	1.84	0.34x10 ⁻¹	
	21.5	25	1200*	0.29x10 ⁻⁴	0.57	0.08	1.01	0.12x10 ⁻¹	
	21.5	39	502*	0.9 x10 ⁻⁶	0.88	0.08	1.45	0.75x10 ⁻²	
	21.5	46	11.6	0.9 x10 ⁻⁵	1.02	0.08	1.23	0.77x10 ⁻²	
	21.5	52	18.9	0.29x10 ⁻⁴	1.24	0.062	1.49	0.56x10 ⁻²	
	BIDIRECTIONAL WOVEN ROVING	24	36	1015*	0.15x10 ⁻⁴	0.298	0.04	0.39	0.12x10 ⁻¹
		24	68	166*	0.9 x10 ⁻⁴	0.68	0.03	0.79	0.74x10 ⁻²
		24	88	1183*	0.4 x10 ⁻⁵	0.94	0.04	1.25	0.13x10 ⁻¹
BIDIRECTIONAL WOVEN ROVING AT ± 45°	24	12	74.5*	0.0 x10 ⁻⁶	0.45	0.19	1.26	0.37x10 ⁻¹	
	24	24	74	0.25x10 ⁻⁵	0.95	0.27	3.86	0.59x10 ⁻¹	
	24	33	7.5	0.16x10 ⁻⁵	2.6	0.25	4.38	0.16x10 ⁻¹	
UNIDIRECTIONAL WOVEN ROVING	45.5	78	1015*	0.45x10 ⁻⁴	0.43	0.008	0.45	0.17x10 ⁻²	
	54	75	1015*	0.79x10 ⁻⁵	0.39	0.010	0.42	0.95x10 ⁻³	
	54	102	1015*	0.93x10 ⁻⁴	0.46	0.009	0.49	0.13x10 ⁻²	

* SIGNIFIES TEST TERMINATED BEFORE MATERIAL FAILURE

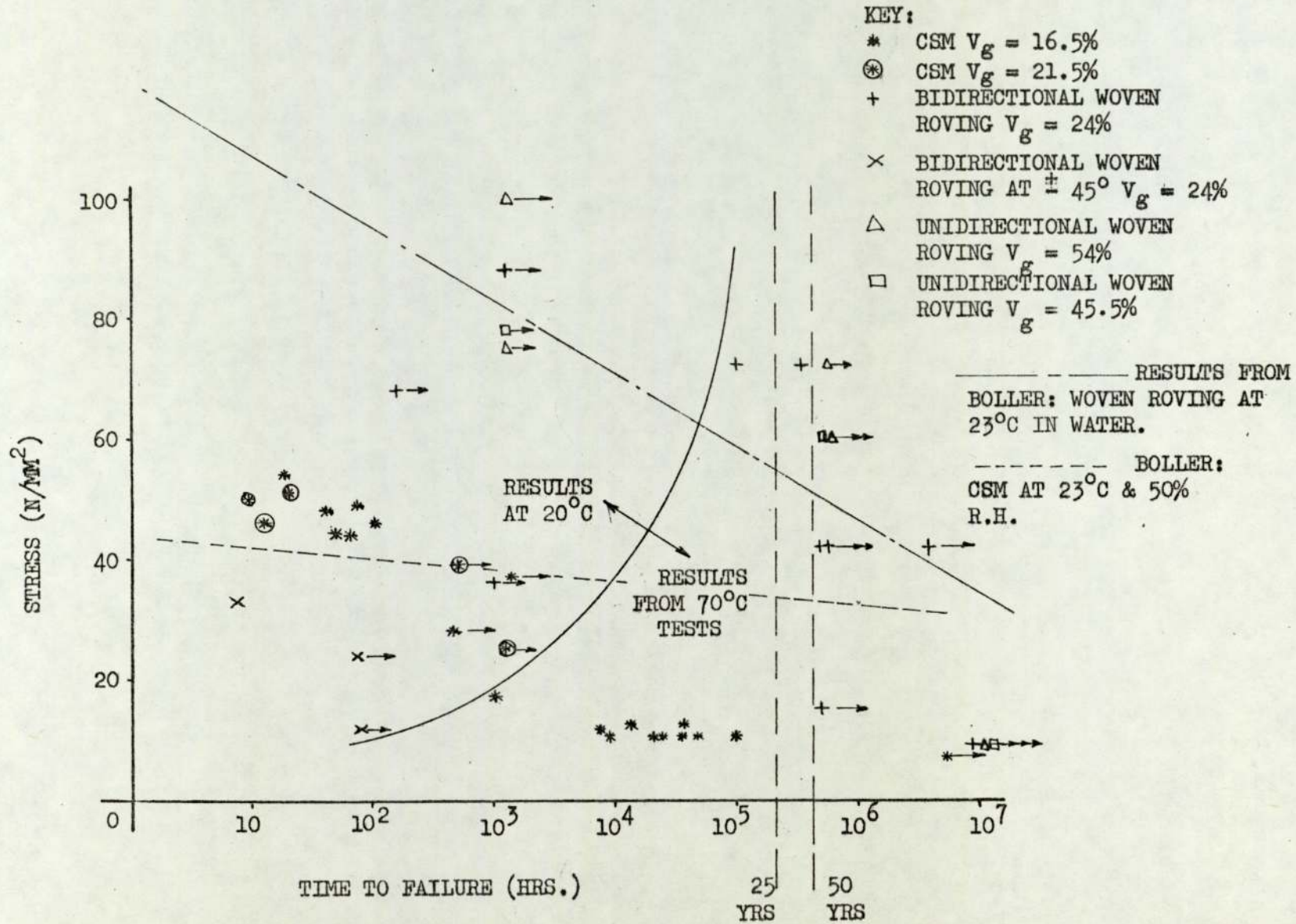
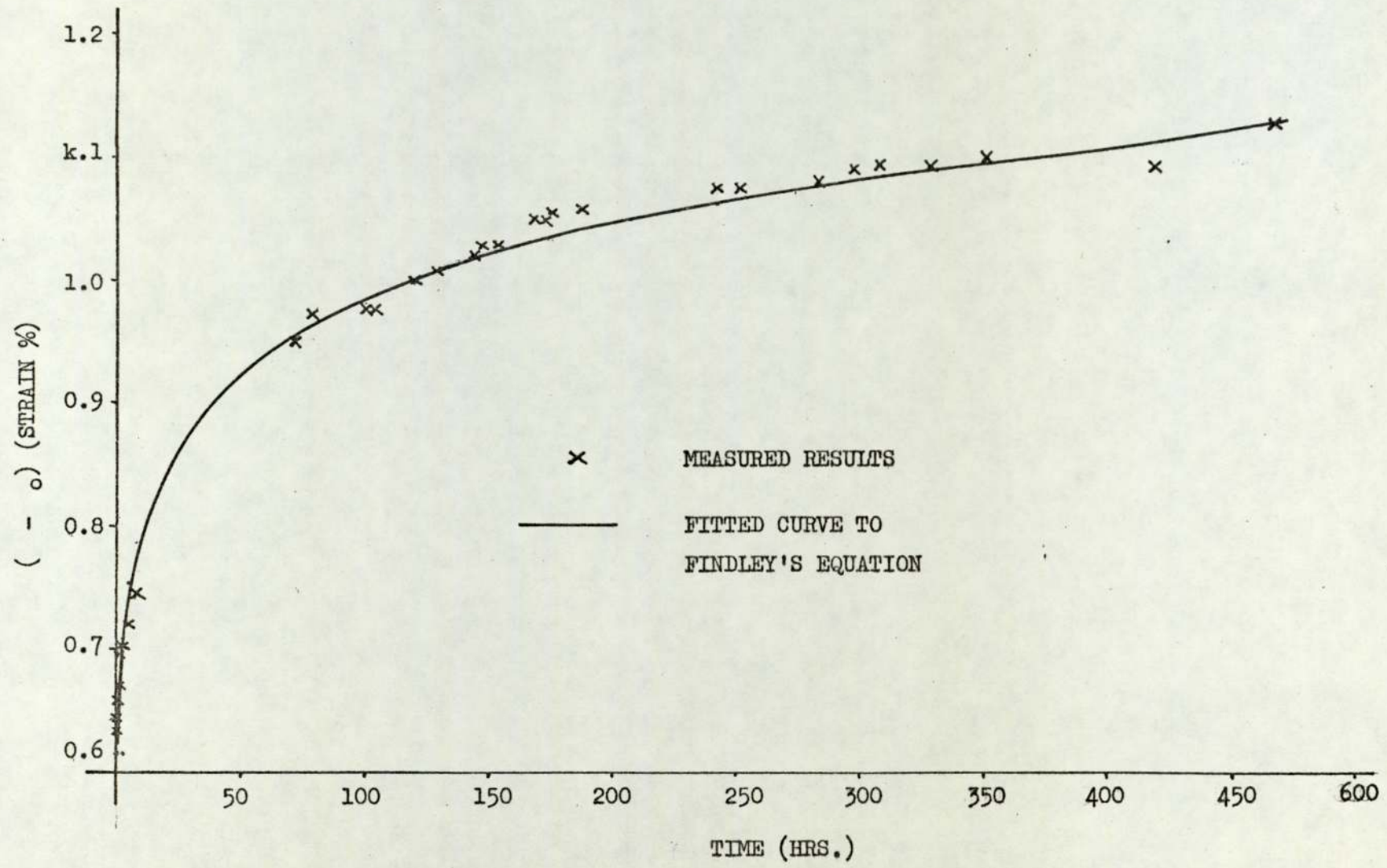


FIG. 3.22 GRAPH OF STRESS RUPTURE RESULTS AT 20°C AND 100% R.H.

FIG. 3.23 GRAPH OF CREEP RESULTS FOR CSM ($V_f = 16.5$)
AP STRESS = 28 N/MM²



RESULTS FITTED TO
FINDLEY EQUATION

66% CONFIDENCE
LIMITS

* TEST TERMINATION BEFORE
MATERIAL FAILURE

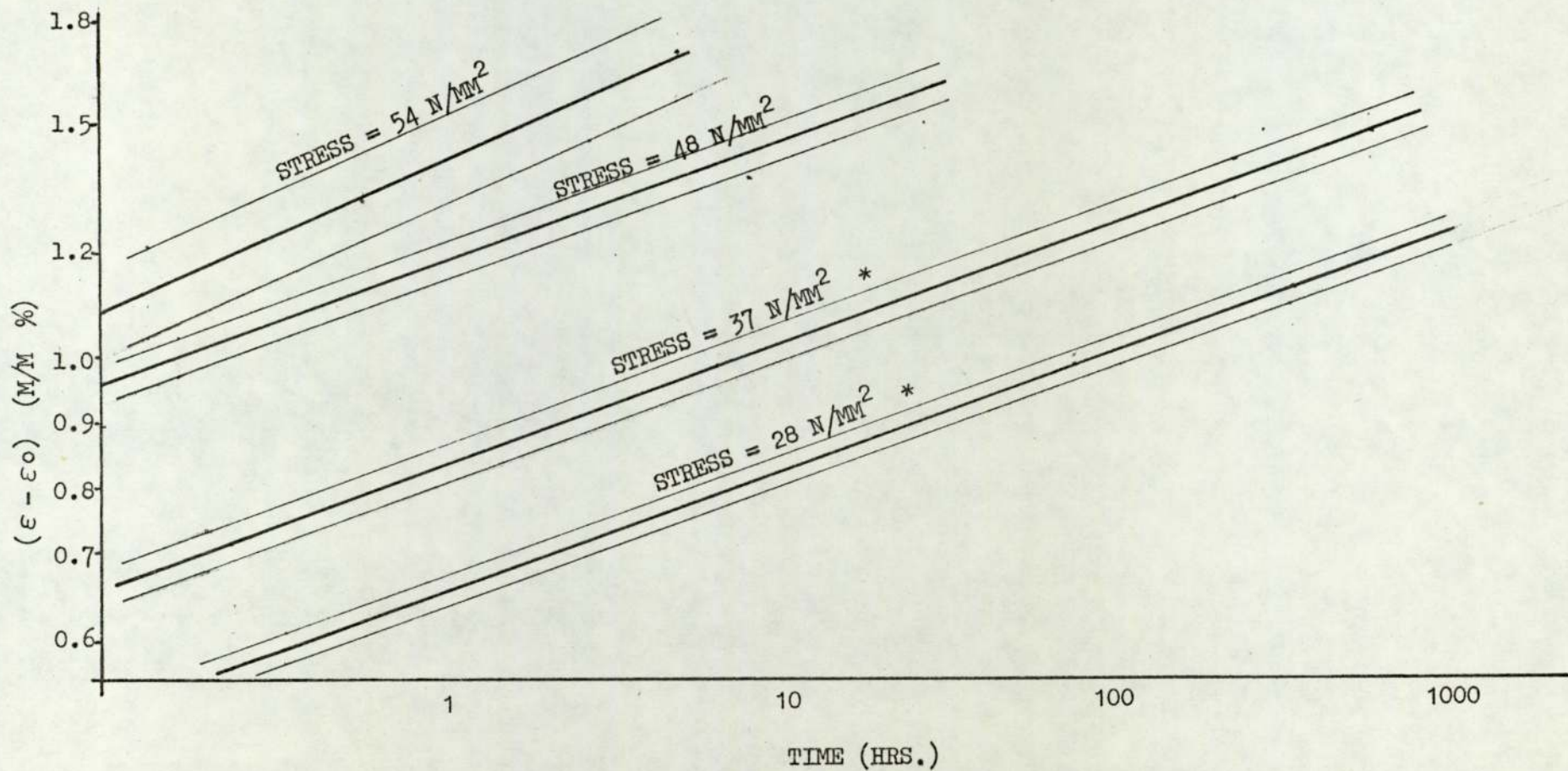


FIG. 3.24

SELECTED CREEP RESULTS OF

CSM : $V_f = 16.5\%$

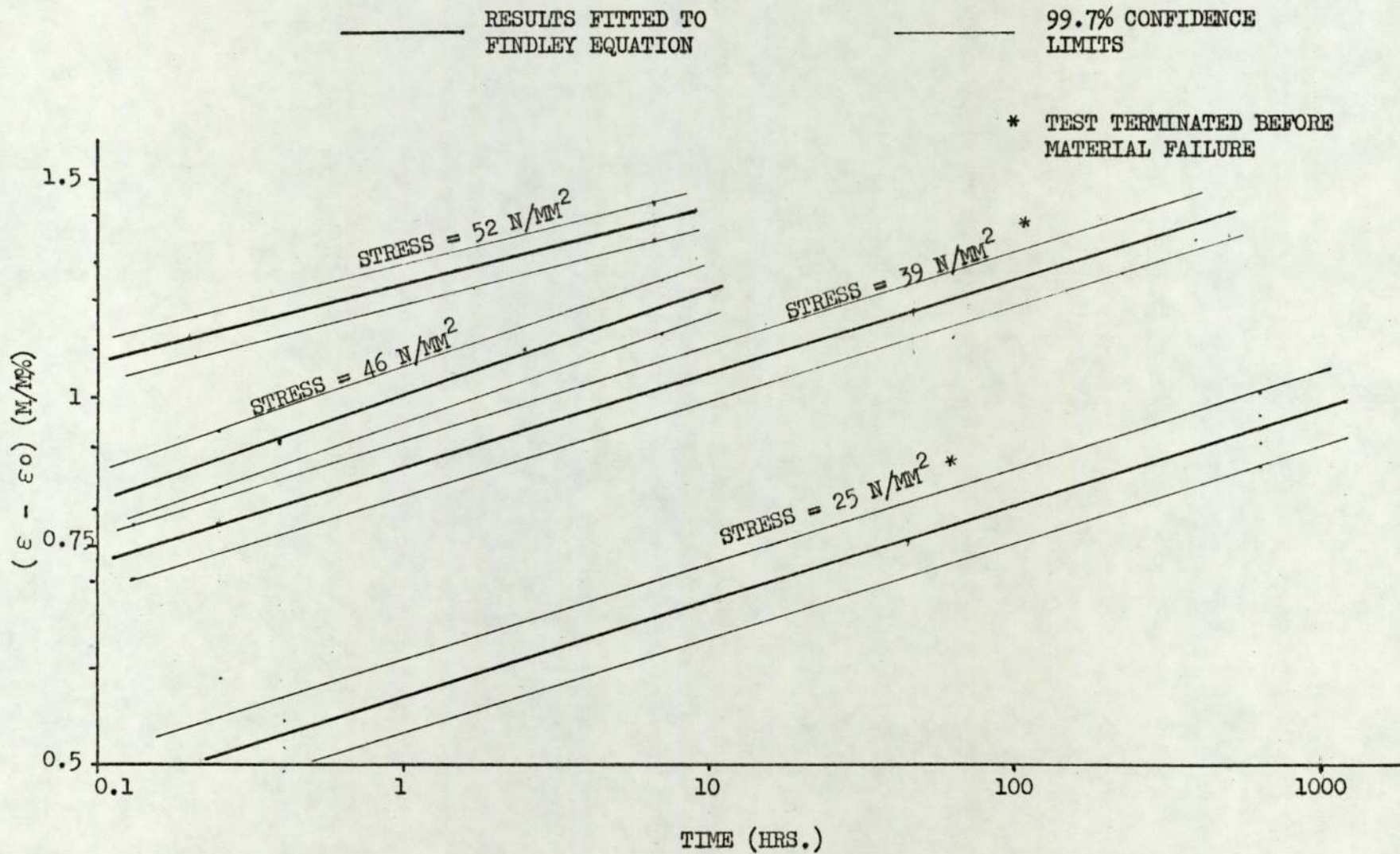


FIG. 3.25 CREEP RESULTS : CSM $V_f = 21.5\%$

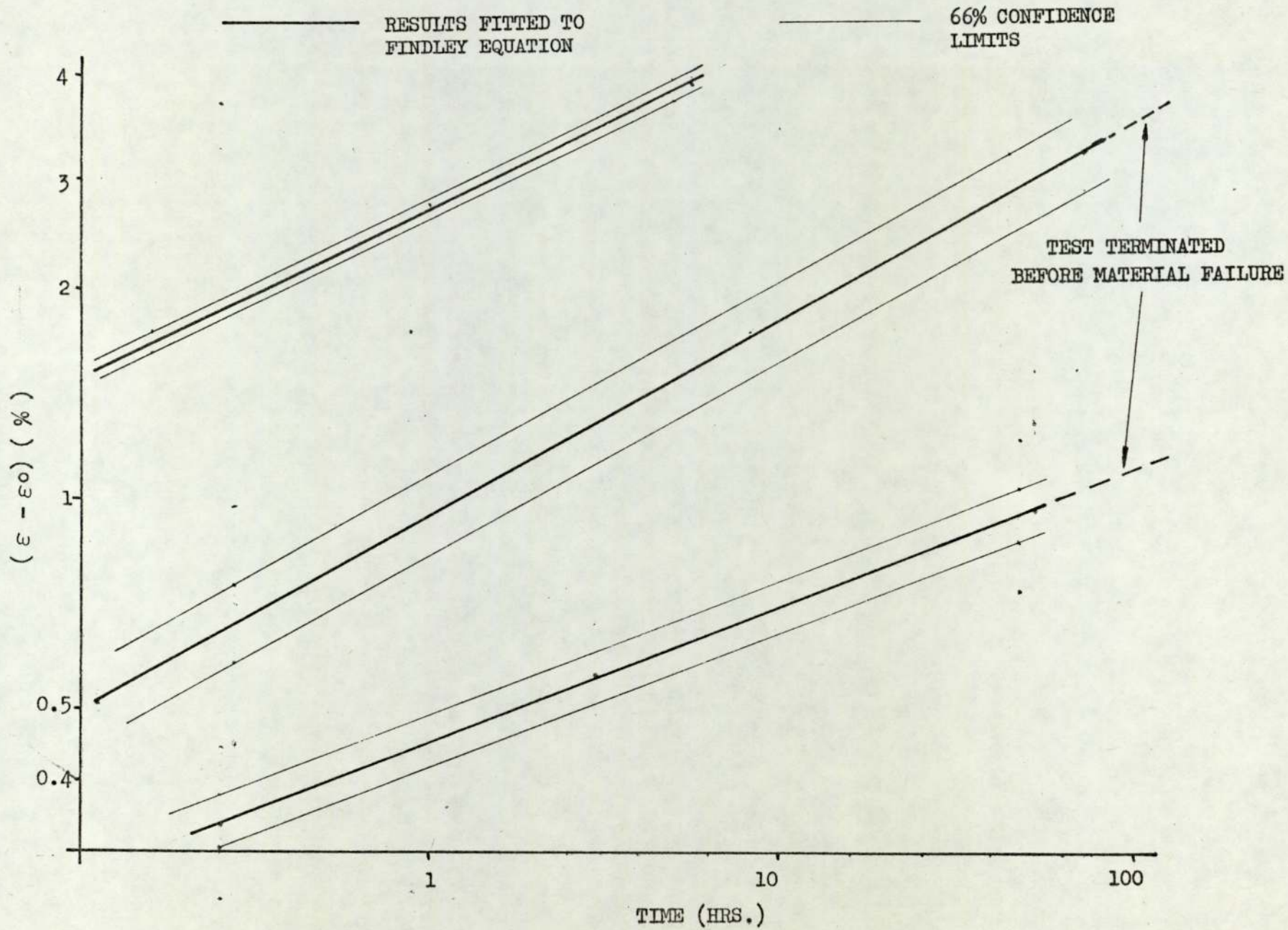


FIG. 3.26 CREEP RESULTS: + 45° BIDIRECTIONAL WOVEN ROVING

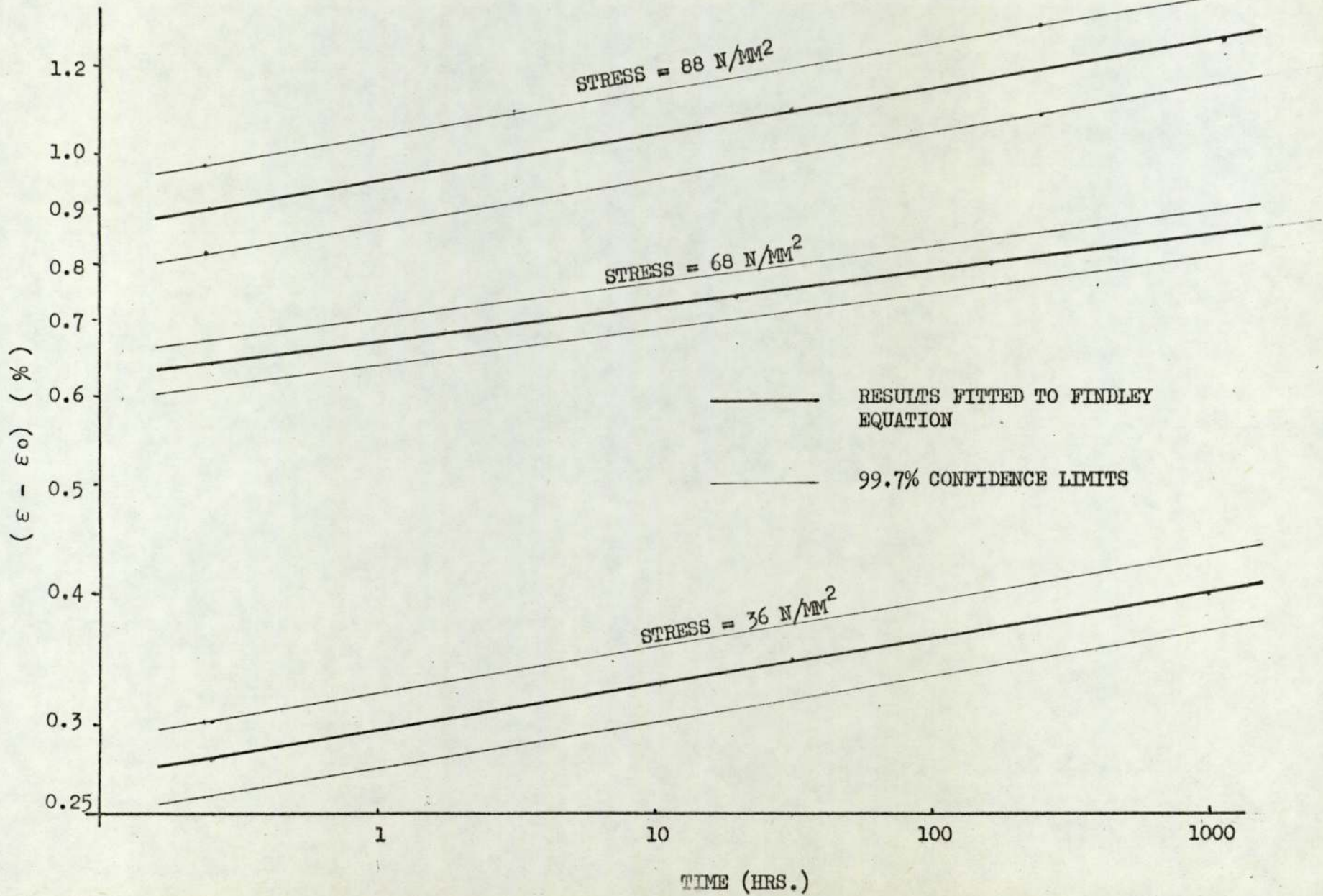


FIG. 3.27

CREEP RESULTS: BIDIRECTIONAL WOVEN

ROVING $\nu_g = 24\%$

———— RESULTS FITTED TO FINDLEY EQUATION
———— 99.7% CONFIDENCE LIMITS ON FIT

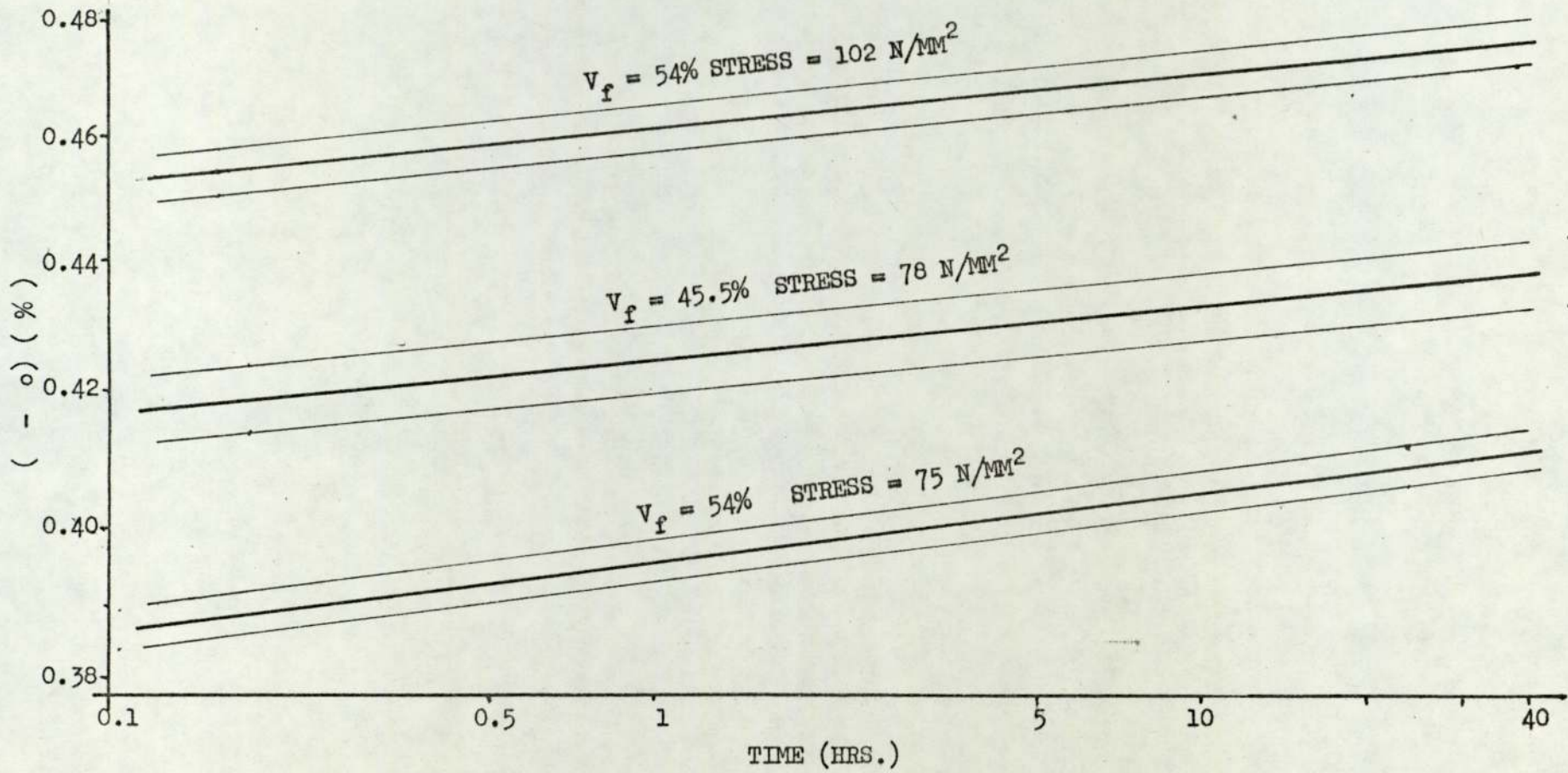
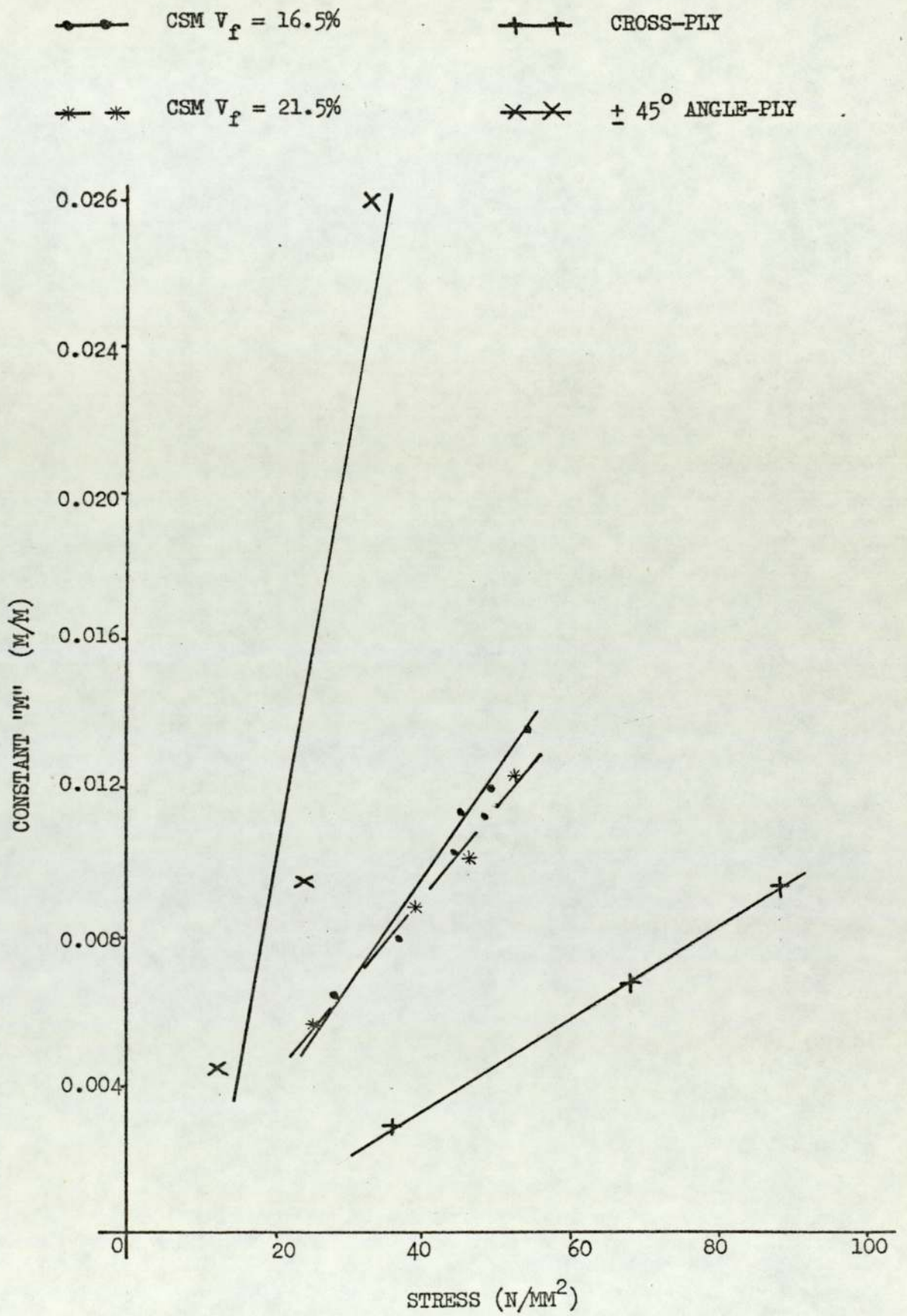


FIG. 3.28 CREEP RESULTS: UNIDIRECTIONAL MATERIAL.

FIG. 3.29 GRAPH OF CONSTANT "M" AGAINST STRESS



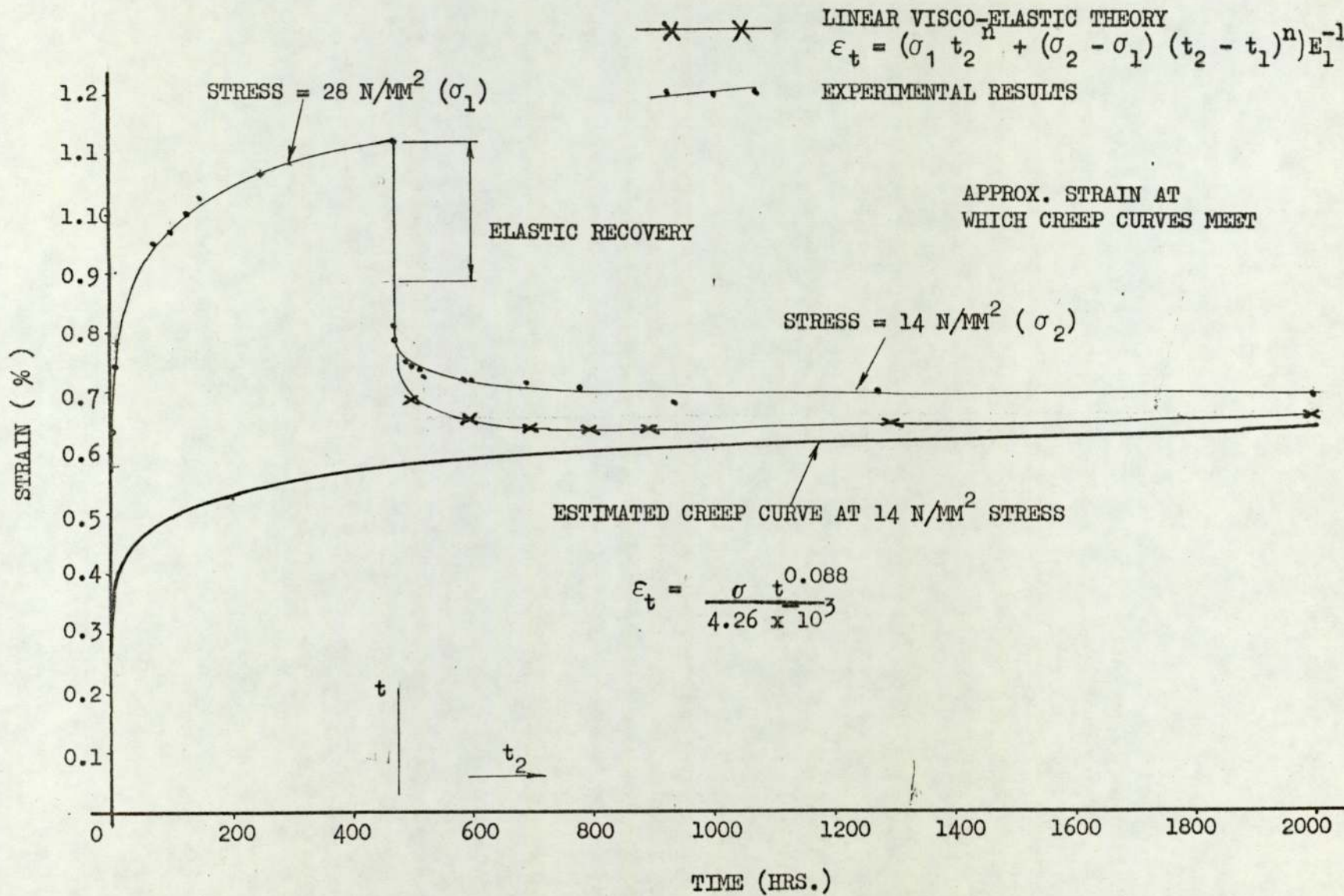


FIG. 3.30 CREEP RECOVERY

FIG. 3.31

CREEP SPECIMENS - CSM

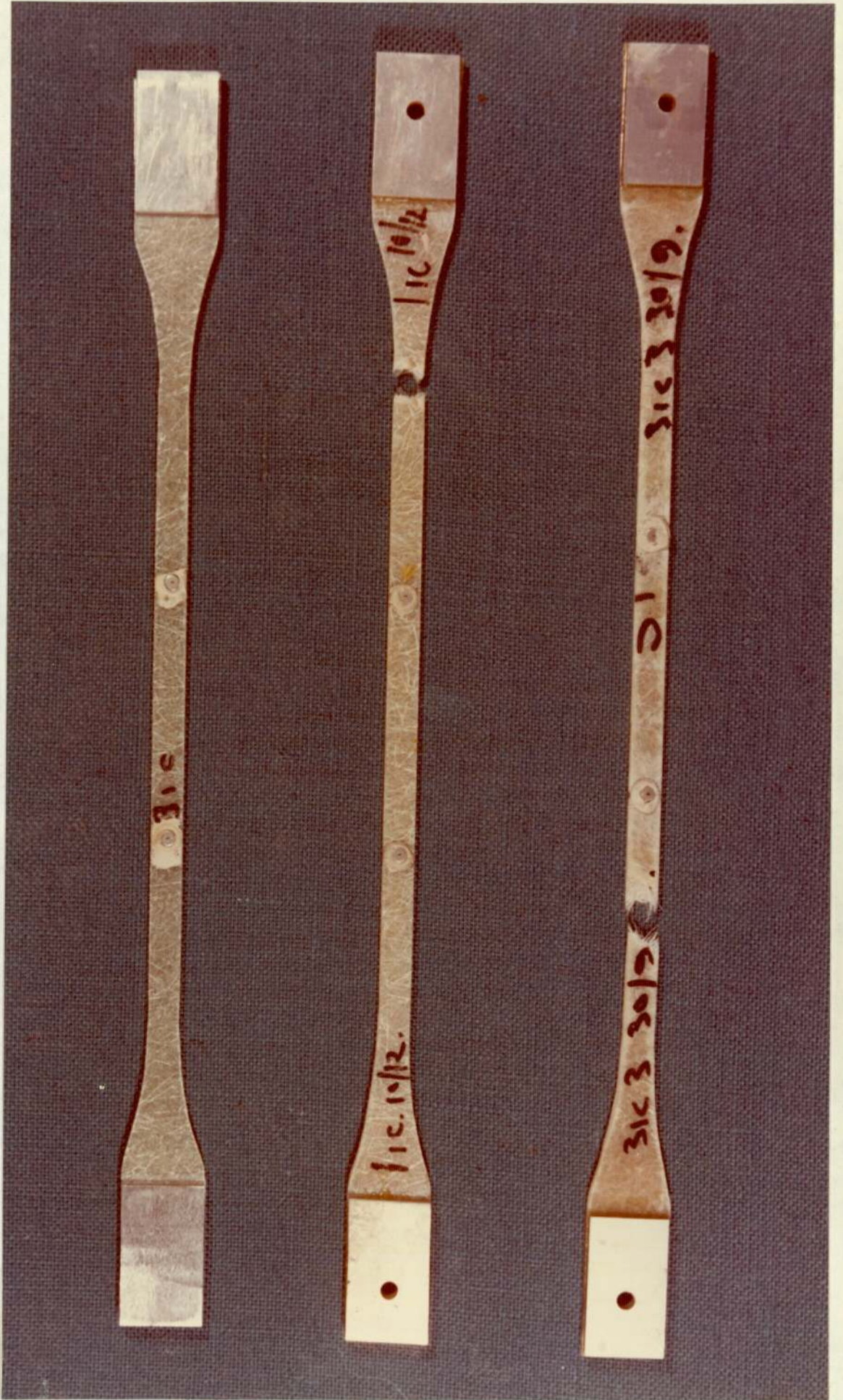


FIG. 3.32 CREEP SPECIMENS - BIDIRECTIONAL

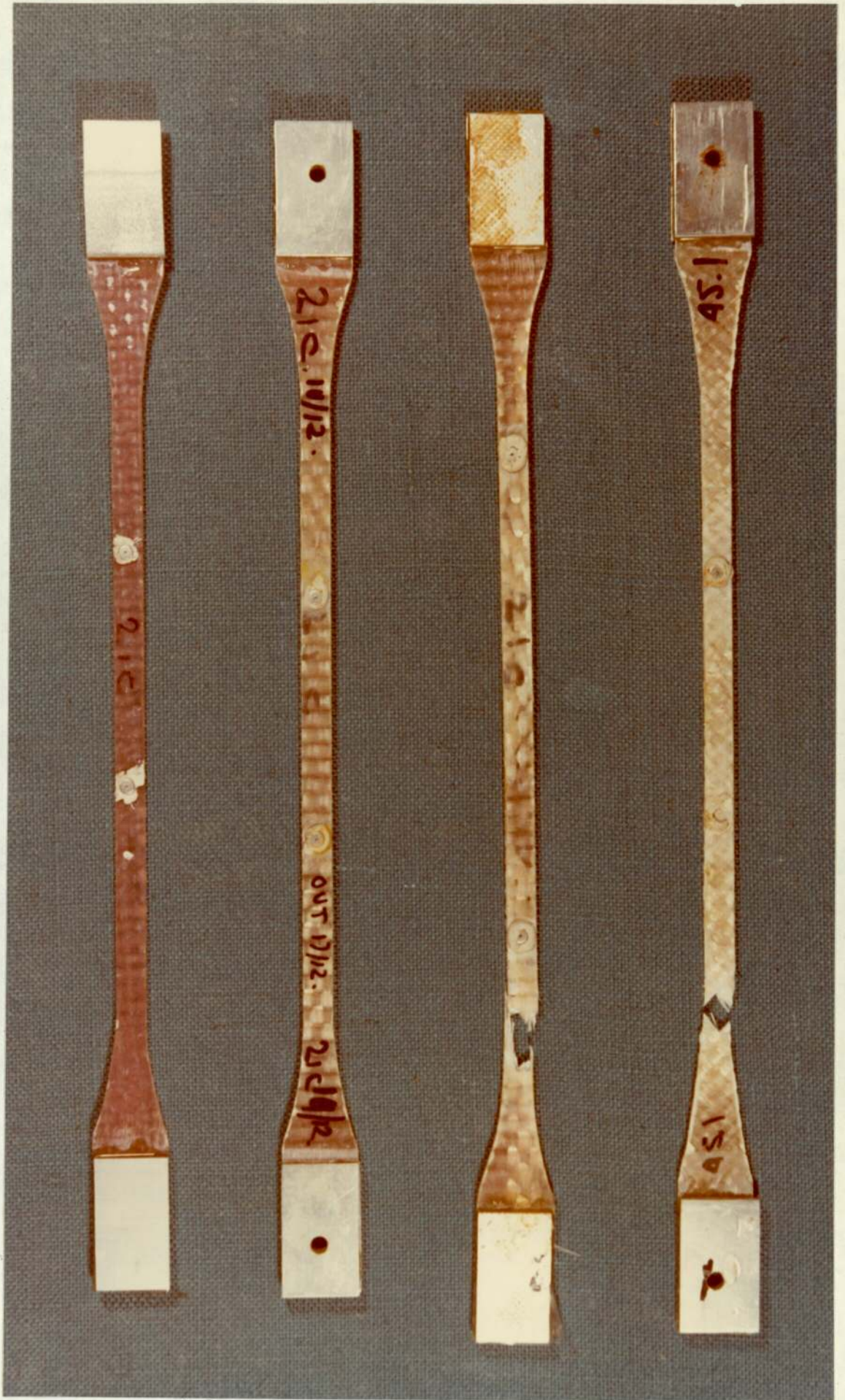


FIG. 3.33 CREEP SPECIMENS - UNIDIRECTIONAL



CHAPTER 4

STRUCTURAL ENGINEERING DESIGN WITH GRP

CHAPTER FOUR

Structural Engineering Design with GRP

4.1

Introduction

In previous chapters the structural properties of grp have been described. In the light of this the design process and the design of grp structures will be discussed. Information will be presented to assist in obtaining the most cost-effective solution.

In order to design well, the designer should thoroughly understand the materials with which he is working. This is imperative when composite materials such as grp are being used. In addition to the normal case, where the engineer just selects the material, when composites are used he must then go on and design the form of the material. Failure to do this will invariably lead to a product which is more costly than is necessary.

The result of material design will often be an anisotropic laminate. Consequently, the engineer will require a more general knowledge of elastic theory. However, stress analysis can often be simplified with judicious choice of the overall structural form. This need not lead to a loss in structural efficiency, since a design that simplified the stress analysis may also be an optimum design. For instance, the "Least Weight Design" of structures leads to a situation where all the stresses are either tensile or compressive [4.1]. A special case of this is where the structure conforms to the shape of its funicular polygon. Al-Khyatt [4.2] found that the optimum fibre orientation for a plate in pure shear to resist buckling was at 45° to the plate axes, which coincides with the direction of the tensile principal stress. In situations such as these, orientated and possibly unidirectional material can be used, and economy of materials obtained. The significance of this to the design process is that there is an important interaction between the overall structural design and material design.

Important considerations in the choice of overall design are: cost, durability and the aesthetic potential of the materials used. Structural designs where the "monochoque" principle is employed will fully utilise the potential of grp and offset its high cost. Hence designs in grp consisting of a superstructure and cladding as separate entities will not exploit the material to the full.

Material design is limited by the moulding techniques available, so that on occasions the ideal fibre orientation is not practicable. On the other hand, the mouldability of grp allows the designer to use efficient structural forms more readily than with other structural materials. The ability to use folded plates, singly and doubly curved shells, stressed skin space structures, sandwich structures, stiffened plates, and changes in thickness without greatly increasing production costs, assists relatively expensive and extensible grp to compete with other structural materials.

To summarise, the design process may be considered in four stages, viz.,

- a) Overall structural, or macroscopic design,
- b) Material, or microscopic design,
- c) Choice of moulding technique,
- d) Reappraisal and integration of a), b) and c)
for the optimum solution.

There are many different forms of glass fibres available commercially, such as chopped strand mat, rovings and woven rovings. The cost per unit weight of these different forms varies considerably; the roving being the cheapest, and combination products of chopped strands and woven rovings being the most expensive. The practicable fibre volume fraction also varies significantly from product to product (Fig. 4.10). Thus for a given structural use the best fibre orientation may not be the most cost effective.

To determine the relative cost effectiveness of the various laminates, the thickness (H) of a unit, 1 m^2 , is calculated for the range of fibre volume fractions.

$$H = (C_f D_f V_f + C_m D_m V_m)^{-1} \quad 4.1$$

where C_f = Cost of the fibre

D_f = Density of the fibre

C_m = Cost of the resin

D_m = Density of the resin

The structural properties are then calculated for the laminates from fibre and resin properties using the Tasi approach (with $C = 0$) and the laminate theory outlined in Chapter 3. The cost effectiveness is then given by :

$$\text{Cost effectiveness} = \frac{\text{Structural property value at } V_f}{\text{Structural property value at } V_f = 0}$$

Various basic structural properties have been studied for two ratios of fibre cost to resin cost ($CF = \frac{C_f}{C_m}$) i.e. 1 and 1.5, together with four different fibre orientations: unidirectional, cross-ply, $\pm 45^\circ$ angle-ply and quasi-isotropic where $\alpha = 0^\circ, \pm 45^\circ, 90^\circ$. E-glass and BIP 836 polyester resin properties were used. The computer program used for the calculation is designed to handle any fibre and resin properties and all 4-fibre orthotropic systems, and is shown in Appendix B together with an example of the results.

4.3.1 Axial Stiffness

The axial stiffness cost-effectiveness (\overline{EEAN}) is given by:

$$\overline{EEAN} = \frac{(H \times E_1)}{(H \times E_1)} \frac{V_f}{V_f} = 0 \quad 4.2$$

Fig. 4.1 & 2 show graphs of cost effectiveness against fibre volume fraction for the material designs considered.

Unidirectional material is by far the most cost-effective, as may be expected, and generally the order of superiority follows the order in which the laminates have the highest proportion of fibres in the $\alpha = 0^\circ$ direction. The advantage gained by using unidirectional material is so great that even when the cost factor (CF) is 1.5 this material is superior to other fibre orientations when the cost factor is 1, assuming the same resin is used. In general, the cost-effectiveness is improved by increasing the fibre volume fraction.

4.3.2 Flexural Stiffness

The flexural stiffness investigated here is that which is appropriate to a narrow beam, but for simplicity the geometry of the laminate will be determined on the basis outlined above.

The flexural stiffness cost-effectiveness (FLEXN) is given by :

$$\text{FLEXN} = \frac{(E_1 H^3/12)_{V_f}}{(E_1 H^3/12)_{V_f = 0}} \quad 4.3$$

Figs. 4.3 & 4 summarise this investigation. For a particular cost factor (CF) the order of superiority of fibre orientation is the same as for axial stiffness since the elastic constant E_1 appears in both equations. The effect of changing the volume fraction is not so straightforward.

In several of the laminate designs examined the graphs show that there is an optimum volume fraction within the practical ranges. This is true for unidirectional materials at both CF values and is true for angle-ply and quasi-isotropic materials when $CF = 1$. With this value of CF, angle-ply is found to be most cost-effective at high and low volume fractions, and least when the fibre volume fraction is approximately 0.4.

When the cost factor is 1.5 the majority of laminates reduce in cost effectiveness with increasing fibre volume fraction within the practical ranges. The rate of reduction varies however, so that

a random reinforcement, which is basically an inferior material design for this property, becomes more cost-effective at low volume fractions than other orientations at the higher end of their practical ranges.

4.3.3 Shear Stiffness

The shear stiffness studied in this section is the inplane shear stiffness, and the corresponding cost-effectiveness is given by :

$$EGN = \frac{(G_{12} \cdot H)_{V_f}}{(G_{12} \cdot H)_{V_f = 0}} \quad 4.4$$

Cost-effectiveness in this case (Fig. 4.5) increases with increasing fibre volume fraction. The order of merit for material designs follows the order in which the materials have the largest proportion of their fibres in the $\pm 45^\circ$ directions, the unidirectional and cross-ply materials being equivalent.

As the practical range of fibre volume fractions varies for different material forms it is possible for unidirectional material to become more cost-effective than random or quasi-isotropic materials. This is the case for both cost factor values considered. For example, the range of cost-effectiveness for unidirectional material is from 1 to 2.2 whereas for chopped strand mat it is about 1.5 to 1.75 when $CF = 1.5$.

4.3.4 Plate Buckling

The buckling load of rectangular orthotropic plates under axial compression is given by [4.14]:

$$P_{cr} = \frac{k \pi^2 \left((D_1 \times D_2)^{\frac{1}{2}} + D_3 \right)}{b}$$

where k = a factor depending upon the aspect ratio and boundary conditions of the plate

b = width of the plate

$$D_1 = \frac{H^3 E_1}{12(1 - \mu_{12} \mu_{21})}$$

$$D_2 = \frac{H^3 E_2}{12(1 - \mu_{12} \mu_{21})}$$

$$D_3 = 0.5 (\mu_{12} D_2 + \mu_{21} D_1) + \frac{H^3 G_{12}}{6}$$

The cost-effectiveness is, therefore, given by :

$$PCRN = \frac{\left((D_1 D_2)^{\frac{1}{2}} + D_3 \right)_{V_f}}{\left((D_1 D_2)^{\frac{1}{2}} + D_3 \right)_{V_f} = 0} \quad 4.5$$

Figs. 4.6 & 7 illustrate the results on this basis. The most cost-effective fibre orientation at any particular volume fraction is $\pm 45^\circ$. The next most effective is the quasi-isotropic material, followed by cross-plyed and then unidirectional materials. The optimum fibre orientation of $\pm 45^\circ$ is also reported by Rothwell [4.11] after considering structural properties only.

In this case the cost factor is found to be dominant, so that all the materials with a CF of 1 are shown to be superior than those with a CF of 1.5. Thus for a given resin cost, materials incorporating the cheaper fibres ($\frac{2}{3}$ of the cost of the expensive ones) will be more effective no matter what fibre orientation is adopted. Thus rovings at 58p/kg used unidirectionally are superior to angle-ply woven rovings at 87p/kg even though the angle-ply orientation is more effective. These prices were approximately correct in February 1975. Although prices will change with time the ratios may be expected to remain similar and so the conclusions will remain valid.

When $CF = 1$ there are optimum fibre volume fractions for angle-ply, quasi-isotropic and cross-ply materials at approximately $V_f = 0.3$. For $CF = 1.5$ within the practical range of volume fractions, materials become less cost-effective with increasing volumes of fibre. However, because of the difference in the ranges of practical volume fractions the range of cost-effectiveness for isotropic materials is similar to that for $\pm 45^\circ$ angle-ply.

4.3.5 Cylinder Buckling

The buckling load of orthotropic, homogeneous cylinder walls under the action of axial compression is given, for long cylinders, by [4.12] :

$$\text{CYCR} = 2 \pi H^2 (0.666 \left(A_{12} + (A_1 + A_2)^{\frac{1}{2}} \right) A_3)^{\frac{1}{2}}$$

$$\text{where } A_1 = \frac{E_1}{1 - \mu_{12} \mu_{21}}$$

$$A_2 = \frac{E_2}{1 - \mu_{12} \mu_{21}}$$

$$A_3 = G_{12}$$

$$A_{12} = \frac{E_1 \mu_{21}}{1 - \mu_{12} \mu_{21}}$$

The cost-effectiveness is given by :

$$\text{CYCRN} = \frac{(\text{CYCR})_{V_f}}{(\text{CYCR})_{V_f} = 0} = 0 \quad 4.6$$

Figs. 4.8 & 9 show the cost-effectiveness against fibre volume fraction based on the above equation. The material order of merit is the same as for plate buckling for a given volume fraction. Under certain circumstances there are optimum fibre volume fractions as has previously been found when the cost-effectiveness has been a function of thickness (H) to a power greater than unity. In this particular case when CF = 1.5 the angle-plyed and quasi-isotropic materials are optimum when the fibre volume fraction is approximately 0.25.

4.4

Process Economics

In section 4.2 it was stated that there was a large number of production processes available and choice of a process was an integral part of good design. In this section the economics of several production processes will be considered and compared. The

processes chosen for examination are thought to be relevant to long span structures, and were described briefly in Chapter 2.

To compare the processes it will be assumed that four types of product are to be manufactured; two simple and two relatively complicated (Figs. 4.11 & 12). One of each type will be small and the other large. The direct production costs of the products will be calculated at various production rates to broaden the comparison. The production costs will be divided into fixed costs per product and costs which depend upon the production rate. In calculating the costs, the following assumptions will be made :

- 1) Working hours - three 8 hour shifts per day, 5 days per week and 49 weeks per year.
- 2) Capital Amortisation - Capital goods will be amortised over a period of 5 years.
- 3) Labour costs - £4,000/an. per Foreman for 40 hours per week = £2.04/hr.; Semi-skilled men - £3,300/an. = £1.68/hr.; Unskilled labour £2,900/an. = £1.47/hr.
- 4) Costs of less than £0.01 will be rounded off to £0.01.

The hand lay-up process is treated as the basic process and the others as modifications to this.

4.4.1 The Hand Lay-up Process

Labour Costs :

Labour times and activities may be divided as follows for each moulding :

1) Mould preparation time (WT): it is assumed that moulds require treating with release agent after every sixth moulding and that this takes 2 man minutes/unit surface area of the mould.

$$\therefore WT = \frac{SA \cdot 2}{60 \cdot 6}$$

$$= \frac{SA}{180} \quad (\text{m hrs.}) \quad 4.7$$

where SA = Product surface area.

(All times are measured in man hours.)

2) Material preparation time (MPT): the time for material preparation per product is taken to be a linear function of the product edge length.

$$MPT = (PEL \times 0.0028 + 0.017) \quad 4.8$$

where PEL = Product edge length.

3) Lay-up time : the lay-up time depends upon the weight of the product and the lay-up rate. The lay-up rate (LUR) is a function of the surface area of the mould and its complexity. The complexity is measured as the quotient of the plan area (PA) and the surface area (SA) of the mould.

$$LUR = \left(11 - \frac{6}{(1 + SA + SA^2/2)} \right) \frac{PA}{SA} \quad 4.9$$

Thus a maximum lay-up rate of 11 kg/hr. is assumed. The lay-up time is given by :

$$LUT = \frac{W}{LUR} \quad 4.10$$

where W = Weight of product.

4) Stripping Mould Time : the time required to remove the finished product from its mould is based upon the edge length of the product and its complexity.

$$\text{Stripping mould time (SMT)} = \frac{PEL}{240} \times \frac{SA}{PA} \quad 4.11$$

5) Product Trimming Time : the trimming time is assumed to be a function of the edge length and the thickness (TK) of the material to be cut.

$$\text{Trimming time (TT)} = \frac{PEL \times 2 \times TK}{60 \times 0.003} \quad 4.12$$

All the above activities may be carried out by unskilled labour with the exception of the laminating procedure which requires semi-skilled labour. However, the semi-skilled labour time is much greater than the unskilled labour time so that only semi-skilled labour will be used.

$$\therefore \text{Total man hours} = WT + SMT + TT + MPT + LUT \quad 4.13$$

Labour costs are calculated assuming that labour works at 85% efficiency. Provision for a foreman is made by allowing $12\frac{1}{2}\%$ of a foreman's salary to be added to each worker's wage.

From the above, the labour costs for each product can be calculated for various production levels. At least one of the production levels chosen will be one at which labour is used to the maximum efficiency so that the labour cost is at a minimum.

Mould Costs:

To calculate the cost of mould the following will be assumed:

1) The production moulds are made from mould masters which are made from a master mould which in turn is made from a pattern.

2) The production moulds are made of glass-reinforced epoxy resin.

3) The life of production moulds and mould masters is 500 products.

4) The cost of patterns and mould masters is written off over 5 years.

5) Cost of patterns and master moulds

$$= (100 \cdot SA + 100) \frac{SA}{PA}^{0.14} \quad 4.14$$

$$= CPAMM (\pounds)$$

Cost of one mould master = 0.65 CPAMM

Cost of one production mould = 0.5 CPAMM

Mould Usage :

The number of production moulds required depends upon the production rate and the time that the mould is in use for each product (MT). A mould utilisation factor of 0.9 is allowed.

$$MT = (WT + LUT + CT + SMT) \frac{1}{0.9} \quad 4.15$$

$$\text{Cure Time (CT)} = (1.5 + 0.6 \cdot (\text{weight of resin per unit area kg/m}^2))$$

The number of moulds required (NOMR) is therefore:

$$NOMR = \frac{MT \cdot PRPD}{24} \quad 4.16$$

One mould master will be allowed for every 5 production moulds. Hence the number of mould masters required is:

$$NOMM = \frac{NOMR}{5} \quad 4.17$$

Mould costs per product:

$$\text{Cost per product for one mould master} = \frac{0.65 \times \text{CPAMM}}{500}$$

Total cost per product for mould masters =

$$\frac{NOMM \times 0.65 \cdot \text{CPAMM}}{PRPD \cdot 1225}$$

From equation 4.16 and 4.17 this can be simplified to:

$$\text{Cost of mould masters/product} = \dots \quad 4.18$$

$$MT \cdot \text{CPAMM} \cdot 0.44 \cdot 10^{-5}$$

$$\text{Production mould cost per product} = \frac{0.5 \text{ CPAMM}}{500} \quad 4.19$$

Cost of pattern and master mould per product

$$= \frac{\text{CPAMM}}{\text{PRPD } 1225} \quad 4.20$$

Thus the cost per product of the production moulds and the mould masters is independent of the production rate.

Factory Costs :

Factory costs are based upon the plan area of the product, and provision for floor space for material preparation, product storage and administration with a factory rent per unit area per annum of £7.3 $\boxed{4.3}$.

$$\text{Factory area per mould (APM)} = (\text{PA}^{\frac{1}{2}} \times 1.73)^2 \cdot 1.3 \quad 4.21$$

Factory costs per product (FC) are therefore given by :

$$\text{FC} = \frac{\text{APM} \cdot \text{NOMR} \cdot 7.3}{\text{PRPD} \cdot 5.49}$$

With the use of equation 4.16 this simplifies to:

$$\text{FC} = \text{APM} \cdot \text{MT} \cdot 0.124 \times 10^{-2} \quad 4.22$$

Energy Costs :

Since no large machinery is used in this process the energy used will be for environmental purposes. Therefore, it will be assumed that the power consumed will be proportional to the floor area and thus the factory costs.

$$\text{Energy cost per product} = \frac{1}{3} \text{FC} \quad 4.23$$

Product Handling Equipment :

This equipment is only required for large products A and B and is used for lifting them from their moulds.

Capital cost of equipment = £1,000

$$\text{Cost per product} = \frac{1000}{\text{PRPD } 1225} \quad 4.24$$

The results of the hand lay-up process cost analysis are shown in tabular form in Figs. 4.13 & 14 and in graphical form in Figs. 4.25 - 28.

4.4.2 The Basic Spray-up Process

Labour Costs :

Labour costs in this case may be divided into those appropriate to unskilled labour and those which must be carried out by semi-skilled labour as follows:

Unskilled Activities:

- 1) Trimming - time as hand lay-up.
- 2) Mould preparation - time as hand lay-up.
- 3) Mould stripping - time as hand lay-up.
- 4) Material Preparation.
- 5) Material Consolidation.

Semi-skilled Activities:

1) Spray-Up.

Labour times unique to the activities of the spray-up process are as follows:

a) Material Preparation : the time involved in this activity per product is, compared to the hand lay-up process, very small since the spray-up machine can draw resin from bulk supplies and the glass fibre does not require tailoring. This activity is assumed to take 0.25 minutes per 10kg of laminate.

b) Spray-Up : the spray-up rate is normally between 5 - 10 lb of laminate per minute depending upon the size and complexity of the mould.

The spray-up time (SUT) is given by:

$$SUT = \frac{W}{0.454 \cdot 8.60} \frac{SA}{PA}^{\frac{1}{2}} + 0.2 \quad 4.26$$

c) Material Consolidation Time : this time is calculated as:

$$RDT = 2 \cdot SUT \quad 4.27$$

Hence, total unskilled labour time (ULT) is given by :

$$ULT = (TT + WT + SMT + MPT + RDT) \frac{1}{0.85} \quad 4.28$$

Total semi-skilled labour time (SST) is:

$$SST = \frac{SUT}{0.85} \quad 4.29$$

Labour Costs :

Labour costs are calculated with a minimum labour force of 1 foreman and 1 semi-skilled operator. In this case all the operations are carried out by the semi-skilled workman. The labour costs are also calculated with both semi-skilled and unskilled operators fully utilised.

Spray-Up Machine Costs :

It is assumed that a machine utilisation factor of 0.75 applies. As indicated earlier capital equipment is written off over 5 years.

Cost of machine = £2,500

Machine cost per product = $\frac{2,500}{\text{PRPD } 1225}$ 4.30

where PRPD = number of products produced per day per
machine

$\text{PRPD}_{\text{max}} = \frac{0.75}{\text{SUT}}$ 4.30

Mould Costs :

Mould costs are calculated on the same basis as for the hand lay-up process.

Factory Costs :

Again, these are based on the principles outlined under the hand lay-up process.

Energy Costs :

$$\text{Cost per product} = \text{PA} \times 0.0096 \quad 4.31$$

The above formula is based upon information taken from a Pilkington internal report [4.3].

Product Handling Equipment Costs :

These are calculated in the same way as for the hand lay-up process.

Costs at various production levels considered are tabulated in Figs. 4.15 & 16 and are shown graphically in Figs. 4.25 - 28.

4.4.3 The Robot Spray-up Process

This process is essentially the same as the basic spray-up process except that a machine performs the semi-skilled operator's function of spraying-up the laminate. Consequently, the only difference in the cost calculations is that the semi-skilled labour cost is replaced by an increased machine cost.

The capital cost of the robot spray machine is taken to be five times that of the basic spray-up machine at £12,500.

Tables in Figs. 17 & 18 show production costs which are also illustrated graphically in Figs. 4.25 - 28.

4.4.4 The Continuous Spray-up Process

The continuous spray-up process is similar to the continuous laminating process described in Chapter 2, except that discrete moulds are used rather than a continuous mould. Unlike the previous spray-up processes where the spray gun is passed over the mould, in this process the mould is passed under the gun. The gun is held by a machine which is capable of making reciprocating movements in a transverse direction relative to the mould. Thus as in the robot spray-up process only unskilled labour is required. Although the robot is more versatile in movement and in directing the spray the continuous spray-up machine is capable of depositing 4 times the quantity of material per unit time.

Labour and energy costs are calculated by the same procedure as that for the robot spray-up process. Product handling equipment, factory costs and mould costs are calculated on the same basis as for the hand lay-up process. The machine cost calculations, based upon an acquisition cost of £12,000, follow the same procedure used for the costing of the basic spray-up machine.

A cost summary is tabulated in Figs. 4.19 & 20 and illustrated graphically in Figs. 4.25 - 28.

4.4.5 The Resin Injection Process

Labour Costs :

Mould preparation time : this is taken as twice that required for the hand lay-up process since it is a closed mould process.

Material preparation time : as hand lay-up.

Resin injection time (IT) : this is based upon a resin injection rate of 8 lb/min.

$$IT = \frac{W \times 0.75}{8 \times 60} \quad 4.32$$

Stripping mould time : as hand lay-up.

Trimming time : this is taken as half that required for hand lay-up since the edge of the product is pinched between the two halves of the mould. The glass fibre in this area is starved of resin, making cutting easier.

Mould costs :

Mould costs are based upon those calculated for hand lay-up moulds, but modified as follows: for products C and D, production mould costs are assumed to be 2.5 times those for hand lay-up. For products A and B, costs are taken as 3 x hand lay-up costs. The larger factor employed for products A and B is to allow for mould-opening devices. These devices are necessary due to the weight of the moulds. In calculating the cost per product of the mould master,

equation 4.18 is modified by replacing the mould committed time (MT) by a cycle time (CYT) as follows:

$$\text{Mould master cost per product} = \text{CYT} \cdot 0.49 \cdot 10^{-15} \times \text{CPAMM} \quad 4.33$$

$$\text{where CYT} = 0.019 \times W + 0.066 \quad 4.34$$

Machine costs : machine costs are based on an acquisition cost of £3,000 and a utilisation factor of 90%.

Product handling equipment : as hand lay-up.

Energy costs : as spray-up.

Factory costs : again these costs are based upon the hand lay-up process calculation but the mould committed time (MT) is replaced by cycle time; CYT.

4.4.6 The Hot Press Process

Labour costs : for the analysis of this process it is assumed that there is a minimum labour force of three: a press operator, a material preparation labourer and a product deflashing labourer. Hourly labour costs are therefore:

$$3 \times \text{£}1.47 = \text{£}4.41/\text{hr.}$$

$$\text{Labour cost per product} = \frac{4.41 \times 24}{\text{PRPD}} \quad 4.35$$

Press costs : the costs adopted for the presses are based upon information received from FRP. Applications Dept., Fibreglass Ltd.

For products A & B Press Cost = £50,000

For products C & D Press Cost = £5,300

Press costs per unit produced are calculated on the same principles used for the basic spray-up process with a machine utilisation factor of 0.85. The maximum production level per day is given by:

$$\text{PRPD}_{\text{max}} = \frac{0.80 \cdot 24 \cdot 60}{\text{CYT}} \quad 4.36$$

where 0.80 = a factor allowing for labour and machine inefficiency.

CYT = Cycle time (mins.)

$$\text{CYT} = \text{TK} \times 0.42 \times 10^3 + \text{PA} \cdot 0.23 + 1.5$$

TK = thickness of product (M)

Mould costs : these costs are again based upon information recieved from Fibreglass Ltd.

$$\text{Cost of Mould (TC)} = 1500 \cdot \frac{\text{SA}}{\text{PA}} \text{SA}^{0.14} + 2500 \quad 4.37$$

The life of hot press moulds are taken as 10,000 products therefore:

$$\text{Cost of moulds per product} = \frac{\text{TC}}{10,000} \quad 4.38$$

Factory costs : the same cost per unit floor area is used as for hand lay-up i.e. £7.3/m²/an. The floor area required is based upon the plan area of the press being equal to that of the product plus an additional area round the press 3M wide; a further

factor of 1.3 is allowed for storage etc. Thus factory costs are given by:

$$FC = \frac{7.3 \text{ APM}}{\text{PRPD } 5 \times 49} \quad 4.39$$

Energy costs : these are assumed to be 3 x hand lay-up costs.

Hence :

$$\text{Energy costs} = FC \quad 4.40$$

Product handling equipment : as hand lay-up.

Calculations are summarised in Figs. 4.23 - 28.

4.4.7 Discussion of Process Analysis

The tables shown in Figs. 4.13 - 24 reveal that in general, labour is still the major direct production cost even when machinery is used, although in the resin injection and hot press processes the production mould is also a major cost area.

In interpreting the graphs, Figs. 4.25 - 28 the important aspects are the cost at which the graphs level out and at what production rate this happens. The hot press process is shown to be most economical for product types A, B and D at high production rates. Graphs for the hand lay-up process level out at the lowest production rates, but usually at a much higher cost level. In the majority of cases there is little to choose between resin injection and basic spray-up. However, resin injection costs reduce to a more economical

level when the product is complicated, and vice versa when the product is plain. Little difference is shown between robot and continuous spray processes but robot spray is more economical than the basic spray-up process at high production levels. The choice between the various spray-up processes and resin injection will be based upon factors other than production costs such as: the type of reinforcement required, whether two smooth surfaces are required, and whether changes in material thickness are required.

When direct production costs are compared to material costs, based on a laminate cost of 65p/kg, at medium to high production levels, products A and B show material costs approximately ten times greater than those for production. Hence, at these production rates if some material can be saved or cheaper material used, for marginal increases in production costs, significant savings could be made on large products.

The effect of changing the capital amortisation period to two years would have little effect on the relative merits of the various processes considered. This is the case since the capital repayment costs per product are normally of the order of 10% of the total direct production costs. If the number of shifts per day was reduced but the production level kept constant the main effect would be to reduce the competitiveness of the capital-intensive processes, since the production rate per machine per unit time would be reduced and the initial capital outlay increased.

In simple stress fields such as pure tension, compression or pure shear it can be seen from the sections on material cost-effectiveness (4.3) and theoretical material properties (3.2 & 3.3) that the strongest, stiffest and cheapest laminates are obtained when the fibres lie in the directions of the principal stresses. When the secondary principal stress approaches zero, unidirectional material may be used. In more complicated stress fields, for example around bolt holes, the situation is not as clear.

Since the equations for Mohr's stress circle are independent of material properties [4.4] they apply equally to anisotropic and isotropic materials. Thus under a given set of loads the principal planes are always in the same direction. If it is accepted that the fibres are the main strength and stiffness giving constituent and that they are best used in pure tension or compression the fibres should follow the directions of the principal stresses.

In many circumstances the principal planes will change direction frequently and in a complicated manner, and it will not be practical for the fibres to follow. However, in such circumstances compromises between the ideal and the practical may be beneficial. For example, the fibre orientation shown in Fig. 4.29 would be expected to give a higher tensile strength to the component when loaded via a bolt, than a pure unidirectional laminate.

The design of joints in grp requires more care than is normally necessary in steel, because grp is brittle and joints usually cause stress concentrations. Brittle materials cannot stress-relieve in areas of stress concentration and thus these high stresses must be borne by the material elastically. This disadvantage is compounded by the fact that stress concentrations are often larger in anisotropic materials. The use of additional material in areas of high stress is one solution to the problem, but this is likely to be expensive, due to the high cost of the material, and also, in extreme cases, ugly.

There are three basic types of jointing system which are applicable to grp and will be discussed below:

- a) Adhesive
- b) Mechanical
- c) Combination of a) and b)

It should be noted that when thermosetting resins, such as polyester, are used there is no jointing process equivalent to welding.

4.6.1 Adhesive Joints

Good joint design in grp will minimise the stress concentrations associated with the joint. Adhesive joints provide the best

opportunity for doing this. In general the stress flow lines should be interrupted as little as possible and joints should be based on shear, tensile or compressive stresses; peeling stress situations should be avoided (Fig. 4.30).

Joints between adherends fall into three categories: butts, laps and scarfs (Fig. 4.31). Simple configurations of each of these have been treated theoretically [4.5]. However, only in the case of lap joints in tension is it possible to calculate analytically the stress concentration, and then only when the adherends are isotropic.

For a simple tensile joint the scarf type is preferable with a stress concentration factor of 1.45 or less having been determined empirically. The scarf joint is also recommended for compressive joints. Fig. 4.31 shows a variation of the pure scarf joint known as a landed scarf joint. Landed scarf joints are useful for taking compressive loads, controlling the thickness of the adhesive and location of the adherends during assembly. However, they need to be used carefully if high stress concentrations are to be avoided.

By increasing the area of the scarf joint it is possible to obtain a joint of greater strength than the adherends and so failure may be expected to occur in the adherends rather than in the adhesive. In many cases the joint strength will be limited by the interlamina shear strength of the adherend.

Butt joints (Fig. 4.31) are special cases of scarf joints in which the scarf angle is 90° . The joint area in this case is limited to the cross-sectional area of the adherends and is therefore

not normally suitable for tensile use. However, like scarf joints, butt joints are relatively free of stress concentrations and under compressive conditions the full strength of the adherend may be developed.

Single flat lap joints in tension experience considerable stress concentrations due to shear and bending forces in the adherends. Goland and Reissner [4.6] have developed a theory for predicting the shear and normal stresses throughout the joint. They found that the maximum stresses occurred at the ends of the adhesive and that the ratio of the maximum stress to the mean stress increased with increasing lap length. Consequently, it is more effective to increase the width of the joint rather than the length of the lap. Stress concentrations can be reduced by bevelling the ends of the adherends (Fig. 4.31).

Double flat lap joints, fig. 4.31, are stronger in tension and compression than single lap joints since bending and hence stress concentrations are reduced, due to the symmetry of the joint.

Adhesive joints suffer from three main disadvantages. Firstly, the adherends often have to be held in position for considerable periods of time whilst the adhesive cures. In many civil engineering structures this could prolong erection time and lead to additional expense. Strong adhesives, usually being polymers, are subject to creep and stress rupture. As a result, structures which are loaded for long periods may not be best served by adhesive joints. Lastly, the quality of these joints is difficult to guarantee under site conditions because of the difficulty in maintaining cleanliness and the difficulty in checking whether a finished joint is upto the required standard.

Some of these problems can be partly overcome: heat may be applied to the adhesive but cure time may still be up to an hour or more; film adhesives ensure that the adhesive thickness is uniform and reduces the number of voids but the quality of the adherends' faces still remains a problem.

4.6.2 Mechanical Joints

Mechanical joints, in this case, may be divided into two sections: those joints which rely upon the shear strength of bolts or rivets; and those which depend on friction to transmit forces. In the second category it is usual to use high tensile bolts which compress the joining components together. High shear forces are then required to overcome the friction between the components. This type of joint is not considered suitable for use with grp because this material will creep under the bolt force and thereby relieve the tension in the bolt and weaken the joint. Also, crushing of the grp under the bolt may cause premature cracking and lead to failure.

Mechanical shear joints inevitably cause considerable stress concentrations in the region of the bolt or rivet. Lap and flange joints are the most common types, a few of which are shown in Fig. 4.32. As with adhesive joints, lower stresses in double lap joints lead to higher strength than is the case with single lap joints.

Bolted shear joints have the advantages that they are convenient to assemble and that they are not permanent, so that components may be replaced without difficulty.

In contrast to the situation with joints in steel, only a limited amount of experience has been documented on bolted joints in grp. Youngs [4.7] found that in order to prevent joint failure to the side or edge of a laminate the following rules should be applied: the distance from the centre of the bolt hole to the edge should be at least 4.5 times the hole diameter (D), and the distance from the side should be 3.0 D for woven fabrics. For CSM the side distance should be increased to a minimum of 3.5 D. It was found that with the failure to the sides and edge of the laminates suppressed, failure occurred by crushing of the material under the bearing load. The bearing failure load was found to be an undefined function of the laminate's compressive strength.

Several other "rules of thumb" are also available from the works of Youngs, Weiss and Strauss [4.7 - 9]. Several small diameter bolts are preferable to a smaller number of larger - diameter bolts. The ratio of the diameter of the bolt (d) to the thickness of the section (t) is significant and a d/t ratio of 1 gave higher strengths than a ratio of 1.5. Bolt holes may be punched or drilled and should have a 0.4 mm clearance on the diameter, they should also be well aligned to avoid unnecessarily high stresses. Excessive torque applied to the bolts should be avoided since this can lead to crushing of the material under the nut and bolt head.

4.6.3 Combination Joints

Combination joints have been designed in an attempt to avoid some of the disadvantages and combine some of the advantages of bolted

and adhesive joints. In one type of combination joint a ductile metal is used in combination with grp. The metal is moulded in situ during laminating and is used for bolting through. Fig. 4.33 shows some examples of this type. This figure also shows an adhesive lap joint with bolts near the ends of the laps. It is suggested [4.10] that this combination may be advantageous under fatigue loading. In addition the bolts would provide positive location for the joint and support during cure of the adhesive.

4.7

Safety Factors

Makowski [4.13] suggested the following safety factors :

Static loads of short duration	1.5 - 2
Static loads of prolonged duration	3 - 4
Cyclic loads	4
Fatigue loading	6
Impact loads	10

These safety factors are based on stress considerations alone, and are to be employed to obtain allowable working stresses. Further factors have to be used if there is any ignorance of the level of the applied stress. An alternative approach is to design on the basis of allowable strain. In a proposed B.S.I. specification for "Vessels and Tanks in Grp" the allowable strain (ϵ_w) is given by the smaller of

$$\epsilon_w = 0.05 \quad \epsilon_r$$

$$\epsilon_w = 0.2\%$$

where ϵ_r is the percentage elongation to failure of the resin. This approach is convenient when designing against creep.

Neither of the approaches described above allow for the time-dependent nature of the properties of grp in any precise manner. This can lead to over-conservative design or at the other extreme, an inadequate design. . Further, when designing on the basis of allowable strain, the fact that some materials (Boller - woven roving [3.26]) fail at larger strains with increasing time but at reduced stress, and other materials at reduced stress and strain, makes this approach more unsatisfactory.

For efficient design in grp it is necessary to know both the creep and stress rupture properties of the laminate used. As these properties depend upon the environment this must also be known. A "design life" must also be chosen for grp structures. With this information available, economy in the use of grp may be achieved and its full potential for efficient structural design realised by the choice of realistic safety factors.

FIG. 4.1 MATERIAL COST EFFECTIVENESS

- AXIAL STIFFNESS

—●— UDR $\alpha = 0^\circ$
—+— BIR $\alpha = 0^\circ, 90^\circ$

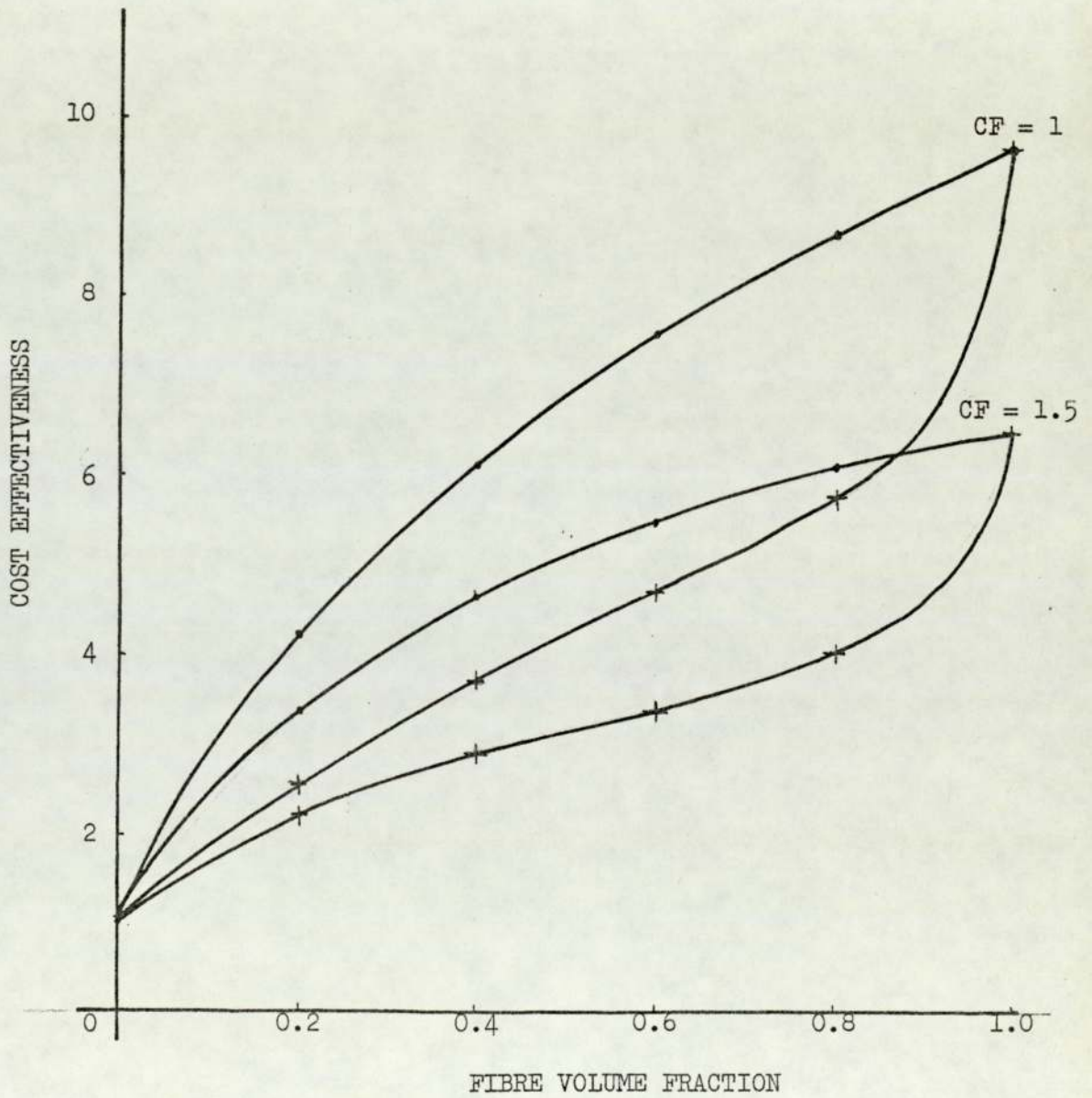


FIG. 4.2 MATERIAL COST EFFECTIVENESS

- AXIAL STIFFNESS

— * — * — * ANGLE-PLY $\alpha = \pm 45^\circ, 90^\circ, 0^\circ$

— x — x — x ANGLE-PLY $\alpha = \pm 45^\circ$

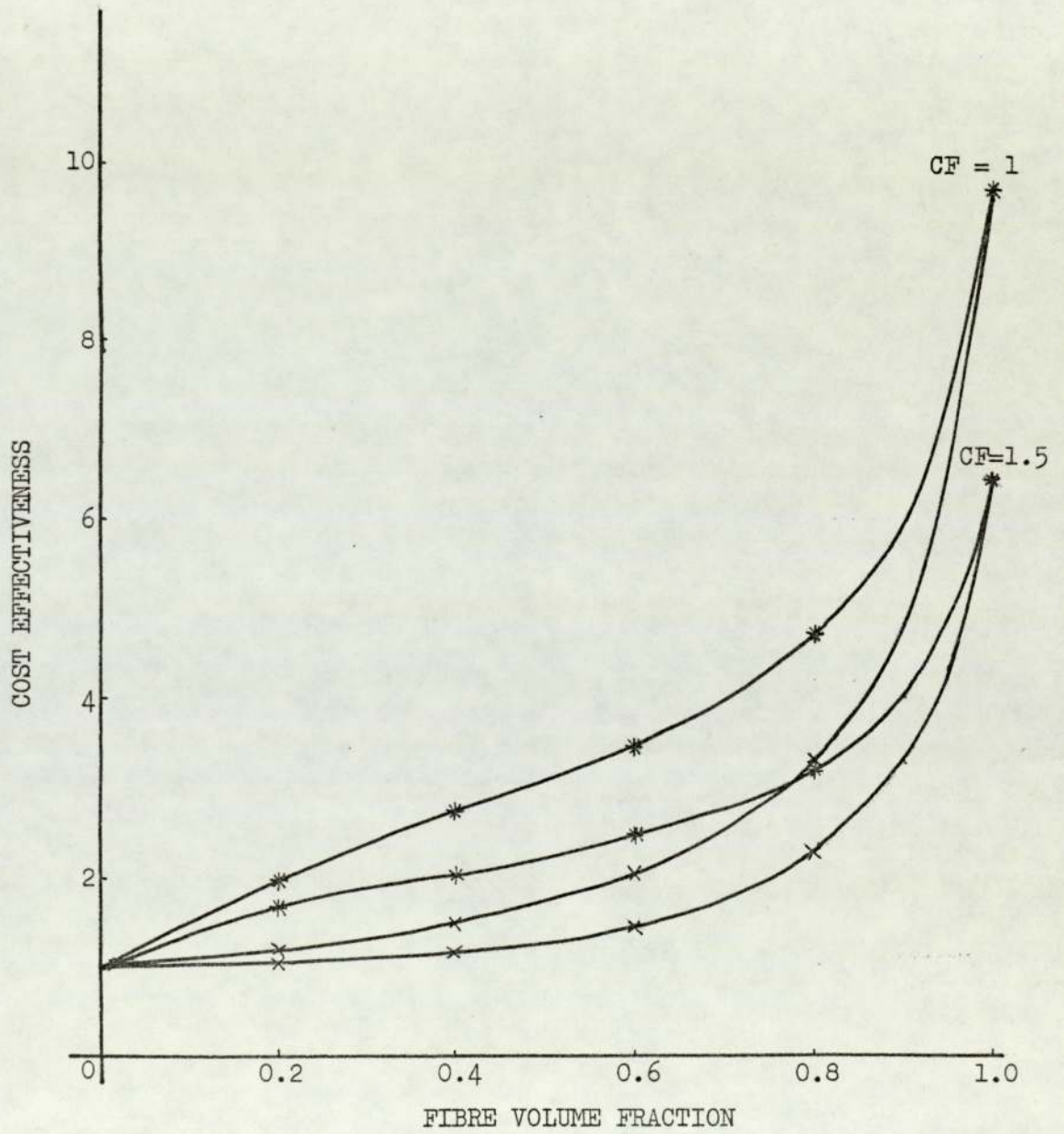


FIG. 4.3 MATERIAL COST EFFECTIVENESS

- FLEXURAL RIGIDITY

● — $\alpha = 0^\circ$
+ — $\alpha = 0^\circ, 90^\circ$

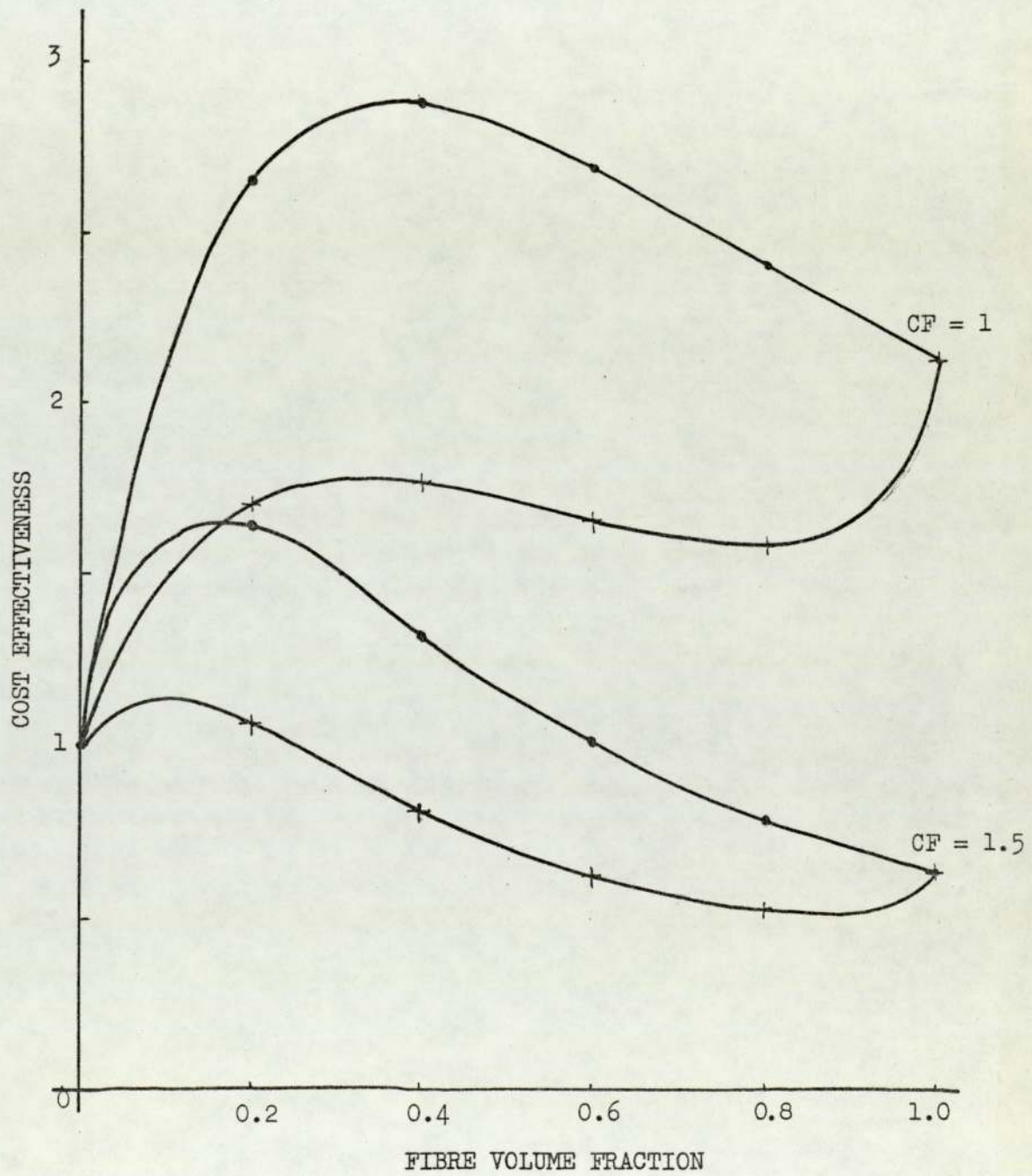


FIG. 4.4 MATERIAL COST EFFECTIVENESS

- FLEXURAL STIFFNESS

* * * $\alpha = \pm 45^\circ, 90^\circ, 0^\circ$
 x x x $\alpha = \pm 45^\circ$

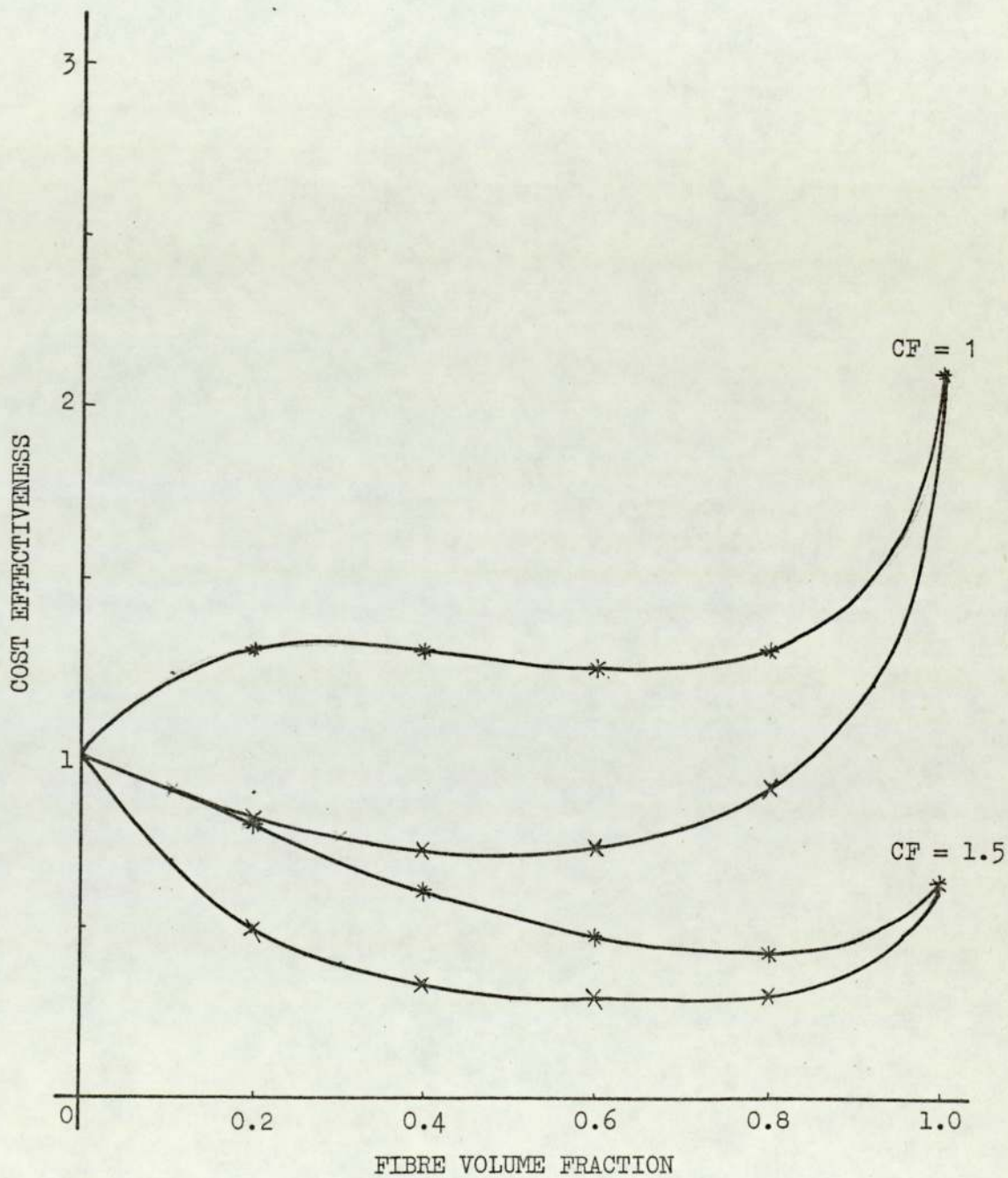


FIG. 4.5 MATERIAL COST EFFECTIVENESS

- SHEAR STIFFNESS

- $\alpha = 0^\circ \text{ \& \ } 0^\circ, 90^\circ$
- ×—×—×— $\alpha = \pm 45^\circ$
- *—*—*— $\alpha = 0^\circ, 90^\circ, \pm 45^\circ$

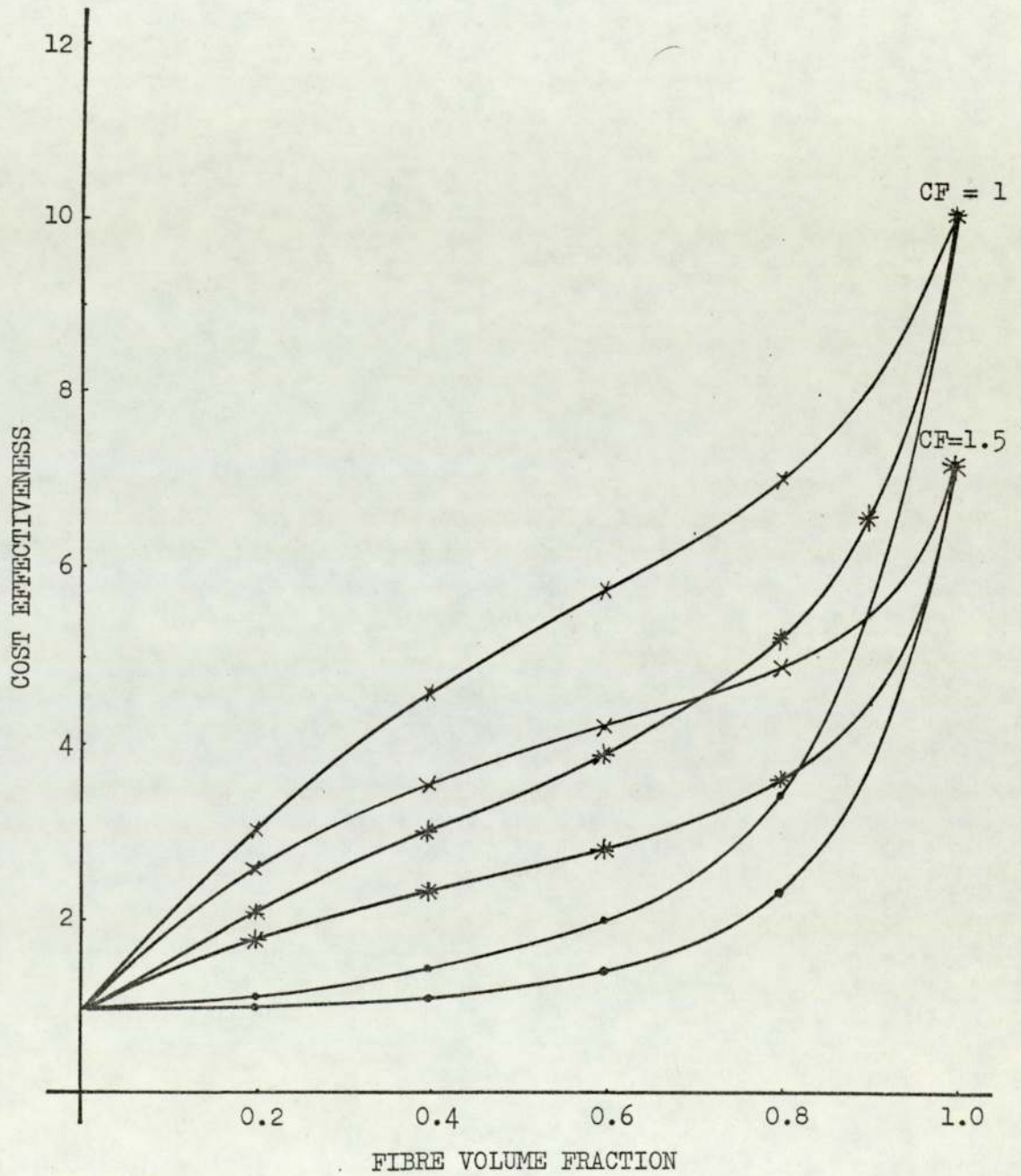


FIG. 4.6 MATERIAL COST EFFECTIVENESS

- PLATE BUCKLING

—•—•—•— $\alpha = 0^\circ$
—+—+—+— $\alpha = 0^\circ \text{ \& \ } 90^\circ$

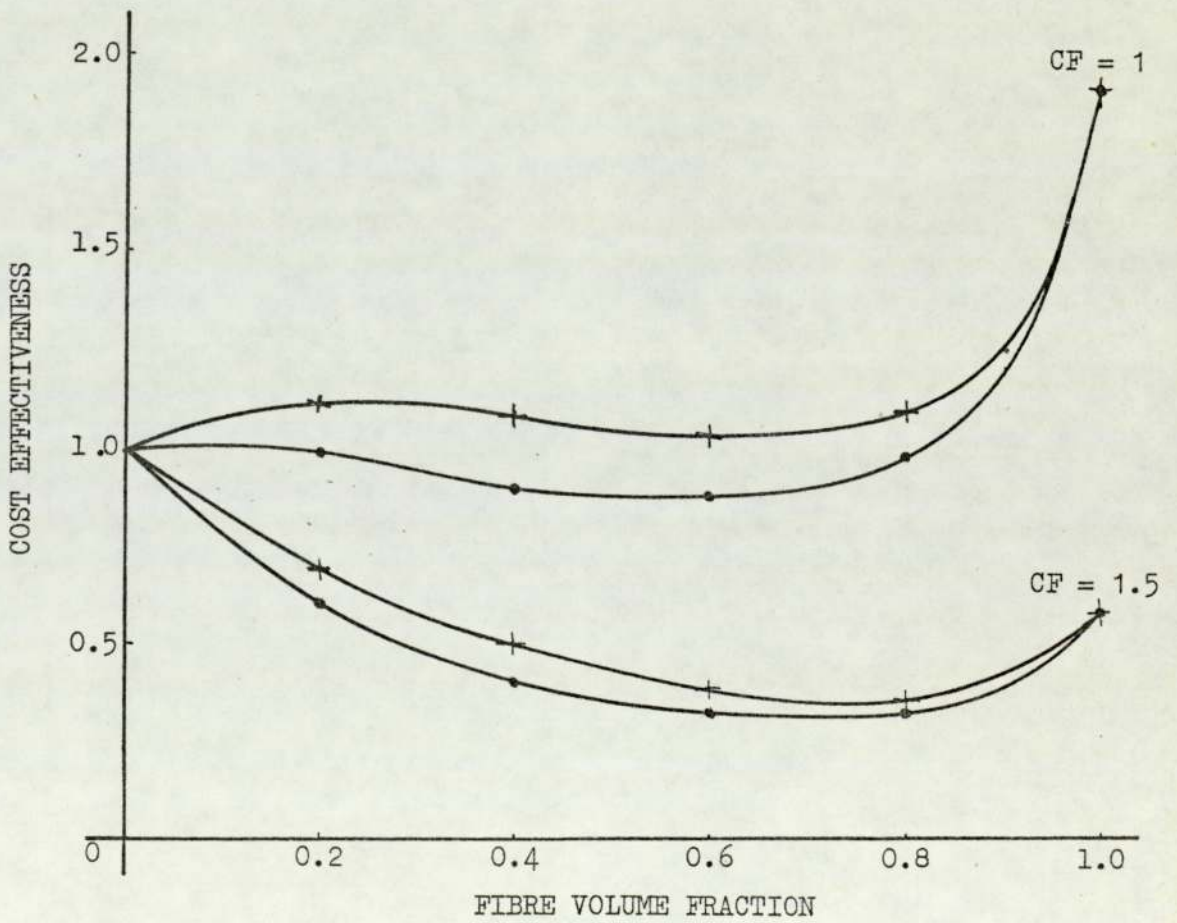


FIG. 4.7 MATERIAL COST EFFECTIVENESS

- PLATE BUCKLING

— x — x — x $\alpha = \pm 45^\circ$
— * — * — * $\alpha = 0^\circ, \pm 45^\circ, 90^\circ$

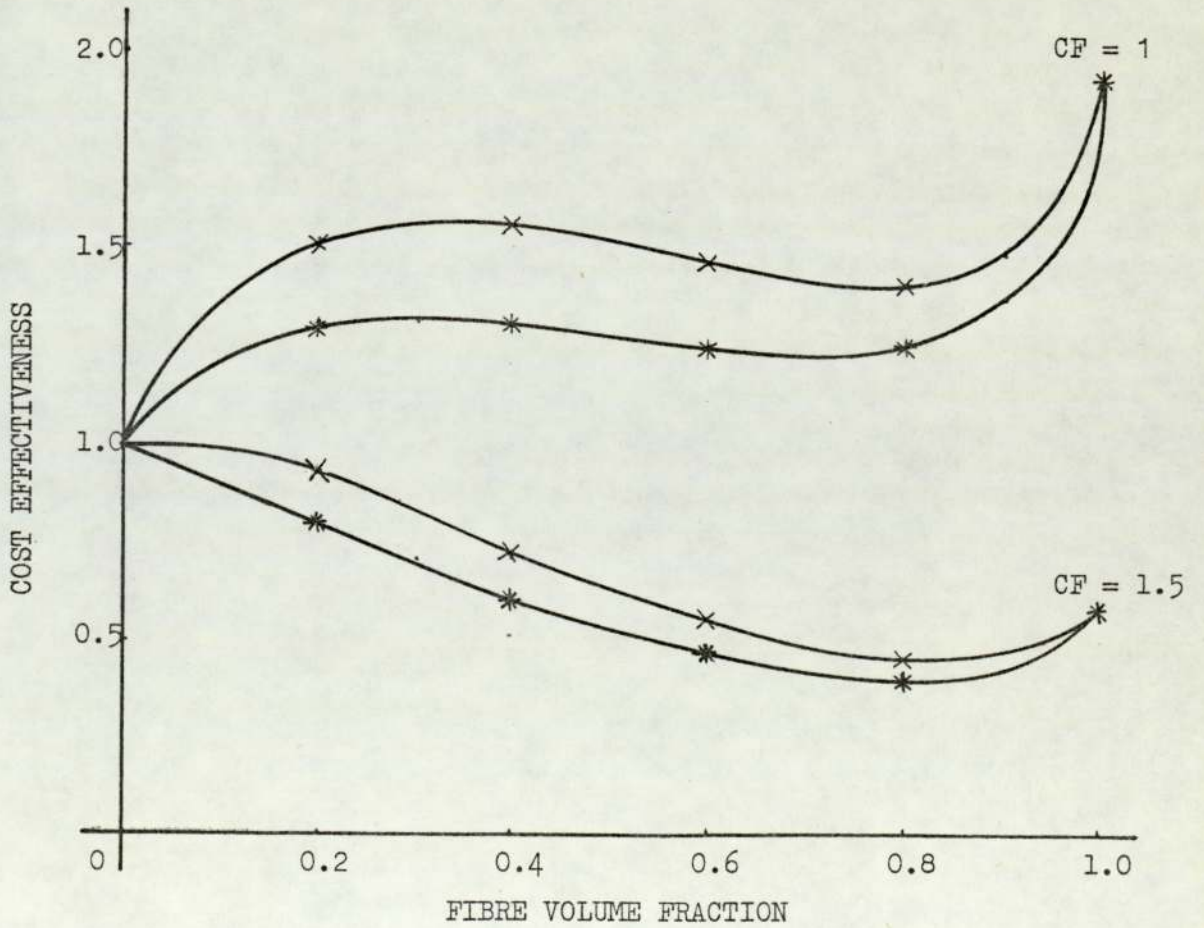


FIG. 4.8 MATERIAL COST EFFECTIVENESS

- CYLINDER BUCKLING

—•—•—•— $\alpha = 0^\circ$
—+—+—+— $\alpha = 0^\circ, 90^\circ$

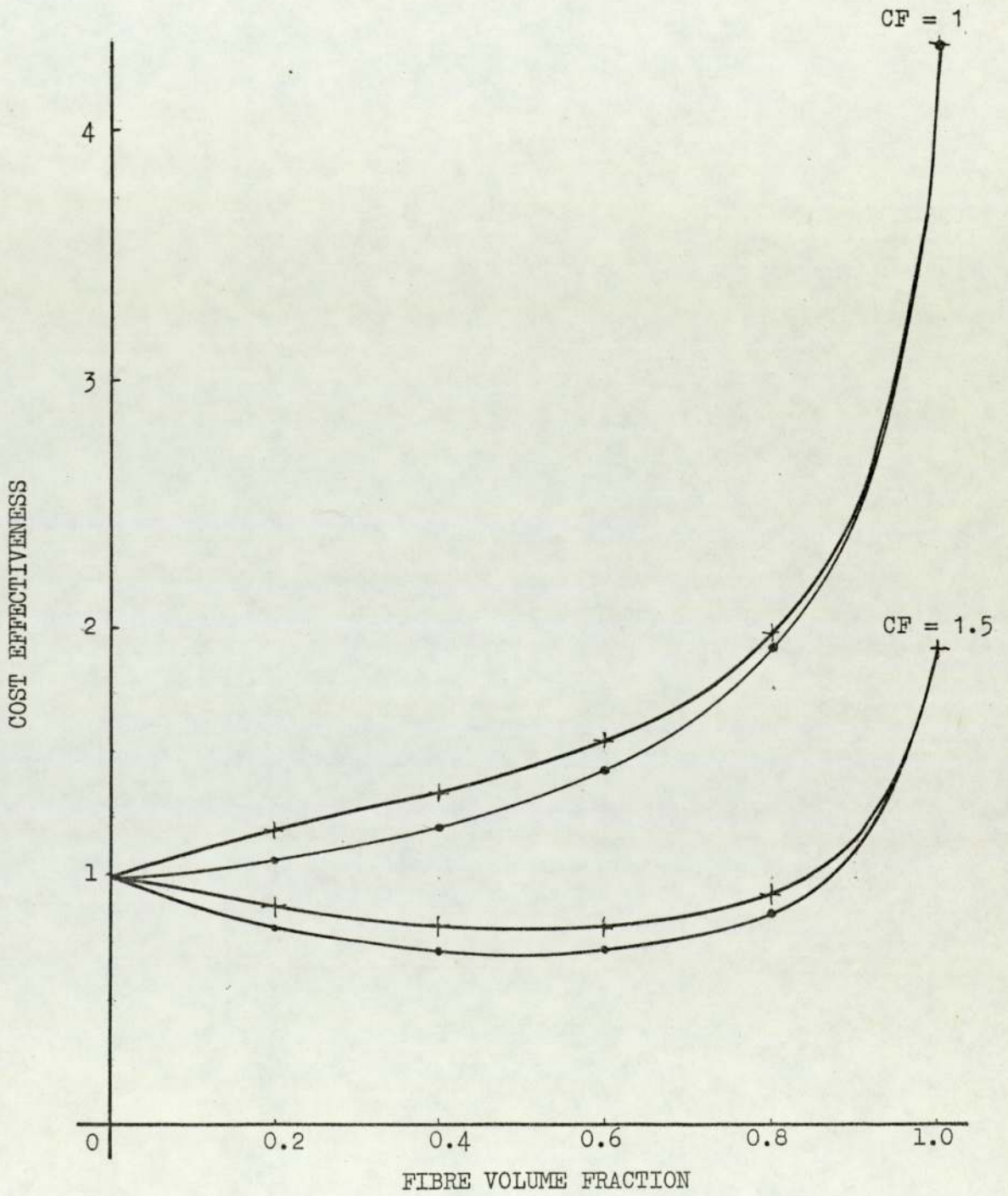


FIG. 4.9 MATERIAL COST EFFECTIVENESS
 - CYLINDER BUCKLING

$\times \times \times$ $\alpha = \pm 45^\circ$
 $* * *$ $\alpha = 0^\circ, \pm 45^\circ, 90^\circ$

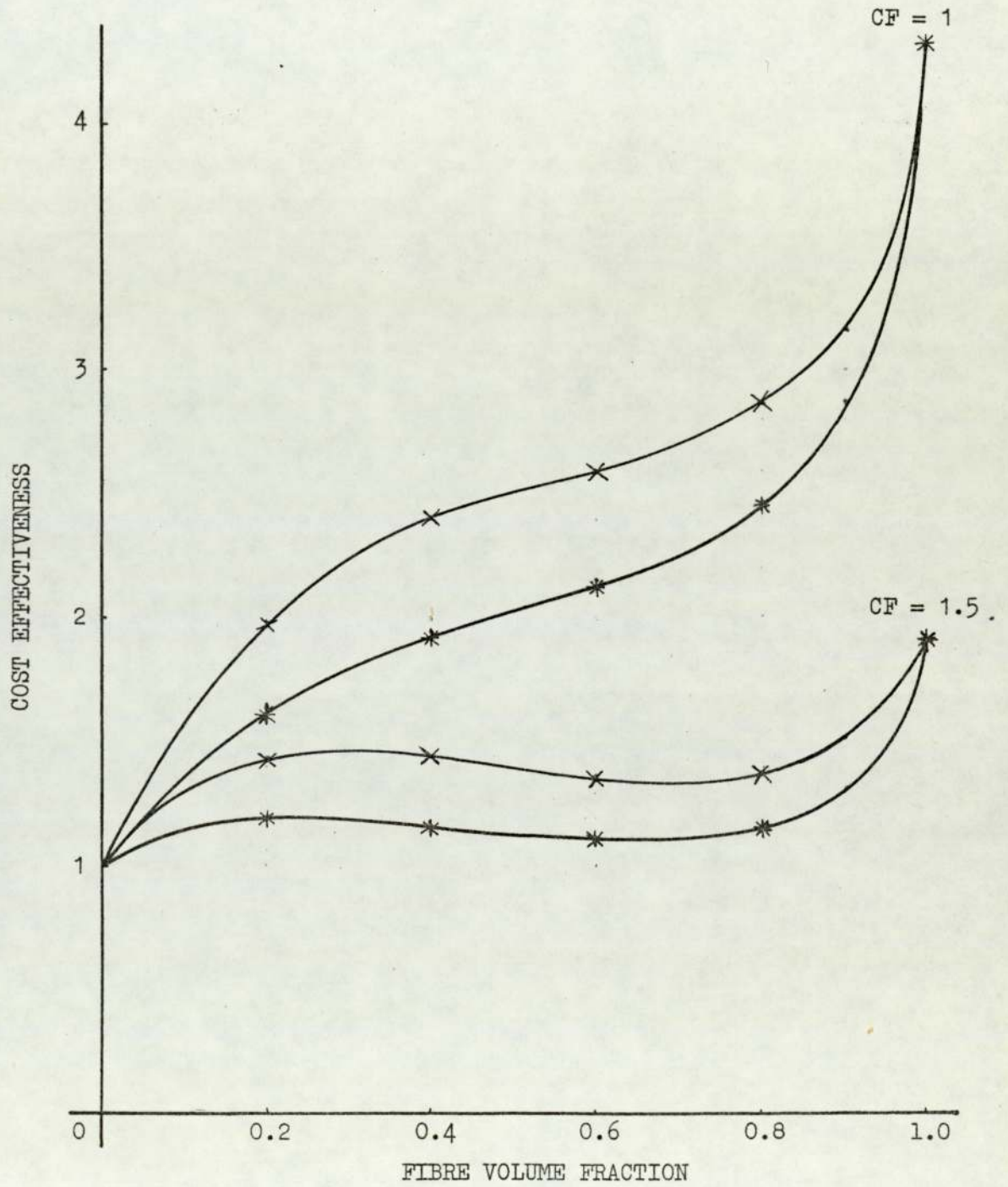


FIG. 4.10 PRACTICAL FIBRE VOLUME FRACTIONS

FOR VARIOUS MATERIALS

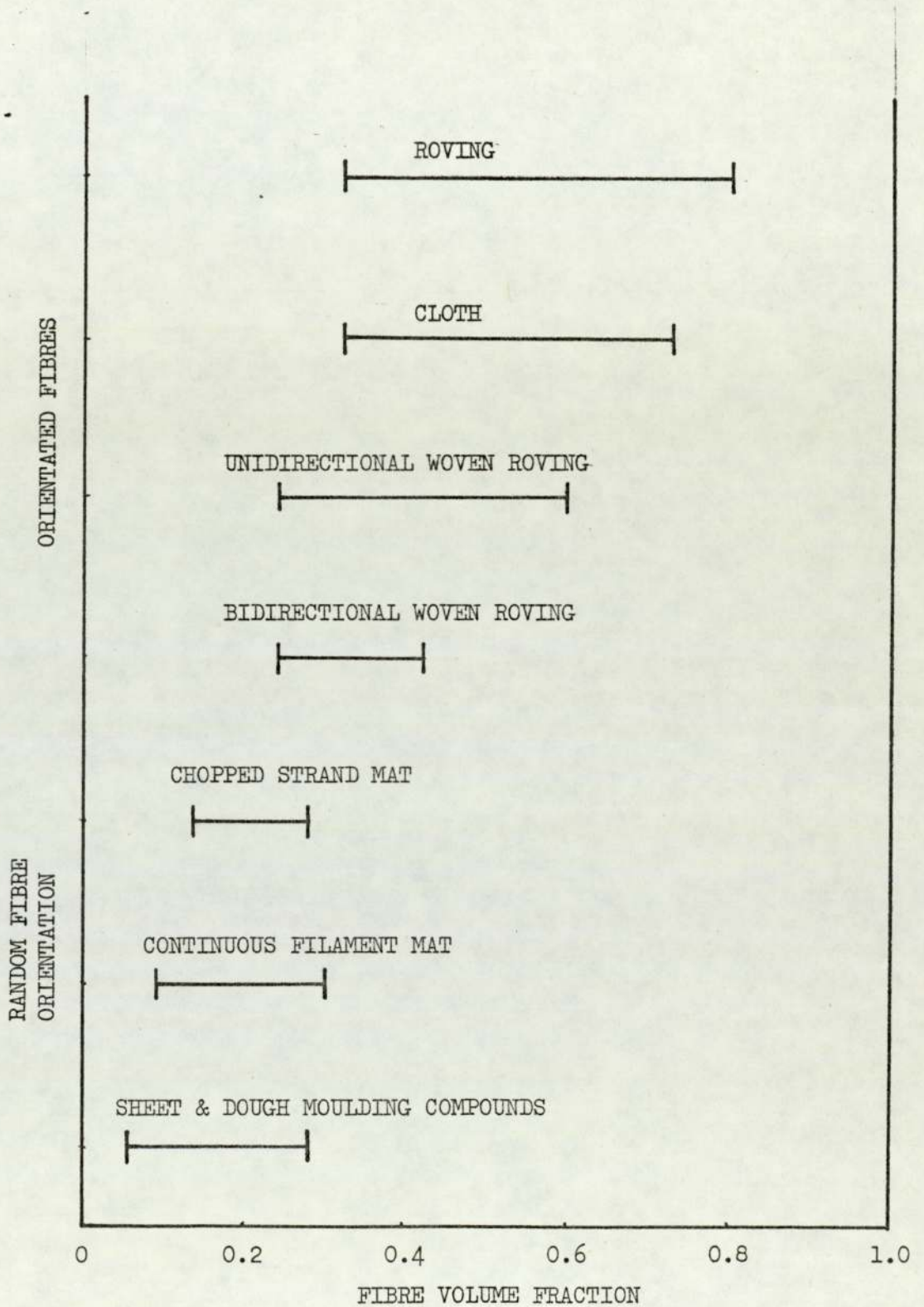
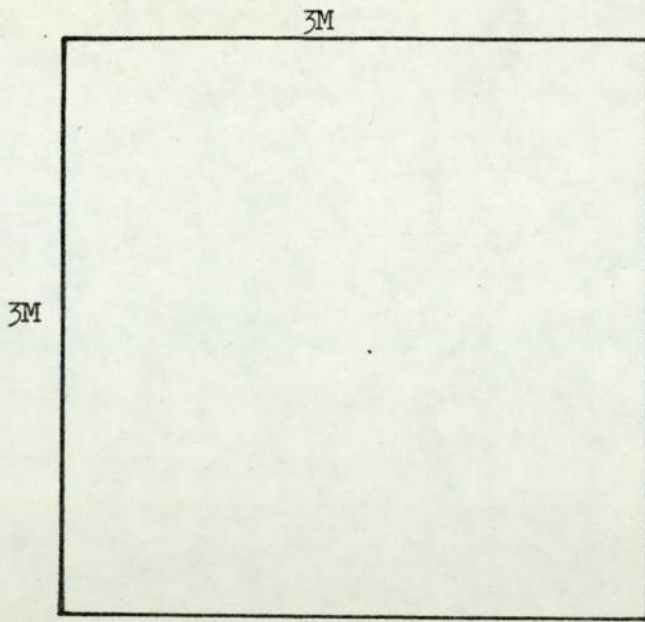


FIG. 4.11 PRODUCTS A AND B



PRODUCT TYPE A

$$TK = 0.006 \text{ M}$$

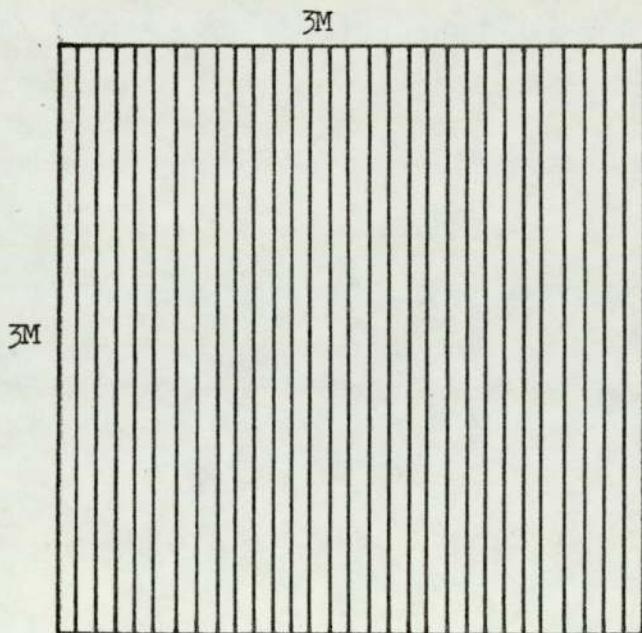
$$\text{WEIGHT (W)} = 86.5 \text{ kg.}$$

$$SA = 9 \text{ M}^2$$

$$PA = 9 \text{ M}^2$$

$$\frac{SA}{PA} = 1$$

$$PEL = 12 \text{ M}$$



PRODUCT TYPE B

$$TK = 0.006 \text{ M}$$

$$\text{WEIGHT (W)} = 176 \text{ kg.}$$

$$SA = 18.3 \text{ M}^2$$

$$PA = 9 \text{ M}^2$$

$$\frac{SA}{PA} = 2.033$$

$$PEL = 18.2 \text{ M}$$

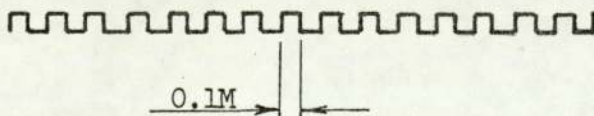
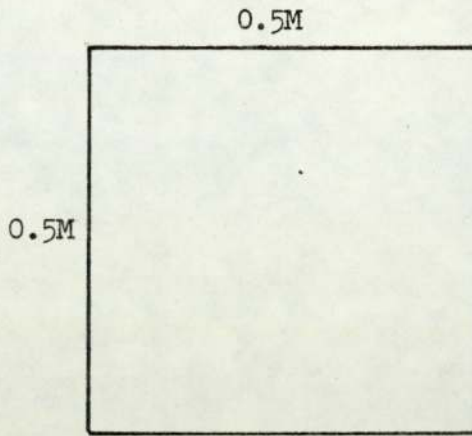


FIG. 4.12 PRODUCTS C AND D



PRODUCT TYPE C

$$TK = 0.006 \text{ M}$$

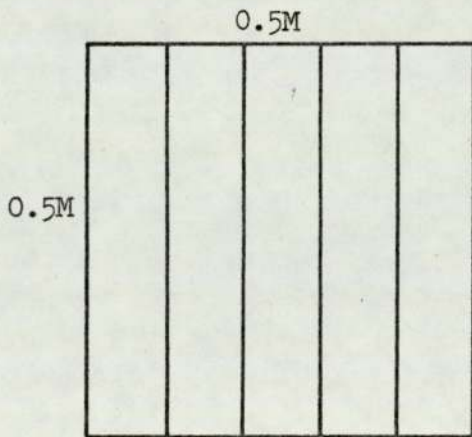
$$\text{WEIGHT (W)} = 2.4 \text{ kg.}$$

$$SA = 0.25 \text{ M}^2$$

$$PA = 0.25 \text{ M}^2$$

$$\frac{SA}{PA} = 1$$

$$PEL = 2 \text{ M}$$



PRODUCT TYPE D

$$TK = 0.006 \text{ M}$$

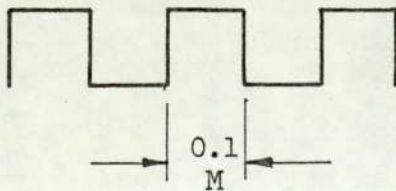
$$\text{WEIGHT (W)} = 5.28 \text{ kg.}$$

$$SA = 0.55 \text{ M}^2$$

$$PA = 0.25 \text{ M}^2$$

$$\frac{SA}{PA} = 2.2$$

$$PEL = 3.2 \text{ M}$$



COST AREA	<u>PRODUCT TYPE A</u>						<u>PRODUCT TYPE B</u>					
	FIXED COSTS	PRPD					FIXED COSTS	PRPD				
		0.5	2	10	40	200		0.5	2	10	40	200
FACTORY	0.27						0.76					
ENERGY	0.09						0.25					
PRODUCTION MOULD	1.00						2.10					
MOULD MASTER	0.06						0.34					
PATTERN & MASTER MOULD		1.64	0.41	0.08	0.02	0.01		3.42	0.85	0.17	0.04	0.01
LABOUR		93.00	23.30	23.30	23.30	23.30		93.00	93.00	93.00	93.00	93.00
PRODUCT HANDLING EQUIP.		1.63	0.41	0.08	0.02	0.01		1.63	0.41	0.08	0.02	0.01
FIXED COSTS TOTAL	1.42	1.42	1.42	1.42	1.42	1.42	3.45	3.45	3.45	3.45	3.45	3.45
TOTAL COSTS (£)		97.69	25.54	24.88	24.76	24.74		101.50	97.71	96.70	96.51	96.47

FIG. 4.13 HAND LAY-UP COSTS TABLE

COST AREA	<u>PRODUCT TYPE C</u>						<u>PRODUCT TYPE D</u>					
	FIXED COSTS	PRPD					FIXED COSTS	PRPD				
		0.5	2	10	40	200		0.5	2	10	40	200
FACTORY	0.01						0.02					
ENERGY	0.01						0.01					
PRODUCTION MOULD	0.13						0.17					
MOULD MASTER	0.01						0.01					
PATTERN & MASTER MOULD		0.20	0.05	0.01	0.01	0.01		0.28	0.07	0.01	0.01	0.01
LABOUR		93.00	23.30	4.70	1.20	1.20		93.00	23.30	4.70	4.70	4.70
FIXED COSTS TOTAL	0.16	0.16	0.16	0.16	0.16	0.16	0.31	0.31	0.31	0.31	0.31	0.31
TOTAL COSTS (£)		93.36	23.51	4.87	1.37	1.37		93.59	23.68	5.02	5.02	5.02

FIG. 4.14 HAND LAY-UP COSTS TABLE

COST AREA	<u>PRODUCT TYPE A</u>					<u>PRODUCT TYPE B</u>				
	FIXED COSTS	PRPD				FIXED COSTS	PRPD			
		2	3	9.4	49		2	4	17.5	52.5
FACTORY	0.12					0.15				
ENERGY	0.09					0.09				
PRODUCTION MOULD	1.00					0.10				
MOULD MASTER	0.03					0.07				
PATTERN & MASTER MOULD		0.41	0.27	0.09	0.02		0.86	0.43	0.10	0.03
LABOUR		44.68	29.80	9.51	5.45		44.68	22.34	13.22	10.01
PRODUCT HANDLING EQUIP.		0.41	0.27	0.09	0.02		0.40	0.20	0.05	0.02
SPRAY M/C		1.02	0.68	0.22	0.05		1.02	0.51	0.13	0.13
FIXED COSTS TOTAL	1.24	<u>1.24</u>	<u>1.24</u>	<u>1.24</u>	<u>1.24</u>	2.41	<u>2.41</u>	<u>2.41</u>	<u>2.41</u>	<u>2.41</u>
TOTAL COSTS (£)		47.86	32.26	11.15	6.78		49.37	25.89	15.91	12.60

FIG. 4.15 BASIC SPRAY-UP COSTS TABLE

COST AREA	<u>PRODUCT TYPE C</u>				<u>PRODUCT TYPE D</u>					
	FIXED COSTS	2	20	PRPD 127	648	FIXED COSTS	2	49	PRPD 369	738
FACTORY	0.01					0.02				
ENERGY	0.01					0.01				
PRODUCTION MOULD	0.01					0.02				
MOULD MASTER	0.01					0.01				
PATTERN & MASTER MOULD		0.05	0.01	0.01	0.01		0.07	0.01	0.01	0.01
LABOUR		44.68	4.47	0.70	0.36		44.68	1.82	0.92	0.80
SPRAY M/C		1.02	0.10	0.02	0.02		1.02	0.04	0.01	0.01
FIXED COSTS TOTAL	0.04	<u>0.04</u>	<u>0.04</u>	<u>0.04</u>	<u>0.04</u>	0.06	<u>0.06</u>	<u>0.06</u>	<u>0.06</u>	<u>0.06</u>
TOTAL COSTS (£)		45.79	4.62	0.77	0.43		46.83	1.93	1.00	0.88

FIG. 4.16 BASIC SPRAY-UP COSTS TABLE

COST AREA	<u>PRODUCT TYPE A</u>					<u>PRODUCT TYPE B</u>				
	FIXED COSTS	PRPD				FIXED COSTS	PRPD			
		2	11.6	40	104.4		2	5.3	15	82
FACTORY	0.12					0.15				
ENERGY	0.09					0.09				
PRODUCTION MOULD	1.00					2.10				
MOULD MASTER	0.03					0.07				
PATTERN & MASTER MOULD		0.41	0.07	0.02	0.01	0.85	0.32	0.11	0.02	
LABOUR		42.25	9.35	3.89	3.58	42.25	15.94	10.37	8.16	
ROBOT M/C		5.10	0.88	0.26	0.26	5.10	1.93	0.68	0.66	
PRODUCT HANDLING EQUIP.		0.41	0.07	0.02	0.01	0.41	0.15	0.05	0.01	
FIXED COSTS TOTAL	1.24	<u>1.24</u>	<u>1.24</u>	<u>1.24</u>	<u>1.24</u>	2.41	<u>2.41</u>	<u>2.41</u>	<u>2.41</u>	<u>2.41</u>
TOTAL COSTS (£)		49.41	11.61	5.43	5.10	51.02	20.75	13.62	11.26	

FIG. 4.17 ROBOT SPRAY-UP COSTS TABLE

COST AREA	FIXED COSTS	<u>PRODUCT TYPE C</u>				<u>PRODUCT TYPE D</u>			
		2	11.6	158	470	2	11.6	57	158
FACTORY	0.01								
ENERGY	0.01								
PRODUCTION MOULD	0.01								
MOULD MASTER	0.01								
PATTERN & MASTER MOULD		0.05	0.01	0.01	0.01	0.07	0.01	0.01	0.01
LABOUR		42.25	7.28	0.54	0.33	42.25	7.28	1.48	0.98
ROBOT M/C		5.10	0.88	0.06	0.07	5.10	0.88	0.18	0.06
FIXED COSTS TOTAL	0.04	<u>0.04</u>	<u>0.04</u>	<u>0.04</u>	<u>0.04</u>	0.06	<u>0.06</u>	<u>0.06</u>	<u>0.06</u>
TOTAL COSTS (£)		47.44	8.21	0.65	0.45	47.48	8.23	1.73	1.11

FIG. 4.18 ROBOT SPRAY-UP COSTS TABLE

COST AREA	<u>PRODUCT TYPE A</u>				<u>PRODUCT TYPE B</u>			
	FIXED COSTS	1	2	PRPD 11.6 140	FIXED COSTS	1	2	PRPD 5.3 62
FACTORY	0.13				0.15			
ENERGY	0.09				0.09			
PRODUCTION MOULD	1.00				2.10			
MOULD MASTER	0.03				0.07			
PATTERN & MASTER MOULD		0.82	0.41	0.07 0.01		1.71	0.86	0.32 0.03
LABOUR		84.49	42.25	7.28 3.39		84.49	42.25	15.97 7.66
PRODUCT HANDLING EQUIP.		0.82	0.41	0.07 0.01		0.82	0.41	0.15 0.01
SPRAY M/C		9.80	4.90	0.84 0.07		9.80	4.90	1.85 0.16
FIXED COSTS TOTAL	1.25	<u>1.25</u>	<u>1.25</u>	<u>1.25</u> <u>1.25</u>	2.41	<u>2.41</u>	<u>2.41</u>	<u>2.41</u> <u>2.41</u>
TOTAL COSTS (£)		97.18	49.22	9.51 4.73		99.23	50.83	20.70 10.27

FIG. 4.19 CONTINUOUS SPRAY-UP COSTS TABLE

COST AREA	FIXED COSTS	<u>PRODUCT TYPE C</u>				FIXED COSTS	<u>PRODUCT TYPE D</u>			
		2	11.6	158	1732		PRPD	2	11.6	57
FACTORY	0.01					0.01				
ENERGY	0.01					0.01				
PRODUCTION MOULD	0.01					0.02				
MOULD MASTER	0.01					0.01				
PATTERN & MASTER MOULD		0.05	0.01	0.01	0.01		0.07	0.01	0.01	0.01
LABOUR		42.25	7.28	0.69	0.27		42.25	7.28	1.90	0.69
SPRAY M/C		4.48	0.84	0.06	0.01		4.88	0.84	0.17	0.01
FIXED COSTS TOTAL	0.04	<u>0.04</u>	<u>0.04</u>	<u>0.04</u>	<u>0.04</u>	0.05	<u>0.05</u>	<u>0.05</u>	<u>0.05</u>	<u>0.05</u>
TOTAL COSTS (£)		47.23	8.17	0.80	0.33		47.26	8.16	2.13	0.76

FIG. 4.20 CONTINUOUS SPRAY-UP COSTS TABLE

COST AREA	FIXED COSTS	<u>PRODUCT TYPE A</u>				PRPD	23.1	<u>PRODUCT TYPE B</u>			
		2	5	10	PRPD			2	4	9	18.9
FACTORY	0.09						0.19				
ENERGY	0.09						0.09				
PRODUCTION MOULD	3.00						6.30				
MOULD MASTER	0.02						0.08				
PATTERN & MASTER MOULD		0.41	0.16	0.08	0.04		0.86	0.43	0.19	0.09	
LABOUR		42.25	16.90	8.45	3.68		42.25	21.12	9.39	4.47	
PRODUCT HANDLING EQUIP.		0.41	0.16	0.08	0.04		0.41	0.20	0.09	0.04	
INJECTION M/C		1.23	0.49	0.24	0.11		1.23	0.61	0.27	0.13	
FIXED COSTS TOTAL	3.20	<u>3.20</u>	<u>3.20</u>	<u>3.20</u>	<u>3.20</u>		6.66	<u>6.66</u>	<u>6.66</u>	<u>6.66</u>	
TOTAL COSTS (£)		47.50	20.09	12.05	7.07		51.41	29.02	16.60	11.39	

FIG. 4.21 RESIN INJECTION COSTS TABLE

COST AREA	FIXED COSTS	<u>PRODUCT TYPE C</u>				FIXED COSTS	<u>PRODUCT TYPE D</u>			
		PRPD					PRPD			
		2	10	100	400		2	5	20	125
FACTORY	0.01					0.01				
ENERGY	0.01					0.01				
PRODUCTION MOULD	0.33					0.43				
MOULD MASTER	0.01					0.01				
PATTERN & MASTER MOULD		0.05	0.01	0.01	0.01		0.07	0.02	0.01	0.01
LABOUR		42.25	9.45	0.84	0.21		42.25	16.90	4.22	0.68
INJECTION M/C		0.01	0.02	0.20	0.01		1.23	0.49	0.12	0.02
FIXED COSTS TOTAL	0.36	<u>0.36</u>	<u>0.36</u>	<u>0.36</u>	<u>0.36</u>	0.46	<u>0.46</u>	<u>0.46</u>	<u>0.46</u>	<u>0.46</u>
TOTAL COSTS (£)		43.66	9.02	1.23	0.59		44.01	17.87	4.81	1.17

FIG. 4.22 RESIN INJECTION COSTS TABLE

COST AREA	<u>PRODUCT TYPE A</u>				<u>PRODUCT TYPE B</u>			
	PRPD							
	2	10	100	200	2	10	100	200
FACTORY	0.70	0.14	0.02	0.01	0.70	0.14	0.02	0.01
ENERGY	0.70	0.14	0.02	0.01	0.70	0.14	0.02	0.01
PRODUCTION MOULD	1.60	1.60	1.60	1.60	3.20	3.20	3.20	3.20
LABOUR	46.00	9.20	1.41	1.41	46.00	9.20	1.41	1.41
PRODUCT HANDLING EQUIP.	0.41	0.08	0.01	0.01	0.41	0.08	0.01	0.01
PRESS	<u>24.00</u>	<u>4.80</u>	<u>0.48</u>	<u>0.24</u>	<u>24.00</u>	<u>4.80</u>	<u>0.48</u>	<u>0.24</u>
TOTAL COST (£)	73.41	15.96	3.54	3.28	80.01	17.56	6.53	4.87

FIG. 4.23 HOT PRESS COSTS TABLE

COST AREA	<u>PRODUCT TYPE C</u>				<u>PRODUCT TYPE D</u>			
	PRPD							
	2	10	100	400	2	10	100	400
FACTORY	0.25	0.05	0.03	0.01	0.25	0.05	0.01	0.01
ENERGY	0.25	0.05	0.03	0.01	0.25	0.05	0.01	0.01
PRODUCTION MOULD	0.28	0.28	0.28	0.28	0.34	0.34	0.34	0.34
LABOUR	46.00	9.20	0.92	0.35	46.00	9.20	0.92	0.35
PRESS	2.55	0.51	0.05	0.02	2.55	0.51	0.05	0.02
TOTAL COSTS (£)	49.33	10.09	1.31	0.67	49.39	10.15	1.33	0.73

FIG. 4.24 HOT PRESS COSTS TABLE

FIG. 4.25 PRODUCTION COSTS OF PRODUCT A

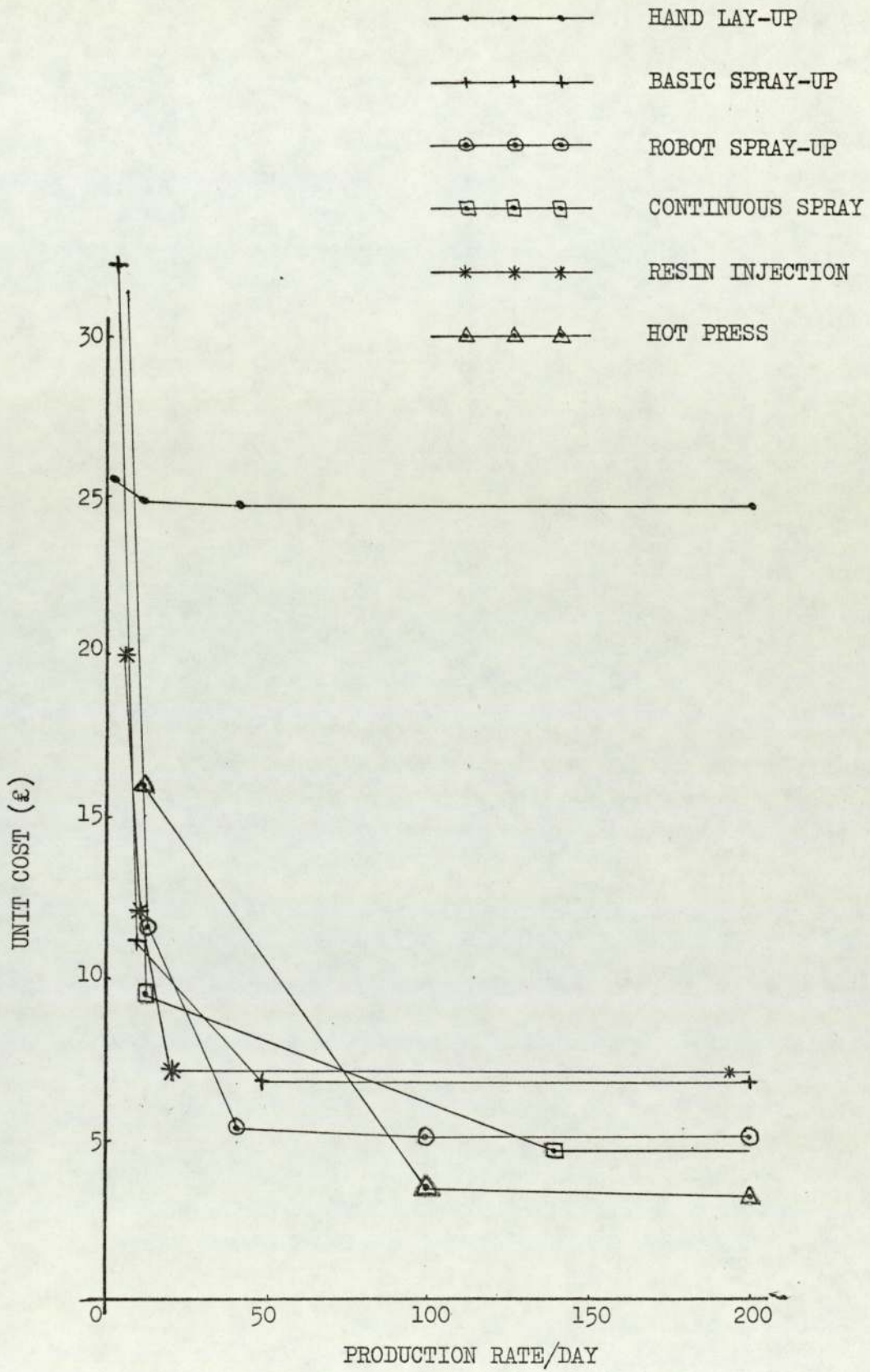
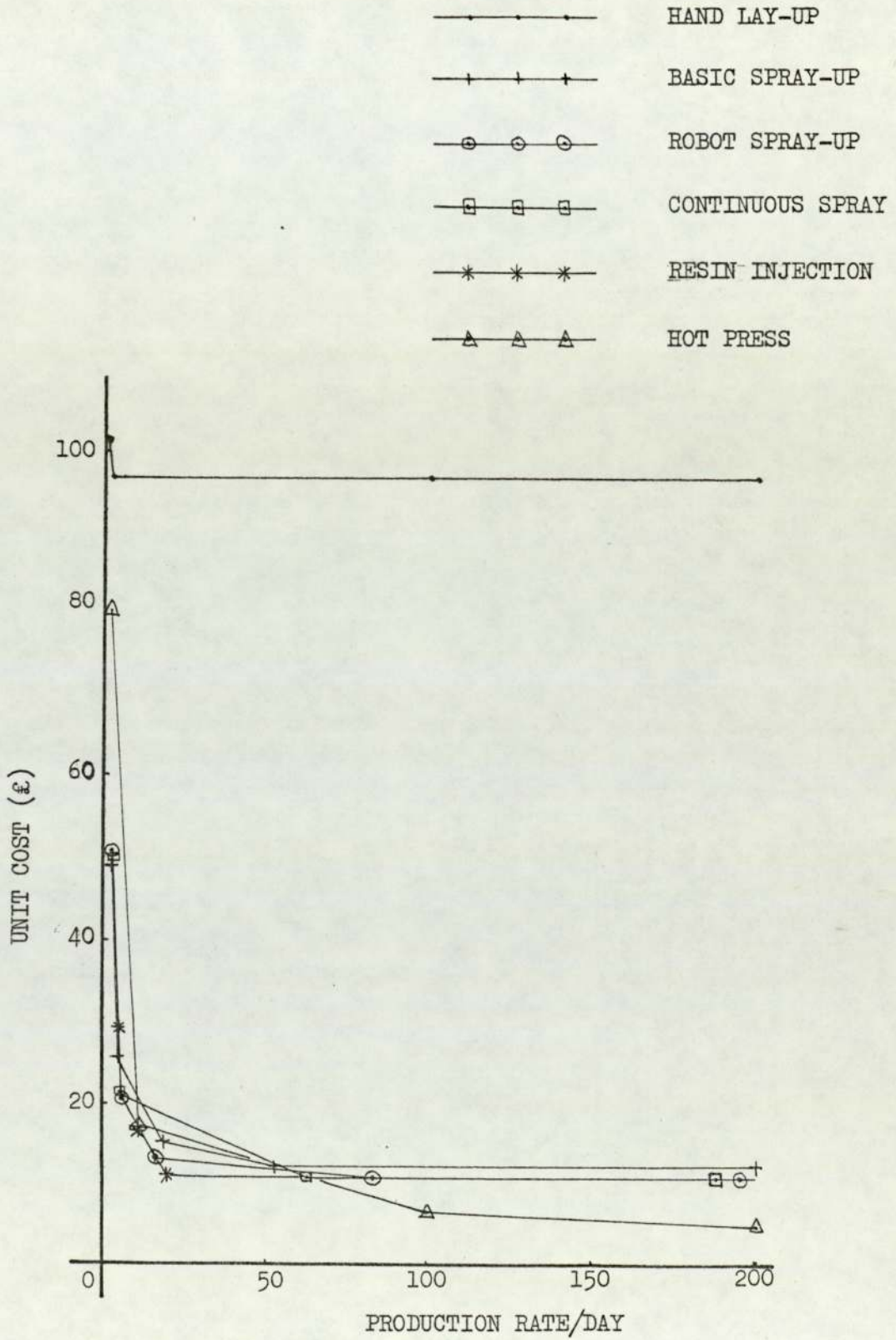


FIG. 4.26 PRODUCTION COSTS OF PRODUCT B



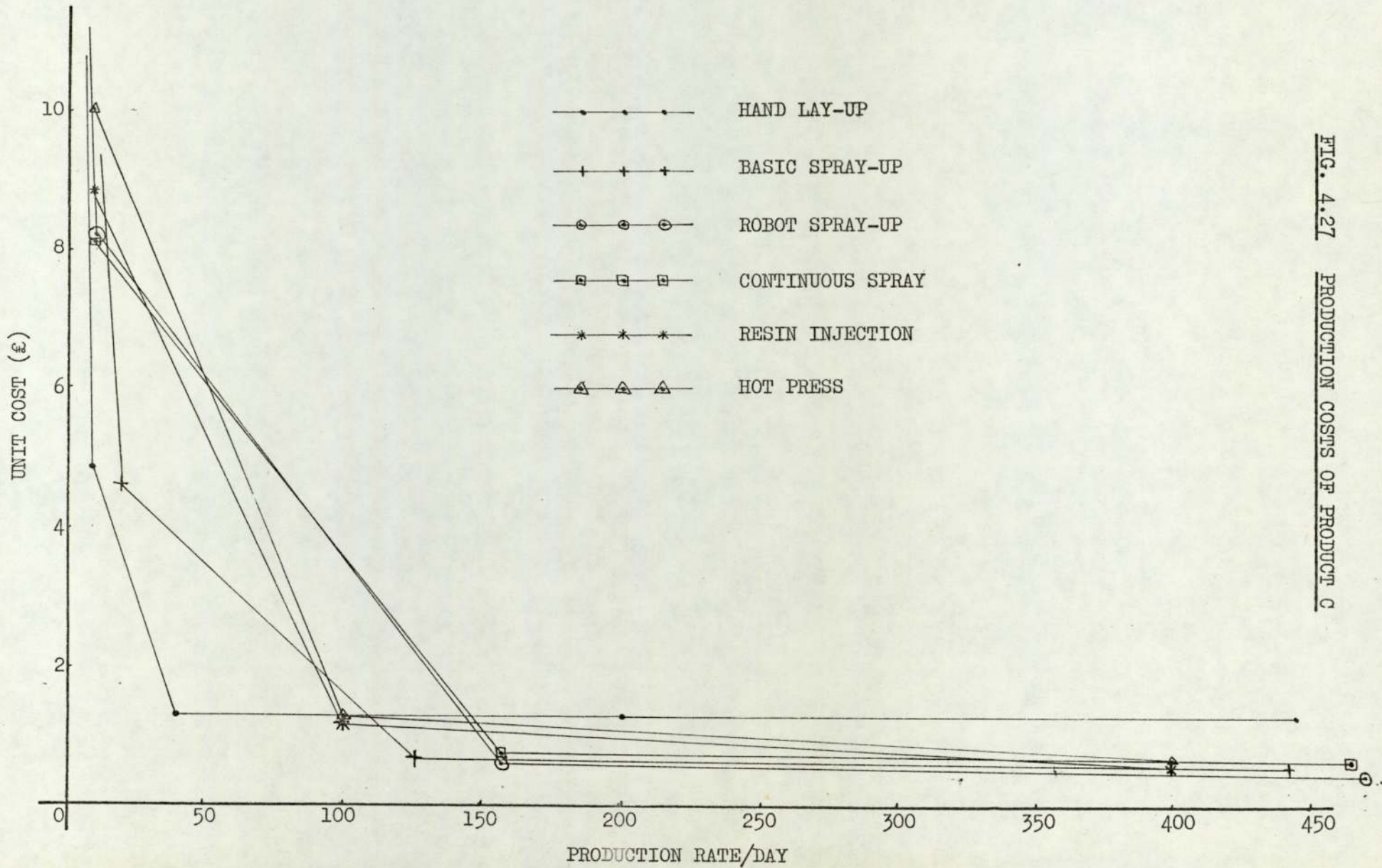


FIG. 4.27

PRODUCTION COSTS OF PRODUCT C

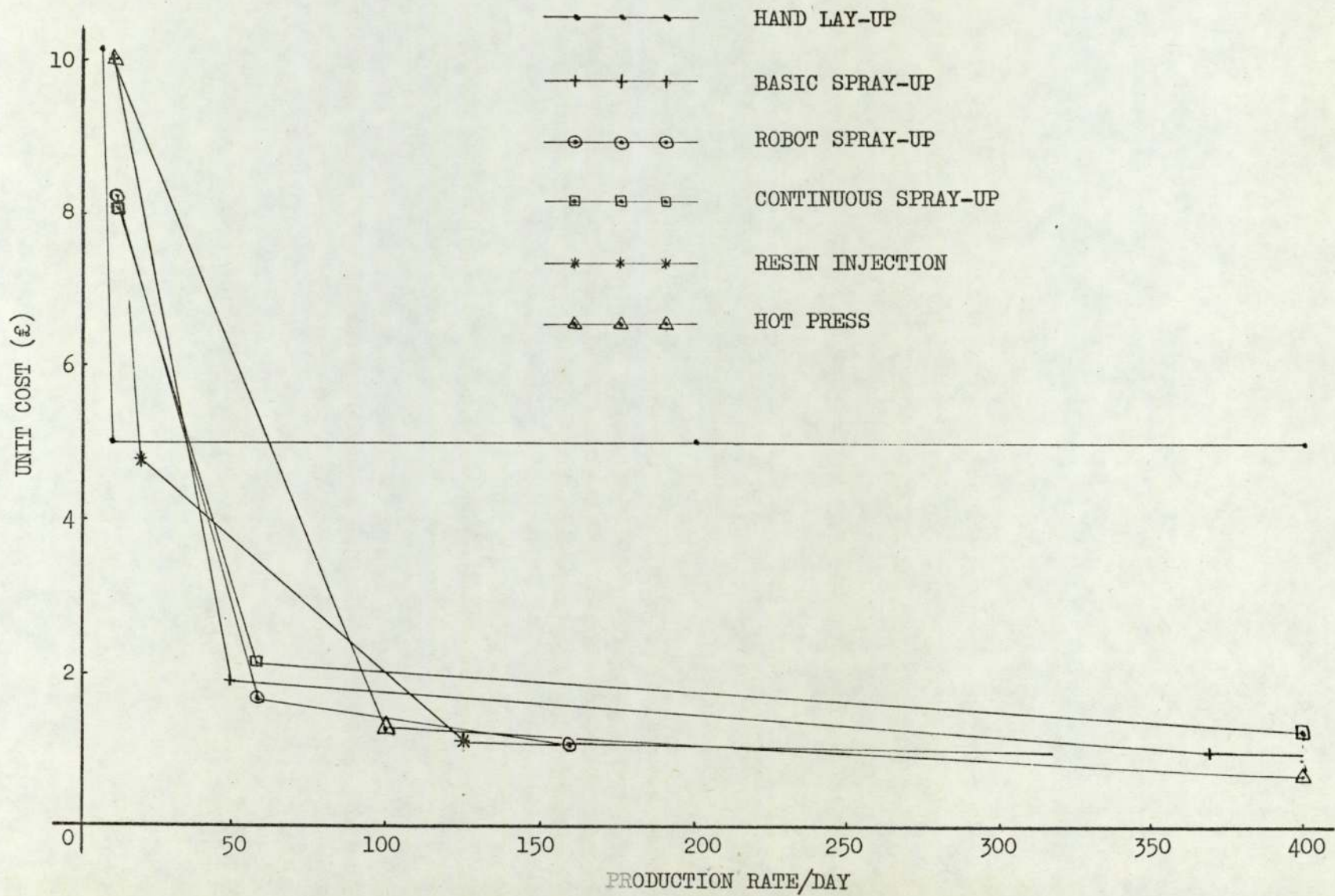


FIG. 4.28 PRODUCTION COSTS OF PRODUCT D

FIG. 4.29 IMPROVED FIBRE ORIENTATION

ROUND BOLT IN A TENSILE

JOINT

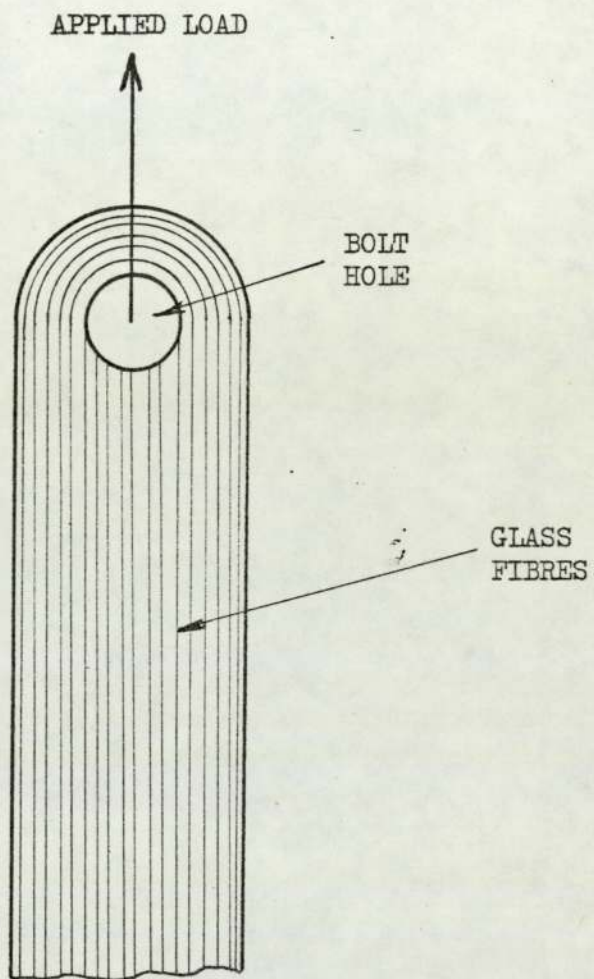


FIG. 4.30 TYPES OF ADHESIVE LOADING

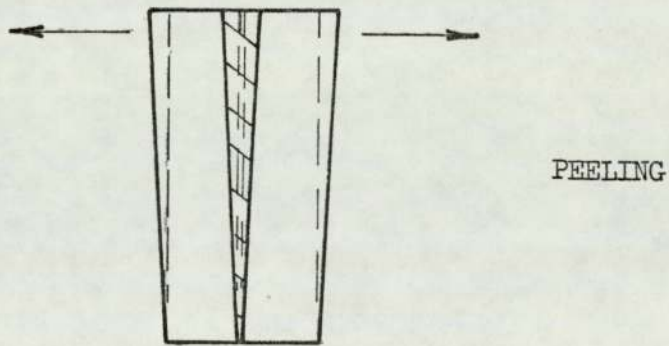
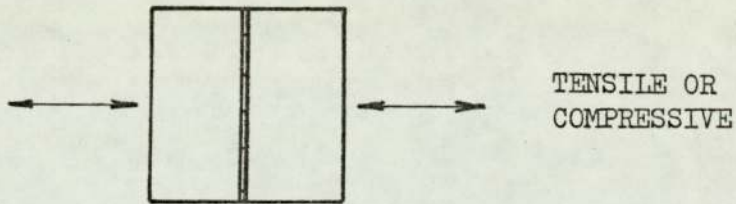
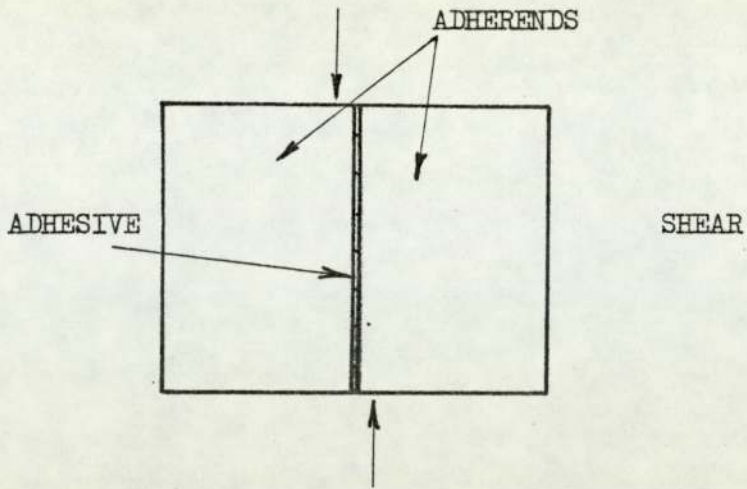
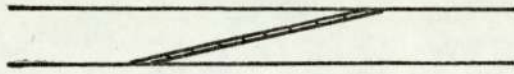
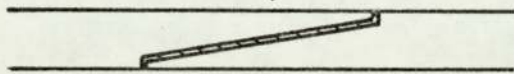


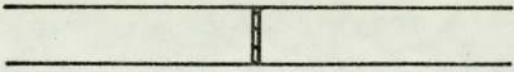
FIG. 4.31 ADHESIVE JOINTS



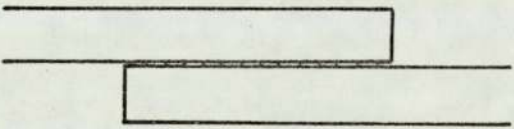
PURE SCARF



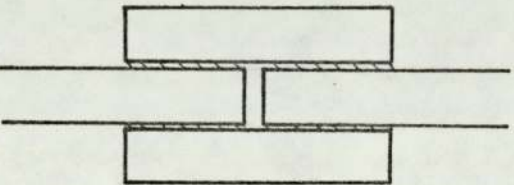
LANDED SCARF



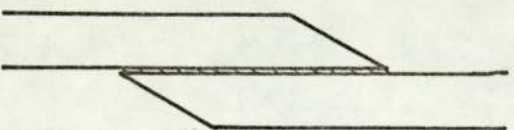
BUTT



SINGLE FLAT
LAP

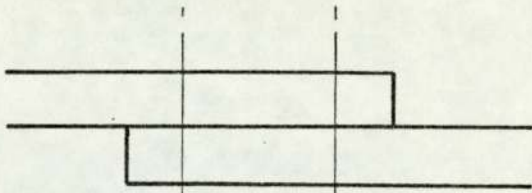


DOUBLE FLAT
LAP

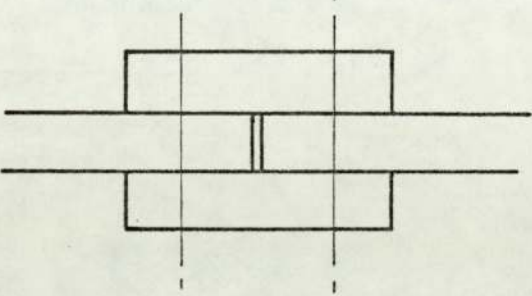


BEVELLED LAP

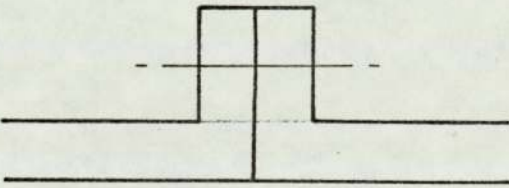
FIG. 4.32 MECHANICAL JOINTS



SINGLE LAP



DOUBLE LAP



FLANGE

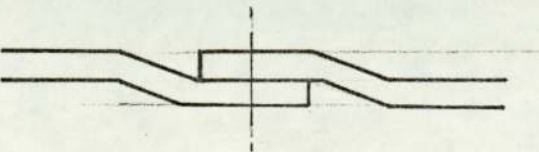
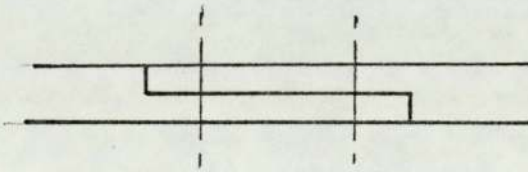
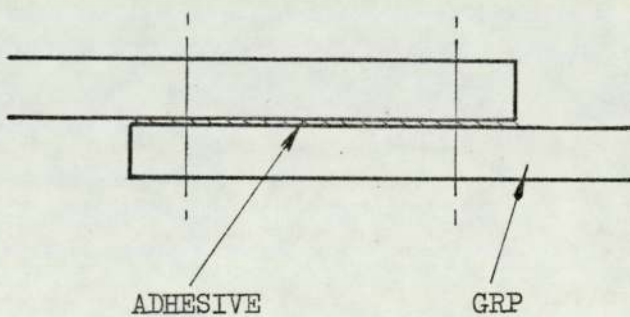
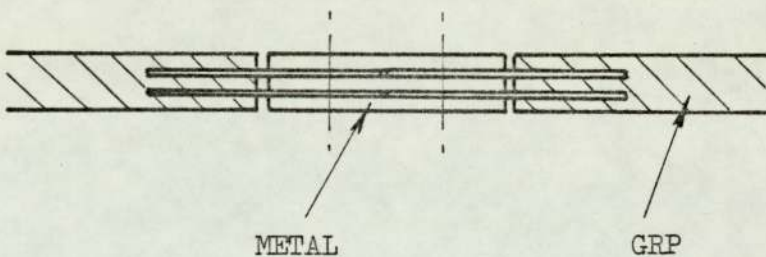
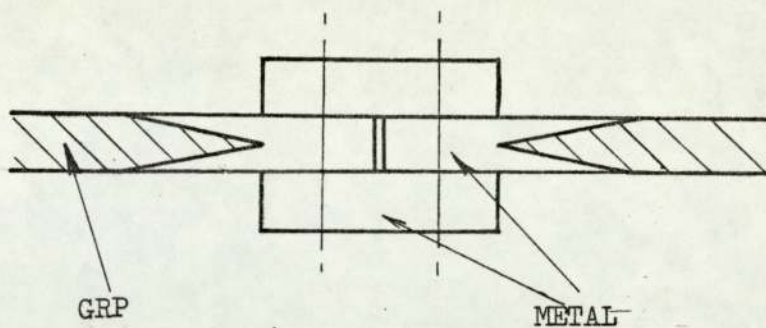


FIG. 4.33 COMBINATION JOINTS



CHAPTER 5

DISCUSSION AND PRELIMINARY DESIGN OF
A STRUCTURAL SYSTEM

CHAPTER FIVE

Discussion and Preliminary Design of a Structural System

5.1

Introduction

In previous chapters the characteristics of grp have been studied theoretically and empirically, and from these studies certain design philosophies and guidelines have been presented. With this knowledge, an argument will be presented for the selection of a particular structural system. The system will then be the subject of a preliminary design study.

Long-span lightly loaded structures have been chosen for study since the stress and deflection of these structures is, to a greater extent, dependent upon the self-weight of the structure. Grp is a low-density material and is therefore potentially capable of forming a light structure. Further weight, and hence material, should be saved, since less material is then required to support the structure itself. In the extreme case, where the structure's loading is its self-weight only, the maximum possible span is dependent upon grp's most outstanding property: its strength to weight ratio.

To show, satisfactorily, the feasibility of long-span grp structures, it is considered necessary to study both the economic and the structural aspects. Rather than study appropriate structures in abstract it would be beneficial to select a particular structure for analysis and assessment. A suitable structural function will be one that uses grp's relatively good properties to the full and one in which its weak properties are avoided or mitigated. Structures with a large potential market would be desirable.

It is of particular importance that a high modulus of elasticity should not be of overriding importance to the structure and that deflections may be limited by suitable choice of geometry. Further, if large deflections are not fundamentally unacceptable in the structure then the structural function is most suitable.

Long-span roof structures are an example of lightly-loaded structures which exploit the attributes of grp and mitigate the short-

comings adequately for this study. They offer a market which is large enough to warrant further investigation. Fire restrictions are not as stringent for roofs as for other parts of buildings. The good weathering properties of grp are used to the full. A roof structure, for the majority of its life, has only its own weight to support, thus reducing the severity of the creep problem compared with other structures which may be fully loaded continuously.

5.3

The Preliminary Design of a Long-Span Grp Roof

5.3.1 Introduction

Having chosen a particular structure for study it is now possible to carry out a preliminary design study. This will demonstrate the use of grp structurally, and will enable information for an economic study to be obtained.

5.3.2 Roof Loading

The normal major loading which a roof has to sustain is:

- a) Self-weight
- b) Snow loading
- c) Wind loading

The simultaneous action of the self-weight and snow load is normally the greatest load. It is not possible to determine the self-weight at this stage, however. British Standards code of practice CP3 : Ch V : Part 1 1972 lays down two possible snow loads for roofs with slopes of 30° or less. The lighter of the two loads must only be used when access to the roof is limited to that required for maintenance. The lower load of 0.75 KN/M^2 is considered more appropriate to this study and will be adopted for design purposes. The major roof load may therefore be considered a uniformly distributed load. (Hereafter referred to as a udl.)

The wind load will normally act in the opposite sense to that of the self-weight and snow load, and may or may not be a udl. The wind load cannot be determined until the size and shape of the roof is known.

5.3.3 Macroscopic Design

Approximately 72% of the industrial buildings in Great Britain are based on portal frame, and steel truss and stanchion structural systems [5.1]. It may be concluded, therefore, that most of the market for industrial buildings is based upon a rectangular plan shape. Also, 40 - 44% of new industrial ground area is for extensions and thus it is important that the initial structural design should be versatile in this respect. For these reasons a rectangular roof shape will be assumed for the design study.

It was stated earlier that stressed skin structures were particularly suitable for design in grp. Also it has been acknowledged for some time that stressed skin roof structures can lead to material and financial savings. Thus for this study it is appropriate to choose a stressed skin type of structure.

It is often proposed that roofs in grp should be based upon such efficient structures as domes, hyperbolic paraboloids and other synclastic and anticlastic shapes. The dome has not been chosen in this case since the demand for circular based buildings does not appear to be high. Neither is the dome versatile when extensions are required. The hyperbolic paraboloid is most compatible with grp when the distance between supports is small enough for the whole structure to be made from one mould. In the case of large spans many moulds could be required. Also, for large hyperbolic paraboloids it is usual to use heavy solid cantilever-like edge beams for which grp is not likely to be the most economical material.

In a recent publication [5.2] concerning long-span roofs, all the systems described were made up from two-dimensional beam-like structures, i.e. portal frames, trusses, tee beams or barrel vaults. It is therefore reasonable to think in terms of a two-dimensional module, many of which may be used together to form a stressed skin roof structure. In addition, industrial buildings requiring large spans may also require large doors or openings for the movement of goods or other objects. Two-dimensional roof structures, only requiring support on two sides, automatically have provision for this.

The overall structural design chosen for study is shown in Figs. 5.1 & 2. The structure consists of two parabolic surfaces

meeting at the roof edges and separated by vertical stays and cross bracing. The roof may be considered as being split up into many beam-like sections, each placed side by side to cover the total area. In each section the upper surface is analogous to an arch, being in compression for its full length, and the lower tensile surface to an inverted arch (not a cable or membrane since it has significant flexural rigidity). Similar structures have been used previously: by Brunnel for the Saltash railway bridge, and for the "Ahoy" exhibition and sports centre, Rotterdam. The "Ahoy" structure was chosen in preference to lattice beams, roof shells, suspended roof and space frames, each of which were considered. The maximum span of the "Ahoy" complex was 90m [5.3].

The structural system conforms to the principles of design in grp according to Section 4.2 in the following ways:

- a) Grp is used according to the "monochoque" principle.
- b) The aesthetic potential of grp is used in providing clean outer and inner surfaces which may be pigmented as required.
- c) The major stress system is simple (similar to the flanges of "I" beams) allowing maximum economy of material.
- d) The symmetry of the structure will lead to economies in production.

The roof span chosen for analysis has to be large enough for grp's properties to be significant. Also it is necessary to compare the design of the roof with conventional structures and, therefore, the span must be reasonably common. 60m is considered

to be a suitable span. The span to depth ratio chosen is slightly ~~larger~~ ^{smaller} than usual, at 12:1, to compensate for the low modulus of elasticity.

5.3.4 Analysis of Roof Structure

5.3.4.1 Proposed Design of Roof Surface Element Cross-Section

The major loads that the surface elements have to take are axial. Secondary stresses are induced by bending moments and shear forces. The upper compressive surface also has to be able to take a load of 0.9 KN concentrated over an area of 0.09m^2 in any position in addition to the snow load. Also, local and Euler buckling must be resisted. Accordingly, a cylindrical shell shape as shown in Fig. 5.3 was chosen.

Since the major forces are axial the "edge-beams" are of unidirectional material ($V_f = 54\%$). The shell, which must resist local buckling, should be made, according to Section 4.3.5, from $\pm 45^\circ$ angle-ply since this was shown to be most cost-effective. However, in Chapter 3 this material was shown to be relatively weak and very susceptible to creep. Further, this material has to be tailored from rolls of woven roving at $\pm 90^\circ$, and considerable wastage results. Quasi-isotropic reinforcement has been shown to be next most cost-effective and has better strength and creep properties. CSM reinforcement has, therefore, been chosen for the cylindrical section

$(V_f = 16.5\%)$.

The use of stiffened cylindrical section greatly improves the efficiency of the shell in resisting local buckling. The addition of the longitudinal stiffeners, known as stringers, restricts the wavelength and so increases the theoretical buckling load. Isotropic cylinders have been found to be very unreliable in local buckling due to their high sensitivity to local imperfections. However, the addition of ring stiffeners has been found to considerably reduce this sensitivity by constraining buckling to the axisymmetric mode. This results in linear theory agreeing with empirical experience to within $\pm 10\%$ [5.4].

An acceptable design life for a building will depend upon the function of that building. A factory may only be designed for 25 years whereas a civic building will often be designed to last considerably longer. For this design study a life of approximately 50 years is considered reasonable. After periods of time of this order grp failure stresses and strains change slowly with time. Consequently, the additional cost incurred through choosing this life as against, say, 25 years will be small.

As the strength and stiffness of grp reduces with time, it is necessary to calculate the material properties at the end of the design life and use these to determine not only the safety factors as described in the previous chapter (Section 4.7) but also the geometric properties such as the flexural rigidity of the roof's surface unit. The flexural rigidity will be influenced by the relative loss of stiffness between CSM and unidirectional materials.

Unfortunately, it is difficult to define the roof's environment for a period of 50 years. This is the case for many reasons, including the unpredictability of weather and the fact that the precise location of the roof is unknown. However, the environment used in the time-dependent tests described in Section 3.5 is considered to be as severe as a typical British outdoor environment. The results of this section will be used to predict the performance of the design roof.

5.3.4.2 Verification of the Proposed Roof Design

Roof Loading

The self-weight of the roof is 0.28 KN/M^2 ; of this, grp accounts for 0.17 KN/M^2 . It is now possible to calculate the effective snow and wind loads.

Wind Loading

The wind pressure distribution across the upper curved surface of the roof cannot be calculated completely from British Code of Practice CP3 Ch.5 Part 2 1973 since this roof shape is not dealt with. However, Sachs [5.5] reports American recommendations for curved roofs and these have been used to determine the external pressure coefficients across the roof's surface. CP3 has been used to determine the internal pressure coefficients (C_{p_i}). The design wind speed chosen was 33.6 m/s . This allows the roof to be built in any of the large English cities or their surrounding countryside providing:

- i) the building site is in unexceptional topographical surroundings.
- ii) the overall height of the roof is not greater than 12m and that there are many wind breaks in the surrounding areas such as found in small towns or the outskirts of a small city.
- iii) There are no extraordinary safety requirements for the building.

Based on the above and the self-weight of the roof, the effective wind loads in the two principal directions are shown in Fig. 5.4a.

Snow Loading

The combined snow load and self-weight of the roof is shown, in Fig. 5.4b, to be the major load at 1.03 KN/M^2 . However, the wind load is considerable and there is justification for roof symmetry about the horizontal mid-plane.

Although the roof members have been designed and the roof loads calculated, it is not possible to compute directly the roof deflections and member forces. This is a result of the visco-elastic nature of grp which leads to the member properties being dependent upon the roof's loading history. The loading history of a roof over 50 years is very complex. However, for the purposes of this analysis the loading history will be taken as:

- 1) roof self-weight only for the initial 4×10^5 hrs.
- 2) self-weight plus snow load for the following 800 hrs. (approximately 1 month).

Thus it is assumed that creep resulting from other loads (wind, rain, snow) cancel each other out.

To calculate the roof's deflections and member forces the following procedure was adopted:

- 1) Approximate axial force in the roof's surfaces.

This was calculated from the maximum bending moment applied to the roof, plus an allowance of 5% for the shear force.

$$F = \frac{wl^2}{8d} \quad 1.05 \quad 5.1$$

where: F = axial force per metre width

w = load per unit area

l = roof span

d = maximum depth of roof

The force 'F' was calculated for both load intensities:

$$F_1 \text{ (due to self-weight only)} = 26.5 \text{ KN}$$

$$F_2 \text{ (due to self-weight plus snow load)} = 98 \text{ KN.}$$

- 2) Approximate axial strain in grp members at the end of the design life.

$$F_i = \sigma_i \text{ CYL} A_{\text{CYL}} + \sigma_i \text{ EB} A_{\text{EB}} \quad i = 1,2 \quad 5.2$$

where: σ = axial stress (N/mm^2)

A = cross-sectional area per metre width

Suffix 'CYL' refers to the cylindrical section.

Suffix 'EB' refers to the edge beams.

Since the edge beams are of unidirectional grp (UD) and the cylindrical section is of CSM, from Section 3.5.6.6 the following

equations may be written:

$$\epsilon_t \text{ CSM} = \sigma_{\text{CSM}} t^{0.091} 4149^{-1} \quad 5.3$$

$$\epsilon_t \text{ UD} = \sigma_{\text{UD}} t^{0.010} 20823^{-1} \quad 5.4$$

$$\epsilon_t \text{ UD} = \epsilon_t \text{ CSM} \quad 5.5$$

It is assumed for equation 5.5 that there is a uniform strain distribution across the width of the roof surface section. This will not, in fact, be true since there will be bending and shear forces present. Also, in the regions of the joints between sections there will be complicated strain patterns. However, these are expected to be second order effects. The bending and shear forces have been kept to a minimum by the parabolic shape of the surfaces.

From equations 5.2 to 5.5 the axial stresses and strains may be estimated after 4×10^5 hrs.:

$$\epsilon_t = 4 \times 10^5 = 7.592 \times 10^{-4}$$

$$\sigma_1 \text{ CSM} = 0.974 \text{ N/mm}^2$$

$$\sigma_1 \text{ UD} = 13.9 \text{ N/mm}^2$$

For the second period of loading

$$\epsilon_{t_2} = \frac{\sigma_1 t_2^n}{E_1} + \frac{(\sigma_2 - \sigma_1) (t_2 - t_1)^n}{E_1} \quad 5.6$$

(See Section 3.5.6.5 and Fig. 3.30.)

From equations 5.2 and 5.6 it may be calculated that:

$$\epsilon_t = 4.008 \times 10^5 = 0.0022\%$$

$$\sigma_2 \text{ CSM} = 4.27 \text{ N/mm}^2$$

$$\sigma_2 \text{ UD} = 41.5 \text{ N/mm}^2$$

3) Grp elastic properties at the end of the design life.

The apparent modulus (\bar{E}) of the two types of grp at the end of the design life may now be obtained:

$$\bar{E}_{\text{CSM}} = \frac{\sigma_2 \text{ CSM}}{\epsilon_{t2}} = 1.97 \times 10^3 \text{ N/mm}^2 \quad 5.7$$

$$\bar{E}_{\text{UD}} = \frac{\sigma_2 \text{ UD}}{\epsilon_{t2}} = 19.1 \times 10^3 \text{ N/mm}^2 \quad 5.8$$

4) Geometric properties of the grp roof members.

Now that the approximate "design life" elastic properties of the grp are known it is possible to estimate the geometric properties of the roof surface units by the method of equivalent sections. Changing the unidirectional grp of the edge-beams to the equivalent area of CSM A'_{EB} as follows:

$$A'_{\text{EB}} = A_{\text{EB}} \times \frac{\bar{E}_{\text{UD}}}{\bar{E}_{\text{CSM}}} \quad 5.9$$

it can be shown that:

- i) The roof surfaces' cross-sectional area per metre width (A_S) = $2.29 \times 10^{-2} \text{ m}^2$
- ii) The roof surfaces' second moment of area per metre width (I_S) = $3.093 \times 10^{-4} \text{ m}^4$.

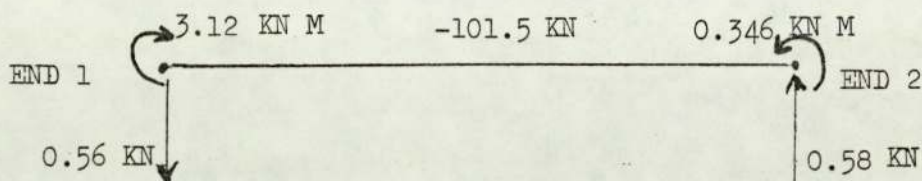
5) Computer Calculations

Using the design life structural properties of the grp members, an existing University computer programme [5.6], based upon load-displacement techniques, was used to analyse the roof structure. The idealised structural system analysed is shown in Fig. 5.5. Only the tensile half of the diagonal cross-bracing was included, since the bracing was not designed to withstand compressive forces.

The most highly-stressed part of the roof was found to be near the supports in member 3; see Figs. 5.5 and 5.6.

Grp member stresses.

Member 3 : This member was shown to be subject to the highest axial load at 101.5 KN. This force is approximately 2% greater than that used in the approximate calculations. The general loading of this member is shown below:



Again using equivalent sections theory, the purely axial stress was found to be:

-4,440 KN/M^2 in CSM material and
-43,224 KN/M^2 in UD material

The mean shear stress in the member was $64.8 \text{ KN}/\text{M}^2$, which is insignificant.

Considering end No. 1.

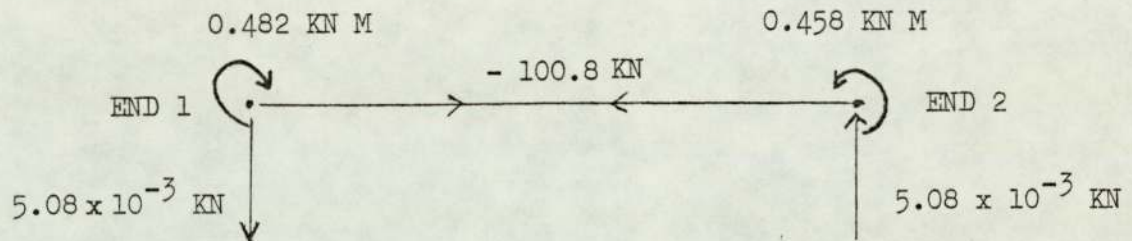
Maximum combined axial and bending stress in the CSM was found to be: $-8,247 \text{ KN}/\text{M}^2$, and the corresponding strain: -0.419% .

The maximum combined stress in the unidirectional material was $-58,680 \text{ KN}/\text{M}^2$ and the corresponding strain: -0.307% .

Considering end No. 2.

The maximum combined stress in the CSM material was calculated as $-4,854 \text{ KN}/\text{M}^2$ and in the unidirectional material as $-44,128 \text{ KN}/\text{M}^2$.

In the approximate analysis, used to calculate the referred cross-sectional area and the second moment of area, bending stresses were not considered. Hence the properties used in the computer analysis were not strictly valid. However, the regions where high bending stresses occur are very limited. The eight members with the highest bending moments, ± 3.21 KN M or ± 3.12 KN M, experience these only at one end. In the majority of members the bending moments are only 10 - 20% of these. The stresses in a typical member (11) are as follows:



The axial stress calculated for CSM was -4407 KN/M^2 and for unidirectional material $-42,704 \text{ KN/M}^2$. The shear stresses were again negligible.

End 1

The maximum combined stress was again in the unidirectional material at $-44,244 \text{ KN/M}^2$. The maximum combined stress in the CSM was found to be -4984 KN/M^2 .

End 2

The maximum combined stress in the CSM laminate
 $= - 4955 \text{ KN/M}^2$.

The maximum combined stress in the unidirectional material
 $= - 44,168 \text{ KN/M}^2$.

Thus it can be seen that although there are small regions of high bending stresses, the majority of the grp is under principally axial stress. Further, the axial stress was found to vary only about $4\frac{1}{2}\%$ across the span in the upper and lower surface.

Since the forces used in the approximate approach agree well with those determined with the use of a computer, it is considered that the design approach is satisfactory.

Roof Deflection

The maximum deflection of the roof under the action of its own weight and the snow load at the end of the design life as calculated by the computer

$$= 0.56 M = \frac{\text{span}}{107}$$

Stability of Roof Members

1) The Cross-Bracing

The diagonal cross-bracing members were designed to take tension only, and in the analysis their stiffness in compression was not taken into account. The vertical members are in compression under the snow load. The most critical member in this respect is the central vertical member 5 m. long under a load of -2.72 KN. For the purposes of analysis this member was considered as a built-in strut because of the far greater flexural stiffness of the grp surface units to which it is connected. Under these circumstances there was found to be a safety factor of 25 on the Euler buckling load.

2) Grp Roof Surface Members

Euler Buckling

The maximum compressive force occurs in members 3 and 21 under the action of the self-weight and snow load and is equal to 101.5 KN. These members are considered as simply-supported struts. In fact the unit would experience some end-restraint due to the flexural rigidity of the cross-bracing but this would be small because of the relative flexural stiffnesses. On this basis there is a factor of safety of 2.37 on the Euler buckling load (P_E) where:

$$P_E = \frac{\pi^2 E I}{l^2} \quad 5.10$$

and the symbols have their usual meaning.

Local Buckling of Cylindrical Section

Lakshmikantham and Gerard [5.4] have presented results to show that provided certain geometrical constraints were applied, the following formula was reliable in determining the local buckling loads of symmetrically stiffened cylinders:

$$N = \frac{2 (1 - \mu)^{\frac{1}{2}} (B_2)^{\frac{1}{2}}}{r D_1} \quad 5.11$$

where N = buckling load per unit width

r = cylinder radius

μ = Poisson's ratio

$$B_2 = E \left(t_s + \frac{A_r}{L_t} \right) (1 - \mu^2)^{-1}$$

$$D_1 = E I_{st} (1 - \mu^2)^{-1}$$

The conditions imposed for reliability were that:

$$\frac{B_1 D_2}{B_2 D_1} > 1.8 \quad \& \quad \frac{r}{h_r} > 100$$

and
$$B_1 = E \left(t_s + \frac{A_{st}}{L_{st}} \right) (1 - \mu^2)^{-1}$$

$$D_2 = E I_r (1 - \mu^2)^{-1}$$

t_s = skin thickness

A_r = ring area

A_{st} = stringer area

I_r = ring second moment of area

L_{st} = stringer pitch

h_r = ring depth

The proposed roof surface cylindrical section meets the above conditions and the value for N was calculated as:

$$N = -31 \text{ KN/metre width}$$

The equivalent axial stress is:

$$\sigma_{cr} = 12,550 \text{ KN/M}^2$$

The maximum mean axial stress in the cylindrical section at the end of the design life was $-4,440 \text{ KN/M}^2$. The maximum combined bending and axial stress was $-8,247 \text{ KN/M}^2$. The safety factor on the mean axial stress is 2.82 and on the combined stress 1.52.

Support of Secondary Loads

Although the skin of the cylindrical section of the roof unit is thin (2 mm) the rib stiffening system will rapidly dissipate local loads. The statutory requirement for local loading on the roof

as mentioned earlier is 0.9 KN, concentrated on a square of sides 300 mm. Such a square would be supported by at least one stringer and one ring stiffener.

5.3.5 Discussion and Assessment of Roof Design

The maximum stress in the CSM has been calculated in the previous section to be $-8,247 \text{ KN/M}^2$. Since the stress that CSM can be expected to endure continuously is approximately $35,000 \text{ KN/M}^2$ (See Fig. 3.22) and CSM in the short term tests was found to be stronger in compression, the safety factor here of over 4 is adequate. The maximum stress predicted in the unidirectional material is $-58,680 \text{ KN/M}^2$. A conservative estimate (Fig. 3.22) of the stress level that this material could withstand continuously for 50 years is $70,000 \text{ KN/M}^2$. Since this is a conservative estimate and the roof is expected to be under maximum load for only 800 hrs. the safety margin is considered satisfactory.

The short term strengths of the two materials are as follows:

(See Section 3.4)

CSM: compression = $200,000 \text{ KN/M}^2$
tension = $75,000 \text{ KN/M}^2$

Unidirectional Laminate: compression = $425,000 \text{ KN/M}^2$
tension = $640,000 \text{ KN/M}^2$

The safety factors on the short term strengths are considerably in excess of the factors recommended by Makowski (Section 4.7).

The slenderness ratio of the roof surface units is 43, and as such a safety factor of 2.37 at the end of the design life is considered satisfactory against failure by Euler buckling. Local buckling of the cylindrical section is not considered to be as critical as Euler buckling, since in itself it does not cause catastrophic failure. The safety factor of 1.52 against buckling in localised areas of high bending stresses is considered satisfactory. A safety factor of 2.82 against the mean axial stress is adequate.

The deflection of the roof at 0.56 m is considerably greater than is normally allowed in conventional roof structures. For steel structures the deflection is often limited to $1/360 \times \text{span}$, and for aluminium structures to $1/240 \times \text{span}$. The deflection ratio for the grp roof is $1/107 \times \text{span}$. This deflection is considered acceptable, however, since the stresses involved are safe and the structure does not appear to be grossly distorted (see Fig. 5.7). In a particular application of this roof structure this deflection would have to be reconsidered in the light of that application. For instance, the deflection of the roof must not damage any internal fittings.

It is apparent at this stage that designing structures in grp is considerably more complex than is the case with steel. Considerably more data on the material and the structure is required. Unfortunately, all of this data was not available for the design of the grp roof and assumptions were made. It is considered, however, that the assumptions made have been conservative but at the same time not too unrealistic. For instance, the environment chosen for estimating the creep and stress rupture of the grp was very damp. In fact the outer surface of the roof would be dry for long periods of time and at other times would be covered in water. Similar

comments could also be made about temperature. Also the upper roof surface would be frequently subject to U.V. light. To balance this however, the lower surface would be dry. An important point leading to the net effect of the assumptions being conservative is that creep was assumed to take place at 20°C. In fact creep of the roof under the snow load would take place at a temperature well below this.

To assess the efficiency of the design of the roof in grp the weight of the grp roof may be compared with the weights of conventional roof structures (Fig. 5.8). The weight of the grp roof is considerably below that of other roofing systems and in particular approximately $\frac{1}{3}$ of the weight of a portal frame roof. (The conventional roof weights were supplied kindly by I.D.C. Limited, Stratford.)

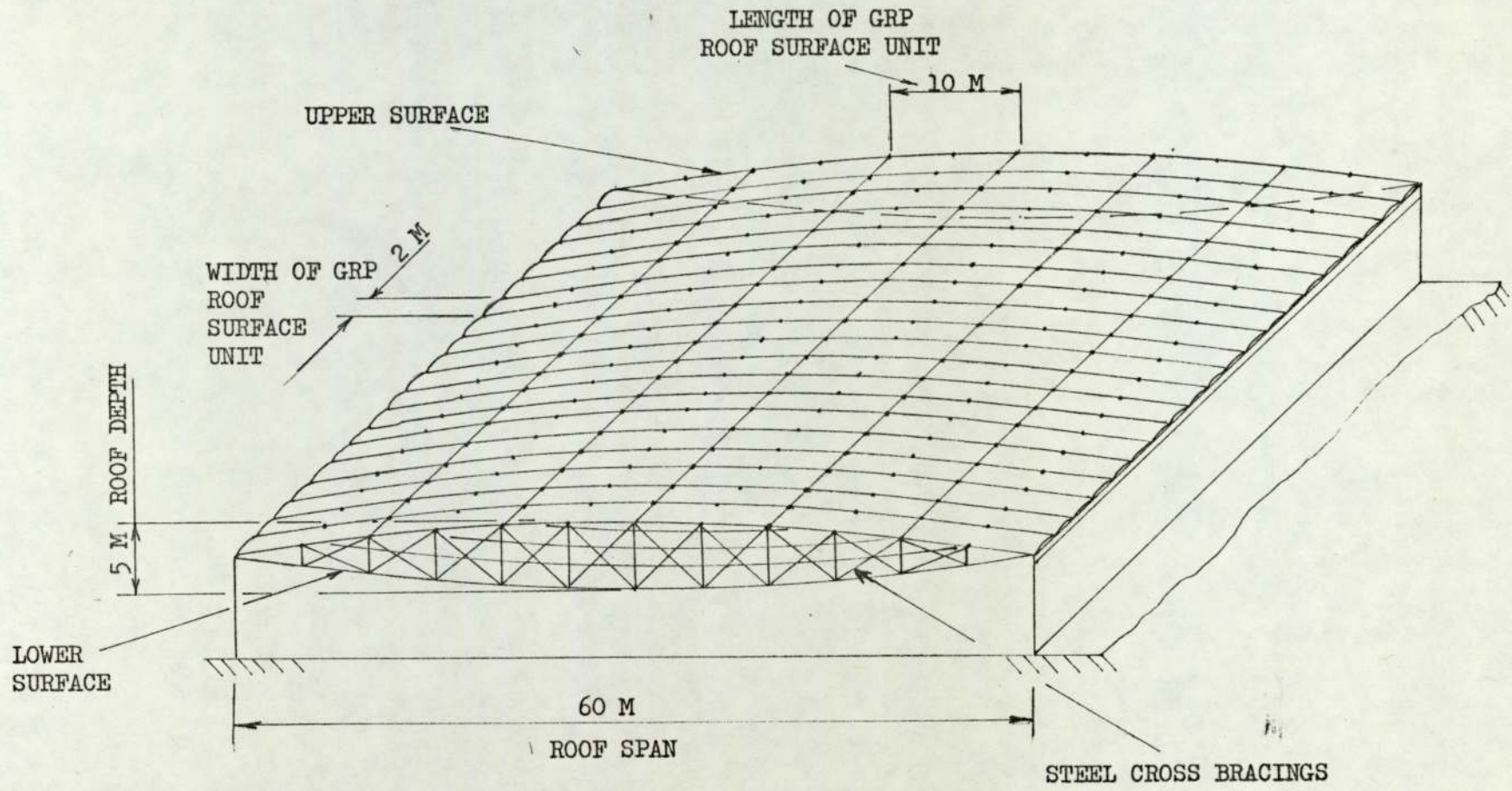


FIG. 5.1 GRP ROOF DESIGN

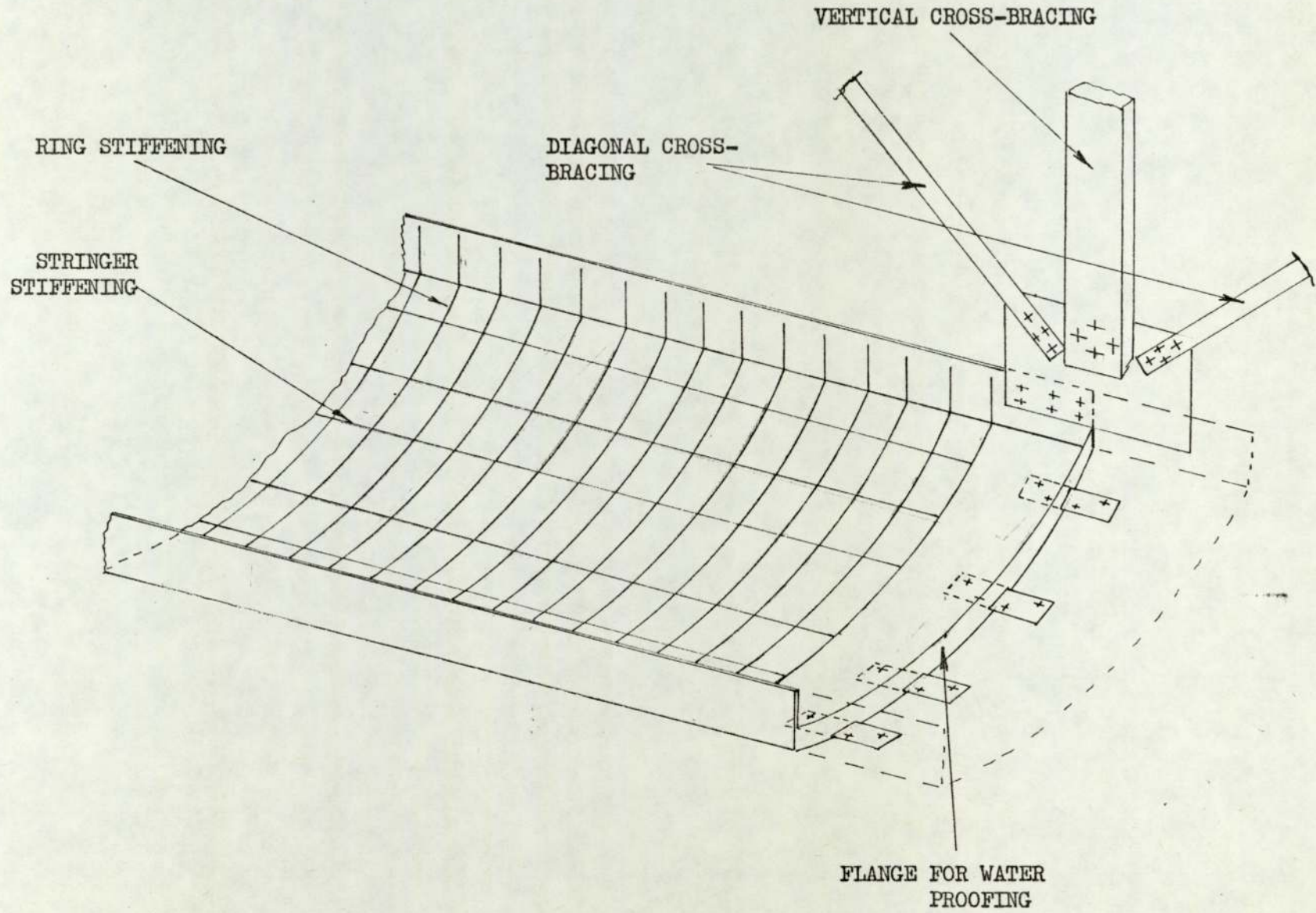


FIG. 5.2 VIEW OF LOWER SURFACE UNIT JOINT REGION

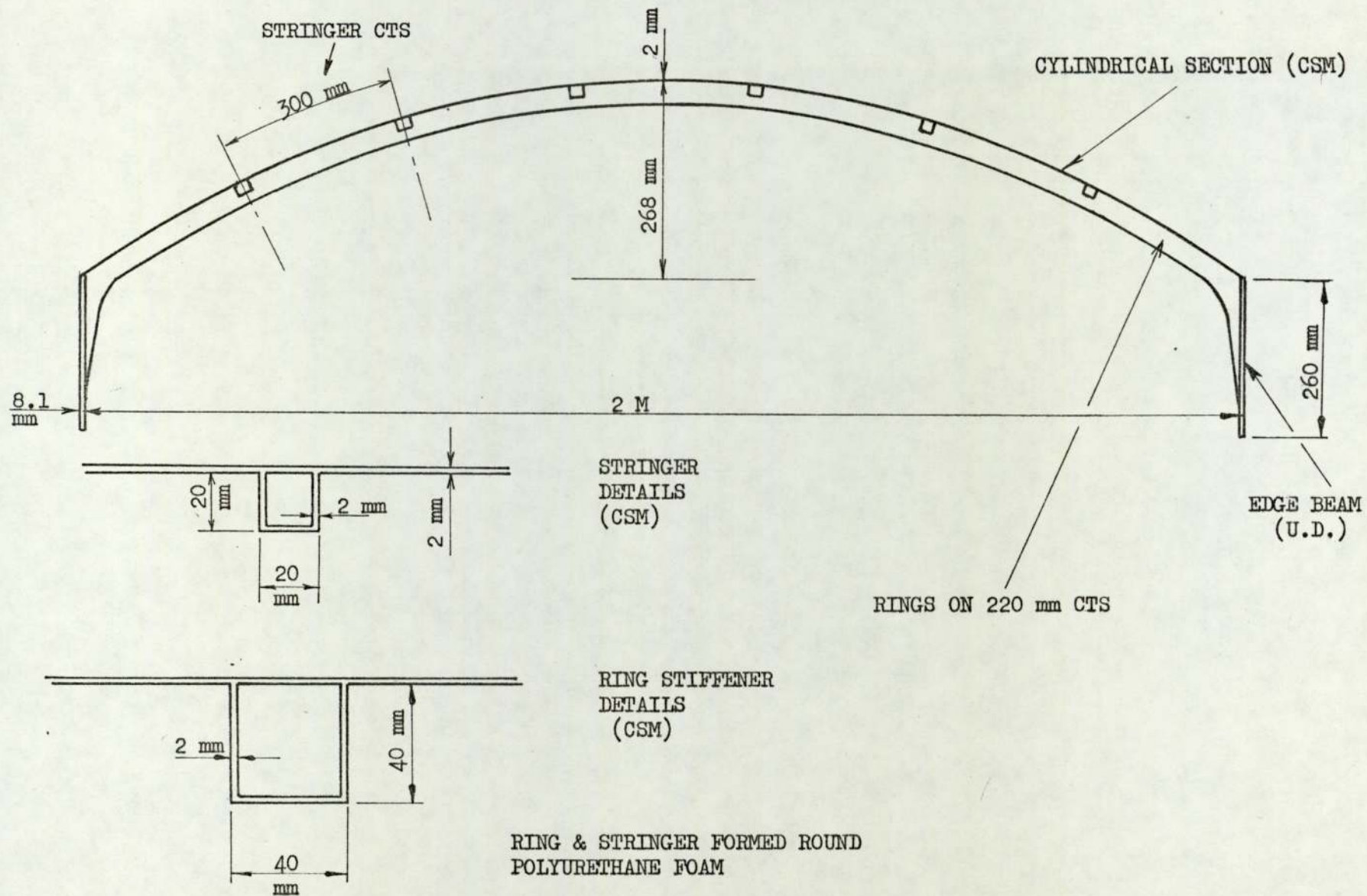
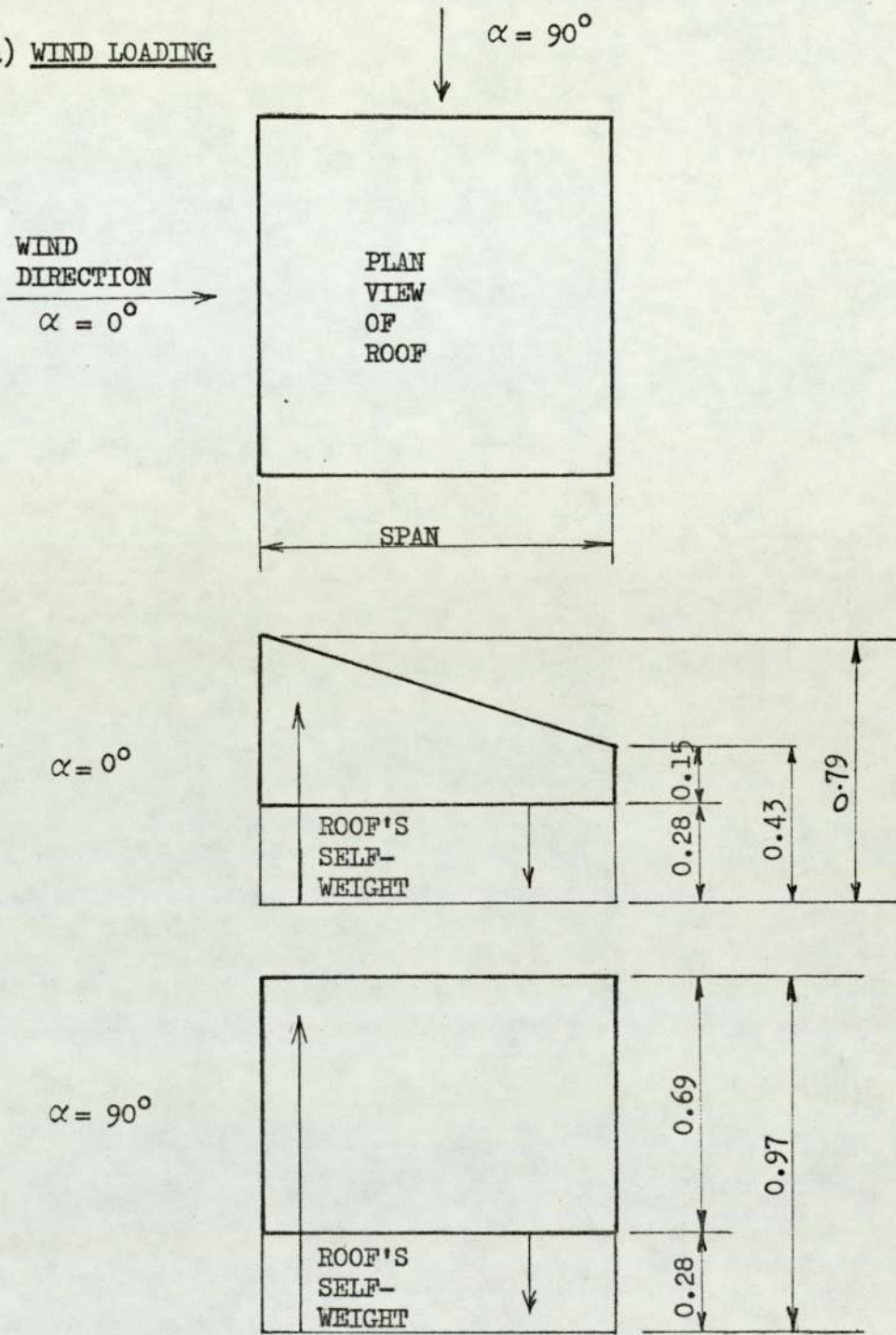


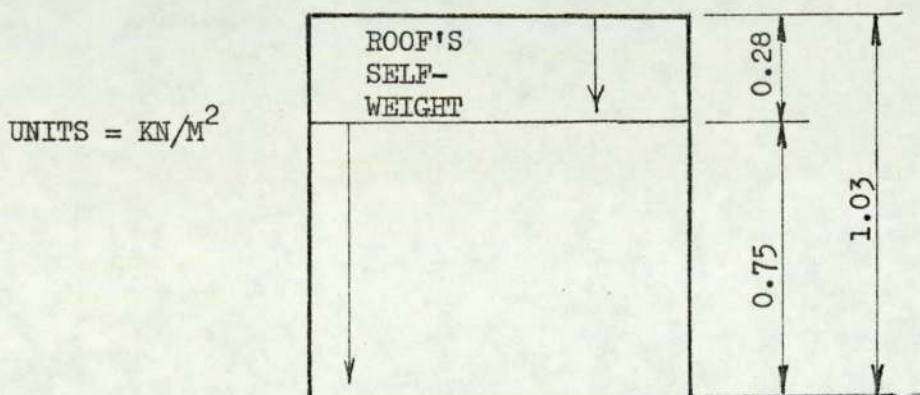
FIG. 5.3 ROOF SURFACE UNIT: CROSS-SECTIONAL DETAILS

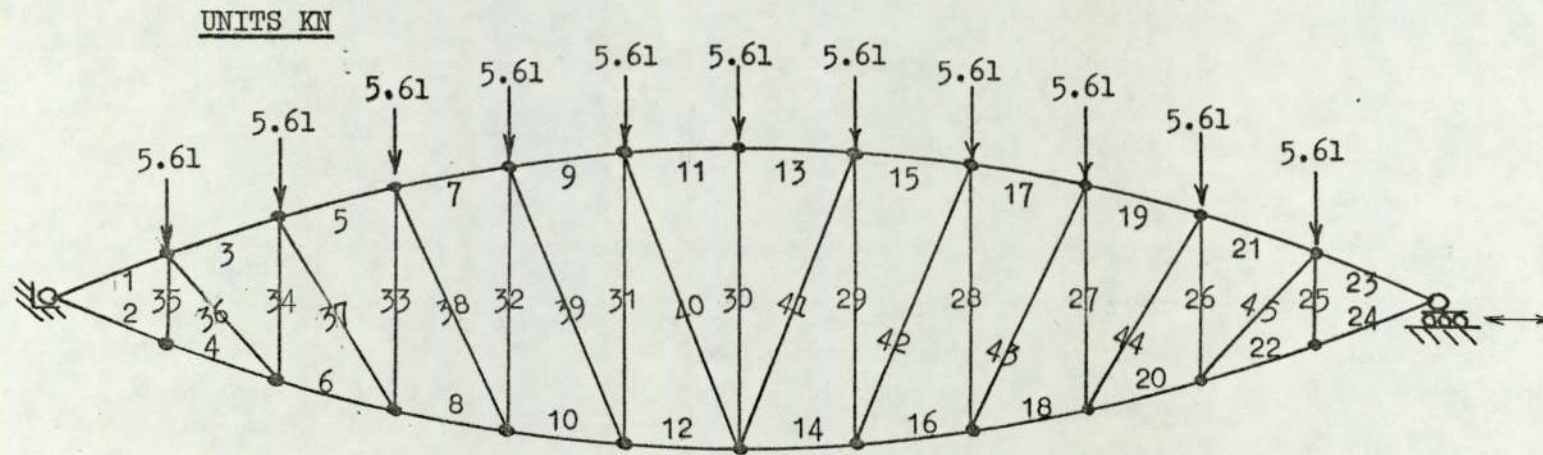
FIG. 5.4 ROOF LOADING

a) WIND LOADING



b) SNOW LOADING + SELF-WEIGHT





- PINNED JOINT
- RIGID JOINT

MEMBER PROPERTIES

	E	A _s	I _B
GRP ROOF UNITS	1.97	22.9x10 ⁻³	3.09x10 ⁻⁴
VERTICAL CROSS-BRACING	203	1.58x10 ⁻³	2.13x10 ⁻⁷
DIAGONAL CROSS-BRACING	203	1.77x10 ⁻⁴	1.0 x10 ⁻⁸

x10⁶ KN/M² M² M⁴

FIG. 5.5 IDEALISED STRUCTURAL SYSTEM

FIG. 5.6 MEMBER LOADING

MEMBER NO.	AXIAL FORCE (KN)	SHEAR FORCE (KN)	B.MOMENT END 1 (KN M)	B.MOMENT END 2 (KN M)
1	- 98	0.64	0	-3.21
2	98	-0.64	0	3.21
3	-101.5	-0.56	3.12	-0.34
4	97.6	0.56	-3.12	0.34
5	-101.1	0.07	0.37	-0.71
6	101.3	-0.07	-0.37	0.70
7	-101	-0.05	0.71	-0.48
8	100.9	0.05	-0.71	0.48
9	-100.9	0	0.48	-0.47
10	100.9	0	-0.49	0.47
11	-100.8	0	0.47	-0.45
12	100.8	0	-0.47	0.45
30	-2.7	0	0	0
31	-2.7	0	0	0
32	-2.7	0	0	0
33	-2.7	0	0	0
34	-2.2	-0.02	-0.03	-0.03
35	-1.7	0.12	0.09	0.09
36	4.3	0	0	0
37	-0.21	0	0	00
38	0.22	0	0	0
39	0	0	0	0
40	0.05	0	0	0

SIGN CONVENTION : THE RIGHT HAND SCREW RULE IS ASSUMED. TRANSLATIONS AND ROTATIONS IN A POSITIVE SENSE WITH RESPECT TO THIS RULE ARE POSITIVE.

SCALE 1:250

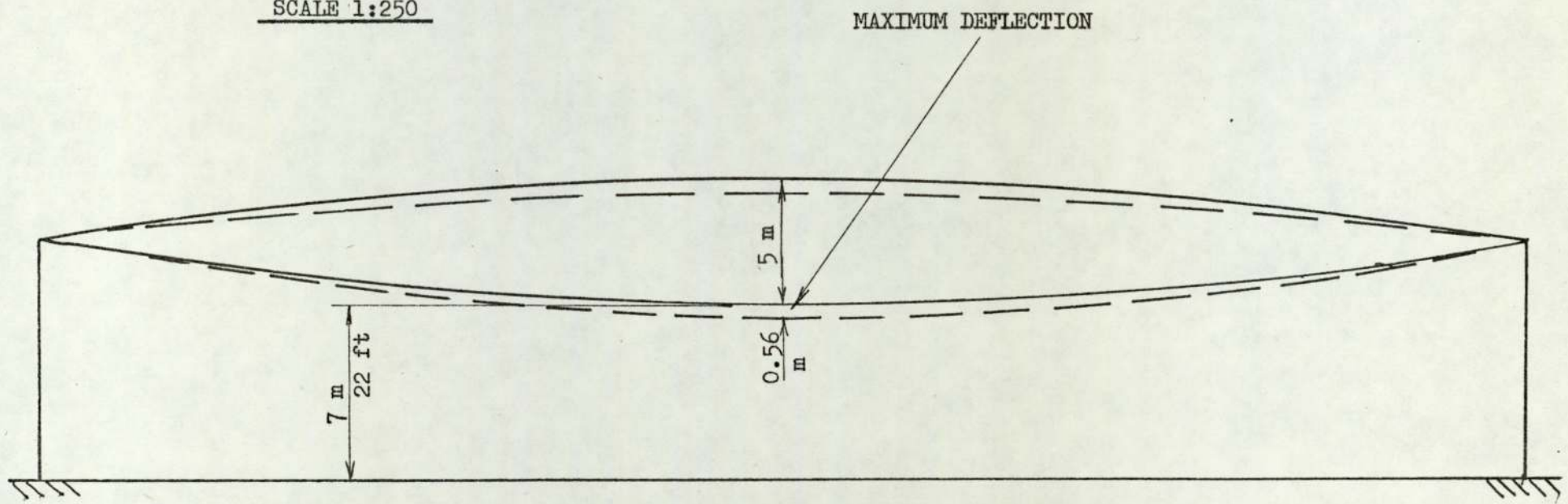
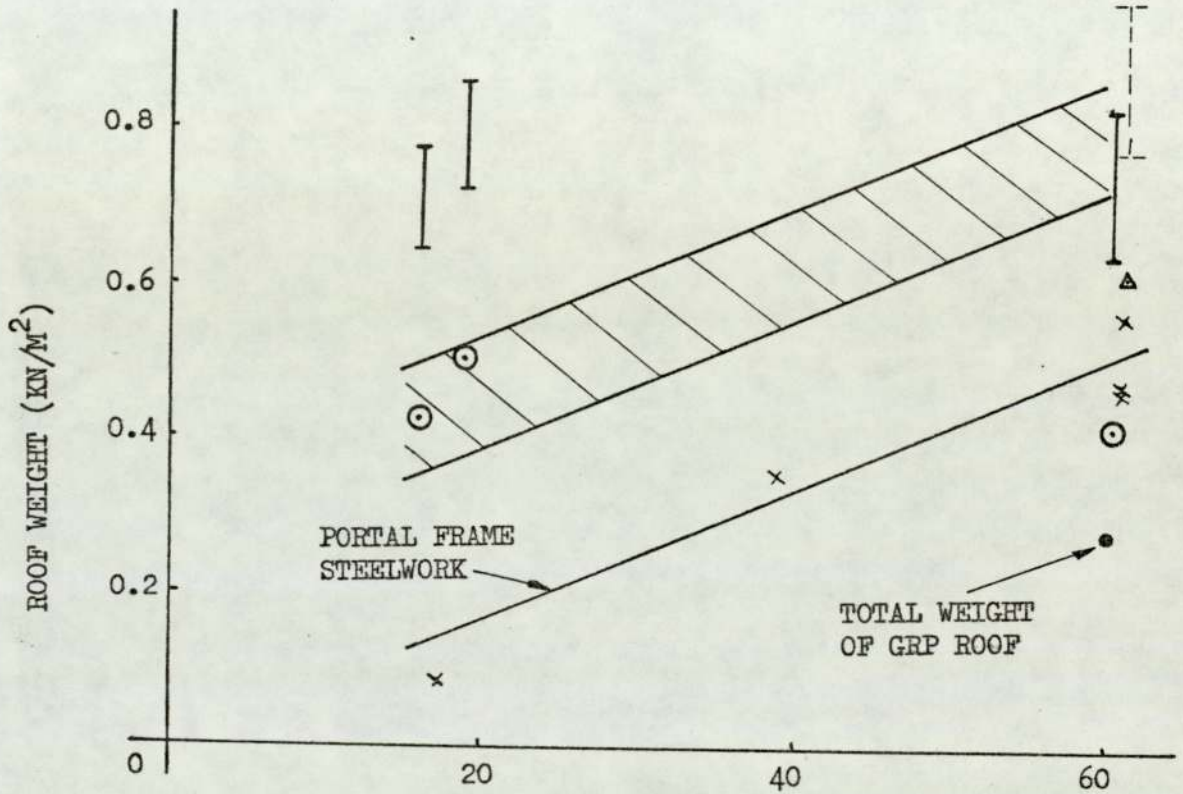





FIG. 5.7 ROOF DEFLECTION

FIG. 5.8 ROOF WEIGHT AGAINST SPAN



<u>STEEL WORK WEIGHTS</u>		<u>RANGE OF CLADDING WEIGHTS</u>	
x	PORTAL FRAME		PORTAL FRAME
⊙	LATTICE FRAMES (VARIOUS TYPES)		LATTICE FRAMES
△	POST-TENSIONED PRECAST CONCRETE ARCH		POST-TENSIONED PRECAST CONCRETE ARCH

CHAPTER 6

DESIGN, MANUFACTURE AND TESTING OF

A MODEL LONG SPAN ROOF

CHAPTER SIX

Design, Manufacture and Testing of a Model Long Span Roof

6.1

Introduction

In the previous chapter a preliminary design of a 60 m span grp roof was presented. In this chapter a model roof will be designed using similar principles. This will be followed by a brief description of the manufacture of the roof.

The purpose of the model roof is: a) to enable various tests to be applied so that the accuracy of the structural analysis may be examined, and b) to confirm the predicted structural behaviour of the roof as a whole and hence the suitability of grp as a structural material.

The model roof testing will be carried out in three stages: the roof will be tested under a uniformly distributed load simulating snow loading; secondly, under an unsymmetrical load to simulate behaviour under wind loading, and finally the roof will be left for an extended period under a simulated snow load so that the creep characteristics of the roof may be studied.

6.2

Scale of Model Roof

The size of the designed roof makes it impossible to build for testing within the resources of this project. Instead, a scaled down roof will be designed. A suitable scale for the model roof is 1/6th of the full size. This scale is large enough for the model to be reasonably realistic in shape and proportion, and small enough to be within the project's resources.

Although the major dimensions of the roof, such as span-to-depth ratio, will be designed to this scale, it will in some cases be impractical and in others imprudent to do so. For instance, the length of the surface units will be designed to a 1/5th scale so that the model surface unit's resistance to Euler buckling will be reduced to a level closer to that of the full scale roof. Also the manufacture of the model is simplified.

6.3.1 Surface Unit Design

The cross-section of the model surface unit is shown in Fig. 6.1. It will be noticed that orthotropic stiffening has not been included in the design. As it is not practical to reduce the skin thickness of the 60 m roof (2 mm) by a factor of 6, the model roof's skin is relatively thick at 1.49 mm, and stiffening is not required.

The distance between joints has been reduced by a factor of 5 to 1 M, making the length of each surface unit 2 m and the distance between cross-bracing joints 1 m.

The edge-beam stiffening shown in Fig. 6.1 is to be included on the outer edges of the compressive surface of the model. In this position there are no adjacent units to support the edge-beams against buckling. The diaphragm shown in the cross-sectional view is included in all the compressive surface units to prevent "flattening" of the cylindrical section.

6.3.2 Cross-bracing Design

The design of the cross-bracing is mainly influenced by the test loading technique. It is proposed to load the model using dead

weights slung below the roof. Thus all the cross-bracing may be designed for tensile forces only. This arrangement has the disadvantage that the vertical cross-bracing members are not used in precisely the same way as they would be under the snow load in the full size roof. However, this is not considered to be a serious disadvantage, since it does not affect greatly the grp members which are of most interest and concern. The arrangements considered to avoid this were either too complicated, expensive, inaccurate or required equipment which was not available. It should also be realised that the arrangement adopted is realistic in the case of wind loads, i.e. the vertical cross-bracing members would be expected to be in tension under this load.

The cross-sectional area, A_S , of the vertical cross-bracing is 600 mm^2 and the diagonals are 300 mm^2 and the second moment of areas, I_S , are 2290 mm^4 and 271 mm^4 respectively.

6.3.3 Joint Design

The joints between the grp surface units may be divided into two groups. Firstly, the joints in the cylindrically shaped part and secondly the edge-beam joints. The cylindrical section joints are shown in Fig. 6.2 and the edge-beam joints are shown together with a typical cross-bracing joint in Fig. 6.3.

6.3.4 End Fixing Design

The roof support and end joints are shown in Fig. 6.4. The knife edges employed effectively make the joints pinned, as was assumed in the analysis of the 60 m roof in Chapter 5 (Fig. 5.5). A small amount of horizontal movement was allowed for in the size of the "vee" support locating holes at one end.

6.3.5 Materials Summary

Fig. 6.5 shows the overall design of the model roof structure. The width of the roof, is 1 m, i.e. three beam-like elements. For two main reasons this width is considered to be the minimum required for testing. Firstly, a narrower roof would be susceptible to lateral buckling. The two outside beams are special cases since they have support only on one side. This is particularly important in the compressive surface which is subject to instability effects. Thus only the centre beam is a typical roof beam-like element.

The materials required for the roof structure as shown in Fig. 6.5 are as follows:

CSM 21 kg or 2.1 kg/m^2

Roving 12.6 kg or 1.26 kg/m^2

Polyester resin 65 kg or 6.5 kg/m^2

Total weight of grp in roof 98.6 kg or 9.9 kg/m^2

Total weight of steel 140 kg or 14 kg/m^2

Total self-weight of the roof is 0.23 KN/m^2 .

6.3.6 Analysis of Model

The analysis of the model roof will be carried out in three stages as follows:

- 1) Analysis based upon the theoretically determined elastic properties of grp.
- 2) Analysis based upon the experimentally determined elastic properties (Section 3.4).
- 3) Analysis based upon the visco-elastic properties of grp (Section 3.5) under prolonged loading.

6.3.6.1 Theoretical Elastic Analysis

The approach to the loading of the model roof will be similar to that adopted in the previous chapter. The uniformly distributed snow load will be idealised to nine discrete equal loads. The idealised system is shown in Fig. 6.6. The non-symmetrical wind loading is also idealised as shown in Fig. 6.6.

Based on the theories discussed in Sections 3.2 and 3.3 the following moduli may be calculated:

$$E_{\text{CSM}} (V_f = 0.16) = 7.74 \times 10^6 \text{ KN/M}^2 \text{ (See Fig. 3.10)}$$

$$E_{\text{UD}} (V_f = 0.32) = 25.58 \text{ KN/M}^2 \text{ (See Fig. 3.6)}$$

On the same basis it follows that:

$$\mu_{12, \text{CSM}} = \mu_{21, \text{CSM}} = 0.32 (V_f = 0.16)$$

By changing the unidirectional material of the edge-beams to an equivalent volume of CSM by the method of equivalent sections according to equation 5.9 it may be shown that:

$$A_S = 4.49 \times 10^{-3} \text{ m}^2$$

$$I_S = 3.27 \times 10^{-6} \text{ m}^4$$

On feeding these properties into the computer programme [5.6] the following were obtained:

Snow Loading

$$F_{\text{max}} = - 11.6 \text{ KN (Member 10 and 12)}$$

Max. bending moment applied to grp roof unit

$$= \pm 9.35 \times 10^{-2} \text{ KN M (Members 1, 2, 19 and 20)}$$

Max. deflection of roof = 12.7 mm (At centre line).

Wind Loading

$$F_{\text{max}} = - 5.73 \text{ KN (Member 4)}$$

Max. bending moment applied to grp roof unit

$$= - 5.0 \times 10^{-2} \text{ KN M (Member 2)}$$

Max. deflection of roof = 9.40 mm (At centre line).

6.3.6.2 Empirical Elastic Analysis

The applied loading for this analysis is identical to that used for the above computations.

From graph 3.6 and 3.10 it may be determined that the actual elastic moduli of the grp materials used are:

$$E_{\text{CSM}} = 7.05 \times 10^6 \text{ KN/M}^2$$

$$E_{\text{UD}} = 20.0 \times 10^6 \text{ KN/M}^2$$

Again using the method of equivalent sections, the following may be determined:

$$A_S = 4.13 \times 10^{-3} \text{ m}^2$$

$$I_S = 3.10 \times 10^{-6} \text{ m}^4$$

Computations based upon the modified data above lead to member loadings as tabulated in Figs. 6.7 and 6.8 for snow and wind loadings respectively. The tables show that the highest stresses are, as expected, due to the snow loading. The maximum deflection is shown to be 14.5 mm in table: Fig. 6.9.

The tabulated forces and moments and the equation below may be used to calculate the various stresses and strains.

$$\sigma = \frac{F}{A_S} \pm \frac{M y}{I_S} \quad 6.1$$

where σ = direct stress referred to CSM

F = member axial force

M = applied bending moment

y = distance from the neutral axis

y_{max} = 46 mm for the cylindrical section and
39 mm for the edge-beams.

Shear stresses have been neglected as insignificant and

will be less than 15 KN/M^2 .

From equation 6.1 it may be shown that the stress due to solely the snow load are:

1) For CSM: a) the maximum compressive stress, predicted in the cylindrical sections, is in members 10 and 12 and equal to $-2,800 \text{ KN/M}^2$.

b) the maximum compressive stress, predicted in the edge-beams, is in members 2 and 20:- $- 3500 \text{ KN/M}^2$.

c) the maximum tensile stress is in members 1 and 19:- $3,700 \text{ KN/M}^2$.

2) For unidirectional material:

a) the maximum compressive stress occurs in members 2 and 20:- $- 9,950 \text{ KN/M}^2$.

b) the maximum tensile stress occurs in members 9 and 11:- $7,800 \text{ KN/M}^2$.

To calculate stress in the unidirectional material, equation 6.1 is multiplied by a factor: $\frac{E_{UD}}{E_{CSM}}$

In cases 1b) and 2a) the maximum stresses occur at a cross-bracing node where there is some local reinforcement. The maximum stresses will, therefore, be very slightly lower.

If the self-weight of the model roof is allowed for, the stresses are increased by the following factor:

$$\frac{\text{model self-weight} + \text{snow load}}{\text{snow load}} = 1.31$$

6.2

The maximum stresses then become:

- 1) a) - 3,670 KN/M²
 b) - 4,590 KN/M²
 c) 4,850 KN/M²
- 2) a) - 13,000 KN/M²
 b) 10,200 KN/M²

The short term strength for CSM in tension, which is less than the compressive strength, is approximately 75×10^3 KN/M², giving a short-term safety factor of over 15. The corresponding strength of the unidirectional material is approximately 300×10^3 KN/M² giving a minimum safety factor of over 20.

Stability of cylindrical section

The critical stress for a cylinder subjected to an axial compressive load is given by Timoshenko 6.1 as:

$$\sigma_{cr} = \frac{E h}{a \left(\frac{3}{1 - \mu^2} \right)^{\frac{1}{2}}} \quad 6.3$$

However, cylinders are known to be very susceptible to imperfections of the cylinder wall so that the stress level predicted by equation 6.3 is never reached in practice. A more reliable equation is suggested by Little [6.2] as follows:

$$\sigma_{cr} = \frac{0.33 E h}{a \left(\frac{3}{1 - \mu^2} \right)^{\frac{1}{2}}} \quad 6.4$$

where h = cylinder wall thickness
 a = cylinder radius

Based upon equation 6.4 the critical stress of the cylindrical section is -6350 KN/M^2 giving a safety factor of 1.73 on the stress in the cylindrical section due to the snow load and self-weight. This, however, will be a slightly conservative estimate since the section is under combined bending and axial compression. Timoshenko [6.1] estimates an increase of about 30% in the critical stress for the pure bending case.

Euler buckling of surface unit

Treating the roof surface units as simply supported struts as in the previous chapter the buckling load is given by equation 5.10:

$$P_E = \frac{\pi^2 EI_s}{l^2} = 216 \text{ KN}$$

The maximum compressive axial force occurs in members 10 and 12, -11.6 KN, giving a factor of safety of 18.6.

Buckling of Steel Cross-bracing

Under wind loading steel work members 34 are under compression. There is a danger, therefore, of Euler buckling. As there is a large difference between the rigidities of the grp surface members and the cross-bracing, member 34 will be treated as a strut with rigid ends. Thus the buckling load (P_E) is given by:

$$P_E = \frac{4 \pi^2 E I}{l^2} = 1.27 \text{ KN/M width of roof}$$

The theoretical member load is given in Fig. 6.8 as 0.27 KN giving an adequate safety factor of 4.7.

6.3.6.3 Visco-elastic Analysis

It is intended to load the model roof simulating snow loading for a period of 4 weeks (672 hrs.). To calculate the approximate change in deflection over this period of time equations 5.2 to 5.5 will be used. In this case F equals the mean axial force in the grp members computed from table Fig. 6.7 and is equal to 10.95 KN.

$$\begin{aligned}\sigma_{\text{CSM}} &= 1266 \text{ KN/M}^2 \\ \sigma_{\text{UD}} &= 10,923 \text{ KN/M}^2 \\ \bar{E}_{\text{CSM}} &= 2.30 \times 10^6 \text{ KN/M}^2 \\ \bar{E}_{\text{UD}} &= 19.3 \times 10^6 \text{ KN/M}^2 \\ I_{\text{S}} &= 4.36 \times 10^{-6} \text{ m}^4 \\ A_{\text{S}} &= 8.50 \times 10^{-3} \text{ m}^2\end{aligned}$$

The deflection at the end of the loading period (δ_v) may be estimated in the following way:

$$\delta_v = \frac{\delta_{\text{EP}} \times (\bar{E}_{\text{CSM}} \times A_{\text{S}})_{\text{EP}}}{(\bar{E}_{\text{CSM}} \times A_{\text{S}})_v} \quad 6.4a$$

where suffix v refers to visco-elastic term suffix EP refers to an empirical elastic term.

$$\delta_v = 20.7 \text{ mm}$$

It is assumed here that the change in deflection is due to the change in axial stiffness of the grp members of the model roof structure. It is also assumed that the change in stiffness will not

lead to a large redistribution of load within the structure. This is supported by the fact that the difference in the loads in the grp members in the two elastic analyses was small. The axial force in members 10 and 12 remained unchanged and maximum bending moment in member 2 changed by only 10%.

The flexural rigidity (EI_g) of the grp members is reduced, i.e. from 21.9 KN M^2 to 10 KN M^2 , leading to a reduced but still adequate safety factor (≈ 7) against Euler buckling.

6.4

Preliminary Tests

6.4.1 Surface Unit Compression Test

6.4.1.1 Introduction

It is proposed to test the model roof upto a load equivalent to 1.75 times the snow load. Thus, at this maximum short term load, including the roof's self-weight, the safety factor of Section 6.3.6.2 will be reduced by a factor of 1.57. The safety factor for local buckling thus becomes 1.1. This may be inadequate to prevent local buckling due to the empirical nature of equation 6.4.

Local buckling of the cylindrical section will lead to a redistribution of stress in the surface unit. This, in turn, may lead to further buckling. In addition, thin-walled open sections have

been known to buckle in unexpected modes and thus it is considered necessary to carry out a preliminary compression test on a surface unit. Further, such a test provides an opportunity to examine:

- a) the compressive strength of joints similar to the surface unit joints, and
- b) the accuracy of the buckling formula, equation 6.4.

6.4.1.2 Description of Test

Fig. 6.13 shows a general view of the test specimen and equipment. The roof unit is shown as a column with its edges stiffened with special aluminium channel. The purpose of the edge stiffening is to simulate the support given to the edges, in the roof, by adjacent units. Fig. 6.14 shows a more detailed view of this arrangement. Of the several fixing screws in each stiffening section only one is tightened firmly. The others are "finger-tightened" only. This ensures that the aluminium does not take any axial load.

The column is mounted between two concrete blocks which are located in a large testing frame. The joints between the test specimen and the concrete blocks are equivalent to the inter-unit joints of the roof shown in Figs. 6.2 and 6.3. The steel joint plates are, however, set into the concrete blocks rather than in adjoining units.

The load was applied to the test specimen by use of a large calibrated hydraulic jack. The maximum load applied was built up in increments of 2.5 KN to 20 KN.

Electrical resistance strain gauges were used to detect the onset of local buckling (see Fig. 6.15). A dial test indicator was placed level with the web of the cylindrical section, where local buckling would not occur, to detect bending of the column. The electrical resistance strain gauges were used in conjunction with a computerised data logger. This enabled the time between load increments to be kept to a minimum and hence minimise the effect of creep.

6.4.1.3 Results of Test

Table, Fig. 6.16 shows strain gauge results and Fig. 6.17 shows a graph of lateral deflection against load as measured by the dial test indicator. These results indicate that the strain is approximately uniform throughout the section and that it is directly proportional to load up until the onset of local buckling. However, on close examination it can be determined that the strain and hence the axial load is greater in the edge-beams than in the cylindrical section. In fact, at a load of 12.5 KN the mean strain of all the edge-beam strain gauges is $- 1.374 \times 10^{-3}$ M/M, whereas in the cylindrical section the mean measured strain is $- 1.194 \times 10^{-3}$ M/M. The theoretical strain at this load is $- 1.290 \times 10^{-3}$ M/M. This compares well with the mean of all the strain gauge results, $- 1.284 \times 10^{-3}$ M/M. Fig. 6.18 shows the strain distribution at section A-A (Fig. 6.15) and the tendency for lower strain in the cylindrical section. This may be explained by the propensity of stress to be attracted to the stiffer elements of structures at the expense of the less stiff. Imperfections in the cylindrical part of the specimen will cause local

bending. This effectively reduces the axial stiffness of the material causing higher stresses to be taken by the relatively stiff edge-beams and the regions close to the corners between the cylindrical section and edge-beams.

The onset of buckling was observed visually (Fig. 6.19) at a load of 12.8 KN which corresponds to an overall mean strain of $- 1.330 \times 10^{-3}$ M/M. Allowing for the non-uniform strain distribution between the sections of the specimen the mean strain in the cylindrical section was $- 1.200 \times 10^{-3}$ M/M. The corresponding stress is $8,600 \text{ KN/M}^2$. From equation 6.4 the theoretical buckling stress is $6,350 \text{ KN/M}^2$ which is a factor of 1.35 lower.

Figs. 6.20 and 6.21 show the effect of buckling on the load-strain relationship is to cause sharp discontinuities. On further increases of load, buckling develops further until at 20 KN local buckling was general throughout the specimen including the short unsupported lengths of the edge-beams (see Fig. 6.22). However, no material failure occurred and on unloading, the specimen recovered its original geometry.

Fig. 6.17 shows a graph of lateral displacement of the specimen, as measured by the dial test indicator, against load. Again the graph is linear upto buckling, whereupon a sharp discontinuity occurs. The maximum deflection, however, was approximately 1.3 mm and occurred after buckling. This corresponds to a span to deflection ratio of 770:1 and indicates that little bending took place.

The joints showed no signs of damage as a result of the test. The maximum axial stress in the CSM material was $- 14,500 \text{ KN/M}^2$ and

the maximum compressive stress expected in the model roof is
- 7200 KN/M².

6.4.1.4 Conclusions

- 1) The local buckling stress of the cylindrical section was 8,600 KN/M². Equation 6.4 was shown to be conservative in this case. On the basis of this result the equation may be modified to:

$$\sigma_{cr} = \frac{0.45 E h}{a \left(3 (1 - \mu^2) \right)^{\frac{1}{2}}}$$

However, a wide range of values for buckling stress would be expected from a large number of test specimens, and would depend upon the irregularities of each specimen.

- 2) No indication of Euler buckling of the specimen was found before or after local buckling.
- 3) Grp is capable of complete recovery after buckling.
- 4) The joints are capable of sustaining greater loads than they are expected to encounter during tests of the model roof.
- 5) There is a tendency for the cylindrical section to take less load than expected theoretically.

- 6) The design is adequate for use in testing the model roof.

6.4.2 Tensile Joint Tests

6.4.2.1 Introduction

Insufficient theory or data is available to be able to design reliably the joints for the model roof. In the previous section a joint design was proved in compression; in this section the joints will be tested in tension. Other similar joints will be also tested for comparison.

6.4.2.2 Description of Tests

The grp lay-up for all the joints was as shown in Figs. 6.2 and 6.3; the details of the proposed model roof joints, which are denoted as Type A. The details of the other joints to be tested are shown in Figs. 6.23 and 24. In all cases the joints were tested in a Denison testing machine at a strain rate causing failure within 1.5 to 2.5 mins.

6.4.2.3 Results of Tests

Cylindrical Section Joints

The strongest joint was type B, Fig. 6.23, which failed at 11.6 KN. Fig. 6.25 shows the failed specimen. Joint type A Fig. 6.2 failed at a marginally lower load of 10.2 KN and is shown in Fig. 6.25. The weakest joint was type C, Fig. 6.26 with a failure load of $0.6 T_f$.

Edge-beam Joints

Of the two types of edge-beam joints tested, type A, Fig. 6.3 was the stronger with a failure load of 25.3 KN. Type B, Fig. 6.24 failed at 23.5 KN. The failed specimens are shown in Fig. 6.27.

6.4.2.4 Discussion of Results

The failed specimens in general show clear evidence of material crushing at the bolts, which is an indication that the edge and side distances, measured from the holes, are adequate (see Section 4.6.2). Modification of these distances would, therefore, not be expected to increase the strength of the joints for a given hole arrangement.

Although previous evidence suggests that several small bolts are preferable to a smaller number of large bolts (see Section 4.6.2) this was not found to be the case in this instance for the cylindrical section joints.

The strength of the cylindrical section joint, A, used in the model roof design is capable of producing a stress in the section of $63,400 \text{ KN/M}^2$, whereas the maximum tensile stress expected in the section under the design load is 4850 KN/M^2 giving a safety factor of about 13. The safety factor for the edge-beam joint is greater than this.

Although the cylindrical section joint B is stronger than the designed model joint A, it is not proposed to use the joint B as its large hole is more difficult to manufacture than the two smaller holes of joint A.

6.4.2.5 Conclusions

- 1) The strongest joints were found to be cylindrical section joint B and edge-beam joint A.
- 2) The joints used in the design of the model roof (types A) are adequate.

6.5

Model Roof Manufacture

The grp roof members were manufactured by the hand lay-up process described in Sections 2.10.1 and 4.4.1 using a female mould.

The steel work was manufactured from hot-rolled mild steel and required only cutting to size and drilling.

The roof was assembled on its side using a floor to mark out the roof shape. The roof, having been bolted together, was correctly orientated and lifted onto its supports with the aid of hydraulic fork lifts.

Typical inter-surface section joints are shown in Figs. 6.2 and 6.3 and a cross-bracing node where sections are not joined is shown in Fig. 6.10. The roof supports are shown in Fig. 6.4 and a general view of the roof can be seen in Fig. 6.11.

6.6

Model Roof Testing

6.6.1 Introduction

In this section the model roof testing technique will be described. To prove the roof design and to confirm its predicted behaviour, the testing will be carried out in three stages: firstly a uniform load, equivalent to the statutory snow load x 1.75, will be applied to the roof over a short period of time to examine the elastic behaviour; this will be followed by a test under non-uniform loading to examine the elastic response to wind loading; and finally the roof will be tested under prolonged snow loading and the creep behaviour of the roof observed.

6.6.2 Loading Details

The loading system of the model roof corresponds in principle to the system shown in Fig. 6.6. The dead-weights were supported by means of specially made trays and nylon ropes from the lower cross-bracing nodes as shown in Fig. 6.12. The dead-weights themselves consisted of rectangular buckets filled to various degrees with scrap iron so that the maximum load of 1.75 x the snow load could be applied in seven increments. Unfortunately, for practical reasons it was not possible to simply add additional buckets for each increment: it was necessary to replace buckets leading to an irregular loading cycle. Three groups of buckets, corresponding to $\frac{1}{4}$, $\frac{1}{2}$ and 1 x the snow load, were used in the following ways.

A) Snow Load:

Increment	Buckets (x snow load)
1	$\frac{1}{4}$
2	$\frac{1}{2}$
3	$\frac{1}{4} + \frac{1}{2}$
4	1
5	$1 + \frac{1}{4}$
6	$1 + \frac{1}{2}$
7	$1 + \frac{1}{4} + \frac{1}{2}$

B) Wind Load:

Increment	Buckets (x snow load)		
	Joint Nos.	Joint Nos.	Joint Nos.
	16,18,14,12	10	8,6,4,2
1	$\frac{1}{2}$	$\frac{1}{4}$	0
2	$\frac{1}{4} + \frac{1}{2}$	$\frac{1}{2}$	$\frac{1}{4}$
3	1	$\frac{1}{4} + \frac{1}{2}$	$\frac{1}{2}$
4	$1 + \frac{1}{4}$	1	$\frac{1}{4} + \frac{1}{2}$
5	$1 + \frac{1}{2}$	$1 + \frac{1}{4}$	1
6	$1 + \frac{1}{4} + \frac{1}{2}$	$1 + \frac{1}{2}$	$1 + \frac{1}{4}$

C) Creep Test Loading:

Load intensity was constant as per increment 4 of the snow loading test.

For cases A) and B) 10 mins. were allowed inbetween increments of load.

6.6.3 Gauging

The behaviour of the roof was monitored by the use of electrical resistance strain gauges, in conjunction with a computerised data logger, and dial test indicators for the short term tests. The dial test indicators were used alone for the creep test.

176 strain gauges were used to detect the onset of buckling and to check the predicted member forces. All strain gauges were used in pairs: one on each side of the section to be gauged. By taking the mean reading of these pairs, the effect of local bending in the direction of the roof beams' axis could be eliminated. Three main roof sections were examined with the gauges: the central regions of members 19 and 20, 17 and 18 and members 11 and 12. Steel work members 21, 22, 36 and 37 between beams A and B and beams B and C were also gauged.

Four dial test indicators were used to measure the deflection of the lower surface of the roof as follows:

Dial Test Indicator	Joint No.	Beam No.
1	4	B
2	10	B
3	10	A
4	16	B

The location of indicator 1 may be seen in Fig. 6.12.

The temperature of the environment varied between 14' - 16°C during testing.

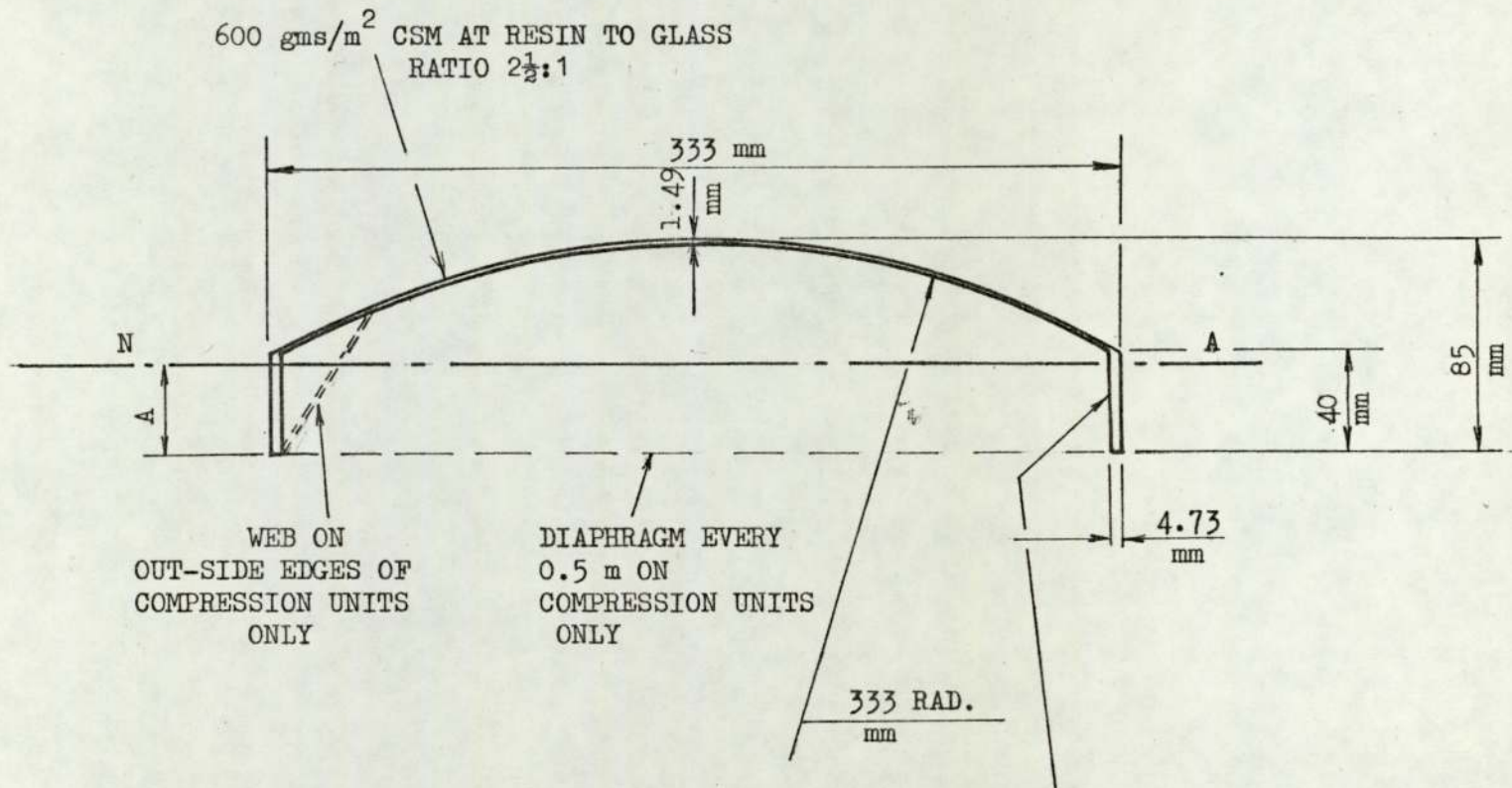


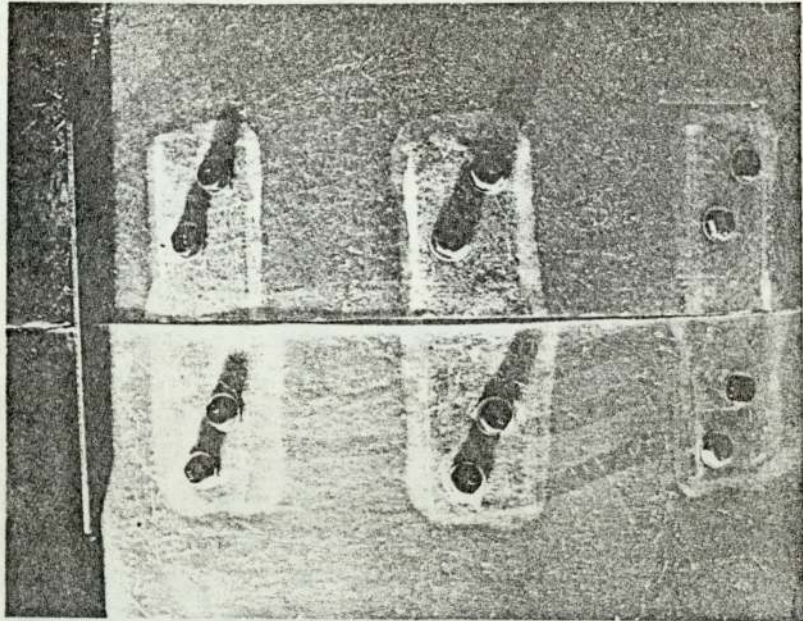
FIG. 6.1 CROSS-SECTION OF ROOF SURFACE UNIT

DIMENSION A
 THEORETICAL MODULUS A = 37.5 mm
 EMPIRICAL MODULUS A = 39 mm

600 gms/m² CSM AT 2½:1
 PLUS 2600 gms/m² ROVINGS
 AT 1:1 RESIN TO GLASS RATIO

FIG. 6.2 SURFACE UNIT CYLINDRICAL SECTION JOINT
(TYPE A)

GENERAL VIEW



PARTIAL VIEW AT CROSS-SECTION ON
CENTRE LINE

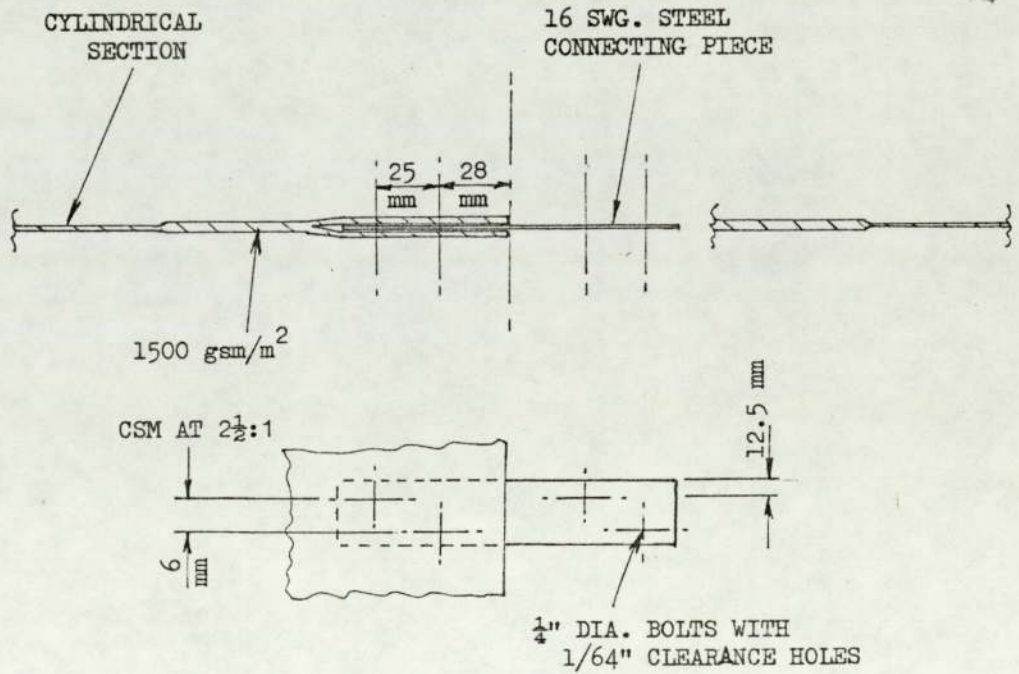
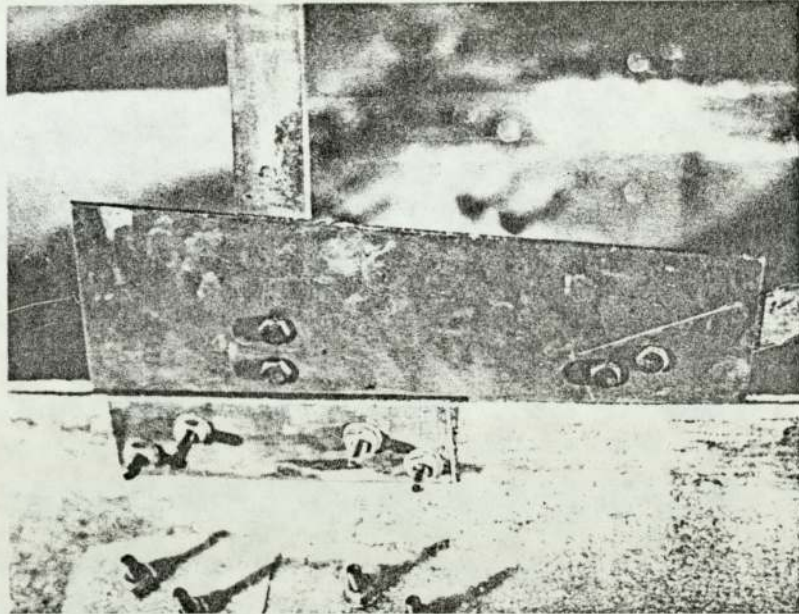


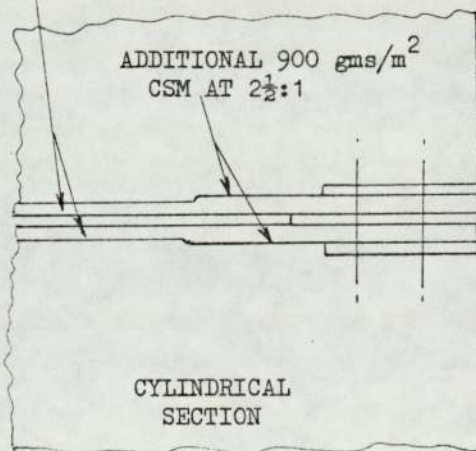
FIG. 6.3 EDGE-BEAM AND CROSS-BRACING JOINT
(TYPE A)

GENERAL VIEW



VIEW SHOWING LOCAL REINFORCEMENT
AND JOINT DETAILS

EDGE-BEAMS
SEE FIG. 6.1



JOINT FISH
PLATES

CROSS-BRACING
JOINT PLATE

¼" DIA. BOLTS WITH
1/64" CLEARANCE HOLES

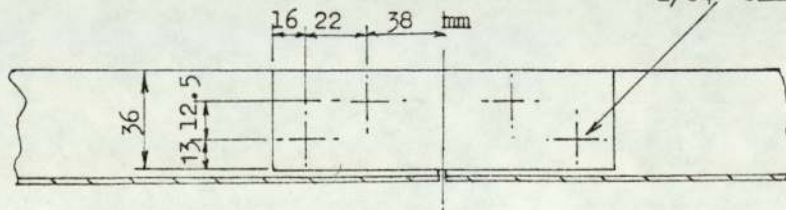
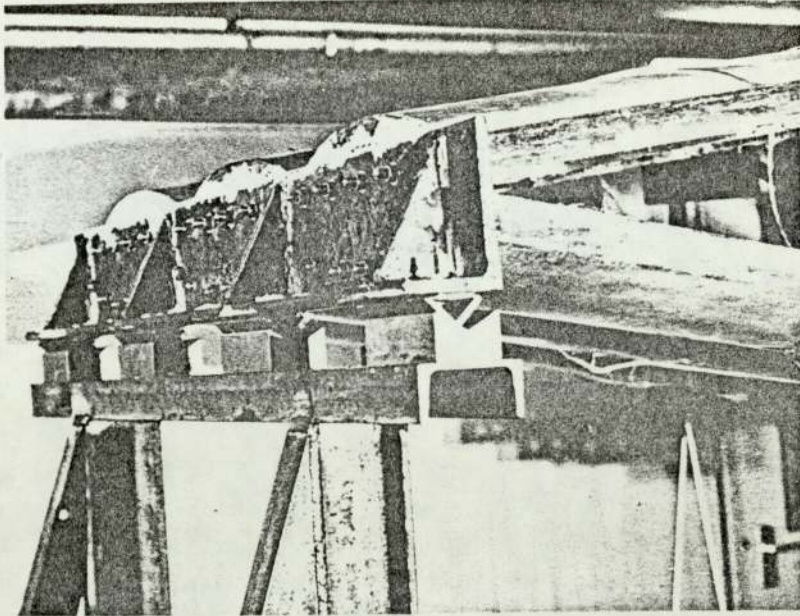
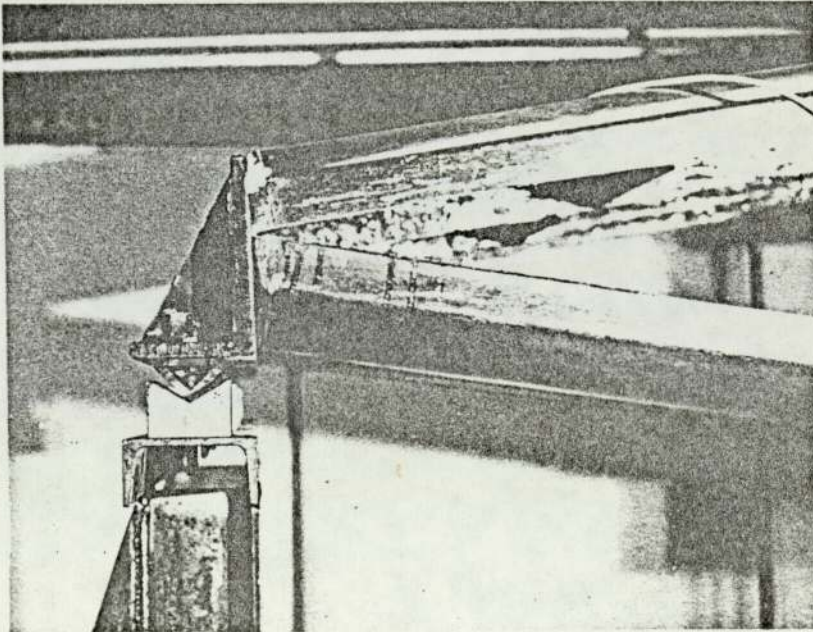


FIG. 6.4 ROOF SUPPORT AND END JOINTS

GENERAL VIEW



END ELEVATION



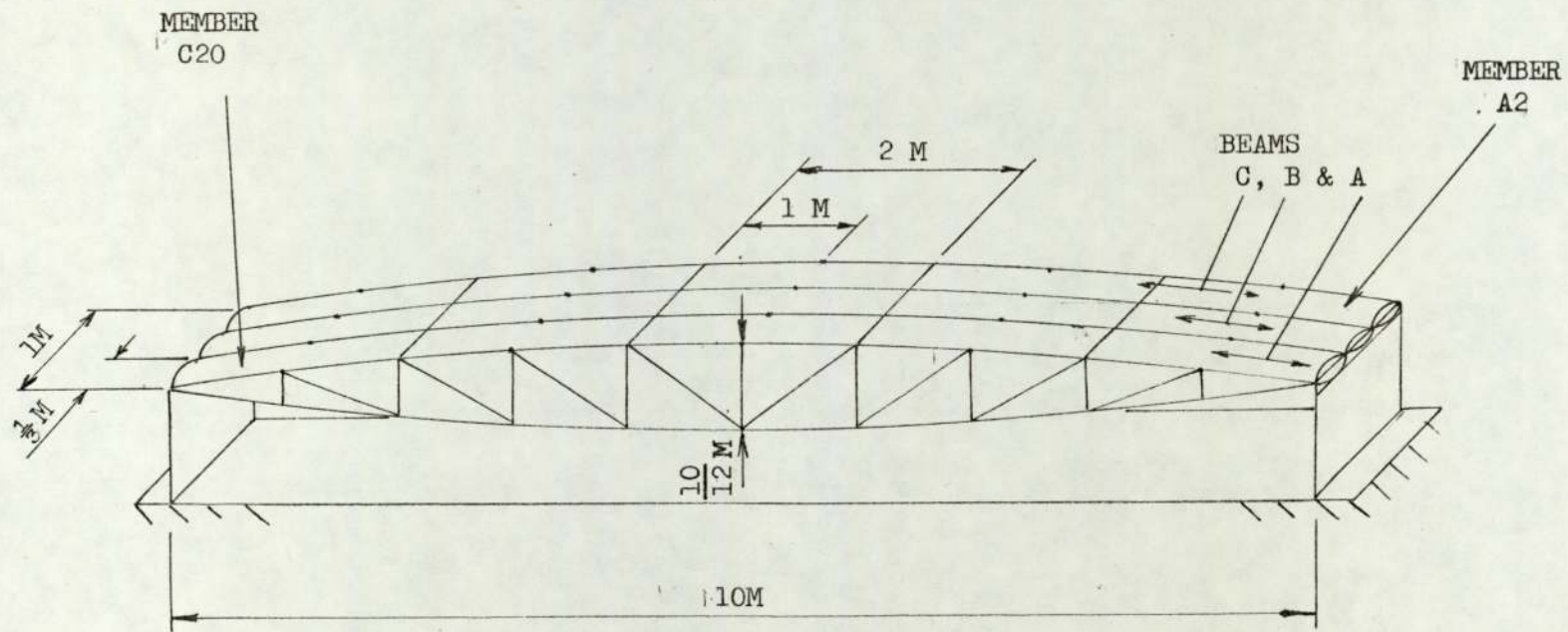


FIG. 6.5 DIAGRAM OF MODEL ROOF

- PINNED JOINTS
- RIGID JOINTS
- 3 MEMBER NO.
- 3 JOINT NO.

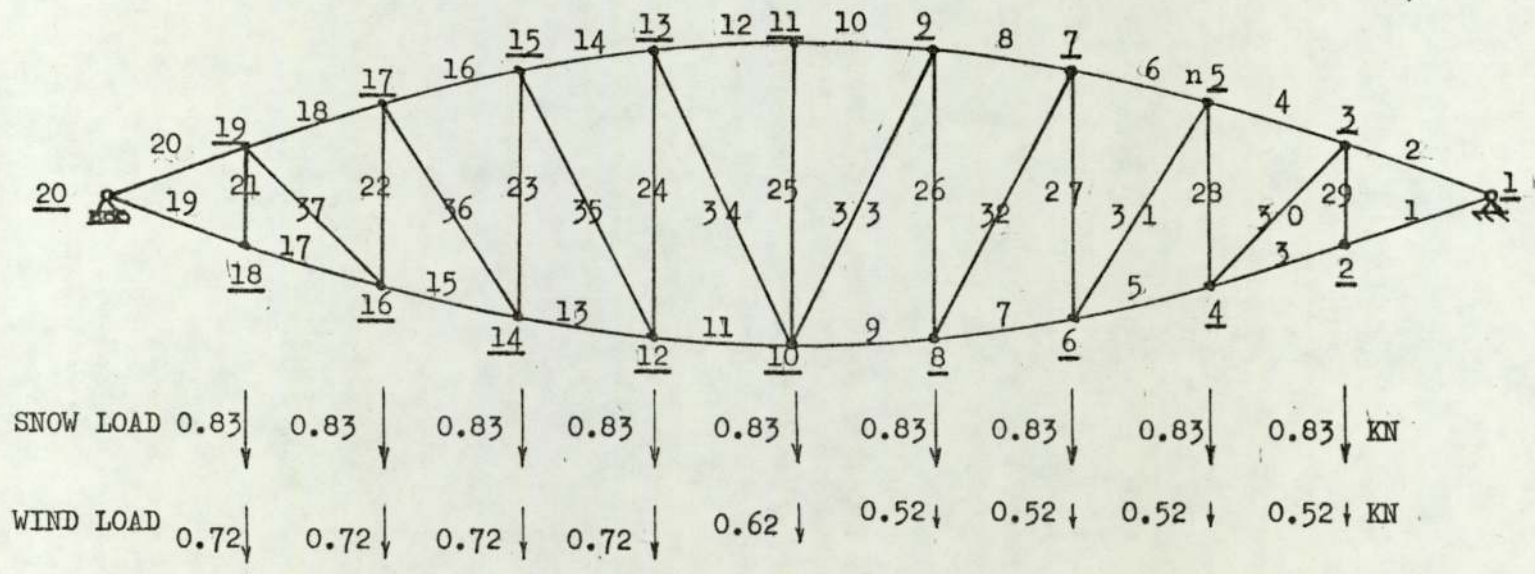


FIG. 6.6 LOADING OF MODEL ROOF

FIG. 6.7 ROOF MEMBER LOADING - SNOW LOAD

MEMBER NO.	AXIAL FORCE KN	SHEAR FORCE KN	MOMENT END 1 KN M	MOMENT END 2 KN M
1	9.88	-0.09	0	0.087
2	-9.88	0.09	0	-0.087
3	9.93	0.05	-0.058	0.014
4	-9.93	-0.04	0.053	-0.015
5	11.1	0	-0.022	0.018
6	-11.4	0	0.019	-0.019
7	11.4	0	-0.021	0.015
8	-11.5	0	0.019	-0.016
9	11.5	0	-0.017	0.017
10	-11.6	0	0.016	-0.017
25	0.37	0	0	0
26	0.34	0	0	0
27	0.25	0	0	0
28	0.06	-0.02	0.006	
29	0.06	0.15	-0.029	-0.028
30	1.32	0	-0.006	0.002
31	0.43	0	-0.002	0.002
32	0.17	0	-0.002	0.002
33	0.72	0	-0.001	0.002

FORCES AND MOMENTS ARE PER METRE WIDTH OF ROOF.

OTHER MEMBER FORCES AND MOMENTS MAY BE OBTAINED BY SYMMETRY.

POSITIVE ROTATIONS AND TRANSLATIONS CONFORM TO THE "RIGHT HAND SCREW RULE".

FIG. 6.8 ROOF MEMBER LOADING - WIND LOAD

MEMBER NO.	AXIAL FORCE KN	SHEAR FORCE KN	MOMENT END 1 KN M	MOMENT END 2 KN M
1	6.78	-0.067	0	0.068
2	-6.78	0.069	0	-0.070
3	6.81	0.035	-0.046	0.008
4	-7.77	0.032	0.045	-0.013
5	7.71	0	-0.018	0.015
6	-8.10	0	0.015	-0.016
7	8.07	0.005	-0.018	0.013
8	-8.34	-0.001	0.015	-0.014
9	8.34	-0.001	-0.015	0.014
10	-8.61	0.002	0.012	-0.014
11	8.79	- .001	-0.015	0.016
12	-8.61	0	0.015	-0.015
13	8.88	-0.007	-0.013	0.020
14	-8.82	0.004	0.014	-0.018
15	8.73	-0.003	-0.017	0.020
61	-8.91	0	0.018	-0.019
17	7.89	-0.033	-0.012	0.055
18	-8.79	0.039	0.014	-0.053
19	7.86	0.080	-0.080	0
20	-7.86	-0.081	0.081	0
21	0.10	-0.132	0.025	0.024
22	0.14	0.021	-0.061	-0.006
23	0.33	0	0	0
24	0.48	0	0	0
25	0.27	0	0	0
26	0.36	0	0	0
27	0.33	0	0	0
28	-0.05	-0.015	0.004	0.005
29	-0.02	0.118	-0.022	-0.021
30	1.03	0	0	0
31	0.45	0	0	0
32	0.34	0	0	0
33	0.36	0	0	0
34	-0.27	0	0	0
35	-0.08	0	0	0
36	0.19	0	0	0
37	0.99	0	0	0

FIG. 6.9 DEFLECTION OF MODEL ROOF - EMPIRICAL
ELASTIC ANALYSIS

JOINT NO.	DEFLECTION (mm)	
	SNOW LOAD	WIND LOAD
1	0	0
2	6.5	4.6
4	10.2	7.3
6	12.7	9.2
8	14.0	10.3
10	14.5	10.7
12	14.0	10.5
14	12.7	9.6
16	10.2	7.8
18	6.5	5.0
20	0	0

FIG. 6.10 ROOF CROSS-BRACING NODE

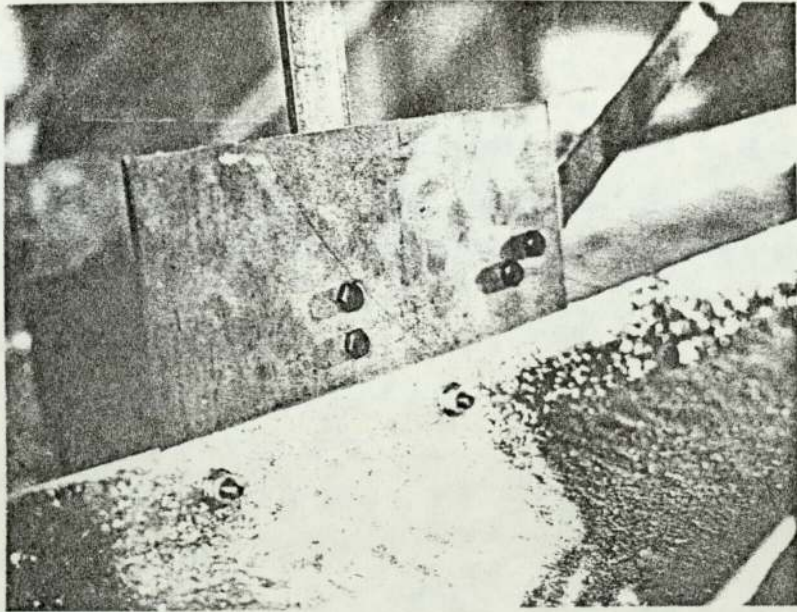


FIG. 6.11 GENERAL VIEW OF MODEL ROOF

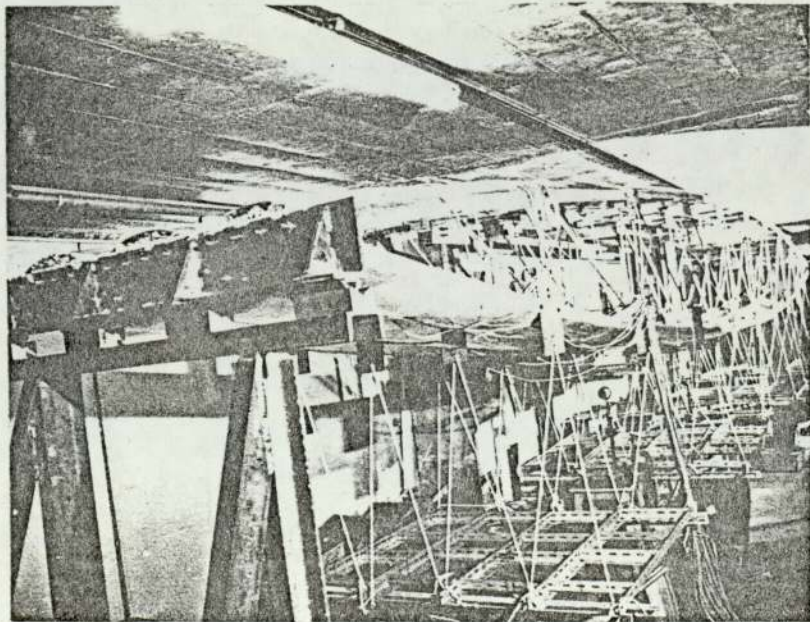


FIG. 6.12 LOAD SUPPORT ARRANGEMENTS

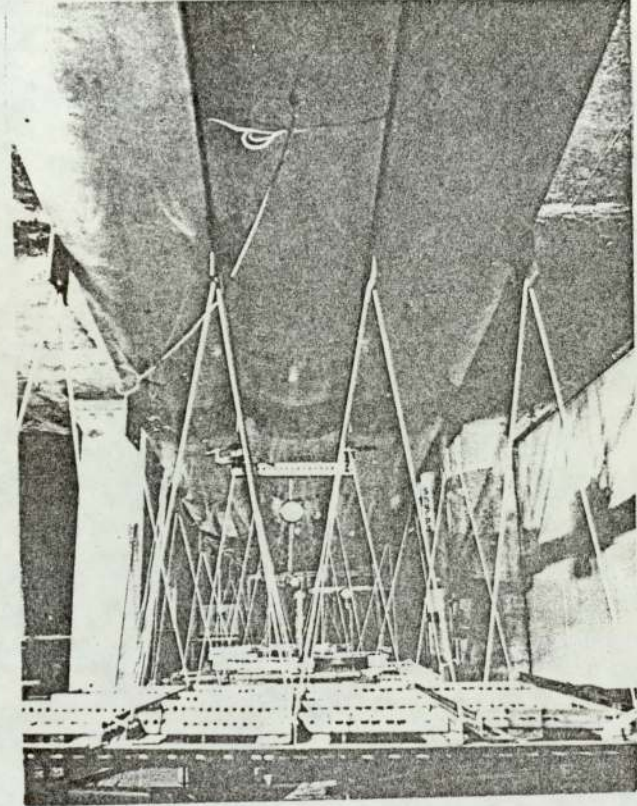


FIG. 6.13 GENERAL VIEW OF PRELIMINARY COMPRESSION TEST

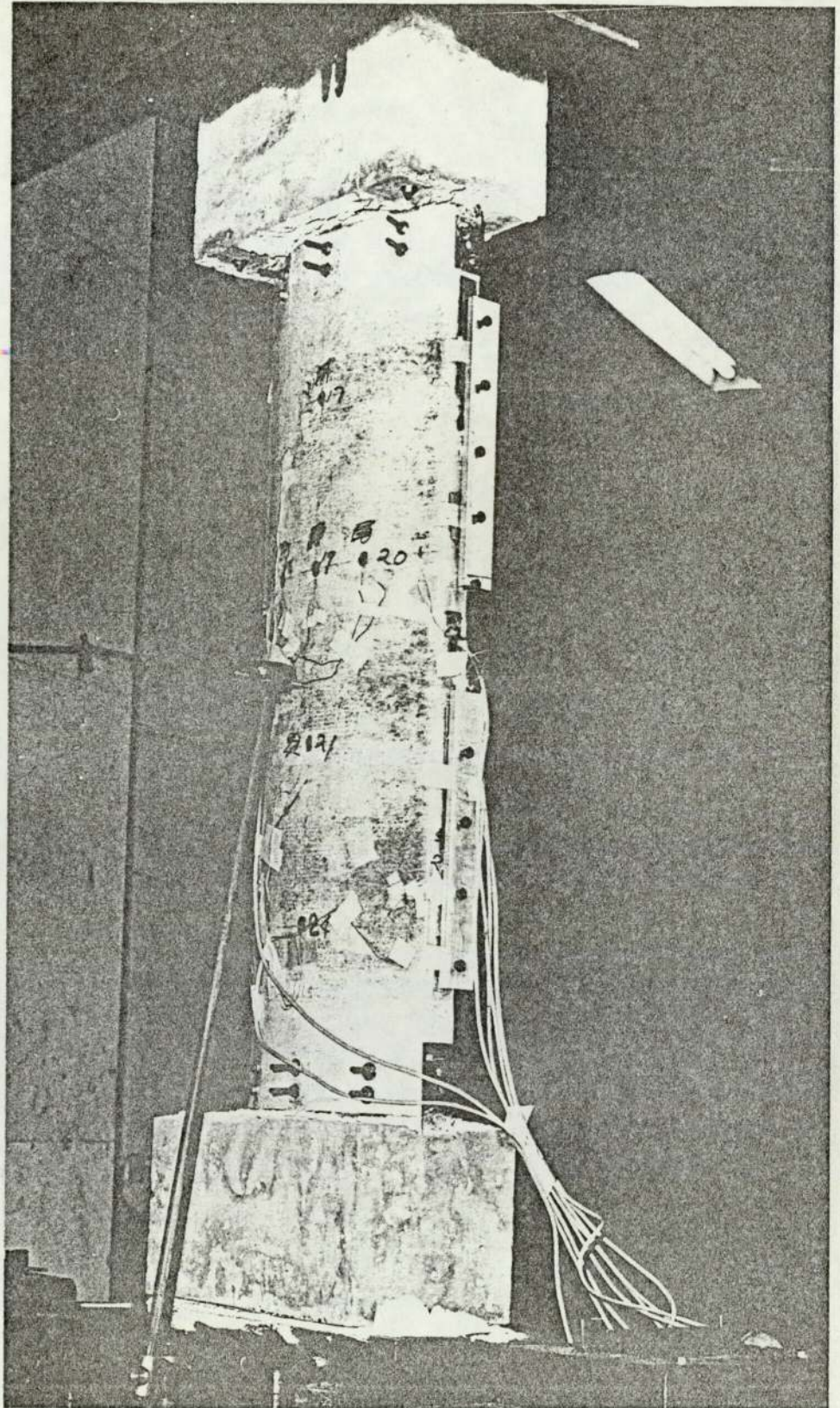
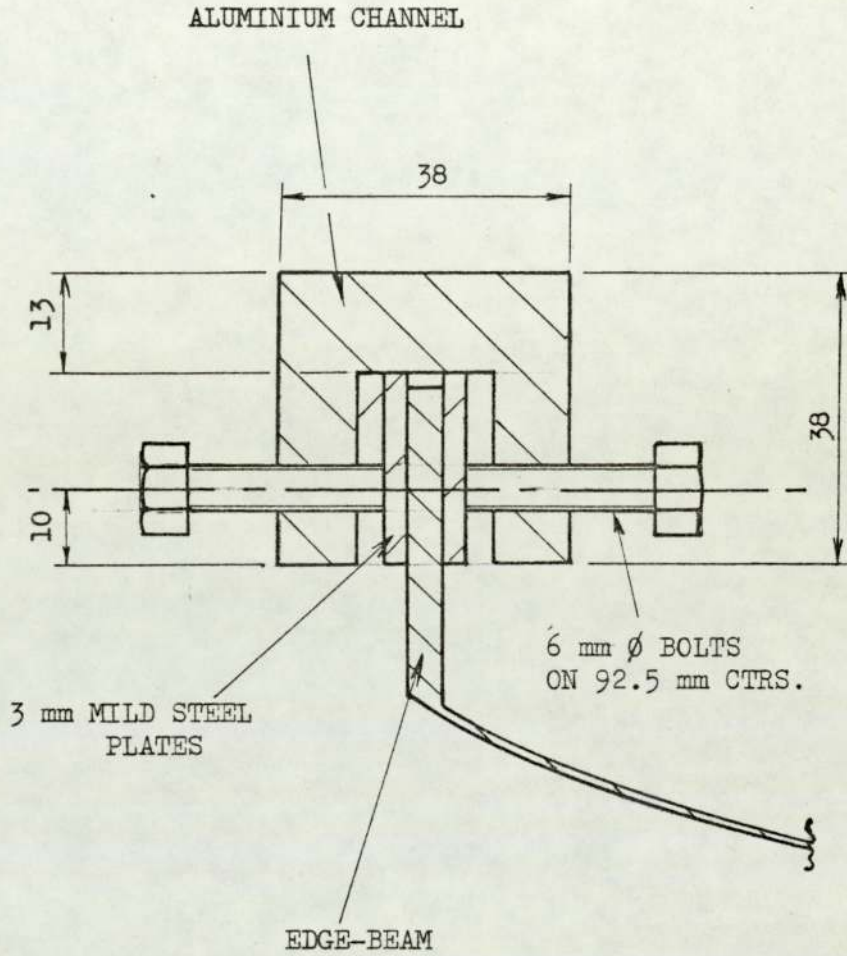


FIG. 6.14 COMPRESSION SPECIMEN EDGE-BEAM
SUPPORT



DIMENSIONS IN MILLIMETERS

FIG. 6.15 DEPLOYMENT OF STRAIN GAUGES

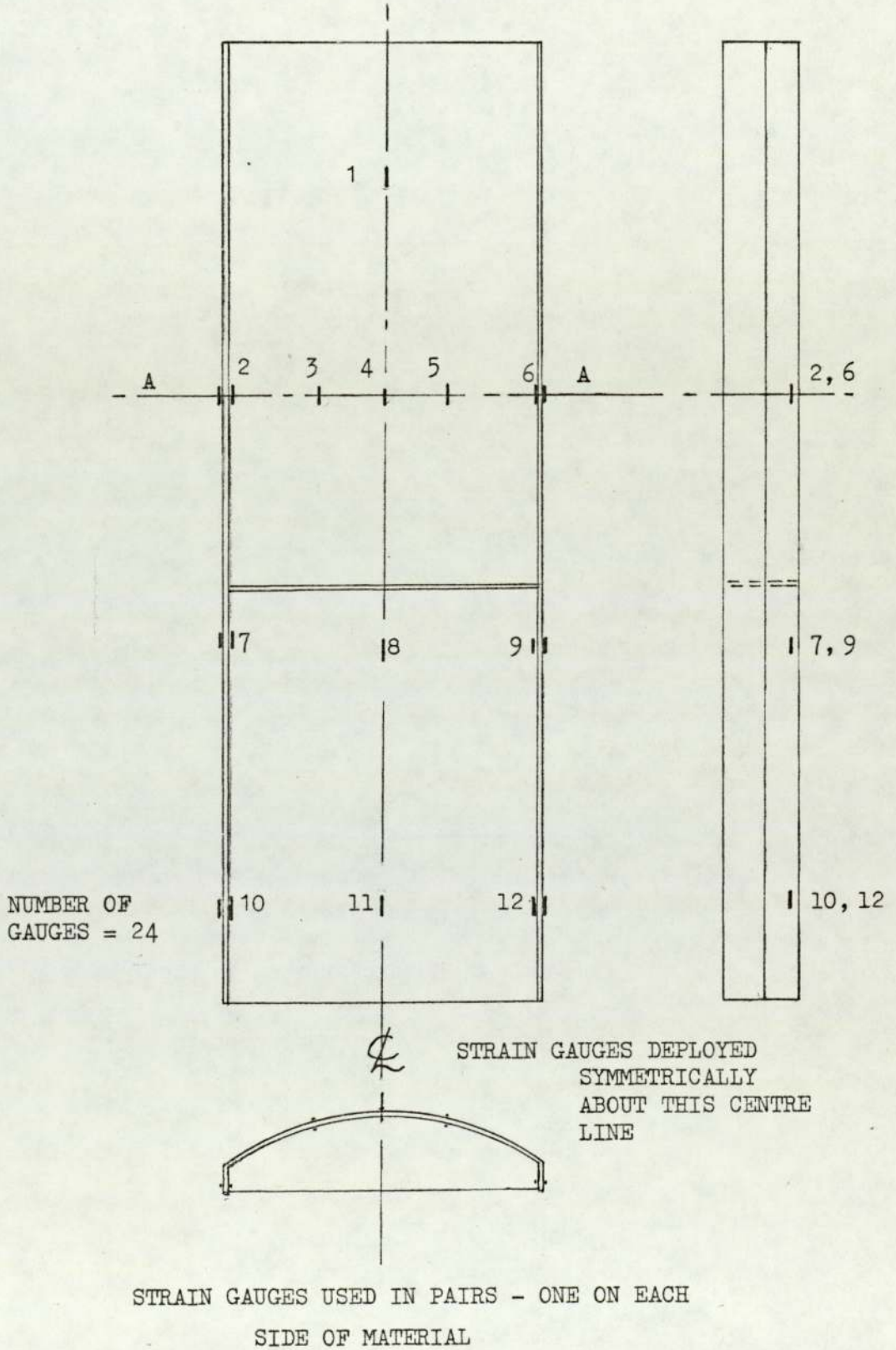


FIG. 6.16 STRAIN GAUGE RESULTS

LOAD (KN x 10)	MEAN OF STRAIN GAUGE PAIRS (SEE FIG. 6.15) (M/M x 10 ⁻³)					
	1	2	3	4	5	6
0	0	0	0	0	0	0
0.25	-0.409	-0.390	-0.271	-0.296	-0.322	-0.344
0.5	-0.643	-0.641	-0.450	-0.496	-0.558	-0.585
0.75	-0.892	-0.900	-0.637	-0.701	-0.816	-0.858
1.0	-1.117	-1.134	-0.805	-0.878	-1.049	-1.071
1.25	-1.376	-1.395	-1.001	-1.072	-1.355	-1.296
1.5	-1.279	-1.838	-0.466	-1.208	-0.304	-1.598
1.75	-1.339	-2.160	-0.369	-2.007	-0.220	-1.854
2.0	-0.689	-2.594	+0.024	-2.312	-0.242	-2.203
	7	8	9	10	11	12
0.25	-0.324	-0.304	-0.372	-0.365	-0.275	-0.319
0.5	-0.620	-0.520	-0.636	-0.619	-0.464	-0.552
0.75	-0.922	-0.754	-0.937	-0.904	-0.702	-0.828
1.0	-1.184	-0.964	-1.189	-1.142	-0.921	-1.028
1.25	-1.473	-1.205	-1.452	-1.418	-1.158	-1.210
1.5	-1.946	-0.866	-1.959	-2.008	-0.531	-1.527
1.75	-2.195	-0.546	-2.451	-2.300	-0.225	-1.710
2.0	-2.418	-0.114	-2.922	-2.515	-0.151	-1.650

FIG. 6.17 LATERAL DEFLECTION OF SPECIMEN IN
PRELIMINARY COMPRESSION TEST

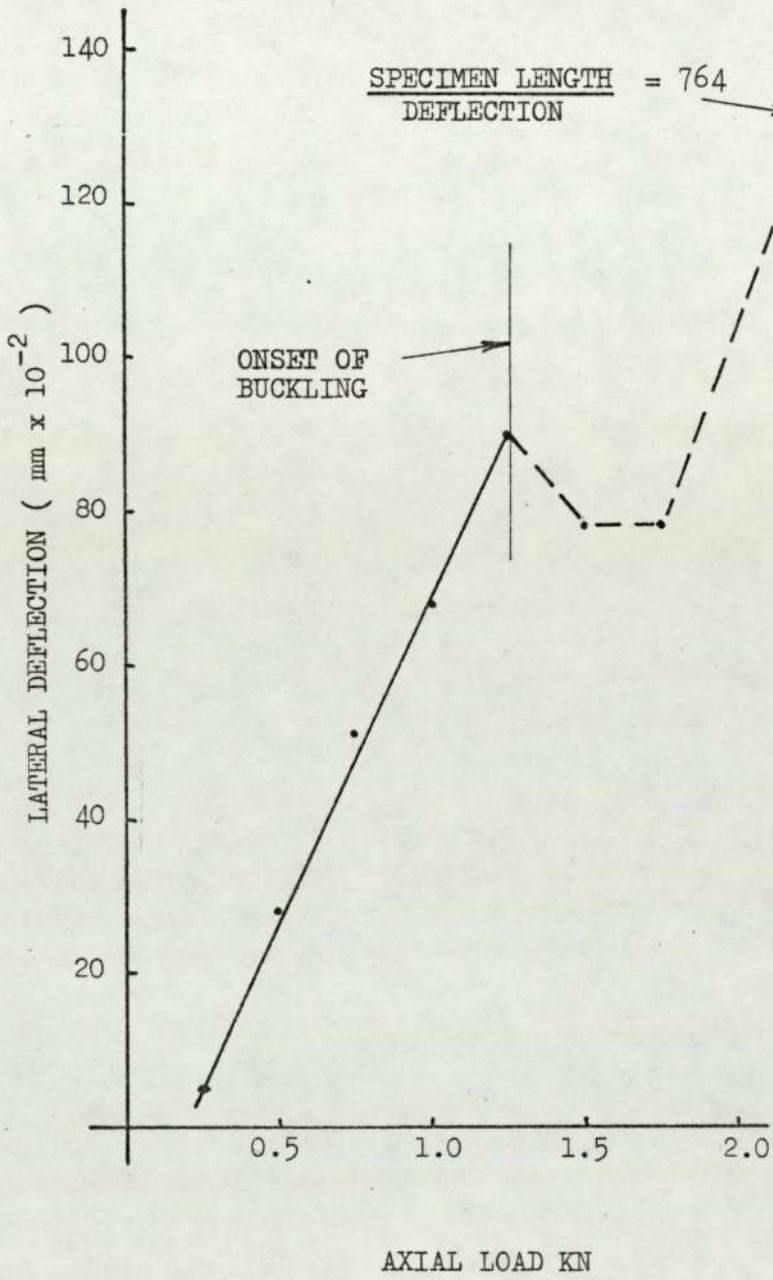


FIG. 6.18 STRAIN DISTRIBUTION ACROSS THE SPECIMEN

AT SECTION A-A AT LOAD 12.5 KN

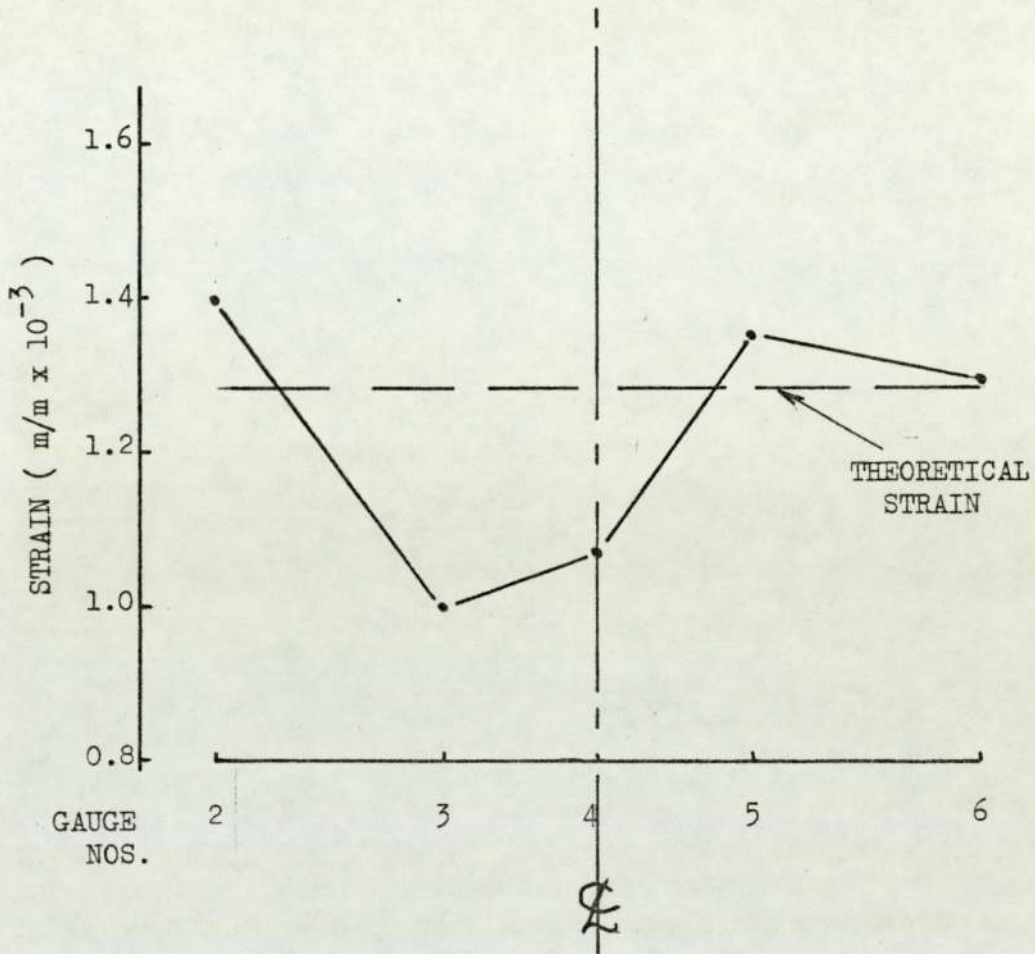


FIG. 6.20 GRAPH OF LOAD AGAINST STRAIN AT SECTION

A-A. (FIG. 6.15)

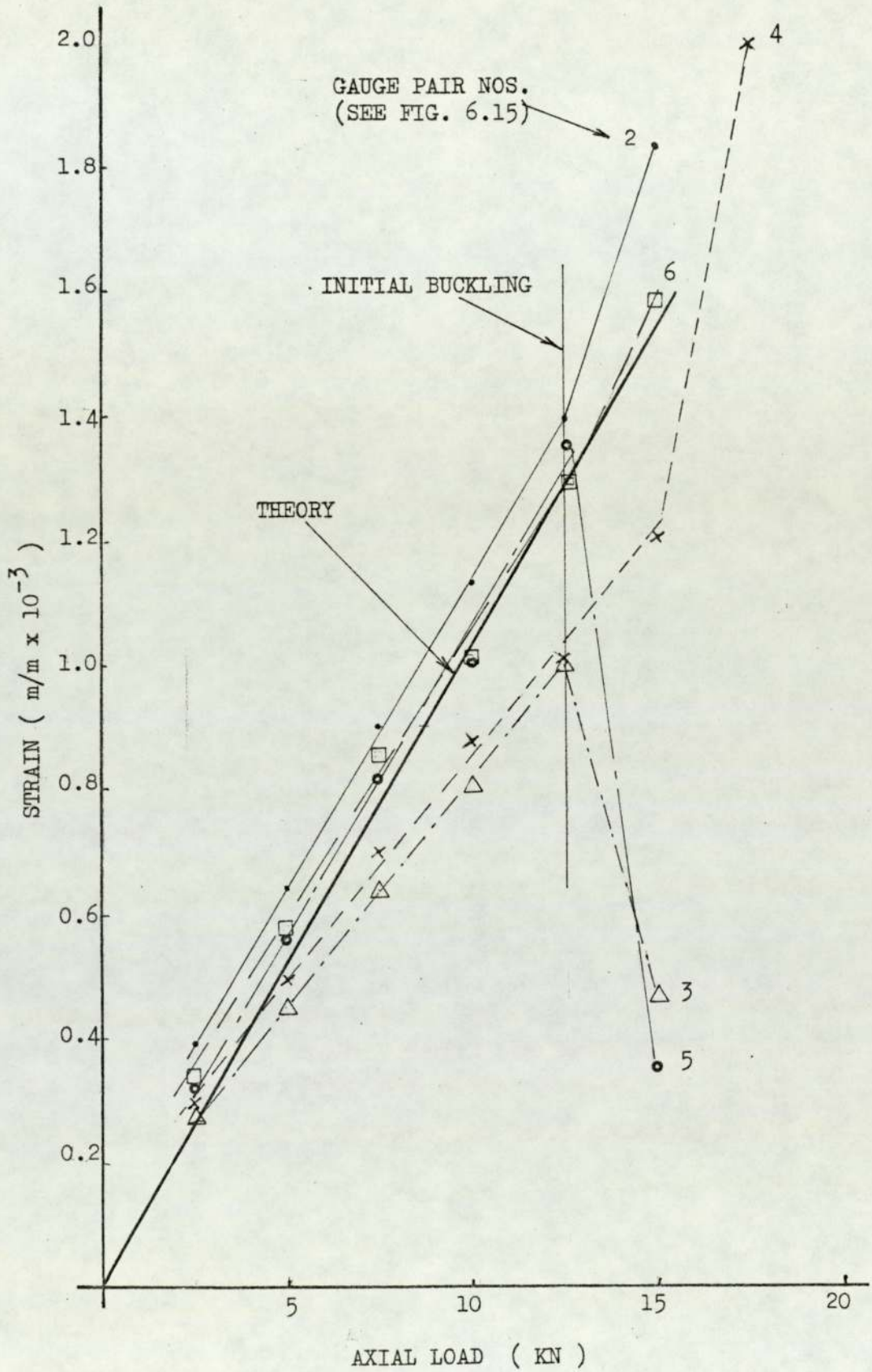


FIG. 6.21 GRAPH OF STRAIN AGAINST LOAD FOR
STRAIN GAUGE PAIR 11

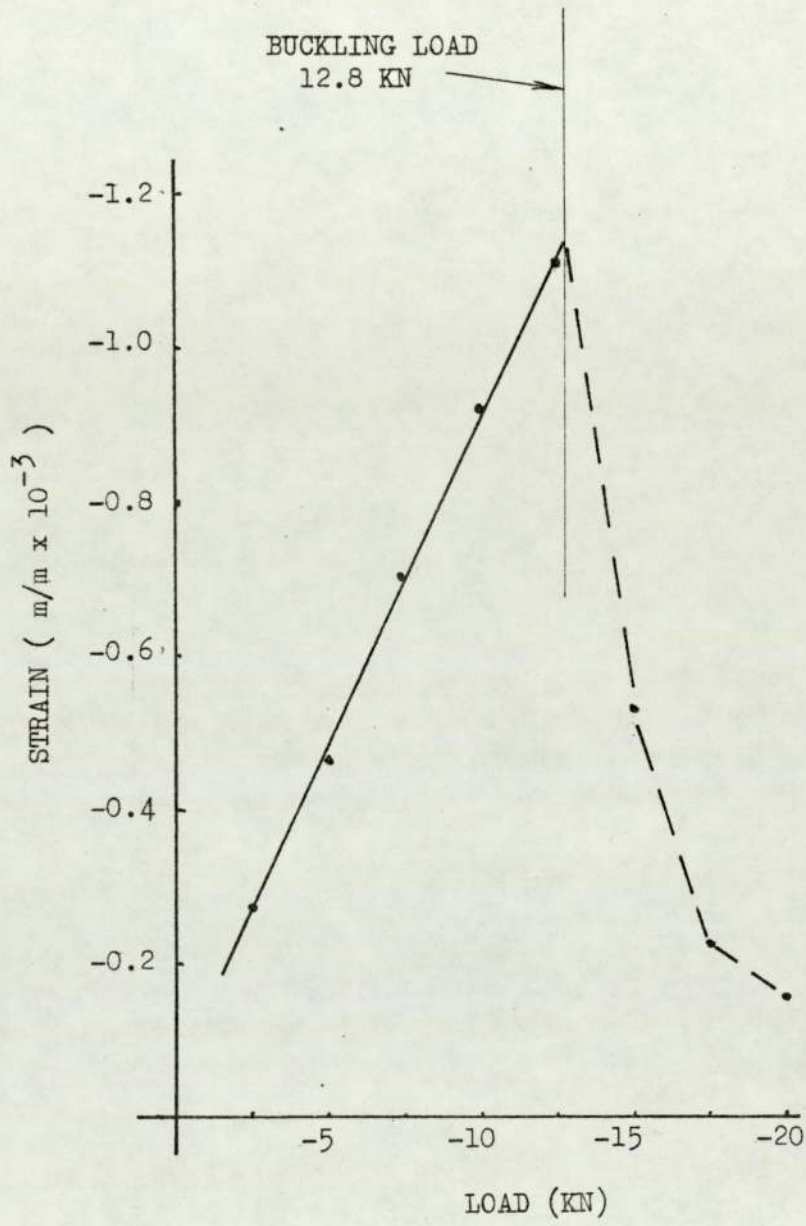


FIG. 6.22 COMBINED BUCKLING OF CYLINDRICAL SECTION

AND EDGE-BEAM

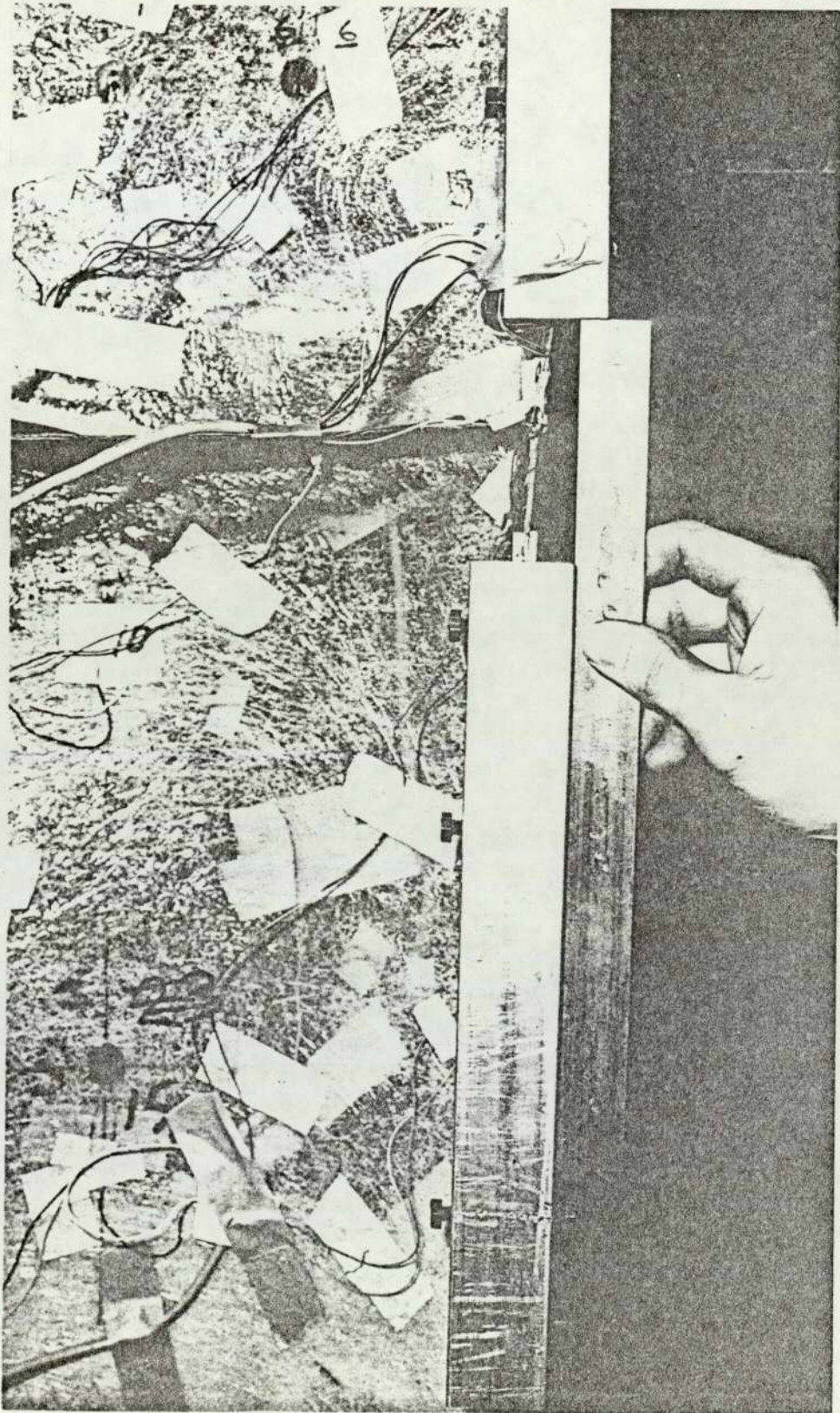


FIG. 6.23 CYLINDRICAL SECTION JOINTS

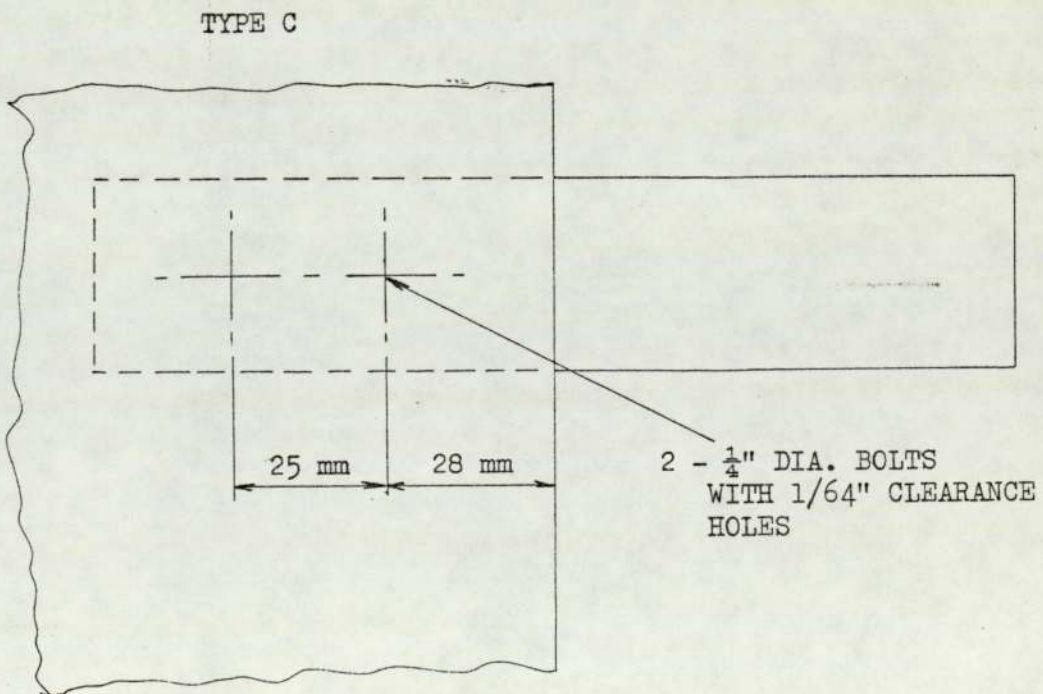
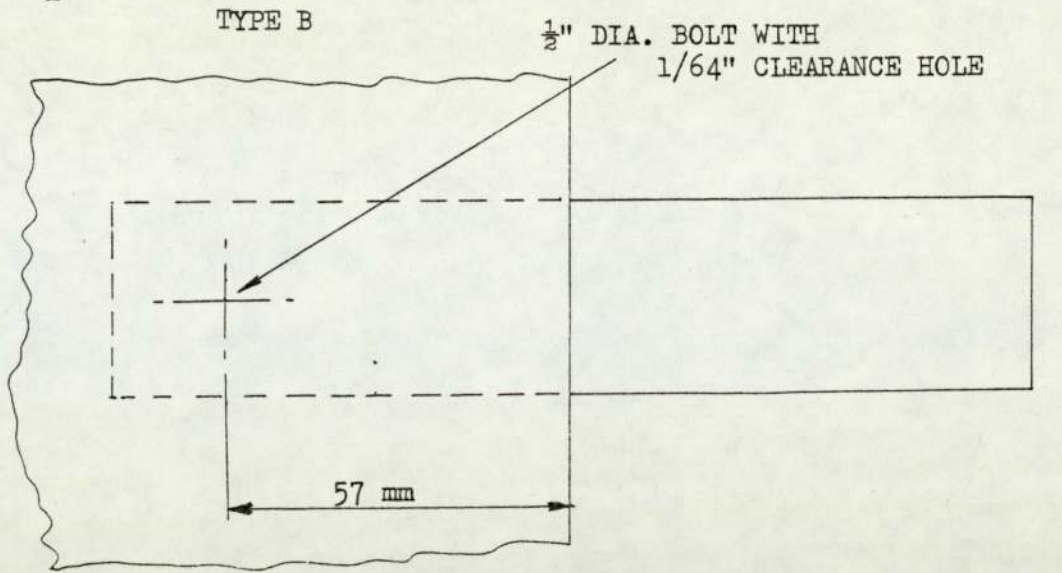
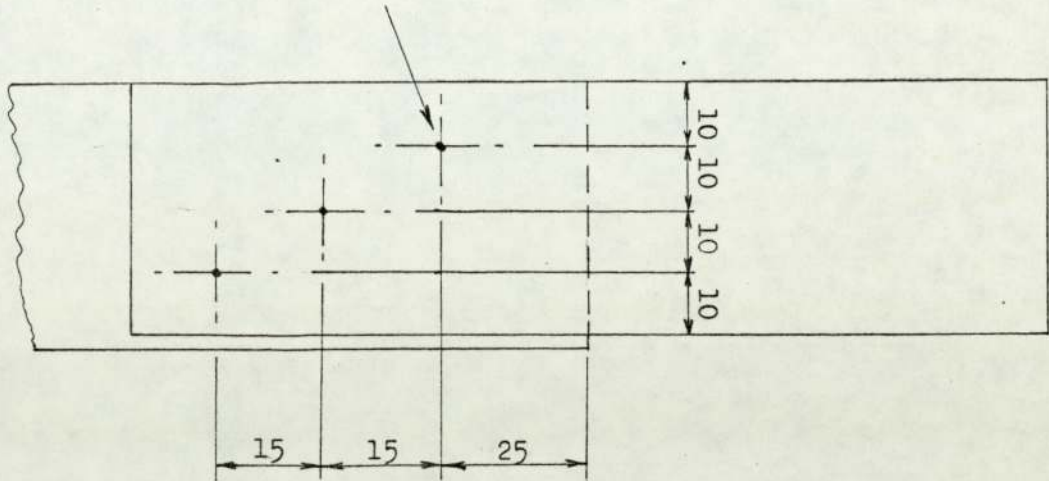


FIG. 6.24 EDGE-BEAM JOINT TYPE B

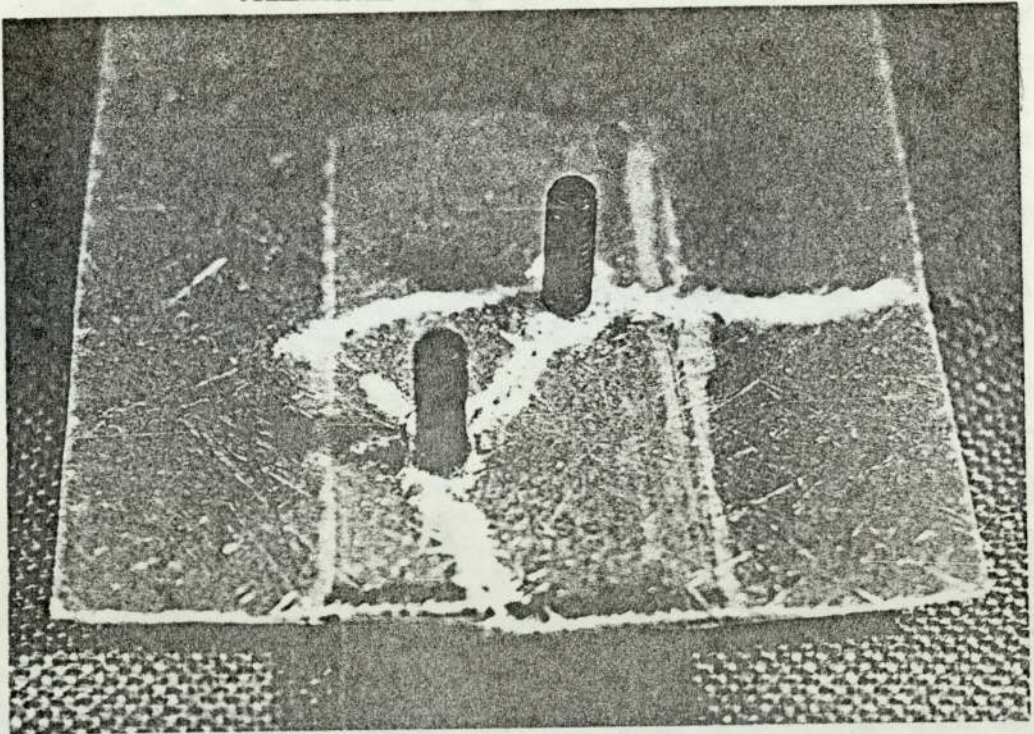
3 - BOLTS $\frac{1}{4}$ " DIA. WITH
1/64" CLEARANCE HOLES



DIMENSIONS IN MILLIMETERS

FIG. 6.25 JOINT FAILURE MODES

CYLINDRICAL SECTION JOINT TYPE A



CYLINDRICAL SECTION JOINT TYPE B

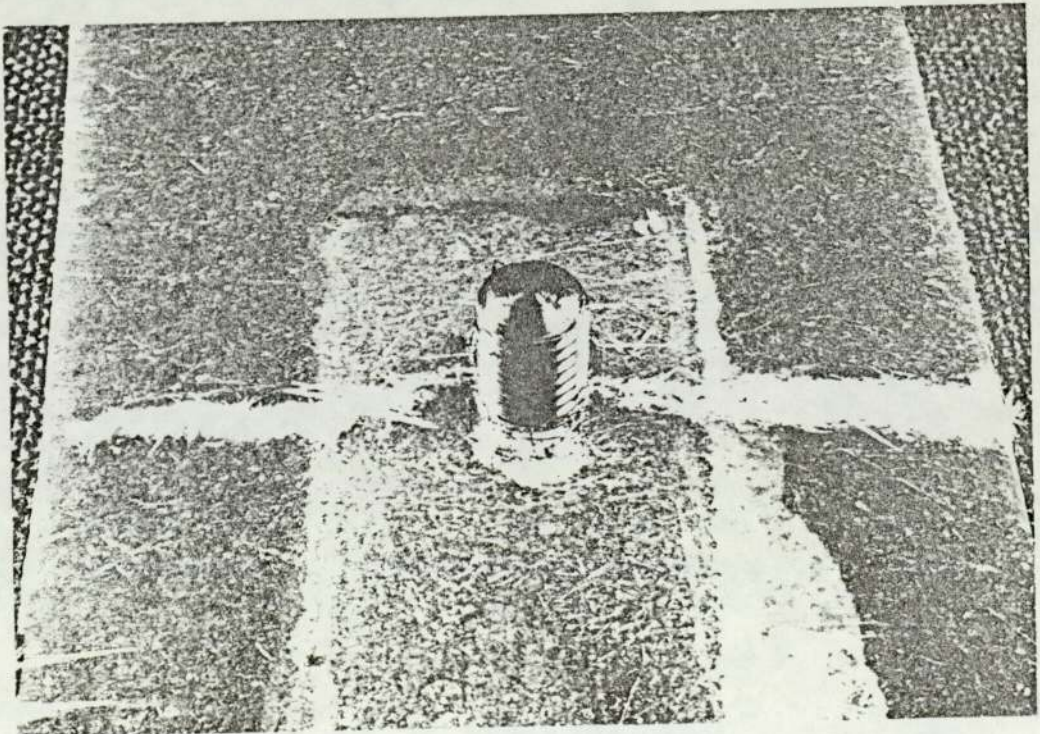
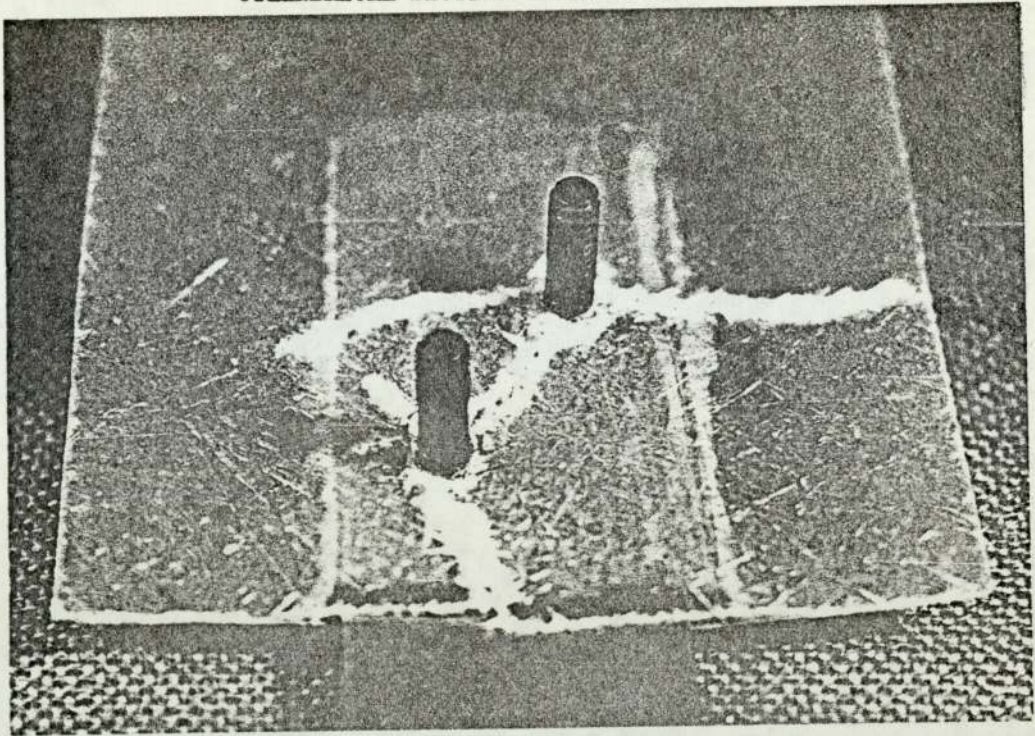


FIG. 6.25 JOINT FAILURE MODES

CYLINDRICAL SECTION JOINT TYPE A



CYLINDRICAL SECTION JOINT TYPE B

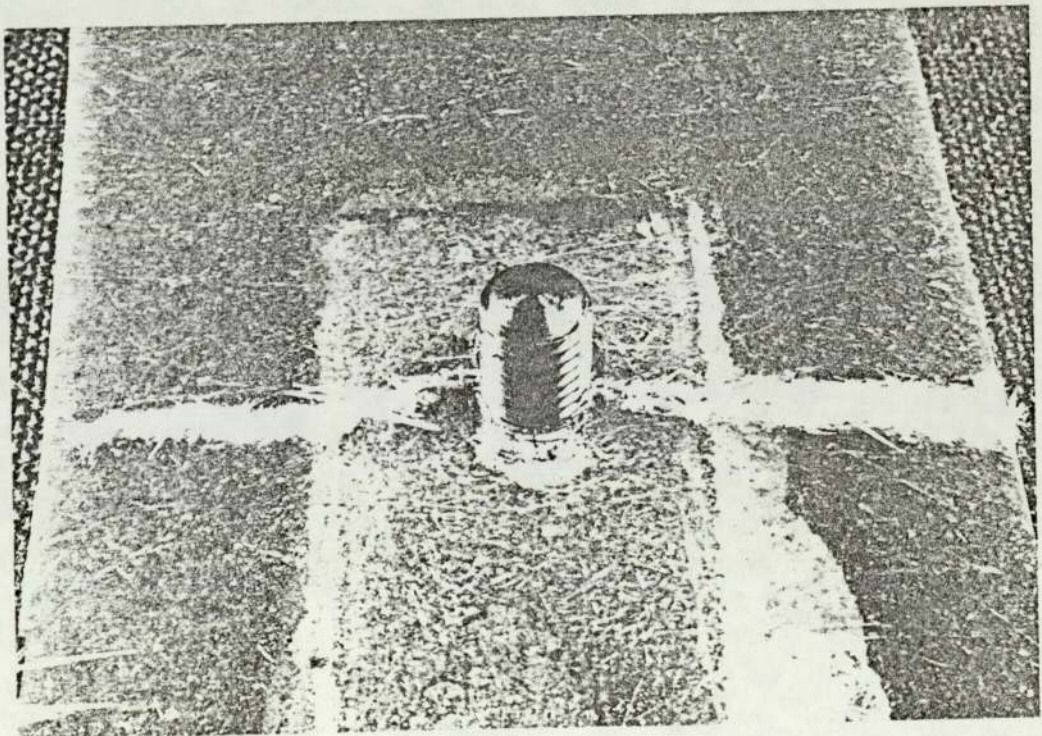


FIG. 6.26 JOINT FAILURE MODES

CYLINDRICAL SECTION JOINT TYPE C

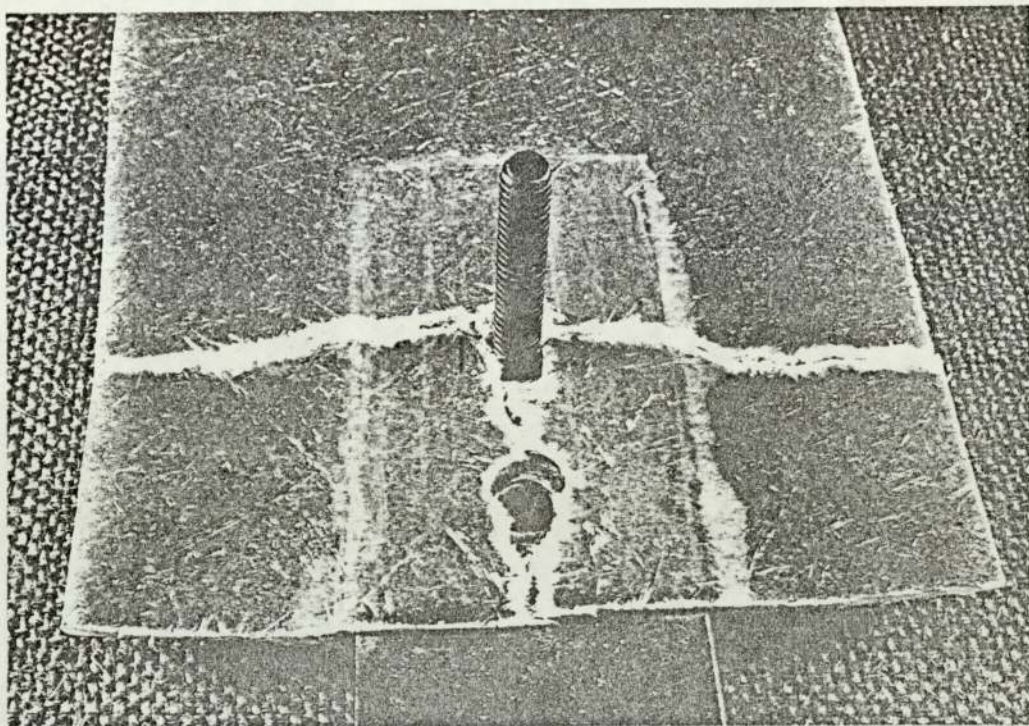
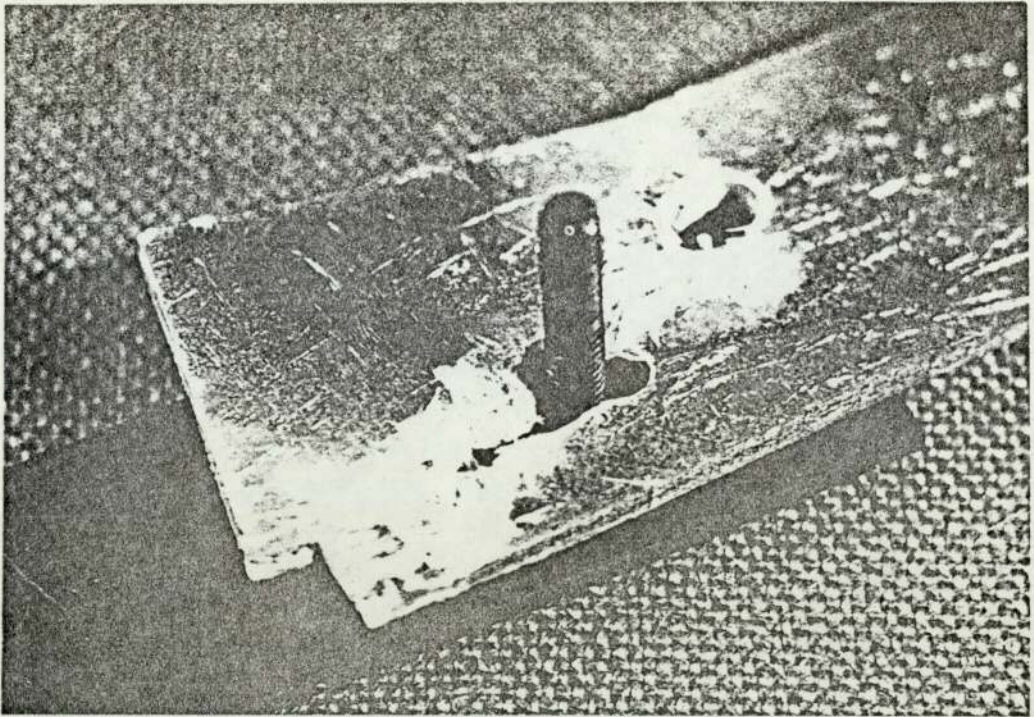
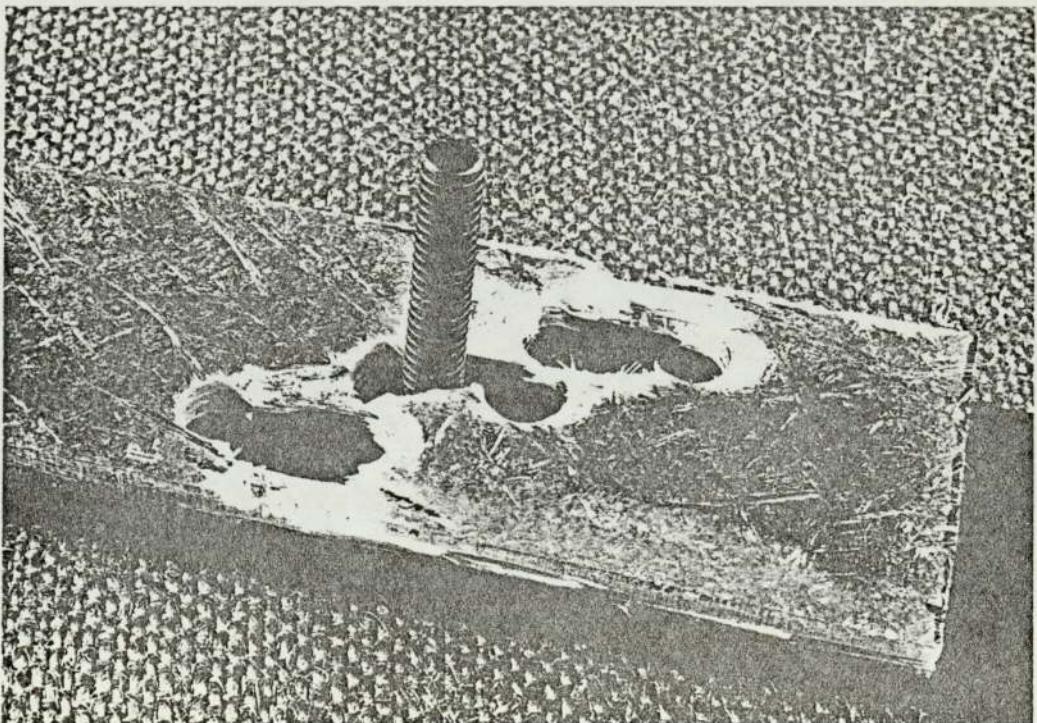


FIG. 6.27 JOINT FAILURE MODES

EDGE-BEAM JOINT TYPE A



EDGE-BEAM JOINT TYPE B



CHAPTER 7

DISCUSSION BETWEEN THEORY & EXPERIMENTAL

MODEL TEST RESULTS

CHAPTER SEVEN

Discussion Between Theory and Experimental Model Test Results

7.1

Introduction

This chapter is concerned with the comparison between the predicted behaviour of the model roof and that which was experienced under test. The test procedure has been described in Chapter 6. The comparison will enable conclusions to be drawn concerning the structural feasibility of the 60 m span roof designed in Chapter 5.

7.2.1 Deflection

Table Fig. 7.1 compares the theoretically (empirical modulus) determined deflections with those obtained experimentally. The latter were marginally greater than those predicted, with the exception of the deflection at point B (See Fig. 7.2). In both the snow and wind loading tests the deflection at point B was less than predicted.

Fig. 7.3 shows graphically the deflections of the model roof at mid-span plotted against load. Theoretical deflection was plotted on the basis of both theoretical modulus and empirical modulus. Experimental results are in close agreement with the empirically-determined modulus theory, particularly if the mean of the two central deflections is considered (points B & C). Although the experimental results also agree reasonably well with the theory based on the theoretical modulus, the discrepancy is greater. Consequently only the empirically based modulus theory will now be considered.

On unloading, the roof did not return to its original position, but maintained a 1.5 mm deflection. Thus the roof did not behave perfectly elastically.

The deflections of points A and D (Fig. 7.2) are presented in Fig. 7.4. In both cases the deflection was a linear function of load, and compared reasonably well with theory. Point D however, deflected more than point A, whereas in theory their deflection is

identical due to symmetry. The deflection of point A was 9% greater than theory, and point B 15% greater. Again, permanent deflection was experienced on unloading.

The central deflection under the action of wind loading is shown in Fig. 7.5. Point C again deflected more than point B, and again experimental results were in close agreement with theory. As was the case with the roof behaviour under snow loading, permanent deflection was observed after unloading.

Fig. 7.6 shows the deflections of point A and D. Point D deflected more than point A, as expected, but the error between observed and predicted deflection was 22% in the case of point D, and 7% in the case of point A.

The time-dependent nature of the deflection of the roof under snow load is shown in Fig. 7.7. The logarithm of the deflection is shown to vary approximately linearly with the logarithm of time according to the following equation:

$$\log \delta = 0.0316 \log t + 1.12 \quad 7.1$$

Equation 7.1 is analogous to the equation describing the creep behaviour of grp as discussed in Chapter 3, and may be written:

$$\delta = 13.18 t^{0.0316} \quad 7.2$$

Fig. 7.8 shows the creep behaviour on a linear scale and also the recovery of the roof on unloading. The observed deflection of the roof after 672 hrs. (4 weeks) is substantially less than the predicted deflection calculated in Section 6.3.6.3, which was based on grp's creep properties at 20°C and a relative humidity of 100%.

By analogy with the equation

$$\varepsilon = \frac{\sigma t^n}{E_1}$$

established in Chapter 3, equation 7.2 may be written:

$$\delta = \frac{W t^{0.0316}}{k} \quad 7.3$$

where k = a term representing the roof stiffness

W = the total applied load

$$\frac{W}{k} = 1.12$$

As the snow load (W) = $10 \times 0.75 \text{ KN/M}^2$

$$\therefore k = \frac{10 \times 0.75}{1.12} = 0.569 \text{ KN/M}$$

Applying the Boltzmann superposition principle to the deflection of the roof after unloading and neglecting the roof's self-weight and previous loading cycles:

$$\delta = \left(7.5 t_n^{0.0316} - 7.5 (t_n - t_{872})^{0.0316} \right) \quad 7.4$$

The recovery curve predicted by equation 7.4 is also plotted in Fig. 7.8 and is in reasonable agreement with the empirical results.

7.2.2 Member Loads, Strains and Buckling

The theoretical and experimental strains for the grp roof members are tabulated in Figs. 7.9 & 10. Each of the experimental strains tabulated is the mean of two strain gauge readings. Fig. 7.11 shows the deployment of the strain gauges on the members. In general the observed and predicted strains are not equal.

Figs. 7.12 - 7.17 show theoretical and typical experimental load-strain relationships for the grp members. In general the load-strain relationship is linear, but in Figs. 7.12, 13 and 15 sharp discontinuities were observed in the strain gauge results between the sixth and seventh load increments. These discontinuities coincided with the local buckling of the grp members 14C and 4B. Fig. 7.18 shows a photograph of a locally buckled member. The graphs (Fig. 7.12 - 17) confirm the lack of agreement between theoretical and experimental strain, and in general, the theory provides either an upper or lower bound to the observed results.

Figs. 7.19 to 7.21 show the strain distribution at snow load, across sections of the roof's upper and lower surfaces. Again the discrepancy between theory and experiment is shown.

Typical results of steelwork strain measurement are shown in Fig. 7.22, and it is apparent that the experimental results bear little relationship to the predicted strains. Unlike the grp experimental results, the steelwork measured strain is not a linear function of load intensity. Although, theoretically all the steelwork members were in tension, member 34 on the outside of beam C was observed to buckle at a load intensity of $1.25 \times$ snow load, illustrating a compressive load.

Figs. 7.23 - 26 illustrate that the experimentally determined strain in the grp members under wind loading compares with theory in a similar way to the strain under snow loading. That is:

- a) the load/strain relationship is approximately linear.
- and b) in general the theoretical strain curve provides an upper or lower bound to the experimental results.

Local buckling of the grp members was not observed under wind loading. However, two steelwork members were observed to buckle prematurely under the first increment of load; i.e. members 34 on the outside of beams A and C.

7.3

Discussion of Results

7.3.1 Deflection

In general the predicted and experimental elastic (short term) deflections correlated satisfactorily. There are discrepancies between the two however, which are considered to be the result of the following:

- 1) joint slippage; leading to non-rigid joints which behave in a manner between rigid and pin-jointed.
- 2) creep; the durations of the roof tests were 70 mins. for the snow loading test and 60 mins. for the wind loading test. Consequently, some creep is bound to have taken place even though the structure was not loaded continuously.
- 3) geometric inaccuracies of the structure as a whole and within the material, stemming from all stages of manufacture. On a microscopic scale the hand lay-up process used to manufacture the grp components will have led to areas of gross inhomogeneity and anisotropy. On a larger scale the mould used for laminating would not have been geometrically perfect, leading to an

imperfect moulding shape. On a macroscopic scale geometric inaccuracies will have been built into the roof during assembly.

The non-recovered deflections observed are considered to be best explained by 1) and 2) above. The lack of symmetry observed in the deflections may be explained by a combination of joint slippage and macroscopic geometric inaccuracies distributed within the roof unsymmetrically. These phenomena could lead to unpredicted bending and twisting of the surface units.

The large discrepancy between the predicted and experimental long term deflection of the roof (See Fig. 7.8) was due mainly to the environmental difference between the roof test and the material characterisation tests of Chapter 3. However, the same basic creep law was found to apply approximately as well to the structure as a whole as to the constituent materials (See Fig. 7.7). On unloading the roof, deflection recovery was found to follow, reasonably well, the recovery curve as predicted on the basis of the Boltzmann superposition principle. The small discrepancy between the two may be explained in part by the fact that neither the total roof loading history nor the self-weight was taken into account. However, the roof had been assembled and the short term tests completed approximately three months before the creep test was carried out, so that the effect of these factors is expected to have been small. In addition, any contribution to deflection which did not result in the storage of strain energy, such as joint slippage or debonding of the glass fibres and resin, would contribute to the discrepancy.

7.3.2 Member Forces, Strains and Buckling

The three main causes of the discrepancies between theoretical and experimental deflection are also considered to be the main causes of the differences between measured and predicted strain, and therefore stress, in the roof members.

Joint slippage would reduce the predicted bending strains in the members, and the difference between maximum and minimum strains would be reduced. The theoretical strains in the cylindrical section and the edge-beams will form upper and lower bounds to the experimental results. As pointed out in Section 7.2 this was generally the case as observed. However, the discrepancies were too large for this to totally explain the results. Not only can joint slippage cause the roof to behave more like a pin-jointed structure, but it can also cause unpredicted bending in the plane of the roof surface units and also out-of-plane twisting. These phenomena can cause principal stress and strains in directions other than the predicted axial stresses and strains. This can lead to incorrect interpretation of the strain gauge readings, since the results have been assumed to be principal strains resulting from uni-axial stresses. Although the strain gauge readings in general increase linearly with increasing load, if the results are closely examined it can be seen that in many cases strain increases spasmodically (see Fig. 7.13). This is considered to be due to a combination of joint slippage and the loading method where the load was occasionally removed before being increased (as described in Chapter 6); on reloading, different joints may slip.

Geometric inaccuracies can also lead to stresses and strains in non-principal axis directions. For example, there will be at least a two-dimensional stress field round a resin-rich or resin starved area. Also, small areas of anisotropy will cause local bending and twisting of the laminates. This is particularly likely to occur in the edge-beams where the unidirectional material may not be perfectly straight as a result of stippling during lamination.

Creep may also be a factor in the variance due to the non-homogeneous nature of grp. There is likely to be a time-dependent strain distribution between a resin-rich surface and the main body of the laminate. This effect however, is considered to be of little significance.

Since the measured deflections of the roof compare well with those predicted, the mean theoretical and experimental member strains would be expected to be similar. The mean of all the theoretical strains at snow load was 0.353×10^{-3} m/m and the mean of all the measured strains was 0.307×10^{-3} m/m. The discrepancy here is 13%. The maximum strain expected to be measured in the roof at snow load was -4.43×10^{-4} m/m in the edge-beams of members 18 A, B and C. The largest strain actually measured was -5.74×10^{-4} m/m in the cylindrical section of member 8c, which is 30% greater than the predicted maximum strain.

During the snow loading test, measured strain in the steel cross-bracing was grossly different from that predicted. Indeed, one member (member 34) was observed to buckle when it was theoretically a tensile member. During the wind loading test the same member

buckled again, plus one other member as described in Section 7.2.2. However, under wind loading these members were expected to be under compression. The theoretical buckling load for these members was 1.27 KN and the theoretical load at buckling was 0.09 KN. The buckling load is small compared with the forces in the grp surface units, and so bending or twisting of these units could cause buckling. There are four cross-bracing members at the particular section where the members buckled, but only two actually buckled. This would seem to support the above view. This cross-bracing buckling is undesirable but does not have any significant effect on the design of the 60 m roof, since its cross-bracing was designed on the cross-wire principle. Also the buckling apparently did not have any significant effect on the deflection of the model roof.

The strains, and therefore the stresses, in the cylindrical section of the grp compression members tended to be greater than predicted, occasionally by a factor of 2. It is, therefore, to be expected that local buckling would occur, as observed, since the safety factor at maximum load was only 1.73. The effect of local buckling, however, was small since the relationship between load and deflection remained sensibly linear after buckling. Further, on unloading, the buckled areas returned to their original shape without any apparent material damage.

Finally, it would appear that where there was a large variance between theory and experiment, joint slippage was a major cause. Bolted joints are known to frequently give problems in this respect. In this case, however, it is thought that the problem was exacerbated by the rough grp surfaces to which the fishplates were bolted. The rough surfaces were a result of the hand lay-up manufacturing process.

- 1) The short term elastic deflection of the model roof was predicted with adequate accuracy under uniform and unsymmetric loads using empirically determined material moduli.
- 2) The creep behaviour of the roof structure as a whole was similar to that of grp as a material.
- 3) The visco-elastic character of grp causes significant increases in the deflection (28%) over a period of one month in addition to the elastic deflection.
- 4) The environment has a considerable effect on the rate of creep.
- 5) Creep strain is largely recoverable after a period of unloading equal to the loading period. This may only be the case when the maximum strains do not approach the failure strains.
- 6) Locally, strains were not predicted accurately but the maximum and mean theoretical and experimental strains of the roof were in reasonable agreement.
- 7) Local buckling of the cylindrical section of the grp members did not have any immediate serious effect.

- 8) Bolted joints were a major source of variance between theoretical and experimental results.
- 9) The roof's structural design is efficient compared with conventional roof structures when measured in terms of weight per unit area.
- 10) The structural properties of grp adequately meet the requirements of roof structures, as tested in this project.
- 11) The 60 m span grp roof, designed in Chapter 5 is structurally feasible.

FIG. 7.1 COMPARISON BETWEEN THEORETICAL
ELASTIC ANALYSIS DEFLECTION AND
EXPERIMENTAL DEFLECTION

SNOW LOAD (0.75 KN/M)

MEASURING POINT (SEE FIG. 7.2)	THEORETICAL mm	EXPERIMENTAL mm
A	10.2	10.6
B	14.5	13.5
C	14.5	15.2
D	10.2	12.2

WIND LOAD (INCREMENT 3)

MEASURING POINT (SEE FIG. 7.2)	THEORETICAL mm	EXPERIMENTAL mm
A	7.3	7.4
B	10.7	9.7
C	10.7	11.4
D	7.8	9.4

FIG. 7.2 DEFLECTION MEASURING POINTS

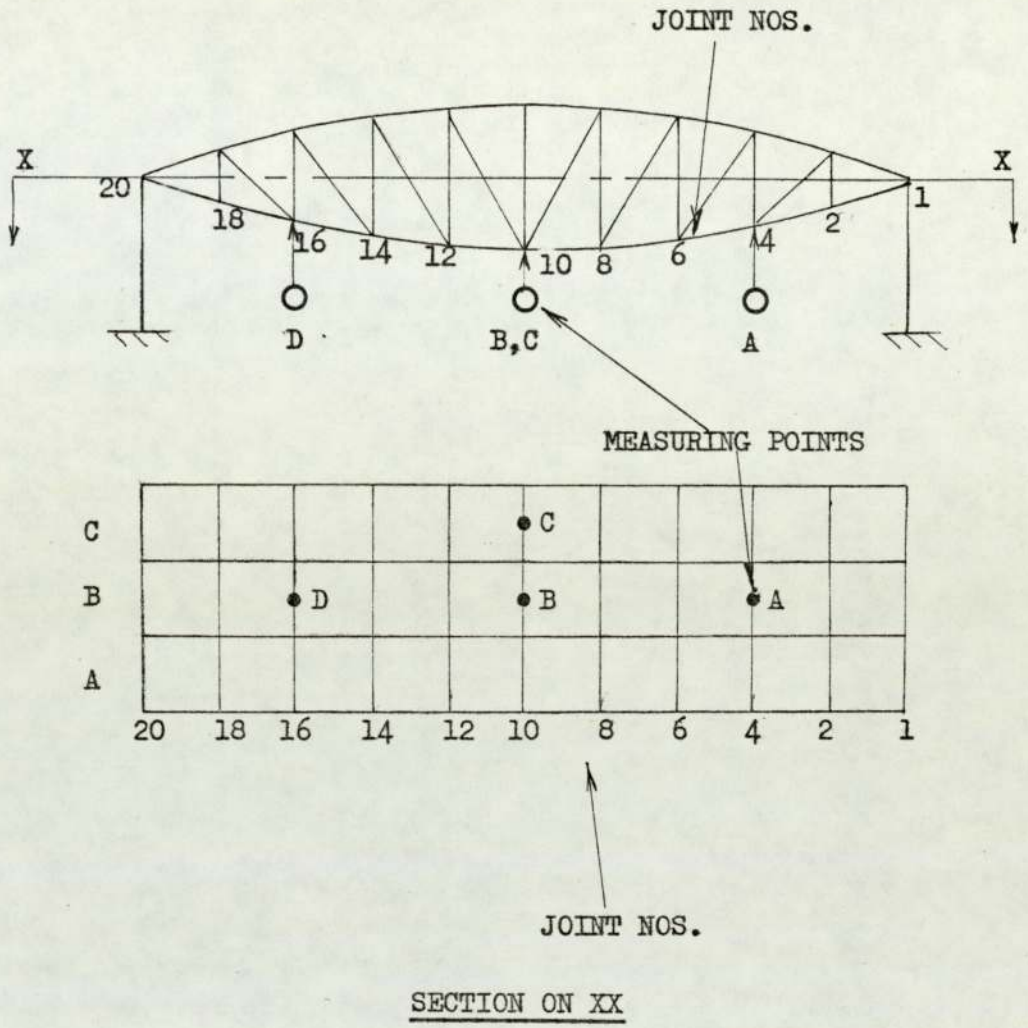


FIG. 7.3 COMPARISON BETWEEN THEORETICALLY DETERMINED
AND EMPIRICALLY DETERMINED MODEL ROOF
DEFLECTIONS
SNOW LOADING

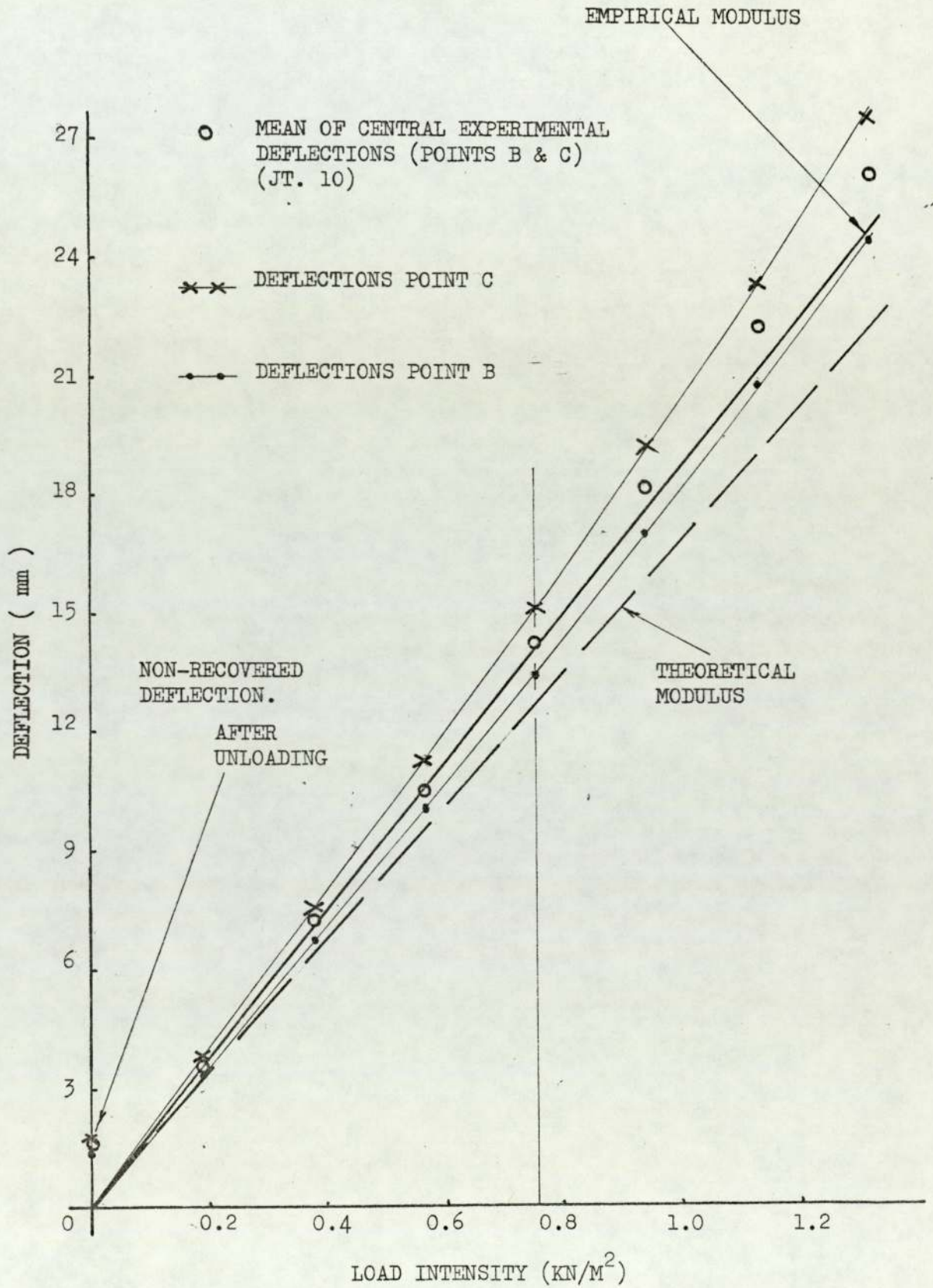


FIG. 7.4 DEFLECTION OF JOINTS 4 AND 16 (POINTS A & D)
SNOW LOADING

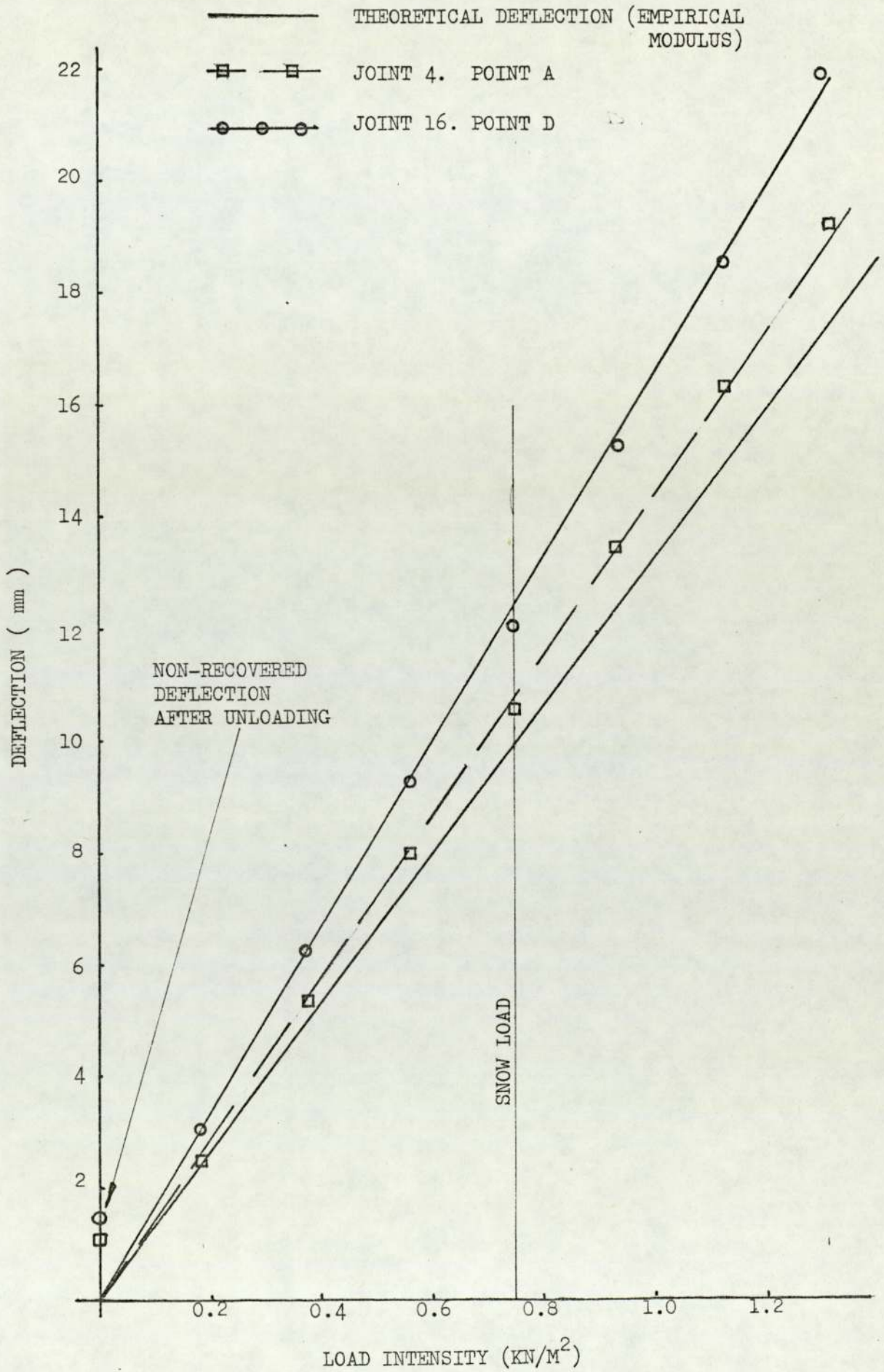


FIG. 7.5 COMPARISON BETWEEN THEORETICAL AND
EXPERIMENTAL CENTRAL ROOF
DEFLECTIONS. WIND LOAD

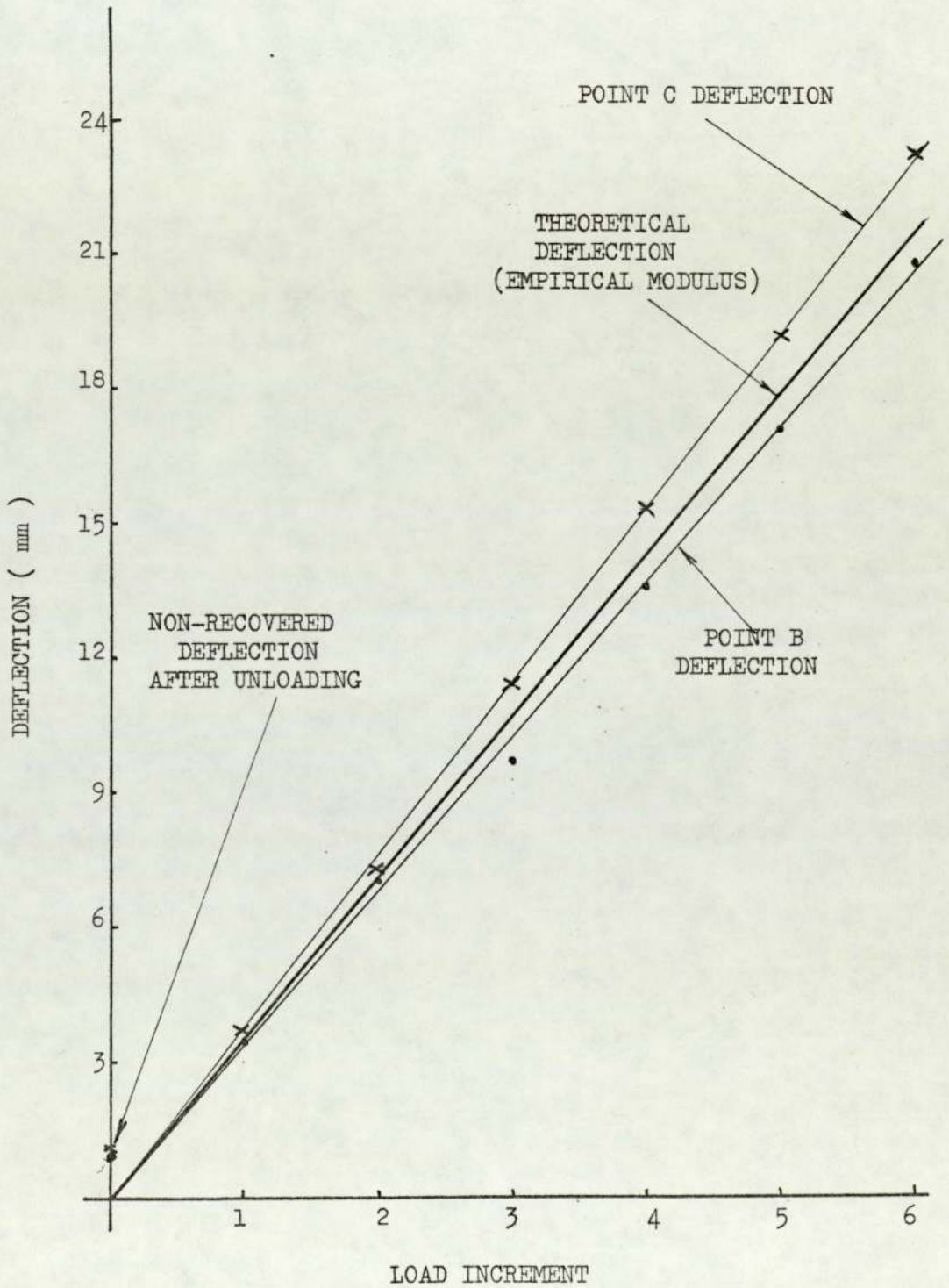
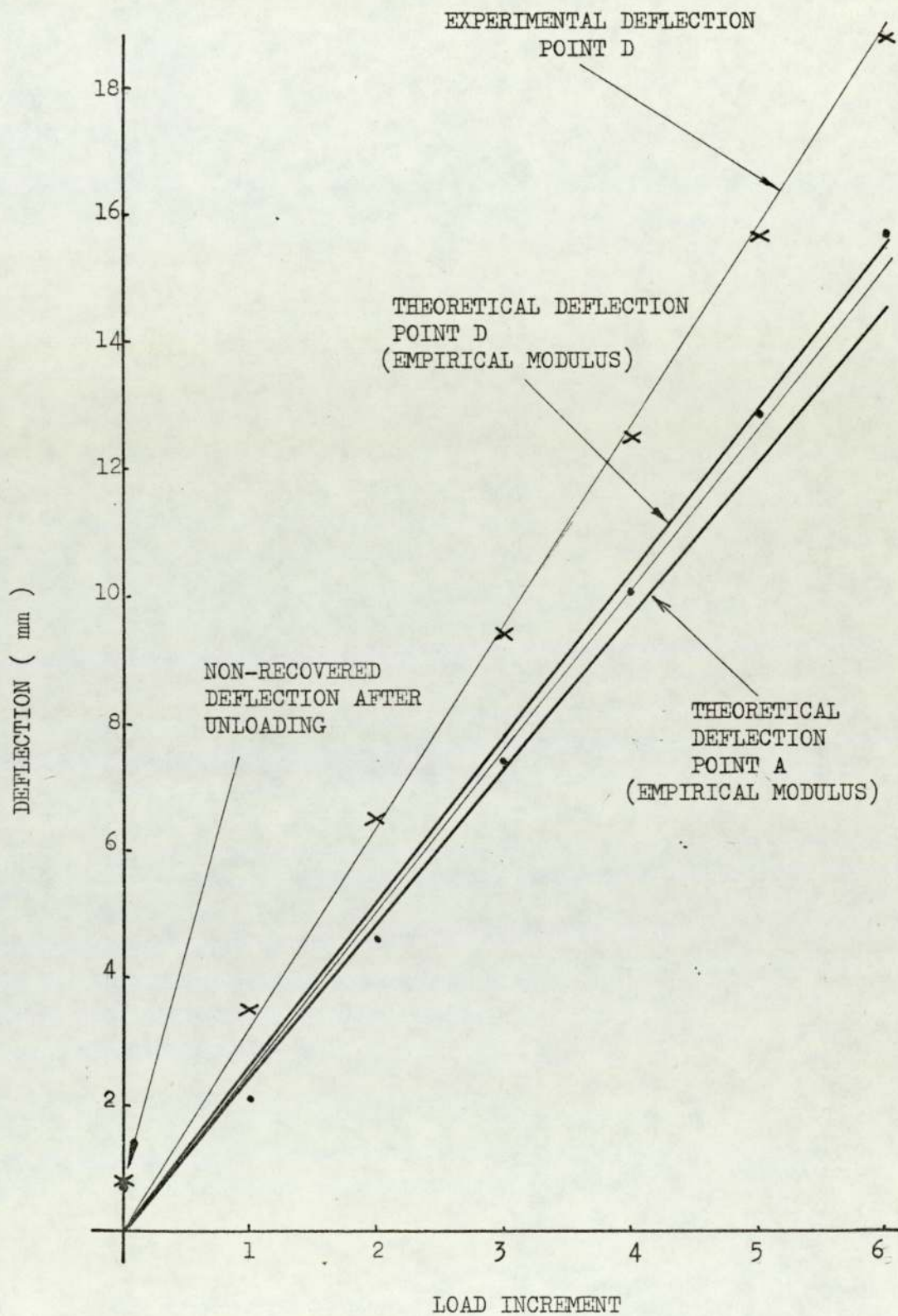


FIG. 7.6 DEFLECTION OF JOINTS 4 AND 16 (POINTS A & D)
WIND LOADING



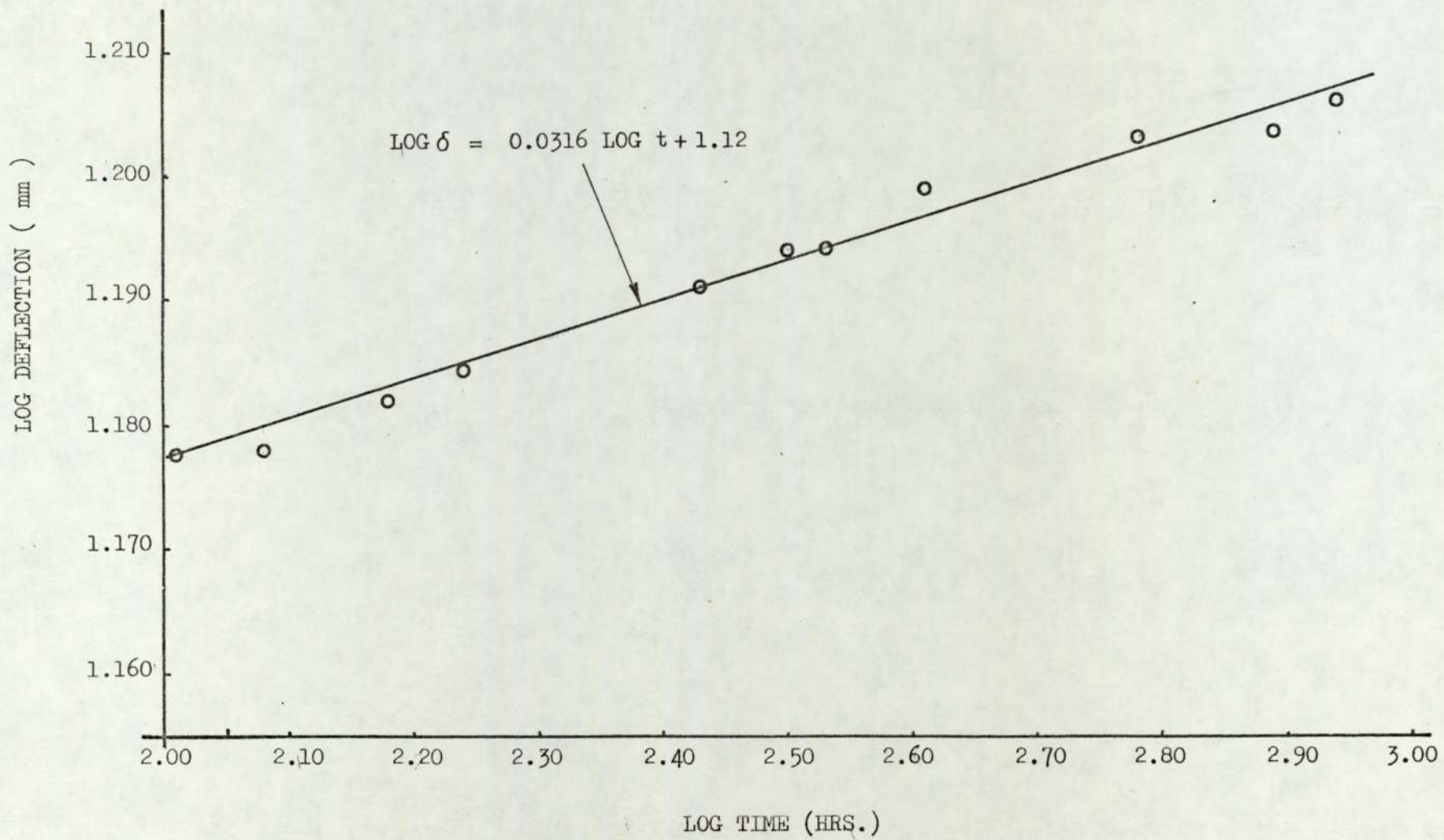


FIG. 7.7 ROOF CREEP: GRAPH OF LOG TIME
AGAINST LOG DEFLECTION

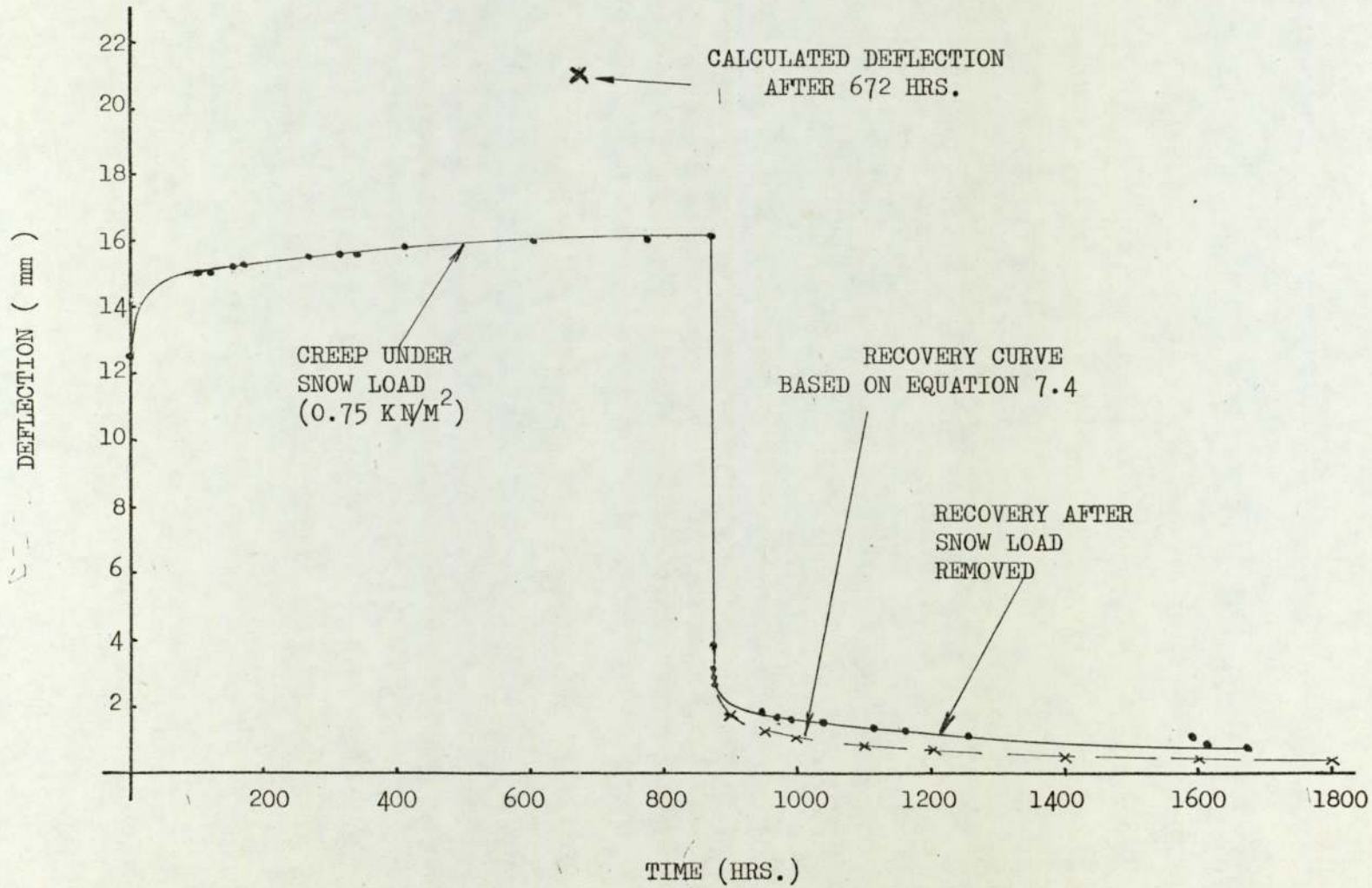


FIG. 7. 8 ROOF CREEP: GRAPH OF TIME AGAINST DEFLECTION

MEMBER	STRAIN GAUGE NOS. (SEE FIG. 7.9)	STRAIN ($M/M \times 10^{-4}$)															
		1		2		3		4		5		6		7		8	
		THRY	EXP	THRY	EXP	THRY	EXP	THRY	EXP	THRY	EXP	THRY	EXP	THRY	EXP	THRY	EXP
20A		-4.07	-2.18	-4.07	-0.94	-2.48	-2.47										
20B		-4.07	-3.40	-4.07	-1.82	-2.48	-1.98	-2.68	-2.51	-2.68	-2.76	-2.87	-1.69	-2.87	-1.04	-2.72	-0.80
20C		-4.07	-4.06	-4.07	-3.10	-2.48	-3.38										
19A		2.77	2.28	2.77	-0.73	4.30	0.56										
19B		2.77	1.89	2.77	1.86	4.30	3.22										
18A		-4.43	-1.68	-4.43	-2.86	-2.84	-4.50										
18B		-4.43	-3.43	-4.43	-2.74	-3.84	-4.16	-2.84	-4.33	-2.84	-4.14	-2.93	-4.03	-2.93	-3.52	-2.79	-4.67
18C		-4.43	-3.17	-4.43	-1.32	-2.84	-5.74										
17A		2.86	2.62	2.86	3.03	4.16	4.53										
17B		2.86	4.56	2.86	2.82	4.16	0.51										
17C		2.86	4.42	2.86	2.63	4.16	3.05										
12B		-4.24	-3.27	-4.24	-3.67	-3.63	-	-3.91	-4.12	-3.91	-3.59						
11B		3.64	3.20	3.64	3.12	4.31	2.70	3.98	2.29	3.98	3.18						

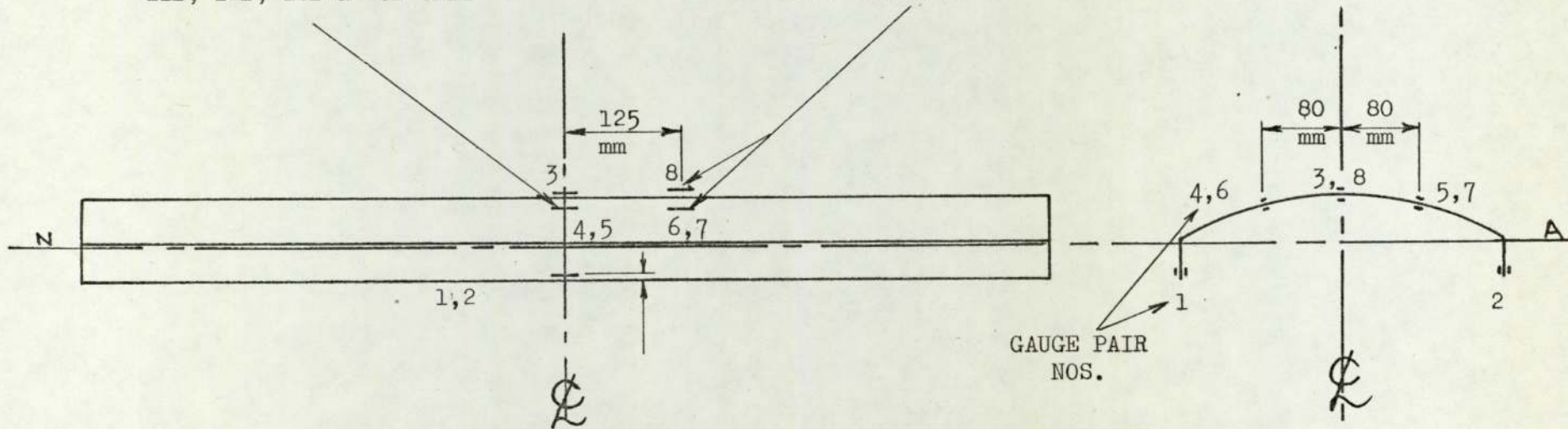
FIG. 7.9. TABLE OF THEORETICAL AND EXPERIMENTAL STRAINS AT SNOW LOAD ($0.75 \times KN/M^2$)

MEMBER	STRAIN GAUGE NOS. (SEE FIG. 7.11)	STRAIN ($M/M \times 10^{-4}$)					
		1		2		3	
		THYR	EXP	THYR	EXP	THYR	EXP
12A		-4.24	-3.68	-4.24	-4.20	-3.63	-4.59
11A		3.64	4.54	3.64	3.52	4.31	4.68
10B		-4.24	-3.48	-4.24	-2.96	-3.63	-3.97
9B		3.64	3.38	3.64	2.82	4.31	3.41
2B		-4.07	-4.58	-4.07	-3.16	-2.48	-2.36
1B		2.77	4.11	2.77	2.93	4.30	-

FIG. 7.10 TABLE OF THEORETICAL AND EXPERIMENTAL
STRAINS AT SNOW LOAD (0.75 KN/M²)

GAUGES IN THIS
POSITION ON MEMBERS:
11B, 12B, 18B & 20B ONLY

GAUGES IN THESE
POSITIONS ON MEMBERS:
18B & 20B ONLY



GAUGES USED IN PAIRS: ONE ON
EACH SIDE OF SECTION

FIG. 7.11 POSITION OF STRAIN GAUGES

FIG. 7.12 GRAPH OF EDGE-BEAM STRAIN AGAINST LOAD

FOR MEMBERS 20 A, B & C

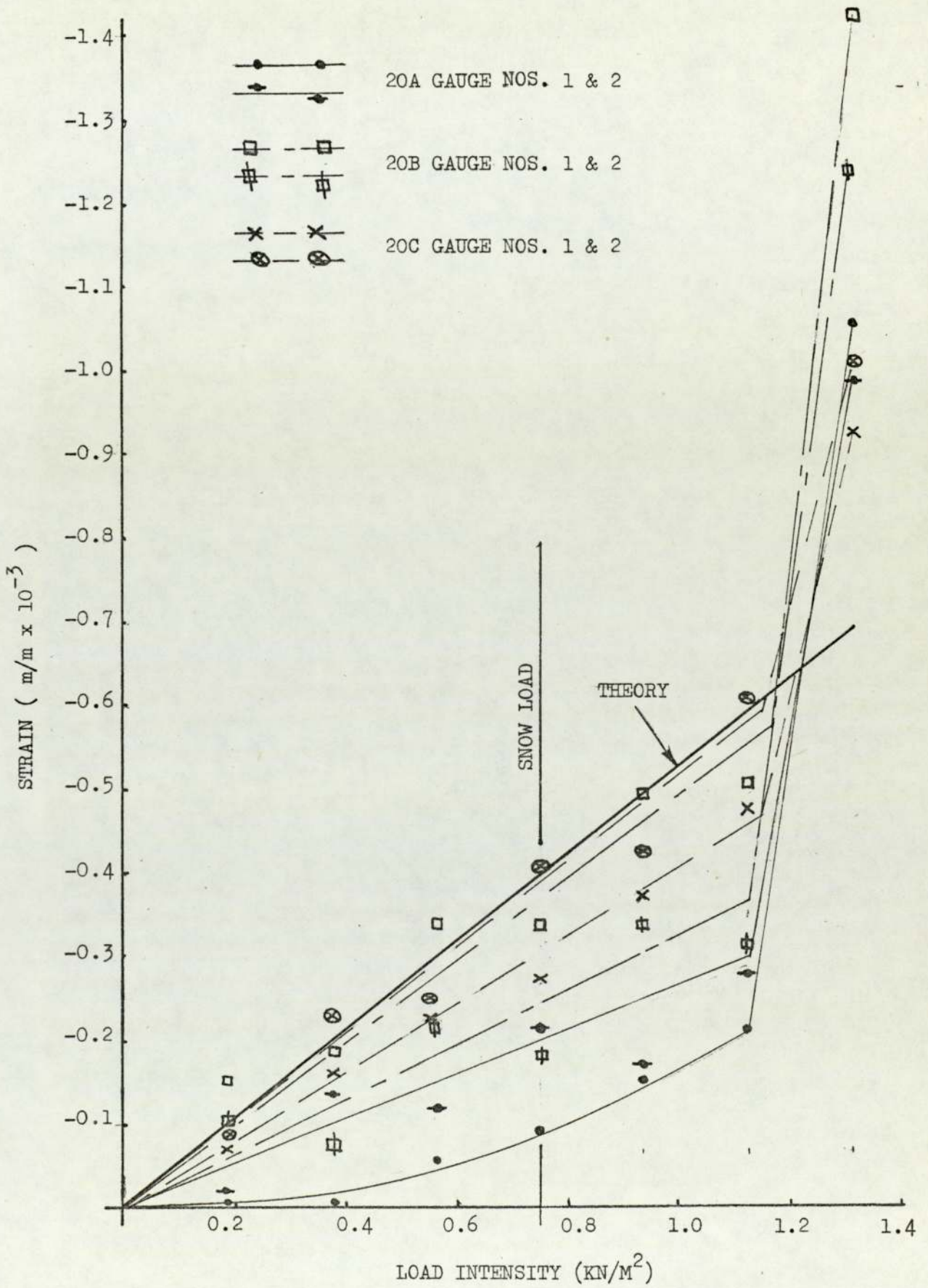


FIG. 7.13 GRAPH OF CYL. SECTION SUMMIT STRAIN

AGAINST LOAD FOR MEMBERS

20 A, B & C

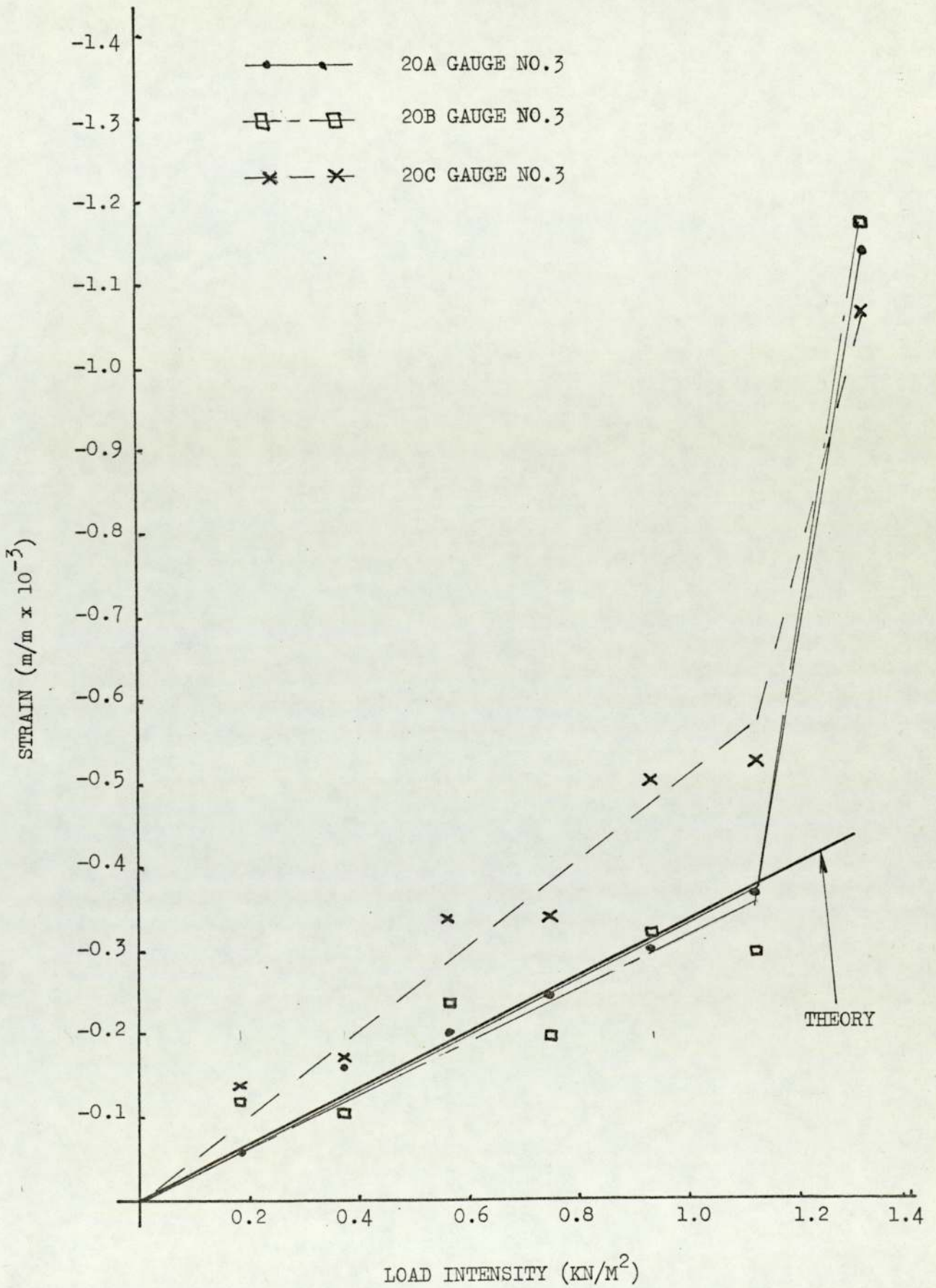


FIG. 7.14 GRAPH OF EDGE-BEAM STRAINS AGAINST LOAD
FOR MEMBERS 18 (STRAIN GAUGE NOS. 1 & 2)

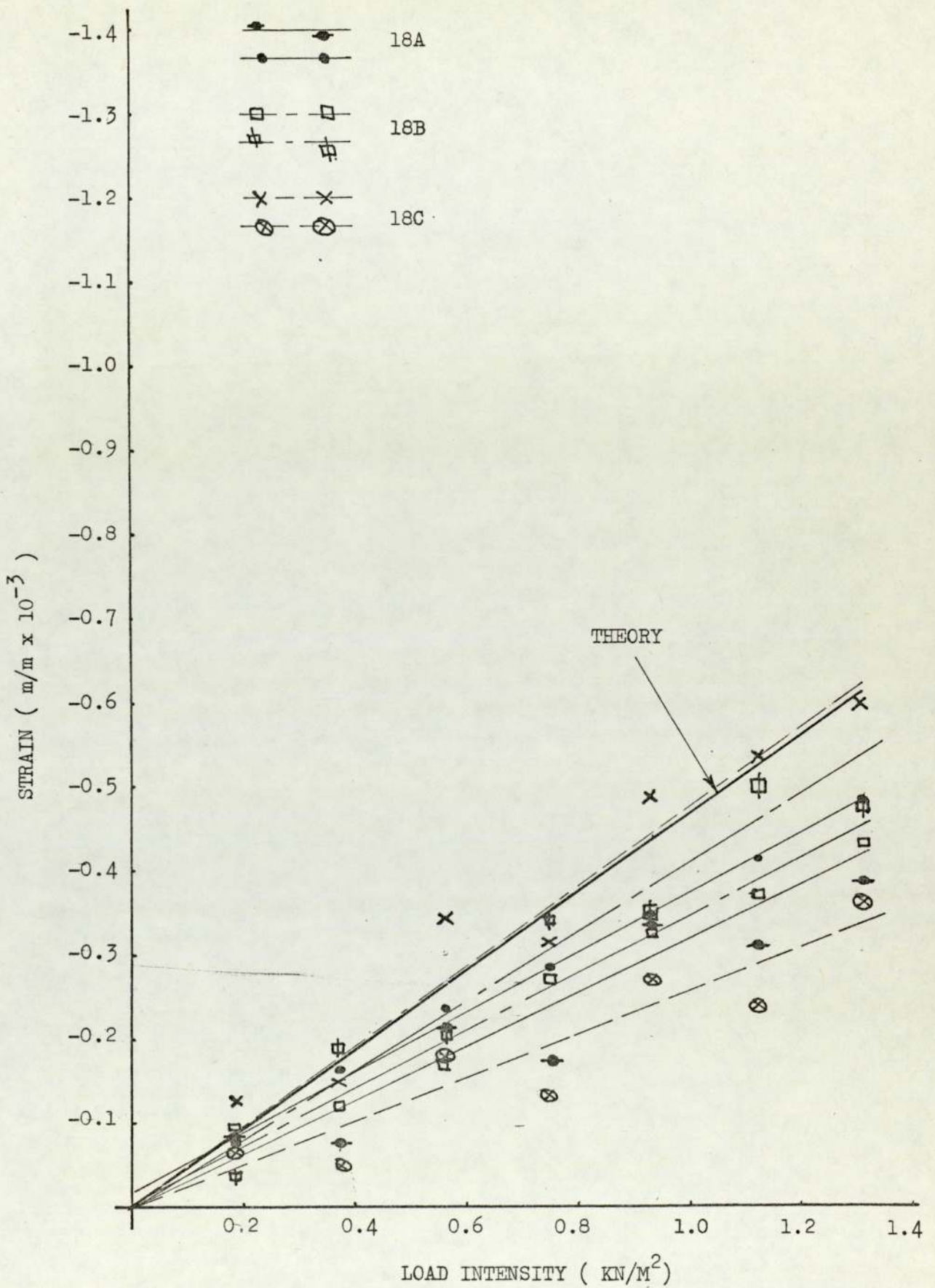


FIG. 7.15 GRAPH OF CYLINDRICAL SECTION SUMMIT

STRAIN AGAINST LOAD FOR MEMBERS

18 A, B & C (GAUGE NO. 3)

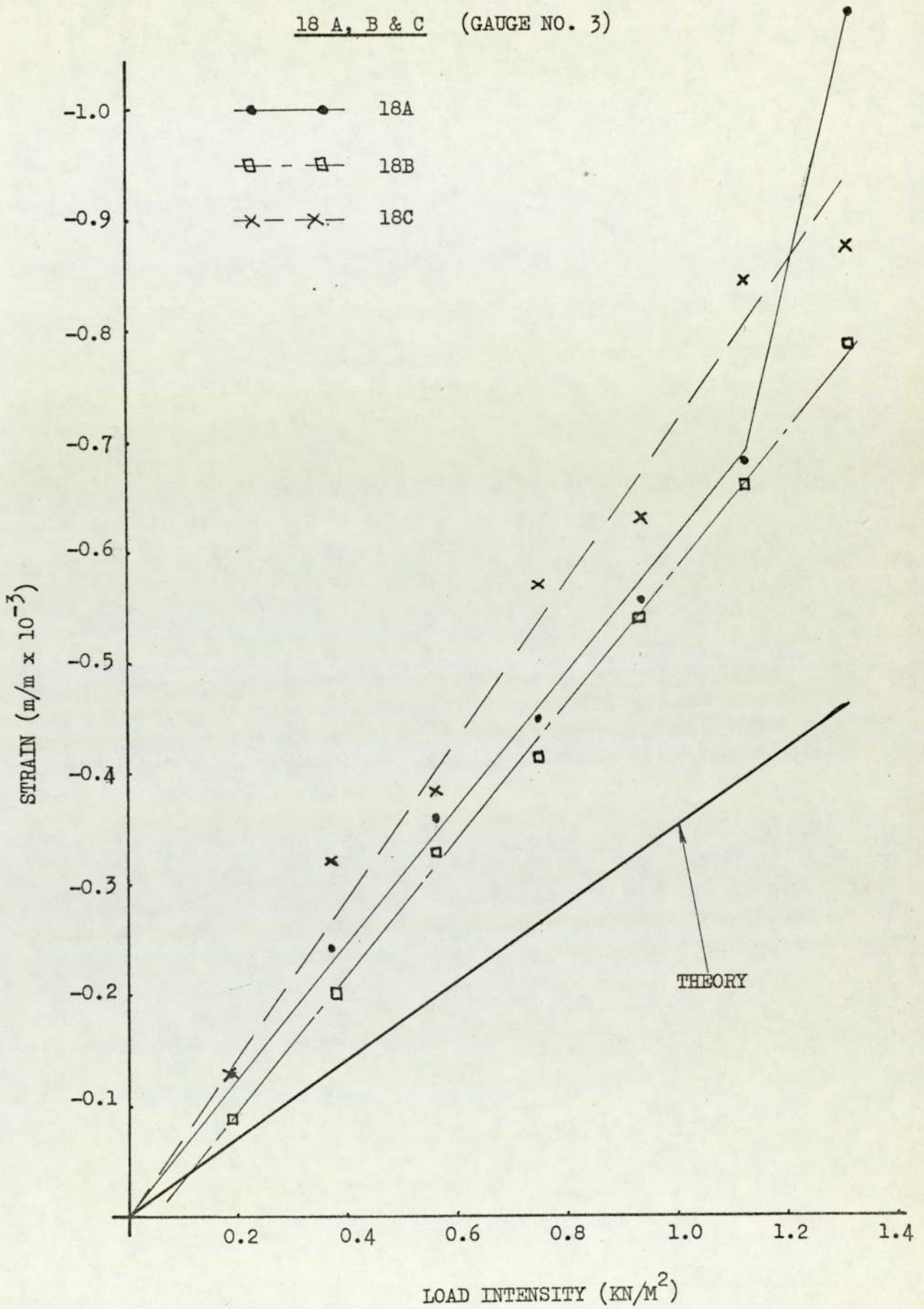


FIG. 7.16 GRAPH OF EDGE-BEAM STRAIN AGAINST

LOAD FOR MEMBERS 17 A, B & C
(GAUGE NOS. 1 & 2)

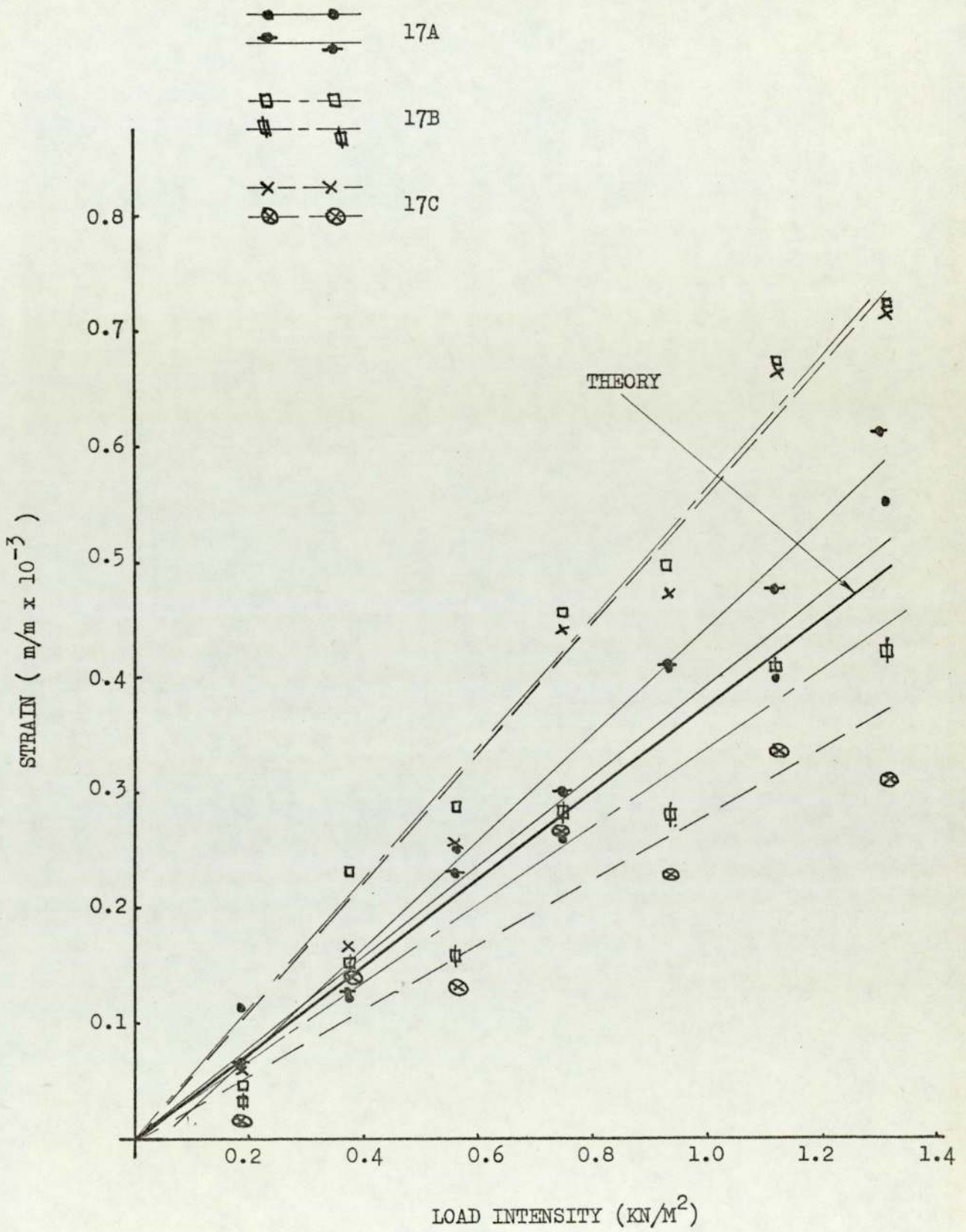


FIG. 7.1⁷
GRAPH OF CYLINDRICAL SECTION SUMMIT
STRAIN AGAINST LOAD FOR MEMBERS
17 A, B & C (GAUGE NO. 3)

- — ● 17A
- — □ 17B
- × — × 17C

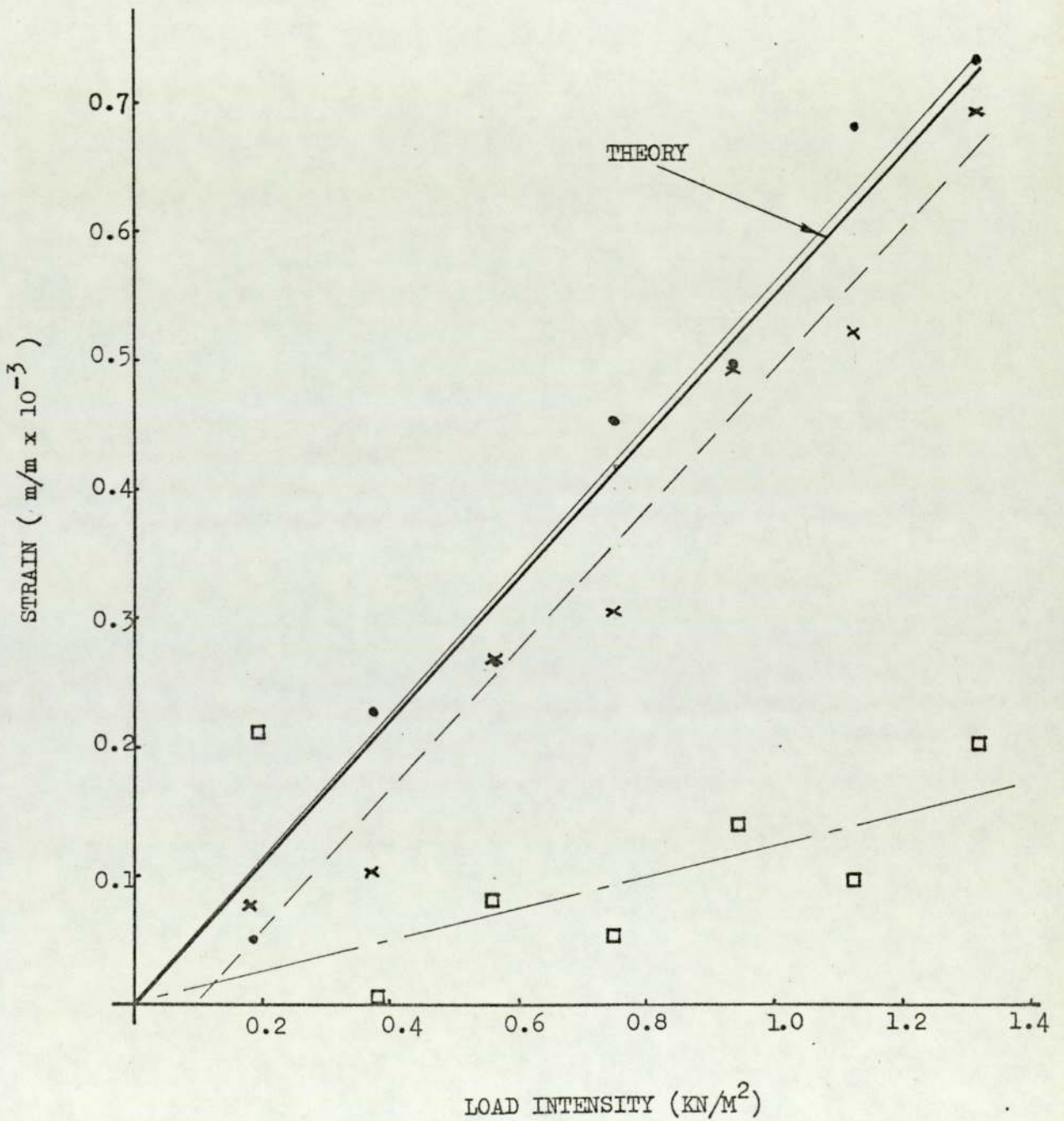


FIG. 7.18 ROOF MEMBER AFTER LOCAL BUCKLING

EXPERIMENTAL STRAIN IN MEMBERS 20
AT SNOW LOAD (0.75 KN/M²)

THEORY

EXPERIMENTAL RESULTS

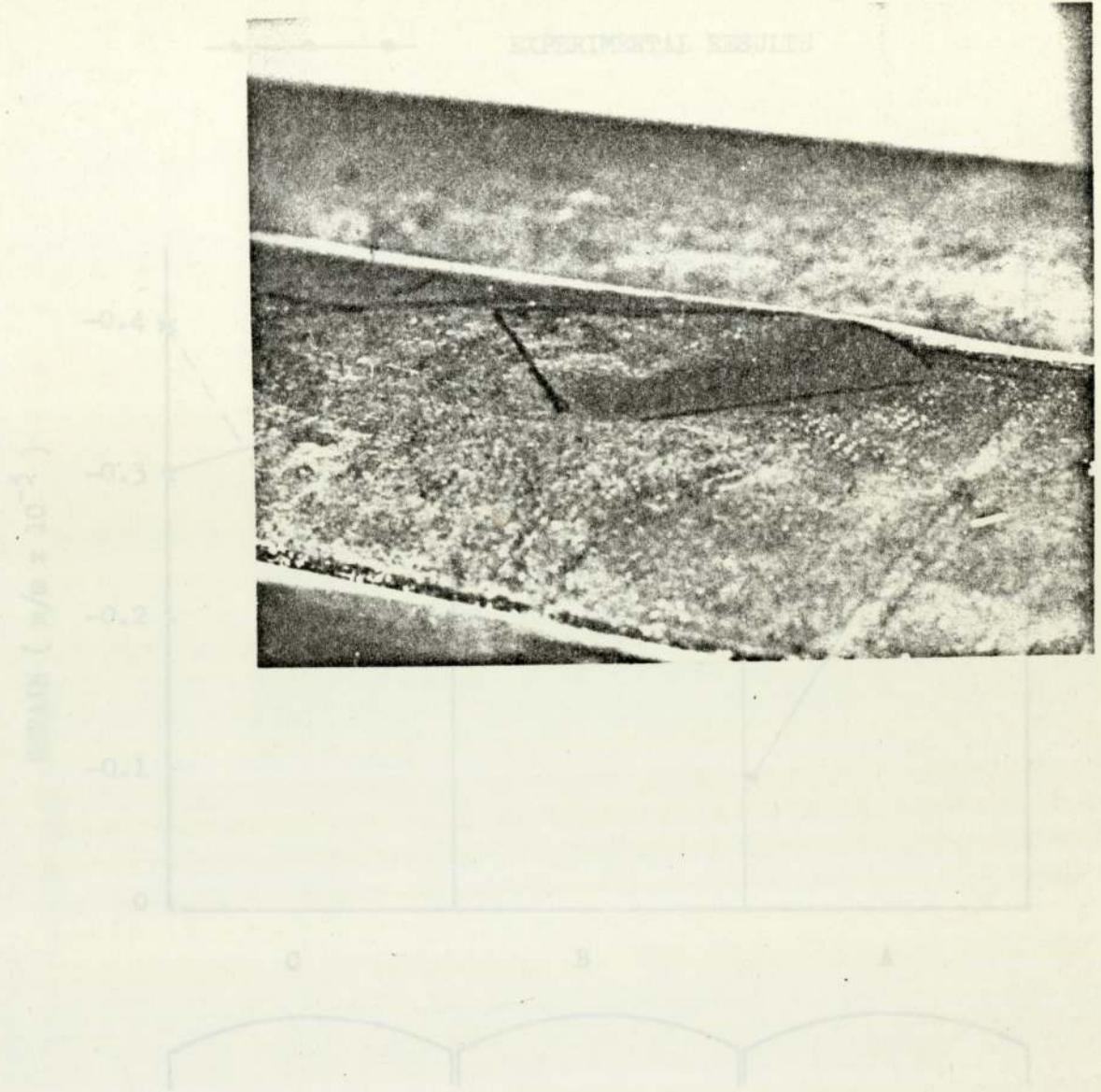


FIG. 7.20 COMPARISON BETWEEN THEORETICAL AND EXPERIMENTAL
STRAIN IN MEMBERS 19 A, B & C UNDER SNOW LOADING

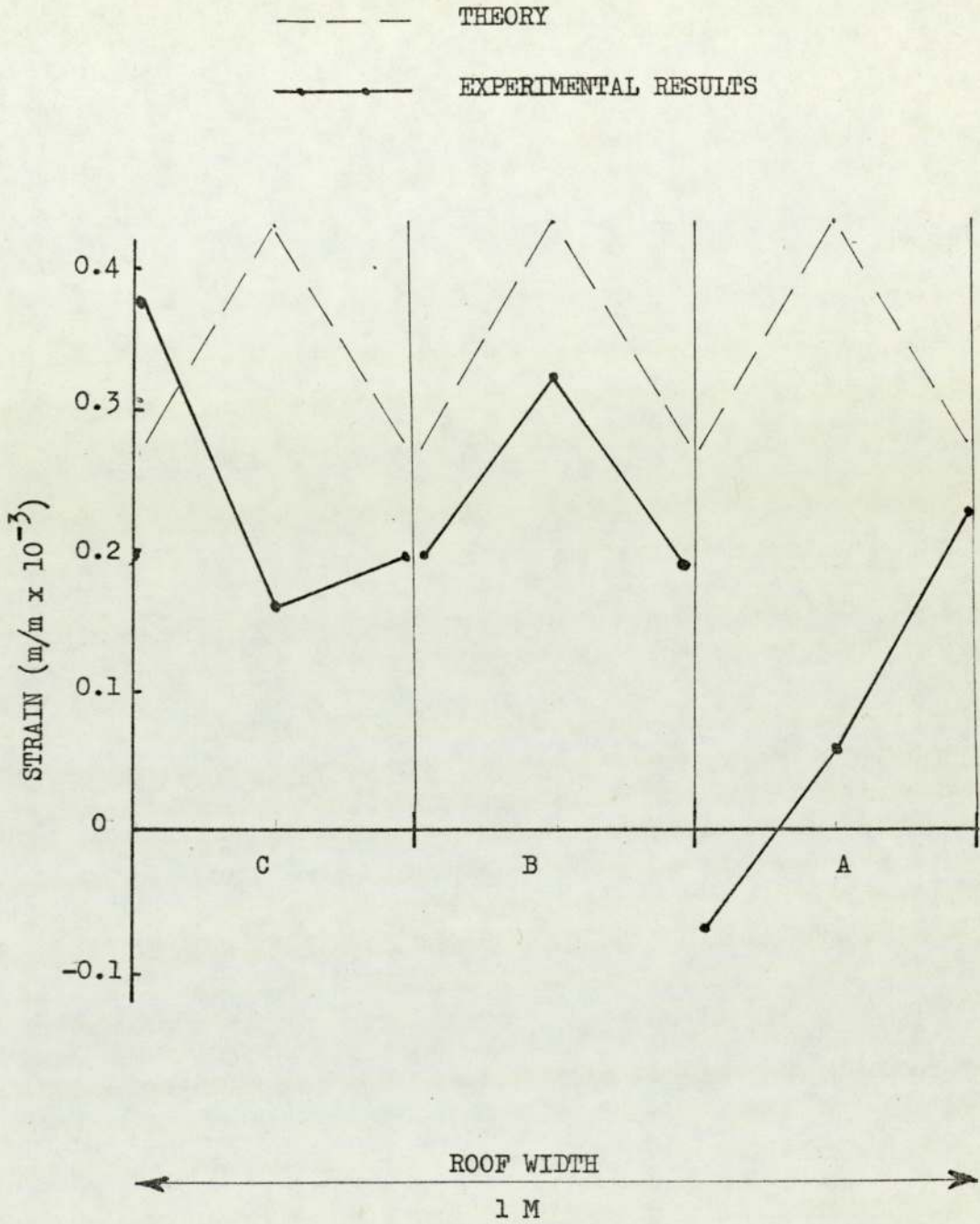


FIG. 7.21 COMPARISON BETWEEN THEORETICAL AND
EXPERIMENTAL STRAIN IN MEMBERS 18
AT SNOW LOAD (0.75 KN/M²)

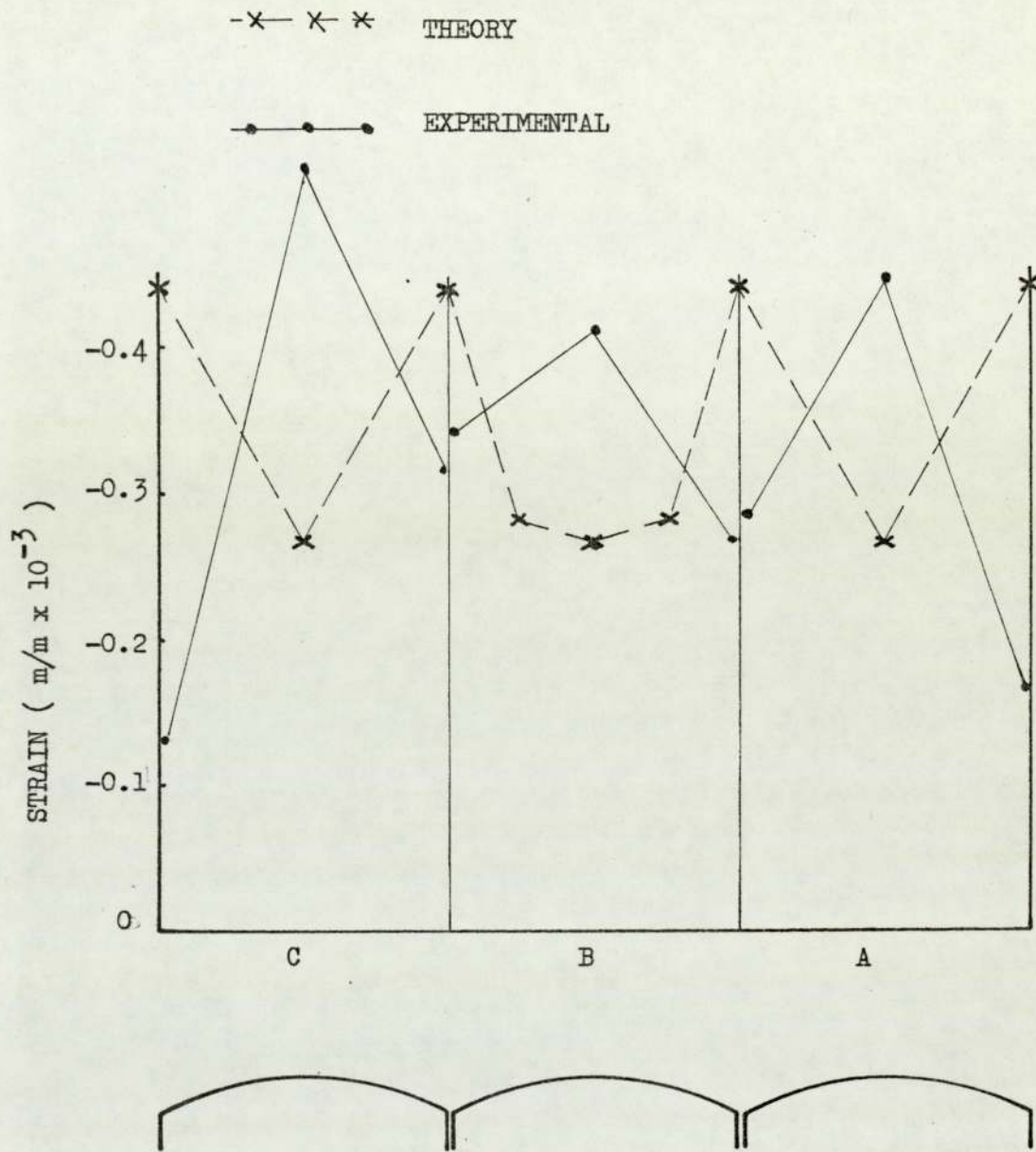


FIG. 7.22 GRAPH OF STEEL MEMBERS 21, 36 & 37

STRAIN AGAINST LOAD - SNOW LOADING

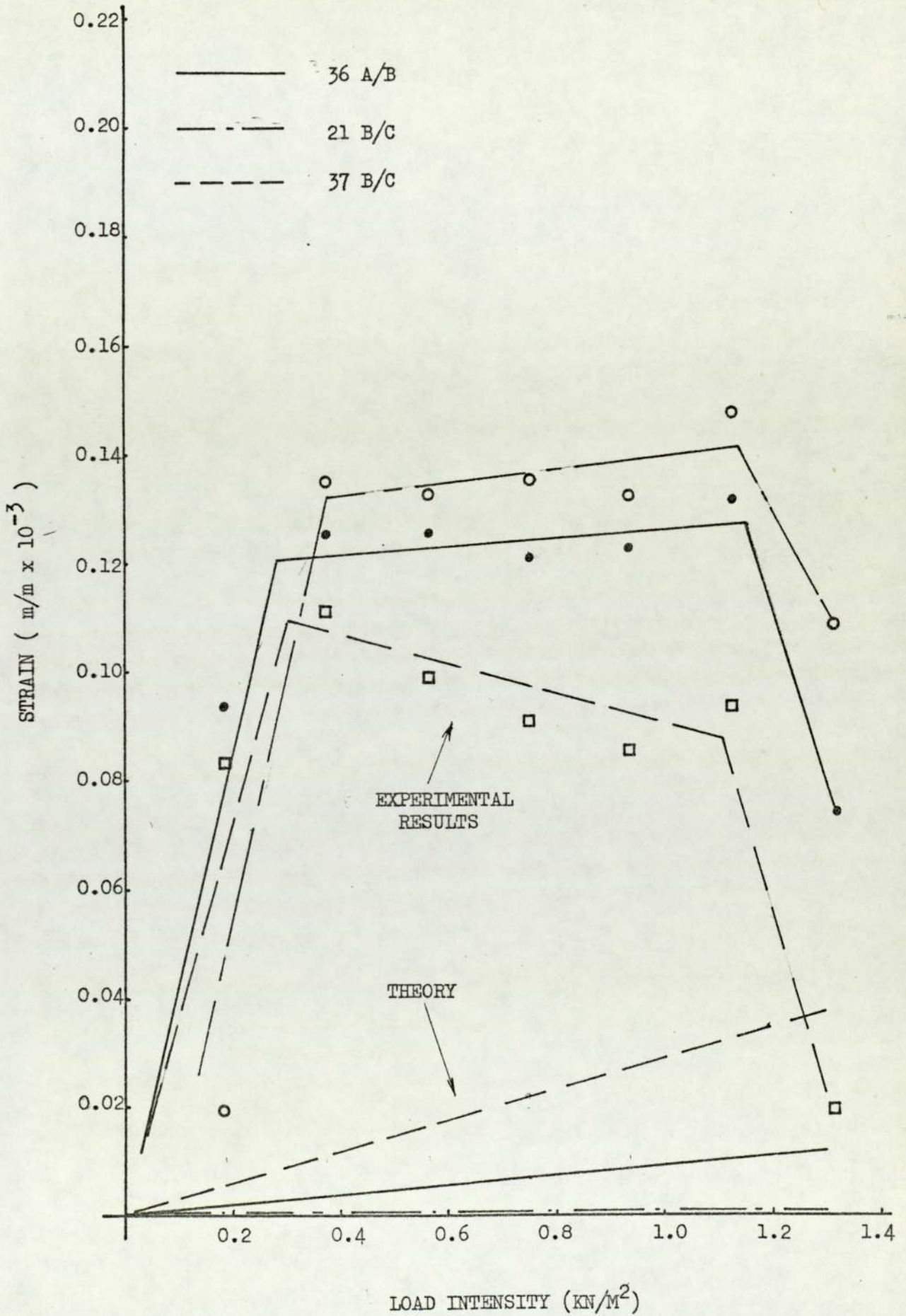


FIG. 7.23 GRAPH OF EDGE-BEAM STRAIN AGAINST LOAD FOR
MEMBERS 18 A, B & C - WIND LOADING (GAUGES 1 & 2)

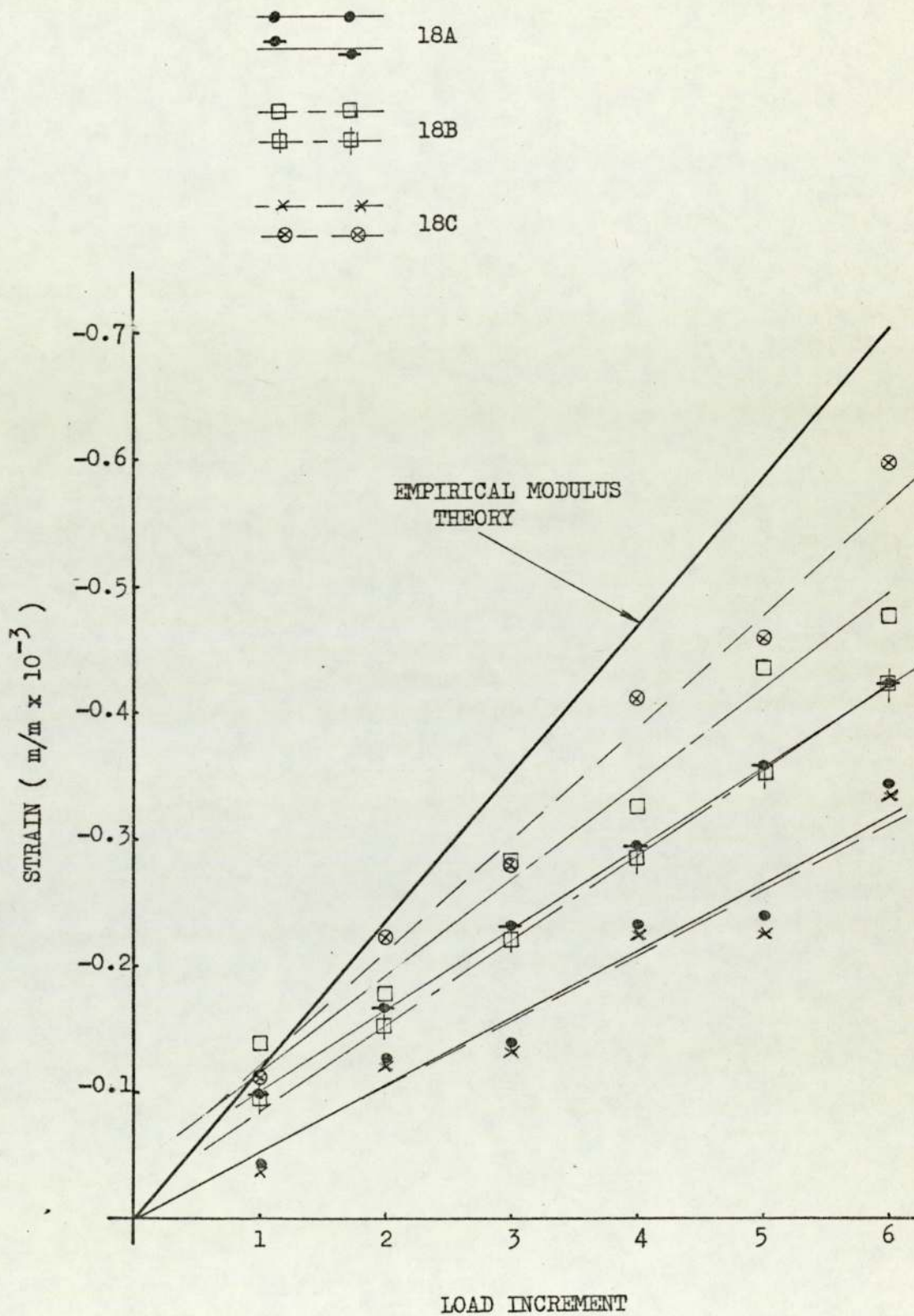


FIG. 7.24 GRAPH OF CYL. SECTION SUMMIT STRAIN AGAINST
LOAD FOR MEMBERS 18 A, B & C - WIND LOADING
STRAIN GAUGE NO. 3

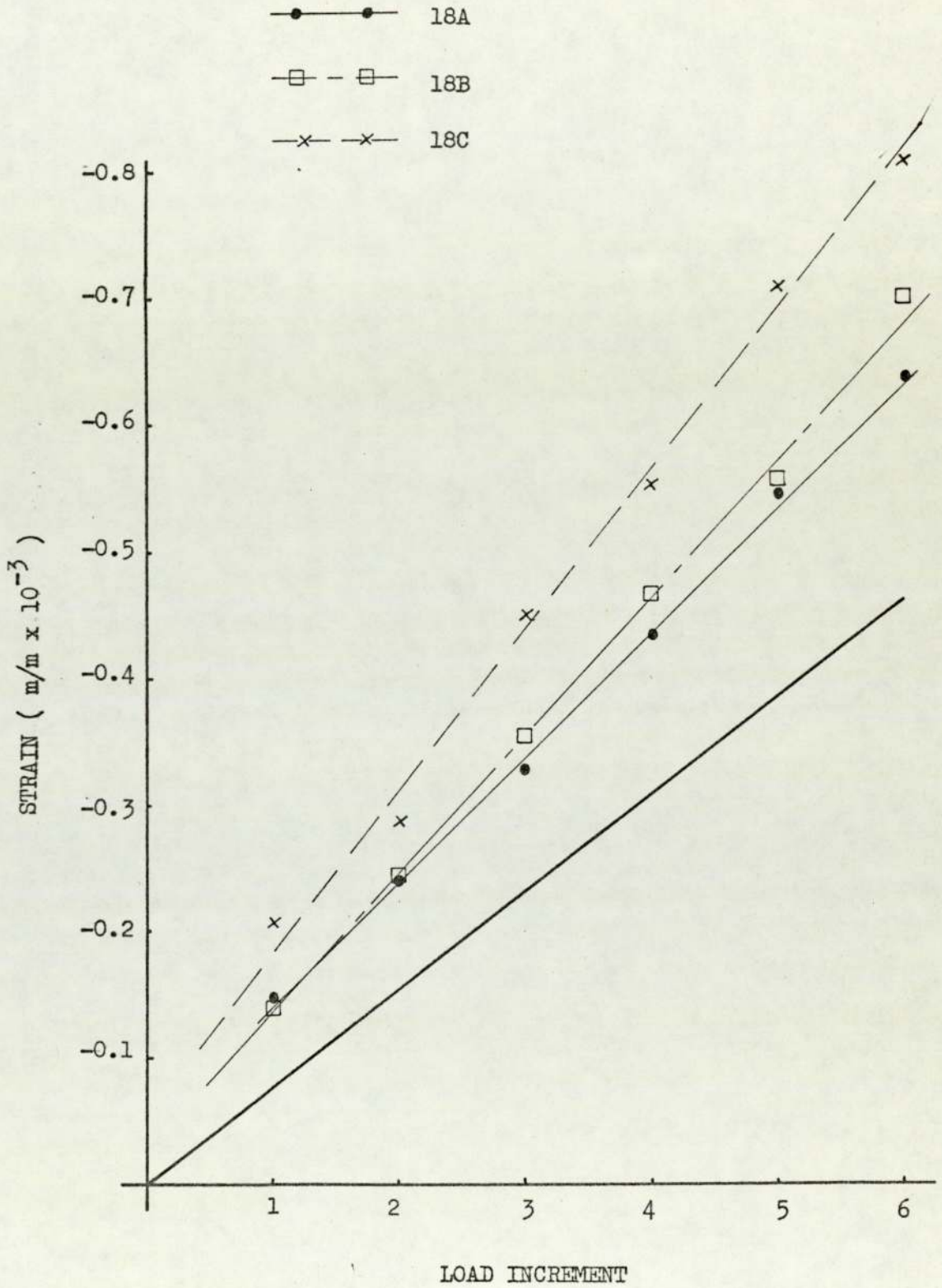


FIG. 7.25 GRAPH OF EDGE-BEAM STRAIN AGAINST LOAD FOR
MEMBERS 17 A, B & C - WIND LOADING
(GAUGE NOS. 1 & 2)

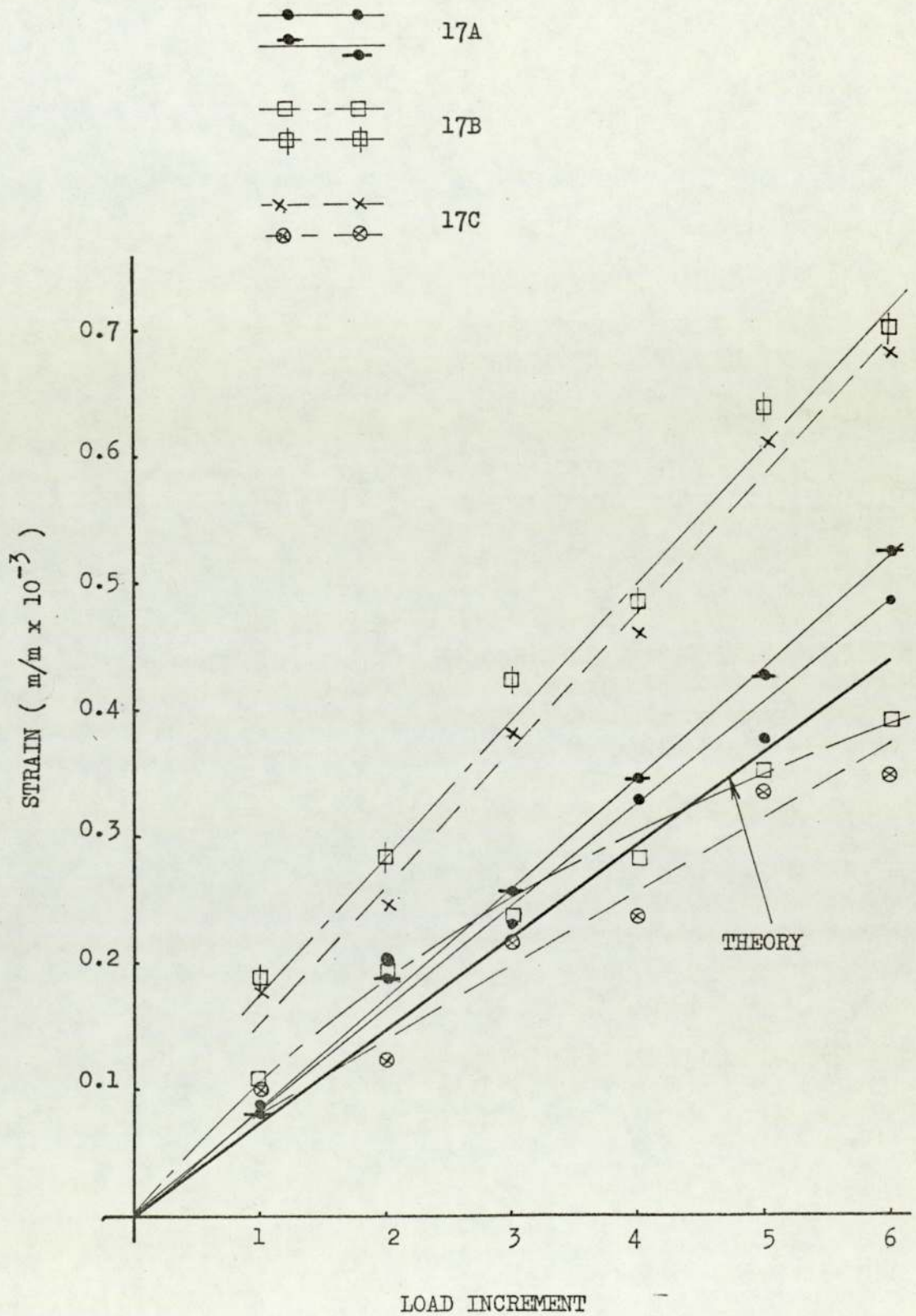
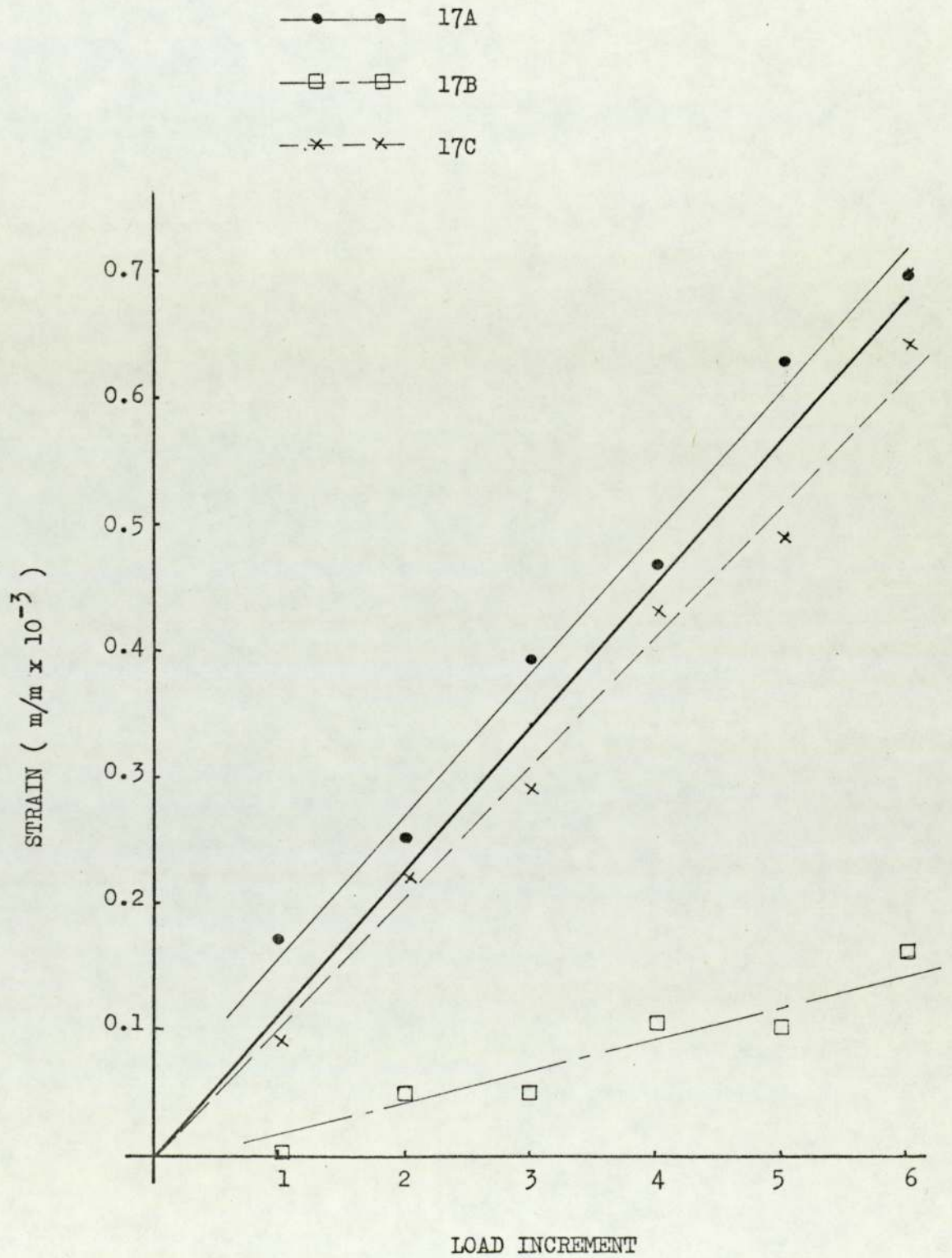


FIG. 7.26 GRAPH OF CYL. SECTION SUMMIT STRAIN AGAINST
LOAD FOR MEMBERS 17 A, B & C - WIND LOADING
(STRAIN GAUGE NO. 3)



CHAPTER 8

ECONOMIC ASPECTS

CHAPTER EIGHT

Economic Aspects

8.1

Introduction

In the previous chapters the structural feasibility of long-span lightly loaded structures has been investigated. In Chapter 4, the basis for an economic feasibility study was laid by analysing the production costs of grp components. The concern, therefore, of this chapter is to investigate the economics of long span roofs and in particular the 60 m roof designed in Chapter 5. The cost of the designed roof will be estimated and compared with conventional roof structures.

The costs of the conventional roof structures, the steel work for the grp roof and all erection costs are based on information supplied by I.D.C. Limited, Stratford. Grp raw material cost

figures were supplied by Fibreglass Limited. Profits have not been allowed for in the costings which are based on February 1975 figures. Many of the conventional roofs have actually been built for some years; accordingly their costs have been up-dated with the use of a "Building Costs Chart" published by "Building" [8.1].

8.2

The Cost of Long Span Grp Roofs

8.2.1 Selection of a Grp Production Process

In order to produce the grp roof surface units designed in Chapter 5 it is envisaged that two production processes would be utilised; i.e. the robot spray-up process for the unit as a whole, but with the unidirectional laminate in the edge-beams being produced using a crude "home-made" pultrusion process. In the latter process, rovings would be pulled firstly through a resin bath and then through a steel die. Finally, the laminate would be cured on a waxed flat surface at room temperature. The robot spray-up process has been chosen, in preference to the other processes considered in Chapter 4, for the following reasons:

- 1) Low cost glass reinforcement may be used.
- 2) Non-skilled labour used predominantly.
- 3) The laminate quality is more easily controlled and reproducible.
- 4) Efficient at reasonably low production rates.
- 5) Less initial capital investment required than for the hot press process.

8.2.2 Calculation of Roof Cost

For the purposes of calculating the grp surface units' production costs, a production rate of 5.3 units per day will be assumed. The significance of this assumption will be discussed in section 8.3. It will also be assumed that the production costs for product B, Chapter 4, expressed in terms of £/unit weight may be applied to the production of the surface unit including the pultruded edge-beams. The capital outlay required for the pultrusion process would be nominal, and the productivity of the process at least as high as the robot spray-up process. For the purposes of this study an additional allowance will be made for overheads based on 50% of the direct labour costs.

Costs of Product B

Direct Production Cost	£20.75 (See Fig. 4.17)
Overheads at 50% of labour	
Costs	<u>£ 7.97</u>
Total Production Cost	£28.72

Weight of Product B = 176 kg (1.8 KN)

Cost per unit weight = £0.163 kg (£16.6/KN)

The self-weight of grp in the 60 M roof = 0.172 KN/M^2

∴ Production cost of grp = $£2.86/\text{M}^2$ or the production cost of one surface unit = £28.6.

Roof Surface Units' Raw Material Costs

Initially, general purpose polyester resin will be assumed.

Basic cost of resin	£0.50/kg
Basic cost of glass fibre	£0.58/kg
Basic cost of polyurethane foam	£24/m ³
Weight of resin in roof	4.48 kg/m ²
Weight of glass fibre	4.30 kg/m ²
Volume of foam	12.7x10 ⁻³ m ³ /m ² of roof
Cost of glass fibres	£4.99/m ² of roof
Cost of resin	£4.48/m ² of roof
Cost of polyurethane foam	£0.30/m ² of roof
Allowance for wastage (10%)	£0.98/m ² of roof
Total cost of materials	£10.75/m ² of roof

Cost of Steel Work

The cost of steel work is based on a combined cost for raw materials and fabrication of £280/Tonne.

Roofs' steel work self-weight = 11.0 kg/m² (0.108 KN/M²).

Steel work raw materials and production cost = £3.08/m².

Roof Erection Costs

Erection costs are based on a figure of £25/Tonne.

Total self-weight of the roof 28.6 kg/m² (0.28 KN/M²).

Cost of erecting roof £0.98/m²

8.2.4 Possible Developments and Modifications

From Fig. 8.2 it is apparent that the raw materials constitute the major cost area for 60 m grp roof. Thus any raw material cost savings can have an important effect on the overall roof cost. Unfortunately, there does not appear to be any potential for reducing the cost of the glass fibre reinforcement since the cheapest form of fibres is already being utilised.

There is a possibility for making savings with regard to the resin, however. Various low-cost fillers may be combined with the resin, so that for a constant volume laminate upto 30% of the resin cost may be saved [8.3]. This corresponds to an 8% saving on the total roof costs. The effect the filler would have on the long term properties of grp is, however, unknown.

Polyester resins have been developed continuously for many years and there are now many different types to meet various requirements. Of particular interest to the roof construction industry is the possibility of using transparent or translucent resin in a roof to give a controlled natural lighting effect at little or no extra cost. Glazing in conventional roofs often increases the cost substantially. Natural lighting could also have an important effect on the total life cost of a building. At a time when energy is becoming relatively more expensive the cost of heating and lighting industrial buildings will be taken increasingly into account when choosing a building envelope. A double-skin structure, such as the one designed in this project, has considerably more potential for efficient

thermal insulation than single skin structures. The air between the skins, if prevented from moving, will provide a high degree of thermal insulation.

Roof maintenance is a third area where grp roofs may be expected to show lower operating costs. The low maintenance requirements of grp has now been recognised in the building industry, which has led to its increasingly widespread use as a cladding material.

The effect of reducing the span of the roof on the cost per unit area may be investigated by calculating the cost of the 10 m span model roof. If this is carried out on the basis of the same cost per unit weight per unit area as the 60 m span roof, then the cost of a 10 m span roof is approximately $\text{£}15/\text{m}^2$. As shown in Fig. 8.1, this cost is slightly higher than that of the portal frame. However, assuming a linear relationship between span and grp roof cost, then a grp roof would be competitive with steel lattice frame roofs of 15 m and greater.

On increasing the span of a grp roof beyond 60 m, its competitiveness would be expected to increase, as at greater spans grp may be used more efficiently. The thickness of the cylindrical section of the 60 m roof surface units was chosen as the minimum practical thickness to prevent penetration from incidental and maintenance loads. The stiffening was then designed so as to provide adequate resistance to local buckling. Thus largely secondary loads and considerations determined the amount of randomly-orientated glass reinforcement used. On increasing the span, the minimum thickness may be maintained, and the increased loads taken by optimising the cylinder stiffening, and increasing the proportion of unidirectional

material used. Unidirectional grp is, as established in Chapters 3 and 4, considerably more efficient in resisting axial loads, where buckling is not a problem, than random reinforcement.

A further consequence of enlarging the span is to increase the roof's weight per unit area. Eventually a point would be reached where the self-weight of the roof is greater than the maximum upward thrust of the wind. Under such circumstances it would be possible to replace the lower roof surface, which would always be in tension, by a cable of almost completely unidirectional material; again increasing the efficient use of grp.

Reducing the span-to-depth ratio of the 60 m grp roof so as to reduce the loads in the surfaces, would not be expected to reduce the cost significantly. Any savings made on the grp material costs would be restricted to reducing the amount of efficient unidirectional edge-beam material, and would have to be offset against increased cross-bracing costs. There would, however, be an optimum span-to-depth ratio for minimum cost. Where the deflection of the roof had to be minimised, an increased depth of roof would be most beneficial.

8.3

The Long Span Grp Roof Market

Potential

The market for long span roofs, above 30 m, in Great Britain is growing. In 1963 only 15% of all major industrial buildings were over 30 m in span, by 1969, 24% were greater than 30 m [8.2].

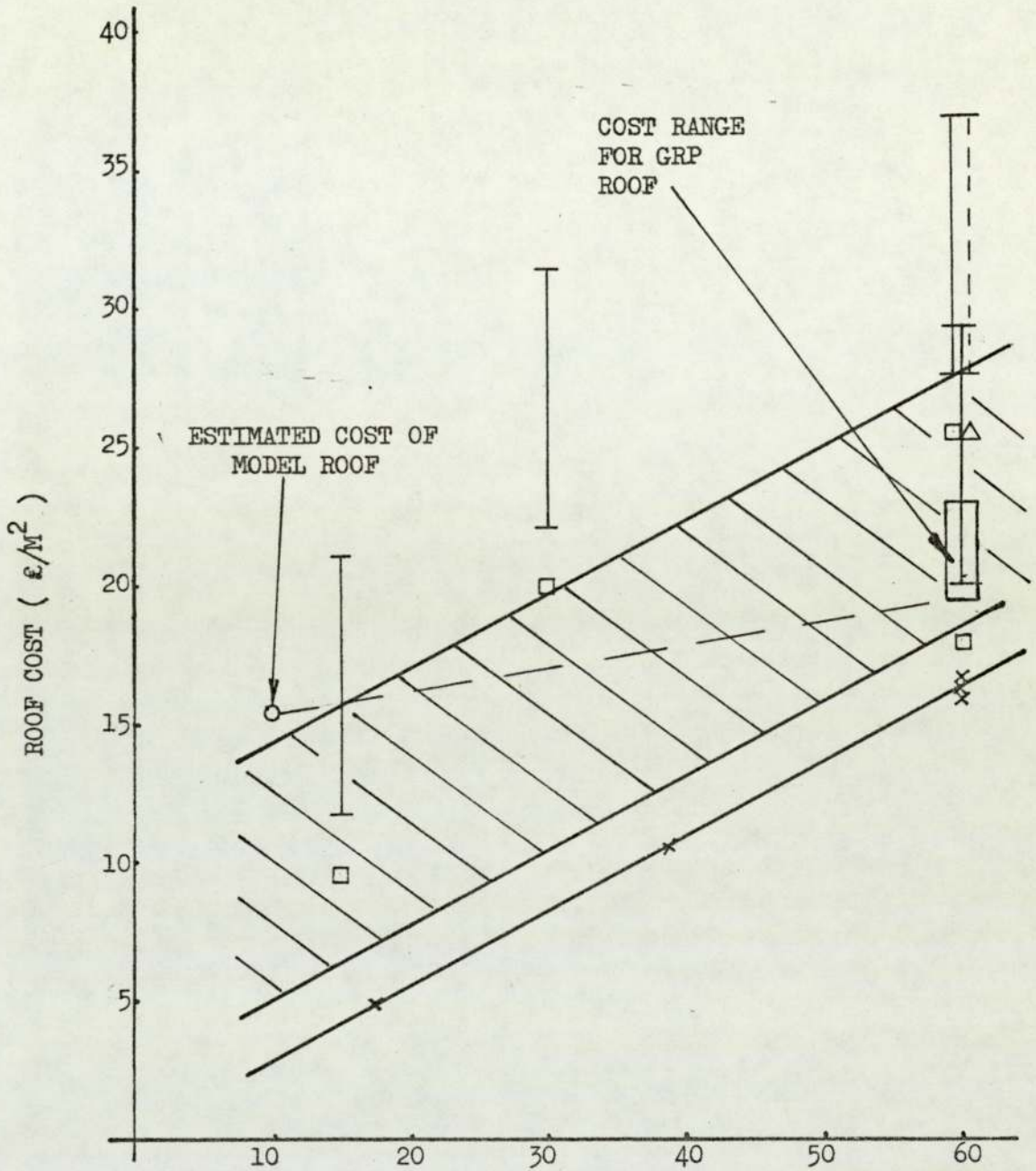
This trend may be expected to continue, since industry in its quest for increasing efficiency during a time of rapid change, requires adaptability from its buildings. Larger spans give more clear space and more versatility.

In 1971 the total area of major (over 925 M² or 10,000 ft²) industrial buildings completed was 3.8×10^6 M². Assuming the same proportion of long-span roofs as in 1969 the total area of buildings with a clear span of over 30 m is 910,000 M². The proportion of this area taken by 60 m span roofs is likely to be small. However, a production rate of 5.3 surface units per day, as was assumed in Section 8.2., is equivalent to a total roof area of 12,985 m²/yr. or 1.43% of the market for roofs over 30 m in span. The assumed production would, therefore, appear to be reasonable and would account for an even smaller proportion of the European or World markets.

Although at spans greater than 60 m the competitive position of grp roofs would be expected to improve, the size of the market would not be of any great commercial interest. At smaller spans, grp roofs are expected to remain competitive with all roofing systems down to approximately 30 m, and competitive with all roofs, with the exception of portal frame roofs, down to approximately 15 m. This gives a total market potential for grp roofs of 1.43×10^6 M². Assuming an average weight of glass fibres in the roofs to be 4 kg/m², the total potential market for glass fibres is 5,600 Tonnes. and for grp as a whole, approximately double this amount.

To conclude: long span grp roofs are competitive with conventional roof systems over a wide range of spans and are therefore economically feasible.

FIG. 8.1 ROOF COST AGAINST SPAN



STEEL WORK COSTS

x

PORTAL FRAME

□

LATTICE FRAME
(VARIOUS TYPES)

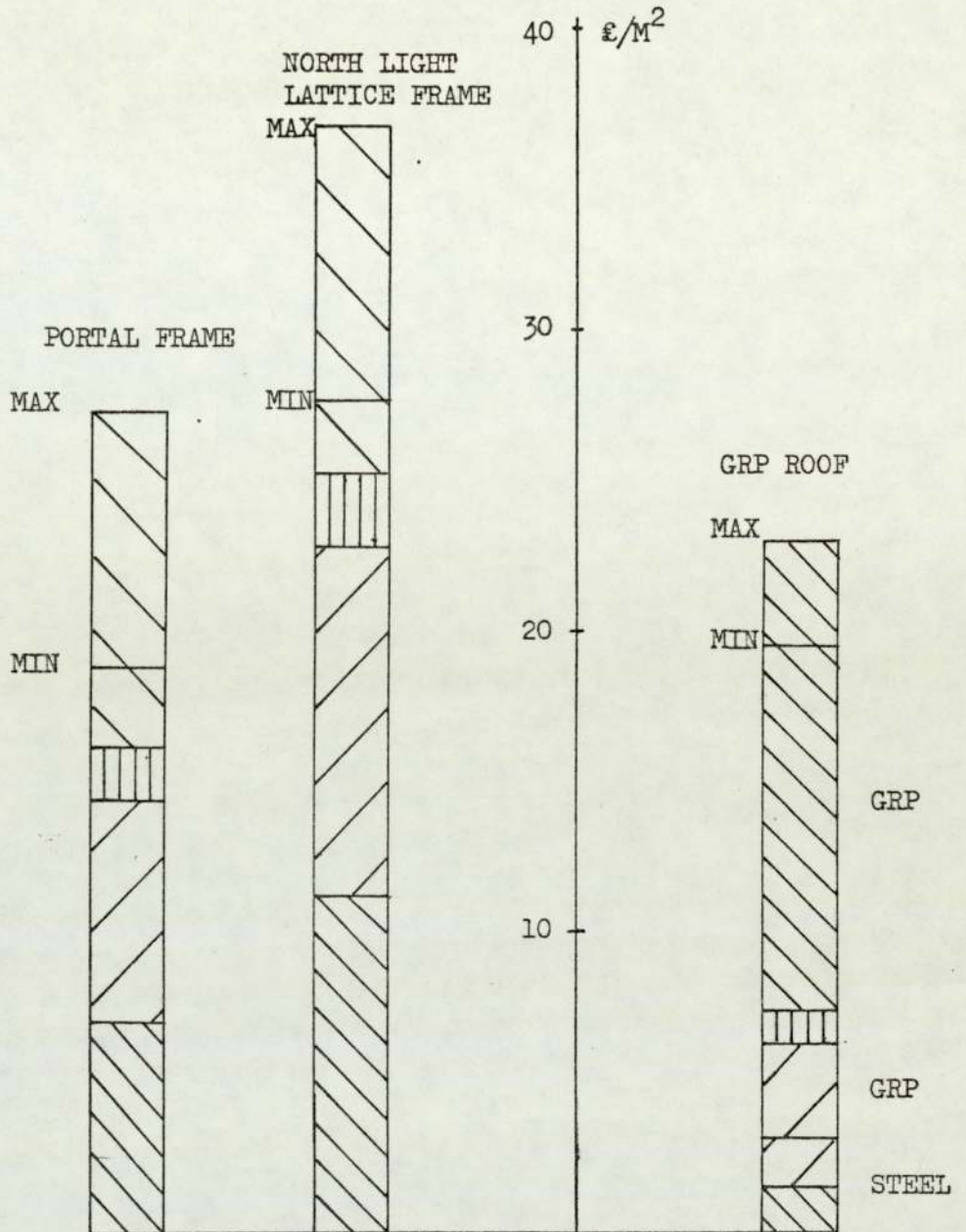
△


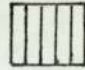
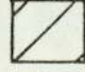

POST-TENSIONED
PRECAST CONCRETE
ARCH

CLADDING COST RANGE



FIG. 8.2 BREAK-DOWN OF ROOF COSTS AT A SPAN OF 60 M



-  CLADDING COSTS (LATTICE & PORTAL FRAMES ONLY)
-  ERECTION COSTS
-  FABRICATION OR PRODUCTION COSTS
-  RAW MATERIAL COSTS

CHAPTER 9

CONCLUSIONS & RECOMMENDATIONS FOR

FURTHER WORK

CHAPTER NINE

Conclusions and Recommendations for Further Work

In this final chapter the general conclusions of the project will be presented. They will be followed by recommendations for further work to: a) aid the development of the roof designed in this project, b) to provide structural designers with useful data, and c) investigate other areas where grp may be applicable.

Conclusions:

- 1) Grp's loss of strength and stiffness over the 50 year life of a long span roof is significant and should be taken into account during design.

- 2) Creep strains, of the order likely to be experienced in long span grp structures, are largely recoverable on unloading.

- 3) Fibre orientation and volume fraction have a significant effect on the cost-effectiveness of laminates under various loading conditions.
- 4) Mechanised laminating processes considerably reduce the manufacturing costs of grp components at production rates relevant to the building industry.
- 5) The mouldability of grp enables the designer to use efficient structural shapes without incurring a financial penalty, and thus compensates for the high raw material costs.
- 6) It is structurally feasible to build a 60 m span roof using the structural design concepts employed in this project.
- 7) The low specific gravity of grp enables structures to be designed which are considerably lighter than conventional structures.
- 8) The cost of large grp components when produced in quantity is due predominantly to the cost of the raw materials.
- 9) Long span grp roof structures are economically feasible.

10) It has been shown that long span lightly loaded grp structures are feasible. However, grp's strength-to-weight ratio is not the major property which compensates for its relatively high material cost, when roof structures are considered, as can be seen from the table below. The long term specific strengths are based on the long term strengths assumed for grp in the design of the 60 m roof.

MATERIAL	ULTIMATE STRENGTH σ_{ULT} (KN/M ²)	SPECIFIC GRAVITY (S.G.)	$\frac{\sigma_{ULT}}{S.G.}$
STEEL (STRUCTURAL)	4.5×10^5	7.8	5.8×10^4
CSM)	7.8×10^4	1.42	5.5×10^4
UDR)	6×10^5	1.88	3.2×10^5
SHORT TERM			
CSM)	3.5×10^4	1.42	2.5×10^4
UDR)	7×10^4	1.88	3.7×10^4
LONG TERM			

Recommendations for Further Work:

- 1) Optimisation of the grp roof's proportions for minimum cost.
- 2) Quantification of the financial benefits due to reduced maintenance and other operating costs for roofs.
- 3) A study, in greater depth, of the economics of roofs of smaller spans than 60 m.
- 4) Investigation of the long term strength of bolted joints.

- 5) Investigation of the effect of low cost fillers on the long term strength and stiffness of grp.
- 6) Investigation of the effect on creep of fibre strength in randomly-orientated fibre laminates.
- 7) Determination of the multi-axial creep characteristics of grp.
- 8) Analysis of the potential of grp in structures other than roof structures where the superstructure and cladding are normally separated, but where grp may be utilised applying the monocoque principle.

APPENDIX

APPENDIX A

In order to fit Findley's equation (3.36) to the creep results obtained, the computer programme below was written. The form of Findley's equation used is:

$$\log_{10} (\epsilon_t - \epsilon_0) = \log m + n \log t.$$

The input data for the programme consists of:

- a) The applied stress to the specimen (STRESS),
- b) The gauge length (LG),
- c) The initial Demec gauge reading (LO),
- d) The time to rupture (TR),
- e) The number of readings (P),
- f) The Demec reading at time t (ET),
- g) The time t (T).

The method of least squares is used and a regression line of $\log_{10} (\epsilon_t - \epsilon_0)$ on $\log t$ found. An interactive procedure is adopted to find the best value of ϵ_0 so that the standard error is minimised.

An example of a typical output from the programme is also given below where:

- LOG TIME = the logarithm of the time at which a reading was taken (hrs.).
- MEAS.Y = $\text{Log}_{10} (\epsilon_t - \epsilon_0)$ using the empirical value of strain ϵ_t and the best value of ϵ .
- EST.Y = $\text{Log}_{10} (\epsilon_t - \epsilon_0)$ computed using Findley's equation with the constants m, n and ϵ_0 as determined by the analysis.
- TIME = Time corresponding to $(\epsilon_t - \epsilon_0)$.
- (E - EO) = $(\epsilon_t - \epsilon_0)$ as computed using Findley's equation.
- MEAS.(E - EO) = $(\epsilon_t - \epsilon_0)$ calculated from empirical values of ϵ_t .
- EO = Best value of ϵ_0 .
- CONST = Constant 'm'.
- SLOPE = Constant 'n'.
- ETR = Strain at failure where appropriate or strain at 50 years.
- VAR = Standard error calculated from the least squares analysis.

```

DIMENSION E(21), T(21), ET(21)

INTEGER P

REAL LIMIT, MOD25, LO, LG

READ(8, 2) STRESS, LO, LG, TR, P

2   FORMAT(4F, 1I)

DO 3 I=1, P

READ(8, 4) ET(I), T(I)

4   FORMAT( 2F)

E(I) = (ET(I)-LO)/LG

WRITE(5, 111) T(I), E(I)

111 FORMAT(/, 5X, 'TIME = ', E15.7, 5X, 'STRAIN = ', E15.7)

3   CONTINUE

VAR=10. **10

L=1

M=E(1)*1000000. 0-1

WRITE(5, 112) L, M, N

N=(M-L)/10

113 FORMAT(/, 3I5)

100 DO 102 J=L, M, N

ZY=0

ZX=0

ZXAS=0

ZXY =0

ZXS=0

ZYS=0

DO 10 I=1, P, 1

EO=J/10000000. 0

E(I) = (ET(I)-LO)/LG

Y=ALOG10(E(I)-EO)

```



```

ZY= ZY+Y
X=ALOG10(T(I) )
ZX=ZX+X
ZXAS = ZX**2
ZYAS = ZY**2
ZYS = ZYS+Y**2
ZXY=ZXY+X*Y
ZXS=ZXS+X**2
10  CONTINUE
CONST = (ZY*ZXS-ZX*ZXY)/(P*ZXS-ZXAS)
SLOPE = (P*ZXY-ZX*ZY)/(P*ZXS-ZXAS)
SXY = SQRT ( (ZYS-CONST*ZY-SLOPE*ZXY)/(P-2) )
IF (SXY.LT.0.000001) GOTO 103
ACC=N/1000000. 0
IF (SXY-VAR)101,101,102
101  VAR=SXY
LIMIT=J
WRITE(5,112)EO,ACC,SXY,CONST,SLOPE,LIMIT
112  FORMAT(/,6E15.7)
102  CONTINUE
IF(ACC-0. 000001)103,103,104
104  L = LIMIT - N
M = LIMIT + N
IF(L-1. 0)120,120,121
120  L=1
121  N=(M-L)/10
IF(N.LT.1) N=1
WRITE(5,113)L,M,N
GOTO 100

```

```

103  CONST=10.**CONST
      ETR=EO=CONST*TR**SLOPE
      WRITE(5,110)EO,CONST,SLOPE,ETR,STRESS,VAR
110  FORMAT(/,5X,'SPECIMEN 31C/5 3/11',//,5X'EO = ',E15.7,/,5X,
      *CONST + ',E.15.7,/,5X,'SLOPE + ',E15.7,/,5X,'ETR=',E15.7,/,
      *5X,'STRESS = ',E15.7,/,5X,'VARR = ',E15.7)
      DO 122 I=1,P
      Y=ALOG10(E(I)-EO)
      X=ALOG10(T(I) )
      YF=ALOG10(CONST)=SLOPE*X
      A=T(I)
      B=CONST*A**SLOPE*100
      C=(E(I)-EO)*100
      WRITE(5,123)X,Y,YF,A,B,C
123  FORMAT(//,5X,'LOG TIME = ',E15.7,5X,'MEAS. Y = ',E15.7,5X,
      *'EST. Y = ',E15.7,/,5X'TIME = ',E15.7,5X,'(E-EO) % = ',
      *E15.7,5X,'MEAS.(E-EO) %=' ,E15.7)
122  CONTINUE
      END

```

SPECIMEN 31C1 3/11

EO = 0.800E-06

CONST = 0.890E-02

SLOPE = 0.120E 00

ETR = 0.157E-01

STRESS = 0.460E 06

VARR(T=1) = 0.262E-01

LOG TIME = -0.100E 01 MEAS. Y = -0.210E 01 EST. Y = -0.217E 01
 TIME = 0.100E 00 (E-EO) % = 0.674E 00 MEAS. (E-EO) % = 0.792E 00
 LOG TIME = -0.698E 00 MEAS. Y = -0.209E 01 EST. Y = -0.213E 01
 TIME = 0.200E 00 (E-EO) % = 0.733E 00 MEAS. (E-EO) % = 0.804E 00
 LOG TIME = -0.522E 00 MEAS. Y = -0.208E 01 EST. Y = -0.211E 01
 TIME = 0.300E 00 (E-EO) % = 0.770E 00 MEAS. (E-EO) % = 0.813E 00
 LOG TIME = -0.397E 00 MEAS. Y = -0.208E 01 EST. Y = -0.209E 01
 TIME = 0.400E 00 (E-EO) % = 0.797E 00 MEAS. (E-EO) % = 0.819E 00
 LOG TIME = -0.301E 00 MEAS. Y = -0.208E 01 EST. Y = -0.208E 01
 TIME = 0.500E 00 (E-EO) % = 0.819E 00 MEAS. (E-EO) % = 0.827E 00
 LOG TIME = -0.124E 00 MEAS. Y = -0.205E 01 EST. Y = -0.206E 01
 TIME = 0.750E 00 (E-EO) % = 0.860E 00 MEAS. (E-EO) % = 0.872E 00
 LOG TIME = 0.000E 00 MEAS. Y = -0.205E 01 EST. Y = -0.205E 01
 TIME = 0.100E 01 (E-EO) % = 0.890E 00 MEAS. (E-EO) % = 0.879E 00
 LOG TIME = 0.969E-01 MEAS. Y = -0.205E 01 EST. Y = -0.203E 01
 TIME = 0.123E 01 (E-EO) % = 0.914E 00 MEAS. (E-EO) % = 0.882E 00
 LOG TIME = 0.176E 00 MEAS. Y = -0.205E 01 EST. Y = -0.202E 01
 TIME = 0.150E 01 (E-EO) % = 0.935E 00 MEAS. (E-EO) % = 0.889E 00
 LOG TIME = 0.301E 00 MEAS. Y = -0.204E 01 EST. Y = -0.201E 01
 TIME = 0.200E 01 (E-EO) % = 0.968E 00 MEAS. (E-EO) % = 0.904E 00
 LOG TIME = 0.397E 00 MEAS. Y = -0.203E 01 EST. Y = -0.200E 01
 TIME = 0.250E 01 (E-EO) % = 0.994E 00 MEAS. (E-EO) % = 0.914E 00
 LOG TIME = 0.477E 00 MEAS. Y = -0.203E 01 EST. Y = -0.199E 01
 TIME = 0.300E 01 (E-EO) % = 0.101E 01 MEAS. (E-EO) % = 0.924E 00
 LOG TIME = 0.602E 00 MEAS. Y = -0.201E 01 EST. Y = -0.197E 01
 TIME = 0.400E 01 (E-EO) % = 0.105E 01 MEAS. (E-EO) % = 0.972E 00
 LOG TIME = 0.698E 00 MEAS. Y = -0.200E 01 EST. Y = -0.196E 01
 TIME = 0.500E 01 (E-EO) % = 0.108E 01 MEAS. (E-EO) % = 0.989E 00
 LOG TIME = 0.778E 00 MEAS. Y = -0.198E 01 EST. Y = -0.195E 01
 TIME = 0.600E 01 (E-EO) % = 0.110E 01 MEAS. (E-EO) % = 0.103E 01

APPENDIX B

The computer programme to calculate the cost-effectiveness of various four fibre laminates is shown below. The input data required is:

- a) Fibre Young's modulus (EF)
- b) Resin Young's modulus (EM)
- c) Fibre Poisson's ratio (PF)
- d) Resin Poisson's ratio (PM)
- e) Density of the fibres (DF) and resin (DM)
- f) Cost of the fibres (CF) and resin (CM)
- g) The four fibre angles (A1, A2, A3 and A4)

The output from the computer programme consists of:

- a) The laminate volume fraction.
- b) The properties of the constituent lamina referred to the natural axes, i.e. the longitudinal modulus (FL), the transverse modulus (ET), Poisson's ration (PLT) and the shear modulus (GLT).
- c) The properties of the laminate referred to principal axes, i e. the longitudinal modulus (EI), the transverse modulus (ET), Poisson's ratio (P12) and the shear modulus (G12).

- d) The plate buckling cost-effectiveness (PCRN)
- e) Cylindrical shell local buckling cost-effectiveness (CYCRN).
- f) Laminate axial stiffness cost-effectiveness (EEAN).
- g) Laminate shear stiffness cost-effectiveness (EGN).
- h) Laminate flexural stiffness cost-effectiveness (FLEXN).

An example of results from the programme is also given below for a quasi-isotropic laminate.

```

DIMENSION CYCR(11),PCR(11),EEA(11),EG(11),FLEX(11)
REAL LND,KF,KM
READ(8,10)EF,EM,PF,PM,DF,DM,CF,CM,A1,A2,A3,A4
10  FORMAT (12F)
WRITE(5,9) EF,EM,PF,PM,DF,DM,CF,CM,A1,A2,A3,A4
9   FORMAT (1H1,2X,F9,3.1X,F7.3,1X,F4.2,1X,F4.2,1X,F5.0,1X,F5.0,1X,
*F4.2,1X,F4.2,1X,F3.1,1X,F4.0,1X,F4.0,1X,F4.0,1X,F4.0)
WRITE(5,11)
11  FORMAT(///,1X,'VF',9X,'EL',13X'ET',12X,'PLT',12X,'GLT',/,
*12X,'EI',13X,'E2',12X,'P12',12X,'G12',//,
11X,'PCRN',10X,
*'CYCRN',11X,'EEAN',11X,'EGN',11X,'FLEXN')
EF=EF*1000000.
EM=EM*1000000.
A1=A1*0.017453
A2=A2*0.017453

```

```

A3=A3*0.017453
A4=A4*0.017453
DO 20 I=1,11
VF=1-VF
EL=VF*EF+VM*EM
KF=EF/(2*(1-PF) )
KM=EM/(2*(1-PM) )
GF=EF/(2*(1+PF) )
GM=EM/(2*(1+PM) )
X1=KF*PF*(2*KM+GM)*VF+KM*PM*(2*KF+GM)*VM
X2=KF*(2*KM+GM)-GM*(KF-KM)*VM
X3=X1/X2
X4=KM*PM*(2*KF+GF)*VM+KF*(2*KM+GF)*VF*PF
X5=KF*(2*KM+GF)+GF*(KM-KF)*VM
X6=X4/X5
C=0.0
X7=(1-C)*(KF*(2*KM+GM)-GM*(KF-KM)*VM)
X8=2*KM+GM+2*(KF-KM)*VM
X9=X7/X8
X10=C*(KF*(2*KM+GF)+GF*(KM-KF)*VM)
X11=2*KM+GF-2*(KM-KF)*VM
X12=X10/X11
PLT=(1-C)*X1/X2+C*X4/X5
ET=2*(1-PF+VM*(PF-PM) )*(X9+X12)
PTL=PTL*ET/EL
X13=(1-C)*GM*(2*GF-(GF-GM)*VM)/(2*GM+(GF-GM)*VM)
X14=C*GF*( (GF+GM)-(GF-GM)*VM)/( (GF+GM)+(GF-GM)*VM)
GLT=X13+X14
LND=1-PLT*PTL

```


$$SC4=(\cos(A1)**4+\cos(A2)**4+\cos(A3)**4+\cos(A4)**4)/4$$

$$SS4=(\sin(A1)**4+\sin(A2)**4+\sin(A3)**4+\sin(A4)**4)/4$$

$$CS21=(\sin(A1)*\cos(A1))**2$$

$$CS22=(\sin(A2)*\cos(A2))**2$$

$$CS23=(\sin(A3)*\cos(A3))**2$$

$$CS24=(\sin(A4)*\cos(A4))**2$$

$$SCS2=(CS21+CS22+CS23+CS24)/4$$

$$CMSS1=(\cos(A1)**2-\sin(A1)**2)**2$$

$$CMSS2=(\cos(A2)**2-\sin(A2)**2)**2$$

$$CMSS3=(\cos(A3)**2-\sin(A3)**2)**2$$

$$CMSS4=(\cos(A4)**2-\sin(A4)**2)**2$$

$$SCMSS=(CMSS1+CMSS2+CMSS3+CMSS4)/4$$

$$SCS4=SC4+SS4$$

$$S3C1=\sin(A1)**3*\cos(A1)$$

$$S3C2=\sin(A2)**3*\cos(A2)$$

$$S3C3=\sin(A3)**3*\cos(A3)$$

$$S3C4=\sin(A4)**3*\cos(A4)$$

$$SS3C=(S3C1+S3C2+S3C3+S3C4)/4$$

$$C3S1=\cos(A1)**3*\sin(A1)$$

$$C3S2=\cos(A2)**3*\sin(A2)$$

$$C3S3=\cos(A3)**3*\sin(A3)$$

$$C3S4=\cos(A4)**3*\sin(A4)$$

$$SC3S=(C3S1+C3S2+C3S3+C3S4)/4$$

$$SB11=(EL*SC4+ET*SS4+(2*EL*PTL+4*LND*GLT)*SCS2)/LND$$

$$SB22=(ET*SC4+EL*SS4+(2*EL*PTL+4*LND*GLT)*SCS2)/LND$$

$$SB33=((EL+ET-2*EL*PTL-2*LND*GLT)*SCS2+GLT*LND*SCS4)/LND$$

$$SB12=((EL+ET-4*LND*GLT)*SCS2+EL*PTL*SCS4)/LND$$

$$SB13=(-ET+EL*PTL+2*LND*GLT)*SS3C+(EL-EL*PTL-2*LND*GLT)*SC3S)/LND$$

$$SB23=(-ET+EL*PTL+2*LND*GLT)*SC3S+(EL-EL*PTL-2*LND*GLT)*SS3C)/LND$$

```

X15 = SB11*SB22*SB33-SB11*SB23**2-SB22*SB13**2
X16 = SB33*SB12**2-2*SB12*SB13*SB23
DELTA = X15-16
E1= DELTA/(SB22*SB33-SB23**2)
E2= DELTA/(SB11*SB33-SB13**2)
P12=(SB12*SB33-SB23*SB13)/(SB22*SB33-SB23**2)
P21=P12*E2/E1
G12=DELTA/(SB11*SB22-SB12**2)
H=1/(VF*DF*CF+VM*DM*CM)
D1= E1*H**3/(12*(1-P12*P21) )
D2= E2*H**2*(12*(1-P12*P21) )
D3= 0.5*(P12*D2+P21*D1)+G12*H**3/6
A12=E1*P21/(1-P12*P21)
A22=E2/(1-P12*P21)
A11=E1/(1-P12*P21)
A33=G12
CYCR(I)=2*3.142*H**2*SQRT(0.666*(A12+SQRT(A11*A22))*A33)
PCR(I)= 2*3.142**2*(SQRT(D1*D2)+D3)
EEA(I)= E1*H
FLEX(I)=E1*H**3/12
EG (I) = G12*H
FLEXN=FLEX(I)/FLEX(1)
CYCRN=CYCR(I)/CYCR(1)
PCRN=PCR(I)/PCR(1)
EEAN=EEA(I)/EEA(1)
EGN=EG(I)/EG(1)
WRITE(5,30)VF,EL,ET,PLT,GLT,E1,E2,P12,G12,
*EG(I),FLEX(I),PCRN,CYCRN,EEAN,EGN,FLEXN
30  FORMAT(///,1X,F4,2,4E15.7,/,5X,4E15.7,///,5X,5E15.7)
20  CONTINUE
END

```


	72.400	3.500	0.22	0.36	2560	1200.	0.72	0.48	45.	0.-45.	90
VF	EL	ET	PLT	GLT							
	EI	E2	P12	G12							
	PCRN	CYCRN	EEAN	EGN	FLEXN						
0.00	0.350E 07	0.350E 07	0.360E 00	0.128E 07							
	0.350E 07	0.350E 07	0.360E 00	0.128E 07							
	0.100E 01	0.100E 01	0.100E 01	0.100E 01	0.100E 01						
0.10	0.103E 08	0.402E 07	0.343E 00	0.154E 07							
	0.608E 07	0.608E 07	0.323E 00	0.229E 07							
	0.931E 00	0.115E 01	0.142E 01	0.146E 01	0.957E 00						
0.20	0.172E 08	0.468E 07	0.327E 00	0.186E 07							
	0.884E 07	0.884E 07	0.313E 00	0.336E 07							
	0.816E 00	0.119E 01	0.175E 01	0.181E 01	0.846E 00						
0.30	0.241E 08	0.550E 07	0.311E 00	0.226E 07							
	0.117E 08	0.117E 08	0.307E 00	0.448E 07							
	0.704E 00	0.119E 01	0.201E 01	0.201E 01	0.732E 00						
0.40	0.310E 08	0.653E 07	0.297E 00	0.277E 07							
	0.147E 08	0.147E 08	0.301E 00	0.568E 07							
	0.609E 00	0.117E 01	0.224E 01	0.235E 01	0.636E 00						
0.50	0.379E 08	0.803E 07	0.283E 00	0.346E 07							
	0.181E 08	0.181E 08	0.294E 00	0.700E 07							
	0.533E 00	0.114E 01	0.246E 01	0.259E 01	0.559E 00						
0.60	0.443E 08	0.101E 08	0.269E 00	0.443E 07							
	0.218E 08	0.218E 08	0.286E 00	0.850E 07							
	0.475E 00	0.113E 01	0.269E 01	0.284E 01	0.500E 00						
0.70	0.517E 08	0.132E 08	0.256E 00	0.589E 07							
	0.264E 08	0.264E 08	0.276E 00	0.102E 08							
	0.434E 00	0.113E 01	0.297E 01	0.316E 01	0.460E 00						

0.80	0.586E 08	0.187E 08	0.243E 00	0.836E 07		
	0.325E 08	0.325E 08	0.262E 00	0.128E 08		
	0.413E 00	0.117E 01	0.336E 01	0.362E 01	0.441E 00	
0.90	0.655E 08	0.304E 08	0.231E 00	0.134E 08		
	0.427E 08	0.427E 08	0.242E 00	0.172E 08		
	0.426E 00	0.132E 01	0.410E 01	0.448E 01	0.461E 00	
1.00	0.724E 08	0.724E 08	0.220E 00	0.296E 08		
	0.724E 08	0.724E 08	0.220E 00	0.296E 08		
	0.577E 00	0.193E 01	0.646E 01	0.720E 01	0.631E 00	

REFERENCES

REFERENCES

REFERENCES CHAPTER 2

1. Cox, H.L., British J. Applied Phys., Vol. 3, 72 (1952).
2. Dow, N.F., General Electric Co., Rep. R63/SD61 (1963).
3. Rosen, B.W. "Mechanics of Composite Strengthening", Fibre Composite Materials, American Soc. Of Metals, Metals Park, Ohio, p.37 (1965).
4. Metcalfe, A.G., Schmitz, G.K., "Effect of Length on the Strength of Glass Fibres", ASTM, Proc., Vol. 64, pp.1075 - 93, (1964).
5. Bartener, G.M., Izmailava, L.K., Soviet Phys. Sol. St., Vol. 6, 920, (1964).
6. Broutman, L.J., Krock, P.R., eds., "Modern Composite Materials", Chapter 13, Addison-Wesley, 1967.
7. Hashin, Z., "Theory of Fibre Reinforced Materials", NASA CR - 1974, 1972.
8. Al-Khayatt, Q.J., "The Structural Properties of Glassfibre Reinforced Plastics", Ph.D. Thesis, University of Aston in Birmingham, 1974.
9. Jones, B.H., Noyes, J.V., "Effect of Voids on the Transverse and In-plane Shear Strength and Elastic Properties of Fibrous Composites", Douglas Paper 4706, McDonnell Douglas Corporation, 1967.

References Chapter 2 Continued

10. As ref. 6 but Chapter 2.
11. Fried, N., Kaminetsky, J., "The Influence of Material Variables on the Compressive Properties of Parallel Filament Reinforced Plastics", Proc. 19th Conf. SPI Reinforced Plastics Division, 1964.
12. Greszczuk, L.B., "Effect of voids on Strength Properties of Filamenting Composites", Proc. 22nd Conf. SPI, Reinforced Plastics Division, 1967.
13. Sands, A.G., Clark, R.C., Kohn, E.J., NRL Rep. 648, 1967.
14. Gibbs and Cox, "Marine Design Manual", McGraw-Hill Book Co. Inc., New York, 1960.
15. Proctor, B.A., Faraday Special Discussion, Paper 6, Nottingham, 1972.
16. Kabelka, J., 5th Int. Reinforced Plastics Conf. Nov. 1966, Paper 17.
17. Boller, K.H., "Effect of Long-term Loading on Glass Reinforced Plastic Laminates", Proc. 14th Conf. SPI Reinforced Plastics Division, 1959.
18. Steel, D.J., "The Creep and Stress Rupture of Reinforced Plastics", Trans. J. Plastics Inst., October 1965.
19. Diggwa, A.D.S., Norman, R.H., "Mechanism of Creep of Grp", Plastics and Polymers, October 1972.
20. Owen, M.J., Dukes, R., Smith, T.R., SPI, 23rd Conf. 1968, Paper 14B.
21. Smith, T.R., Owen, M.J., British Plastics Federation 6th Int. Conf., London, Nov. 1968, Paper 27.

References Chapter 2 Continued

22. Boller, K.H., Modern Plastics, Vol. 34, June 1957 p. 163.
23. Owen, M.J., "Fatigue", in "Glass Reinforced Plastics", ed. Parkyn, Iliffe Books, London, 1970.
24. Thompson, A.W., Trans, Plast. Inst. Vol. 30, 1962, pp. 39-47.
25. Matthon, J., et al, "Ageing and Weathering of Glass Fibre Reinforced Polyester Resins", A Review of the Literature on the Ageing and Weathering of Plastics, Part 4, R.A.P.R.A., 1970.
26. Lovell, R.B., "Influence of Surfacing Mat on Surface Deterioration of Fibre Glass Reinforced Plastics", Proc. 22nd Conf. SPI Reinforced Plastics Div., 1967.
27. Scott and Matthon, "Weathering" as ref. 2.23.
28. Algra, E.A.H., van der Beck, M.H.B., "Ageing of Reinforced Plastics", Kunststoffe, vol. 58, No. 12, 1968.
29. Rugger, G.R., "Weathering of Reinforced Plastics, Jon 1966, Plastics Tech. Evaluation Centre, Picatinny Arsenal, Dover, N.J.
30. Kimball, K.E., "Weathering of Glass-fabric-base Plastic Laminates Under Stress", ASD-TR-61-145, June 1961.
31. Benjamin, B.S., "Structural Design with Plastics", Van Nostrand Reinhold, 1969.
32. Ashton, J.E., et al, "Primer on Composite Materials : Analysis", Technomic, 1969.
33. Brown, G.F., "Cold Press Moulding", British Plastics, April 1970.
34. Anon., "Spray Winding", Europlastics Monthly, July, 1972.
35. Whitehouse, A.A.K., "Resin Systems" as ref. 2.23.
36. Anon., Modern Plastics International, Aug., 1975, p.16.

REFERENCES

REFERENCES CHAPTER 3

1. Tsai, S.W., "Mechanics of Composite Materials", Part II, Technical Report AFML-TR-66-149, November, 1966.
2. Calcote, L.R., "The Analysis of Laminated Composite Materials", Chapter 2, New York, Van Nostrand Reinhold, 1969.
3. Tsai, S.W., "Structural Behaviour of Composite Materials", NASA CR-71, July 1964.
4. Al-Khayatt, Q.J., "The Structural Properties of Glass-fibre Reinforced Plastics", Ph.D. Thesis, University of Aston in Birmingham, 1974.
5. Ashton, J.E., et al, "Primer on Composite Materials : Analysis", Chapter 5, Technomic, 1969.
6. Tsai, S.W., "Strength Characteristics of Composite Materials", NASA CR-224, 1965.
7. As reference 5 but Chapter 4.
8. Jones, B.H., "Predicting the Stiffness and Strength of Filamentary Composites for Design Application", Plastics and Polymers, April 1968.
9. Bishop, P.H.H., "Predicting Mechanical Properties of Fibre Composites", in Glass Reinforced Plastics, ed. B. Parkyn, Ififfe, 1970.

References Chapter 3 continued

10. Tsai, S.W., "Structural Behaviour of Composite Materials", NASA, Contractor Rep., NASA CR-71, 1964.
11. Rosen, S.W., et al, "Mechanical Properties of Fibrous Composites", NASA 65 16806, July 1963.
12. Harris, B., "The Strength of Fibrous Composites", Composites, July 1972, pp 152 - 167.
13. Schuerch, H., "Prediction of Composite Strength in Uniaxial Boron fibre-metal Matrix Material", AIAA Journal, Vol. 4, Jan. 1966.
14. Dow, N.F., Rosen, B.W., "Evaluation of Filament-Reinforced Composites for Aerospace Structural Applications", NASA CR-207, 1965.
15. Shu, L.S., Rosen, B.W., "Strength of Fibre Reinforced Composites by Limit Analysis Methods", Journal of Composite Materials, Vol. 1, 1967.
16. Hasin, Z., "Theory of Fibre Reinforced Materials", NASA CR-1974, 1972.
17. Dimmock, J., Abrahams, M., "Prediction of Composite Properties from Fibre and Matrix Properties", Composites, Vol. 1, No. 2, 1969.
18. "Fatigue and Creep in Reinforced Plastics", British Plastics Federation Review, 1967.
19. Findley, W.N., "The Effect of Temperature and Combined Stresses on Creep of Plastics", B.P.F. 2nd International Reinforced Plastics Conf., London, Dec. 1960.
20. Kabelka, J., "The Behaviour of Glass Reinforced Polyester Under Long Term Stress", B.P.F., 5th International Reinforced Plastics Conf., London, Nov. 1966.

References Chapter 3 continued

21. O'Connor, D.G., and Findley, W.N., "Influence of Normal Stress on Creep in Tension and Compression of Polyethylene and Rigid Poly(Vinyl chloride) Copolymer", J. Eng. Ind., May 1962, pp 237.
22. McCrum, N.G., "A Review of the Science of Fibre Reinforced Plastics", H.M.S.O., 1971.
23. Weidmann, G.W., and Ogorkiewicz, R.M., "Tensile Creep of a Unidirectional Glass Fibre-epoxy Laminate", Composites, May 1974.
24. Schmitz, G.K., and Metcalfe, A.G., "Stress Corrosion of E-Glass Fibres", I & EC Product Research and Development, Vol. 5, No. 1, March 1966.
25. Steel, D.J., "The Creep and Stress-rupture of Reinforced Plastics", J. Plastics Inst., Oct. 1965.
26. Boller, K.H., 14th Annual Meeting of the Reinforced Plastics Div. of the Soc. of the Plastics Ind., Feb. 1959, Paper 10.
27. Findley, W.N., and Peterson, D.B., "Prediction of Long-Time Creep with Ten-Year Creep Data on Four Plastic Laminates", Proc. ASTM, Vol. 58, 1958, pp 841 - 861.
28. Findley, W.N., and Khosla, G., "An Equation for Tension Creep of Three Unfilled Thermoplastics", SPE Journal, Vol. 12, No. 12, 1956, pp 20 - 25.
29. Rawe, A.W., "Environmental Behaviour of Glass-fibre Reinforced Plastics", Ibid, Vol. 30, 1962.
30. McLaughlin, J.R., "A New Creep Law for Plastics", Mod. Plastics, Feb. 1968.
31. Larson, F.R., and Miller, J., "A time-Temperature Relationship for Rupture and Creep Stresses", Trans. ASME, Vol. 74, p 765, 1952.

References Chapter 3 continued

32. "Elevated Temperature Properties of Glass Fabric Base Plastic Laminates", USAF Tech. Report No. 6172, Battelle Memorial Institute, May 1950.
33. "Long-Term Loading of Reinforced Plastic Laminates under Tension and Flexure", Sub-Task 30 of NS-034-045, Contract No. Bu Ships - 1700 S-540, Forest Products Laboratory, Dec. 1956.
34. Goldfein, S., "Time, Temperature, and Rupture Stresses in Reinforced Plastics", Mod. Plastics, Dec. 1954.
35. Monkman, F.C., and Grant, N.C., ASTM Proc. p 593, 1956.
36. Carles, R.J., "Static Fatigue of Glass", Appl. Physics, Vol. 29, p 1549.
37. Cameron, J.B., "The Temperature Limitations of Reinforced Plastics in Aggressive Environments", Trans. J. Plastics Inst., Oct. 1967.
38. Brown, W.E., ed. "Testing of Polymers", Vol. 4, Ch.1& 3 John Wiley Interscience, 1969.
39. Benjamin, B.S., "Structural Design with Plastics", Van Nostrand Reinhold, 1969.

REFERENCES CHAPTER 4

1. Owen, T.B.B., "Analysis and Design of Light Structures", Edward Arnold, 1965.
2. Al-khyatt, Q.J., "The Structural Properties of Glassfibre Reinforced Plastics", Ph.D. Thesis, University of Aston, 1974.
3. Marshall, S., "Duftec" internal report, Pilkington Bros. Ltd.
4. Ryder, G.H., "Strength of Materials", Macmillan Press, 1971.
5. Perry, H.A., "Adhesive Bonding of Reinforced Plastics", McGraw Hill, 1959.
6. Goland, M., and Reissner, E., J. Appl. Mechanics, vol. 11, A-17, 1944.
7. Youngs, R.L., "Bolt-Bearing Properties of Glass Fabric-Base Plastic Laminates", Forest Products Lab., Rept. No. 1824 A, 1955.
8. Weiss, M.D., "Mechanical Fasteners for Glass Reinforced Plastics", Proc. 14th Conf. SPI, Reinforced Plastics Division, 1959.
9. Strauss, E.L., "Effects of Stress Concentration on the Strength of Reinforced Plastic Laminates", Proc. 14th Conf. SPI, Reinforced Plastics Division, 1959.
10. Anon. "Design Principles of Adhesive-bonded Joints", Engrs. Digest, Vol. 28, No. 12, December 1967.
11. Rothwell, A., "Optimum fibre orientations for the buckling of thin plates of composite materials", Fibre Sci. and Techn. Vol. 2, p.111 (1969).

References Chapter 4 continued

12. Boresi, A.P., et al, "Buckling of Axially-Compressed Bilayered Fibre-Reinforced Elastic Cylindrical Shell", Developments in Theoretical and Applied Mechanics, Vol. 2, ed. W. A. Shaw, Pergamon Press, 1965.
13. Makowski, Z.S., EFTA Association Symposium on Plastics in Buildings, 1972.
14. Timoshenko, S.P., and Gere, J.M., "Theory of Elastic Stability", McGraw-Hill Kogakusha, Tokyo. 1961.

REFERENCES

REFERENCES CHAPTER 5

1. Miller, D. M., "Factories and Warehouses : Statistics", Building with Steel, No. 18, British Steel Corporation, Sept. 1974.
2. Briggs, W.R., et al, "Wide Span Structures", Civil Eng. and Public Works Review, Feb. 1973. pp 145.
3. Passchier, G. and Krjgsman A., "The "Ahoy" Complex", Rotterdam (Netherlands) E.C.C.S. Award 1973, Acier. Stahl. Steel, Jan. 1974.
4. Lakshmikantham, C., and Gerard, G., "Minimum Weight Design of Stiffened Cylinders", The Aeronautical Quarterly, Feb. 1970.
5. Sachs, P., "Wind Forces in Eng." Oxford: Pergamon Press, 1972.
6. Bray, K.H.M., "Computer Analysis of Large Civil Engineering Structures", PhD. Thesis, University of Aston in Birmingham, 1973.

REFERENCES

REFERENCES CHAPTER SIX

1. Timoshenko, S.P., and Gere, J.M., "Theory of Elastic Stability",
2nd ed., McGraw-Hill Kogakusha, Tokyo, 1961.
2. Litle, W.A., "Reliability of Shell Buckling Predictions",
M.I.T. Press 1964.

REFERENCES

REFERENCES CHAPTER 8

1. Anon. "Building Costs", Building, 11th July, 1975 pp 51 & 2.
2. Miller, D.M., "Statistics", Building with Steel No. 18,
British Steel Corp., Sept., 1974.
3. Murfitt, P., "Polyester resin - Too precious to be used unfilled?"
Reinforced Plastics, April 1974.

AN INVESTIGATION INTO THE FEASIBILITY OF
THE STRUCTURAL USE OF GLASS REINFORCED PLASTICS
IN LONG SPAN LIGHTLY LOADED STRUCTURES

KEITH WINSTON MOLYNEUX

A THESIS SUBMITTED FOR THE DEGREE OF
DOCTOR OF PHILOSOPHY

624.01178 MOL
204630 18 MAR 1977

DEPARTMENT OF CIVIL ENGINEERING
UNIVERSITY OF ASTON IN BIRMINGHAM

OCTOBER 1976

SYNOPSIS

The problem of feasibility is approached by first reviewing the general properties of grp. In Chapter three, the more relevant properties are discussed in greater depth. Experimentally determined data is presented for both long and short term strength and stiffness characteristics. Results show that elastic properties can be predicted reasonably well by theory, and that empirical creep data can be represented by power laws.

In Chapter four, analyses are presented to determine the effect of fibre volume fraction and the relative cost of fibres and resin on the cost-effectiveness of laminates under various loading conditions. Also, various production processes and their associated costs are analysed at various production levels to assist in making design and manufacturing decisions.

On the basis of the properties of grp, a roof structure is chosen as a suitable structure to investigate, in order to establish economical and structural feasibility of long span lightly loaded grp structures in general. The structural feasibility is tested by the design of a 60 m span roof, and the building and testing of a 10 m span model roof. The economic feasibility is investigated by

comparing the estimated cost of grp roofs with the cost of conventional roof structures.

It is concluded that 60 m grp roofs, and, therefore, long span lightly loaded grp structures are structurally and economically feasible. Grp roofs are competitive with conventional roof structures at a span of 20 - 30 m and their position improves with increasing span. It is estimated that the annual British market for glass fibres in this application is 5600 Tonnes.

ACKNOWLEDGEMENTS

The author would like to thank his supervisors, Prof. M. Holmes, Mr. J. Huddart, Prof. Pick and Prof. Scott for their assistance and advice during the course of this investigation.

The author is also most grateful to Mess. Pilkington Bros. Ltd. for their financial support and permission to carry out the investigation.

Further thanks are also extended to: Mr. W. Parsons, the Civil Engineering Departmental Superintendent and his staff for their willing assistance, Miss N. A. Byrne for her excellent typing of the script, and the author's wife for her help, patience and encouragement.

CONTENTS

		<u>Page No.</u>
SYNOPSIS		(i)
ACKNOWLEDGEMENTS		(iii)
CONTENTS		(iv)
NOMENCLATURE		(xi)
<u>CHAPTER 1</u>	INTRODUCTION	1.1
<u>CHAPTER 2</u>	DISCUSSION OF THE PROPERTIES OF GRP RELEVANT TO STRUCTURAL ENGINEERING	
2.1	Introduction	2.1
2.2	Ultimate Strength	2.2
2.3	Stress Rupture	2.6
2.4	Modulus of Elasticity	2.7
2.5	Creep	2.8
2.6	Dynamic Fatigue	2.9
2.7	Ductility & Fracture Toughness	2.11
2.8	Durability	2.12
2.9	Thermal Properties	2.14
2.10	Mouldability	2.15
	2.10.1 Contact Moulding	2.16
	2.10.2 Spray-up	2.18
	2.10.3 Robot Spray	2.19
	2.10.4 Pressure Bag	2.19
	2.10.5 Vacuum Bag	2.19
	2.10.6 Autoclave	2.20
	2.10.7 Cold Press Moulding & Resin Injection	2.20

CHAPTER 2 (Contd)

Page No.

2.10.8	Hot Press Moulding	2.21
2.10.9	Filament Winding	2.22
2.10.10	Pultrusion	2.22
2.10.11	Continuous Laminating	2.23
2.10.12	Preforming	2.23
2.11	Fire	2.24
2.12	Cost	2.25

CHAPTER 3

THEORETICALLY & EXPERIMENTALLY
DETERMINED PROPERTIES OF GRP

3.1	Introduction	3.1
3.2	Elastic Properties of Orthotropic Laminates	3.2
3.2.1	Introduction	3.2
3.2.2	Prediction of Elastic Constants of the Basic Mono-Layer (Fig. 3.2)	3.3
3.2.2.1	Law of Mixtures	3.3
3.2.2.2	Tasi Approach	3.5
3.2.2.3	Halpin-Tsai Approach	3.6
3.2.3	Stress-Strain Relationships Referred to Natural Axes	3.7
3.2.4	Stress-Strain Relationships Referred to Arbitrary Axes	3.10
3.2.5	Elastic Constants of Laminated Grp	3.13
3.3	Strength Properties of Laminated Grp	3.16
3.3.1	Introduction	3.16
3.3.2	Prediction of the Strength of the Basic Mono-Layer	3.17

3.3.2.1	Longitudinal Tensile Strength	3.18
3.3.2.2	Longitudinal Compressive Strength	3.18
3.3.2.3	Transverse Strengths	3.19
3.3.2.4	Interlamina Shear Strength	3.19
3.3.2.5	Flexural Strength	3.20
3.3.3	Strength Properties of Laminated Grp	3.20
3.3.3.1	Laminate Behaviour Under Load	3.21
3.4	Theoretically & Experimentally Determined Elastic & Strength Properties of Selected Grp Laminates	3.23
3.4.1	Introduction	3.23
3.4.2	Design of Specimens	3.23
3.4.3	Experimentally Determined Properties	3.25
3.4.3.1	Properties of the Basic Lamina & Selected Laminates	3.25
3.4.4	Conclusions	3.28
3.5	Time-Dependent Properties of Grp	3.29
3.5.1	Introduction	3.29
3.5.2	Creep Mechanism	3.29
3.5.3	Nature of Strength Reduction	3.32
3.5.4	Prediction of the Loss of Stiffness with Time	3.32
3.5.4.1	Extrapolation Techniques	3.33
3.5.4.2	The Larson-Miller Parameter	3.35
3.5.5	Prediction of the Loss of Strength with Time	3.37
3.5.5.1	Larson-Miller Parameter	3.37
3.5.5.2	Wohler Method	3.37
3.5.5.3	The Monkman and Grant Relationship	3.38

3.5.5.4 Charles' Equation	3.40
3.5.6 Experimentally Determined Time- Dependent Properties of Grp	3.41
3.5.6.1 Introduction	3.41
3.5.6.2 Design of Test Specimens	3.42
3.5.6.3 Design of Test Equipment	3.43
3.5.6.4 Test Procedure	3.45
3.5.6.5 Results & Discussion of Results	3.46
3.5.6.6 Conclusions	3.51

CHAPTER 4

STRUCTURAL ENGINEERING DESIGN WITH GRP

4.1 Introduction	4.1
4.2 The Design Process in Grp	4.2
4.3 Material Cost-Effectiveness	4.4
4.3.1 Axial Stiffness	4.5
4.3.2 Flexural Stiffness	4.6
4.3.3 Shear Stiffness	4.7
4.3.4 Plate Buckling	4.8
4.3.5 Cylinder Buckling	4.9
4.4 Process Economics	4.10
4.4.1 The Hand Lay-up Process	4.12
4.4.2 The Basic Spray-up Process	4.17
4.4.3 The Robot Spray-up Process	4.20
4.4.4 The Continuous Spray-up Process	4.21
4.4.5 The Resin Injection Process	4.22
4.4.6 The Hot Press Process	4.23
4.4.7 Discussion of Process Analysis	4.25

<u>CHAPTER 4</u> (Contd)	<u>Page No.</u>
4.5 Preferential Fibre Orientation	4.27
4.6 Joint Design	4.28
4.6.1 Adhesive Joints	4.28
4.6.2 Mechanical Joints	4.31
4.6.3 Combination Joints	4.32
4.7 Safety Factors	4.33
<u>CHAPTER 5</u>	DISCUSSION AND PRELIMINARY DESIGN OF A STRUCTURAL SYSTEM
5.1 Introduction	5.1
5.2 Suitable Structural Function	5.2
5.3 The Preliminary Design of a Long-Span Grp Roof	5.3
5.4 5.3.1 Introduction	5.3
5.3.2 Roof Loading	5.3
5.3.3 Macroscopic Design	5.4
5.3.4 Analysis of Roof Structure	5.7
5.3.4.1 Proposed Design of Roof Surface Element Cross-Section	5.7
5.3.4.2 Verification of the Proposed Roof Design	5.9
5.3.5 Discussion & Assessment of Roof Design	5.19
<u>CHAPTER 6</u>	DESIGN, MANUFACTURE & TESTING OF A MODEL SPAN ROOF
6.1 Introduction	6.1
6.2 Scale of Model Roof	6.2
6.3 Design of Model Roof	6.3

6.3.1	Surface Unit Design	6.3
6.3.2	Cross-bracing Design	6.3
6.3.3	Joint Design	6.4
6.3.4	End Fixing Design	6.5
6.3.5	Materials Summary	6.5
6.3.6	Analysis of Model	6.6
6.3.6.1	Theoretical Elastic Analysis	6.6
6.3.6.2	Empirical Elastic Analysis	6.7
6.3.6.3	Visco-elastic Analysis	6.12
6.4	Preliminary Tests	6.13
6.4.1	Surface Unit Compression Test	6.13
6.4.1.1	Introduction	6.13
6.4.1.2	Description of Test	6.14
6.4.1.3	Results of Test	6.15
6.4.1.4	Conclusions	6.17
6.4.2	Tensile Joint Tests	6.18
6.4.2.1	Introduction	6.18
6.4.2.2	Description of Tests	6.18
6.4.2.3	Results of Tests	6.19
6.4.2.4	Discussion of Results	6.19
6.4.2.5	Conclusions	6.20
6.5	Model Roof Manufacture	6.20
6.6	Model Roof Testing	6.21
6.6.1	Introduction	6.21
6.6.2	Loading Details	6.22
6.6.3	Gauging	6.23

	<u>Page No.</u>
<u>CHAPTER 7</u>	DISCUSSION BETWEEN THEORY & EXPERIMENTAL MODEL TEST RESULTS
7.1	Introduction 7.1
7.2	Presentation & Comparison of Results 7.2
	7.2.1 Deflection 7.2
	7.2.2 Member Loads, Strains & Buckling 7.4
7.3	Discussion of Results 7.6
	7.3.1 Deflection 7.6
	7.3.2 Member Forces, Strains & Buckling 7.8
7.4	Conclusions 7.11
<u>CHAPTER 8</u>	ECONOMIC ASPECTS
8.1	Introduction 8.1
8.2	The Cost of Long Span Grp Roofs 8.2
	8.2.1 Selection of a Grp Production Process 8.2
	8.2.2 Calculation of Roof Cost 8.3
	8.2.3 Additional Costs 8.5
	8.2.4 Possible Developments & Modifi- cations 8.6
8.3	The Long Span Grp Roof Market Potential 8.8
<u>CHAPTER 9</u>	CONCLUSIONS & RECOMMENDATIONS FOR FURTHER WORK 9.1
APPENDIX A	A1
APPENDIX B	B1
REFERENCES	R1

NOMENCLATURE

A

- A - Area
- APM - Factory area per mould.
- A_{ij} - Orthotropic cylinder stiffness elements or inplane stiffness matrix.
- A'_{ij} - Inplane compliance matrix.
- a - Cylinder radius.

B

- B - Material Stiffness.
- B_{ij} - Coupling Matrix.
- b - Plate width.

C

- C - Contiguity factor.
- CPMM - Cost of patterns and master moulds.
- CYCRN - Cylinder buckling cost-effectiveness.
- CYT - Cycle Time.
- CF - Fibre cost to resin cost ratio.
- CT - Cure Time.

- C_f - Cost of fibres.
- C_{ij} - Stiffness matrix.
- \bar{c}_{ij} - Transformed stiffness matrix.
- C_m - Cost of resin.

D

- D_f - Density of fibres.
- D_{ij} - Flexural stiffness matrix.
- D_m - Density of resin.
- d - Maximum depth of roof.

E

- E - Modulus of elasticity.
- EEAN - Axial stiffness cost-effectiveness.
- E_f - Fibre elastic modulus.
- E_l - Longitudinal modulus of elasticity.
- E_m - Matrix modulus of elasticity.
- E_t - Transverse modulus of elasticity.
- \bar{E} - Apparent modulus of elasticity.
- E_1 - Apparent modulus after 1 hour of creep.

F

- F, F_1, F_2 - Force in roof surface.
- FC - Factory costs.
- FLEXN - Flexural stiffness cost-effectiveness

$F_{1(T)}, F_{1(C)}$ - Longitudinal tensile strength and compressive strength respectively.

F_t - Transverse strength.

G

G_f - Shear modulus of the fibres.

G_{lt} - Composite shear modulus.

G_m - Shear modulus of the matrix.

H

H - Laminate thickness.

h - Cylinder wall thickness.

I

I - Second moment of area.

IT - Resin injection time.

K

K - Fibre misalignment factor.

k - Stress intensification factor.

k_x, k_y, k_{xy} - Midplane curvatures.

L

LUR - Laminate lay-up rate.

LUT - Laminate lay-up time.

- l - Crack length, roof span.
- l_c - Ineffective fibre strength.

M

- MPT - Material preparation time.
- MT - Mould Committed time.
- M_x, M_y, M_{xy} - Laminate moment resultants.

N

- N - Buckling load per unit width.
- NOMR - Number of moulds required.
- N_x, N_y - Midplane stress resultants in the x or y direction respectively.
- N_{xy} - Midplane shear stress resultant.

P

- PA - Plan area.
- PCRN - Plate buckling cost-effectiveness
- P_E - Euler buckling load.
- PEL - Product edge length.
- PRPD - Production rate per day.

R

- R - Radius of crack tip.
- RDT - Material consolidation time.
- r - Cylinder radius.

S

- SA - Surface Area.
- SUT - Spray-up time.
- S_A - Fatigue stress amplitude.
- S_C - Stress rupture strength.
- S_E - Fatigue strength at stated life.
- S_M - Mean Stress
- S_U - Ultimate strength of material.
- S_{ij} - Compliance matrix.
- \bar{S}_{ij} - Transformed compliance matrix.

T

- T - Absolute temperature.
- TC - Hot press mould cost.
- TK - Thickness.
- T_{ij} - Transformation matrix.
- t - Time.
- t_r - Time to rupture.

U

- ULT - Unskilled labour time.

V

- V_f - Fibre volume fraction.
- V_m - Matrix volume fraction.

W

- W - Weight.
- WT - Mould preparation time.
- w - Load intensity.

GREEK SYMBOLS

α	- Fibre angle or wind angle
γ_{12}	- Shear strain
δ	- Roof deflection
σ	- Normal stress
σ_{ij}	- Stress component
σ_0	- Stress rupture constant
σ_r	- Rupture stress
ϵ	- Normal strain
ϵ_{ij}	- Strain component
ϵ_w	- Allowable strain
ϵ_r	- Resin percentage elongation at failure
ϵ_t	- Strain at time t.
$\epsilon_x^0, \epsilon_y^0, \epsilon_{xy}^0$	- Midplane strains
ϵ_0	- Constant depending upon material stress and environment
ϵ'_0	- Constant depending upon material environment
τ	- Shear stress
μ_f	- Poisson's ratio of the fibres
μ_m	- Poisson's ratio of the matrix
μ_{lt}	- Major or longitudinal Poisson's ratio
μ_{tl}	- Minor or transverse Poisson's ratio

SUFFIXES

f	- Glass fibre
m	- Resin
csm	- Chopped strand mat
UD	- Uni-directional roving
t	- Time, transverse direction
l	- Longitudinal direction
EB	- Edge-beam
r	- Stiffening ring property
S	- Denoting property per unit width
st	- Stringer property
s	- Skin property
v	- Visco-elastic term
EP	- Empirical elastic term

CHAPTER 1

INTRODUCTION

CHAPTER ONE

Introduction

Glass reinforced plastic (grp) has now been available as a structural material for several decades. However, its use as a major load-bearing material has been very limited in civil and structural engineering. In the main, its structural use has been restricted to roofs of moderate span such as the 17 m span roof over the Morpeth Secondary School in London.

The concern of this project is to investigate the feasibility of long span lightly loaded structures where grp is used as the major structural material. Many forms of glass reinforced laminates have exceptionally good strength to weight ratios. Structures in which this property may be used to advantage, and yet are not rendered unsatisfactory by grp's relatively low modulus of elasticity, may be well suited to this material. Long span lightly loaded structures are potentially of this type.

The problem of feasibility will be approached by making a general survey of the properties of glass reinforced plastics, and then investigating in greater depth, theoretically and in some cases experimentally, the more relevant structural properties. With the knowledge gained, general design philosophies will be discussed and the cost effective design of laminates under various loading systems investigated. Also the financial aspects of several production techniques will be studied. Having examined the material and its application, suitable long span structures are discussed and a particular structural function chosen for further investigation. A design study will then be carried out and analysed on a structural and financial basis. The design will be verified by the manufacture and testing of a model structure. Attention will be paid to the potential market of the structure and hence the associated consumption of glass fibres, since the Pilkington Group, who manufacture glass fibres, sponsored this project.

CHAPTER 2

DISCUSSION OF THE PROPERTIES OF GRP
RELEVANT TO STRUCTURAL ENGINEERING

CHAPTER TWO

Discussion of the Properties of Grp Relevant to Structural Engineering.

2.1

Introduction

Grp has been used for some years in structural engineering, although in comparatively small quantities. By far the most common constituent materials used have been 'E' glass fibres, as reinforcement, and polyester resin, as the matrix. The reason for this is that these two materials possess the best combination of economic and structural properties relevant to the construction industry. Consequently, most attention has been directed towards these materials in preparation of this thesis. It should, however, be realised that these materials are available in many forms and thus may have a wide range of properties. Figure 2.1 shows several forms of glass reinforcement.

The following chapter is a brief description of grp's important and relevant properties together with the role played by the constituents.

2.2

Ultimate Strength

As mentioned above, glass reinforcement, the main strength - giving constituent, can be incorporated in grp in many different forms and as a result the material may possess either general anisotropic properties, special cases of anisotropy, or isotropic properties. The materials are never microscopically homogeneous but are often considered to be macroscopically homogeneous. The strongest forms of grp are those with orientated reinforcement. In this case, high strengths are only found in particular directions and the composite is of the anisotropic type. Figure 2.2 demonstrates the strength anisotropy of various designs of laminates in tension. A similar diagram could be drawn for compressive strengths which in general are lower. The difference in these strengths can be explained in terms of the micromechanics of fibre-reinforced plastics.

Composite tensile strength in the direction of the fibres depends upon a strong, stiff bond, either frictional or chemical, between the glass fibres and the resin. This is necessary so that the applied force can be transferred through the resin into the fibres by a shear mechanism. Thus a finite length of fibre is required before the maximum stress in the fibre is reached. This is particularly important for short fibre reinforcements such as chopped strand mat. Fig. 2.3 shows a simple model of a fibre in a matrix and how the load varies in the fibre and matrix. Solutions for this model have been

obtained by Cox [2.1], Dow [2.2], and Rosen [2.3]. Due to the ineffective length of fibre l_c , the longer the fibre then the greater the proportion of the fibre that is used efficiently, and the stronger the composite. Continuous fibres are the ideal, but in practice, although such fibres may have been used in the manufacture of the laminate, fibres will only be continuous at low stress levels. The strength of fibres reduces with increase in length [2.4, 2.5] due to a statistical distribution of flaws.

Resin structural properties have little effect on the longitudinal tensile properties, provided that elongation of the resin at failure is greater than the ultimate strain of the glass fibres [2.6.]

The tensile strength of aligned grp increases approximately linearly with fibre volume fraction within practical limits determined by the type of reinforcement used. Outside these limits, resin - rich or starved regions have a deleterious effect.

The transverse tensile strength of a unidirectional laminate is resin-dominated according to Hashin [2.7] and is of the same order as the strength of the matrix but lower [2.8]. The void content of the resin has a significant adverse effect on the strength; as much as 50% of the unvoided strength can be lost with a 2% voidage [2.9]. Increasing fibre volume fraction also has a deleterious effect.

Since the modulus of elasticity of the glass fibres is far greater than that of the resin the average stress is much greater in the fibres than in the resin. Notwithstanding this, the resin plays a major part in the longitudinal compressive strength of grp. The fibres act as columns supported in a continuous elastic or elastic/plastic medium; the resin. Ultimate failure occurs on fibre

buckling or debonding between the resin and glass [2.10]. Figure 2.4 shows schematically two modes of fibre buckling and the expected compressive strengths on this basis according to Rosen [2.3] for a glass-epoxy laminate. Predicted strengths have never been achieved in practice. The maximum strength is obtained when the fibre volume fraction is about 60 - 65% [2.8, 2.11]. At higher volume fractions the fibres are not adequately supported, and the strength reduces. In general, anything which gives additional support to the fibres improves the compressive strength, particularly high resin yield strengths and stiffnesses [2.11].

Voids again play an important role in decreasing the strength both in the longitudinal and transverse directions [2.9, 2.12].

The transverse compressive strength is largely governed by the compressive strength of the matrix which is an upper bound [2.7].

Flexural strength has been found commonly to lie between the compressive and tensile strengths of the material. Usually failure occurs in the outermost fibres in compression, but with compressive stresses higher than the simple compressive strength. This may be due to fibres closer to the neutral axis, under lower stress, providing the outer fibres with more support than they would receive if all fibres were equally stressed.

Glass fibres, within laminated composites, are rarely found in directions other than in the plane of the composite. This produces the possibility of interlaminar shear (ILS); a phenomenon peculiar to fibre-reinforced composites. The ILS strength may be an order of magnitude lower than the longitudinal tensile or compressive

strengths and must be considered an important weakness of the material. ILS occurs along resin-rich planes where there are very few or no transverse fibres to halt the progression of cracks.

This strength is largely dependent on the resin shear strength and the resin-glass interfacial bond strength. The fibre content has a small but adverse effect on the interlaminar shear strength [2.8].

Voids tend to accumulate in resin-rich areas particularly between layers of cloth or mat, and greatly reduce the ILS strength [2.12, 2.13].

Voids in laminates clearly have an important effect on their strength. The quantity of voids depends upon many factors, particularly the type of glass fibre, mat or fabric used and the laminate manufacturing process. For many commercial laminates the volume of voids can be expected to lie between 1 and 2.5% [2.14]. Reductions in strength of upto 10% to 40% can be expected on the void-free strength.

Figure 2.5 shows a range of tensile and compressive strengths which are found in commercially available grp laminates and sections compared to other structural materials. Steel is grp's strongest competitor but even this material compares poorly with many types of grp on a specific strength basis.

In general, for maximum efficiency, the fibres should be parallel to the direction of the major stresses. Where these stresses occur in more than one direction, fibre reinforced composites become

less efficient. Proctor [2.15] illustrates the reason for this (Figure 2.6); not only is the fibre reduced in the principal directions but also the total fibre volume fraction is reduced.

2.3

Stress Rupture

Stressed grp in normal environments exhibits a loss of strength with time (Figure 2.7). The magnitude of the loss may be significant and should be considered when choosing design stresses. Both the major constituents of the composite, the resin and fibres, together with the interface, contribute to the loss. Water is well accepted as a major cause of the phenomenon. Temperature also greatly affects the rate of reduction in strength.

Figure 2.7 shows the results of several workers in this field [2.16, 2.17, 2.18, 2.19]. Although they all worked with apparently similar material there is clearly a great difference in the results. Consequently the designer must make conservative estimates of strength, which leads to inefficiency unless tests are carried out on the design material.

This topic will be treated more fully both theoretically and experimentally in the following chapter.

Figure 2.8 compares the absolute and specific flexural modulus of commercially available laminates and sections in grp with other structural materials. Grp compares poorly on both bases although better from the specific point of view. As stated previously, laminated grp exhibits in-plane anisotropy unless specially orientated or random reinforcement is used. Figure 2.9 illustrates the stiffness anisotropy for several fibre systems. A derivation of these curves may be found in Chapter 3.

Moduli in the direction of fibres are governed principally by the fibres and increases linearly with increase in fibre volume fraction. Shear and transverse stiffness in unidirectional laminates are similar to the resin moduli. They are increased slightly with fibre volume fraction and the compressive transverse modulus tends to be greater than the tensile. Voids in general have a considerably smaller effect on laminate moduli than strength, but are significant in the case of transverse and shear moduli [2.9].

In the short term, grp is generally accepted as being linearly elastic to failure even though this is only approximately true.

Grp is visco-elastic; that is, its extension under stress is a function of time. Hence, where grp is to be stressed for other than very short periods, which could be as short as a few minutes at relatively high stress levels, the consideration of only the short term modulus of elasticity is insufficient. Examples of the work of Kabelka [2.16] and Boller [2.17] are shown in Figure 2.10 in this respect. The characteristic creep curve, as suggested by Steel [2.18], consists of three stages: initial rapid increase in strain; a comparatively long period of time at a minimum rate of creep; and finally a second period of rapid extension to failure (Figure 2.11). Steel's work was endorsed by Diggwa and Norman [2.19]. However, these workers based their conclusions on flexural creep results. Boller [2.17] and Kabelka [2.18] who were concerned with tensile or compressive creep failed to observe the tertiary stage. This may be explained in that progressive failure in flexure may be extended due to the non-uniform stress distribution; highly stressed outer fibres failing first, causing a loss in flexural rigidity and an increased deflection. Inner fibres having been previously under lower stress would not have lost as much strength and may be expected to resist the increased load for some time. Diggwa and Norman's characteristic curve may be further held in doubt since their equipment design would cause an increase in applied bending moment with increasing strain. Thus it is possible that the creep curve is different under direct stress from that in flexure. There may be a tertiary stage under direct stress but spanning a much shorter

period of time in relation to the secondary stage, than suggested by Steel.

Both the resin and the fibres contribute to the creep but the greater contribution is made by the resin. Consequently, short fibre grp is most prone to creep. Unidirectional continuous fibre grp is the most resistant to creep. The creep mechanism will be considered in greater depth in Chapter 3.

2.6

Dynamic Fatigue

As is the case with other structural materials, repeated loading of grp can cause failure at stresses below the short term ultimate stress. Unlike ferrous metals, however, grp does not have an endurance limit whereby the material can withstand unlimited cycles provided the stress is below this limit.

Owen et al [2.20, 2.21] have observed that failure in chopped strand mat (CSM) occurs in three stages; debonding, cracking and finally separation. After 10^6 cycles CSM was found to endure approximately $4 \times 10^4 \text{ KN/M}^2$ reversed stress before separation and approximately $1.2 \times 10^4 \text{ KN/M}^2$ before debonding and cracking. Boller [2.22], using epoxy resin and 181 fabric reported a reversed stress fatigue strength of $8 \times 10^4 \text{ KN/M}^2$ after 10^6 cycles. After 10^7 cycles polyester laminates can be expected to have a strength of between 18% and 37% of their short term strength [2.23].

In general the order of superiority for reinforcements under uni-axial stress is the same as for other properties; orientated reinforcement is better than random, unidirectional material being best; and unwoven fabric is preferable to woven.

Grp is relatively sensitive to mean stress, and as a consequence the Goodman law:

$$\frac{S_A}{S_E} = 1 - \frac{S_M}{S_U} \quad 2.1$$

where S_A = stress amplitude

S_E = fatigue strength at stated life

S_M = mean stress

S_U = ultimate strength of the material

has been found inadequate [2.22, 2.21]. Boller has suggested a modified law:

$$\frac{S_A}{S_E} = 1 - \frac{S_M}{S_C} \quad 2.2$$

where S_C = stress rupture strength

A further adjustment has been proposed by Owen and Smith [2.21] where the mean stress is tensile:

$$\frac{S_A}{S_E} = \frac{1 - \frac{S_M}{S_C}}{1 + \frac{S_M}{S_C}} \quad 2.3$$

Little work has been done on the anisotropy of fatigue, multi-axial stress and random stress cycles. Water appears to have

little effect on grp when there is a long life span [2.24].

2.7

Ductility and Fracture Toughness

Glass and polyester resin are both brittle materials and their combination produces a brittle composite; that is, the large plastic deformation mild steel and other metals experience before ultimate failure does not occur. This has two important structural implications. Grp cannot stress-relieve as effectively as mild steel at points of stress concentration. Hence mechanical jointing requires more care, and stress redistribution due to plastic deformation cannot be relied upon in statically indeterminate structures. Steel structures exhibit large deformations before catastrophic failure, which may serve as a warning to people in their locality. Such warning signs would not be automatically inherent in a grp structure.

Although grp is brittle it does have fracture toughness. A crack in the resin, which may be caused by a broken or transverse fibre, a void, a pre-existing crack or a surface irregularity, does not necessarily cause failure as it may do in a brittle homogeneous material. Cracks in brittle materials propagate easily because the average field stress is magnified by a factor k where

$$k \doteq 1 + 2\sqrt{l/R} \quad 2.4$$

and l = length of crack

R = radius of crack tip.

Thus sharp cracks are more dangerous than blunt ones.

If the resin-glass interface strength is less than approximately $\frac{1}{3}$ of the cohesive strength of the matrix then an advancing crack encountering a fibre behaves as shown in Figure 2.12. The fibre-resin interface breaks down and the crack spreads along the fibre. In effect, the radius of the crack tip has been increased and the stress concentration factor, k , reduced. It should be noted that there is a conflict of interests between fracture toughness, requiring low interface strengths, and composite strength requiring high interface strength. Normally, a satisfactory compromise is obtained if the interface strength lies between $1/5$ and $1/3$ of the matrix cohesive strength [2.6].

2.8

Durability

It is known that grp may suffer a reduction in strength, modulus and appearance and an increase in brittleness on exposure to the elements. Water and ultra-violet light are the main agents of degradation [2.25]. Hence, resins with low water absorption and which are stabilised against ultra-violet light give better weathering characteristics. Heat can also permanently affect the properties of the composite.

Manufacturing technique and quality control are important if the laminate is to be durable. Resin-rich and resin starved areas, which are crack prone, can lead to rapid deterioration due to the resulting ingress of moisture. However, high resin contents are desirable.

Resin rich surfaces, known as gel coats, have been beneficial to the durability of grp laminates. In addition, when the gel coat is reinforced with a surface tissue its good appearance is prolonged, and where relevant, transparency maintained [2.25, 2.26].

The magnitude of the reduction in mechanical properties has not been satisfactorily established. A loss in strength of 10 and 20% is common after exposure for 3 years [2.27]. Algra and von der Beck [2.28] tested various laminates under several conditions for upto 10 years. They found that bi-phenol A polyester resin was superior to iso-phthalic resin, with phthalic acid anhydride polyester enduring least well. Laminates with the bi-phenol resin showed no deterioration in flexural strength or stiffness after exposure for 5 years. A similar laminate of phthalic acid anhydride resin reduced in strength by under 25% and in stiffness by less than 10%. Fire retardant resins generally have poorer strength retention than other resins, and Rugger [2.29] estimates that a factor of 2 applies.

The degree of degradation depends on the climate of the location of the composite, whether the location is urban or rural; if urban the level of atmospheric pollution is important. Even when these variables are known, one side of a pitched roof may weather differently from the other depending upon the amounts of sunlight each receive.

Weathering under stress has not been widely studied. However, tests in Florida, USA, [2.30] with a chrome finish glass fabric and polyester resin composite unstressed, and stressed in flexure at about 25% of the ultimate strength, showed that upto 40% of the strength was lost over 3 years. The difference between the

stressed and unstressed results was small.

Storage in water at 20^oc was found to be more severe than outdoor exposure in Holland [2.28]. A considerable amount of work has been carried out on creep and stress rupture in water, which could be used as a conservative estimate of durability in northern European climates.

In the past, grp has been marketed as maintenance-free. This is not so if its initial properties are to be retained for as long as possible. Estimates as to the required frequency of maintenance are varied and will depend upon the exposure conditions. Hosing down regularly and refinishing every 7 or 15 years if a special gel coat or pvf film is used, is more than adequate, according to grp manufacturers [2.25].

Grp is a relatively new material, and consequently manufacturers are not yet prepared to give guarantees on the life of products. However, grp boats have been in use for over 20 years, and as this period extends, manufacturers will become more confident. Scott and Metthan [2.17] expect guarantees of 60 years soon to become commonplace.

2.9

Thermal Properties

As with other properties, the thermal properties of grp vary with the form and quantities of the constituents. Polyester resin has a larger coefficient of expansion and is a better thermal insulator

than glass. Grp is a considerably better insulator than either steel or aluminium, and has a lower coefficient of expansion than aluminium. Thermal properties are summarised in Figure 2.13.

Grp is readily combined with low density plastic foams to form sandwich panels which can have exceptionally good insulating properties [2.31].

Since glass and polyester have differing coefficients of expansion, when laminating takes place at temperatures above ambient, residual stresses result. These stresses may reduce the composite strength and cause warping [2.32].

2.10

Mouldability

Grp has often been said to give the designer a new degree of freedom in that he can now design the material as well as the shape of the component. The extent to which he can do this is limited by the economic moulding techniques available to him for producing a particular form of reinforcement. The reinforced plastics industry has developed many moulding techniques, some of which are listed below:

- 1) Contact Moulding
- 2) Spray-up
- 3) Robot-spray
- 4) Pressure bag
- 5) Vacuum bag
- 6) Autoclave

- 7) Cold press moulding and resin injection
- 8) Hot press moulding
- 9) Filament winding
- 10) Pultrusion
- 11) Continuous laminating
- 12) Preform

Basic aspects of these processes are outlined below.

2.10.1 Contact Moulding

Contact moulding, otherwise known as hand lay-up, is the original, most basic and common manufacturing technique. Its widespread adoption is mainly due to the low capital cost involved in setting up production. Only one male or female mould is required. The mould is relatively cheaply made from polyester, or, for longer life, epoxy resin. Ancillary equipment may be limited to brushes, ringed rollers, mixing equipment, trimming knives, and safety equipment, all of which can be bought for tens rather than hundreds of pounds. As the process requires little capital it is most suitable for low production rates.

This process is particularly appropriate to the construction industry since there are no size limitations. Complex shapes and changes in thickness are readily accommodated.

All types of reinforcement can be used, with the exception of continuous filament mat. Unwoven rovings are not often used. Low density plastic foams are frequently incorporated to increase

flexural rigidity.

Since only one mould is used, only one smooth surface is possible. The other surface is rough and shows fibre patterns. The thickness of the composite is difficult to control accurately and depends upon the skill of the laminator. Generally laminate quality is very variable and can lead to high void contents and resin-rich areas.

Although little capital equipment is involved the process is labour intensive. The main operations involved are outlined below, assuming the mould is already in use:

- 1) The mould is treated with release agent to facilitate removal of the product.
- 2) A gel coat and surface tissue are applied if required.
- 3) If only a gel coat is applied this must be allowed to gel.
- 4) Catalysed resin and tailored glass reinforcements are layed-up.
- 5) The laminate is stippled with a brush and rolled to ensure good wet-out and minimum voidage.
- 6) The laminate is allowed to gel. This may take place at room temperature, or heated, quickening the reaction.
- 7) Preliminary trimming may take place once the resin has reached a leathery hardness.
- 8) Full curing.
- 9) Removal from the mould and finishing.

A common time-saving modification to this process is to spray the resin onto the fibreglass.

2.10.2 Spray-up

In spray-up, as the title suggests, the glass and resin are sprayed together from a gun onto a mould. This results in considerable labour saving on contact moulding and, provided the spray-up machine is fully utilised, can result in corresponding cost reductions. The initial investment is higher than in the previous process but is still low compared with other industries.

This process is most applicable where large simple mouldings are required, and strength and accuracy of thickness are not a major requirement. In pure spray-up only one reinforcement is used, i.e. chopped rovings. However, other reinforcements can be hand-layed in position in addition to the sprayed material.

The same moulds may be used for spray-up as for contact moulding and the laminating procedure is similar. Stippling and material tailoring is not necessary but rolling is required.

2.10.3 Robot Spray

Robot spray is a further step towards mechanisation beyond spray-up. In this case the spray gun operator is replaced by a numerically controlled machine. In other respects the process is similar to spray-up.

The removal of the spray gun operator leaves a requirement for only unskilled labour.

2.10.4 Pressure Bag

This process is again similar to contact moulding except that consolidation is achieved with the use of a tailored flexible membrane. The mould is sealed using a pressure plate, and compressed air is pumped between the plate and the membrane.

2.10.5 Vacuum Bag

In this case, rather than applying a pressure as in the preceding process, air is drawn out from between the membrane and the mould surface. Thus atmospheric pressure is used in consolidation.

2.10.6 Autoclave

This system is an adaptation of the previous two processes and can operate in two ways. In one case a positive pressure is applied to the flexible membrane using steam, and in effect the autoclave replaces the pressure plate. Alternatively, steam is used in addition to a vacuum between the membrane and mould. The size of moulds is restricted by the capacity of the autoclave.

2.10.7 Cold Press Moulding & Resin Injection

These processes involve both male and female moulds which are brought together to enclose the product. Both moulding surfaces can thus be of high quality if desired and close thickness tolerances are obtainable. Relatively few voids obtained with these processes lead to high strength laminates. All types of reinforcement may be used, but if chopped strand mat is used it must incorporate an insoluble binder.

The two processes differ primarily in the timing of resin introduction. In cold press moulding resin is poured into position before closure of the moulds. This forces the resin through the reinforcement, pushing air out before it. When the resin is to be injected the moulds are closed before introduction of catalysed resin under pressure.

Size limitations for cold press techniques depend upon the size of the press. There are no size limitations associated with resin injection, but more than one injection point may be required.

Capital outlay is higher for these processes compared with hand lay-up and spray-up. The moulds are between $2\frac{1}{2}$ and 5 times more expensive than simple contact moulds [2.33]. Presses and resin injection equipment also have to be procured. Injection equipment can often be considerably cheaper than a press, but when large mouldings are required, mould-opening equipment is necessary.

2.10.8 Hot Press Moulding

The title "Hot Press Moulding" is normally reserved for processes using sheet-moulding compound or dough-moulding compound, both of which are plasticine-like materials comprising of short glass fibres, resin, and filler. Both types of compound are highly viscous and require high pressure for moulding. They also require heat to cure. Consequently, the cost of presses and moulds leads to much higher capital investment than for other processes.

The main advantage of hot press techniques is that they greatly increase production rates; a factor of 30 or 40 applies when compared to hand lay-up [2.33].

2.10.9 Filament Winding

After passing through a reservoir of resin, continuous reinforcement is wound onto a mandrel-like mould. This process is capable of producing grp of the highest strengths and stiffnesses. However, production rates are normally slow and its use has been mainly in the aero-space industry.

Modifications to the process have been made for the production of pipes where reinforcement is sprayed onto a rotating mould [2.34].

2.10.10 Pultrusion

Pultrusion is a continuous process mainly for producing rod stock. However, any straight section which has a constant thickness along the length is suitable.

Continuous reinforcement is fed through a resin bath, formed in dies and then oven-cured. Production rates of upto 5 or 6 ft. per minute are possible [2.31].

2.10.11 Continuous Laminating

In continuous laminating, reinforcement may be either sprayed or unrolled onto a conveyor belt between two sheets of cellophane. Resin may be either sprayed or applied using a resin dip. Curing takes place as the laminate passes through a heated zone.

This process is the most economical way of producing large quantities of long flat or corrugated sheets which are used typically for cladding purposes.

2.10.12 Preforming

Chopped fibres are drawn onto a preform screen by air suction, together with a binder to hold the fibres in position. The shape of the screen matches the final product, so that material tailoring is eliminated. The preform is transferred to a press where the resin is added and the product finished.

This process is readily automated and is very economical for large numbers of small and medium sized products.

These processes may be studied in greater depth by referring to "SPI Handbook of Technology and Engineering of Reinforced Plastics/Composites" 2nd ed., by Mohr, J.G., Van Nostrand Reinhold, 1973.

Polyester resins inherently have a low resistance to fire compared with other structural materials such as steel and concrete. Grp's fire resistance can be improved, however, by the use of additives such as paraffin wax, chlorinated paraffin [2.35] and Halogen [2.36].

Resins are commercially available which meet standard Class 1 in BS 476 part 7, 1972, for surface spread of flame. The requirements of BS 476, part 3, 1958, Ext FAA and Ext SAA can also be met.

With the use of additional materials, grp cladding panels have achieved Class '0' surface spread of flame standard, which is the most demanding classification. The conventional gel coat, in this case, was replaced by a urethane lacquer [2.36]. Comparatively long fire penetration times have been achieved using phenolic foam, manufactured by SRL. Ltd., Liverpool, in conjunction with grp.

The type of reinforcement used can effect the performance of grp in fires. Woven rovings have been found to act as a fire barrier after the resin has been burnt off. Discontinuous fibres would fall away once the resin was lost.

A major obstacle to the widespread acceptance of grp in the construction industry is its cost. Weight for weight, grp can be 4 or more times as expensive as structural steel. Due to grp's relatively low density it is much more competitive on a volume basis.

In many circumstances it is possible to overcome the cost disadvantages with careful design. The designer must utilise the material to the full by taking into consideration its durability, aesthetic potential, mouldability and strength-to-weight ratio. Normally, economics will lead the designer to use light, thin-walled sections rather than solid ones as may be found in concrete.

FIG. 2.1 TYPES OF GLASS REINFORCEMENT

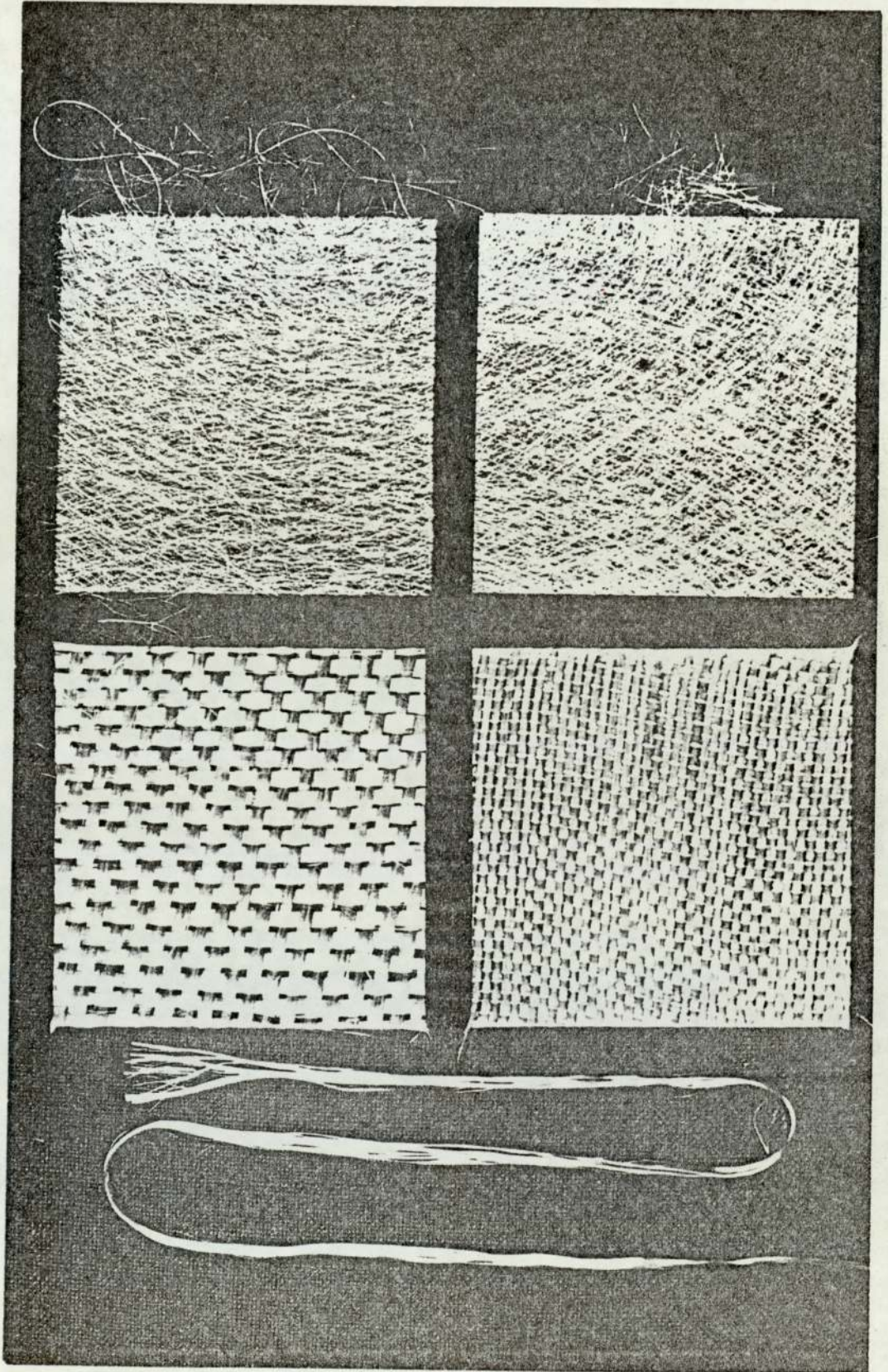


FIG. 2.2 STRENGTH ANISOTROPY

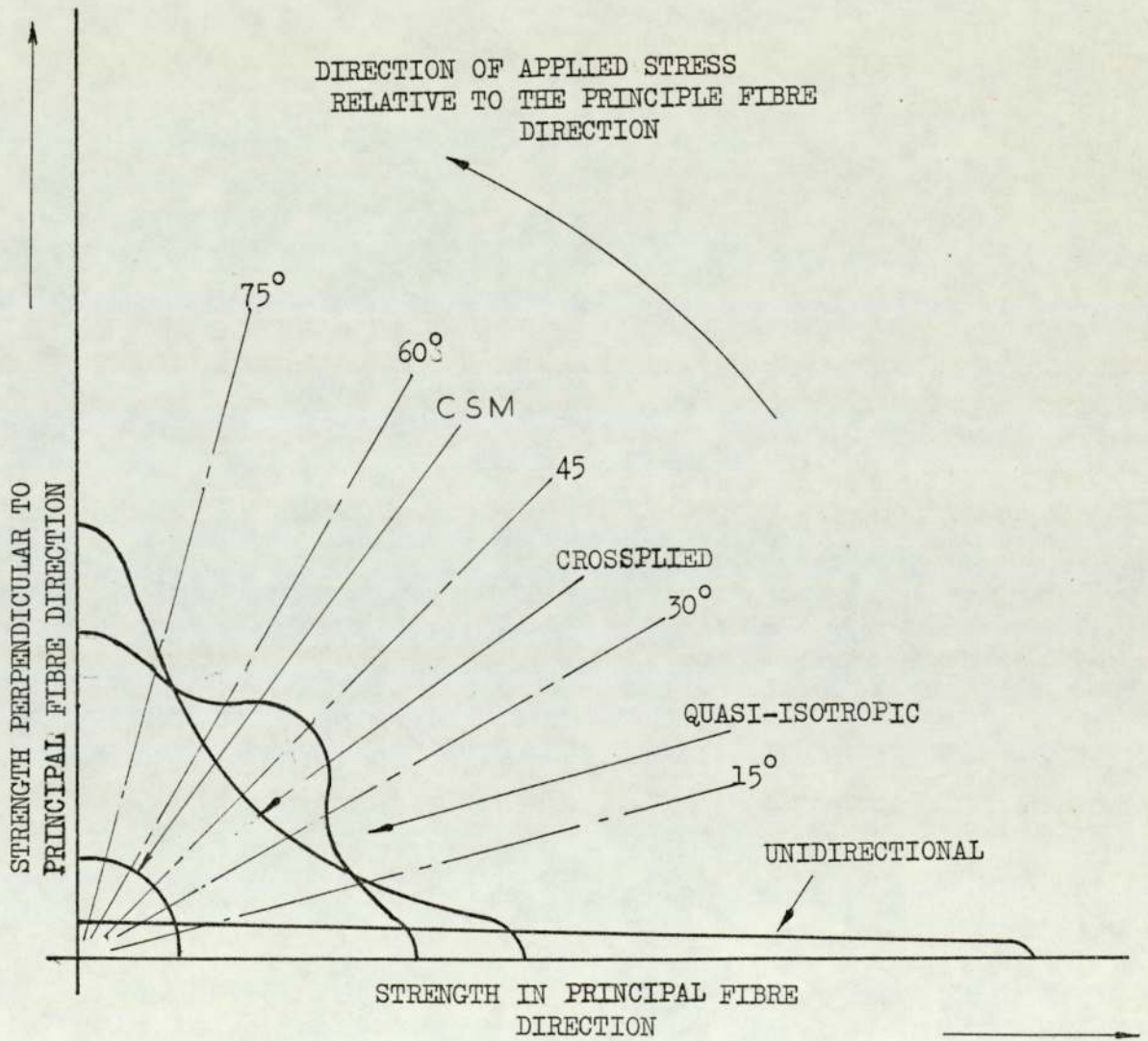
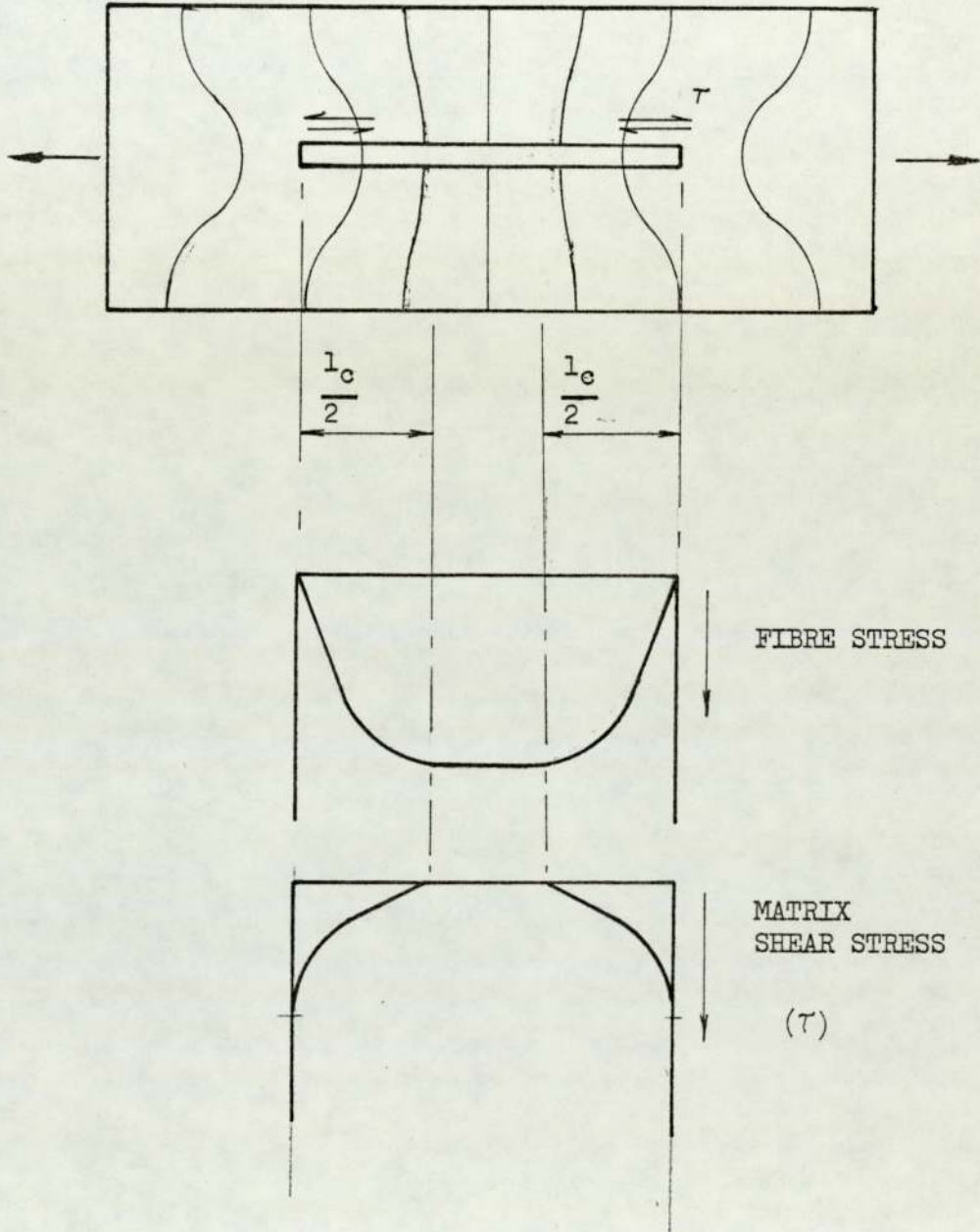


FIG. 2.3 STRENGTHENING MECHANISM



$l_c =$ INEFFECTIVE FIBRE LENGTH

FIG. 2.4 COMPRESSION STRENGTH

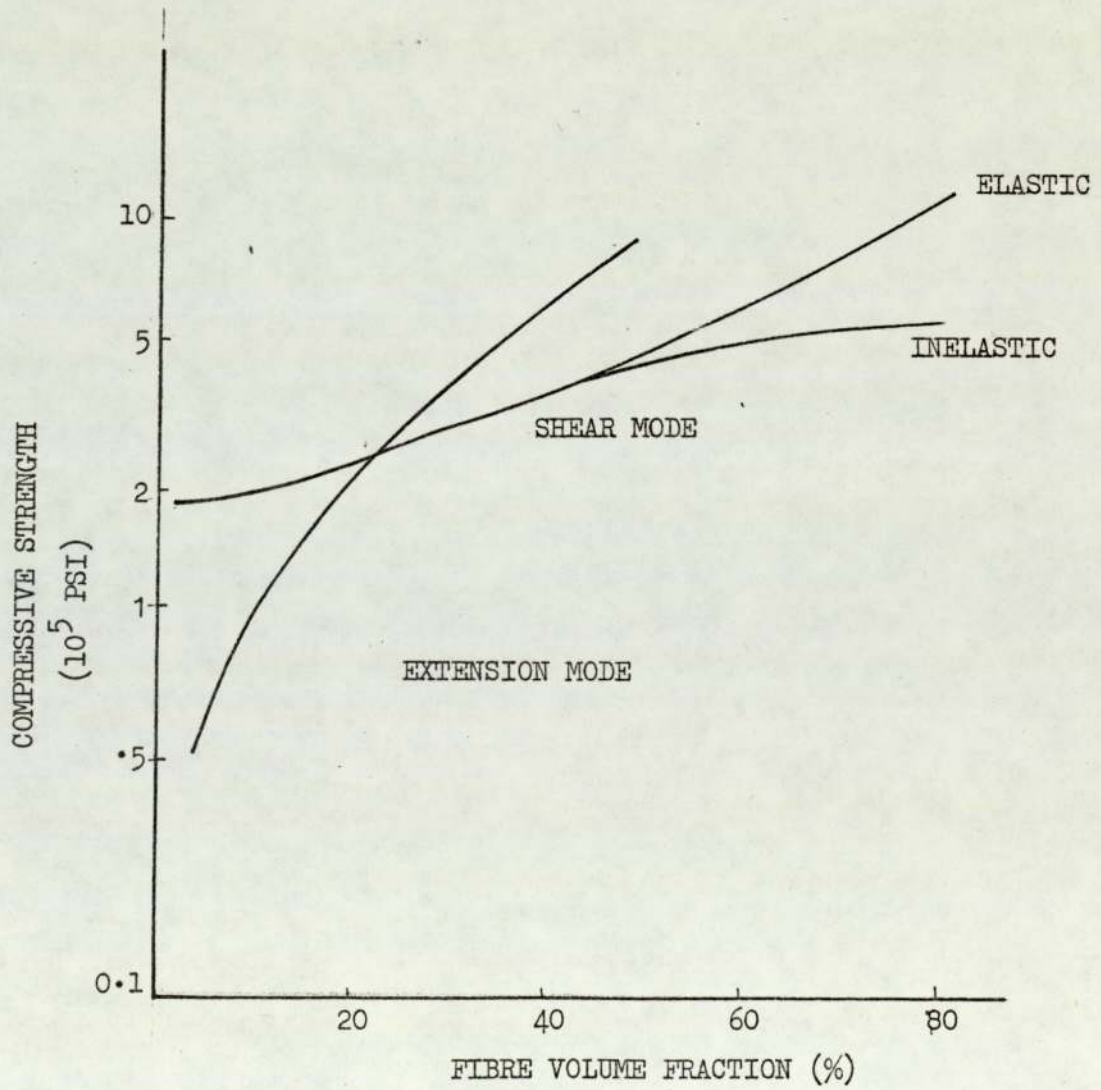
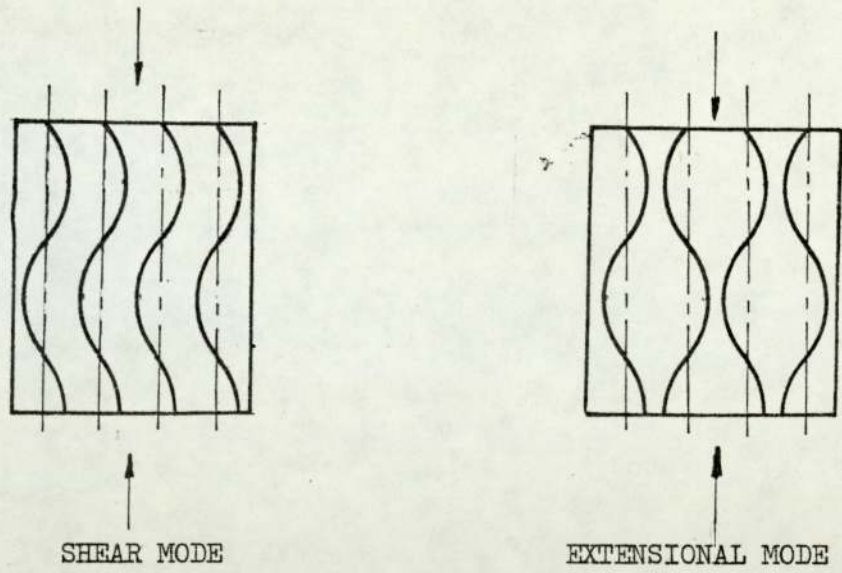
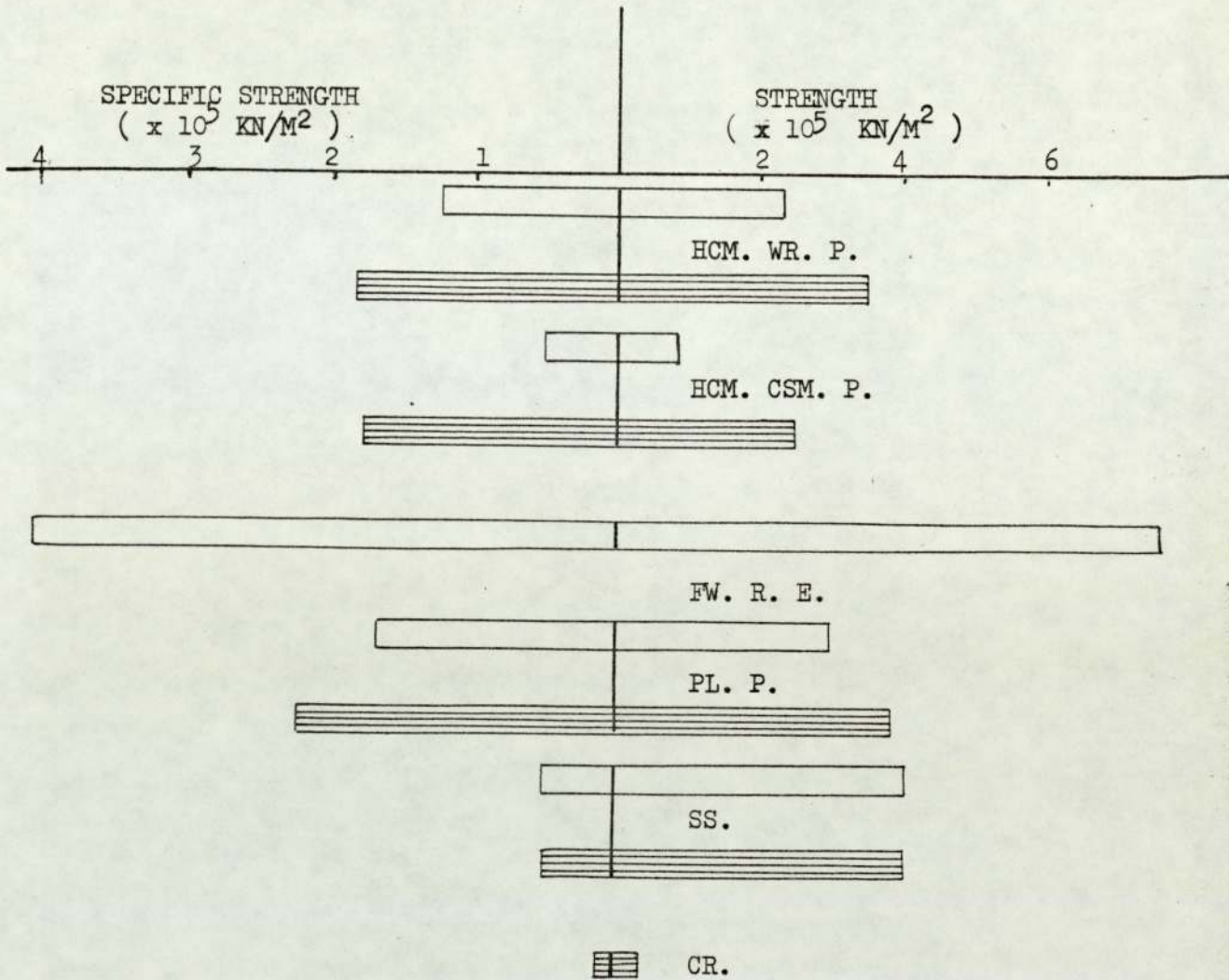


FIG. 2.5 STRENGTH OF STRUCTURAL MATERIALS



KEY

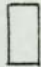



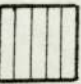
-  - TENSILE STRENGTHS
-  - COMPRESSIVE STRENGTHS
- HCM - HOT COMPRESSION MOULDING
- FW - FILAMENT WINDING
- PL - PULTRUSION
- CSM - CHOPPED STRAND MAT
- WR - WOVEN ROVINGS
- SS - STRUCTURAL STEEL
- CR - CONCRETE
- R - ROVINGS
- P - POLYESTER
- E - EPOXY

FIG. 2.6 FIBRE PACKING DENSITIES & COMPOSITE STRENGTHS

-  - THEORETICAL MAX. FIBRE VOLUME FRACTION
-  - PRACTICAL MAX. VOLUME FRACTION
-  - COMPOSITE PROPERTIES AS A FRACTION OF FIBRE PROPERTIES

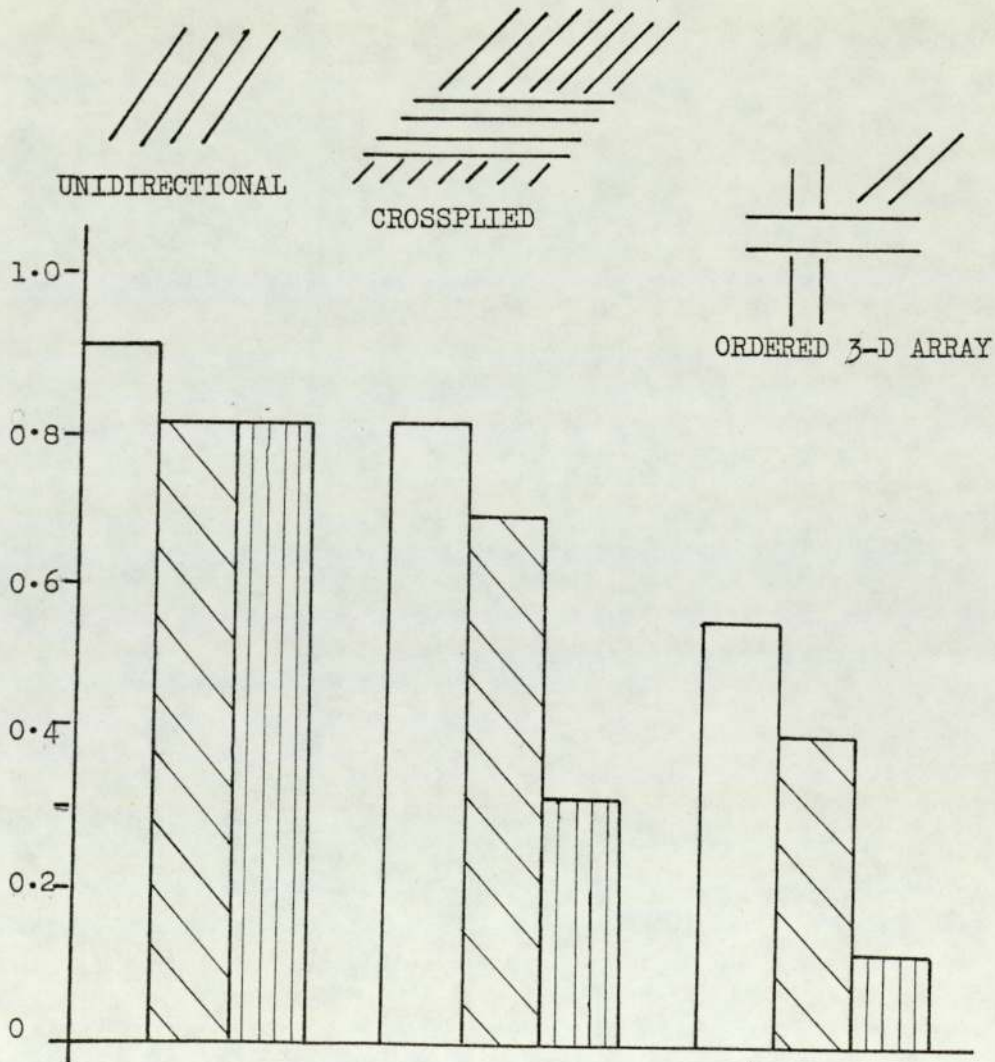


FIG. 2.7 LOSS STRENGTH WITH TIME

1	BOLLER	IN AIR	TENSION	[2.17]
2	BOLLER	IN WATER	TENSION	
3	BENJAMIN	IN WATER	TENSION	[2.31]
4	STEEL	IN AIR	FLEXURAL	[2.18]
5	STEEL	IN AIR	FLEXURAL	
6	KABELKA	IN AIR	COMPRESSION	[2.16]
7	KABELKA	IN AIR	TENSION	

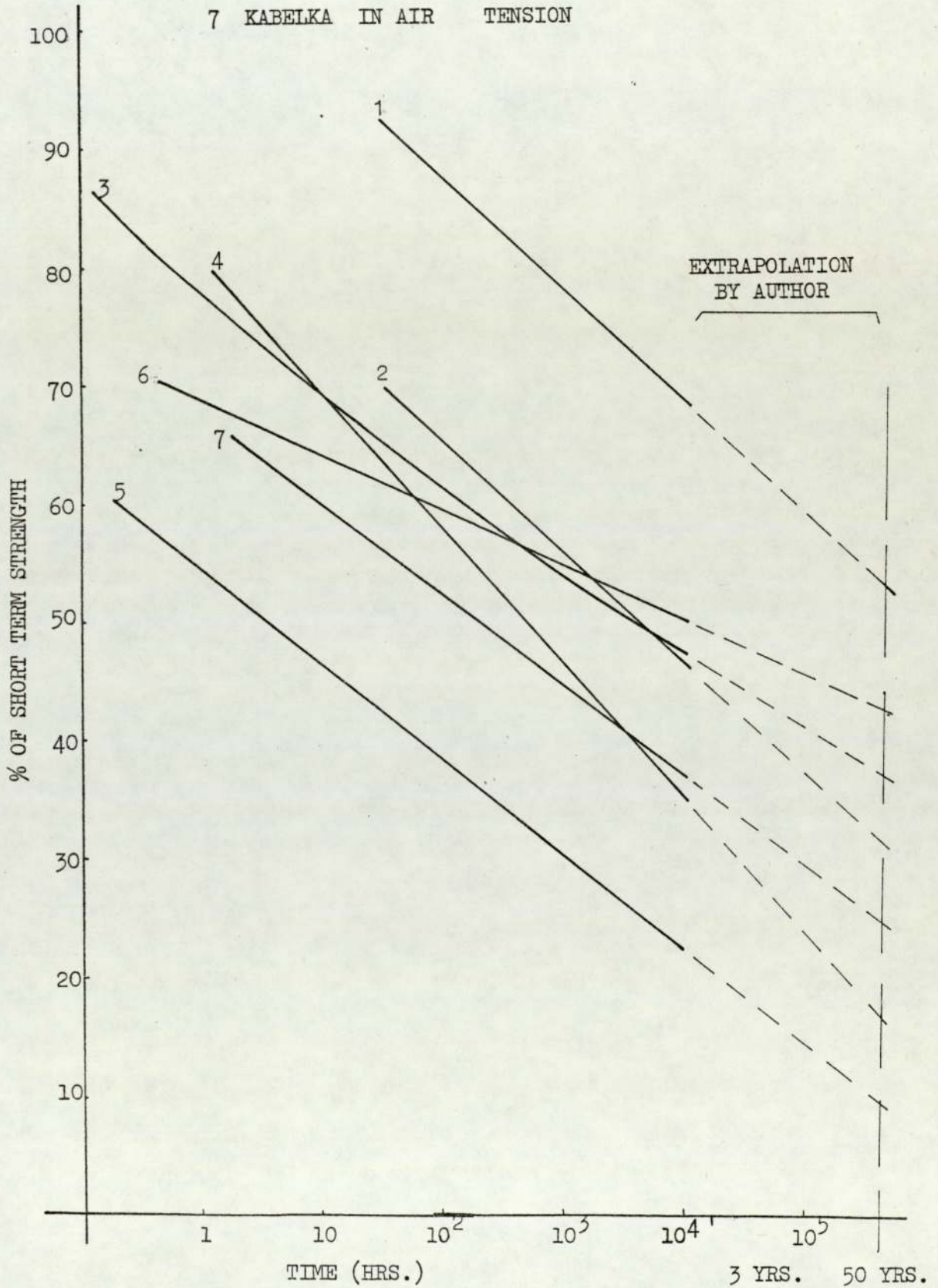
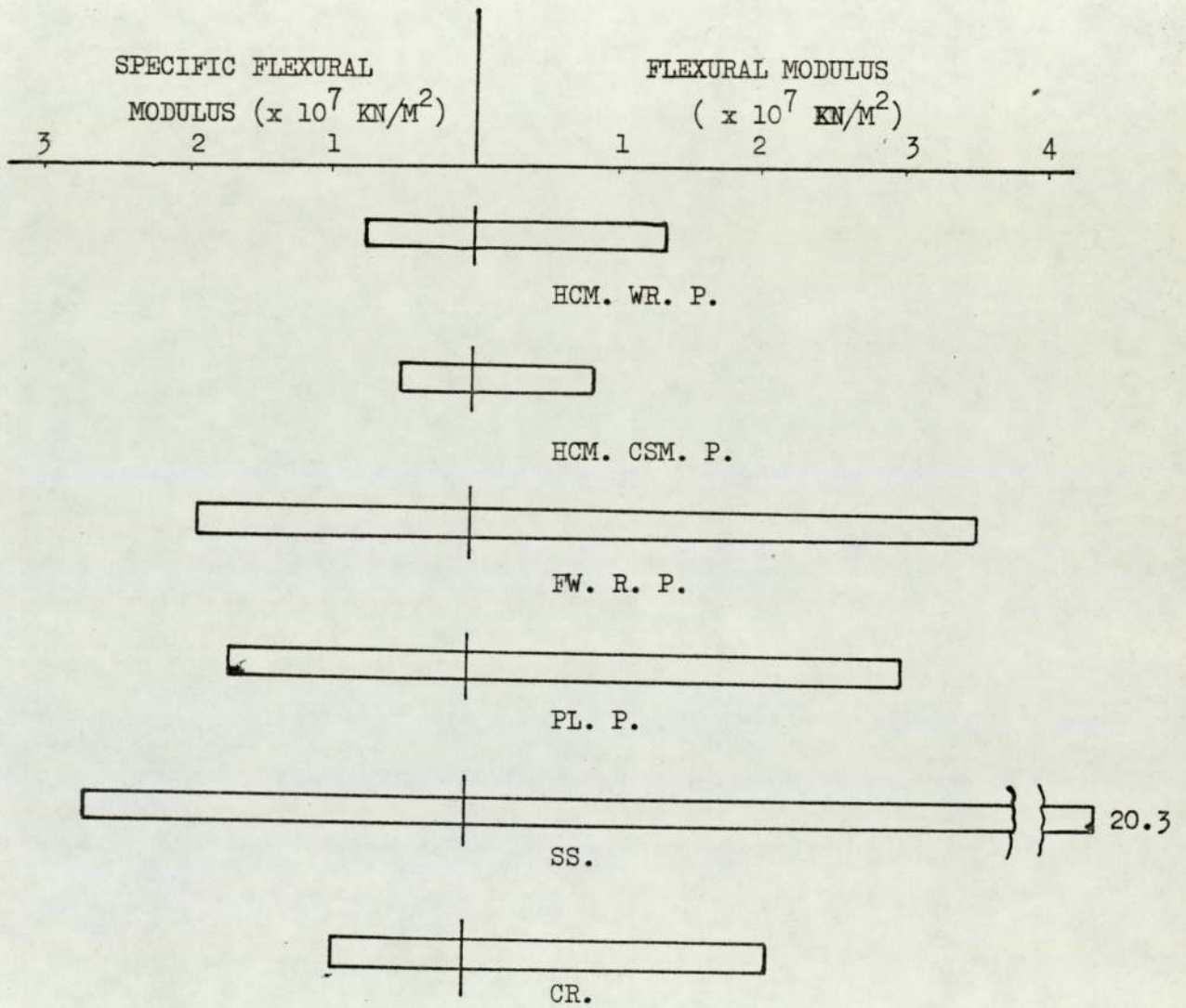
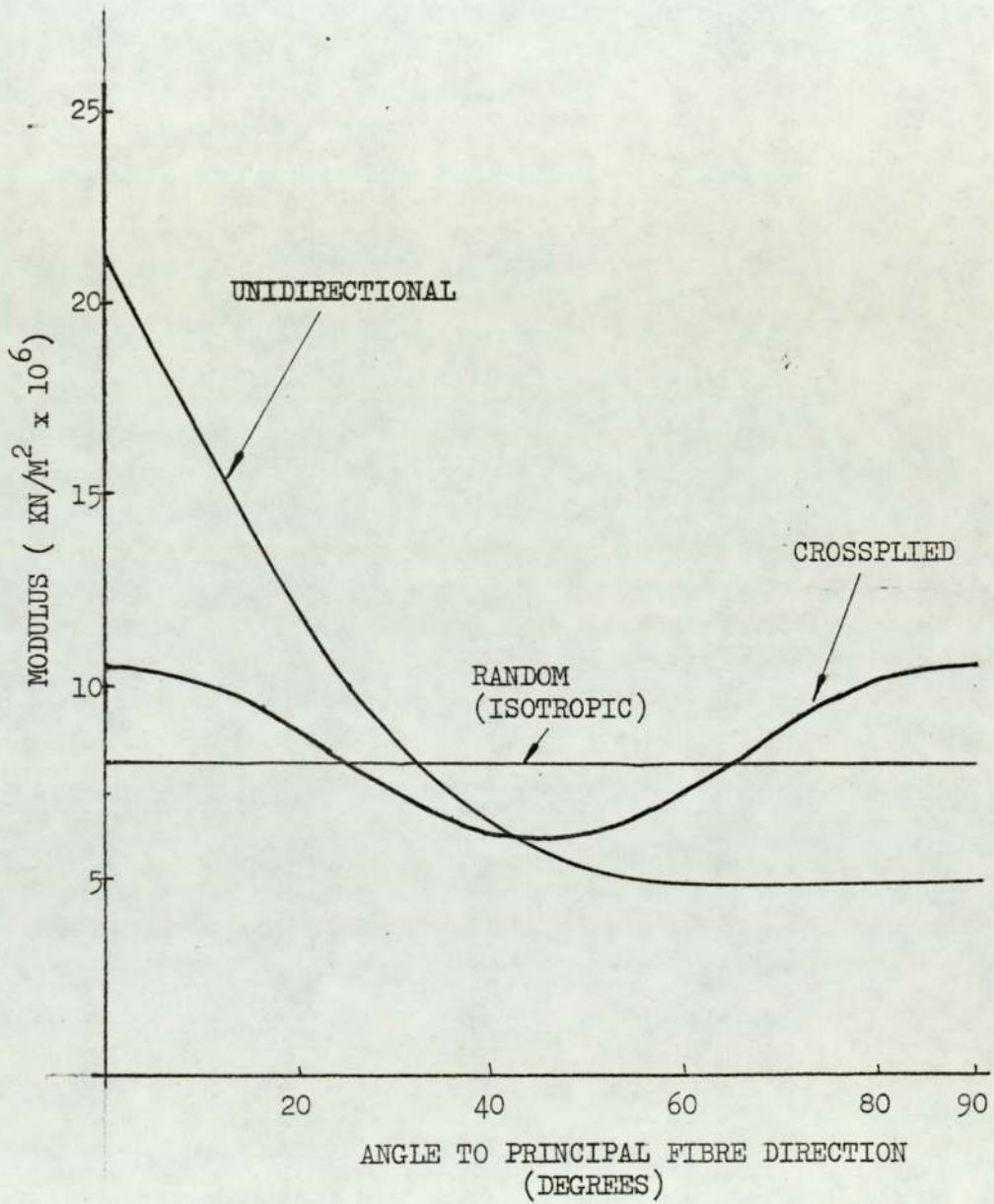


FIG. 2.8 FLEXURAL MODULUS OF STRUCTURAL MATERIALS



FOR ABBREVIATIONS SEE FIG. 2.5

FIG. 2.9 STIFFNESS ANISOTROPY



KABELKA - WOVEN FABRIC, 50% GLASS BY WEIGHT, 18°C, 20,000 KN/M².

BOLLER - WOVEN ROVING, 23°C, 20,000 KN/M².

POLYESTER RESIN WAS USED IN BOTH CASES

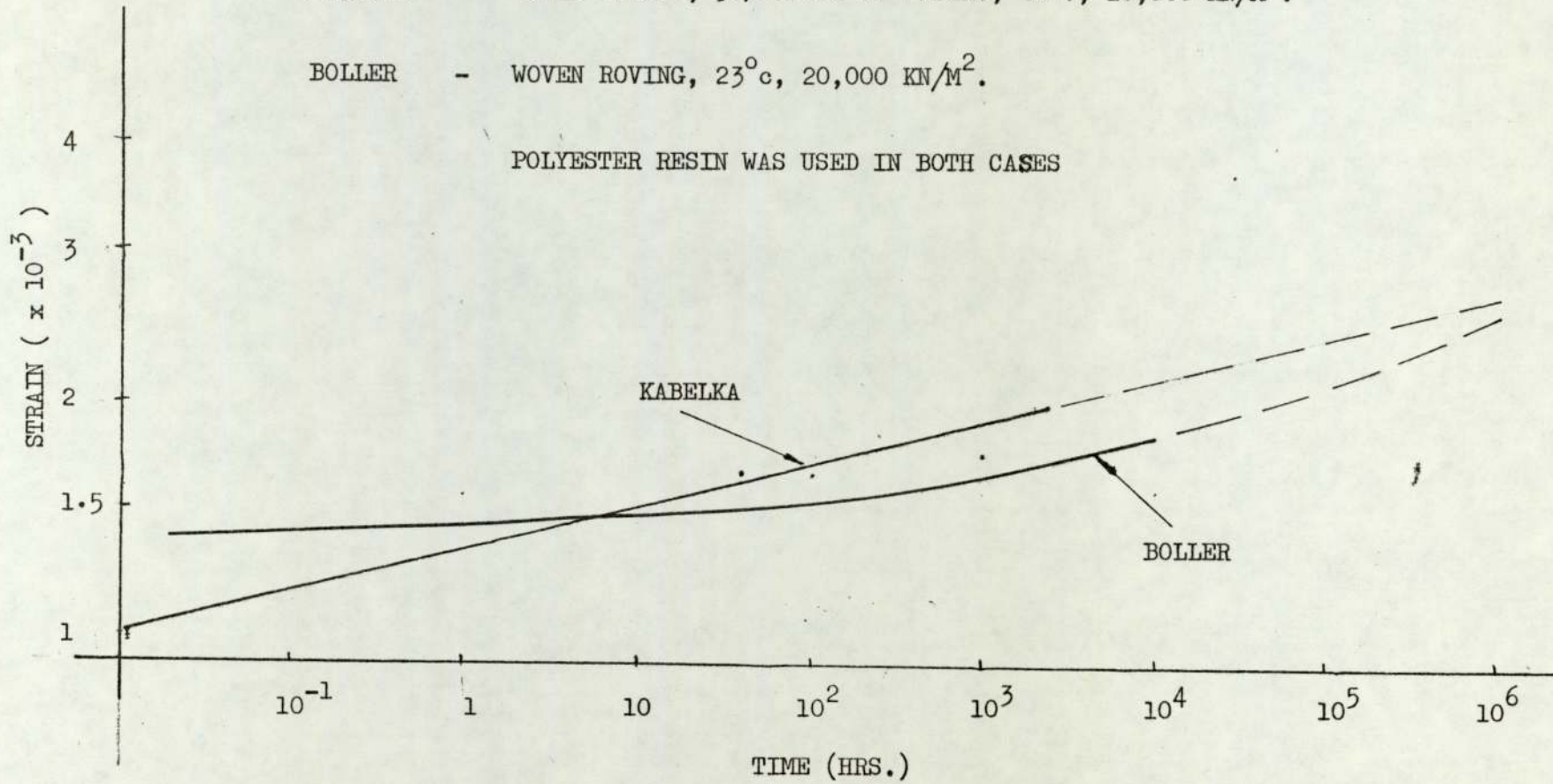


FIG. 2.10 CREEP OF GRP

FIG. 2.11 CHARACTERISTIC CREEP CURVE
ACCORDING TO STEEL [2.18]
(SCHEMATIC)

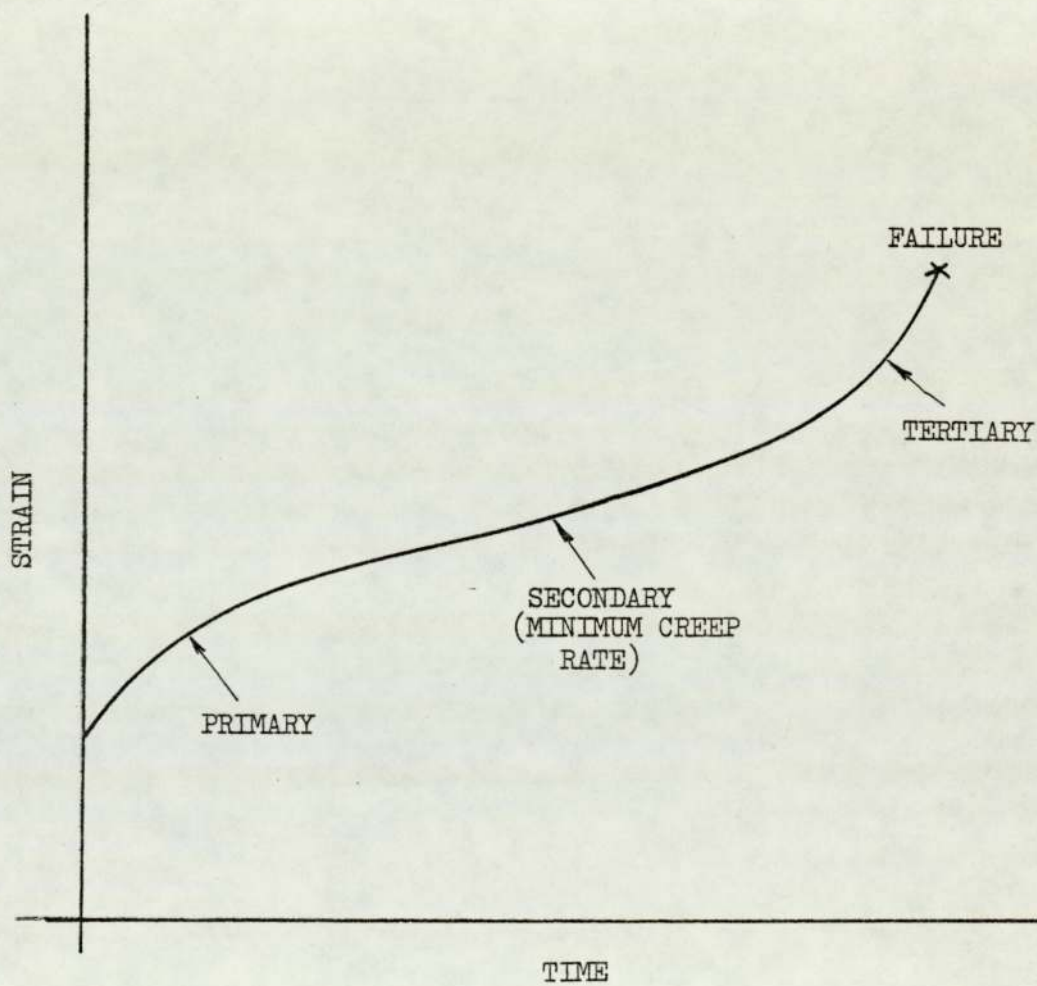


FIG. 2.12 CRACK STOPPING

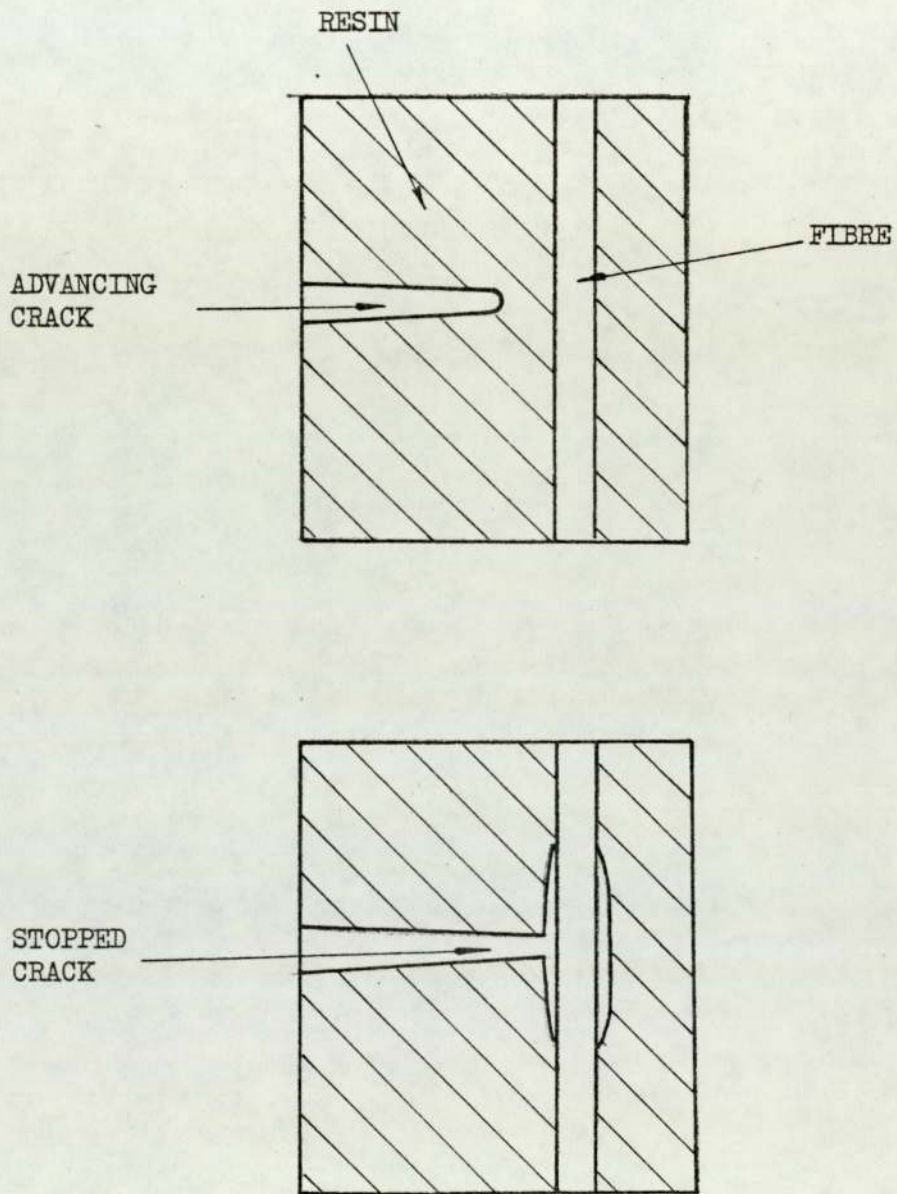


FIG. 2.13 THERMAL PROPERTIES

	COEFF. OF EXPANSION deg. C x 10 ⁻⁶	CONDUCTIVITY W/M deg. C
POLYESTER	9.9 - 18	0.21
GLASS	4.9	1.04
GRP	5 - 18	0.25 - 1
MILD STEEL	11 - 14	46
ALUMINIUM	22 - 23	140 - 190

CHAPTER 3

THEORETICALLY & EXPERIMENTALLY

DETERMINED PROPERTIES OF GRP

CHAPTER THREE

Theoretically and Experimentally Determined

Properties of Grp

3.1

Introduction

The preceding chapter discussed various properties of grp in a qualitative manner, and where relevant in relation to other structural materials. This chapter will deal specifically with grp in a quantitative fashion.

The chapter is in two main parts; that concerning short term properties, and that related to time-dependent properties. A further general division can be made between experimentally and theoretically determined properties.

3.2.1 Introduction

Hooke's law in its most general form is:

$$\sigma_i = C_{ij} \epsilon_j \quad i, j = 1, 2, 3, 4, 5, 6 \quad 3.1$$

where: σ_i are stress components,

C_{ij} is the stiffness matrix,

and ϵ_j are the strain components.

A material requiring this general form of Hooke's law to describe its elastic behaviour is known as a three dimensional anisotropic material. It can be shown that 21 independent elastic constants are required to form the stiffness matrix [3.1]. Such a material has no natural axes of symmetry.

Grp is not commonly used as a three dimensional material because of its relatively high cost, but frequently in laminate form. The number of independent elastic constants required to describe an anisotropic lamina is reduced to six (Figure 3.1a). When such laminas are layed together, to form a laminate, coupling may take place and eighteen elastic coefficients are required (Figure 3.1b).

A special case of the anisotropic lamina exists when the natural axes of the lamina coincide with the principal stress directions.

Such a lamina is known as orthotropic. In this case four elastic constants fully describe the material (Figure 3.1c).

Isotropic materials require only two constants for elastic characterisation (Figure 3.1d). These materials are symmetric about all axes.

It is possible to form laminated composites from anisotropic laminas that behave orthotropically under axial loading. These are known as specially orthotropic laminates. Six elastic constants are sufficient to describe such materials. This will be clarified in section 3.2.5.

Equations, in the following sections, will be presented so that if the basic properties of glass fibres and resin are known, the constitutive equations of a specially orthotropic laminate can be formed, and hence elastic problems solved.

3.2.2 Prediction of Elastic Constants of the Mono-layer (Figure 3.2)

3.2.2.1 Law of Mixtures

This theory is often known as the "mechanics of materials approach". The assumptions in this case are very general and greatly simplify the problem.

a Prediction of the longitudinal modulus of elasticity (E_1)

The main assumption made here is that the strain in the fibres and matrix is equal. Calcote [3.2] derives the following expression:

$$E_1 = V_f E_f + V_m E_m \quad 3.2$$

Where: E_f = Modulus of elasticity of the fibre.

E_m = Modulus of elasticity of the matrix.

V_f = Fibre volume fraction.

V_m = Matrix volume fraction.

b Prediction of the transverse modulus of elasticity (E_t)

In this case it is assumed that the fibres and the matrix experience equal stress [3.2] and the following equation results:

$$E_t = \frac{E_f E_m}{V_f E_m + V_m E_f} \quad 3.3$$

c Prediction of the major Poisson's ratio (μ_{1t})

Again the strain is assumed to be uniform in the fibres and matrix [2].

$$\mu_{1t} = \mu_f V_f + \mu_m V_m \quad 3.4$$

d Prediction of the shear modulus (G_{1t})

The derivation here is similar to that of the transverse modulus.

$$G_{1t} = \frac{G_f G_m}{V_f G_m + V_m G_f} \quad 3.5$$

where G_m = Shear modulus of the matrix and fibre respectively.

a Prediction of E_1

Tsai bases his prediction of E_1 on the "mechanics of materials" approach but modifies it to allow for poor alignment of the fibres.

$$E_1 = K (E_f V_f + E_m V_m) \quad 3.6$$

where K = fibre misalignment factor ≤ 1 .

b Prediction of E_t

The approach here is based upon variational methods, where classical elasticity is used. Using the concept of fibre contiguity, Tsai obtains:

$$E_t = 2 \left[1 - \mu_f + (\mu_f - \mu_m) V_m \right] \left[\frac{(1 - C) K_f (2K_m + G_m) - G_m (K_f - K_m) V_m}{(2K_m + G_m) + 2(K_f - K_m) V_m} \right. \\ \left. + C \frac{K_f (2K_m + G_f) + G_f (K_m - K_f) V_m}{(2K_m + G_f) - 2(K_m - K_f) V_m} \right] \quad 3.7$$

where C = Contiguity factor, $0 \leq C \leq 1$

$$K_f = E_f / 2(1 - \mu_f)$$

$$K_m = E_m / 2(1 - \mu_m)$$

$$G_f = E_f / 2(1 + \mu_f)$$

$$G_m = E_m / 2(1 + \mu_m)$$

c Prediction of μ_{1t}

Using the same approach as before, the following equation is obtained:

$$\begin{aligned} \mu_{1t} = & \frac{(1 - C K_f \mu_f (2 K_m + G_m) V_m + K_m \mu_m (2 K_m + G_f) V_m)}{K_f (2 K_m + G_m) - G_m (K_f - K_m) V_m} \\ & + \frac{C K_m \mu_m (2 K_f + G_f) V_m + K_f \mu_f (2 K_m + G_f) V_f}{K_f (2 K_m + G_f) + G_f (K_m - K_f) V_m} \end{aligned} \quad 3.8$$

d Prediction of G_{1t}

Again in a similar way, the following equation is given:

$$\begin{aligned} G_{1t} = & \frac{(1 - C) \cdot G_m 2 G_f - (G_f - G_m) V_m}{2 G_m + (G_f - G_m) V_m} \\ & + \frac{C G_f (G_f + G_m) - (G_f - G_m) V_m}{(G_f + G_m) + (G_f - G_m) V_m} \end{aligned} \quad 3.9$$

Although contiguity has a significant effect on the values of E_t and G_{1t} Tsai does not give a method of theoretically determining C . He does present results from an E-glass epoxy resin composite, the majority of which lie within the range of $0 \leq C \leq 0.4$, $C = 0.2$ giving a reasonable mean. For the same composite K was found to lie between 0.9 and 1.0. Al-Khyatt [3.4] using polyester resin found that a value of K between 0.8 and 0.9 and $C = 0$ was more appropriate. However, Al-Khyatt used a very low percentage of catalyst (0.01%) which may have presented full polymerisation of the resin and reduced the quality of the bond between the resin and the glass. Tsai's analysis assumes perfect bonding between fibres and matrix. Other fully polymerised polyester systems may give results closer to Tsai's predictions.

3.2.2.3 Halpin-Tsai Approach [3.5]

Halpin and Tsai formulated simple equations based upon more exact elastic solutions. Their equations for E_1 and μ_{1t} are the

same as those for the mechanics of materials approach, equations 3.2 and 3.4.

$$E_t = \frac{E_m (1 + \nu \eta V_f)}{(1 - \eta V_f)} \quad 3.9$$

$$G_{lt} = \frac{G_m (1 + \nu \eta V_f)}{(1 - \eta V_f)} \quad 3.10$$

where $\nu = 1$ for G_t

$\nu = 2$ for E_t

$$\eta = \frac{\frac{G_f}{G_m} - 1}{\frac{G_f}{G_m} + 1} \quad \text{for } G_{lt}$$

$$\eta = \frac{\frac{E_f}{E_m} - 1}{\frac{E_f}{E_m} + 2} \quad \text{for } E_t$$

Micro-Mechanical Methods Closure

The values of the elastic constants of the basic mono-layer can vary widely, depending upon which theory is applied. This is particularly true for E_t and G_{lt} . However, it is possible to predict properties with sufficient accuracy to be of value in the design of composite structures.

3.2.3 Stress-Strain Relationships Referred to Natural Axes

As described in Section 3.2.1 an orthotropic laminate may be characterised by four elastic constants and it can be shown [3.2]

that they are related by the following equation:

$$\begin{bmatrix} \epsilon_1 \\ \epsilon_t \\ \gamma_{1t} \end{bmatrix} = \begin{bmatrix} s_{11} & s_{12} & 0 \\ s_{12} & s_{22} & 0 \\ 0 & 0 & s_{33} \end{bmatrix} \begin{bmatrix} \sigma_1 \\ \sigma_t \\ \tau_{1t} \end{bmatrix} \quad 3.11$$

Equation 3.11 may be inverted to give:

$$\begin{bmatrix} \sigma_1 \\ \sigma_t \\ \tau_{1t} \end{bmatrix} = \begin{bmatrix} c_{11} & c_{12} & 0 \\ c_{12} & c_{22} & 0 \\ 0 & 0 & c_{33} \end{bmatrix} \begin{bmatrix} \epsilon_1 \\ \epsilon_t \\ \gamma_{1t} \end{bmatrix} \quad 3.12$$

$$\text{where } c_{11} = \frac{s_{22}}{\Delta}$$

$$c_{12} = \frac{s_{12}}{\Delta}$$

$$c_{22} = \frac{s_{11}}{\Delta}$$

$$c_{33} = \frac{1}{s_{33}}$$

$$\Delta = s_{11} s_{22} - s_{12}^2$$

The normal engineering constants may be related to the independent constants in the following way: in equation 3.12, if we let σ_1 be the only non zero stress the equation becomes:

$$\sigma_1 = c_{11} \epsilon_1 + c_{12} \epsilon_t$$

$$0 = c_{12} \epsilon_1 + c_{22} \epsilon_t$$

Solving for ϵ_1 and ϵ_t using Cramer's Rule:

$$\epsilon_1 = \frac{\sigma_1 c_{22}}{c_{11} c_{22} - c_{12}^2} \quad 3.13$$

$$\epsilon_t = -\frac{\sigma_1 c_{12}}{c_{11} c_{22} - c_{12}^2}$$

If the modulus E_1 is defined as:

$$E_1 \equiv \frac{\sigma_1}{\epsilon_1}$$

then from 3.13,

$$E_1 = C_{11} - \frac{C_{12}^2}{C_{22}} \quad 3.14$$

Defining μ_{1t} as

$$\mu_{1t} \equiv \frac{-\epsilon_t}{\epsilon_1}$$

yields from equation 3.13

$$\mu_{1t} = \frac{C_{12}}{C_{22}} \quad 3.15$$

If a similar operation is performed with σ_t being the only applied stress then

$$E_t \equiv \frac{\sigma_t}{\epsilon_t} = C_{22} - \frac{C_{12}^2}{C_{11}} \quad 3.16$$

$$\mu_{1t} \equiv \frac{-\epsilon_1}{\epsilon_t} = \frac{C_{12}}{C_{11}} \quad 3.17$$

If only τ_{1t} is non-zero and G_{1t} is defined as

$$G_{1t} \equiv \frac{\tau_{1t}}{\gamma_{1t}} \quad 3.18$$

then similarly it is found that

$$G_{1t} = C_{33}$$

If equations 3.13 and 3.15 are divided and the expressions for μ_{t1} and μ_{1t} are similarly divided it is found that:

$$\frac{E_1}{E_t} = \frac{\mu_{1t}}{\mu_{t1}} = \frac{C_{11}}{C_{22}} \quad 3.20$$

If equations 3.13 to 3.20 are rearranged, the following equations may be derived:

$$\begin{aligned}
C_{11} &= \frac{E_1}{1 - \mu_{1t} \mu_{t1}} \\
C_{12} &= \frac{E_t \mu_{1t}}{1 - \mu_{1t} \mu_{t1}} = \frac{E_1 \mu_{t1}}{1 - \mu_{1t} \mu_{t1}} \\
C_{22} &= \frac{E_t}{1 - \mu_{1t} \mu_{t1}} \\
C_{33} &= G_{1t}
\end{aligned}
\tag{3.21}$$

Substituting equations 3.21 into equations 3.11 and 3.12

yields:

$$\begin{aligned}
S_{11} &= \frac{1}{E_1} \\
S_{12} &= -\frac{\mu_{1t}}{E_1} = -\frac{\mu_{t1}}{E_t} \\
S_{22} &= \frac{1}{E_t} \\
S_{33} &= \frac{1}{G_{1t}}
\end{aligned}
\tag{3.22}$$

3.2.4 Stress-Strain Relationships Referred to Arbitrary Axes

It can be shown [3.5] that stresses and strains on arbitrary axes, 1, 2, (see Figure 3.2) transform to stresses and strains on the natural axes, l, t, as follows:

$$\begin{bmatrix} \sigma_1 \\ \sigma_t \\ \tau_{1t} \end{bmatrix} = T \begin{bmatrix} \sigma_1 \\ \sigma_2 \\ \tau_{12} \end{bmatrix}
\tag{3.23}$$

$$\begin{bmatrix} \epsilon_1 \\ \epsilon_t \\ \frac{1}{2}\gamma_{1t} \end{bmatrix} = T \begin{bmatrix} \epsilon_1 \\ \epsilon_2 \\ \frac{1}{2}\gamma_{12} \end{bmatrix}$$

$$\text{where } T = \begin{bmatrix} \cos^2 \alpha & \sin^2 \alpha & (2 \sin \alpha \cos \alpha) \\ \sin^2 \alpha & \cos^2 \alpha & (-2 \sin \alpha \cos \alpha) \\ -2 \sin \alpha \cos \alpha & \sin \alpha \cos \alpha & (\cos^2 \alpha - \sin^2 \alpha) \end{bmatrix}$$

and tensorial strains are used rather than engineering strains.

Applying equations 3.23 to equation 3.12, with tensorial strains replacing engineering strains:

$$\begin{bmatrix} \sigma_1 \\ \sigma_t \\ \tau_{1t} \end{bmatrix} = [T] \begin{bmatrix} \sigma_1 \\ \sigma_2 \\ \tau_{12} \end{bmatrix} = [C] [T] \begin{bmatrix} \epsilon_1 \\ \epsilon_2 \\ \frac{1}{2}\gamma_{12} \end{bmatrix} \quad 3.24$$

and

$$\begin{bmatrix} \sigma_1 \\ \sigma_2 \\ \tau_{12} \end{bmatrix} = [T]^{-1} [C] [T] \begin{bmatrix} \epsilon_1 \\ \epsilon_2 \\ \frac{1}{2}\gamma_{12} \end{bmatrix} \quad 3.25$$

$$\text{Let } [\bar{C}] = [T]^{-1} [C] [T]$$

then, carrying out the algebra:

$$\bar{C}_{11} = C_{11} \cos^4 \alpha + 2(C_{12} + 2 C_{33}) \sin^2 \alpha \cos^2 \alpha + C_{22} \sin^4 \alpha$$

$$\bar{C}_{12} = (C_{11} + C_{22} - 4 C_{33}) \sin^2 \alpha \cos^2 \alpha + C_{12} (\sin^4 \alpha + \cos^4 \alpha)$$

$$\begin{aligned}
\bar{c}_{13} &= (c_{11} - c_{12} - 2 c_{33}) \sin \alpha \cos^3 \alpha \\
&\quad + (c_{12} - c_{22} + 2 c_{33}) \sin^3 \alpha \cos \alpha \\
\bar{c}_{22} &= c_{11} \sin^4 \alpha + 2 (c_{12} + 2 c_{33}) \sin^2 \alpha \cos^2 \alpha \\
&\quad + c_{22} \cos^4 \alpha \\
\bar{c}_{23} &= (c_{11} - c_{12} - 2 c_{33}) \sin^3 \alpha \cos \alpha \\
&\quad + (c_{12} - c_{22} + 2 c_{33}) \sin \alpha \cos^3 \alpha \\
\bar{c}_{33} &= (c_{11} + c_{22} - 2 c_{12} - 2 c_{33}) \sin^2 \alpha \cos^2 \alpha \\
&\quad + c_{33} (\sin^4 \alpha + \cos^4 \alpha)
\end{aligned} \tag{3.26}$$

In a like manner the compliance matrix \bar{S} can be formed

where:

$$\begin{aligned}
\bar{s}_{11} &= s_{11} \cos^4 \alpha + (2 s_{12} + s_{33}) \sin^2 \alpha \cos^2 \alpha \\
&\quad + s_{22} \sin^4 \alpha \\
\bar{s}_{12} &= s_{12} (\sin^4 \alpha + \cos^4 \alpha) + (s_{11} + s_{22}) \sin^2 \alpha \cos^2 \alpha \\
\bar{s}_{13} &= 2(2 s_{11} - 2 s_{12} - s_{44}) \sin \alpha \cos^3 \alpha \\
&\quad - 2 (2 s_{22} - 2 s_{12} - s_{33}) \sin^3 \alpha \cos \alpha \\
\bar{s}_{22} &= s_{11} \sin^4 \alpha + (2 s_{12} + s_{33}) \sin^2 \alpha \cos^2 \alpha \\
&\quad + s_{22} \cos^4 \alpha \\
\bar{s}_{23} &= 2 (2 s_{11} - 2 s_{12} - s_{33}) \sin^3 \alpha \cos \alpha \\
&\quad - 2 (2 s_{22} - 2 s_{12} - s_{33}) \sin \alpha \cos^3 \alpha \\
\bar{s}_{33} &= 2 (2 s_{11} + 2 s_{22} - 4 s_{12} - s_{33}) \sin^2 \alpha \cos^2 \alpha \\
&\quad + s_{33} (\sin^4 \alpha + \cos^4 \alpha)
\end{aligned} \tag{3.27}$$

Tsai [3.6] has developed relationships between stress and moment resultants at the laminate midplane and the strains and curvatures of the laminate when the working temperature is different from the laminating temperature. This temperature difference depends on the production technique used and is difficult to quantify accurately. Often, where low temperature processes are used, such as hand lay-up, spray-up or cold press, the temperature difference will have little effect. This is particularly so in the case of specially orthotropic laminates, since much of the coupling between constituent laminae is removed. For these reasons the effect of the temperature difference will be neglected in this thesis and Tsai's relationship becomes:

$$\begin{bmatrix} N_x \\ N_y \\ N_{xy} \\ M_x \\ M_y \\ M_{xy} \end{bmatrix} = \begin{bmatrix} A_{11} & A_{12} & A_{13} & B_{11} & B_{12} & B_{13} \\ A_{12} & A_{22} & A_{23} & B_{12} & B_{22} & B_{23} \\ A_{13} & A_{23} & A_{33} & B_{13} & B_{23} & B_{33} \\ B_{11} & B_{12} & B_{13} & D_{11} & D_{12} & D_{13} \\ B_{12} & B_{22} & B_{23} & D_{12} & D_{22} & D_{23} \\ B_{13} & B_{23} & B_{33} & D_{13} & D_{23} & D_{33} \end{bmatrix} \begin{bmatrix} \epsilon_x^0 \\ \epsilon_y^0 \\ \gamma_{xy}^0 \\ k_x \\ k_y \\ k_{xy} \end{bmatrix}$$

3.28

$$\text{or } \begin{bmatrix} N \\ M \end{bmatrix} = \begin{bmatrix} A & B \\ B & D \end{bmatrix} \begin{bmatrix} \epsilon^0 \\ k \end{bmatrix}$$

where N = Midplane stress resultants.

M = Laminate moment resultants

ϵ^0 = Midplane strains

k = Laminate curvatures

$$A_{ij} = \sum_{K=1}^n (\bar{C}_{ij})_K (h_K - h_{K-1}) \quad 3.28a$$

K relates to the layer number.

$$B_{ij} = 0.5 \sum_{K=1}^n (\bar{C}_{ij})_K (h_K^2 - h_{K-1}^2) \quad 3.28b$$

$$D_{ij} = 0.333 \sum_{K=1}^n (\bar{C}_{ij})_K (h_K^3 - h_{K-1}^3) \quad 3.28c$$

Equation 3.28 may be inverted to give:

$$\begin{bmatrix} \varepsilon^0 \\ K \end{bmatrix} = \begin{bmatrix} A' & B' \\ C' & D' \end{bmatrix} \begin{bmatrix} N \\ M \end{bmatrix} \quad 3.29$$

where

$$\begin{aligned} \begin{bmatrix} A' \end{bmatrix} &= \begin{bmatrix} A^* \end{bmatrix} - \begin{bmatrix} B^* \end{bmatrix} \begin{bmatrix} D^{*-1} \end{bmatrix} \begin{bmatrix} C^* \end{bmatrix} \\ \begin{bmatrix} B' \end{bmatrix} &= \begin{bmatrix} B^* \end{bmatrix} \begin{bmatrix} D^{*-1} \end{bmatrix} \\ \begin{bmatrix} C' \end{bmatrix} &= - \begin{bmatrix} D^{*-1} \end{bmatrix} \begin{bmatrix} C^* \end{bmatrix} \\ \begin{bmatrix} D' \end{bmatrix} &= \begin{bmatrix} D^{*-1} \end{bmatrix} \\ \begin{bmatrix} A^* \end{bmatrix} &= \begin{bmatrix} A^{-1} \end{bmatrix} \\ \begin{bmatrix} B^* \end{bmatrix} &= - \begin{bmatrix} A^{-1} \end{bmatrix} \begin{bmatrix} B \end{bmatrix} \\ \begin{bmatrix} C^* \end{bmatrix} &= \begin{bmatrix} B \end{bmatrix} \begin{bmatrix} A^{-1} \end{bmatrix} \\ \begin{bmatrix} D^* \end{bmatrix} &= \begin{bmatrix} D \end{bmatrix} - \begin{bmatrix} B \end{bmatrix} \begin{bmatrix} A^{-1} \end{bmatrix} \begin{bmatrix} B \end{bmatrix} \end{aligned}$$

The complexity of the general anisotropic laminate can be seen from equations 3.28 and 3.29. The normal stress resultants N_x and N_y are developed in part by shearing of the midplane and by twisting of the plate. The shear stress resultant is a ramification of normal strains in the midplane, and bending of the plate. Also, bending and twisting can be induced by normal straining of the midplane as well as bending moments.

From equation 3.28b it is evident that laminates having identical laminae above and below the midplane (that is identical in thickness, distance from the midplane and fibre orientation) have a coupling matrix $[B]$ equal to zero. Such a laminate is known as specially orthotropic and was mentioned earlier. Further simplification can be made if the laminate is symmetrical about its natural axes on both sides of the midplane. That is to say, for each lamina at $+\alpha$ to the x axis there is an adjacent lamina at $-\alpha$ both above and below the midplane. For this type of laminate:

$$\begin{pmatrix} A_{13} \\ A_{23} \end{pmatrix} = \begin{pmatrix} A_{23} \\ A_{13} \end{pmatrix} = 0$$

That is, there is no inplane shear deformation, and four elastic constants describe the inplane behaviour, as is the case with the orthotropic laminae. However, unlike orthotropic laminae the bending behaviour is coupled due to the existence of the coefficients (D_{13}) and (D_{23}) (Equation 3.28c). The use of orthotropic theory in the bending and stability of plates where (D_{13}) and (D_{23}) are not zero leads to non-conservative results [3.7]. There are certain circumstances, however, where (D_{13}) and (D_{23}) are zero, that is, when angle α is 0° or 90° since (\bar{C}_{13}) and (\bar{C}_{23}) (Equation 3.26), are equal to zero. (D_{13}) and (D_{23}) are also equal to zero when $\alpha = \pm 45^\circ$ and balanced woven fabric is used. Furthermore, when the number of pairs of laminates at $\pm \alpha$ becomes large (say ≥ 3) (D_{13}) and (D_{23}) become small [3.7] and their effect may be neglected.

In the remainder of this thesis only specially orthotropic laminates where:

$$(A_{13}) = (A_{23}) = 0 \quad \text{and}$$

$$(D_{13}) = (D_{23}) = 0 \quad \text{or where they are negligible,}$$

will be considered. These laminates are the most commonly used in

strength [3.4, 3.8]. Consequently these theories will only be described briefly. If empirically determined mono-layer strengths are used in conjunction with laminate theory, predictions of adequate accuracy for design purposes can be made.

3.3.2 Prediction of the Strength of the Basic Mono-layer

The important strengths of a grp lamina are:

- a) longitudinal tensile strength
- b) longitudinal compressive strength
- c) transverse tensile strength
- d) transverse compressive strength
- e) interlamina shear (ILS) strength
- f) flexural strength

Broadly, two approaches have been made to predict the various strengths; netting analysis, and continuum analysis. Netting analysis [3.9] assumes that the fibres take all the load and the resin serves only to hold the fibres in position in the longitudinal direction. In shear and transverse directions only the matrix is effective. Continuum analysis is a more rigorous approach, and considers the elastic and strength properties of both constituents [3.10, 3.11]. Results of the latter approach will be outlined briefly here.

3.3.2.1 Longitudinal Tensile Strength ($F_{1(T)}$)

Rosin [3.11] developed the following:

$$F_{1(T)} = V_f (\alpha \beta \delta \rho)^{-1/\beta} \quad 3.31$$

α and β are factors depending upon the relationship between fibre strength and length. δ is the ineffective fibre length (see Fig. 2.3) and ρ is the base of natural logarithms. The equation is applicable when fibre strains are large and Poisson's ratio for the fibres and resin is similar.

Harris [3.12] found that the law of mixtures generally gave adequate accuracy.

$$F_{1(T)} = \sigma_f V_f + \sigma'_m (1 - V_f) \quad 3.32$$

where σ_f = fibre failure stress

σ'_m = resin stress at composite failure strain.

3.3.2.2. Longitudinal Compressive

Strength ($F_{1(c)}$)

In compression, glass fibres are considered to behave as columns supported by a surrounding elastic medium or plastic medium at higher strains. As described in Chapter 2, failure occurs when fibres buckle in one of two modes; shear or extensional. Considerable

effort has been exerted on this basis, to predict the compressive strength [3.11, 3.13], but theories have been found inaccurate and non-conservative. The following factors will contribute to the inaccuracy:

- 1) Misalignment of fibres.
- 2) Crooked fibres.
- 3) Inaccurate knowledge of the resin properties when in the composite.
- 4) The presence of voids in the matrix causing reductions in strength and stiffness.
- 5) Poor bonding between the resin and fibres.

3.3.2.3 Transverse Strengths

Several workers have attempted to model the tensile and compressive transverse strengths [3.14 - 17] but results were inaccurate. Hashin [3.16] concluded that the matrix was the dominant phase in determining strengths.

3.3.2.4 Interlamina Shear (ILS) Strength

No reliable model exists for the prediction of this strength. ILS strength is often assumed to be equal to the shear strength of the resin.

3.3.2.5 Flexural Strength

The flexural strength lies between the tensile and compressive strengths, and the mean will normally give a conservative estimate of sufficient accuracy for design purposes.

3.3.3 Strength Properties of Laminated Grp

The model used for analysing the elastic behaviour may also be used for predicting material failure. It is assumed that the behaviour of an arbitrary lamina within an arbitrary laminate, for given stresses and strains in that lamina natural axis system, is the same as the behaviour measured in the natural axis system when the lamina is part of any other laminate under the same stresses and strains. Plane stress is assumed, and in bending, plane sections remain plane.

$$\text{i.e. } \begin{bmatrix} \epsilon \\ \epsilon \\ \gamma_{xy} \end{bmatrix} = \begin{bmatrix} \epsilon_x \\ \epsilon_y \\ \gamma_{xy} \end{bmatrix} = \begin{bmatrix} \epsilon^0 \end{bmatrix} + Z \begin{bmatrix} k \end{bmatrix} \quad 3.33$$

and from equations (3.30)

$$\begin{bmatrix} \epsilon \end{bmatrix} = \begin{bmatrix} A \end{bmatrix}^{-1} \begin{bmatrix} N \end{bmatrix} + Z \begin{bmatrix} D \end{bmatrix}^{-1} \begin{bmatrix} M \end{bmatrix} \quad 3.34$$

The stresses and strains can now be found for each lamina in the laminate axis system and then transformed to stresses and strains in the lamina natural axis system using equations (3.25 - 3.27)

for which the strengths are known. At this stage failure criteria may be applied to each pair of laminas to test for fracture.

3.3.3.1 Laminate Behaviour Under Load

For design purposes, laminates behave linearly upto initial failure. This initial failure may or may not be ultimate failure, depending upon fibre orientation, and the nature of the stress causing failure. In the case where a tensile load is the cause of lamina failure, e.g. when the laminate is subjected to uniaxial tension, the remaining laminas may be capable of sustaining the load. The remaining laminas must be reappraised by forming a new constitutive equation (3.30) ignoring the failed laminas and retesting for failure. This process may be repeated until all laminas have been found to fail, at which point the ultimate strength has been reached or exceeded. If after initial failure the remaining laminates proved strong enough to take all the load, then the stress-strain relationship would not be linear but would have a "knee" representing the point of initial failure. Fig. 3.3 shows a typical progressive failure curve for a 3 fibre system, 0° , $\pm 45^\circ$, 90° .

Where compressive loads are the cause of failure, initial failure is also considered ultimate. Compressive failure being mainly dependent on the matrix, failure of the matrix in one lamina will cause failure in the other laminas [3.4].

Initial failure in flexure will also be ultimate since it will be precipitated by compressive failure of the outermost fibres.

Behaviour of laminates under complex stress systems is not as yet well defined, and care should be taken if initial failure is not also assumed to be ultimate.

To test a lamina for failure under complex stress the Hill criterion, modified for use with grp by Tsai [3.6] has, generally been accepted as the most applicable.

$$\left[\frac{\sigma_l}{F_l} \right]^2 - \frac{\sigma_l \sigma_t}{F_l^2} + \left[\frac{\sigma_t}{F_t} \right]^2 + \left[\frac{\tau_{lt}}{S} \right]^2 = 1 \quad 3.35$$

where σ = axial stress

F = axial strength

τ = shear stress

S = shear strength

l = longitudinal direction

t = transverse direction

If the axial and shear strengths of the laminate are known then this theory may be applied directly to the laminate.

Other failure theories have been reviewed by Al-Khayatt [3.4].

Theoretically and Experimentally
Determined Elastic and Strength
Properties of Selected Grp Laminates

3.4.1 Introduction

The properties of grp have been shown to be dependent upon the properties of the constituents. The constituents will generally be chosen according to the end use. For example, in a chemical plant a chemically-resistant resin would be chosen, in buildings a fire-resistant resin would frequently be necessary. Since the end use at this stage in the project is not precisely defined, a general-purpose resin will be adopted. Such a resin has been used recently by Al-Khayatt in the characterisation of the basic lamina and several laminates, in the University Department where this project was carried out [3.4]. Hence the work reported here is designed partly as a quality control programme and partly to provide relevant data not provided by Al-Khayatt. In the latter case, where possible, other sources of data have been used for comparison.

3.4.2 Design of Specimens

The design of specimens for the characterisation of fibre-reinforced plastics has been the object of a great deal of work. The traditional designs of test specimens in metal have been found inadequate because they do not allow for the brittle and anisotropic

nature of these materials. The specimen designs adopted in this project are shown in Figs. 3.4 and 3.5. The designs are similar to those adopted by Al-Khayatt, who reviewed the design of test specimens. The necked specimens Fig. 3.4a) were used to determine the tensile strength and modulus for all materials other than chopped strand mat (CSM) reinforced laminates. In the latter case the parallel-sided specimens, Fig. 3.4b) were used. Fig. 3.4c) shows the design of the compression specimens adopted for all materials. In both tensile and compressive tests the elastic properties were obtained with the use of electrical resistance strain gauges.

The materials used in the experimental programme were as follows:

Resin : BIP, Beetle Polyester Resin 836 plus approx.
3% BIP Accelerator B and 1.5% MEKP. catalyst.
The exact proportion of the accelerator and catalyst used was dependent upon the ambient temperature.

Reinforcements : Fothergill and Harvey Limited, uni-directional cloth type Y-996 and bidirectional woven roving Y-023, Fibreglass Limited, "Eque mat".

The preparation of the samples was designed to give a laminate whose properties would be similar to those which could be expected from a good-class hand lay-up laminator. Thus no special techniques were employed to reduce voidage. Laminates were layed-up on a flat steel surface treated with wax release agent. To obtain

smooth, uniform laminates, after lay-up a second steel surface was positioned and pressed on top of the laminate. Spacers were used to control the laminate thickness. Before testing all specimens were post-cured for 3 hrs. at 80°C.

3.4.3 Experimentally Determined Properties

The specimen designs discussed above are such that both elastic and strength properties may be obtained simultaneously. The use of parallel-sided compression specimens may result in slightly lower strengths than if necked specimens were used [3.4] but the difference is not considered significant in this project. The loading rate of both tensile and compressive specimens was such that failure occurred within 1.5 - 2.5 mins.

3.4.3.1 Properties of the Basic Lamina and Selected Laminates

In this section both strength and elastic properties of various laminates will be presented as determined experimentally, and, in the case of elastic properties, compared with theory. Experimental results will be drawn from previous work by Al-Khayatt and work associated with this project. Theories used for comparison will be those of Tsai and Halpin-Tsai, equations 3.6 - 3.9 and 3.9 & 10 respectively.

Fig. 3.6 shows unidirectional material's longitudinal elastic modulus as a function of the fibre volume fraction. Results obtained by Al-Khayatt and the author are in close agreement, as would be expected since similar materials and moulding techniques were employed. However, experimental results were only 80 - 85% of the theoretically predicted modulus. The stress-strain relationship was found to be approximately linear (see Fig. 3.7) as expected for the materials tested.

Fig. 3.8 compares tensile and compressive strengths obtained by the author and Al-Khayatt. Tensile strengths are shown to be 50 - 100% greater than compressive strengths. The greatest difference was at higher glass proportions where the compressive strength begins to reduce.

The axial strengths of several laminates are shown in Fig. 3.9. In tension, cross-ply is shown to be superior to CSM which in turn is stronger than $\pm 45^\circ$ angle-ply. In compression the position of CSM and cross-ply is reversed. In all cases strengths were found to be below those obtained for unidirectional laminates.

Fig. 3.10 compares theoretical and experimental values for the longitudinal and transverse modulus of laminates. The order of superiority is: cross-ply, CSM and $\pm 45^\circ$ angle-ply. In general, theoretical values were marginally higher than empirical ones.

Experimental results obtained by the author were similar to those obtained by Al-Khayatt. The greatest discrepancies occurred

when testing axial strengths of the basic lamina. Al-Khayatt's tensile strengths were greater than those obtained by the author, but in compression the reverse was the case. The proposed reason for this is that the author post-cured specimens before testing, whereas Al-Khayatt did not. Post-curing can be expected to lead to a polymer with more cross-links which give it greater stiffness. Thus fibres would receive greater support against buckling, giving the lamina higher compressive strengths. Post-curing also causes greater resin shrinkage than otherwise would be expected. The high temperature of post-curing induces thermal strains on cooling. These strains then cause premature tensile failure.

Figs. 3.11a & b show photographs of typical tensile and compression failure modes.

Figs. 3.12 and 3.13 compare theoretically determined lamina properties as predicted by Tsai and Halpin-Tsai and empirical properties according to Al-Khayatt. The transverse elastic modulus determined by Al-Khayatt is shown to lie between those predicted theoretically. The Tsai theory, with contiguity factor $C = 0$, gives the most conservative values. With the same value of contiguity factor the Tsai formula for predicting the basic lamina shear modulus is the same as that of Halpin and Tsai. Theoretically and experimentally determined values of the shear modulus agree reasonably well, but the theory is only shown to be conservative at low glass proportions.

The Halpin-Tsai approach, Section 3.2.2.3, adopts the "mechanics of materials" or "law of mixtures" equation for predicting the longitudinal Poisson's ratio. Consequently this equation and

Tsai's theory have been compared to Al-Khayatt's results for the principal Poisson's ratio. Except at high fibre contents, Al-Khayatt's values are marginally lower than those predicted by theory. Again, Tsai's theory is the more conservative.

In Figs. 3.14 and 3.15 three of the more common orthotropic laminates have been treated theoretically. The great effect of fibre orientation on the value of Poisson's ratio is shown in Fig. 3.14. The angle-ply laminate has the largest values, followed by the random fibre laminate and the cross-ply laminate respectively. The same laminate order of superiority is found in the case of the shear modulus; Fig. 3.15.

3.4.4. Conclusions

Experimentally determined property values in this project are, in general, similar to those obtained by Al-Khayatt. Data obtained by Al-Khayatt and the author, therefore, are sufficiently repeatable for design use.

The Halpin-Tsai theory, not reviewed by Al-Khayatt, is shown to be a useful method of predicting the basic lamina elastic properties, but not as accurate as the Tsai approach. However, the Halpin-Tsai equations are simpler and are therefore recommended for preliminary design work.

3.5.1 Introduction

In Chapter 2, the creep and stress rupture properties of grp were outlined. The results of various investigators show that the loss of strength and stiffness is important and must be considered in any structure that is under load, for anything other than very short periods. Further, the results of different workers with similar materials and under similar conditions differ significantly, particularly in the case of stress rupture. In this section the relevant mechanisms will be described in greater depth, and methods of prediction discussed.

3.5.2. Creep Mechanism

Creep is a time-dependent strain in a material, resulting from constant stress. Each phase of the composite contributes to the increase in strain. In grp the resin plays the major role and there is evidence to suggest that for practical purposes creep does not occur in glass [3.18]. However, glass fibres in most composites are buckled or bent due to handling during lamination and/or shrinkage of the resin on cure. Under tension these fibres will tend to straighten, and under compression buckling would advance, thus contributing to creep strain.

The effect of continued stress on polymers, such as polyester resin, is the straining of molecular bonds, and in some cases their rupture. It has been shown that the thermal energy associated with a molecular bond is a function of time [3.19]. Hence, the total amount of energy available to break the bond is not constant. Therefore, under constant stress, bonds near their ultimate strength are not stable, and this results in relative movements between neighbouring segments within molecules and between molecules themselves. Not surprisingly, temperature has been found to play an important role in the creep rate [3.20].

In general, increasing stress and temperature leads to greater mobility of molecules and increased creep rates. Reduction of the creep rate will be achieved by reducing molecular mobility. Thus, highly cross-linked polymers, full curing of the resin and strong resin/fibre bonds are desirable.

Creep has been observed to be less in compression than in tension for some polymers and laminates [3.20, 3.21]. This has been explained with reference to shear stress components and the associated direct stress (Fig. 3.16). If the normal stress, ' σ ', is tensile then a lower value of shear stress, τ , is required for slippage of the molecules than if σ is compressive. Mechanical bonding between molecules will be increased by compression and molecular mobility reduced.

At low loadings it has been observed that about 95% of the creep strain is recoverable after unloading for a period of about

4 times the loaded period [3.18]. This could only occur if strain energy had been stored. Thus at low loads over the time of testing, little failure of the glass fibres and molecular bonds could have occurred. Slippage between unbonded molecules resulting in larger stresses in the fibres could be the mechanism for energy storage provided that the bonds between the glass fibres and the resin remained undamaged.

Water has been commonly observed to increase greatly the rate of creep. This can be explained in terms of the resin, the resin-glass interface, and the glass itself. Water plasticises polyester resin and aids its deformation. In addition, resin has been observed to swell in aqueous environments [3.22] which may lead to strength reduction or failure of the interface bond. A redistribution of stress and an increase in strain would result.

Material construction is an important creep consideration. CSM has been found to be the least creep resistant type of reinforcement, since the resin plays a greater part in load bearing. The resin has to continually transfer the stress from one fibre to another. In addition, the fibre volume fraction is relatively low. Woven fabric has improved creep resistance, provided the warp or weft is parallel to the applied load, since the fibres are continuous, but initially they will not be straight since where perpendicular fibres intersect they have to bend round one another. As mentioned previously, this will contribute to creep. Unidirectional unwoven reinforcement has been found to have the best time-dependent characteristics.

Little work has been carried out on creep and anisotropy. However, Weidmann and Ogorkiewicz [3.23] found that the anisotropy of a unidirectional laminate increases with time under creep conditions.

3.5.3 Nature of Strength Reduction

As pointed out in Chapter 2, grp under stress below its short term strength will eventually fail. The mechanism of failure is closely related to the creep mechanism. Weak bonds in the resin and weak fibres will fail first, causing higher stresses in the remaining material which may lead to further failures. This, associated with a phenomenon known as stress corrosion where the fibres weaken under load with time, eventually causes failure. Loss of fibre strength has been found to accelerate in the presence of water and is associated with crack growth [3.24].

The strain at which failure occurs has been observed to be higher than the short term ultimate strain, particularly when failure occurs after relatively short periods [3.25 & 3.26].

3.5.4 Prediction of the Loss of Stiffness with Time

Interest in the prediction of creep in grp has centred on various empirical methods. These include basic creep modelling,

where a sample of the material is tested in the laboratory under simulated working conditions, and tests in which the environment is modified to accelerate creep.

3.5.4.1 Extrapolation Techniques

a) Findley's Equation [3.21, 27 & 28].

Findley found that the following empirical power function closely described the creep behaviour of several plastics:

$$\epsilon_t = \epsilon_0 + m t^n \quad 3.36$$

where ϵ_t = strain at time t

t = time

ϵ_0 , m , = constants dependent upon the material stress and environment

n = constant depending upon the material and environment.

Using chemical rate theory, Findley modified this equation to take account of the effect of stress on constants ϵ_0 and m .

$$\epsilon_t = \epsilon'_0 \sinh \frac{\sigma}{\sigma_e} + m' t^n \sinh \frac{\sigma}{\sigma_m} \quad 3.37$$

Boller [3.26] in subsequent work found that the equation described the performance of five different forms of grp in both wet and dry conditions. Rawe [3.29] also obtained satisfactory results from the equation for glass-epoxy laminates in several environments.

Finally, Findley [3.19] generalised his equation to take account of multi-axial stress as follows:

$$\begin{aligned} \epsilon_{t1} = \epsilon'_0 & \left[\sinh \frac{\sigma_1}{\sigma_m} - \mu (\sinh \frac{\sigma_2}{\sigma_m} + \sinh \frac{\sigma_3}{\sigma_m}) \right] \\ & + m' \left[\sinh \frac{\sigma_1}{\sigma_m} - 1/2 (\sinh \frac{\sigma_2}{\sigma_m} + \sinh \frac{\sigma_3}{\sigma_m}) \right] t^n \quad 3.38 \end{aligned}$$

where: $\sigma_1, \sigma_2, \sigma_3$ are orthogonal stresses and $\epsilon_{t1}, \epsilon_{t2}, \epsilon_{t3}$ are the corresponding strains.

In the derivation of the above equation it is assumed that the volume of material remains constant, creep in tension and compression is equal, and most importantly that the material is homogeneous and isotropic. The general equation will not, therefore, be applicable to many grp material designs. Further, results have not yet been published verifying the equation, although Findley indicated that work was under way.

b) McLaughlin's Equation [3.30]

McLaughlin proposes an exponential function:

$$-\frac{d \log E_t}{d \log t} = C K \log t$$

where E_t = apparent modulus of elasticity at time t , $= \frac{\sigma}{\epsilon_t}$

C, K = constants,

to describe the creep behaviour of a rigid thermoplastic. McLaughlin demonstrated that his equation could be written:

$$\text{Log} (\text{Log} \epsilon_t - \epsilon_0) = \log m + n \log t \quad 3.39$$

which differs from Findley's equation only in the use of $\log \epsilon_t$ instead of ϵ_t .

McLaughlin claims better accuracy describing polymethyl methacrylate's creep using his equation, than when Findley's is used,

especially when extrapolating from 100 to 10^6 hours. The equation is also used to describe several reinforced plastics in flexural creep for upto 1000 hrs. with good accuracy.

McLaughlin has not extended his equation to accommodate changes in stress as did Findley. However, because of the similarity between the two equations, the hyperbolic relationship used by Findley may be directly applied to McLaughlin's equation thus:

$$\text{Log } \epsilon_t = \epsilon'_0 \sinh \frac{\sigma}{\sigma_\epsilon} + m' t^n \sinh \frac{\sigma}{\sigma_m} \quad 3.40$$

Although Findley's and McLaughlin's equations have been classified as being mainly useful for extrapolation, by testing at higher stresses than the proposed working stresses considerable time may be saved.

3.5.4.2 The Larson-Miller Parameter

Using activation energy theory based upon the Arrhenius equation it can be shown that:

$$K = T (23.78 + \log t)$$

where $K = \text{constant}$

$T = \text{absolute temperature deg. Rankine for materials where the zero strength temperature is much higher than the applied temperature } (T).$ Larson and Miller [3.31] derived empirically the equation:

$$K = T (20 + \log t) \quad 3.41$$

which has been found to work equally well for several materials. Although not derived from work on grp the Larson-Miller parameter has given useful results with this material [3.32, 3.33].

The parameter can be used by testing material at the required stress and at a temperature above the proposed working temperature. The apparent modulus of elasticity is then plotted against parameter K over a period of time as illustrated in Fig. 3.16a. The information may then be used in the following way: suppose a laminate were tested at 150°F and after 100 hours the apparent modulus reduced to $6 \times 10^6 \text{ KW/M}^2$, which was the minimum allowable stiffness, the period of time the material could sustain the test stress before exceeding the creep limit at 75°F would be given by:

$$K = (460 + 150) (20 + \log 100) = (460 + 75) (20 + \log t)$$
$$t \approx 10^5 \text{ hours.}$$

Hence a considerable amount of time can be saved.

Alternatively, the testing time may be kept constant but the temperature varied. A similar plot and calculations can then be made.

The accuracy of predictions depends heavily upon the accuracy of the test temperature. For instance, in the example given, if the actual test temperature was 1° in error at 149°F the creep limit would have been approximately 10% in error.

3.5.5 Prediction of the Loss of Strength with Time

3.5.5.51 Larson-Miller Parameter

In a similar way to creep behaviour, the stress rupture properties of grp have been predicted by the Larson-Miller parameter with useful accuracy [3.32 - 34]. Master curves of K against rupture stress can be drawn, and results at elevated temperatures can be used to calculate strengths at working temperatures over longer periods of time (Fig. 3.17).

3.5.5.52 Wohler Method

In this method specimens are tested in an environment similar to the expected working conditions at various stress levels below their short term ultimate strength. The failure times are then plotted against the testing stress on a semi-log graph.

The relationship between log-time to failure and stress has been found by several investigations [3.20, 25 & 26] to be linear, and Boller proposes the equation:

$$\sigma_R = \sigma_0 - M \log t_R \quad 3.42$$

where σ_R = stress causing rupture

σ_0 = stress causing failure after 1 hour

M = constant

t_r = rupture time

This equation was found to apply over testing periods upto 3×10^4 hrs. Data over longer periods is not available.

3.5.5.3 The Monkman and Grant Relationship

Monkman and Grant discovered empirically that the following equation was applicable to a wide range of alloyed metals.

$$\log t_R = C - b \log (\text{mcr}) \quad 3.43$$

where c, b = constants

mcr = minimum creep rate

'c' and 'b' were found to be almost constant for a wide range of materials and temperatures.

In the discussion following Monkman and Grant's paper, Underwood pointed out that the relationship could be derived from the Arrhenius equation. Thus, although the relationship was derived from work on other materials, useful results may be expected from work on grp since the Larson-Miller parameter may also be derived from the Arrhenius equation. Unfortunately, if the Findley or McLaughlin equation is accepted then there is no minimum creep rate. However, in applying the Arrhenius equation any rate may be used so that the minimum creep rate could be replaced, conveniently, by the creep rate at 1 hour. The Monkman and Grant equation then becomes:

$$\log t_R = c - b \log (\dot{\epsilon}_1) \quad 3.44$$

where $\dot{\epsilon}_1$ = creep rate at $t = 1$ hour

Using the relationship for creep and stress rupture proposed by Findley and Boller, the following calculation can be made:

$$\epsilon = \epsilon_0 + m t^n$$

$$\text{differentiating } \dot{\epsilon} = m n t^{n-1}$$

$$\text{but } m = m' \sinh \frac{\sigma}{\sigma_m}$$

$$\therefore \dot{\epsilon} = n m' \sinh \frac{\sigma}{\sigma_m} t^{n-1}$$

when $t = 1$ hr.

$$\dot{\epsilon}_1 = n m' \sinh \frac{\sigma}{\sigma_m}$$

$$\text{and } \sigma = \sigma_m \sinh^{-1} \left(\frac{\dot{\epsilon}_1}{n m'} \right)$$

$$\sigma_R = \sigma_0 - M \log t_R$$

if $\sigma = \sigma_R$

$$\sigma_m \sinh^{-1} \left(\frac{\dot{\epsilon}_1}{n m'} \right) = \sigma_0 - M \log t_R$$

rearranging the constants gives

$$\sinh^{-1} \left(\frac{\dot{\epsilon}_1}{A} \right) = B - C \log t_R$$

$$\sinh \left(\frac{\dot{\epsilon}_1}{A} \right) = \log \left(\frac{\dot{\epsilon}_1}{A} + \sqrt{\left(\frac{\dot{\epsilon}_1}{A} \right)^2 + 1} \right)$$

$$\therefore \log \left(\frac{\dot{\epsilon}_1}{A} + \sqrt{\left(\frac{\dot{\epsilon}_1}{A} \right)^2 + 1} \right) = B - C \log t_R \quad 3.45$$

This formula is similar in form to that of Monkman and Grant.

At low stresses, i.e. when $\sigma_R < \sigma_m$ the above equation simplifies since $\sinh \frac{\sigma}{\sigma_m} \rightarrow \frac{\sigma}{\sigma_m}$ and it follows that

$$\dot{\epsilon}_1 = B - C \log t_R \quad 3.46$$

3.5.5.4 Charles' Equation [3.36]

Using theories of crack propagation and process rates, Charles developed the following formula for stress rupture of glass fibres

$$\log t_R \approx A \log \frac{1}{\sigma_R} - B \quad 3.47$$

Cameron [3.37] applied this relationship to results of other workers and stated that the agreement was much closer than when the simpler equation $\sigma_R = \sigma_0 - M \log t_R$ was used, but did not demonstrate this statistically.

If the above procedure is repeated using Charles' formula and assuming low stresses it can be shown that

$$\log \dot{\epsilon}_1 = A - B \log t_R \quad 3.48$$

This relationship is similar to the one observed by Monkman and Grant.

3.5.6 Experimentally Determined Time- Dependent Properties of Grp

3.5.6.1 Introduction

As pointed out in Section 3.4.1 the selection of laminate constituents depends upon the end use. However, the choice of resin and the form of the reinforcement have possibly an even greater effect on laminate properties in the long term compared with those in the short term. It is impossible, in a project of this type, to fully characterise all materials and their combinations. Neither sufficient resources nor time are available. Thus, only a limited number of laminates will be tested and will correspond to those used in the short term tests. Also, reliance has to be made upon previous work for data, particularly in the case of stress rupture due to the time involved in testing.

Boller, Steel and Kabelka [3.20, 3.25 & 3.26] have each produced considerable quantities of long-term data from tests in air. Boller and Steel have also presented results from tests in water. Steel's work was concerned with flexural stress. Kabelka's work was with a modified form of flexural stress where the laminates formed part of a composite beam. One side of the beam's neutral axis was grp and the other side, steel. Thus, initially an approximately linear stress distribution would be expected across the thickness of grp. However, since steel does not creep, the stress distribution would be expected to change with time. Boller's work was concerned solely with uniform tensile stresses. Boller's tests covered periods of

time of upto 3 years and examined a wider variety of laminates than did Kabelka and Steel. Consequently, Boller's work is considered the most useful for design data and will be used for comparison with work in this project.

As was the case with Boller's work, only tensile creep will be studied in this project. It will be necessary, therefore, to assume, in design, that the tensile and compressive properties of grp are the same. However, to the best of existing knowledge this assumption is conservative, since as pointed out in Section 3.5.2, lower rates of creep and loss of strength have been observed in compression.

Stress rupture tests at two temperatures will be presented, i.e. at 70°C and at 20°C. Results from the tests at the higher temperature are for use with the Larson-Miller parameter so that rupture may be accelerated as described in Section 3.5.5.1. Creep and stress rupture tests were carried out at 20°C. In both cases tests were carried out at a relative humidity of 100%. This level of humidity was chosen for ease of control.

3.5.6.2 Design of Test Specimens

As is the case in short-term testing, in order to obtain extension and failures in the required mode, anisotropy and the lack of ductility has to be allowed for. Indeed, locally high-stressed areas are not only more prone to short-term failure but can be expected to creep and lose strength more rapidly under extended loading

periods. As a result, loading points require reinforcement, and changes in cross-section have to be gradual.

The measurement of strain must be such that readings can be taken upto the failure strain, where relevant, and the sensitivity should be of the order 0.00001 strain [3.36]. Figure 3.17 shows a typical tensile test specimen. The long parallel section accommodates the strain measurement. The strain measuring technique chosen was that which uses a "Demec" gauge. In this system a dial test indicator is used which is sensitive to 0.0001 ins. and the gauge length can be 2", 4", 6" or 8" depending upon the strain range required. The minimum and maximum strain measurement ranges are 0 - 0.02 strain and 0 - 0.08 strain respectively. The corresponding sensitivities are 0.00005 and 0.0000125 units of strain. The aluminium end-pieces were adhered in position using Araldite epoxy resin. For the 70°C tests high temperature adhesive was used: Araldite HT972/AY105, and for the lower temperature tests Araldite HY951/AY103 was used.

3.5.6.3 Design of Test Equipment

A fundamental requirement of a tensile creep testing machine is that the load should be applied axially to the specimen, and the possibility of moments being applied to the specimen reduced to a minimum. In the machine used for creep testing in this project, moment transmission to the specimen was prevented by the use of orthogonal pin joints in the loading mechanism. The possibility of axial torsion being applied was prevented visually. Assuming that an angle of twist of 10° could be detected visually, and then

corrected, shear stresses of less than 1 KN/M^2 would be prevented. In general, the length of the test specimens greatly reduced the possibility of any significant unwanted stresses.

For accurate results it is important that friction in the loading mechanism be reduced to a minimum. Friction in this situation would lead to a non-constant stress being applied to the specimen. As the specimen extends the loading mechanism should move correspondingly. However, the effect of friction would be to resist and reduce this movement and hence reduce the load applied to the specimen. Where appropriate, knife edges were used to reduce friction.

In order to keep dead weights manageable and still be able to apply satisfactorily high loads, a lever arm of approximately 20:1 was used. No provision was adopted to control the rate of application of load to the specimen, except manual control. Theory, however, assumes instantaneous application of load. The effect of this is to cause the theory to be invalid for periods of time of the order of 10 times the loading period [3.36].

The test environment was controlled by testing the specimens just above the surface of water, the temperature of which was thermostatically controlled. During tests at 70°C , temperature could be controlled to within $\pm 2^{\circ}\text{C}$ and during tests at 20°C , $\pm 4^{\circ}\text{C}$. Stabilisation of the environment was achieved by enclosing with covers positioned just above the specimens. Figure 3.18 shows the design of the loading mechanism.

3.5.6.4 Test Procedure

Although the test equipment was designed to give a loading mechanical advantage of 20:1 it was necessary to calibrate each loading station. This was done using a proving ring (Clockhouse Eng. Ltd. proving ring No. 2998) with attachments made especially to fit the creep machine.

Before testing, specimens were kept in the test environment for 1 hr. before tests at 70°C and 24 hrs. before tests at 20°C.

With the specimens in position, the load was applied in stages but completed within 1 minute. Readings were then taken with a Demec gauge. Demec gauges used in the tests were:

- a) Demec gauge No. 1130 with dial No. 281272 and
- b) Demec gauge No. 876 with dial No. 252253.

The first reading was taken after 0.1 hrs. of creep, being the shortest possible time for meaningful results. Thereafter, intervals between readings were initially 0.1 hrs. and then steadily increased as the test duration increased.

It was necessary to take considerable care not to bend the specimens when taking readings, particularly with low specimen loadings. However, with practice sufficient skill was developed to avoid bending.

Due to the limited time available, tests were, on occasions, terminated before failure of the specimens. This action was taken

when failure appeared to be some considerable time away and sufficient data for creep analysis had been obtained.

3.5.6.5 Results and Discussion of Results

The stress rupture results are as tabulated in Figs. 3.19 and 3.21 for tests at 70°C and 20°C respectively. These results are also shown graphically in Figs. 3.20 and 3.22.

Figure 3.20 shows that CSM at stresses below 10 N/MM² could be expected to last 50 years or more by use of the Larson-Miller parameter. However, when these results are shown together with results from tests at 20°C in Fig. 3.22 they appear rather conservative. CSM tested at 20°C is shown to be superior to Boller's CSM upto approximately 10³ hrs. Results calculated using the Larson-Miller parameter shows Boller's CSM to be far superior from approximately 10³ hrs. onwards. It would appear from these results that the temperature increase resulted in a material modification in addition to the predicted increase in static fatigue rate. The resin manufacturers, however, state that no fundamental chemical changes would be expected at this temperature other than those associated with ageing. It is known that water causes swelling and plasticisation of the resin and this may be exaggerated at higher temperatures. In addition, changes in temperature from the laminating temperature are known to cause internal stresses because of the different thermal expansion coefficients of the constituents. Thus although the applied loads at the two test temperatures were equivalent, the internal

stresses would not be equal. Cracks may have been formed in the resin and at the interface, leading to a change in the physical structure of the laminate. It may be observed that the rate of loss of strength at the two test temperatures does not appear dissimilar. A similar rate would be expected if thermal internal stresses were additive to the applied mechanical stresses. The gradients are also similar to those obtained by Boller for CSM. Discrepancies would also be expected between the results at different temperatures due to the accuracy of the temperature control. It was shown in Section 3.5.4.2 that creep acceleration rates were very sensitive to temperature.

The change in glass volume fraction did not significantly change the stress rupture properties of the CSM laminates. However, the creep properties of the high volume fraction laminate showed a slight improvement (Fig. 3.21).

Results at both temperatures indicate that the cross-ply woven roving tested in this project was superior in strength retention to that tested by Boller.

Unfortunately, there was not sufficient time available in this project to cause failure of the unidirectional material tested. Boller did not test this type of laminate. Results obtained however, show the unidirectional material to sustain higher stresses for longer periods than either the woven roving or the CSM laminates.

The creep results tabulated in Fig. 3.21 show that the order of material superiority in resisting creep is the same as that

in resisting stress rupture. This is in line with expectations, since creep rates and time for rupture have been related earlier in this chapter.

The table, Fig. 3.21, shows that Findley's equation:

$$\epsilon = \epsilon_0 + m t^n$$

can be fitted satisfactorily to individual specimen results since the standard errors, when a regression analysis is performed, are small. The equation used for this analysis is:

$$\log (\epsilon - \epsilon_0) = \log m + n \log t$$

The constant " ϵ_0 " is determined by an iterative procedure which minimises the standard error. The computer programme written to perform this analysis is shown in Appendix A. Fig. 3.23 shows typical results of a creep test together with the curve fitted to the results, using Findley's equation, on a linear scale. Further results are shown on logarithmic scales in Figs. 3.24 to 3.28. Confidence limits are also given in these figures showing the accuracy of fit between theory and experiment.

From the above graphs and the table - Fig. 3.21, constant "n", which according to Findley should be dependent only upon the material and environment, is shown to vary more than can be explained by small variations in material. Thus, it appears that some variation in the test conditions occurred. However, these variations were small compared with the differences in the value of "n" caused by changes in reinforcement type.

In all cases the value of constant ϵ_0 was found to be very small ($< 1 \times 10^{-4}$) and negligible when considering practical

structures. On this basis Findley's equation may be simplified to:

$$\epsilon = m t^n$$

The graph of Fig. 3.29 shows that within the stress range tested, for random and bidirectional laminates, the constant "m" varies approximately linearly with stress. Findley, however, predicts the variation of "m" with stress " σ " as follows:

$$m = m' \sinh \frac{\sigma}{\sigma_m}$$

where m' and σ_m are constants independent of stress. If σ/σ_m is small the above equation simplifies to:

$$m = \frac{m' \sigma}{\sigma_m}$$

Thus Findley's equation extended to account for variations in stress is consistent with the results obtained. Findley's equation for the results obtained may now be written:

$$\epsilon = \frac{m' \sigma t^n}{\sigma_m} \tag{3.49}$$

At time $t = 1$ hr.

$$\epsilon_1 = \frac{m' \sigma}{\sigma_m}$$

Rearranging

$$\frac{\sigma}{\epsilon_1} = \frac{\sigma_m}{m'}$$

Since σ_m and m' are constants which are dependent upon material and environment only, $\frac{\sigma_m}{m'}$ may be considered as the apparent modulus of elasticity after 1 hr. of creep (E_1) which is independent

of stress. Finally, Findley's equation may be amended to:

$$\epsilon = \frac{\sigma t^n}{E_1} \quad 3.50$$

Thus, within the range of stresses used in testing, the creep characteristics of the laminates tested may be determined from tests at one stress only.

In Section 3.5.2 it was stated that creep strain was largely recoverable after a period of 4 times the creep period after unloading. The effect of partial unloading of CSM is shown in Fig. 3.30. In this case the stress was reduced by 50% after a loading period of 468 hrs. After a total time of 2000 hrs. recovery was incomplete. Recovery is considered complete when the two curves at equal stresses meet. That is to say, that the amount of creep is that which would be expected if the stress had been constant at the lower value. It is not possible to state whether total recovery would ever be achieved. The experimentally determined curve shows a constant strain over approximately 1000 hrs. This may continue until the constant stress creep curve, reaches the strain of the partially unloaded creep curve in which case the curves would thereafter coincide. Alternatively, the partially-unloaded creep curve may start to show an increased strain before coincidence of the two curves, and recovery would never be complete. This second alternative is the case if the Boltzmann superposition principle is applied to viscoelastic theory [3.37]. Fig. 3.30 shows that strain begins to increase again after approximately 900 hrs., using this theory and equation 3.50.

Figs. 3.31-33 show creep specimens before and after testing. Fig. 3.31 shows CSM specimens, Fig. 3.32 bidirectional specimens, with

cross-ply and $\pm 45^\circ$ angle-ply reinforcement, and Fig. 3.33 uni-directional reinforcement. A marked change in colour is apparent in the specimens after testing which appear on the right of the photographs. The whitening effect is considered to be due to chemical ageing of the resin, to cracking of the resin, debonding of the resin/glass interface and the ingress of water to the interface. The whitening occurred at both test temperatures but was more marked at the higher temperature as shown in the extreme right hand specimen of Fig. 3.33. At the higher temperature the cause of the colour change appeared to be mainly ageing and the ingress of water. At the lower temperature cracking appeared to be the major cause of colour change. This view is supported by the fact that colour change occurred more in narrow high stress areas than in the broad low stress areas of the specimens.

Failure modes may be seen in Figs. 3.31 & 32 and are similar to the short-term failure modes.

3.5.6.6. Conclusions

Results from tests at 70°C when transformed to 20°C using the Larson-Miller parameter were found to be conservative with respect to data from tests at 20°C .

Laminates with continuous fibres in the direction of the principal stress were shown to be superior in creep and stress rupture resistance than other laminates. The $\pm 45^\circ$ angle-ply laminates

exhibited the greatest propensity for creep.

The results obtained by the author for CSM and bidirectional woven roving at 20°C showed these laminates to be superior to the corresponding laminates tested by Boller.

The following equations may be used to predict the creep behaviour of the laminates tested under the test conditions. Where more than one value of a constant has been obtained the mean value is given:

$$\text{CSM } (V_f = 16.5\%): \epsilon_t = \sigma \cdot t^{0.091} \cdot 4,149^{-1}$$

(Units of stress = N/MM²)

$$\text{CSM } (V_f = 21.5\%): \epsilon_t = \sigma \cdot t^{0.076} \cdot 4,367^{-1}$$

$$\text{CROSS-PLY } (V_f = 24\%): \epsilon_t = \sigma \cdot t^{0.037} \cdot 10,015^{-1}$$

$$\pm 45^\circ \text{ ANGLE-PLY } (V_f = 24\%): \epsilon_t = \sigma \cdot t^{0.237} \cdot 1,729^{-1}$$

UNIDIRECTIONAL WOVEN

$$\text{ROVING } (V_f = 45.5\%): \epsilon_t = \sigma \cdot t^{0.008} \cdot 18,140^{-1}$$

UNIDIRECTIONAL WOVEN

$$\text{ROVING } (V_f = 54\%): \epsilon_t = \sigma \cdot t^{0.010} \cdot 20,823^{-1}$$

Creep recovery for CSM after partial unloading is largely recoverable; total recovery, however, may take a considerable period, if indeed total recovery occurs. The Boltzmann superposition principle gave a reasonable approximation to the recovery curve for CSM but over-estimated the recovery. If this theory is assumed to apply, total recovery is never achieved.

FIG. 3.1 ELASTIC MATERIALS - IN TENSION

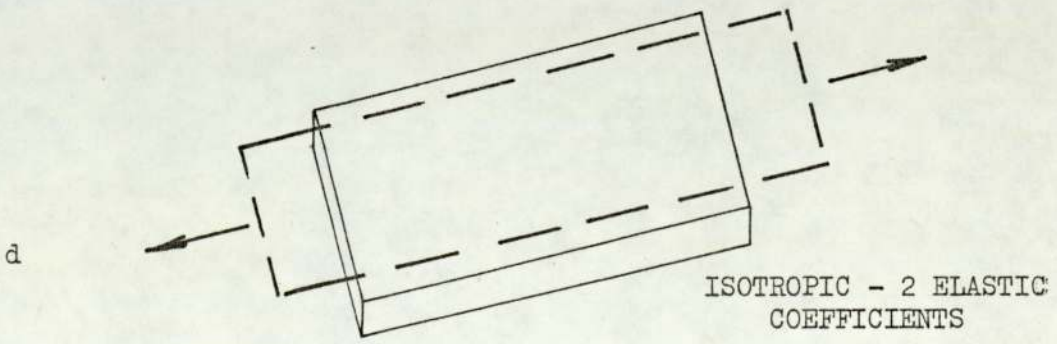
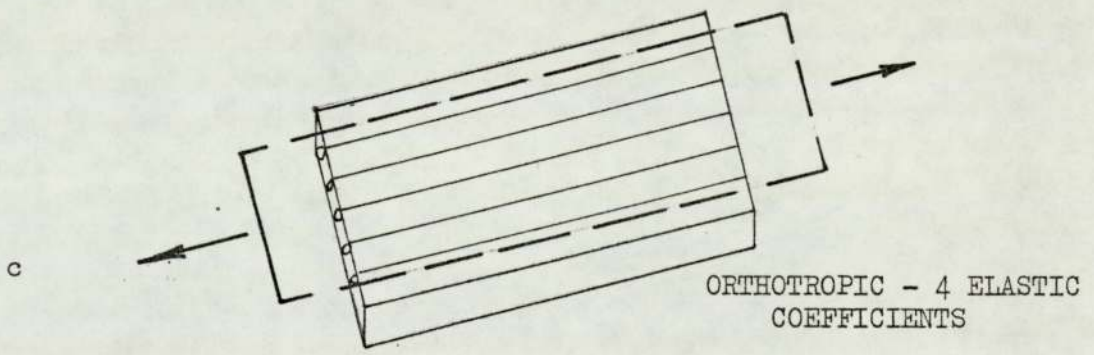
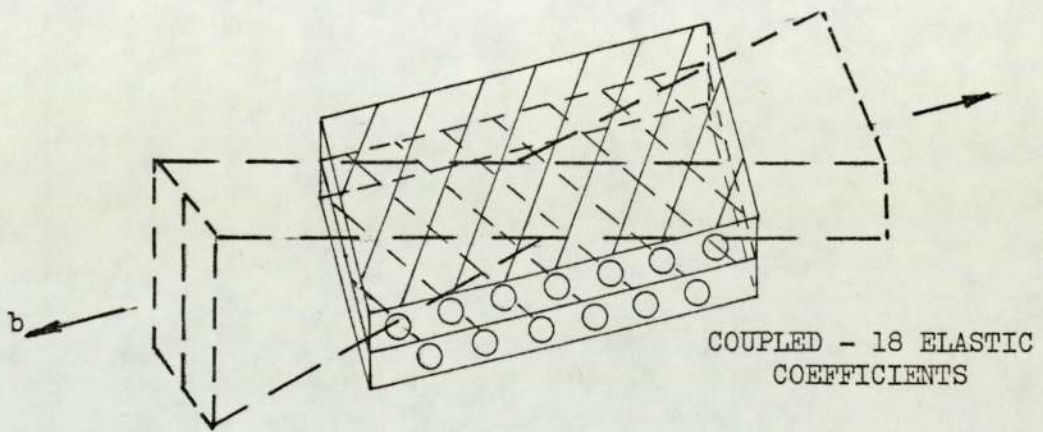
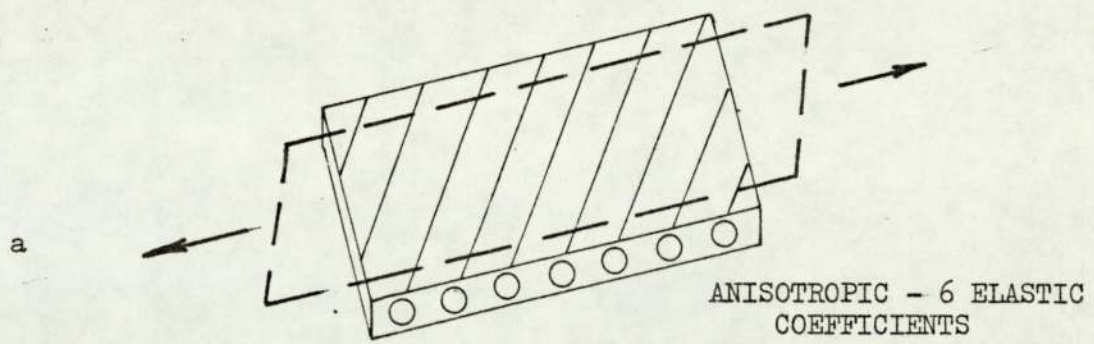
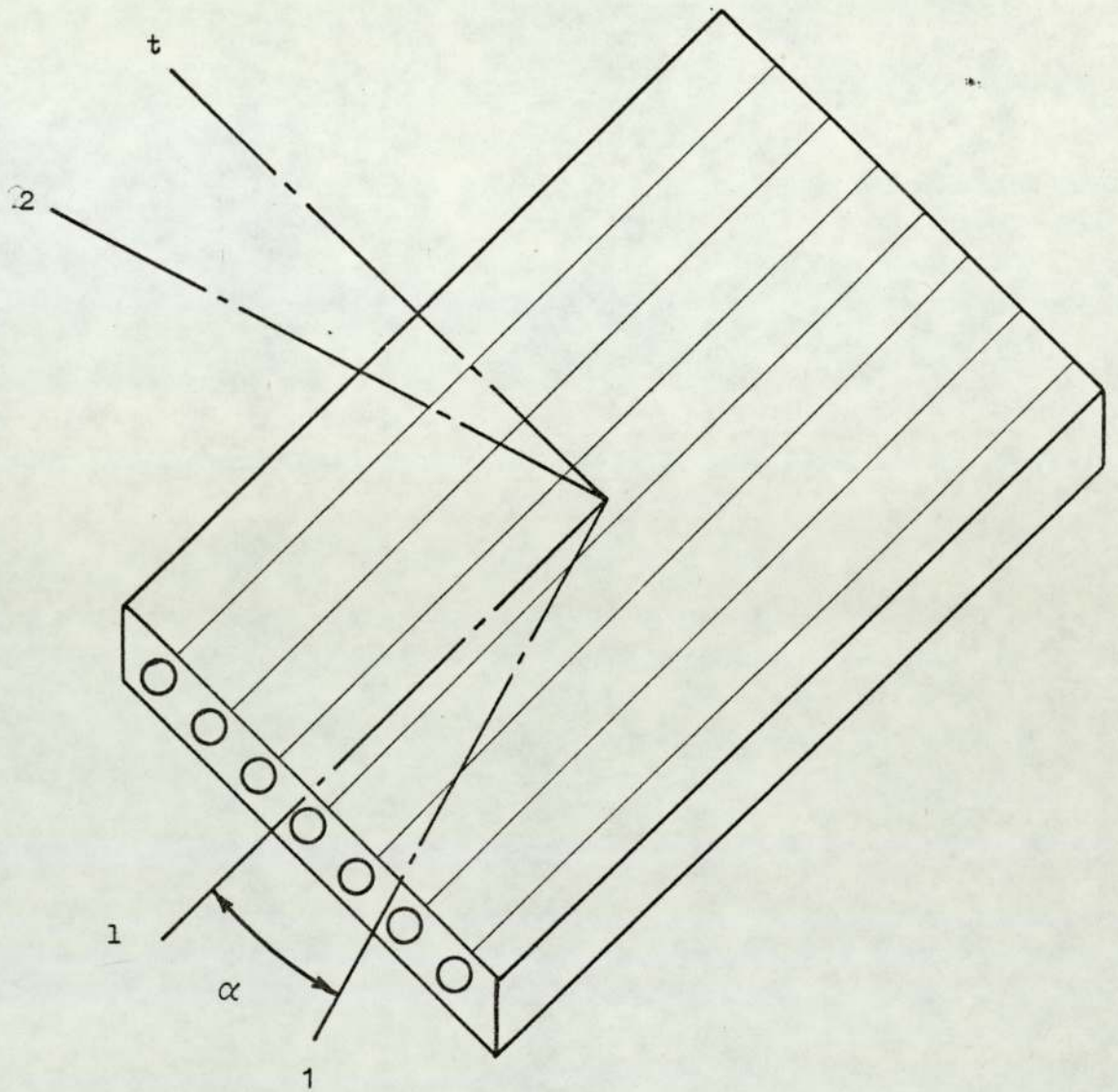


FIG. 3.2 THE BASIC LAMINA



LAMINA PRINCIPLE AXES 1-t
LAMINA ARBITRARY AXES 1-2

FIG. 3.3 FAILURE CURVE FOR A 3-FIBRE SYSTEM

$$\alpha = 0, 45^\circ + 90^\circ$$

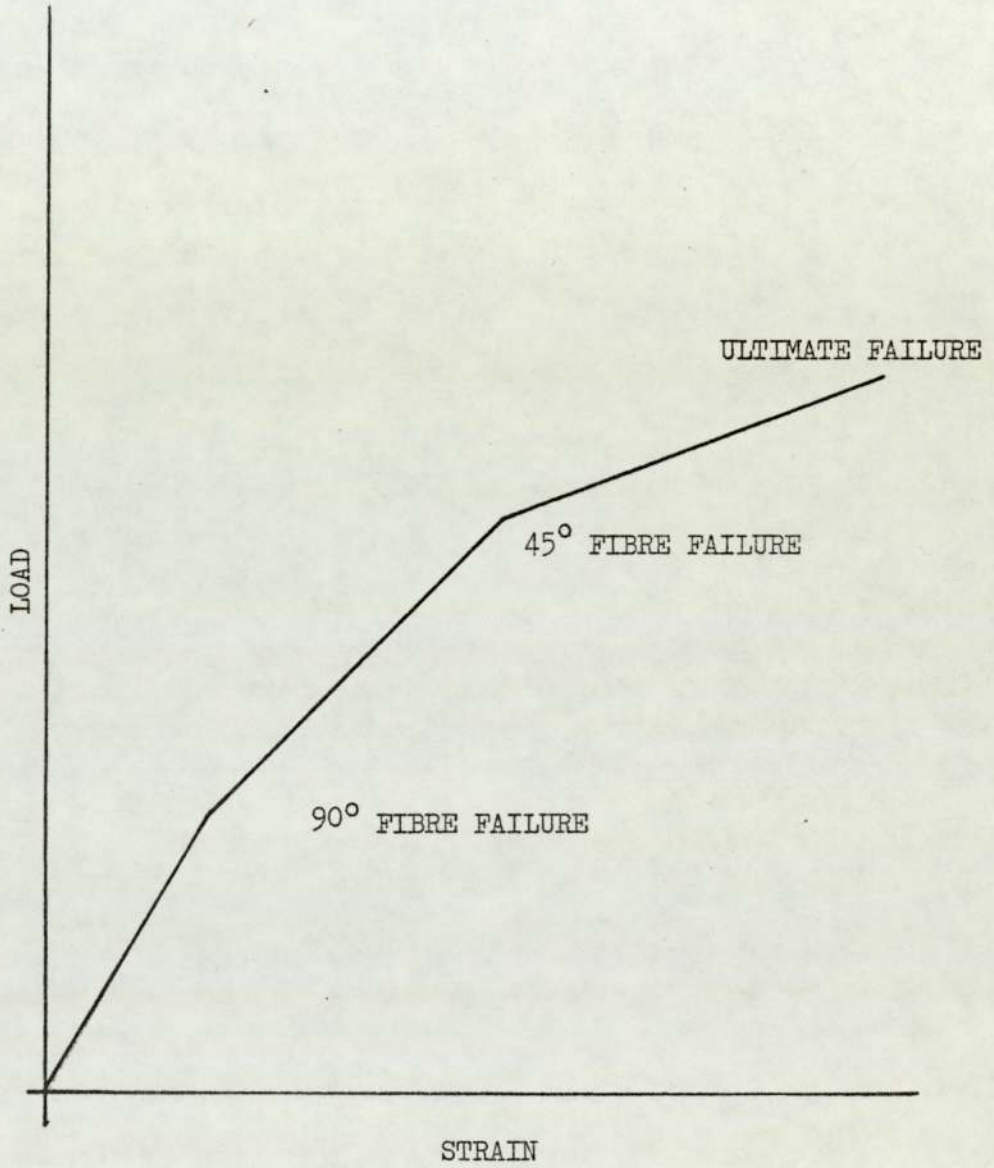
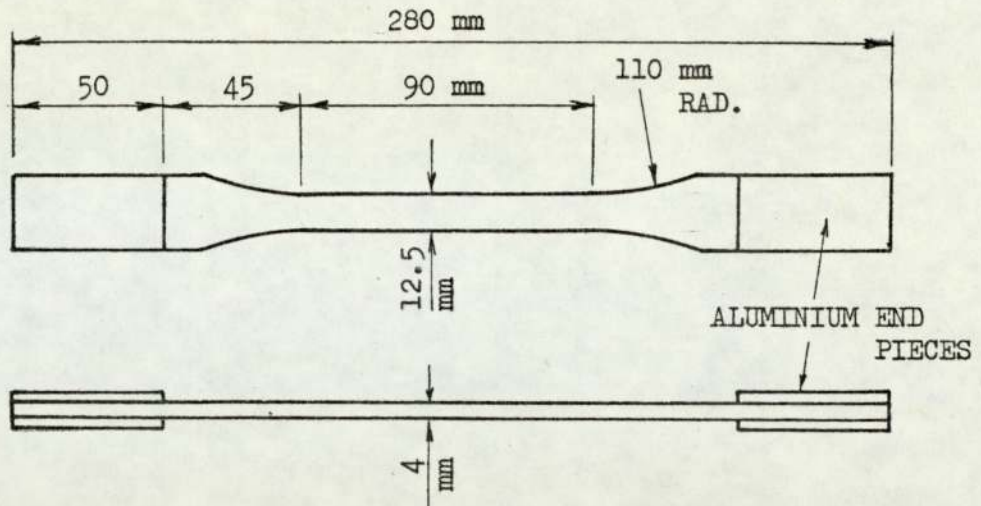
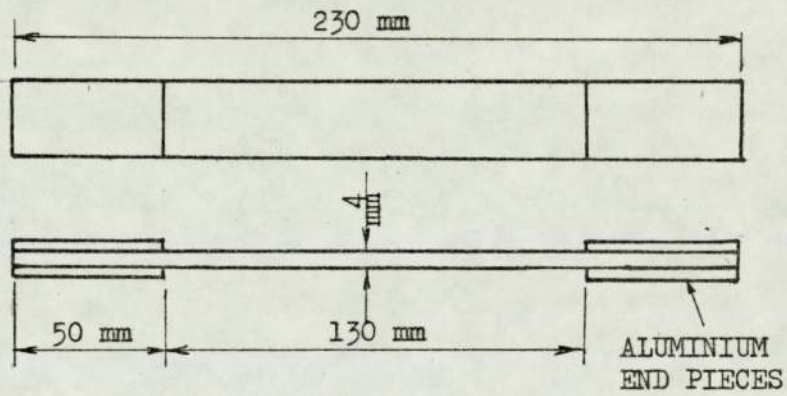


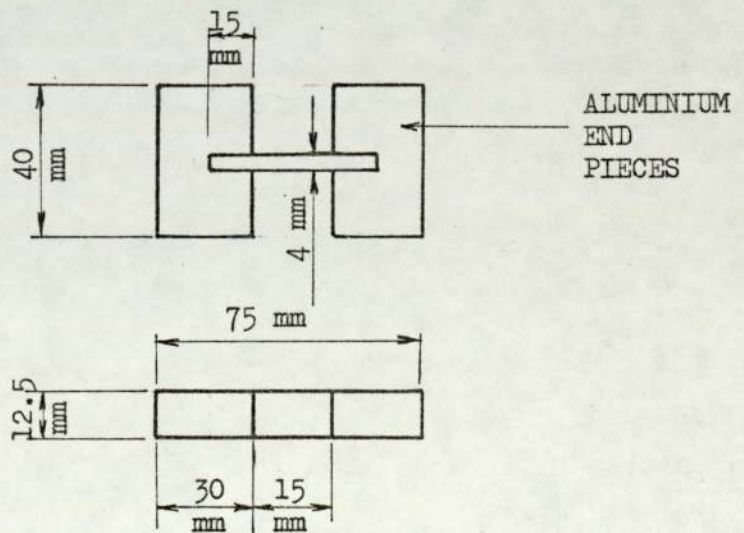
FIG. 3.4 DESIGN OF SHORT TERM TEST SPECIMENS



a) TENSILE SPECIMEN : UNIDIRECTIONAL,
BIDIRECTIONAL & ANGLE-PLY MATERIALS



b) TENSILE SPECIMEN : CSM



c) COMPRESSION SPECIMENS

FIG. 3.5 PHOTOGRAPH OF TYPICAL SHORT TERM SPECIMENS

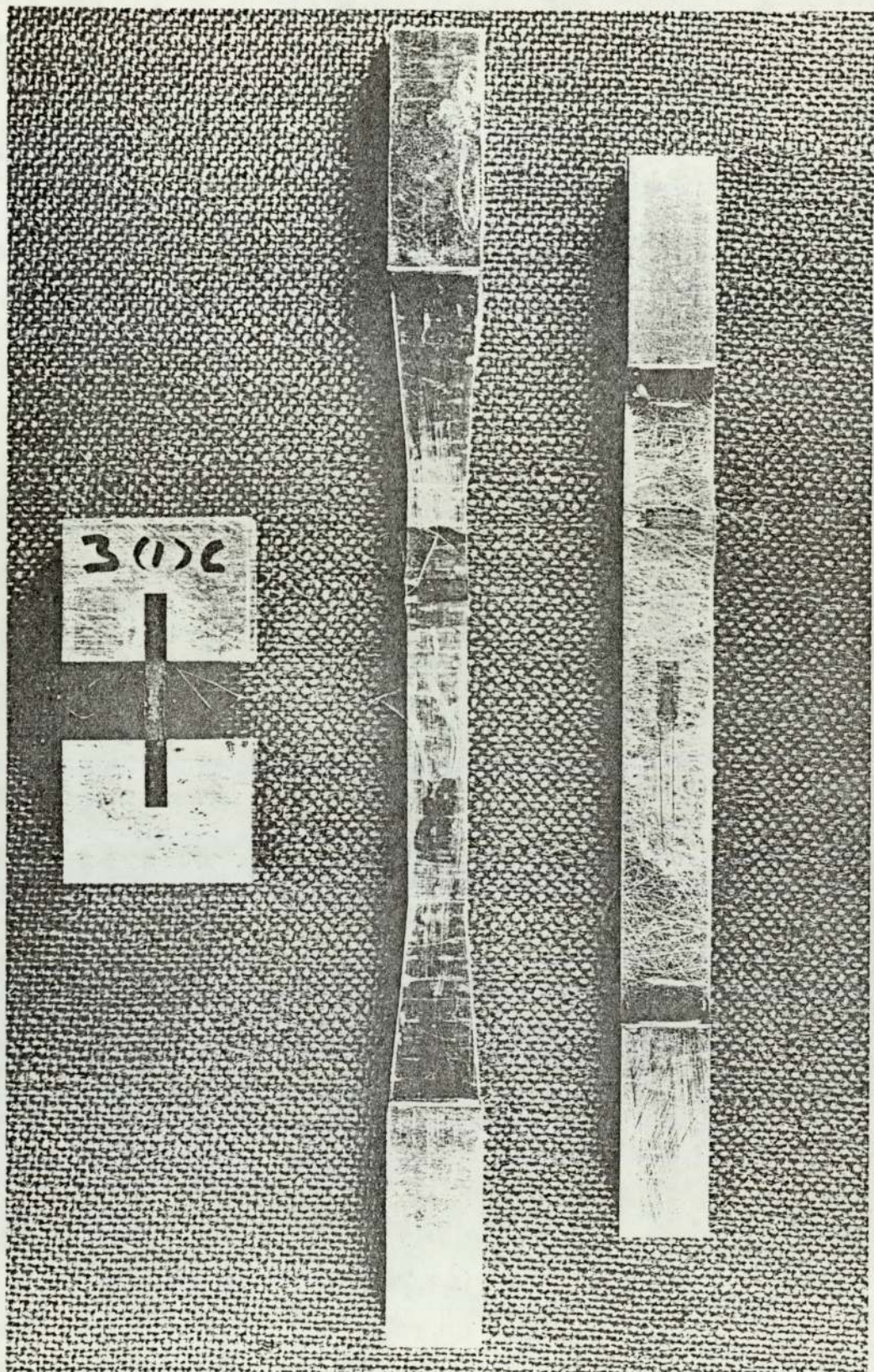


FIG. 3.6 AXIAL ELASTIC MODULUS OF LAMINA

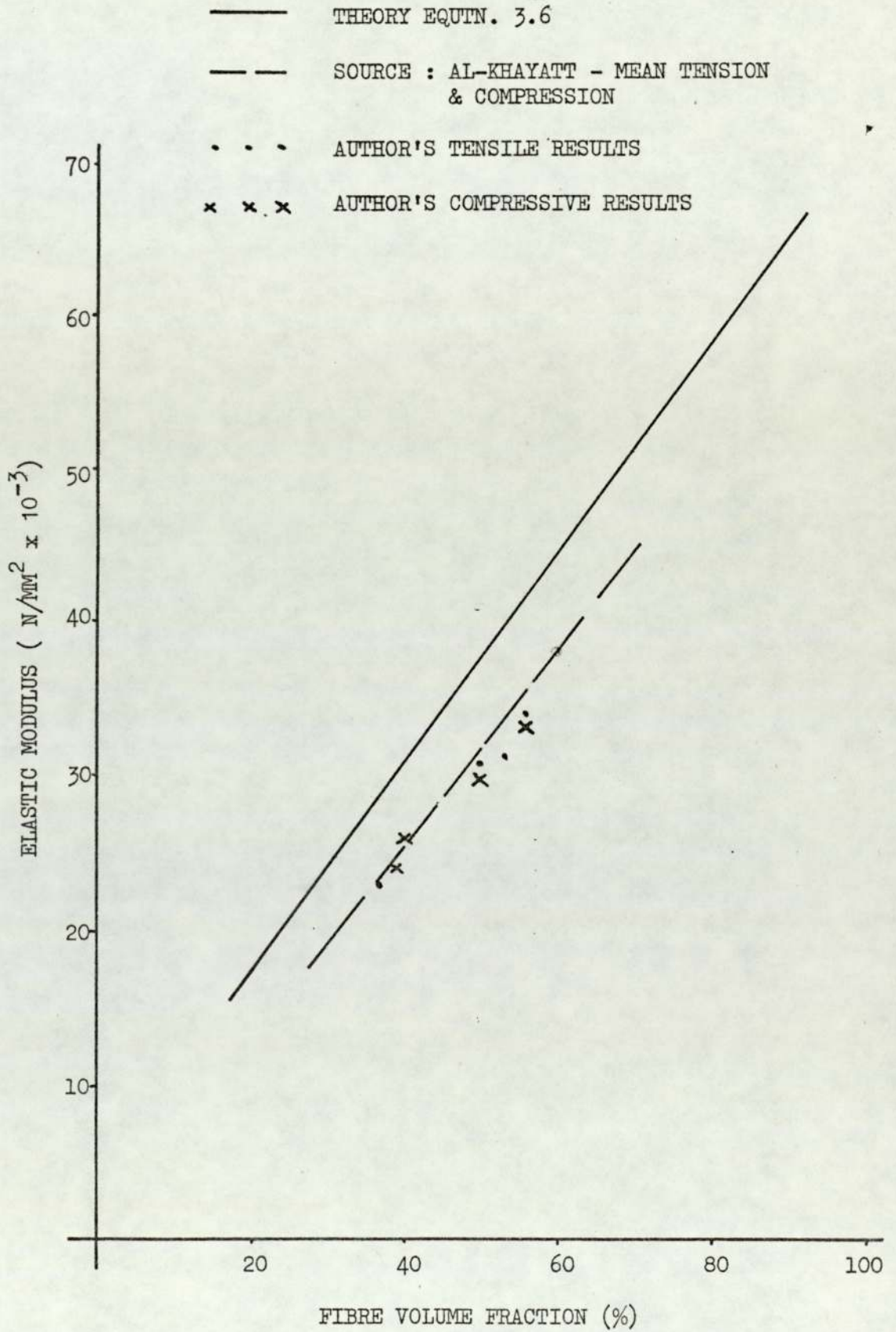


FIG. 3.7 TENSILE STRESS-STRAIN CHARACTERISTICS

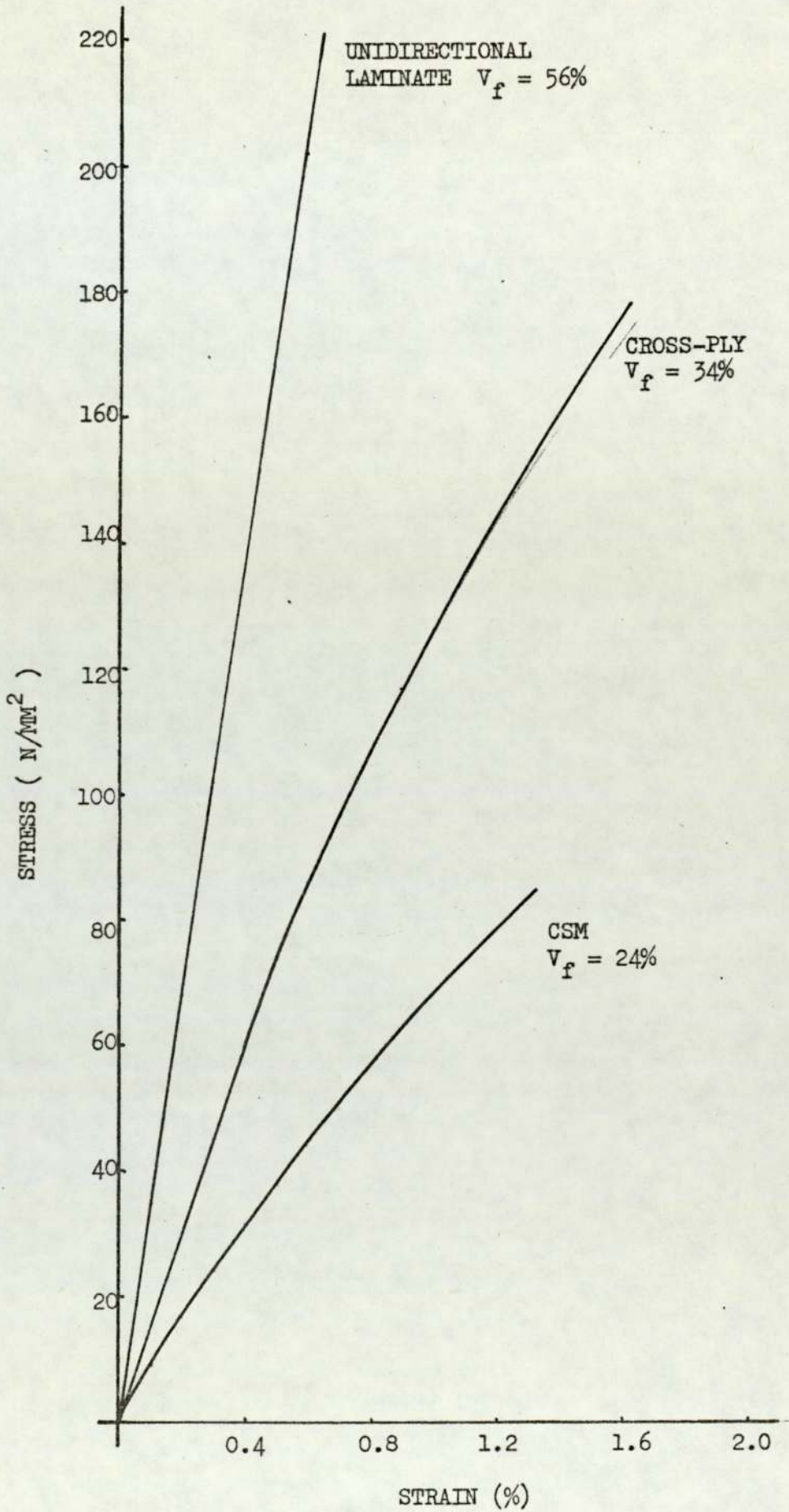


FIG. 3.8 AXIAL STRENGTH OF LAMINA

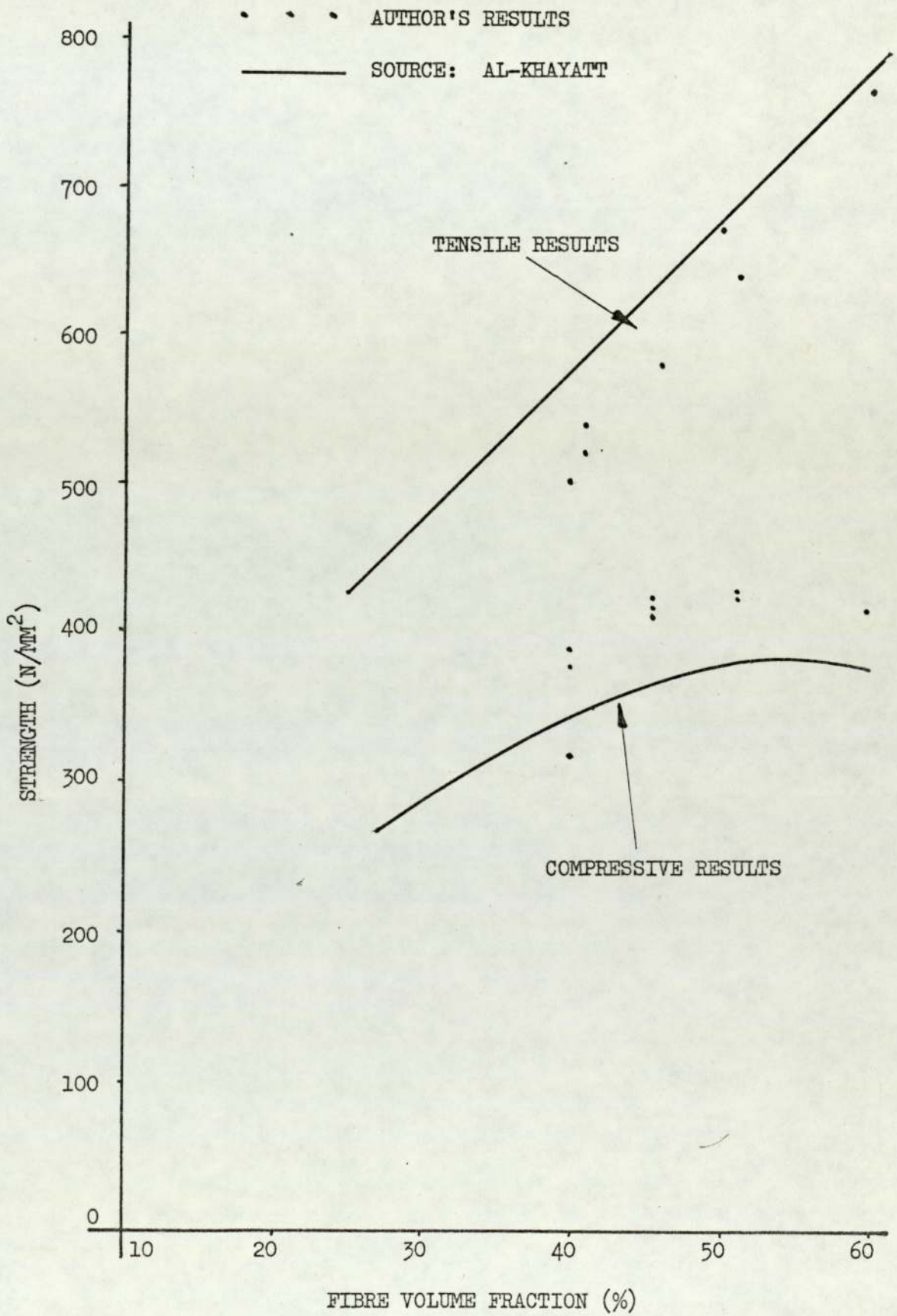


FIG. 3.9 TENSILE & COMPRESSIVE STRENGTHS OF
SEVERAL LAMINATES

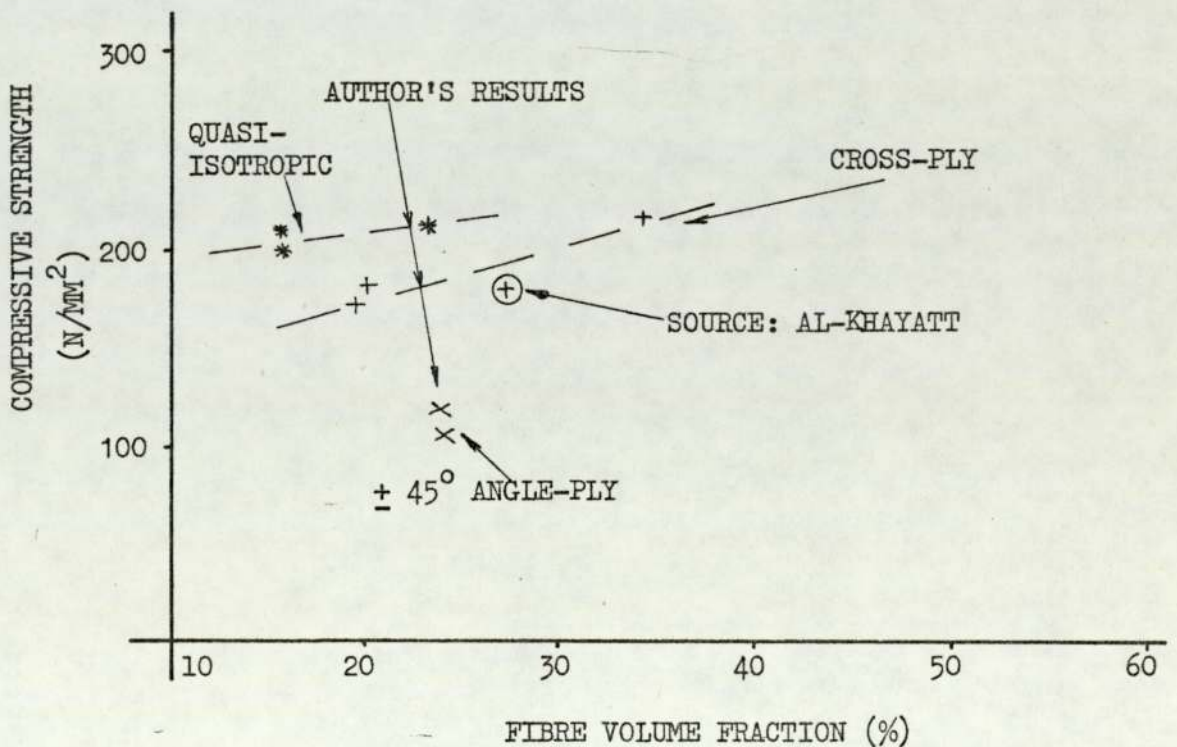
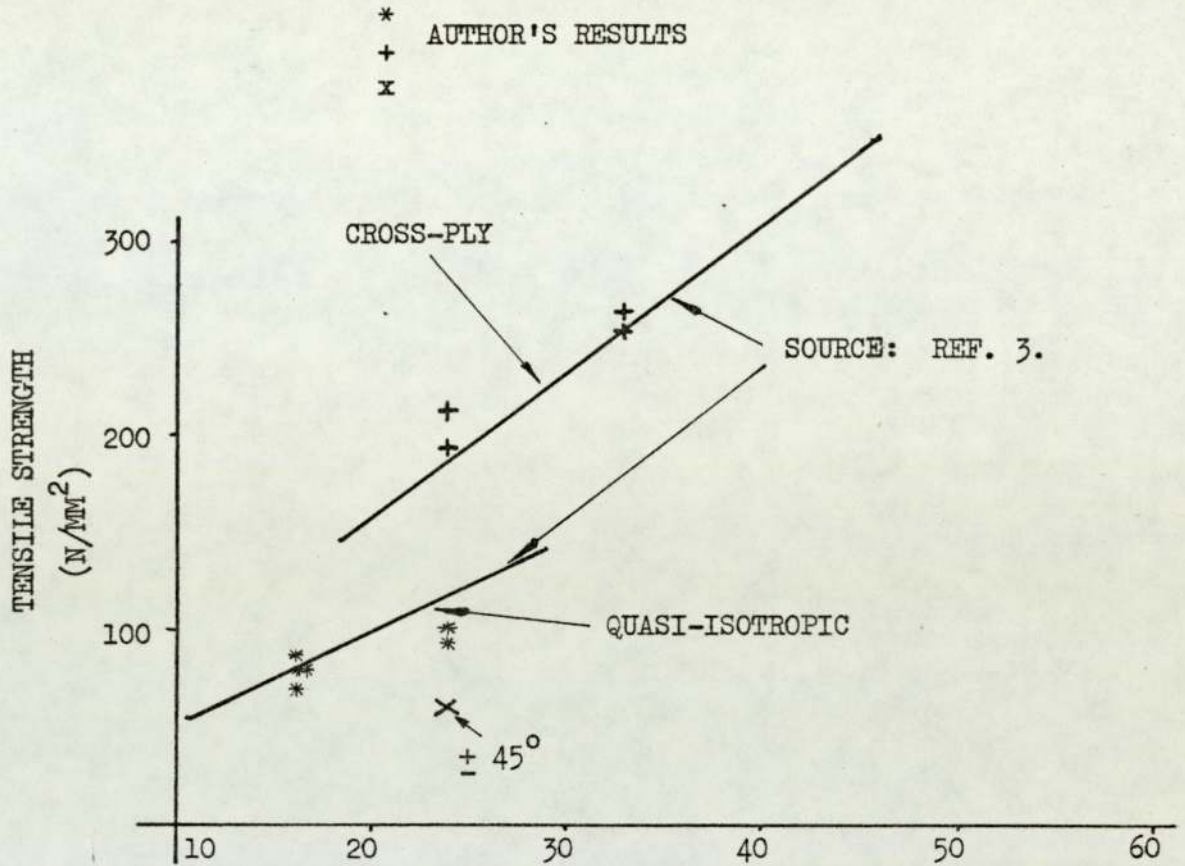


FIG. 3.10 LONGITUDINAL AND TRANSVERSE ELASTIC MODULUS

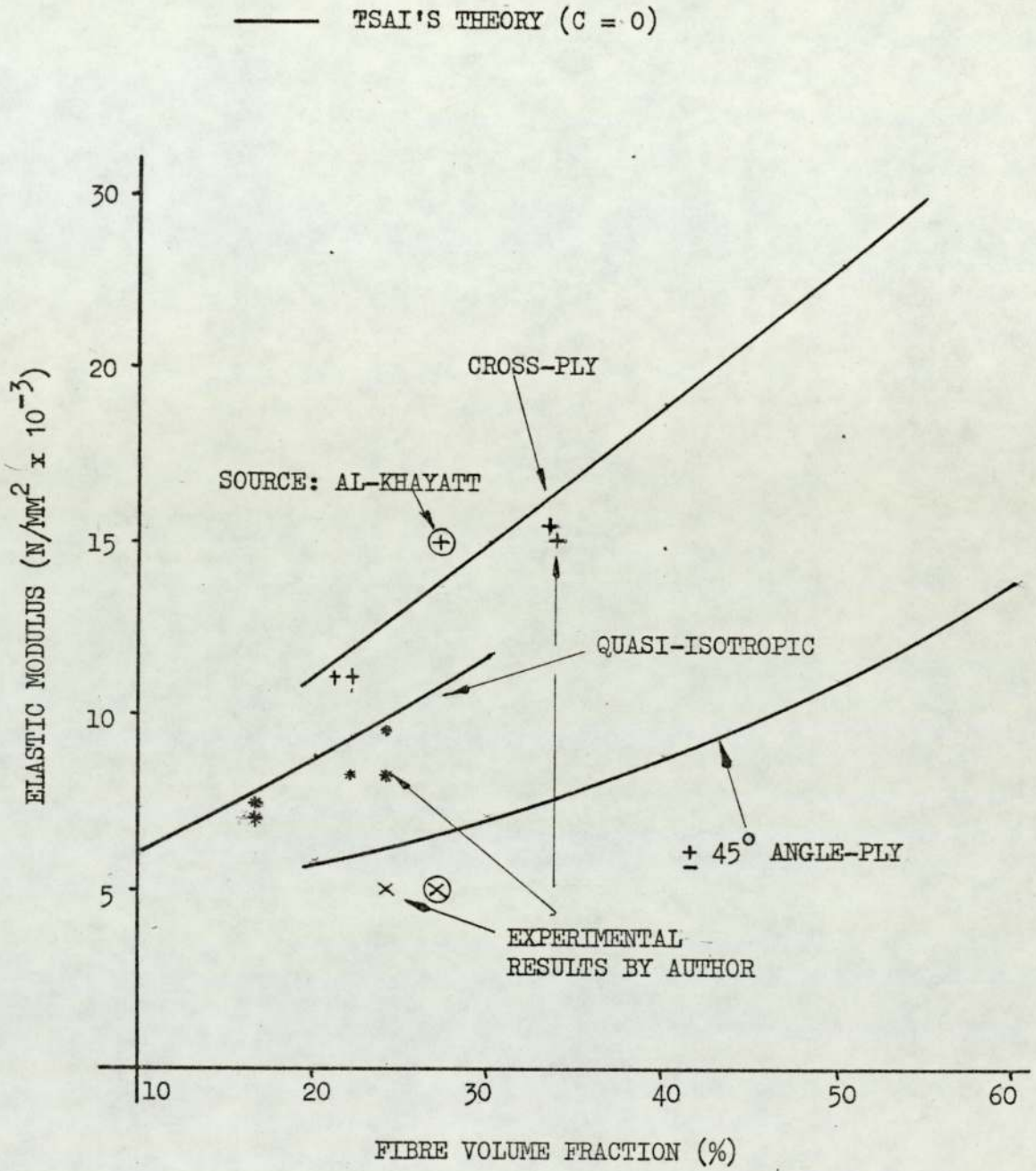
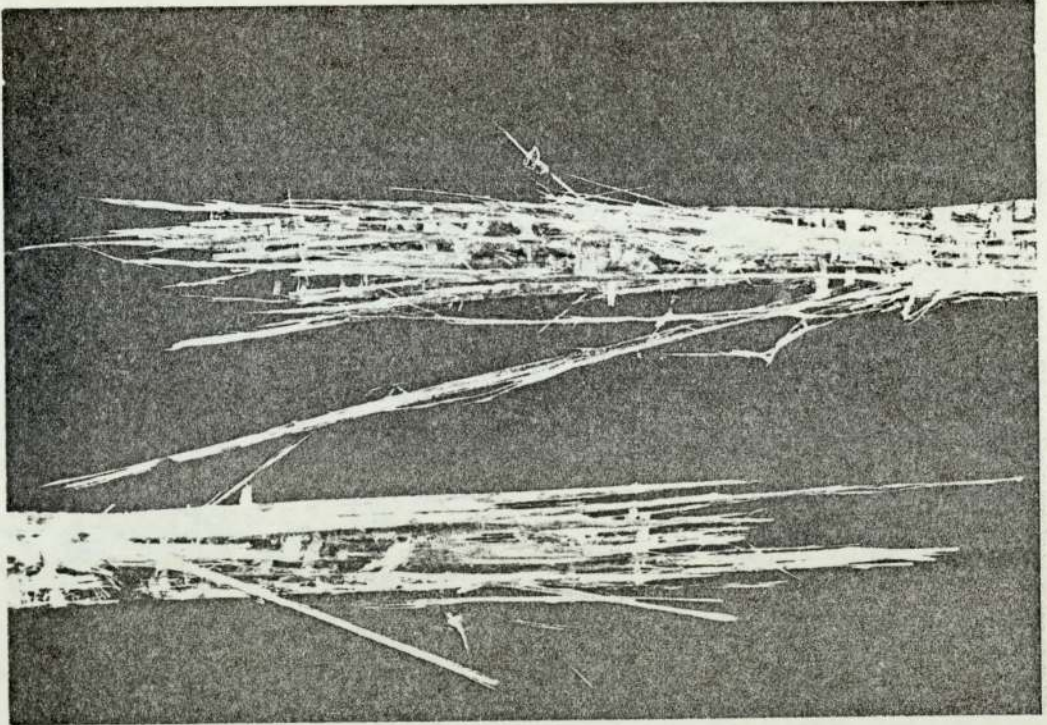
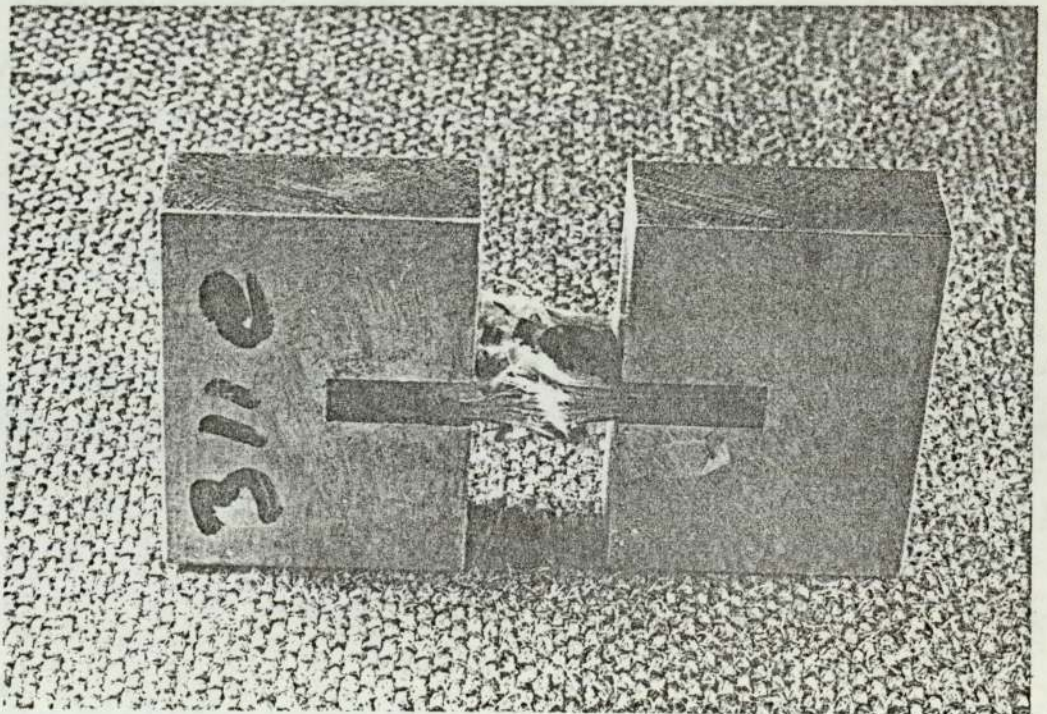


FIG. 3.11 TYPICAL FAILURE MODES

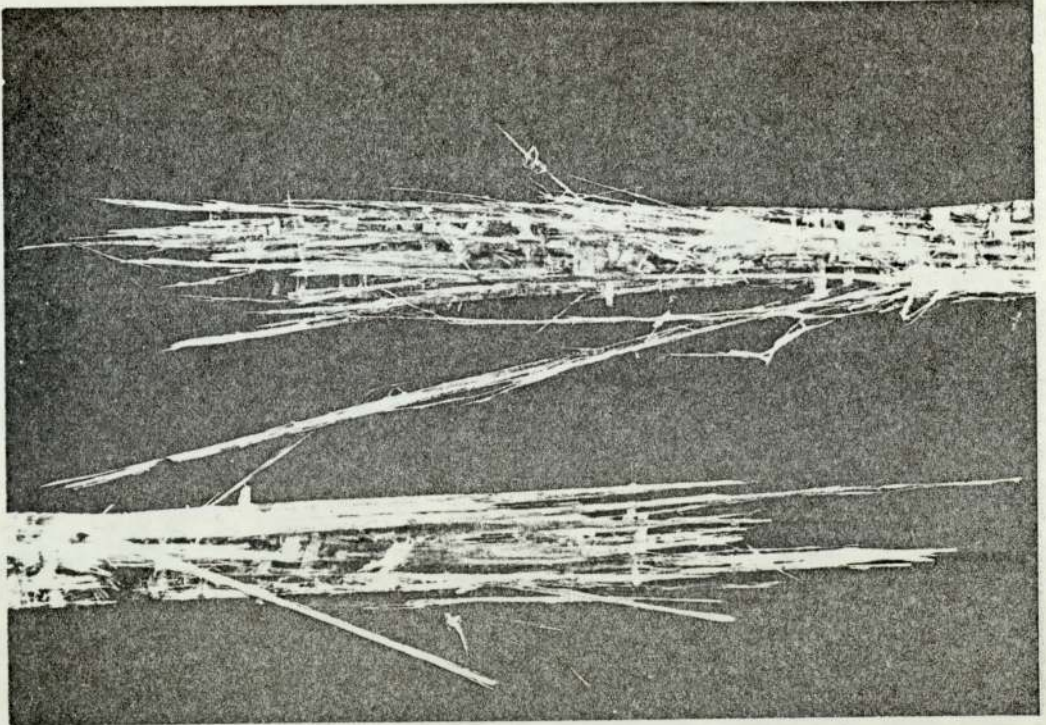


a) TENSILE FAILURE

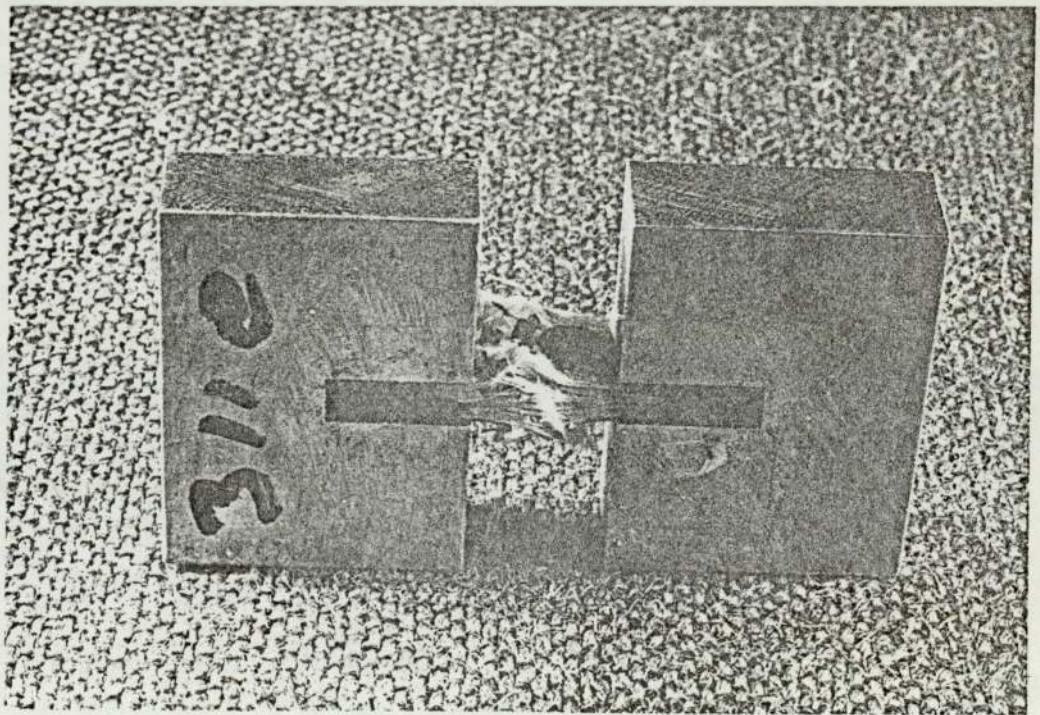


b) COMPRESSION FAILURE

FIG. 3.11 TYPICAL FAILURE MODES



a) TENSILE FAILURE



b) COMPRESSION FAILURE

FIG. 3.12 TRANSVERSE AND SHEAR MODULUS

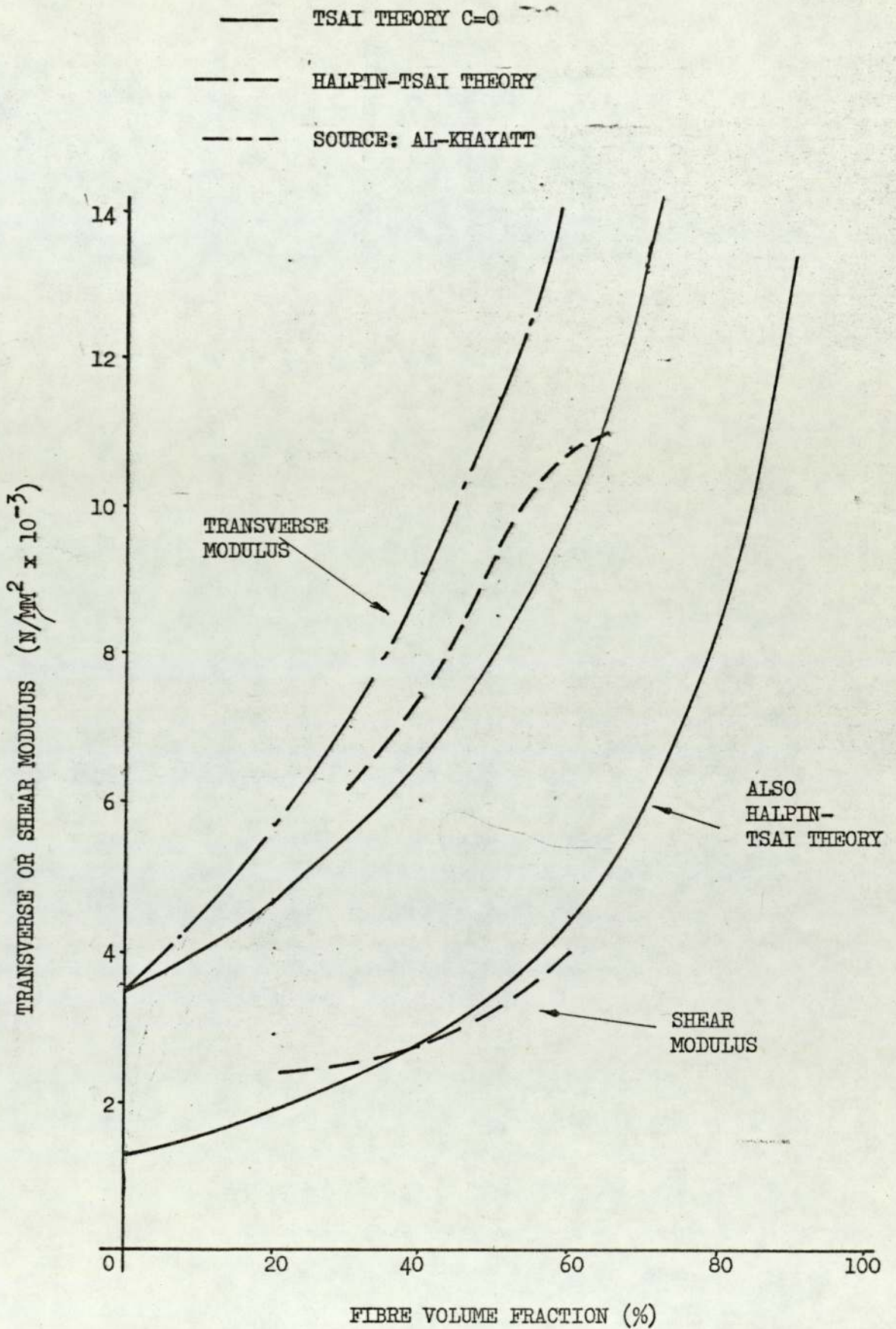


FIG. 3.13 LONGITUDINAL POISSON'S RATIO

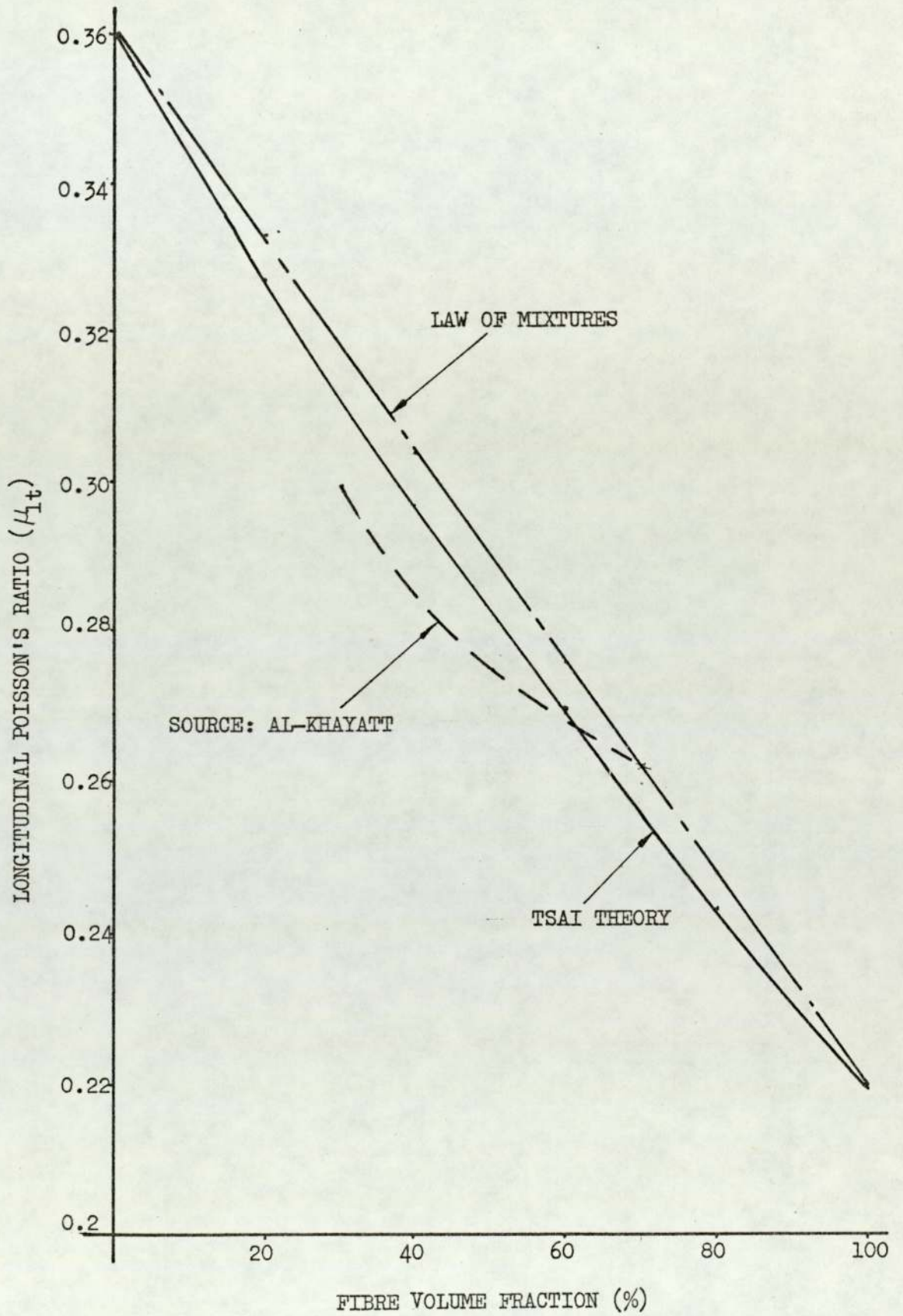


FIG. 3.14 LONGITUDINAL AND TRANSVERSE POISSON'S
RATIO FOR SELECTED LAMINATES

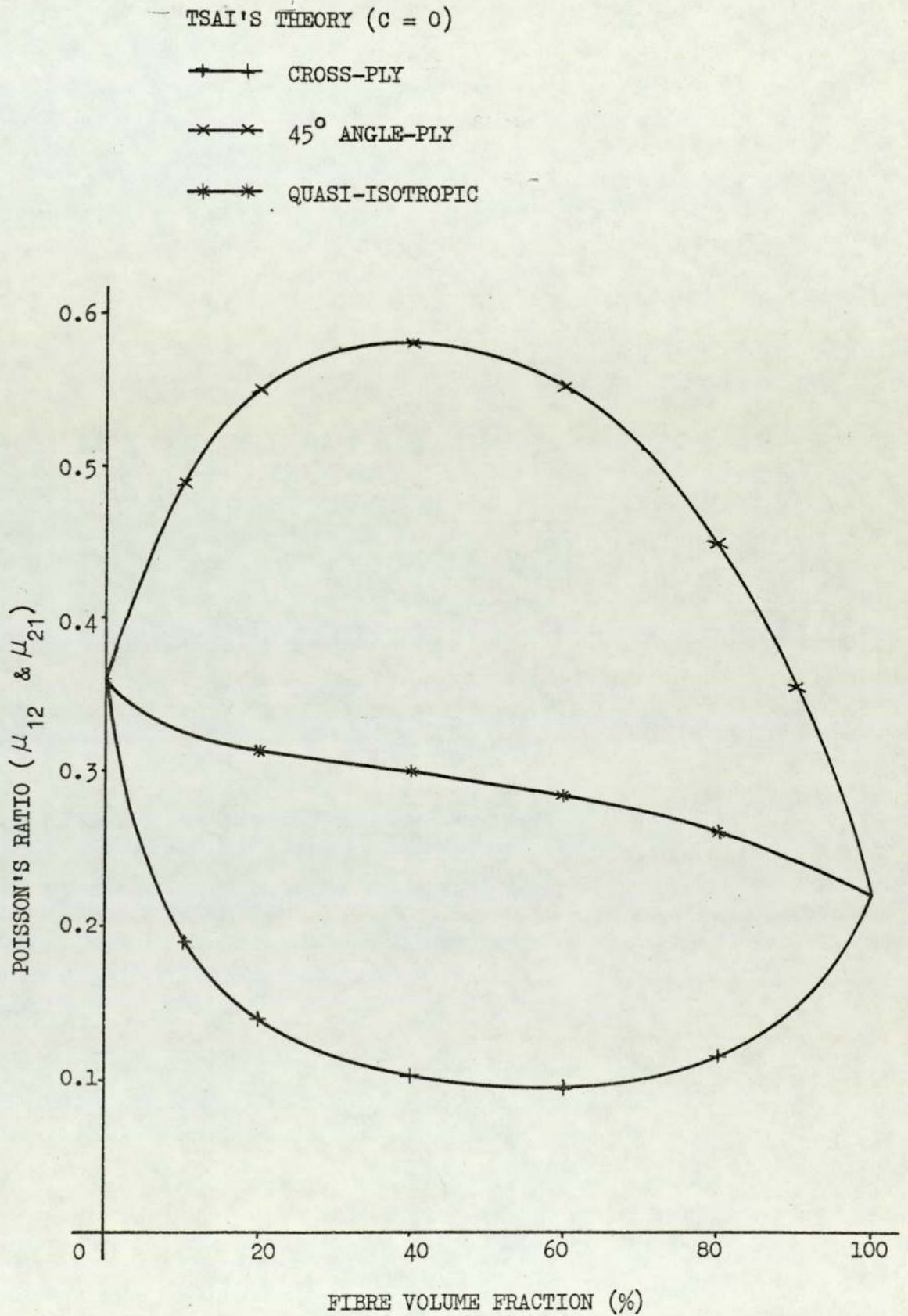


FIG. 3.15 THEORETICAL SHEAR MODULUS FOR
SELECTED LAMINATES

TSAI'S THEORY ($c = 0$)

- +---+ CROSS-PLY
- x---x 45° ANGLE-PLY
- *---* QUASI-ISOTROPIC

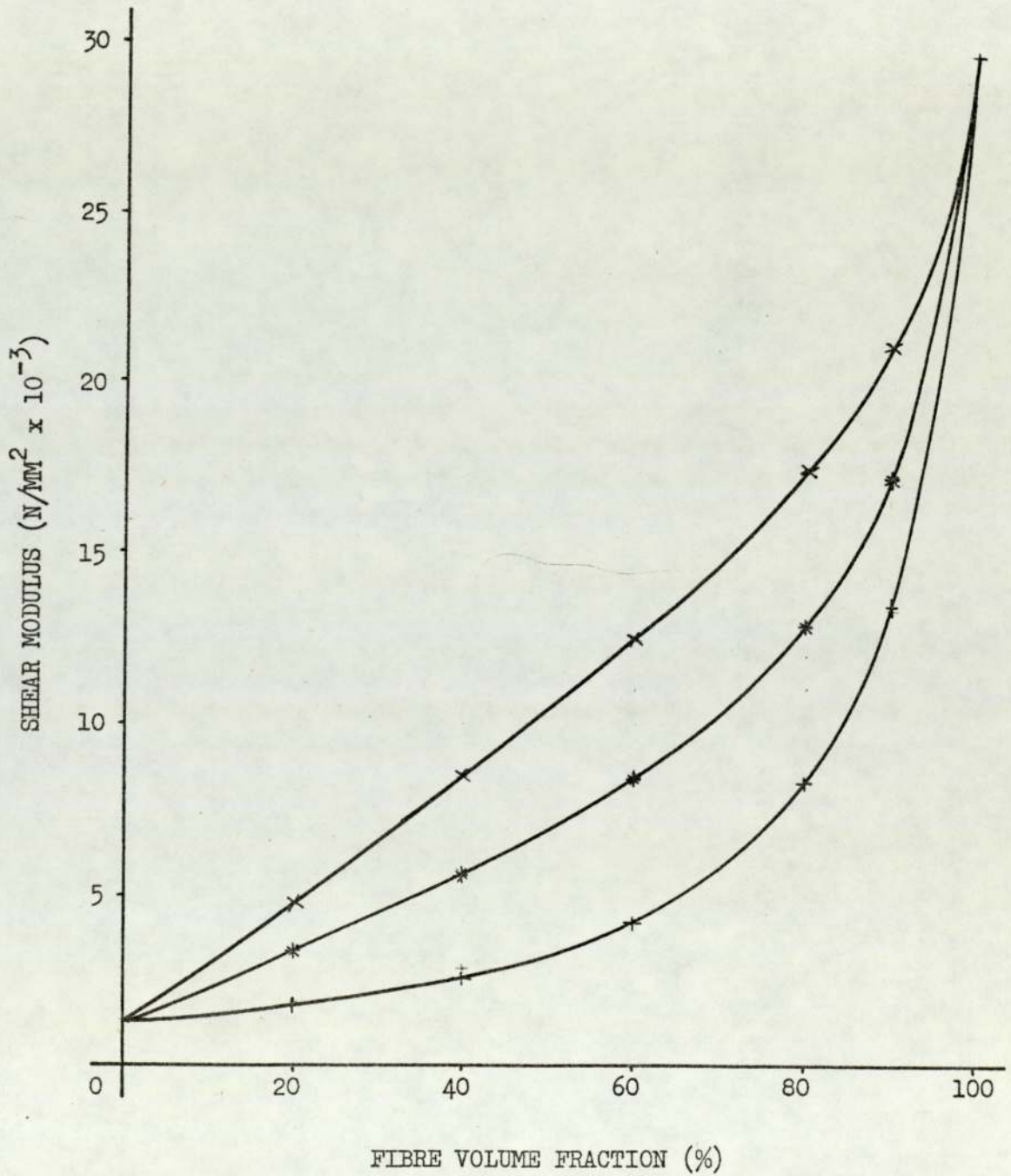


FIG. 3.16

CREEP ACTIVATION STRESS

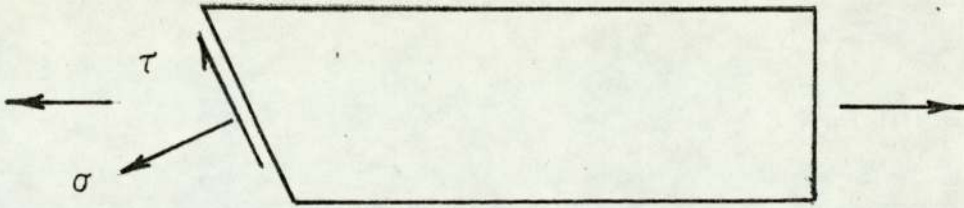


FIG. 3.16a

LARSON-MILLER PARAMETER

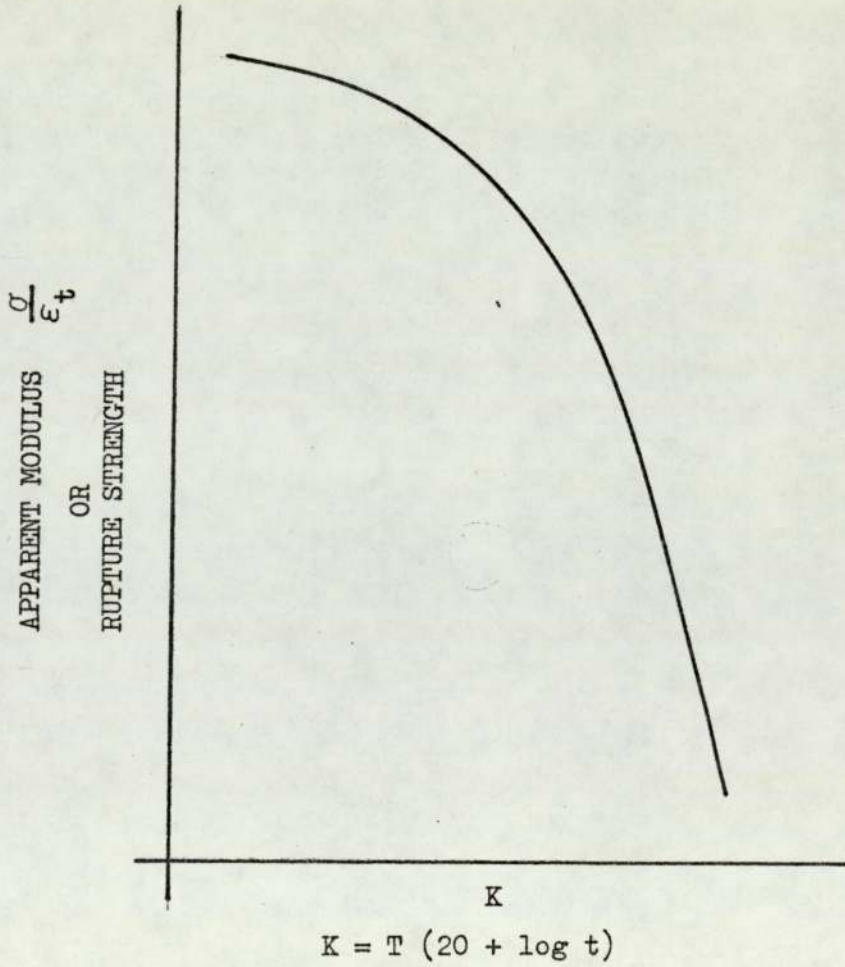
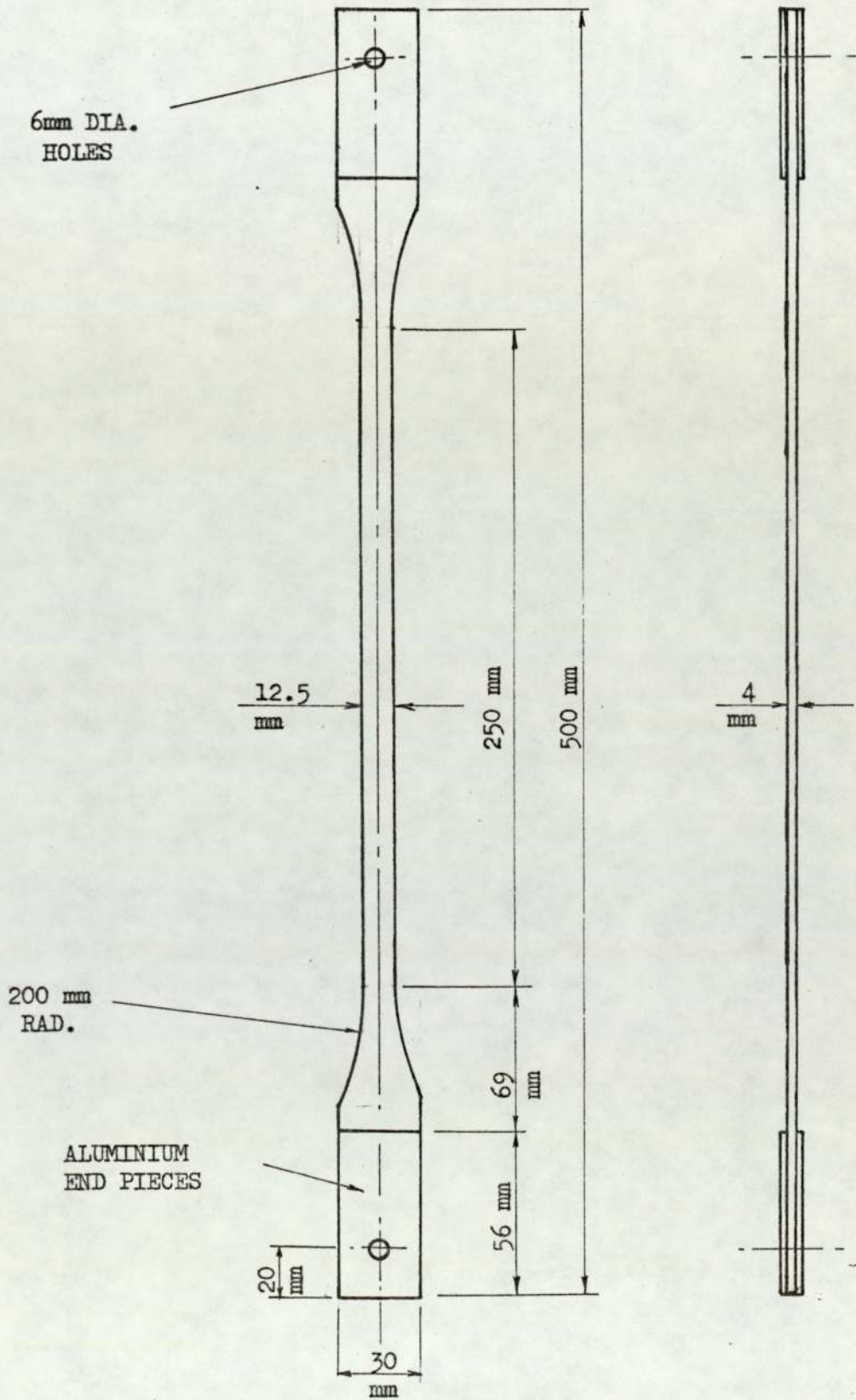


FIG. 3.17 CREEP AND STRESS RUPTURE

SPECIMEN



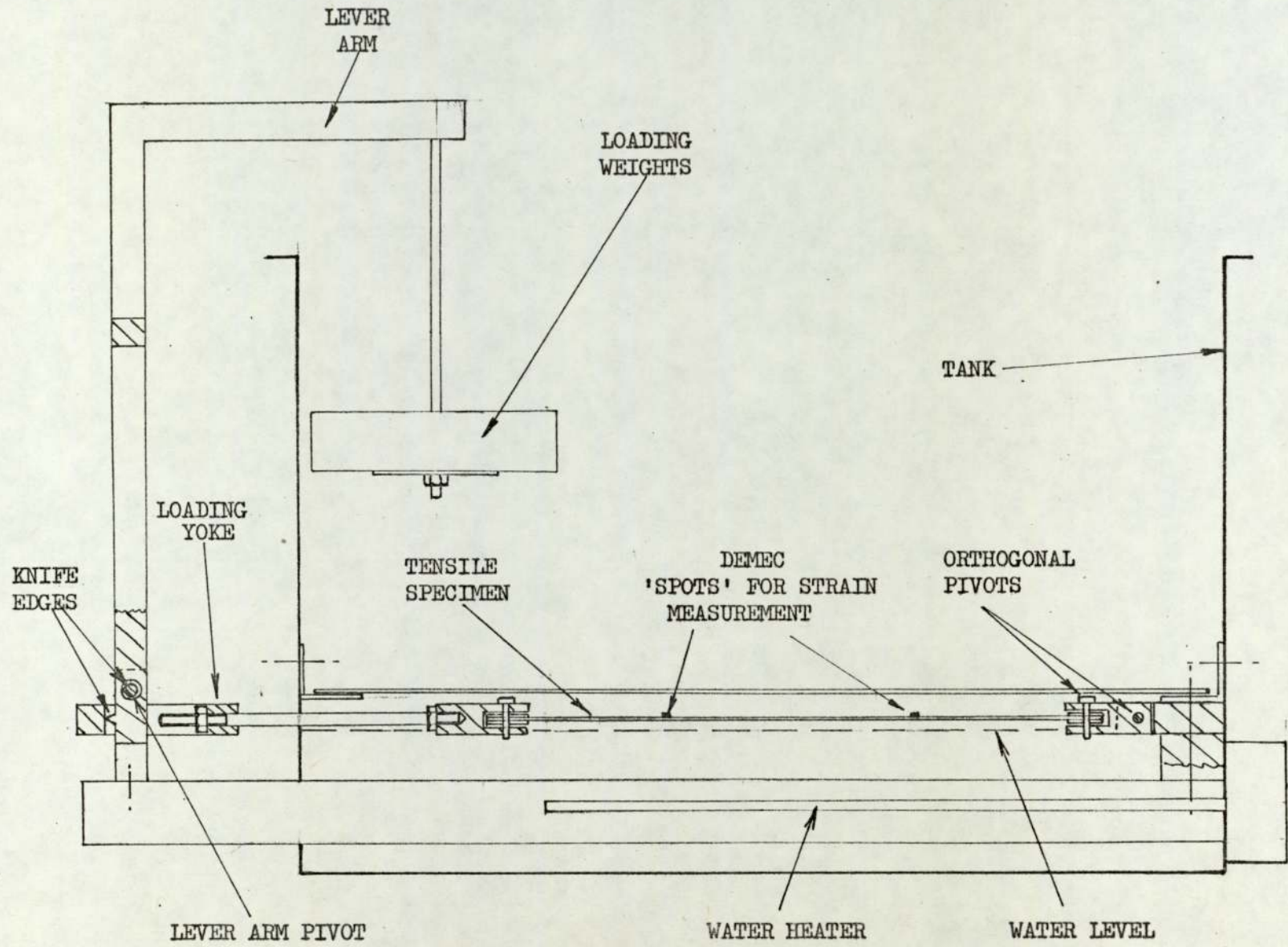


FIG. 3.18 CREEP TEST EQUIPMENT

FIG. 3.19 TABLE OF LONG TERM LOADING RESULTS

AT 70°C & 100% RH.

REINFORCEMENT	VOL. FRAC-TION (V_f) %	STRESS (N/MM ²)	TEST DURA-TION (HRS.)	EQUIVALENT TIME AT 20°C (HRS.)	MAX. STRAIN (%)
CHOPPED STRAND MAT (CSM)	16.5	7	700*	5.5 x 10 ⁶	0.8%
	16.5	10.5	3	9.3 x 10 ³	1.6%
	16.5	10.5	6.75	2.4 x 10 ⁴	2.0%
	16.5	10.5	23	1.0 x 10 ⁵	2.1%
	16.5	10.5	9.25	3.5 x 10 ⁴	2.2%
	16.5	10.5	6.0	2.1 x 10 ⁴	1.8%
	16.5	10.5	12.0	4.7 x 10 ⁴	1.6%
	16.5	10.5	15.0	6.1 x 10 ⁴	1.8%
	16.5	12.25	2.5	7.5 x 10 ³	2.1%
	16.5	12.25	4.0	1.3 x 10 ⁴	1.7%
	16.5	12.25	9.8	3.7 x 10 ⁴	1.7%
	16.5	17.0	0.5	1.1 x 10 ³	-
	BIDIRECTIONAL WOVEN ROVING	24	9	1,104*	9.3 x 10 ⁶
24		15	90*	5.0 x 10 ⁵	
24		42	522*	3.89 x 10 ⁶	0.5%
24		42	90*	5.0 x 10 ⁵	
24		42	96*	5.4 x 10 ⁵	
24		72	25.2	1.1 x 10 ⁵	1.9%
24		72	66	3.5 x 10 ⁵	2.2%
UNIDIRECTIONAL WOVEN ROVING	45.5	9	1,400*	1.27 x 10 ⁷	0.5%
	45.5	60	96*	5.4 x 10 ⁷	
	54	9	1,400*	1.27 x 10 ⁵	0.4%
	54	60	96*	5.4 x 10 ⁵	
		72	96*	5.4 x 10 ⁵	

* SIGNIFIES TEST TERMINATED BEFORE MATERIAL FAILURE

KEY :

* CSM $V_f = 16.5\%$

+ BIDIRECTIONAL WOVEN ROVING $V_f = 24\%$

Δ UNIDIRECTIONAL WOVEN ROVING $V_f = 54\%$

\square UNIDIRECTIONAL WOVEN ROVING $V_f = 45.5$

\rightarrow INDICATES TEST DISCONTINUED BEFORE FAILURE

EQUIVALENT TIME AT 20°C

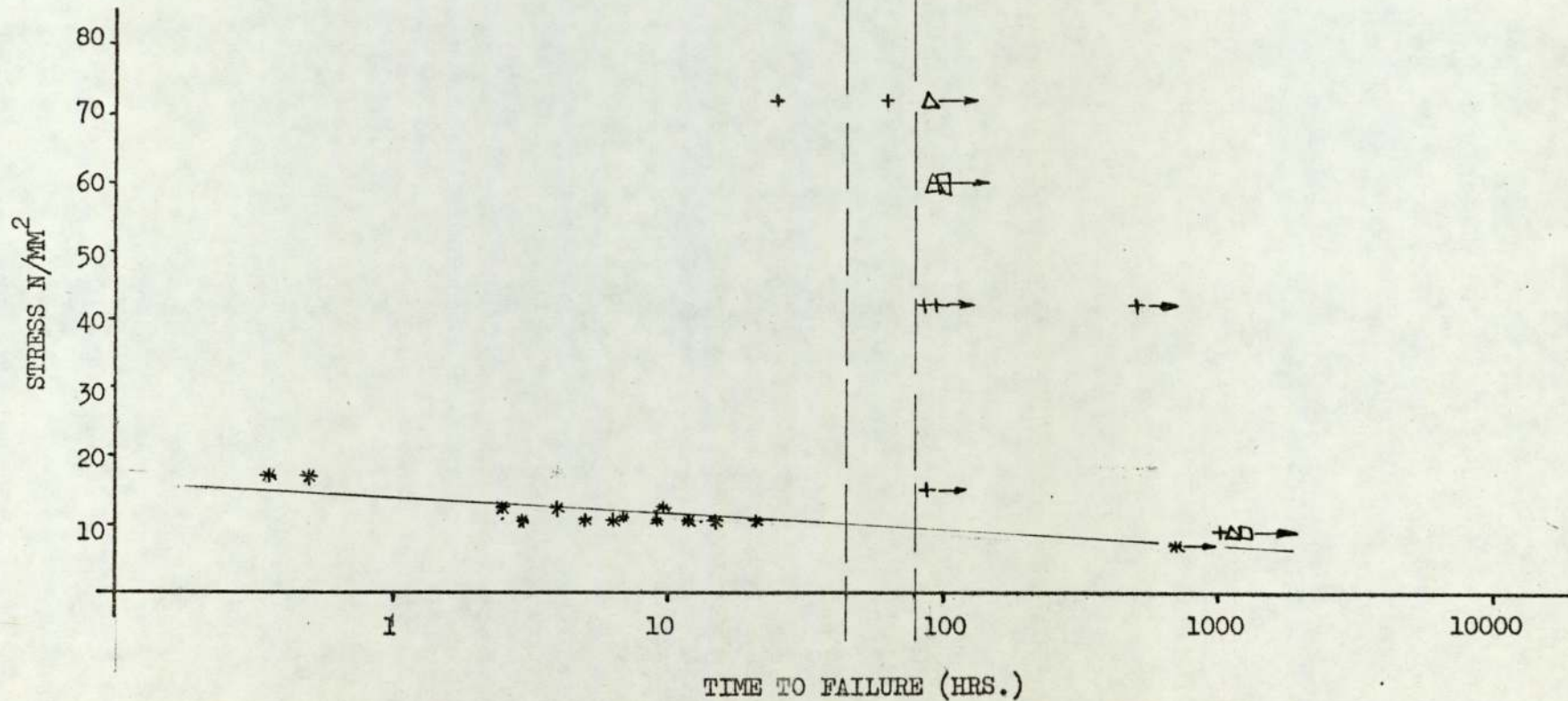


FIG. 3.20 LONG TERM LOADING RESULTS
AT 70°C

FIG. 3.21 TABLE OF LONG TERM PROPERTY RESULTS

AT 20°C & 100% RH.

REINFORCEMENT	VOL. FRAC-TION (V _f) %	STRESS (N/MM ²)	TEST DURA-TION (HRS.)	CREEP CONSTANTS			MAX STRAIN (%)	STD. ERROR lg (t _o)	
				o (M/M)	m (M/M) 10 ⁻²	n			
CHOPPED STRAND MAT (CSM)	16.5	28	468*	0.63x10 ⁻⁵	0.655	0.088	1.13	0.13x10 ⁻¹	
	16.5	37	1430*	0.95x10 ⁻⁵	0.812	0.089	1.55	0.16x10 ⁻¹	
	16.5	44	69	0.39x10 ⁻⁵	1.037	0.111	1.66	0.25x10 ⁻¹	
	16.5	45	45.5	0.55x10 ⁻⁴	1.142	0.086	1.59	0.26x10 ⁻¹	
	16.5	49	78	0.22x10 ⁻⁴	1.214	0.072	1.66	0.15x10 ⁻¹	
	16.5	48	43.5	0.31x10 ⁻⁴	1.13	0.09	1.59	0.23x10 ⁻¹	
	16.5	54	19.5	0.12x10 ⁻⁵	1.36	0.10	1.84	0.34x10 ⁻¹	
	21.5	25	1200*	0.29x10 ⁻⁴	0.57	0.08	1.01	0.12x10 ⁻¹	
	21.5	39	502*	0.9 x10 ⁻⁶	0.88	0.08	1.45	0.75x10 ⁻²	
	21.5	46	11.6	0.9 x10 ⁻⁵	1.02	0.08	1.23	0.77x10 ⁻²	
	21.5	52	18.9	0.29x10 ⁻⁴	1.24	0.062	1.49	0.56x10 ⁻²	
	BIDIRECTIONAL WOVEN ROVING	24	36	1015*	0.15x10 ⁻⁴	0.298	0.04	0.39	0.12x10 ⁻¹
		24	68	166*	0.9 x10 ⁻⁴	0.68	0.03	0.79	0.74x10 ⁻²
		24	88	1183*	0.4 x10 ⁻⁵	0.94	0.04	1.25	0.13x10 ⁻¹
BIDIRECTIONAL WOVEN ROVING AT ± 45°	24	12	74.5*	0.0 x10 ⁻⁶	0.45	0.19	1.26	0.37x10 ⁻¹	
	24	24	74	0.25x10 ⁻⁵	0.95	0.27	3.86	0.59x10 ⁻¹	
	24	33	7.5	0.16x10 ⁻⁵	2.6	0.25	4.38	0.16x10 ⁻¹	
UNIDIRECTIONAL WOVEN ROVING	45.5	78	1015*	0.45x10 ⁻⁴	0.43	0.008	0.45	0.17x10 ⁻²	
	54	75	1015*	0.79x10 ⁻⁵	0.39	0.010	0.42	0.95x10 ⁻³	
	54	102	1015*	0.93x10 ⁻⁴	0.46	0.009	0.49	0.13x10 ⁻²	

* SIGNIFIES TEST TERMINATED BEFORE MATERIAL FAILURE

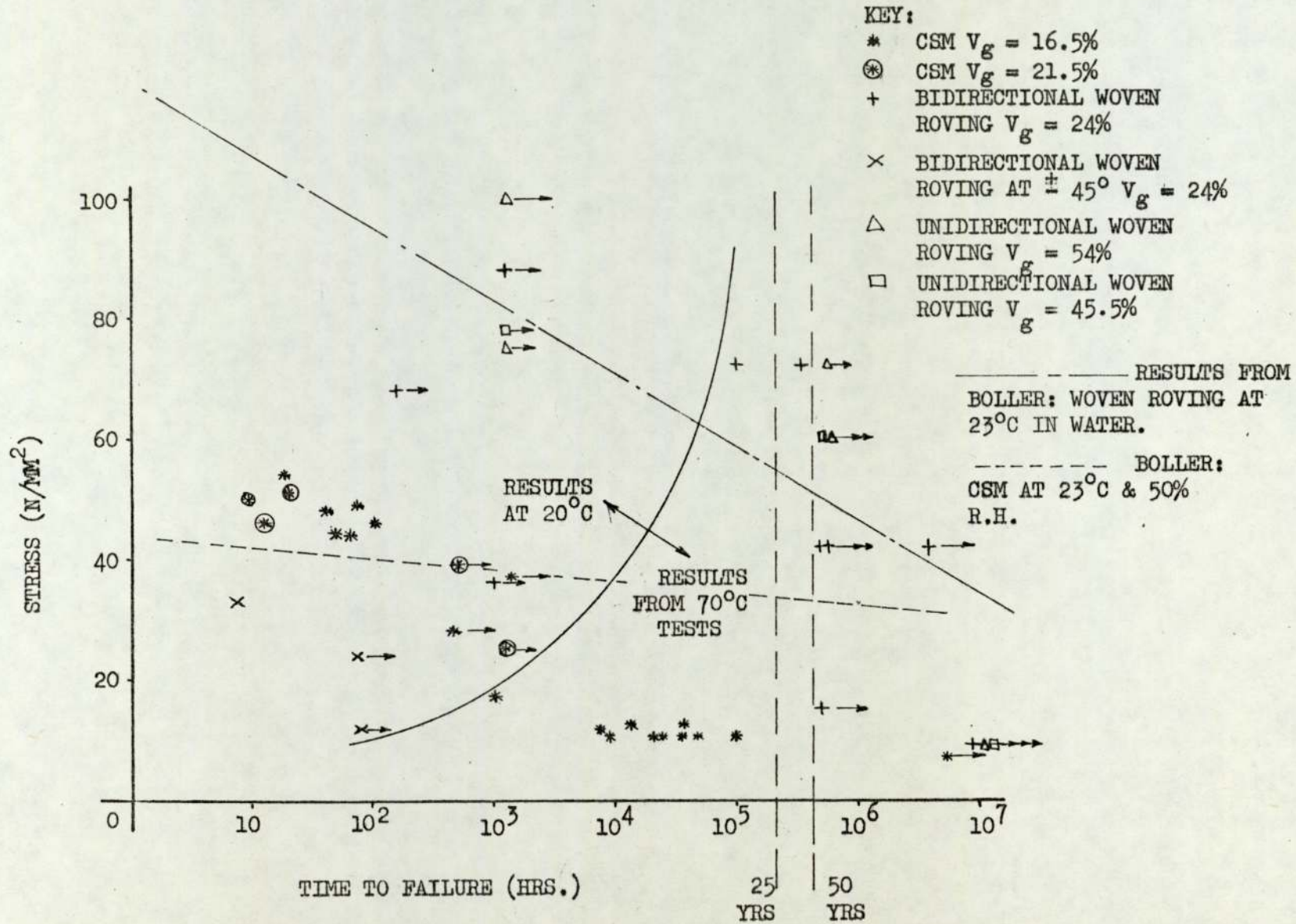
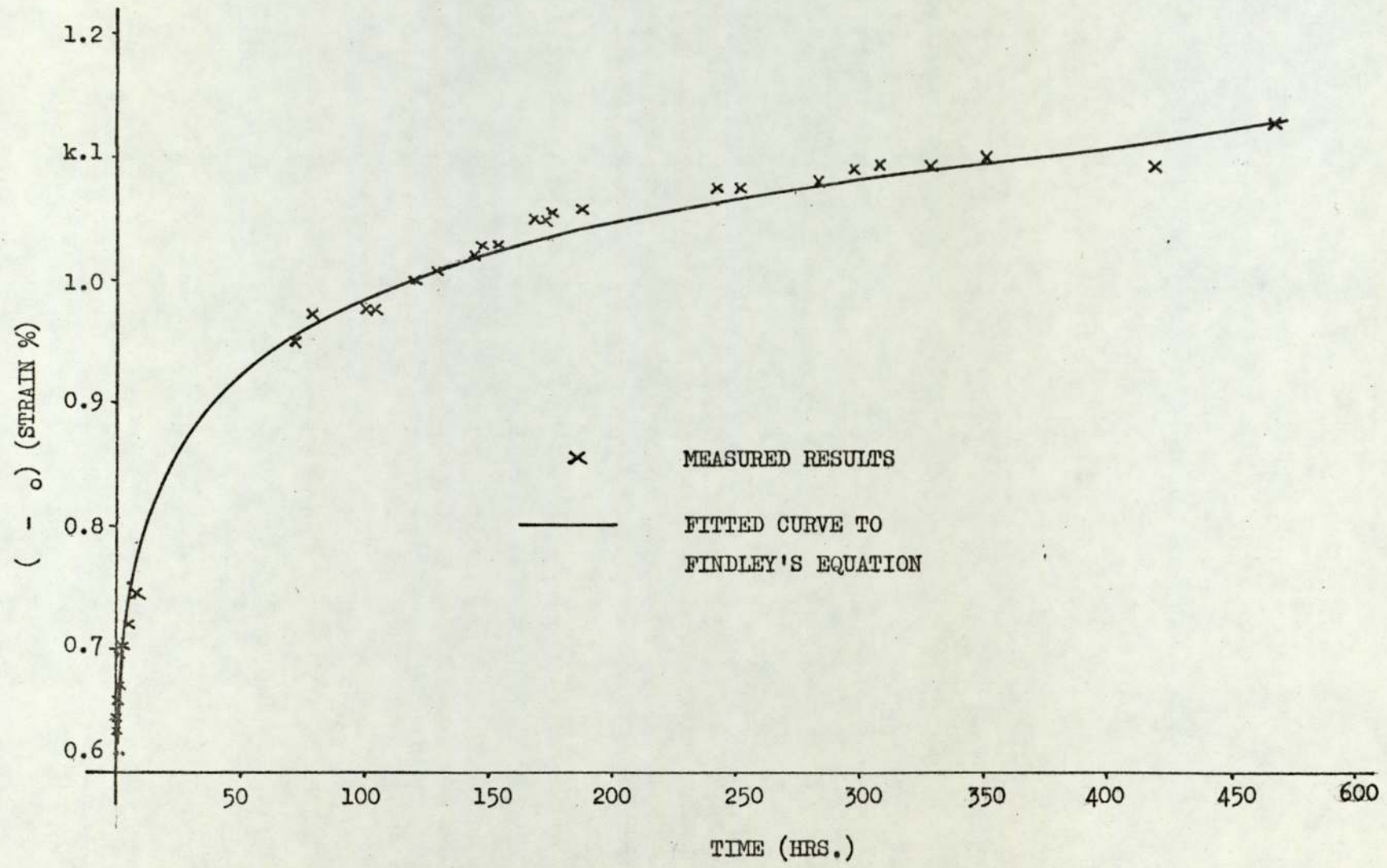


FIG. 3.22

GRAPH OF STRESS RUPTURE RESULTS AT 20°C AND 100% R.H.

FIG. 3.23 GRAPH OF CREEP RESULTS FOR CSM ($V_f = 16.5$)
ALL STRESS = 28 N/MM^2



RESULTS FITTED TO
FINDLEY EQUATION

66% CONFIDENCE
LIMITS

* TEST TERMINATION BEFORE
MATERIAL FAILURE

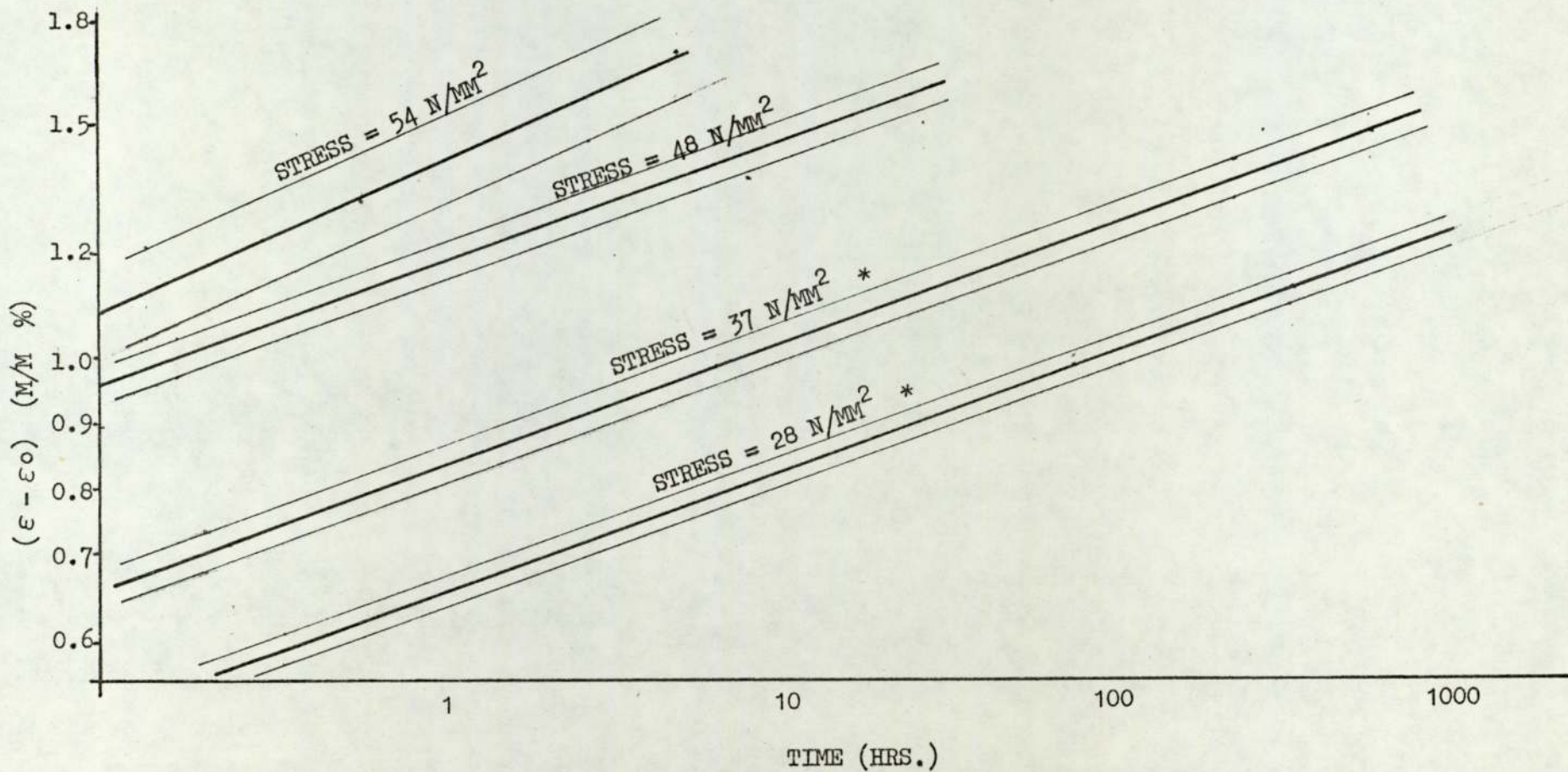


FIG. 3.24

SELECTED CREEP RESULTS OF

CSM : $V_f = 16.5\%$

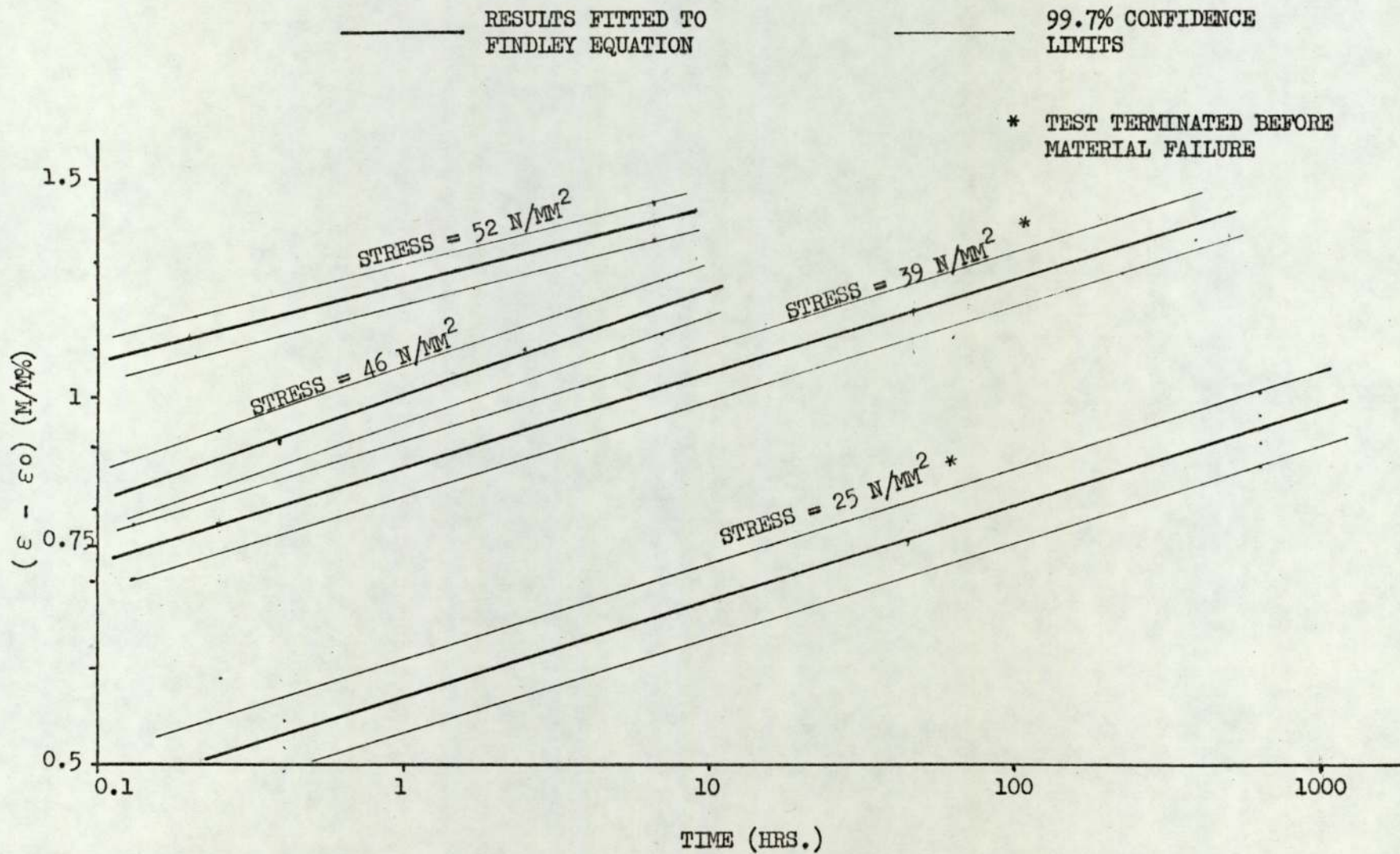


FIG. 3.25 CREEP RESULTS : CSM $V_f = 21.5\%$

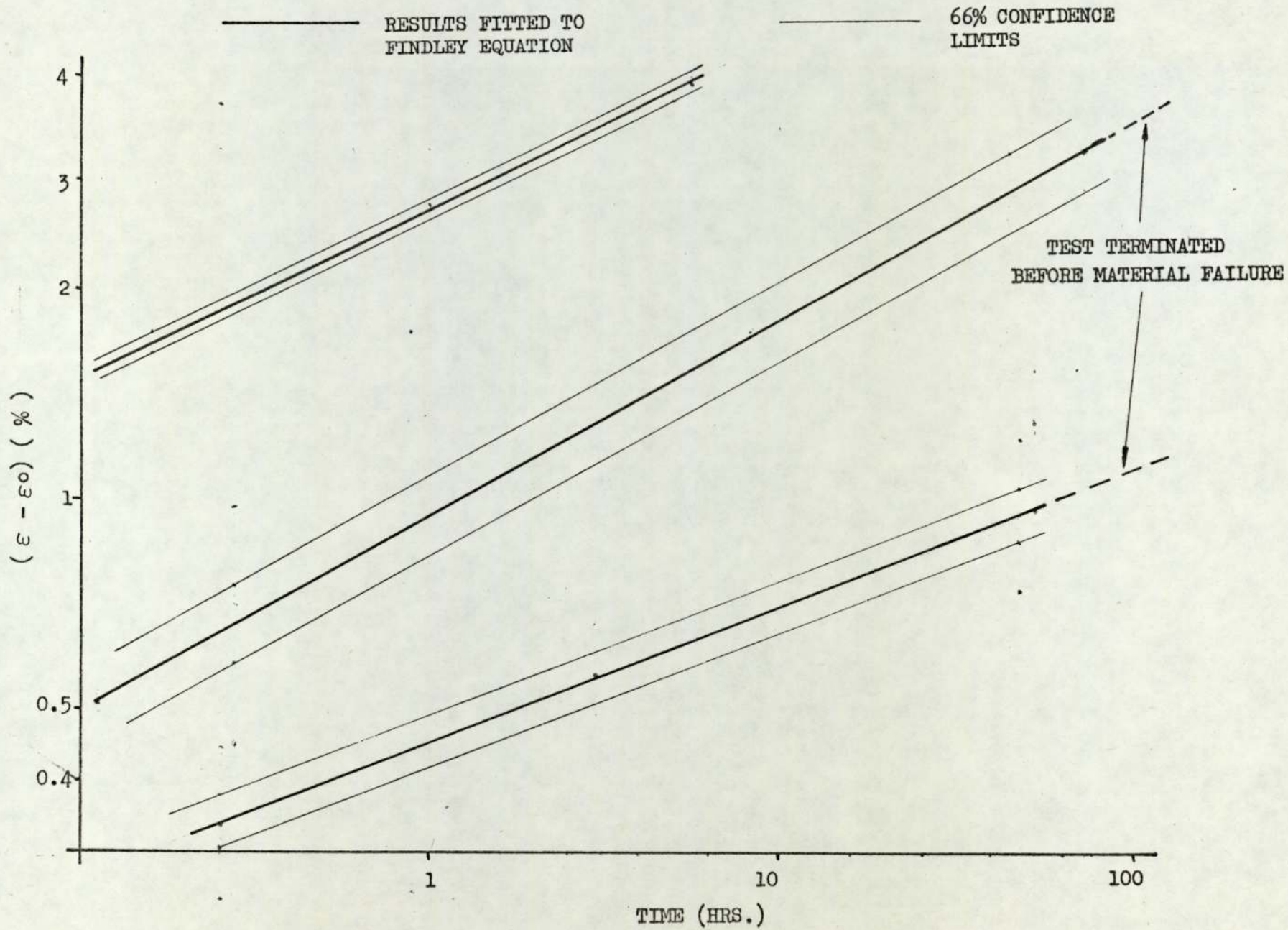


FIG. 3.26 CREEP RESULTS: + 45° BIDIRECTIONAL
WOVEN ROVING

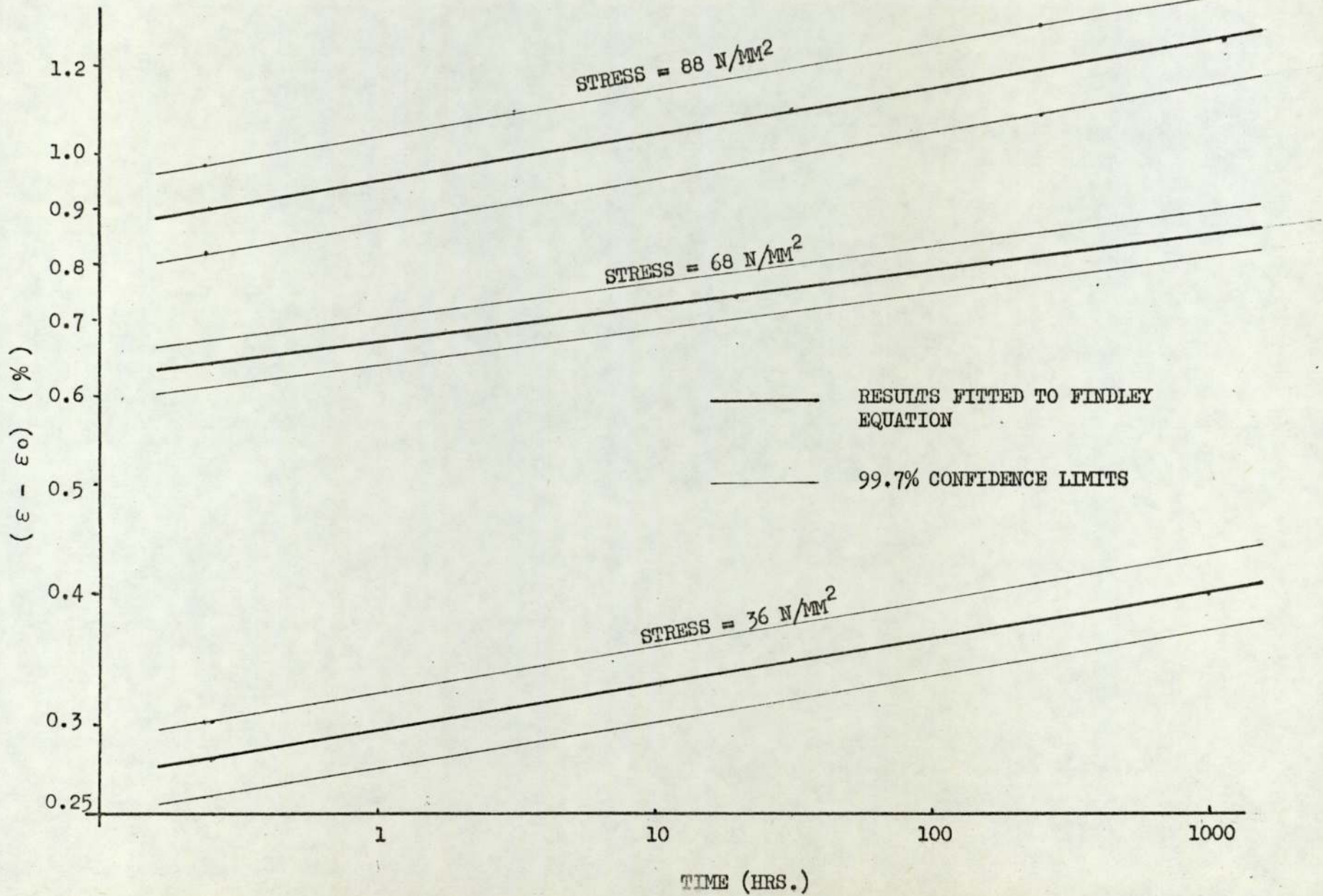


FIG. 3.27

CREEP RESULTS: BIDIRECTIONAL MOVEN

HOVING $\nu_g = 24\%$

———— RESULTS FITTED TO FINDLEY EQUATION
———— 99.7% CONFIDENCE LIMITS ON FIT

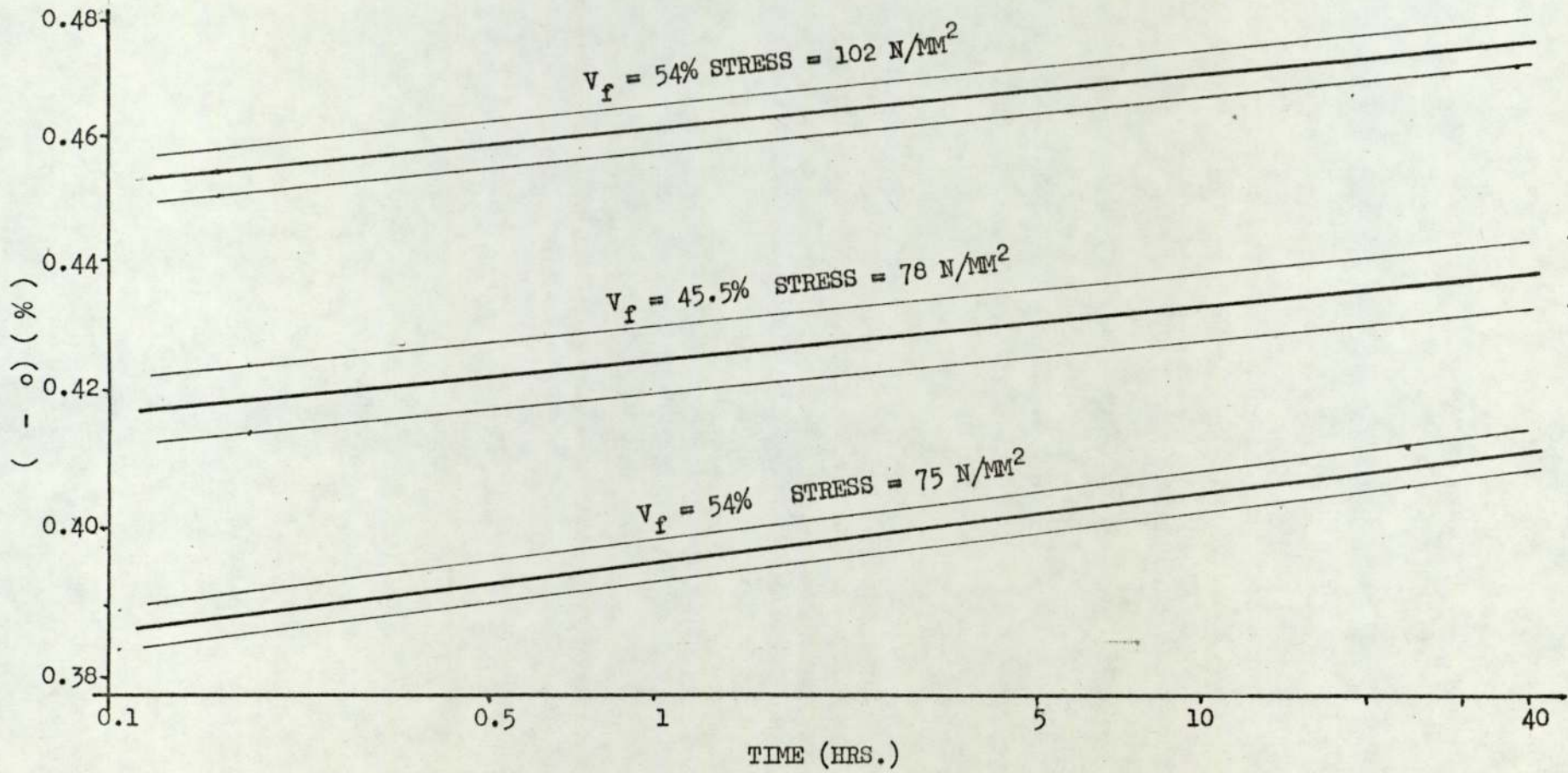
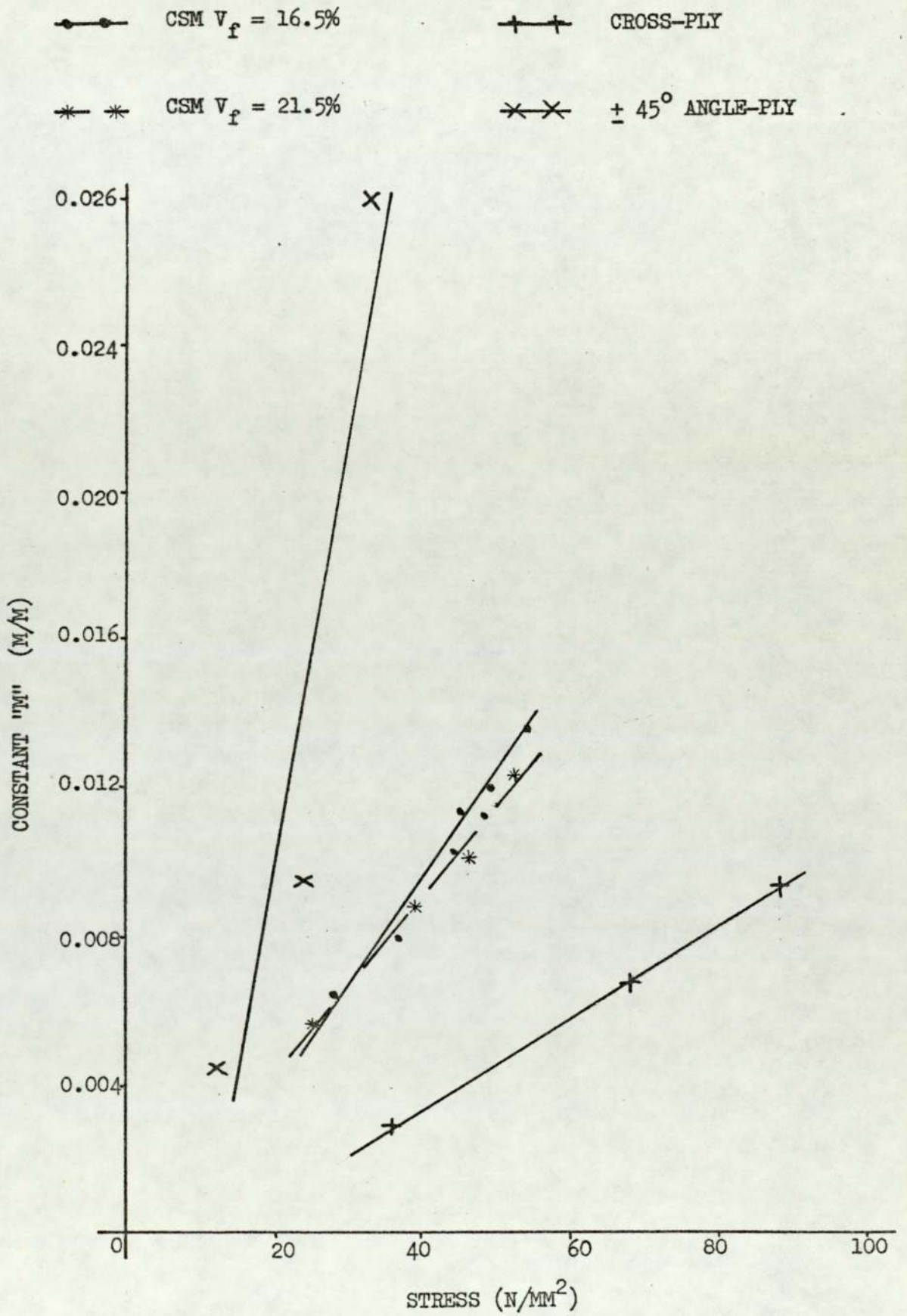


FIG. 3.28 CREEP RESULTS: UNIDIRECTIONAL MATERIAL

FIG. 3.29 GRAPH OF CONSTANT "M" AGAINST STRESS



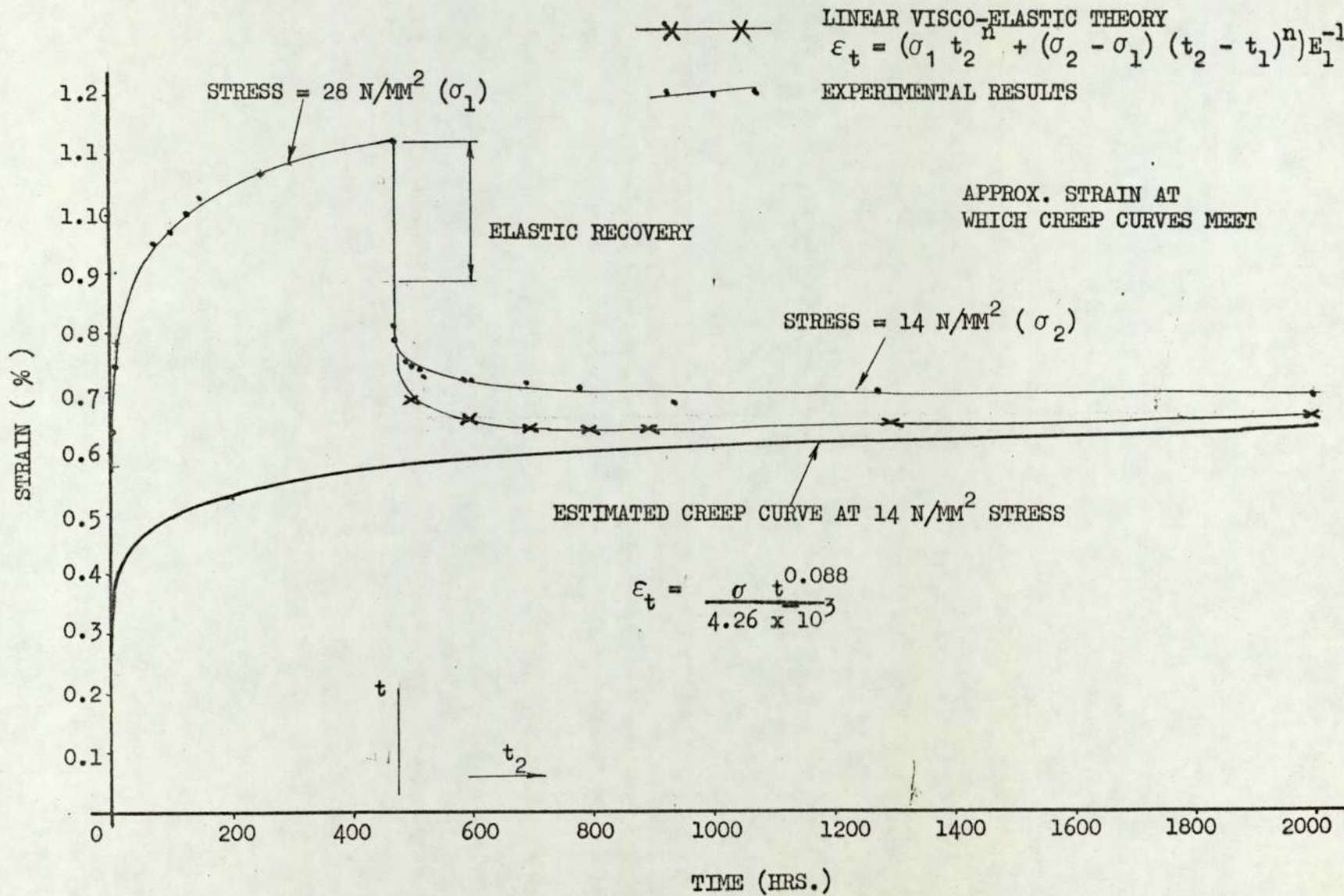


FIG. 3.30 CREEP RECOVERY

FIG. 3.31

CREEP SPECIMENS - CSM

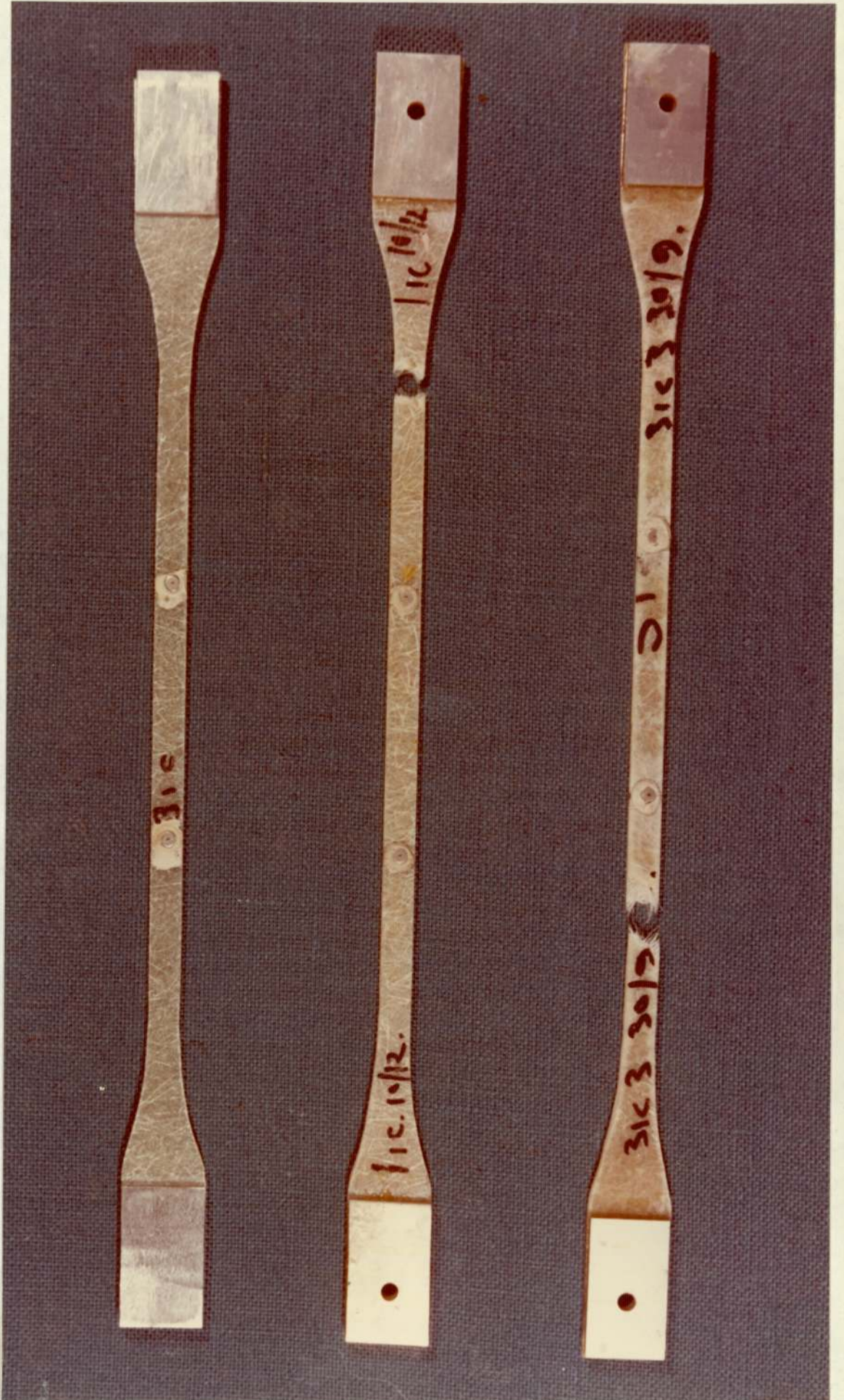


FIG. 3.32 CREEP SPECIMENS - BIDIRECTIONAL

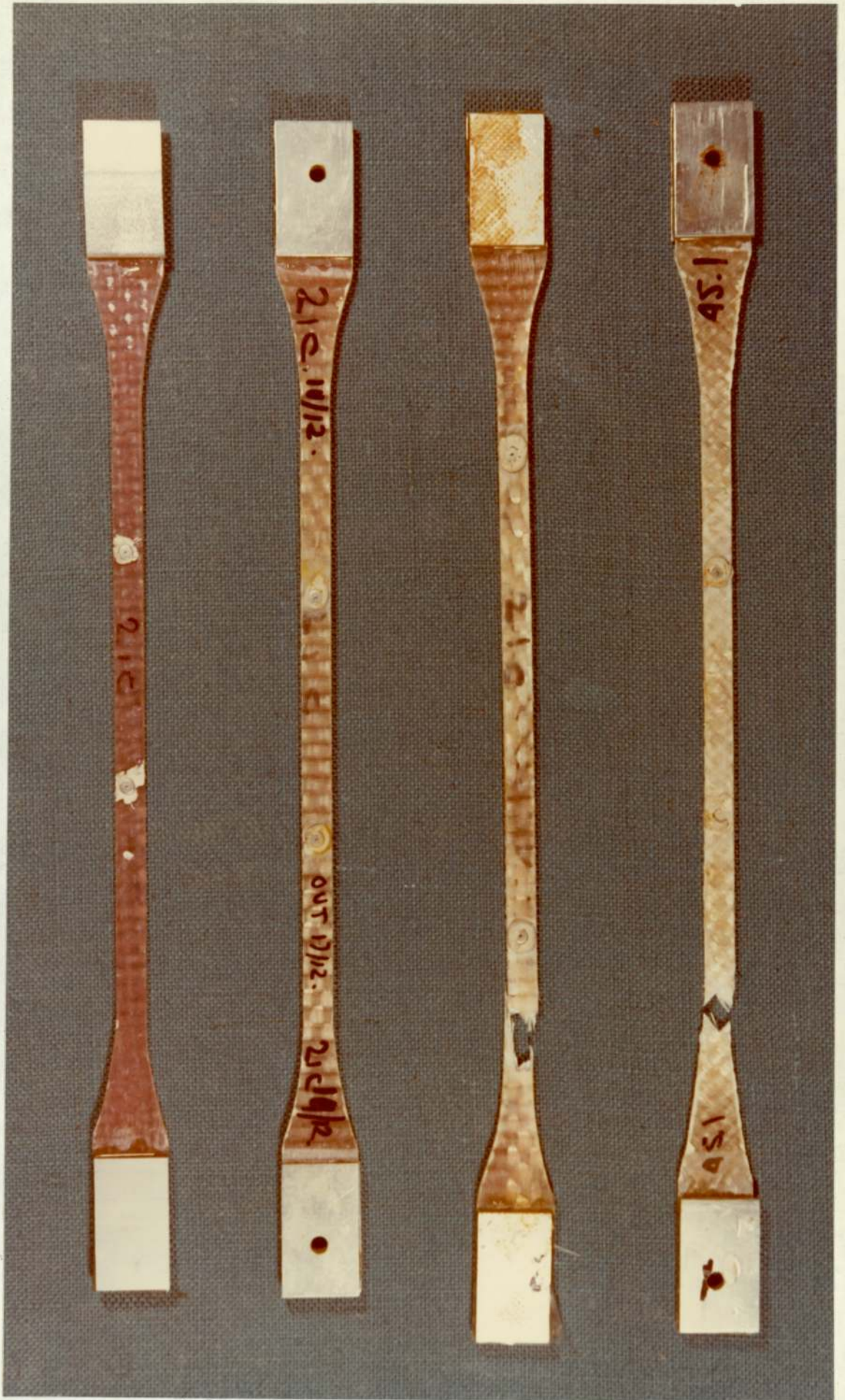


FIG. 3.33 CREEP SPECIMENS - UNIDIRECTIONAL



CHAPTER 4

STRUCTURAL ENGINEERING DESIGN WITH GRP

CHAPTER FOUR

Structural Engineering Design with GRP

4.1

Introduction

In previous chapters the structural properties of grp have been described. In the light of this the design process and the design of grp structures will be discussed. Information will be presented to assist in obtaining the most cost-effective solution.

In order to design well, the designer should thoroughly understand the materials with which he is working. This is imperative when composite materials such as grp are being used. In addition to the normal case, where the engineer just selects the material, when composites are used he must then go on and design the form of the material. Failure to do this will invariably lead to a product which is more costly than is necessary.

The result of material design will often be an anisotropic laminate. Consequently, the engineer will require a more general knowledge of elastic theory. However, stress analysis can often be simplified with judicious choice of the overall structural form. This need not lead to a loss in structural efficiency, since a design that simplified the stress analysis may also be an optimum design. For instance, the "Least Weight Design" of structures leads to a situation where all the stresses are either tensile or compressive [4.1]. A special case of this is where the structure conforms to the shape of its funicular polygon. Al-Khyatt [4.2] found that the optimum fibre orientation for a plate in pure shear to resist buckling was at 45° to the plate axes, which coincides with the direction of the tensile principal stress. In situations such as these, orientated and possibly unidirectional material can be used, and economy of materials obtained. The significance of this to the design process is that there is an important interaction between the overall structural design and material design.

Important considerations in the choice of overall design are: cost, durability and the aesthetic potential of the materials used. Structural designs where the "monochoque" principle is employed will fully utilise the potential of grp and offset its high cost. Hence designs in grp consisting of a superstructure and cladding as separate entities will not exploit the material to the full.

Material design is limited by the moulding techniques available, so that on occasions the ideal fibre orientation is not practicable. On the other hand, the mouldability of grp allows the designer to use efficient structural forms more readily than with other structural materials. The ability to use folded plates, singly and doubly curved shells, stressed skin space structures, sandwich structures, stiffened plates, and changes in thickness without greatly increasing production costs, assists relatively expensive and extensible grp to compete with other structural materials.

To summarise, the design process may be considered in four stages, viz.,

- a) Overall structural, or macroscopic design,
 - b) Material, or microscopic design,
 - c) Choice of moulding technique,
 - d) Reappraisal and integration of a), b) and c)
- for the optimum solution.

There are many different forms of glass fibres available commercially, such as chopped strand mat, rovings and woven rovings. The cost per unit weight of these different forms varies considerably; the roving being the cheapest, and combination products of chopped strands and woven rovings being the most expensive. The practicable fibre volume fraction also varies significantly from product to product (Fig. 4.10). Thus for a given structural use the best fibre orientation may not be the most cost effective.

To determine the relative cost effectiveness of the various laminates, the thickness (H) of a unit, 1 m^2 , is calculated for the range of fibre volume fractions.

$$H = (C_f D_f V_f + C_m D_m V_m)^{-1} \quad 4.1$$

where C_f = Cost of the fibre
 D_f = Density of the fibre
 C_m = Cost of the resin
 D_m = Density of the resin

The structural properties are then calculated for the laminates from fibre and resin properties using the Tasi approach (with $C = 0$) and the laminate theory outlined in Chapter 3. The cost effectiveness is then given by :

$$\text{Cost effectiveness} = \frac{\text{Structural property value at } V_f}{\text{Structural property value at } V_f = 0}$$

Various basic structural properties have been studied for two ratios of fibre cost to resin cost ($CF = \frac{C_f}{C_m}$) i.e. 1 and 1.5, together with four different fibre orientations: unidirectional, cross-ply, $\pm 45^\circ$ angle-ply and quasi-isotropic where $\alpha = 0^\circ, \pm 45^\circ, 90^\circ$. E-glass and BIP 836 polyester resin properties were used. The computer program used for the calculation is designed to handle any fibre and resin properties and all 4-fibre orthotropic systems, and is shown in Appendix B together with an example of the results.

4.3.1 Axial Stiffness

The axial stiffness cost-effectiveness (\overline{EEAN}) is given by:

$$\overline{EEAN} = \frac{(H \times E_1)}{(H \times E_1)} \frac{V_f}{V_f} = 0 \quad 4.2$$

Fig. 4.1 & 2 show graphs of cost effectiveness against fibre volume fraction for the material designs considered.

Unidirectional material is by far the most cost-effective, as may be expected, and generally the order of superiority follows the order in which the laminates have the highest proportion of fibres in the $\alpha = 0^\circ$ direction. The advantage gained by using unidirectional material is so great that even when the cost factor (CF) is 1.5 this material is superior to other fibre orientations when the cost factor is 1, assuming the same resin is used. In general, the cost-effectiveness is improved by increasing the fibre volume fraction.

4.3.2 Flexural Stiffness

The flexural stiffness investigated here is that which is appropriate to a narrow beam, but for simplicity the geometry of the laminate will be determined on the basis outlined above.

The flexural stiffness cost-effectiveness (FLEXN) is given by :

$$\text{FLEXN} = \frac{(E_1 H^3/12)_{V_f}}{(E_1 H^3/12)_{V_f} = 0} \quad 4.3$$

Figs. 4.3 & 4 summarise this investigation. For a particular cost factor (CF) the order of superiority of fibre orientation is the same as for axial stiffness since the elastic constant E_1 appears in both equations. The effect of changing the volume fraction is not so straightforward.

In several of the laminate designs examined the graphs show that there is an optimum volume fraction within the practical ranges. This is true for unidirectional materials at both CF values and is true for angle-ply and quasi-isotropic materials when $CF = 1$. With this value of CF, angle-ply is found to be most cost-effective at high and low volume fractions, and least when the fibre volume fraction is approximately 0.4.

When the cost factor is 1.5 the majority of laminates reduce in cost effectiveness with increasing fibre volume fraction within the practical ranges. The rate of reduction varies however, so that

a random reinforcement, which is basically an inferior material design for this property, becomes more cost-effective at low volume fractions than other orientations at the higher end of their practical ranges.

4.3.3 Shear Stiffness

The shear stiffness studied in this section is the inplane shear stiffness, and the corresponding cost-effectiveness is given by :

$$EGN = \frac{(G_{12} \cdot H)_{V_f}}{(G_{12} \cdot H)_{V_f = 0}} \quad 4.4$$

Cost-effectiveness in this case (Fig. 4.5) increases with increasing fibre volume fraction. The order of merit for material designs follows the order in which the materials have the largest proportion of their fibres in the $\pm 45^\circ$ directions, the unidirectional and cross-ply materials being equivalent.

As the practical range of fibre volume fractions varies for different material forms it is possible for unidirectional material to become more cost-effective than random or quasi-isotropic materials. This is the case for both cost factor values considered. For example, the range of cost-effectiveness for unidirectional material is from 1 to 2.2 whereas for chopped strand mat it is about 1.5 to 1.75 when $CF = 1.5$.

4.3.4 Plate Buckling

The buckling load of rectangular orthotropic plates under axial compression is given by [4.14]:

$$P_{cr} = \frac{k \pi^2 \left((D_1 \times D_2)^{\frac{1}{2}} + D_3 \right)}{b}$$

where k = a factor depending upon the aspect ratio and boundary conditions of the plate

b = width of the plate

$$D_1 = \frac{H^3 E_1}{12(1 - \mu_{12} \mu_{21})}$$

$$D_2 = \frac{H^3 E_2}{12(1 - \mu_{12} \mu_{21})}$$

$$D_3 = 0.5 (\mu_{12} D_2 + \mu_{21} D_1) + \frac{H^3 G_{12}}{6}$$

The cost-effectiveness is, therefore, given by :

$$PCRN = \frac{\left((D_1 D_2)^{\frac{1}{2}} + D_3 \right)_{V_f}}{\left((D_1 D_2)^{\frac{1}{2}} + D_3 \right)_{V_f} = 0} \quad 4.5$$

Figs. 4.6 & 7 illustrate the results on this basis. The most cost-effective fibre orientation at any particular volume fraction is $\pm 45^\circ$. The next most effective is the quasi-isotropic material, followed by cross-plyed and then unidirectional materials. The optimum fibre orientation of $\pm 45^\circ$ is also reported by Rothwell [4.11] after considering structural properties only.

In this case the cost factor is found to be dominant, so that all the materials with a CF of 1 are shown to be superior than those with a CF of 1.5. Thus for a given resin cost, materials incorporating the cheaper fibres ($\frac{2}{3}$ of the cost of the expensive ones) will be more effective no matter what fibre orientation is adopted. Thus rovings at 58p/kg used unidirectionally are superior to angle-ply woven rovings at 87p/kg even though the angle-ply orientation is more effective. These prices were approximately correct in February 1975. Although prices will change with time the ratios may be expected to remain similar and so the conclusions will remain valid.

When $CF = 1$ there are optimum fibre volume fractions for angle-ply, quasi-isotropic and cross-ply materials at approximately $V_f = 0.3$. For $CF = 1.5$ within the practical range of volume fractions, materials become less cost-effective with increasing volumes of fibre. However, because of the difference in the ranges of practical volume fractions the range of cost-effectiveness for isotropic materials is similar to that for $\pm 45^\circ$ angle-ply.

4.3.5 Cylinder Buckling

The buckling load of orthotropic, homogeneous cylinder walls under the action of axial compression is given, for long cylinders, by [4.12] :

$$\text{CYCR} = 2 \pi H^2 (0.666 \left(A_{12} + (A_1 + A_2)^{\frac{1}{2}} \right) A_3)^{\frac{1}{2}}$$

$$\text{where } A_1 = \frac{E_1}{1 - \mu_{12} \mu_{21}}$$

$$A_2 = \frac{E_2}{1 - \mu_{12} \mu_{21}}$$

$$A_3 = G_{12}$$

$$A_{12} = \frac{E_1 \mu_{21}}{1 - \mu_{12} \mu_{21}}$$

The cost-effectiveness is given by :

$$\text{CYCRN} = \frac{(\text{CYCR})_{V_f}}{(\text{CYCR})_{V_f} = 0} = 0 \quad 4.6$$

Figs. 4.8 & 9 show the cost-effectiveness against fibre volume fraction based on the above equation. The material order of merit is the same as for plate buckling for a given volume fraction. Under certain circumstances there are optimum fibre volume fractions as has previously been found when the cost-effectiveness has been a function of thickness (H) to a power greater than unity. In this particular case when CF = 1.5 the angle-ply and quasi-isotropic materials are optimum when the fibre volume fraction is approximately 0.25.

4.4

Process Economics

In section 4.2 it was stated that there was a large number of production processes available and choice of a process was an integral part of good design. In this section the economics of several production processes will be considered and compared. The

processes chosen for examination are thought to be relevant to long span structures, and were described briefly in Chapter 2.

To compare the processes it will be assumed that four types of product are to be manufactured; two simple and two relatively complicated (Figs. 4.11 & 12). One of each type will be small and the other large. The direct production costs of the products will be calculated at various production rates to broaden the comparison. The production costs will be divided into fixed costs per product and costs which depend upon the production rate. In calculating the costs, the following assumptions will be made :

- 1) Working hours - three 8 hour shifts per day,
5 days per week and 49 weeks per year.
- 2) Capital Amortisation - Capital goods will be
amortised over a period of 5 years.
- 3) Labour costs - £4,000/an. per Foreman for 40
hours per week = £2.04/hr.; Semi-skilled men -
£3,300/an. = £1.68/hr.; Unskilled labour
£2,900/an. = £1.47/hr.
- 4) Costs of less than £0.01 will be rounded off
to £0.01.

The hand lay-up process is treated as the basic process and the others as modifications to this.

4.4.1 The Hand Lay-up Process

Labour Costs :

Labour times and activities may be divided as follows for each moulding :

1) Mould preparation time (WT): it is assumed that moulds require treating with release agent after every sixth moulding and that this takes 2 man minutes/unit surface area of the mould.

$$\therefore WT = \frac{SA \cdot 2}{60 \cdot 6}$$

$$= \frac{SA}{180} \quad (\text{m hrs.}) \quad 4.7$$

where SA = Product surface area.

(All times are measured in man hours.)

2) Material preparation time (MPT): the time for material preparation per product is taken to be a linear function of the product edge length.

$$MPT = (PEL \times 0.0028 + 0.017) \quad 4.8$$

where PEL = Product edge length.

3) Lay-up time : the lay-up time depends upon the weight of the product and the lay-up rate. The lay-up rate (LUR) is a function of the surface area of the mould and its complexity. The complexity is measured as the quotient of the plan area (PA) and the surface area (SA) of the mould.

$$LUR = \left(11 - \frac{6}{(1 + SA + SA^2/2)} \right) \frac{PA}{SA} \quad 4.9$$

Thus a maximum lay-up rate of 11 kg/hr. is assumed. The lay-up time is given by :

$$LUT = \frac{W}{LUR} \quad 4.10$$

where W = Weight of product.

4) Stripping Mould Time : the time required to remove the finished product from its mould is based upon the edge length of the product and its complexity.

$$\text{Stripping mould time (SMT)} = \frac{PEL}{240} \times \frac{SA}{PA} \quad 4.11$$

5) Product Trimming Time : the trimming time is assumed to be a function of the edge length and the thickness (TK) of the material to be cut.

$$\text{Trimming time (TT)} = \frac{PEL \times 2 \times TK}{60 \times 0.003} \quad 4.12$$

All the above activities may be carried out by unskilled labour with the exception of the laminating procedure which requires semi-skilled labour. However, the semi-skilled labour time is much greater than the unskilled labour time so that only semi-skilled labour will be used.

$$\therefore \text{Total man hours} = WT + SMT + TT + MPT + LUT \quad 4.13$$

Labour costs are calculated assuming that labour works at 85% efficiency. Provision for a foreman is made by allowing $12\frac{1}{2}\%$ of a foreman's salary to be added to each worker's wage.

From the above, the labour costs for each product can be calculated for various production levels. At least one of the production levels chosen will be one at which labour is used to the maximum efficiency so that the labour cost is at a minimum.

Mould Costs:

To calculate the cost of mould the following will be assumed:

1) The production moulds are made from mould masters which are made from a master mould which in turn is made from a pattern.

2) The production moulds are made of glass-reinforced epoxy resin.

3) The life of production moulds and mould masters is 500 products.

4) The cost of patterns and mould masters is written off over 5 years.

5) Cost of patterns and master moulds

$$= (100 \cdot SA + 100) \frac{SA}{PA}^{0.14} \quad 4.14$$

$$= CPAMM (\pounds)$$

Cost of one mould master = 0.65 CPAMM

Cost of one production mould = 0.5 CPAMM

Mould Usage :

The number of production moulds required depends upon the production rate and the time that the mould is in use for each product (MT). A mould utilisation factor of 0.9 is allowed.

$$MT = (WT + LUT + CT + SMT) \frac{1}{0.9} \quad 4.15$$

$$\text{Cure Time (CT)} = (1.5 + 0.6 \cdot (\text{weight of resin per unit area kg/m}^2))$$

The number of moulds required (NOMR) is therefore:

$$NOMR = \frac{MT \cdot PRPD}{24} \quad 4.16$$

One mould master will be allowed for every 5 production moulds. Hence the number of mould masters required is:

$$NOMM = \frac{NOMR}{5} \quad 4.17$$

Mould costs per product:

$$\text{Cost per product for one mould master} = \frac{0.65 \times \text{CPAMM}}{500}$$

Total cost per product for mould masters =

$$\frac{NOMM \times 0.65 \cdot \text{CPAMM}}{PRPD \cdot 1225}$$

From equation 4.16 and 4.17 this can be simplified to:

$$\text{Cost of mould masters/product} = \dots \quad 4.18$$

$$MT \cdot \text{CPAMM} \cdot 0.44 \cdot 10^{-5}$$

$$\text{Production mould cost per product} = \frac{0.5 \text{ CPAMM}}{500} \quad 4.19$$

Cost of pattern and master mould per product

$$= \frac{\text{CPAMM}}{\text{PRPD } 1225} \quad 4.20$$

Thus the cost per product of the production moulds and the mould masters is independent of the production rate.

Factory Costs :

Factory costs are based upon the plan area of the product, and provision for floor space for material preparation, product storage and administration with a factory rent per unit area per annum of £7.3 $\boxed{4.3}$.

$$\text{Factory area per mould (APM)} = (\text{PA}^{\frac{1}{2}} \times 1.73)^2 \cdot 1.3 \quad 4.21$$

Factory costs per product (FC) are therefore given by :

$$\text{FC} = \frac{\text{APM} \cdot \text{NOMR} \cdot 7.3}{\text{PRPD} \cdot 5.49}$$

With the use of equation 4.16 this simplifies to:

$$\text{FC} = \text{APM} \cdot \text{MT} \cdot 0.124 \times 10^{-2} \quad 4.22$$

Energy Costs :

Since no large machinery is used in this process the energy used will be for environmental purposes. Therefore, it will be assumed that the power consumed will be proportional to the floor area and thus the factory costs.

$$\text{Energy cost per product} = \frac{1}{3} \text{FC} \quad 4.23$$

Product Handling Equipment :

This equipment is only required for large products A and B and is used for lifting them from their moulds.

Capital cost of equipment = £1,000

$$\text{Cost per product} = \frac{1000}{\text{PRPD } 1225} \quad 4.24$$

The results of the hand lay-up process cost analysis are shown in tabular form in Figs. 4.13 & 14 and in graphical form in Figs. 4.25 - 28.

4.4.2 The Basic Spray-up Process

Labour Costs :

Labour costs in this case may be divided into those appropriate to unskilled labour and those which must be carried out by semi-skilled labour as follows:

Unskilled Activities:

- 1) Trimming - time as hand lay-up.
- 2) Mould preparation - time as hand lay-up.
- 3) Mould stripping - time as hand lay-up.
- 4) Material Preparation.
- 5) Material Consolidation.

Semi-skilled Activities:

1) Spray-Up.

Labour times unique to the activities of the spray-up process are as follows:

a) Material Preparation : the time involved in this activity per product is, compared to the hand lay-up process, very small since the spray-up machine can draw resin from bulk supplies and the glass fibre does not require tailoring. This activity is assumed to take 0.25 minutes per 10kg of laminate.

b) Spray-Up : the spray-up rate is normally between 5 - 10 lb of laminate per minute depending upon the size and complexity of the mould.

The spray-up time (SUT) is given by:

$$SUT = \frac{W}{0.454 \cdot 8.60} \frac{SA}{PA}^{\frac{1}{2}} + 0.2 \quad 4.26$$

c) Material Consolidation Time : this time is calculated as:

$$RDT = 2 \cdot SUT \quad 4.27$$

Hence, total unskilled labour time (ULT) is given by :

$$ULT = (TT + WT + SMT + MPT + RDT) \frac{1}{0.85} \quad 4.28$$

Total semi-skilled labour time (SST) is:

$$SST = \frac{SUT}{0.85} \quad 4.29$$

Labour Costs :

Labour costs are calculated with a minimum labour force of 1 foreman and 1 semi-skilled operator. In this case all the operations are carried out by the semi-skilled workman. The labour costs are also calculated with both semi-skilled and unskilled operators fully utilised.

Spray-Up Machine Costs :

It is assumed that a machine utilisation factor of 0.75 applies. As indicated earlier capital equipment is written off over 5 years.

Cost of machine = £2,500

Machine cost per product = $\frac{2,500}{\text{PRPD } 1225}$ 4.30

where PRPD = number of products produced per day per machine

$\text{PRPD}_{\text{max}} = \frac{0.75}{\text{SUT}}$ 4.30

Mould Costs :

Mould costs are calculated on the same basis as for the hand lay-up process.

Factory Costs :

Again, these are based on the principles outlined under the hand lay-up process.

Energy Costs :

$$\text{Cost per product} = \text{PA} \times 0.0096 \qquad 4.31$$

The above formula is based upon information taken from a Pilkington internal report [4.3].

Product Handling Equipment Costs :

These are calculated in the same way as for the hand lay-up process.

Costs at various production levels considered are tabulated in Figs. 4.15 & 16 and are shown graphically in Figs. 4.25 - 28.

4.4.3 The Robot Spray-up Process

This process is essentially the same as the basic spray-up process except that a machine performs the semi-skilled operator's function of spraying-up the laminate. Consequently, the only difference in the cost calculations is that the semi-skilled labour cost is replaced by an increased machine cost.

The capital cost of the robot spray machine is taken to be five times that of the basic spray-up machine at £12,500.

Tables in Figs. 17 & 18 show production costs which are also illustrated graphically in Figs. 4.25 - 28.

4.4.4 The Continuous Spray-up Process

The continuous spray-up process is similar to the continuous laminating process described in Chapter 2, except that discrete moulds are used rather than a continuous mould. Unlike the previous spray-up processes where the spray gun is passed over the mould, in this process the mould is passed under the gun. The gun is held by a machine which is capable of making reciprocating movements in a transverse direction relative to the mould. Thus as in the robot spray-up process only unskilled labour is required. Although the robot is more versatile in movement and in directing the spray the continuous spray-up machine is capable of depositing 4 times the quantity of material per unit time.

Labour and energy costs are calculated by the same procedure as that for the robot spray-up process. Product handling equipment, factory costs and mould costs are calculated on the same basis as for the hand lay-up process. The machine cost calculations, based upon an acquisition cost of £12,000, follow the same procedure used for the costing of the basic spray-up machine.

A cost summary is tabulated in Figs. 4.19 & 20 and illustrated graphically in Figs. 4.25 - 28.

4.4.5 The Resin Injection Process

Labour Costs :

Mould preparation time : this is taken as twice that required for the hand lay-up process since it is a closed mould process.

Material preparation time : as hand lay-up.

Resin injection time (IT) : this is based upon a resin injection rate of 8 lb/min.

$$IT = \frac{W \times 0.75}{8 \times 60} \quad 4.32$$

Stripping mould time : as hand lay-up.

Trimming time : this is taken as half that required for hand lay-up since the edge of the product is pinched between the two halves of the mould. The glass fibre in this area is starved of resin, making cutting easier.

Mould costs :

Mould costs are based upon those calculated for hand lay-up moulds, but modified as follows: for products C and D, production mould costs are assumed to be 2.5 times those for hand lay-up. For products A and B, costs are taken as 3 x hand lay-up costs. The larger factor employed for products A and B is to allow for mould-opening devices. These devices are necessary due to the weight of the moulds. In calculating the cost per product of the mould master,

equation 4.18 is modified by replacing the mould committed time (MT) by a cycle time (CYT) as follows:

$$\text{Mould master cost per product} = \text{CYT} \cdot 0.49 \cdot 10^{-15} \times \text{CPAMM} \quad 4.33$$

$$\text{where CYT} = 0.019 \times W + 0.066 \quad 4.34$$

Machine costs : machine costs are based on an acquisition cost of £3,000 and a utilisation factor of 90%.

Product handling equipment : as hand lay-up.

Energy costs : as spray-up.

Factory costs : again these costs are based upon the hand lay-up process calculation but the mould committed time (MT) is replaced by cycle time; CYT.

4.4.6 The Hot Press Process

Labour costs : for the analysis of this process it is assumed that there is a minimum labour force of three: a press operator, a material preparation labourer and a product deflashing labourer. Hourly labour costs are therefore:

$$3 \times \text{£}1.47 = \text{£}4.41/\text{hr.}$$

$$\text{Labour cost per product} = \frac{4.41 \times 24}{\text{PRPD}} \quad 4.35$$

Press costs : the costs adopted for the presses are based upon information received from FRP. Applications Dept., Fibreglass Ltd.

For products A & B Press Cost = £50,000

For products C & D Press Cost = £5,300

Press costs per unit produced are calculated on the same principles used for the basic spray-up process with a machine utilisation factor of 0.85. The maximum production level per day is given by:

$$\text{PRPD}_{\text{max}} = \frac{0.80 \cdot 24 \cdot 60}{\text{CYT}} \quad 4.36$$

where 0.80 = a factor allowing for labour and machine inefficiency.

CYT = Cycle time (mins.)

$$\text{CYT} = \text{TK} \times 0.42 \times 10^3 + \text{PA} \cdot 0.23 + 1.5$$

TK = thickness of product (M)

Mould costs : these costs are again based upon information recieved from Fibreglass Ltd.

$$\text{Cost of Mould (TC)} = 1500 \cdot \frac{\text{SA}}{\text{PA}} \text{SA}^{0.14} + 2500 \quad 4.37$$

The life of hot press moulds are taken as 10,000 products therefore:

$$\text{Cost of moulds per product} = \frac{\text{TC}}{10,000} \quad 4.38$$

Factory costs : the same cost per unit floor area is used as for hand lay-up i.e. £7.3/m²/an. The floor area required is based upon the plan area of the press being equal to that of the product plus an additional area round the press 3M wide; a further

factor of 1.3 is allowed for storage etc. Thus factory costs are given by:

$$FC = \frac{7.3 \text{ APM}}{\text{PRPD } 5 \times 49} \quad 4.39$$

Energy costs : these are assumed to be 3 x hand lay-up costs.

Hence :

$$\text{Energy costs} = FC \quad 4.40$$

Product handling equipment : as hand lay-up.

Calculations are summarised in Figs. 4.23 - 28.

4.4.7 Discussion of Process Analysis

The tables shown in Figs. 4.13 - 24 reveal that in general, labour is still the major direct production cost even when machinery is used, although in the resin injection and hot press processes the production mould is also a major cost area.

In interpreting the graphs, Figs. 4.25 - 28 the important aspects are the cost at which the graphs level out and at what production rate this happens. The hot press process is shown to be most economical for product types A, B and D at high production rates. Graphs for the hand lay-up process level out at the lowest production rates, but usually at a much higher cost level. In the majority of cases there is little to choose between resin injection and basic spray-up. However, resin injection costs reduce to a more economical

level when the product is complicated, and vice versa when the product is plain. Little difference is shown between robot and continuous spray processes but robot spray is more economical than the basic spray-up process at high production levels. The choice between the various spray-up processes and resin injection will be based upon factors other than production costs such as: the type of reinforcement required, whether two smooth surfaces are required, and whether changes in material thickness are required.

When direct production costs are compared to material costs, based on a laminate cost of 65p/kg, at medium to high production levels, products A and B show material costs approximately ten times greater than those for production. Hence, at these production rates if some material can be saved or cheaper material used, for marginal increases in production costs, significant savings could be made on large products.

The effect of changing the capital amortisation period to two years would have little effect on the relative merits of the various processes considered. This is the case since the capital repayment costs per product are normally of the order of 10% of the total direct production costs. If the number of shifts per day was reduced but the production level kept constant the main effect would be to reduce the competitiveness of the capital-intensive processes, since the production rate per machine per unit time would be reduced and the initial capital outlay increased.

In simple stress fields such as pure tension, compression or pure shear it can be seen from the sections on material cost-effectiveness (4.3) and theoretical material properties (3.2 & 3.3) that the strongest, stiffest and cheapest laminates are obtained when the fibres lie in the directions of the principal stresses. When the secondary principal stress approaches zero, unidirectional material may be used. In more complicated stress fields, for example around bolt holes, the situation is not as clear.

Since the equations for Mohr's stress circle are independent of material properties [4.4] they apply equally to anisotropic and isotropic materials. Thus under a given set of loads the principal planes are always in the same direction. If it is accepted that the fibres are the main strength and stiffness giving constituent and that they are best used in pure tension or compression the fibres should follow the directions of the principal stresses.

In many circumstances the principal planes will change direction frequently and in a complicated manner, and it will not be practical for the fibres to follow. However, in such circumstances compromises between the ideal and the practical may be beneficial. For example, the fibre orientation shown in Fig. 4.29 would be expected to give a higher tensile strength to the component when loaded via a bolt, than a pure unidirectional laminate.

The design of joints in grp requires more care than is normally necessary in steel, because grp is brittle and joints usually cause stress concentrations. Brittle materials cannot stress-relieve in areas of stress concentration and thus these high stresses must be borne by the material elastically. This disadvantage is compounded by the fact that stress concentrations are often larger in anisotropic materials. The use of additional material in areas of high stress is one solution to the problem, but this is likely to be expensive, due to the high cost of the material, and also, in extreme cases, ugly.

There are three basic types of jointing system which are applicable to grp and will be discussed below:

- a) Adhesive
- b) Mechanical
- c) Combination of a) and b)

It should be noted that when thermosetting resins, such as polyester, are used there is no jointing process equivalent to welding.

4.6.1 Adhesive Joints

Good joint design in grp will minimise the stress concentrations associated with the joint. Adhesive joints provide the best

opportunity for doing this. In general the stress flow lines should be interrupted as little as possible and joints should be based on shear, tensile or compressive stresses; peeling stress situations should be avoided (Fig. 4.30).

Joints between adherends fall into three categories: butts, laps and scarfs (Fig. 4.31). Simple configurations of each of these have been treated theoretically [4.5]. However, only in the case of lap joints in tension is it possible to calculate analytically the stress concentration, and then only when the adherends are isotropic.

For a simple tensile joint the scarf type is preferable with a stress concentration factor of 1.45 or less having been determined empirically. The scarf joint is also recommended for compressive joints. Fig. 4.31 shows a variation of the pure scarf joint known as a landed scarf joint. Landed scarf joints are useful for taking compressive loads, controlling the thickness of the adhesive and location of the adherends during assembly. However, they need to be used carefully if high stress concentrations are to be avoided.

By increasing the area of the scarf joint it is possible to obtain a joint of greater strength than the adherends and so failure may be expected to occur in the adherends rather than in the adhesive. In many cases the joint strength will be limited by the interlamina shear strength of the adherend.

Butt joints (Fig. 4.31) are special cases of scarf joints in which the scarf angle is 90° . The joint area in this case is limited to the cross-sectional area of the adherends and is therefore

not normally suitable for tensile use. However, like scarf joints, butt joints are relatively free of stress concentrations and under compressive conditions the full strength of the adherend may be developed.

Single flat lap joints in tension experience considerable stress concentrations due to shear and bending forces in the adherends. Goland and Reissner [4.6] have developed a theory for predicting the shear and normal stresses throughout the joint. They found that the maximum stresses occurred at the ends of the adhesive and that the ratio of the maximum stress to the mean stress increased with increasing lap length. Consequently, it is more effective to increase the width of the joint rather than the length of the lap. Stress concentrations can be reduced by bevelling the ends of the adherends (Fig. 4.31).

Double flat lap joints, fig. 4.31, are stronger in tension and compression than single lap joints since bending and hence stress concentrations are reduced, due to the symmetry of the joint.

Adhesive joints suffer from three main disadvantages. Firstly, the adherends often have to be held in position for considerable periods of time whilst the adhesive cures. In many civil engineering structures this could prolong erection time and lead to additional expense. Strong adhesives, usually being polymers, are subject to creep and stress rupture. As a result, structures which are loaded for long periods may not be best served by adhesive joints. Lastly, the quality of these joints is difficult to guarantee under site conditions because of the difficulty in maintaining cleanliness and the difficulty in checking whether a finished joint is upto the required standard.

Some of these problems can be partly overcome: heat may be applied to the adhesive but cure time may still be up to an hour or more; film adhesives ensure that the adhesive thickness is uniform and reduces the number of voids but the quality of the adherends' faces still remains a problem.

4.6.2 Mechanical Joints

Mechanical joints, in this case, may be divided into two sections: those joints which rely upon the shear strength of bolts or rivets; and those which depend on friction to transmit forces. In the second category it is usual to use high tensile bolts which compress the joining components together. High shear forces are then required to overcome the friction between the components. This type of joint is not considered suitable for use with grp because this material will creep under the bolt force and thereby relieve the tension in the bolt and weaken the joint. Also, crushing of the grp under the bolt may cause premature cracking and lead to failure.

Mechanical shear joints inevitably cause considerable stress concentrations in the region of the bolt or rivet. Lap and flange joints are the most common types, a few of which are shown in Fig. 4.32. As with adhesive joints, lower stresses in double lap joints lead to higher strength than is the case with single lap joints.

Bolted shear joints have the advantages that they are convenient to assemble and that they are not permanent, so that components may be replaced without difficulty.

In contrast to the situation with joints in steel, only a limited amount of experience has been documented on bolted joints in grp. Youngs [4.7] found that in order to prevent joint failure to the side or edge of a laminate the following rules should be applied: the distance from the centre of the bolt hole to the edge should be at least 4.5 times the hole diameter (D), and the distance from the side should be 3.0 D for woven fabrics. For CSM the side distance should be increased to a minimum of 3.5 D. It was found that with the failure to the sides and edge of the laminates suppressed, failure occurred by crushing of the material under the bearing load. The bearing failure load was found to be an undefined function of the laminate's compressive strength.

Several other "rules of thumb" are also available from the works of Youngs, Weiss and Strauss [4.7 - 9]. Several small diameter bolts are preferable to a smaller number of larger - diameter bolts. The ratio of the diameter of the bolt (d) to the thickness of the section (t) is significant and a d/t ratio of 1 gave higher strengths than a ratio of 1.5. Bolt holes may be punched or drilled and should have a 0.4 mm clearance on the diameter, they should also be well aligned to avoid unnecessarily high stresses. Excessive torque applied to the bolts should be avoided since this can lead to crushing of the material under the nut and bolt head.

4.6.3 Combination Joints

Combination joints have been designed in an attempt to avoid some of the disadvantages and combine some of the advantages of bolted

and adhesive joints. In one type of combination joint a ductile metal is used in combination with grp. The metal is moulded in situ during laminating and is used for bolting through. Fig. 4.33 shows some examples of this type. This figure also shows an adhesive lap joint with bolts near the ends of the laps. It is suggested [4.10] that this combination may be advantageous under fatigue loading. In addition the bolts would provide positive location for the joint and support during cure of the adhesive.

4.7

Safety Factors

Makowski [4.13] suggested the following safety factors :

Static loads of short duration	1.5 - 2
Static loads of prolonged duration	3 - 4
Cyclic loads	4
Fatigue loading	6
Impact loads	10

These safety factors are based on stress considerations alone, and are to be employed to obtain allowable working stresses. Further factors have to be used if there is any ignorance of the level of the applied stress. An alternative approach is to design on the basis of allowable strain. In a proposed B.S.I. specification for "Vessels and Tanks in Grp" the allowable strain (ϵ_w) is given by the smaller of

$$\epsilon_w = 0.05 \quad \epsilon_r$$

$$\epsilon_w = 0.2\%$$

where ϵ_r is the percentage elongation to failure of the resin. This approach is convenient when designing against creep.

Neither of the approaches described above allow for the time-dependent nature of the properties of grp in any precise manner. This can lead to over-conservative design or at the other extreme, an inadequate design. . Further, when designing on the basis of allowable strain, the fact that some materials (Boller - woven roving [3.26]) fail at larger strains with increasing time but at reduced stress, and other materials at reduced stress and strain, makes this approach more unsatisfactory.

For efficient design in grp it is necessary to know both the creep and stress rupture properties of the laminate used. As these properties depend upon the environment this must also be known. A "design life" must also be chosen for grp structures. With this information available, economy in the use of grp may be achieved and its full potential for efficient structural design realised by the choice of realistic safety factors.

FIG. 4.1 MATERIAL COST EFFECTIVENESS

- AXIAL STIFFNESS

—●— UDR $\alpha = 0^\circ$
—+— BIR $\alpha = 0^\circ, 90^\circ$

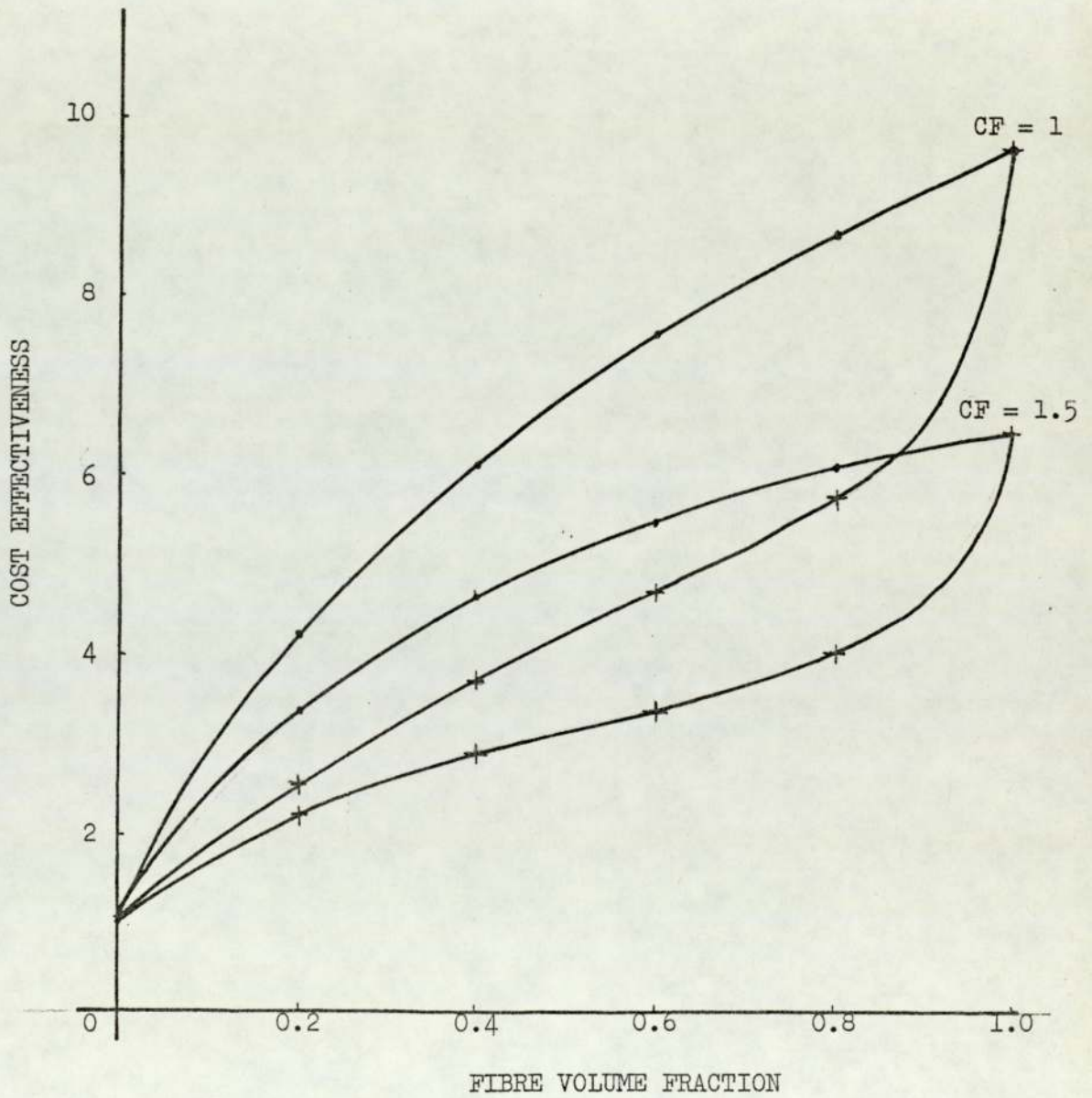


FIG. 4.2 MATERIAL COST EFFECTIVENESS

- AXIAL STIFFNESS

—*—*—*—* ANGLE-PLY $\alpha = \pm 45^\circ, 90^\circ, 0^\circ$

—x—x—x—x ANGLE-PLY $\alpha = \pm 45^\circ$

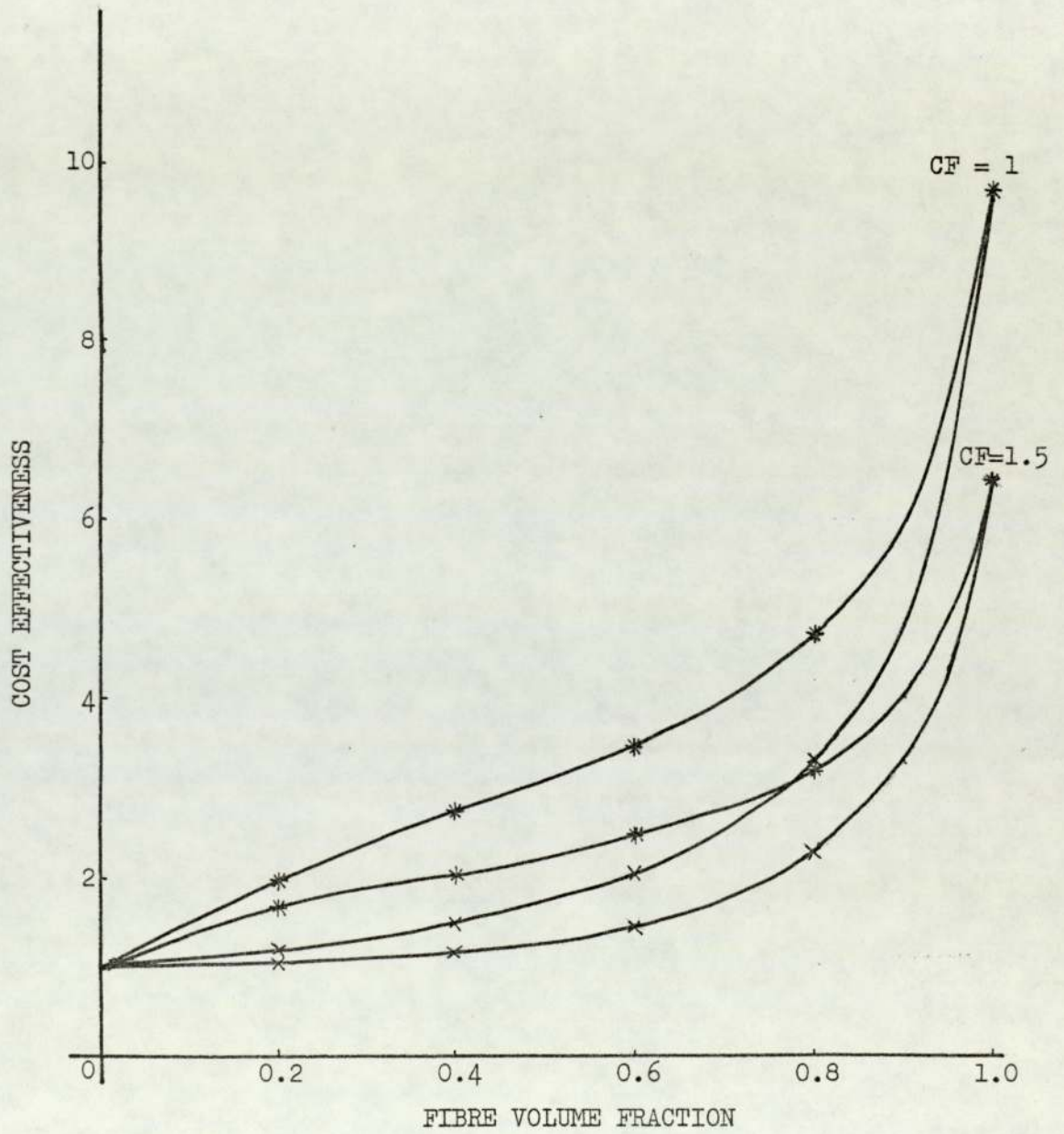


FIG. 4.3 MATERIAL COST EFFECTIVENESS

- FLEXURAL RIGIDITY

—•—•—•— $\alpha = 0^\circ$
—+—+—+— $\alpha = 0^\circ, 90^\circ$

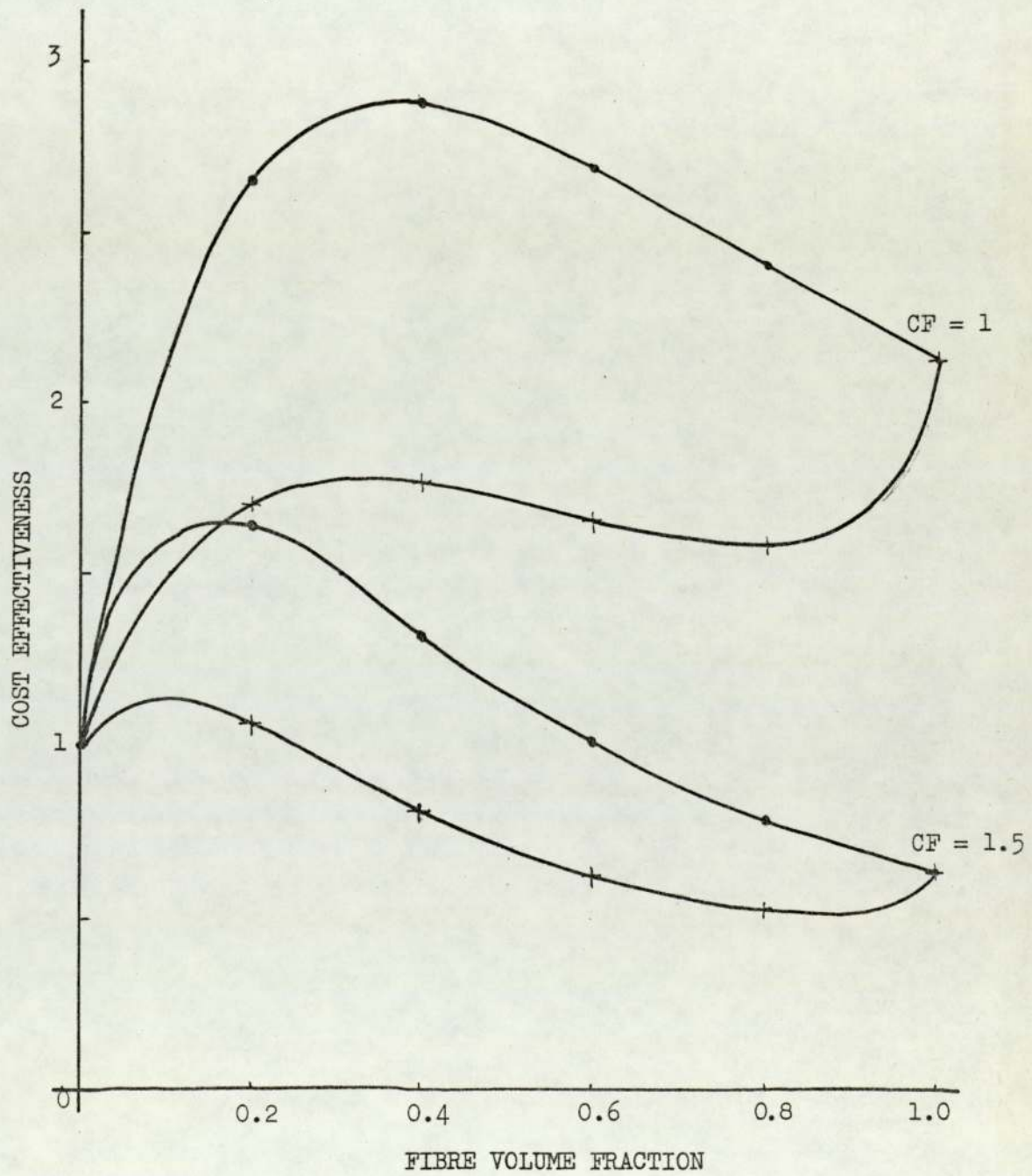


FIG. 4.4 MATERIAL COST EFFECTIVENESS

- FLEXURAL STIFFNESS

* * * $\alpha = \pm 45^\circ, 90^\circ, 0^\circ$
 x x x $\alpha = \pm 45^\circ$

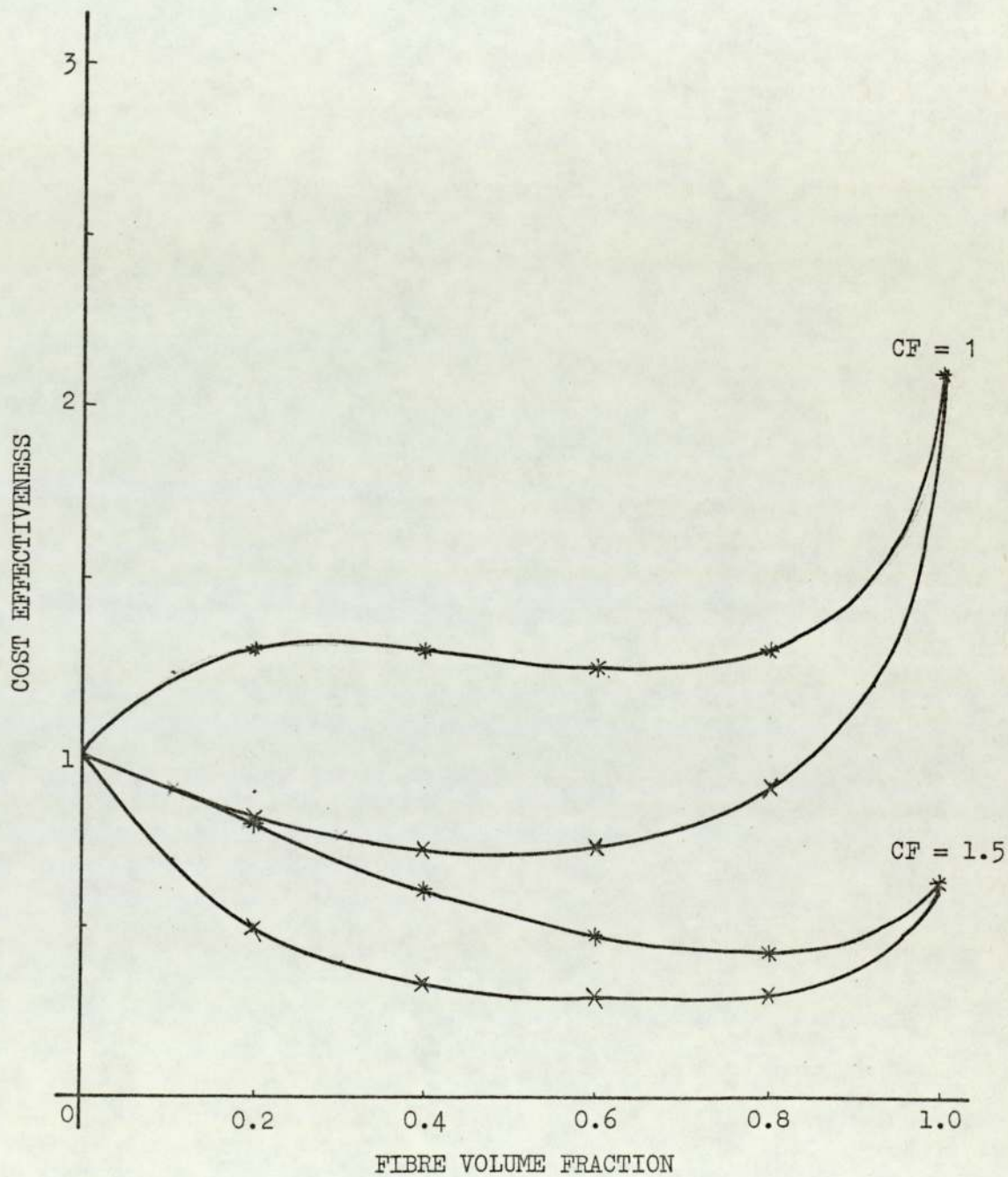


FIG. 4.5 MATERIAL COST EFFECTIVENESS

- SHEAR STIFFNESS

- $\alpha = 0^\circ \text{ \& \ } 0^\circ, 90^\circ$
- ×—×—×— $\alpha = \pm 45^\circ$
- *—*—*— $\alpha = 0^\circ, 90^\circ, \pm 45^\circ$

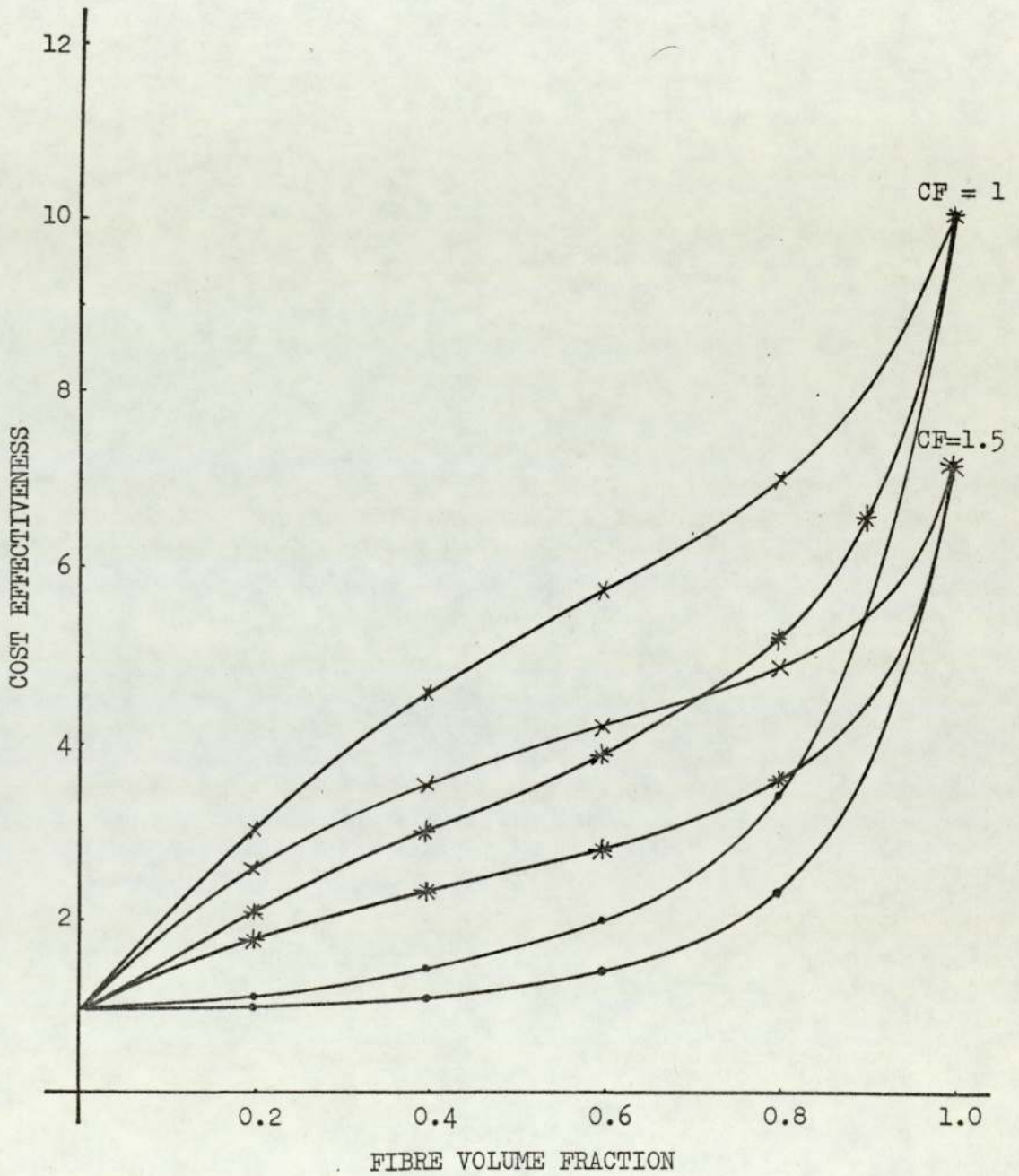


FIG. 4.6 MATERIAL COST EFFECTIVENESS

- PLATE BUCKLING

—•—•—•— $\alpha = 0^\circ$
—+—+—+— $\alpha = 0^\circ \text{ \& \ } 90^\circ$

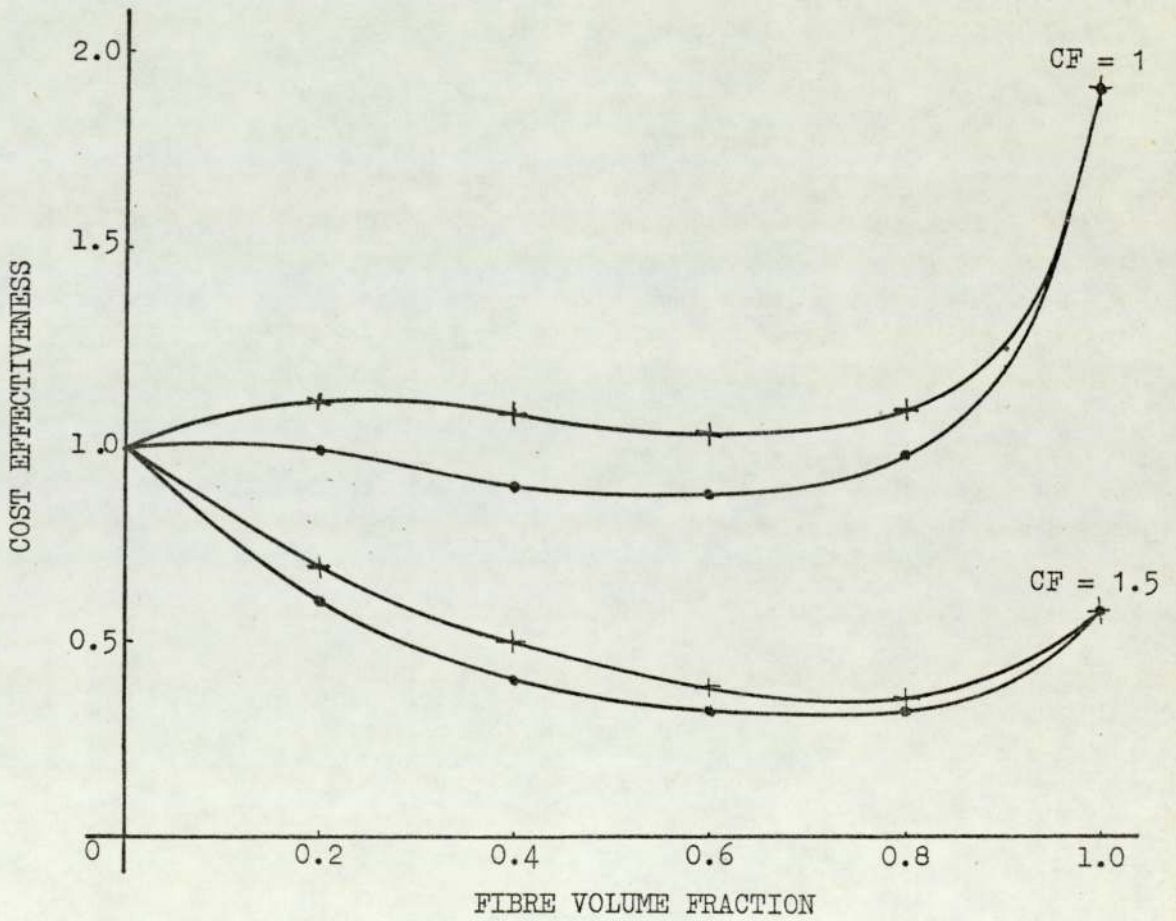


FIG. 4.7 MATERIAL COST EFFECTIVENESS

- PLATE BUCKLING

— x — x — x $\alpha = \pm 45^\circ$
— * — * — * $\alpha = 0^\circ, \pm 45^\circ, 90^\circ$

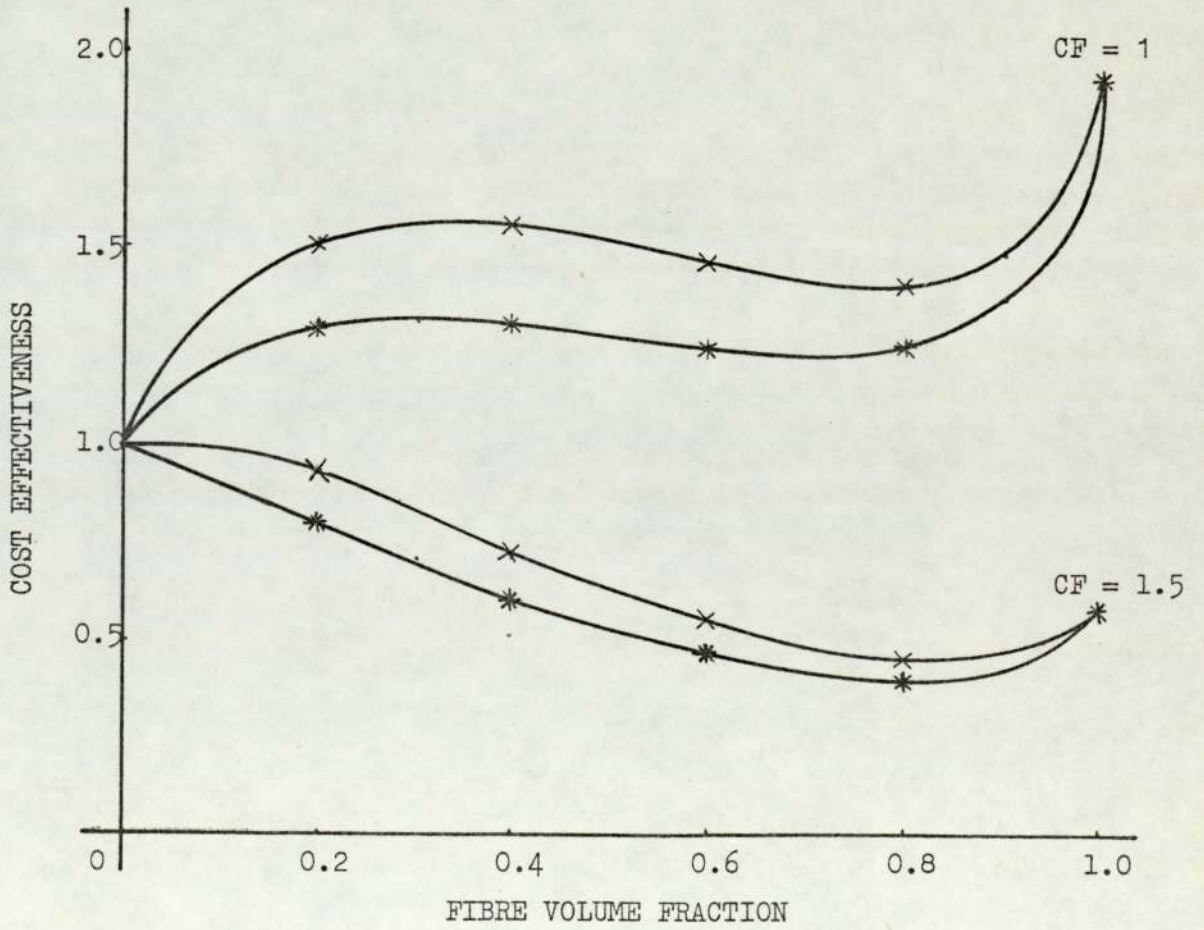


FIG. 4.8 MATERIAL COST EFFECTIVENESS

- CYLINDER BUCKLING

—•—•—•— $\alpha = 0^\circ$
—+—+—+— $\alpha = 0^\circ, 90^\circ$

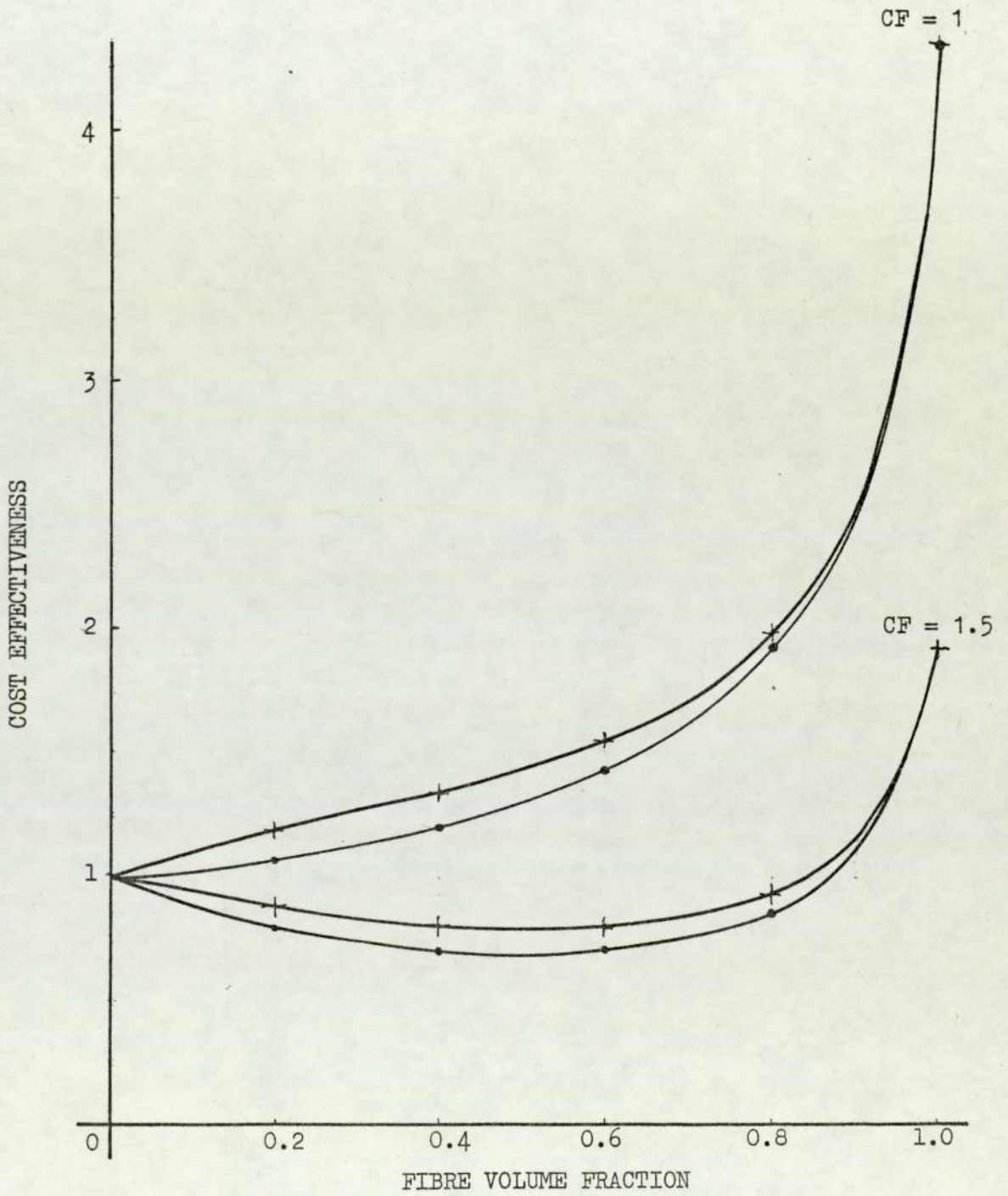


FIG. 4.9 MATERIAL COST EFFECTIVENESS
 - CYLINDER BUCKLING

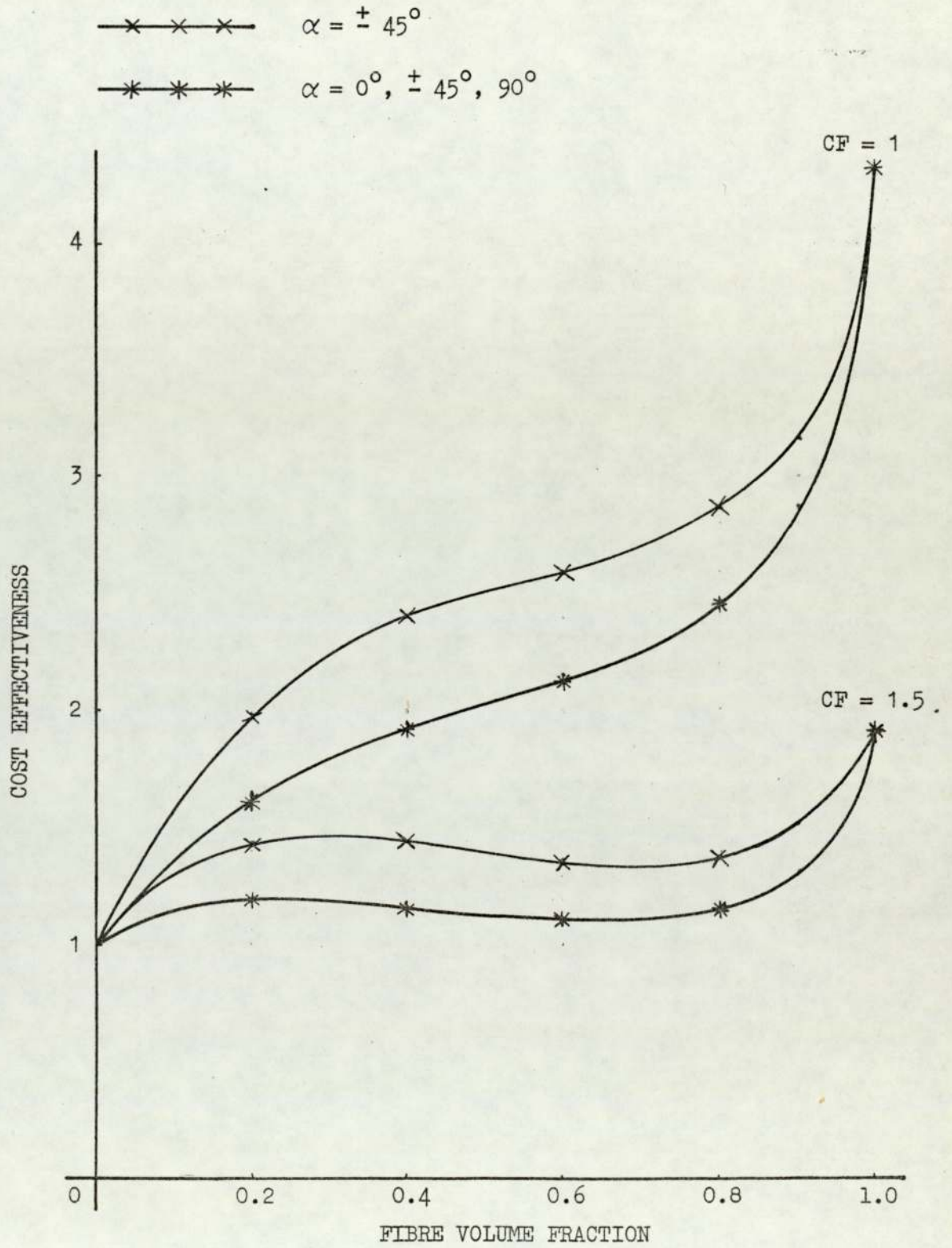


FIG. 4.10 PRACTICAL FIBRE VOLUME FRACTIONS

FOR VARIOUS MATERIALS

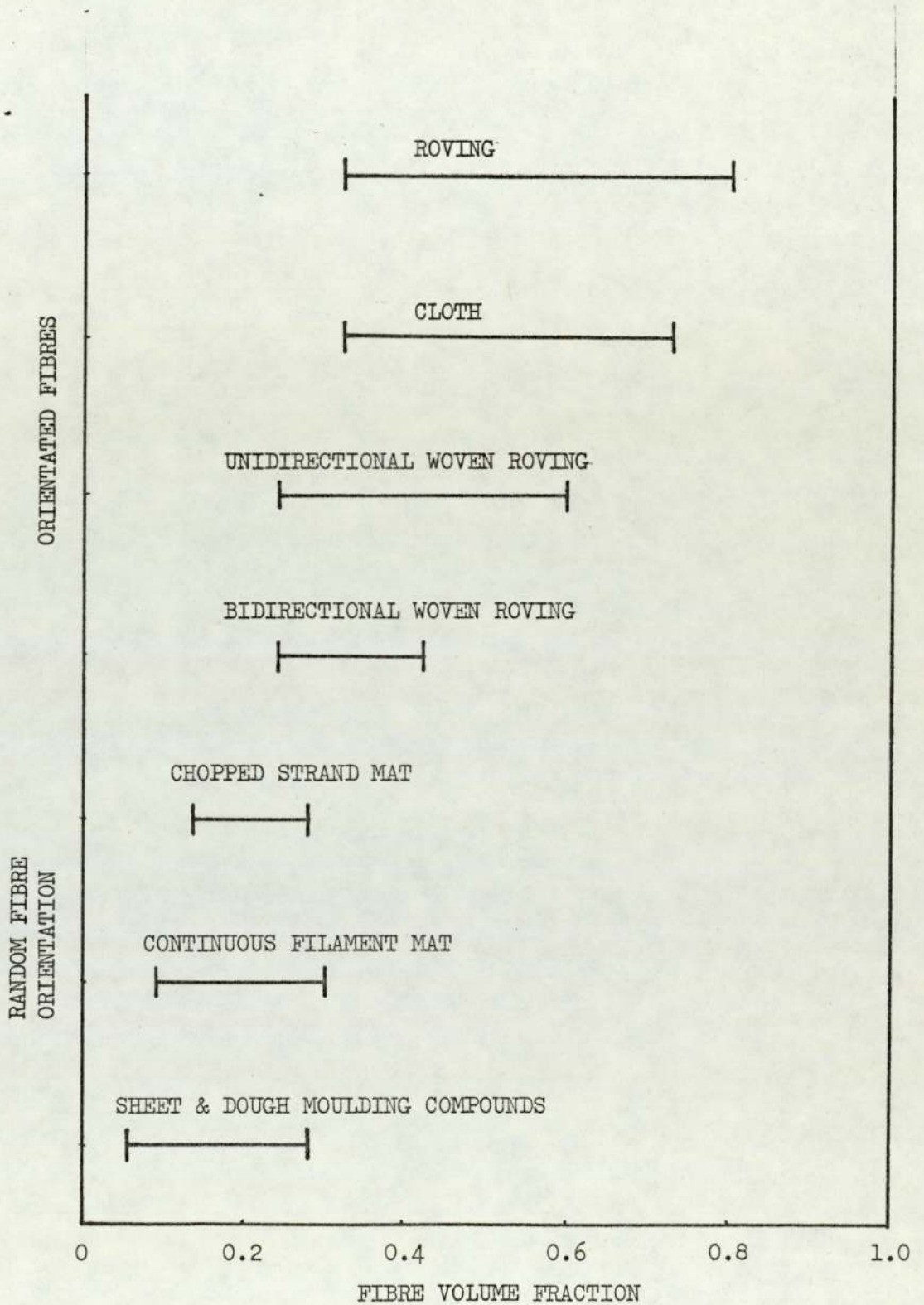
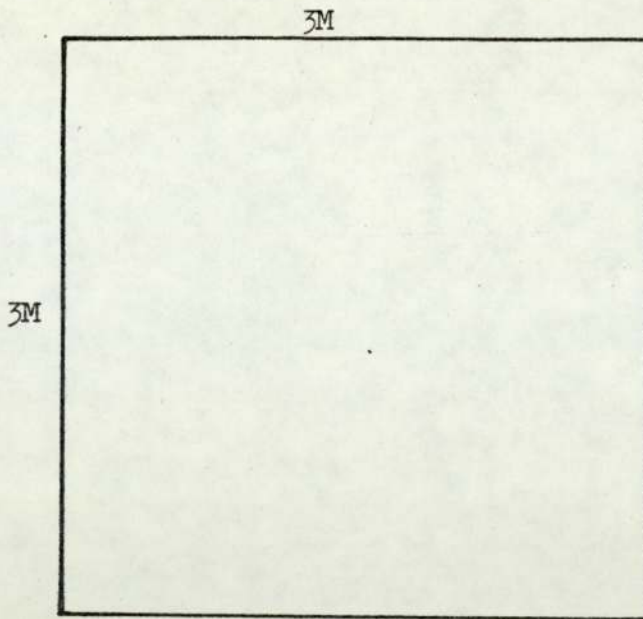


FIG. 4.11 PRODUCTS A AND B



PRODUCT TYPE A

$TK = 0.006 \text{ M}$

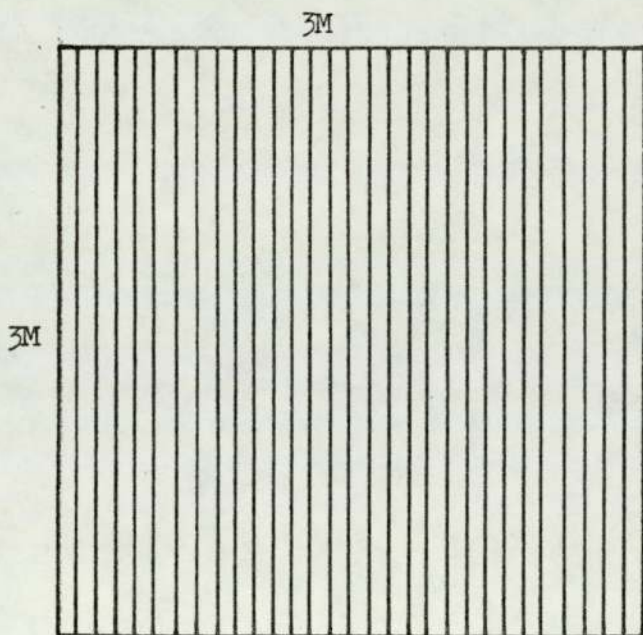
$WEIGHT (W) = 86.5 \text{ kg.}$

$SA = 9 \text{ M}^2$

$PA = 9 \text{ M}^2$

$\frac{SA}{PA} = 1$

$PEL = 12 \text{ M}$



PRODUCT TYPE B

$TK = 0.006 \text{ M}$

$WEIGHT (W) = 176 \text{ kg.}$

$SA = 18.3 \text{ M}^2$

$PA = 9 \text{ M}^2$

$\frac{SA}{PA} = 2.033$

$PEL = 18.2 \text{ M}$

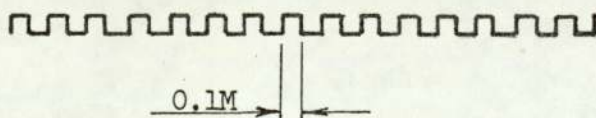
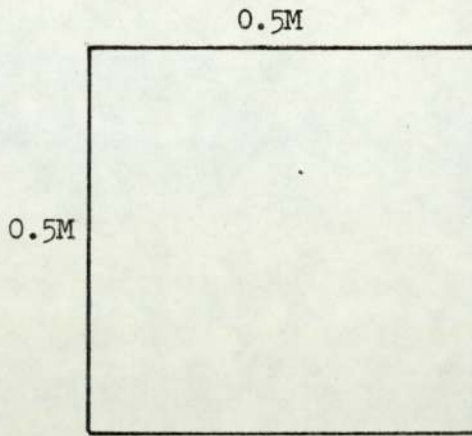


FIG. 4.12 PRODUCTS C AND D



PRODUCT TYPE C

TK = 0.006 M

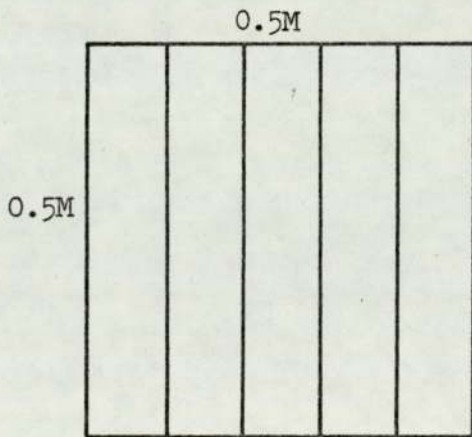
WEIGHT (W) = 2.4 kg.

SA = 0.25 M²

PA = 0.25 M²

$\frac{SA}{PA} = 1$

PEL = 2 M



PRODUCT TYPE D

TK = 0.006 M

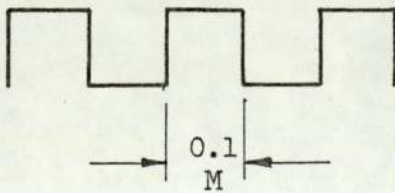
WEIGHT (W) = 5.28 kg.

SA = 0.55 M²

PA = 0.25 M²

$\frac{SA}{PA} = 2.2$

PEL = 3.2 M



COST AREA	<u>PRODUCT TYPE A</u>						<u>PRODUCT TYPE B</u>					
	FIXED COSTS	PRPD					FIXED COSTS	PRPD				
		0.5	2	10	40	200		0.5	2	10	40	200
FACTORY	0.27						0.76					
ENERGY	0.09						0.25					
PRODUCTION MOULD	1.00						2.10					
MOULD MASTER	0.06						0.34					
PATTERN & MASTER MOULD		1.64	0.41	0.08	0.02	0.01		3.42	0.85	0.17	0.04	0.01
LABOUR		93.00	23.30	23.30	23.30	23.30		93.00	93.00	93.00	93.00	93.00
PRODUCT HANDLING EQUIP.		1.63	0.41	0.08	0.02	0.01		1.63	0.41	0.08	0.02	0.01
FIXED COSTS TOTAL	1.42	1.42	1.42	1.42	1.42	1.42	3.45	3.45	3.45	3.45	3.45	3.45
TOTAL COSTS (£)		97.69	25.54	24.88	24.76	24.74		101.50	97.71	96.70	96.51	96.47

FIG. 4.13 HAND LAY-UP COSTS TABLE

COST AREA	<u>PRODUCT TYPE C</u>						<u>PRODUCT TYPE D</u>					
	FIXED COSTS	PRPD					FIXED COSTS	PRPD				
		0.5	2	10	40	200		0.5	2	10	40	200
FACTORY	0.01						0.02					
ENERGY	0.01						0.01					
PRODUCTION MOULD	0.13						0.17					
MOULD MASTER	0.01						0.01					
PATTERN & MASTER MOULD		0.20	0.05	0.01	0.01	0.01		0.28	0.07	0.01	0.01	0.01
LABOUR		93.00	23.30	4.70	1.20	1.20		93.00	23.30	4.70	4.70	4.70
FIXED COSTS TOTAL	0.16	0.16	0.16	0.16	0.16	0.16	0.31	0.31	0.31	0.31	0.31	0.31
TOTAL COSTS (£)		93.36	23.51	4.87	1.37	1.37		93.59	23.68	5.02	5.02	5.02

FIG. 4.14 HAND LAY-UP COSTS TABLE

COST AREA	<u>PRODUCT TYPE A</u>					<u>PRODUCT TYPE B</u>				
	FIXED COSTS	PRPD				FIXED COSTS	PRPD			
		2	3	9.4	49		2	4	17.5	52.5
FACTORY	0.12					0.15				
ENERGY	0.09					0.09				
PRODUCTION MOULD	1.00					0.10				
MOULD MASTER	0.03					0.07				
PATTERN & MASTER MOULD		0.41	0.27	0.09	0.02		0.86	0.43	0.10	0.03
LABOUR		44.68	29.80	9.51	5.45		44.68	22.34	13.22	10.01
PRODUCT HANDLING EQUIP.		0.41	0.27	0.09	0.02		0.40	0.20	0.05	0.02
SPRAY M/C		1.02	0.68	0.22	0.05		1.02	0.51	0.13	0.13
FIXED COSTS TOTAL	1.24	<u>1.24</u>	<u>1.24</u>	<u>1.24</u>	<u>1.24</u>	2.41	<u>2.41</u>	<u>2.41</u>	<u>2.41</u>	<u>2.41</u>
TOTAL COSTS (£)		47.86	32.26	11.15	6.78		49.37	25.89	15.91	12.60

FIG. 4.15 BASIC SPRAY-UP COSTS TABLE

COST AREA	<u>PRODUCT TYPE C</u>					<u>PRODUCT TYPE D</u>				
	FIXED COSTS	PRPD				FIXED COSTS	PRPD			
		2	20	127	648		2	49	369	738
FACTORY	0.01					0.02				
ENERGY	0.01					0.01				
PRODUCTION MOULD	0.01					0.02				
MOULD MASTER	0.01					0.01				
PATTERN & MASTER MOULD		0.05	0.01	0.01	0.01		0.07	0.01	0.01	0.01
LABOUR		44.68	4.47	0.70	0.36		44.68	1.82	0.92	0.80
SPRAY M/C		1.02	0.10	0.02	0.02		1.02	0.04	0.01	0.01
FIXED COSTS TOTAL	0.04	<u>0.04</u>	<u>0.04</u>	<u>0.04</u>	<u>0.04</u>	0.06	<u>0.06</u>	<u>0.06</u>	<u>0.06</u>	<u>0.06</u>
TOTAL COSTS (£)		45.79	4.62	0.77	0.43		46.83	1.93	1.00	0.88

FIG. 4.16 BASIC SPRAY-UP COSTS TABLE

COST AREA	<u>PRODUCT TYPE A</u>					<u>PRODUCT TYPE B</u>				
	FIXED COSTS	PRPD				FIXED COSTS	PRPD			
		2	11.6	40	104.4		2	5.3	15	82
FACTORY	0.12					0.15				
ENERGY	0.09					0.09				
PRODUCTION MOULD	1.00					2.10				
MOULD MASTER	0.03					0.07				
PATTERN & MASTER MOULD		0.41	0.07	0.02	0.01	0.85	0.32	0.11	0.02	
LABOUR		42.25	9.35	3.89	3.58	42.25	15.94	10.37	8.16	
ROBOT M/C		5.10	0.88	0.26	0.26	5.10	1.93	0.68	0.66	
PRODUCT HANDLING EQUIP.		0.41	0.07	0.02	0.01	0.41	0.15	0.05	0.01	
FIXED COSTS TOTAL	1.24	<u>1.24</u>	<u>1.24</u>	<u>1.24</u>	<u>1.24</u>	2.41	<u>2.41</u>	<u>2.41</u>	<u>2.41</u>	<u>2.41</u>
TOTAL COSTS (£)		49.41	11.61	5.43	5.10	51.02	20.75	13.62	11.26	

FIG. 4.17 ROBOT SPRAY-UP COSTS TABLE

COST AREA	FIXED COSTS	<u>PRODUCT TYPE C</u>				FIXED COSTS	<u>PRODUCT TYPE D</u>			
		2	11.6	158	470		2	11.6	57	158
FACTORY	0.01					0.02				
ENERGY	0.01					0.01				
PRODUCTION MOULD	0.01					0.02				
MOULD MASTER	0.01					0.01				
PATTERN & MASTER MOULD		0.05	0.01	0.01	0.01		0.07	0.01	0.01	0.01
LABOUR		42.25	7.28	0.54	0.33		42.25	7.28	1.48	0.98
ROBOT M/C		5.10	0.88	0.06	0.07		5.10	0.88	0.18	0.06
FIXED COSTS TOTAL	0.04	<u>0.04</u>	<u>0.04</u>	<u>0.04</u>	<u>0.04</u>	0.06	<u>0.06</u>	<u>0.06</u>	<u>0.06</u>	<u>0.06</u>
TOTAL COSTS (£)		47.44	8.21	0.65	0.45		47.48	8.23	1.73	1.11

FIG. 4.18 ROBOT SPRAY-UP COSTS TABLE

COST AREA	<u>PRODUCT TYPE A</u>					<u>PRODUCT TYPE B</u>				
	FIXED COSTS	PRPD				FIXED COSTS	PRPD			
		1	2	11.6	140		1	2	5.3	62
FACTORY	0.13					0.15				
ENERGY	0.09					0.09				
PRODUCTION MOULD	1.00					2.10				
MOULD MASTER	0.03					0.07				
PATTERN & MASTER MOULD		0.82	0.41	0.07	0.01	1.71	0.86	0.32	0.03	
LABOUR		84.49	42.25	7.28	3.39	84.49	42.25	15.97	7.66	
PRODUCT HANDLING EQUIP.		0.82	0.41	0.07	0.01	0.82	0.41	0.15	0.01	
SPRAY M/C		9.80	4.90	0.84	0.07	9.80	4.90	1.85	0.16	
FIXED COSTS TOTAL	1.25	<u>1.25</u>	<u>1.25</u>	<u>1.25</u>	<u>1.25</u>	2.41	<u>2.41</u>	<u>2.41</u>	<u>2.41</u>	<u>2.41</u>
TOTAL COSTS (£)		97.18	49.22	9.51	4.73	99.23	50.83	20.70	10.27	

FIG. 4.19 CONTINUOUS SPRAY-UP COSTS TABLE

COST AREA	FIXED COSTS	<u>PRODUCT TYPE C</u>				PRPD	<u>PRODUCT TYPE D</u>			
		2	11.6	158	1732		2	11.6	57	684
FACTORY	0.01									
ENERGY	0.01									
PRODUCTION MOULD	0.01									
MOULD MASTER	0.01									
PATTERN & MASTER MOULD		0.05	0.01	0.01	0.01		0.07	0.01	0.01	0.01
LABOUR		42.25	7.28	0.69	0.27		42.25	7.28	1.90	0.69
SPRAY M/C		4.48	0.84	0.06	0.01		4.88	0.84	0.17	0.01
FIXED COSTS TOTAL	0.04	<u>0.04</u>	<u>0.04</u>	<u>0.04</u>	<u>0.04</u>	0.05	<u>0.05</u>	<u>0.05</u>	<u>0.05</u>	<u>0.05</u>
TOTAL COSTS (£)		47.23	8.17	0.80	0.33		47.26	8.16	2.13	0.76

FIG. 4.20 CONTINUOUS SPRAY-UP COSTS TABLE

COST AREA	FIXED COSTS	<u>PRODUCT TYPE A</u>				23.1	FIXED COSTS	<u>PRODUCT TYPE B</u>				18.9
		2	5	10	PRPD			2	4	9	PRPD	
FACTORY	0.09					0.19						
ENERGY	0.09					0.09						
PRODUCTION MOULD	3.00					6.30						
MOULD MASTER	0.02					0.08						
PATTERN & MASTER MOULD		0.41	0.16	0.08	0.04		0.86	0.43	0.19	0.09		
LABOUR		42.25	16.90	8.45	3.68		42.25	21.12	9.39	4.47		
PRODUCT HANDLING EQUIP.		0.41	0.16	0.08	0.04		0.41	0.20	0.09	0.04		
INJECTION M/C		1.23	0.49	0.24	0.11		1.23	0.61	0.27	0.13		
FIXED COSTS TOTAL	3.20	<u>3.20</u>	<u>3.20</u>	<u>3.20</u>	<u>3.20</u>	6.66	<u>6.66</u>	<u>6.66</u>	<u>6.66</u>	<u>6.66</u>	6.66	
TOTAL COSTS (£)		47.50	20.09	12.05	7.07		51.41	29.02	16.60	11.39		

FIG. 4.21 RESIN INJECTION COSTS TABLE

COST AREA	FIXED COSTS	<u>PRODUCT TYPE C</u>				FIXED COSTS	<u>PRODUCT TYPE D</u>			
		PRPD					PRPD			
		2	10	100	400		2	5	20	125
FACTORY	0.01					0.01				
ENERGY	0.01					0.01				
PRODUCTION MOULD	0.33					0.43				
MOULD MASTER	0.01					0.01				
PATTERN & MASTER MOULD		0.05	0.01	0.01	0.01		0.07	0.02	0.01	0.01
LABOUR		42.25	9.45	0.84	0.21		42.25	16.90	4.22	0.68
INJECTION M/C		0.01	0.02	0.20	0.01		1.23	0.49	0.12	0.02
FIXED COSTS TOTAL	0.36	<u>0.36</u>	<u>0.36</u>	<u>0.36</u>	<u>0.36</u>	0.46	<u>0.46</u>	<u>0.46</u>	<u>0.46</u>	<u>0.46</u>
TOTAL COSTS (£)		43.66	9.02	1.23	0.59		44.01	17.87	4.81	1.17

FIG. 4.22 RESIN INJECTION COSTS TABLE

COST AREA	<u>PRODUCT TYPE A</u>				<u>PRODUCT TYPE B</u>			
	PRPD				PRPD			
	2	10	100	200	2	10	100	200
FACTORY	0.70	0.14	0.02	0.01	0.70	0.14	0.02	0.01
ENERGY	0.70	0.14	0.02	0.01	0.70	0.14	0.02	0.01
PRODUCTION MOULD	1.60	1.60	1.60	1.60	3.20	3.20	3.20	3.20
LABOUR	46.00	9.20	1.41	1.41	46.00	9.20	1.41	1.41
PRODUCT HANDLING EQUIP.	0.41	0.08	0.01	0.01	0.41	0.08	0.01	0.01
PRESS	<u>24.00</u>	<u>4.80</u>	<u>0.48</u>	<u>0.24</u>	<u>24.00</u>	<u>4.80</u>	<u>0.48</u>	<u>0.24</u>
TOTAL COST (£)	73.41	15.96	3.54	3.28	80.01	17.56	6.53	4.87

FIG. 4.23 HOT PRESS COSTS TABLE

COST AREA	<u>PRODUCT TYPE C</u>				<u>PRODUCT TYPE D</u>			
	PRPD							
	2	10	100	400	2	10	100	400
FACTORY	0.25	0.05	0.03	0.01	0.25	0.05	0.01	0.01
ENERGY	0.25	0.05	0.03	0.01	0.25	0.05	0.01	0.01
PRODUCTION MOULD	0.28	0.28	0.28	0.28	0.34	0.34	0.34	0.34
LABOUR	46.00	9.20	0.92	0.35	46.00	9.20	0.92	0.35
PRESS	2.55	0.51	0.05	0.02	2.55	0.51	0.05	0.02
TOTAL COSTS (£)	<u>49.33</u>	<u>10.09</u>	<u>1.31</u>	<u>0.67</u>	<u>49.39</u>	<u>10.15</u>	<u>1.33</u>	<u>0.73</u>

FIG. 4.24 HOT PRESS COSTS TABLE

FIG. 4.25 PRODUCTION COSTS OF PRODUCT A

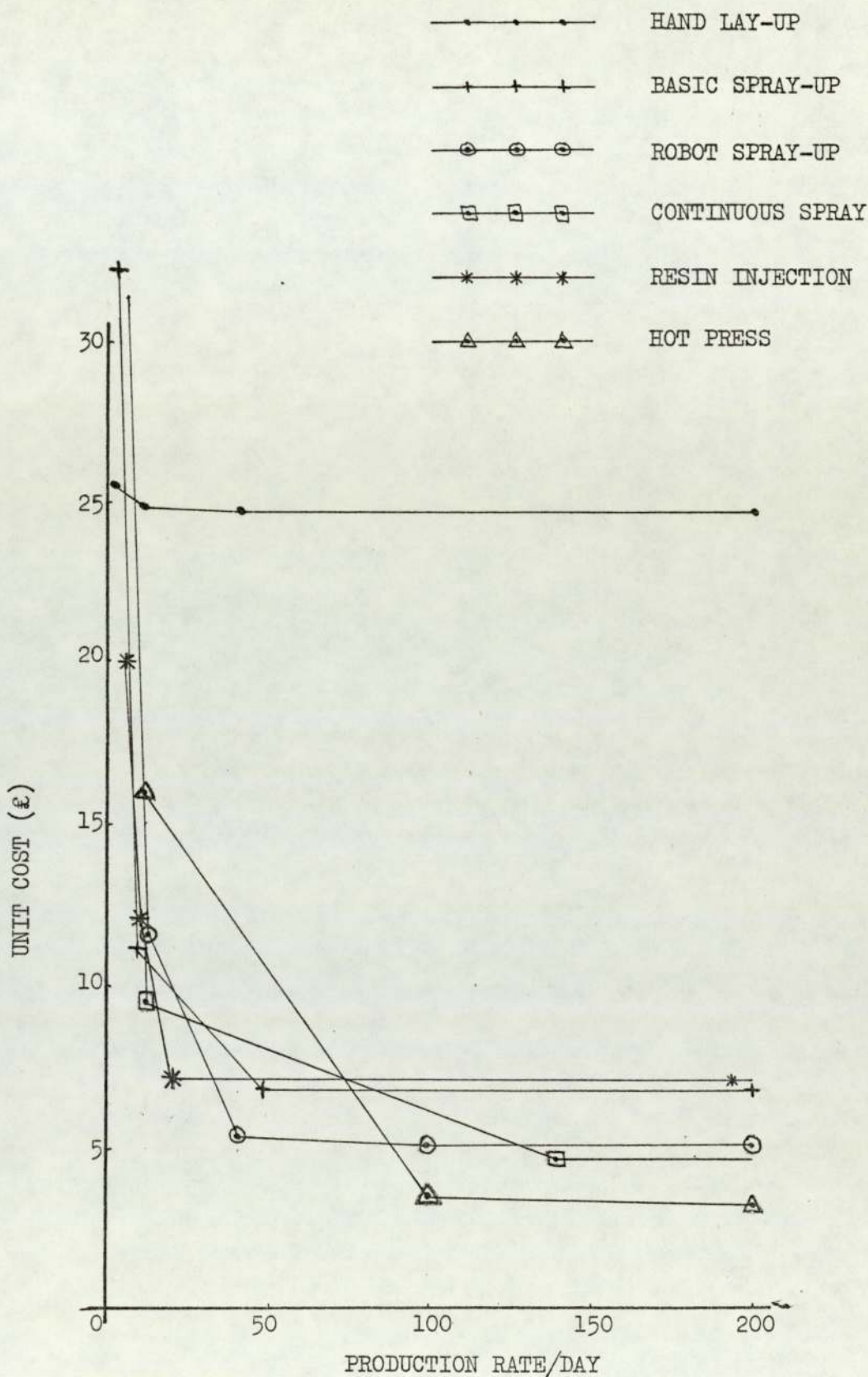
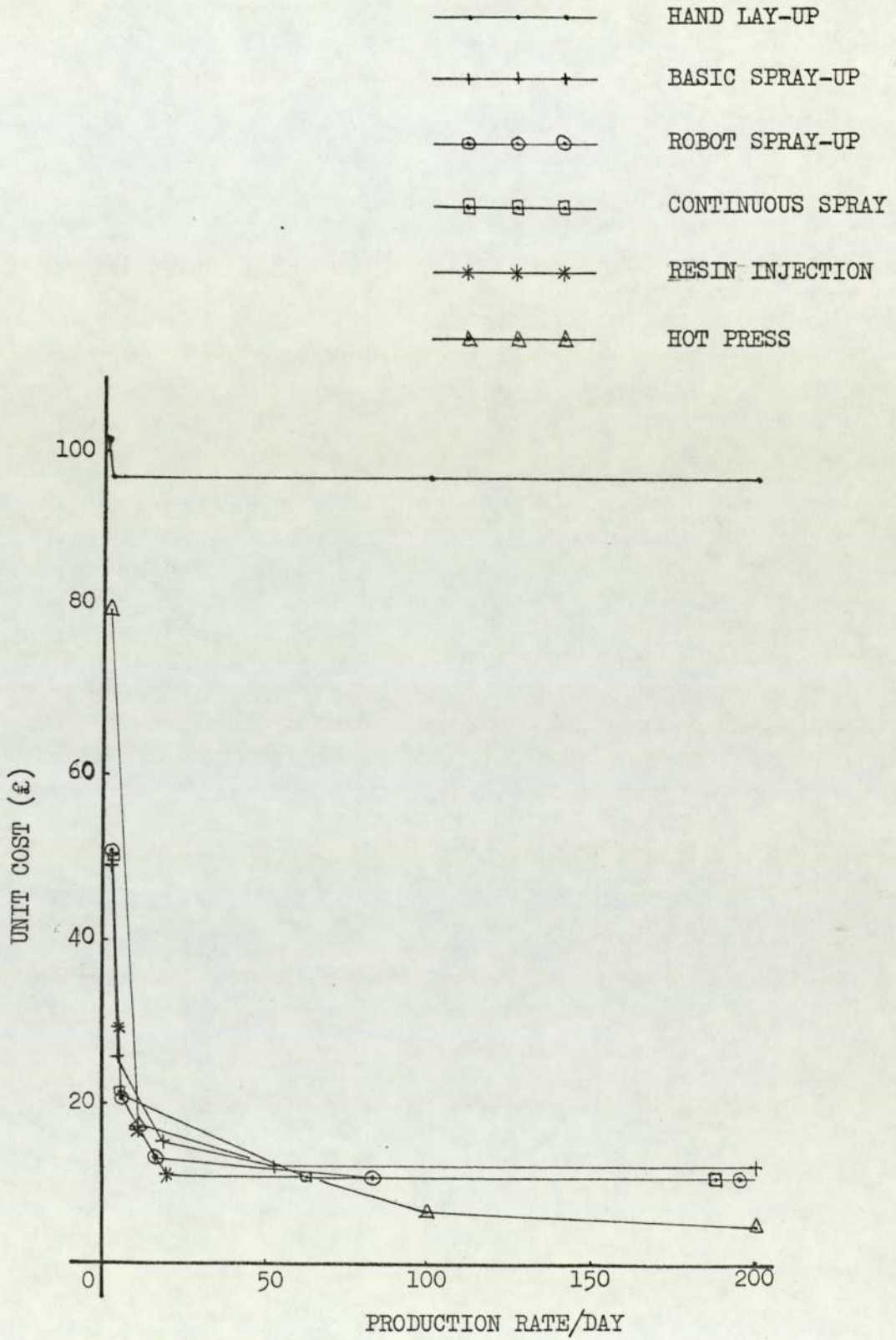


FIG. 4.26 PRODUCTION COSTS OF PRODUCT B



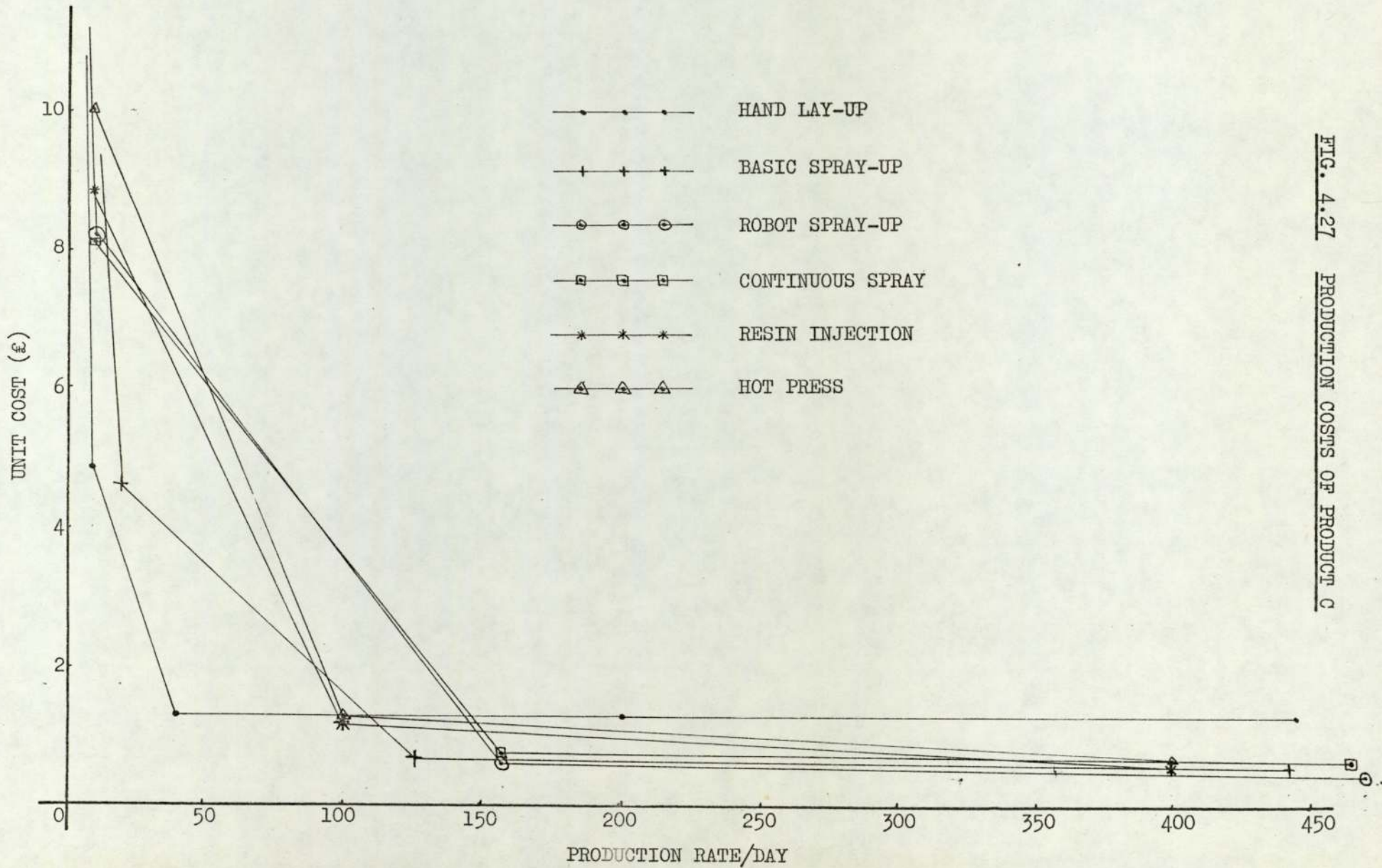


FIG. 4.27 PRODUCTION COSTS OF PRODUCT C

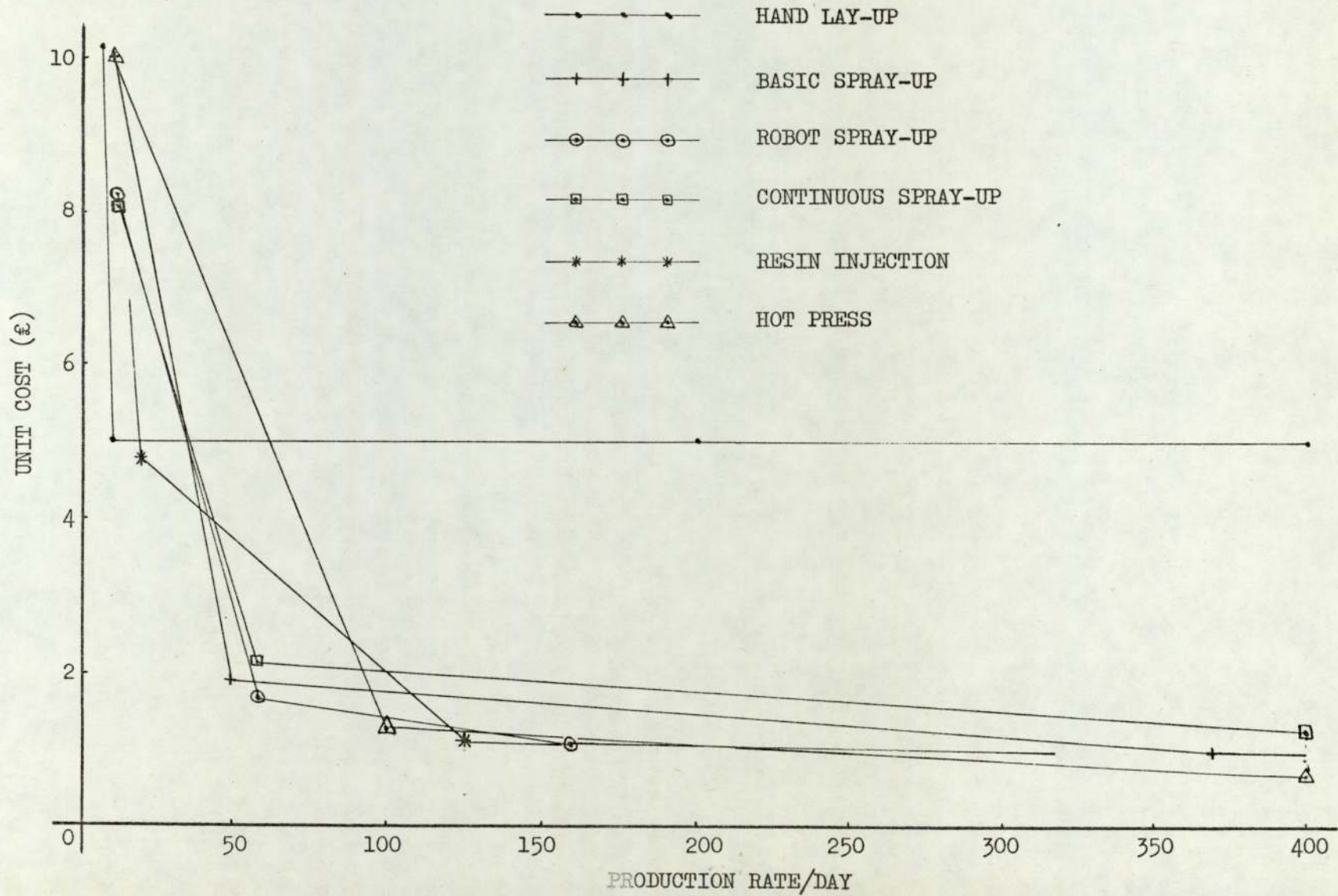


FIG. 4.28

PRODUCTION COSTS OF PRODUCT D

FIG. 4.29 IMPROVED FIBRE ORIENTATION
ROUND BOLT IN A TENSILE
JOINT

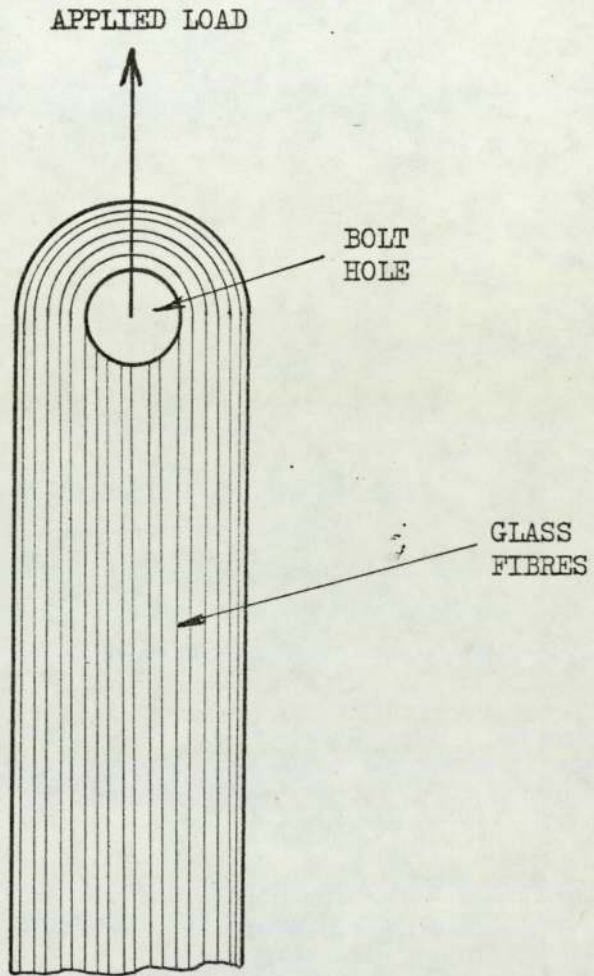


FIG. 4.30 TYPES OF ADHESIVE LOADING

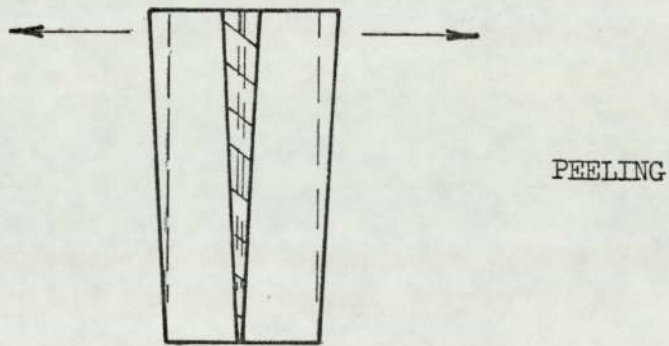
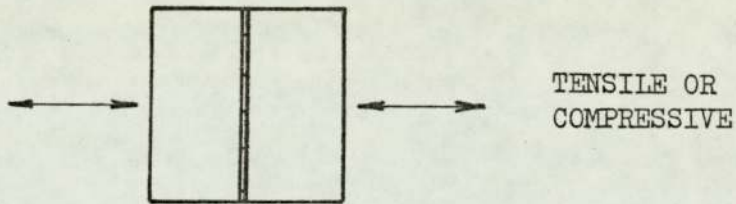
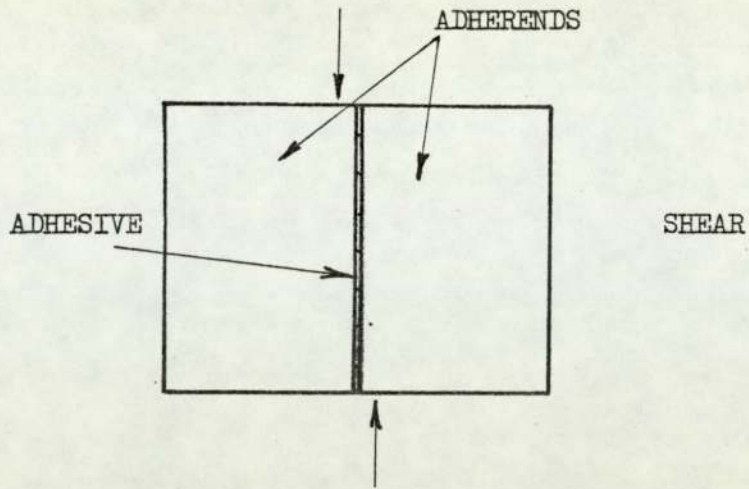
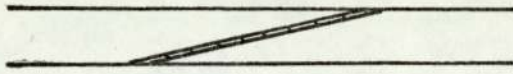
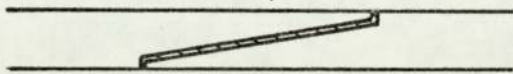


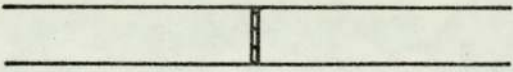
FIG. 4.31 ADHESIVE JOINTS



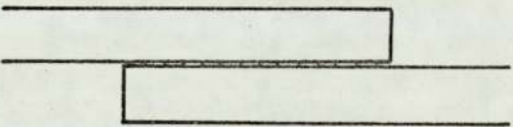
PURE SCARF



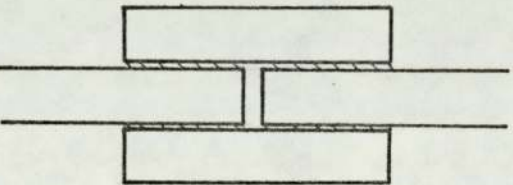
LANDED SCARF



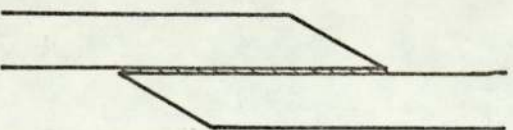
BUTT



SINGLE FLAT
LAP

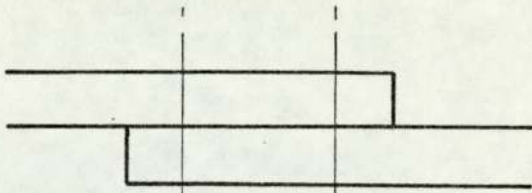


DOUBLE FLAT
LAP

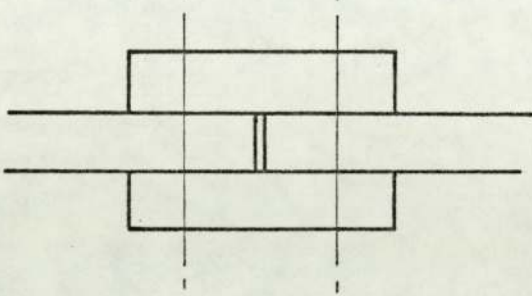


BEVELLED LAP

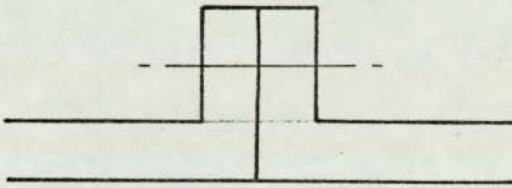
FIG. 4.32 MECHANICAL JOINTS



SINGLE LAP



DOUBLE LAP



FLANGE

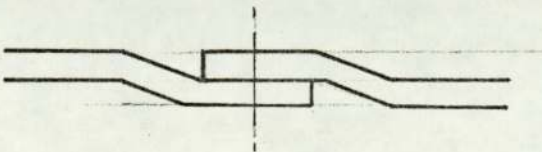
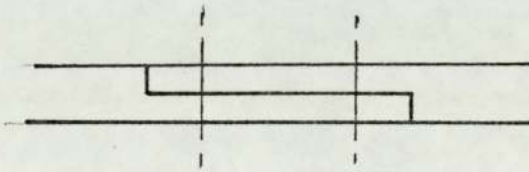
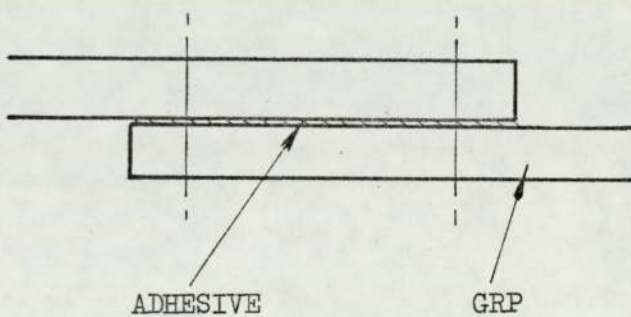
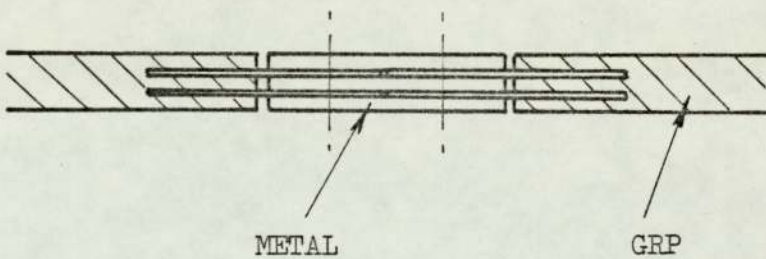
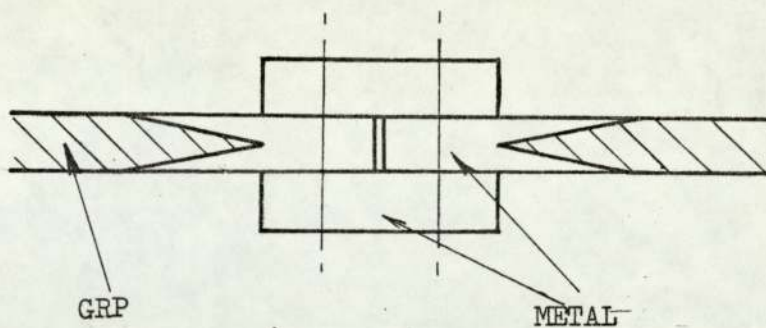


FIG. 4.33 COMBINATION JOINTS



CHAPTER 5

DISCUSSION AND PRELIMINARY DESIGN OF
A STRUCTURAL SYSTEM

CHAPTER FIVE

Discussion and Preliminary Design of a Structural System

5.1

Introduction

In previous chapters the characteristics of grp have been studied theoretically and empirically, and from these studies certain design philosophies and guidelines have been presented. With this knowledge, an argument will be presented for the selection of a particular structural system. The system will then be the subject of a preliminary design study.

Long-span lightly loaded structures have been chosen for study since the stress and deflection of these structures is, to a greater extent, dependent upon the self-weight of the structure. Grp is a low-density material and is therefore potentially capable of forming a light structure. Further weight, and hence material, should be saved, since less material is then required to support the structure itself. In the extreme case, where the structure's loading is its self-weight only, the maximum possible span is dependent upon grp's most outstanding property: its strength to weight ratio.

To show, satisfactorily, the feasibility of long-span grp structures, it is considered necessary to study both the economic and the structural aspects. Rather than study appropriate structures in abstract it would be beneficial to select a particular structure for analysis and assessment. A suitable structural function will be one that uses grp's relatively good properties to the full and one in which its weak properties are avoided or mitigated. Structures with a large potential market would be desirable.

It is of particular importance that a high modulus of elasticity should not be of overriding importance to the structure and that deflections may be limited by suitable choice of geometry. Further, if large deflections are not fundamentally unacceptable in the structure then the structural function is most suitable.

Long-span roof structures are an example of lightly-loaded structures which exploit the attributes of grp and mitigate the short-

comings adequately for this study. They offer a market which is large enough to warrant further investigation. Fire restrictions are not as stringent for roofs as for other parts of buildings. The good weathering properties of grp are used to the full. A roof structure, for the majority of its life, has only its own weight to support, thus reducing the severity of the creep problem compared with other structures which may be fully loaded continuously.

5.3

The Preliminary Design of a Long-Span Grp Roof

5.3.1 Introduction

Having chosen a particular structure for study it is now possible to carry out a preliminary design study. This will demonstrate the use of grp structurally, and will enable information for an economic study to be obtained.

5.3.2 Roof Loading

The normal major loading which a roof has to sustain is:

- a) Self-weight
- b) Snow loading
- c) Wind loading

The simultaneous action of the self-weight and snow load is normally the greatest load. It is not possible to determine the self-weight at this stage, however. British Standards code of practice CP3 : Ch V : Part 1 1972 lays down two possible snow loads for roofs with slopes of 30° or less. The lighter of the two loads must only be used when access to the roof is limited to that required for maintenance. The lower load of 0.75 KN/M^2 is considered more appropriate to this study and will be adopted for design purposes. The major roof load may therefore be considered a uniformly distributed load. (Hereafter referred to as a udl.)

The wind load will normally act in the opposite sense to that of the self-weight and snow load, and may or may not be a udl. The wind load cannot be determined until the size and shape of the roof is known.

5.3.3 Macroscopic Design

Approximately 72% of the industrial buildings in Great Britain are based on portal frame, and steel truss and stanchion structural systems [5.1]. It may be concluded, therefore, that most of the market for industrial buildings is based upon a rectangular plan shape. Also, 40 - 44% of new industrial ground area is for extensions and thus it is important that the initial structural design should be versatile in this respect. For these reasons a rectangular roof shape will be assumed for the design study.

It was stated earlier that stressed skin structures were particularly suitable for design in grp. Also it has been acknowledged for some time that stressed skin roof structures can lead to material and financial savings. Thus for this study it is appropriate to choose a stressed skin type of structure.

It is often proposed that roofs in grp should be based upon such efficient structures as domes, hyperbolic paraboloids and other synclastic and anticlastic shapes. The dome has not been chosen in this case since the demand for circular based buildings does not appear to be high. Neither is the dome versatile when extensions are required. The hyperbolic paraboloid is most compatible with grp when the distance between supports is small enough for the whole structure to be made from one mould. In the case of large spans many moulds could be required. Also, for large hyperbolic paraboloids it is usual to use heavy solid cantilever-like edge beams for which grp is not likely to be the most economical material.

In a recent publication [5.2] concerning long-span roofs, all the systems described were made up from two-dimensional beam-like structures, i.e. portal frames, trusses, tee beams or barrel vaults. It is therefore reasonable to think in terms of a two-dimensional module, many of which may be used together to form a stressed skin roof structure. In addition, industrial buildings requiring large spans may also require large doors or openings for the movement of goods or other objects. Two-dimensional roof structures, only requiring support on two sides, automatically have provision for this.

The overall structural design chosen for study is shown in Figs. 5.1 & 2. The structure consists of two parabolic surfaces

meeting at the roof edges and separated by vertical stays and cross bracing. The roof may be considered as being split up into many beam-like sections, each placed side by side to cover the total area. In each section the upper surface is analogous to an arch, being in compression for its full length, and the lower tensile surface to an inverted arch (not a cable or membrane since it has significant flexural rigidity). Similar structures have been used previously: by Brunnel for the Saltash railway bridge, and for the "Ahoy" exhibition and sports centre, Rotterdam. The "Ahoy" structure was chosen in preference to lattice beams, roof shells, suspended roof and space frames, each of which were considered. The maximum span of the "Ahoy" complex was 90m [5.3].

The structural system conforms to the principles of design in grp according to Section 4.2 in the following ways:

- a) Grp is used according to the "monochoque" principle.
- b) The aesthetic potential of grp is used in providing clean outer and inner surfaces which may be pigmented as required.
- c) The major stress system is simple (similar to the flanges of "I" beams) allowing maximum economy of material.
- d) The symmetry of the structure will lead to economies in production.

The roof span chosen for analysis has to be large enough for grp's properties to be significant. Also it is necessary to compare the design of the roof with conventional structures and, therefore, the span must be reasonably common. 60m is considered

to be a suitable span. The span to depth ratio chosen is slightly ~~larger~~ ^{smaller} than usual, at 12:1, to compensate for the low modulus of elasticity.

5.3.4 Analysis of Roof Structure

5.3.4.1 Proposed Design of Roof Surface Element Cross-Section

The major loads that the surface elements have to take are axial. Secondary stresses are induced by bending moments and shear forces. The upper compressive surface also has to be able to take a load of 0.9 KN concentrated over an area of 0.09m^2 in any position in addition to the snow load. Also, local and Euler buckling must be resisted. Accordingly, a cylindrical shell shape as shown in Fig. 5.3 was chosen.

Since the major forces are axial the "edge-beams" are of unidirectional material ($V_f = 54\%$). The shell, which must resist local buckling, should be made, according to Section 4.3.5, from $\pm 45^\circ$ angle-ply since this was shown to be most cost-effective. However, in Chapter 3 this material was shown to be relatively weak and very susceptible to creep. Further, this material has to be tailored from rolls of woven roving at $\pm 90^\circ$, and considerable wastage results. Quasi-isotropic reinforcement has been shown to be next most cost-effective and has better strength and creep properties. CSM reinforcement has, therefore, been chosen for the cylindrical section

$(v_f = 16.5\%)$.

The use of stiffened cylindrical section greatly improves the efficiency of the shell in resisting local buckling. The addition of the longitudinal stiffeners, known as stringers, restricts the wavelength and so increases the theoretical buckling load. Isotropic cylinders have been found to be very unreliable in local buckling due to their high sensitivity to local imperfections. However, the addition of ring stiffeners has been found to considerably reduce this sensitivity by constraining buckling to the axisymmetric mode. This results in linear theory agreeing with empirical experience to within $\pm 10\%$ [5.4].

An acceptable design life for a building will depend upon the function of that building. A factory may only be designed for 25 years whereas a civic building will often be designed to last considerably longer. For this design study a life of approximately 50 years is considered reasonable. After periods of time of this order grp failure stresses and strains change slowly with time. Consequently, the additional cost incurred through choosing this life as against, say, 25 years will be small.

As the strength and stiffness of grp reduces with time, it is necessary to calculate the material properties at the end of the design life and use these to determine not only the safety factors as described in the previous chapter (Section 4.7) but also the geometric properties such as the flexural rigidity of the roof's surface unit. The flexural rigidity will be influenced by the relative loss of stiffness between CSM and unidirectional materials.

Unfortunately, it is difficult to define the roof's environment for a period of 50 years. This is the case for many reasons, including the unpredictability of weather and the fact that the precise location of the roof is unknown. However, the environment used in the time-dependent tests described in Section 3.5 is considered to be as severe as a typical British outdoor environment. The results of this section will be used to predict the performance of the design roof.

5.3.4.2 Verification of the Proposed Roof Design

Roof Loading

The self-weight of the roof is 0.28 KN/M^2 ; of this, grp accounts for 0.17 KN/M^2 . It is now possible to calculate the effective snow and wind loads.

Wind Loading

The wind pressure distribution across the upper curved surface of the roof cannot be calculated completely from British Code of Practice CP3 Ch.5 Part 2 1973 since this roof shape is not dealt with. However, Sachs [5.5] reports American recommendations for curved roofs and these have been used to determine the external pressure coefficients across the roof's surface. CP3 has been used to determine the internal pressure coefficients (C_{p_i}). The design wind speed chosen was 33.6 m/s . This allows the roof to be built in any of the large English cities or their surrounding countryside providing:

- i) the building site is in unexceptional topographical surroundings.
- ii) the overall height of the roof is not greater than 12m and that there are many wind breaks in the surrounding areas such as found in small towns or the outskirts of a small city.
- iii) There are no extraordinary safety requirements for the building.

Based on the above and the self-weight of the roof, the effective wind loads in the two principal directions are shown in Fig. 5.4a.

Snow Loading

The combined snow load and self-weight of the roof is shown, in Fig. 5.4b, to be the major load at 1.03 KN/M^2 . However, the wind load is considerable and there is justification for roof symmetry about the horizontal mid-plane.

Although the roof members have been designed and the roof loads calculated, it is not possible to compute directly the roof deflections and member forces. This is a result of the visco-elastic nature of grp which leads to the member properties being dependent upon the roof's loading history. The loading history of a roof over 50 years is very complex. However, for the purposes of this analysis the loading history will be taken as:

- 1) roof self-weight only for the initial 4×10^5 hrs.
- 2) self-weight plus snow load for the following 800 hrs. (approximately 1 month).

Thus it is assumed that creep resulting from other loads (wind, rain, snow) cancel each other out.

To calculate the roof's deflections and member forces the following procedure was adopted:

- 1) Approximate axial force in the roof's surfaces.

This was calculated from the maximum bending moment applied to the roof, plus an allowance of 5% for the shear force.

$$F = \frac{wl^2}{8d} \quad 1.05 \quad 5.1$$

where: F = axial force per metre width

w = load per unit area

l = roof span

d = maximum depth of roof

The force 'F' was calculated for both load intensities:

$$F_1 \text{ (due to self-weight only)} = 26.5 \text{ KN}$$

$$F_2 \text{ (due to self-weight plus snow load)} = 98 \text{ KN.}$$

- 2) Approximate axial strain in grp members at the end of the design life.

$$F_i = \sigma_i \text{ CYL} A_{\text{CYL}} + \sigma_i \text{ EB} A_{\text{EB}} \quad i = 1,2 \quad 5.2$$

where: σ = axial stress (N/mm^2)

A = cross-sectional area per metre width

Suffix 'CYL' refers to the cylindrical section.

Suffix 'EB' refers to the edge beams.

Since the edge beams are of unidirectional grp (UD) and the cylindrical section is of CSM, from Section 3.5.6.6 the following

equations may be written:

$$\epsilon_t \text{ CSM} = \sigma_{\text{CSM}} t^{0.091} 4149^{-1} \quad 5.3$$

$$\epsilon_t \text{ UD} = \sigma_{\text{UD}} t^{0.010} 20823^{-1} \quad 5.4$$

$$\epsilon_t \text{ UD} = \epsilon_t \text{ CSM} \quad 5.5$$

It is assumed for equation 5.5 that there is a uniform strain distribution across the width of the roof surface section. This will not, in fact, be true since there will be bending and shear forces present. Also, in the regions of the joints between sections there will be complicated strain patterns. However, these are expected to be second order effects. The bending and shear forces have been kept to a minimum by the parabolic shape of the surfaces.

From equations 5.2 to 5.5 the axial stresses and strains may be estimated after 4×10^5 hrs.:

$$\epsilon_t = 4 \times 10^5 = 7.592 \times 10^{-4}$$

$$\sigma_1 \text{ CSM} = 0.974 \text{ N/mm}^2$$

$$\sigma_1 \text{ UD} = 13.9 \text{ N/mm}^2$$

For the second period of loading

$$\epsilon_{t_2} = \frac{\sigma_1 t_2^n}{E_1} + \frac{(\sigma_2 - \sigma_1) (t_2 - t_1)^n}{E_1} \quad 5.6$$

(See Section 3.5.6.5 and Fig. 3.30.)

From equations 5.2 and 5.6 it may be calculated that:

$$\epsilon_t = 4.008 \times 10^5 = 0.0022\%$$

$$\sigma_2 \text{ CSM} = 4.27 \text{ N/mm}^2$$

$$\sigma_2 \text{ UD} = 41.5 \text{ N/mm}^2$$

3) Grp elastic properties at the end of the design life.

The apparent modulus (\bar{E}) of the two types of grp at the end of the design life may now be obtained:

$$\bar{E}_{\text{CSM}} = \frac{\sigma_2 \text{ CSM}}{\epsilon_{t2}} = 1.97 \times 10^3 \text{ N/mm}^2 \quad 5.7$$

$$\bar{E}_{\text{UD}} = \frac{\sigma_2 \text{ UD}}{\epsilon_{t2}} = 19.1 \times 10^3 \text{ N/mm}^2 \quad 5.8$$

4) Geometric properties of the grp roof members.

Now that the approximate "design life" elastic properties of the grp are known it is possible to estimate the geometric properties of the roof surface units by the method of equivalent sections. Changing the unidirectional grp of the edge-beams to the equivalent area of CSM A'_{EB} as follows:

$$A'_{\text{EB}} = A_{\text{EB}} \times \frac{\bar{E}_{\text{UD}}}{\bar{E}_{\text{CSM}}} \quad 5.9$$

it can be shown that:

- i) The roof surfaces' cross-sectional area per metre width (A_S) = $2.29 \times 10^{-2} \text{ m}^2$
- ii) The roof surfaces' second moment of area per metre width (I_S) = $3.093 \times 10^{-4} \text{ m}^4$.

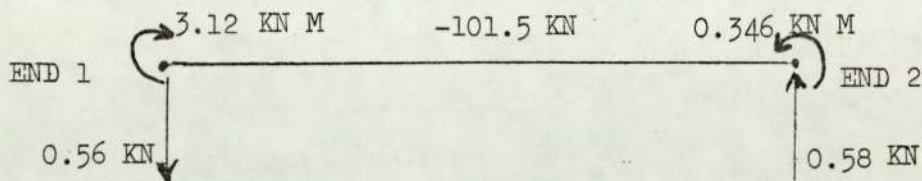
5) Computer Calculations

Using the design life structural properties of the grp members, an existing University computer programme [5.6], based upon load-displacement techniques, was used to analyse the roof structure. The idealised structural system analysed is shown in Fig. 5.5. Only the tensile half of the diagonal cross-bracing was included, since the bracing was not designed to withstand compressive forces.

The most highly-stressed part of the roof was found to be near the supports in member 3; see Figs. 5.5 and 5.6.

Grp member stresses.

Member 3 : This member was shown to be subject to the highest axial load at 101.5 KN. This force is approximately 2% greater than that used in the approximate calculations. The general loading of this member is shown below:



Again using equivalent sections theory, the purely axial stress was found to be:

-4,440 KN/M^2 in CSM material and
-43,224 KN/M^2 in UD material

The mean shear stress in the member was $64.8 \text{ KN}/\text{M}^2$, which is insignificant.

Considering end No. 1.

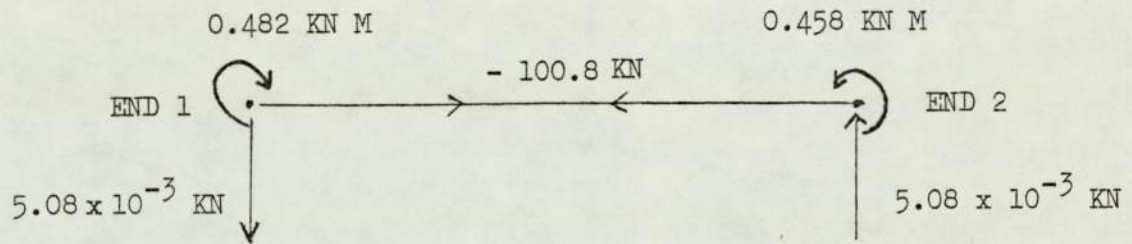
Maximum combined axial and bending stress in the CSM was found to be: $-8,247 \text{ KN}/\text{M}^2$, and the corresponding strain: -0.419% .

The maximum combined stress in the unidirectional material was $-58,680 \text{ KN}/\text{M}^2$ and the corresponding strain: -0.307% .

Considering end No. 2.

The maximum combined stress in the CSM material was calculated as $-4,854 \text{ KN}/\text{M}^2$ and in the unidirectional material as $-44,128 \text{ KN}/\text{M}^2$.

In the approximate analysis, used to calculate the referred cross-sectional area and the second moment of area, bending stresses were not considered. Hence the properties used in the computer analysis were not strictly valid. However, the regions where high bending stresses occur are very limited. The eight members with the highest bending moments, ± 3.21 KN M or ± 3.12 KN M, experience these only at one end. In the majority of members the bending moments are only 10 - 20% of these. The stresses in a typical member (11) are as follows:



The axial stress calculated for CSM was -4407 KN/M^2 and for unidirectional material $-42,704 \text{ KN/M}^2$. The shear stresses were again negligible.

End 1

The maximum combined stress was again in the unidirectional material at $-44,244 \text{ KN/M}^2$. The maximum combined stress in the CSM was found to be -4984 KN/M^2 .

End 2

The maximum combined stress in the CSM laminate
 $= - 4955 \text{ KN/M}^2$.

The maximum combined stress in the unidirectional material
 $= - 44,168 \text{ KN/M}^2$.

Thus it can be seen that although there are small regions of high bending stresses, the majority of the grp is under principally axial stress. Further, the axial stress was found to vary only about 4 $\frac{1}{2}$ % across the span in the upper and lower surface.

Since the forces used in the approximate approach agree well with those determined with the use of a computer, it is considered that the design approach is satisfactory.

Roof Deflection

The maximum deflection of the roof under the action of its own weight and the snow load at the end of the design life as calculated by the computer

$$= 0.56 M = \frac{\text{span}}{107}$$

Stability of Roof Members

1) The Cross-Bracing

The diagonal cross-bracing members were designed to take tension only, and in the analysis their stiffness in compression was not taken into account. The vertical members are in compression under the snow load. The most critical member in this respect is the central vertical member 5 m. long under a load of -2.72 KN. For the purposes of analysis this member was considered as a built-in strut because of the far greater flexural stiffness of the grp surface units to which it is connected. Under these circumstances there was found to be a safety factor of 25 on the Euler buckling load.

2) Grp Roof Surface Members

Euler Buckling

The maximum compressive force occurs in members 3 and 21 under the action of the self-weight and snow load and is equal to 101.5 KN. These members are considered as simply-supported struts. In fact the unit would experience some end-restraint due to the flexural rigidity of the cross-bracing but this would be small because of the relative flexural stiffnesses. On this basis there is a factor of safety of 2.37 on the Euler buckling load (P_E) where:

$$P_E = \frac{\pi^2 E I}{l^2} \quad 5.10$$

and the symbols have their usual meaning.

Local Buckling of Cylindrical Section

Lakshmikantham and Gerard [5.4] have presented results to show that provided certain geometrical constraints were applied, the following formula was reliable in determining the local buckling loads of symmetrically stiffened cylinders:

$$N = \frac{2 (1 - \mu)^{\frac{1}{2}} (B_2)^{\frac{1}{2}}}{r D_1} \quad 5.11$$

where N = buckling load per unit width

r = cylinder radius

μ = Poisson's ratio

$$B_2 = E \left(t_s + \frac{A_r}{L_t} \right) (1 - \mu^2)^{-1}$$

$$D_1 = E I_{st} (1 - \mu^2)^{-1}$$

The conditions imposed for reliability were that:

$$\frac{B_1 D_2}{B_2 D_1} > 1.8 \quad \& \quad \frac{r}{h_r} > 100$$

and
$$B_1 = E \left(t_s + \frac{A_{st}}{L_{st}} \right) (1 - \mu^2)^{-1}$$

$$D_2 = E I_r (1 - \mu^2)^{-1}$$

t_s = skin thickness

A_r = ring area

A_{st} = stringer area

I_r = ring second moment of area

L_{st} = stringer pitch

h_r = ring depth

The proposed roof surface cylindrical section meets the above conditions and the value for N was calculated as:

$$N = -31 \text{ KN/metre width}$$

The equivalent axial stress is:

$$\sigma_{cr} = 12,550 \text{ KN/M}^2$$

The maximum mean axial stress in the cylindrical section at the end of the design life was $-4,440 \text{ KN/M}^2$. The maximum combined bending and axial stress was $-8,247 \text{ KN/M}^2$. The safety factor on the mean axial stress is 2.82 and on the combined stress 1.52.

Support of Secondary Loads

Although the skin of the cylindrical section of the roof unit is thin (2 mm) the rib stiffening system will rapidly dissipate local loads. The statutory requirement for local loading on the roof

as mentioned earlier is 0.9 KN, concentrated on a square of sides 300 mm. Such a square would be supported by at least one stringer and one ring stiffener.

5.3.5 Discussion and Assessment of Roof Design

The maximum stress in the CSM has been calculated in the previous section to be $-8,247 \text{ KN/M}^2$. Since the stress that CSM can be expected to endure continuously is approximately $35,000 \text{ KN/M}^2$ (See Fig. 3.22) and CSM in the short term tests was found to be stronger in compression, the safety factor here of over 4 is adequate. The maximum stress predicted in the unidirectional material is $-58,680 \text{ KN/M}^2$. A conservative estimate (Fig. 3.22) of the stress level that this material could withstand continuously for 50 years is $70,000 \text{ KN/M}^2$. Since this is a conservative estimate and the roof is expected to be under maximum load for only 800 hrs. the safety margin is considered satisfactory.

The short term strengths of the two materials are as follows:

(See Section 3.4)

CSM: compression = $200,000 \text{ KN/M}^2$

tension = $75,000 \text{ KN/M}^2$

Unidirectional Laminate: compression = $425,000 \text{ KN/M}^2$

tension = $640,000 \text{ KN/M}^2$

The safety factors on the short term strengths are considerably in excess of the factors recommended by Makowski (Section 4.7).

The slenderness ratio of the roof surface units is 43, and as such a safety factor of 2.37 at the end of the design life is considered satisfactory against failure by Euler buckling. Local buckling of the cylindrical section is not considered to be as critical as Euler buckling, since in itself it does not cause catastrophic failure. The safety factor of 1.52 against buckling in localised areas of high bending stresses is considered satisfactory. A safety factor of 2.82 against the mean axial stress is adequate.

The deflection of the roof at 0.56 m is considerably greater than is normally allowed in conventional roof structures. For steel structures the deflection is often limited to $1/360$ x span, and for aluminium structures to $1/240$ x span. The deflection ratio for the grp roof is $1/107$ x span. This deflection is considered acceptable, however, since the stresses involved are safe and the structure does not appear to be grossly distorted (see Fig. 5.7). In a particular application of this roof structure this deflection would have to be reconsidered in the light of that application. For instance, the deflection of the roof must not damage any internal fittings.

It is apparent at this stage that designing structures in grp is considerably more complex than is the case with steel. Considerably more data on the material and the structure is required. Unfortunately, all of this data was not available for the design of the grp roof and assumptions were made. It is considered, however, that the assumptions made have been conservative but at the same time not too unrealistic. For instance, the environment chosen for estimating the creep and stress rupture of the grp was very damp. In fact the outer surface of the roof would be dry for long periods of time and at other times would be covered in water. Similar

comments could also be made about temperature. Also the upper roof surface would be frequently subject to U.V. light. To balance this however, the lower surface would be dry. An important point leading to the net effect of the assumptions being conservative is that creep was assumed to take place at 20°C. In fact creep of the roof under the snow load would take place at a temperature well below this.

To assess the efficiency of the design of the roof in grp the weight of the grp roof may be compared with the weights of conventional roof structures (Fig. 5.8). The weight of the grp roof is considerably below that of other roofing systems and in particular approximately $\frac{1}{3}$ of the weight of a portal frame roof. (The conventional roof weights were supplied kindly by I.D.C. Limited, Stratford.)

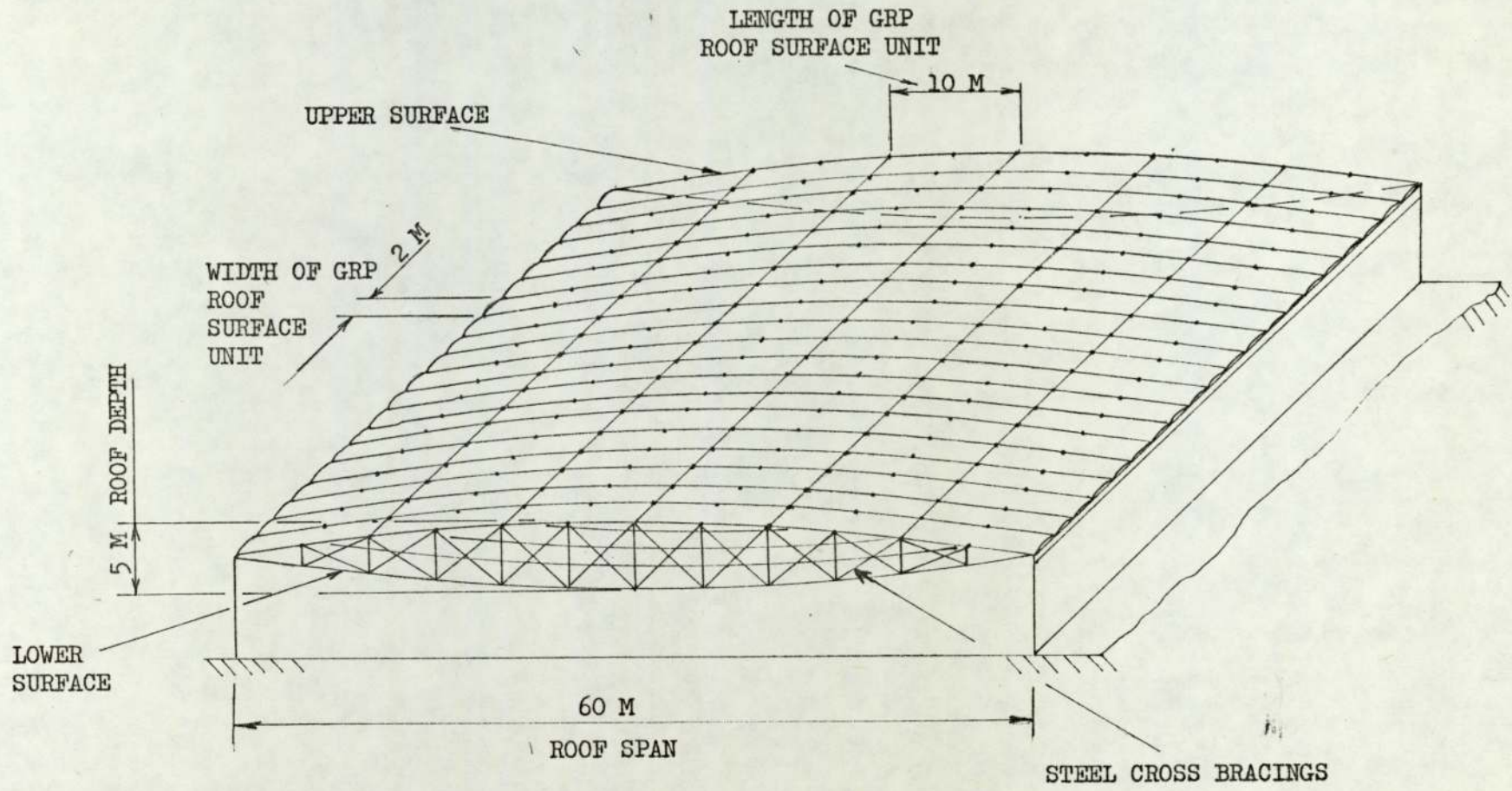


FIG. 5.1 GFRP ROOF DESIGN

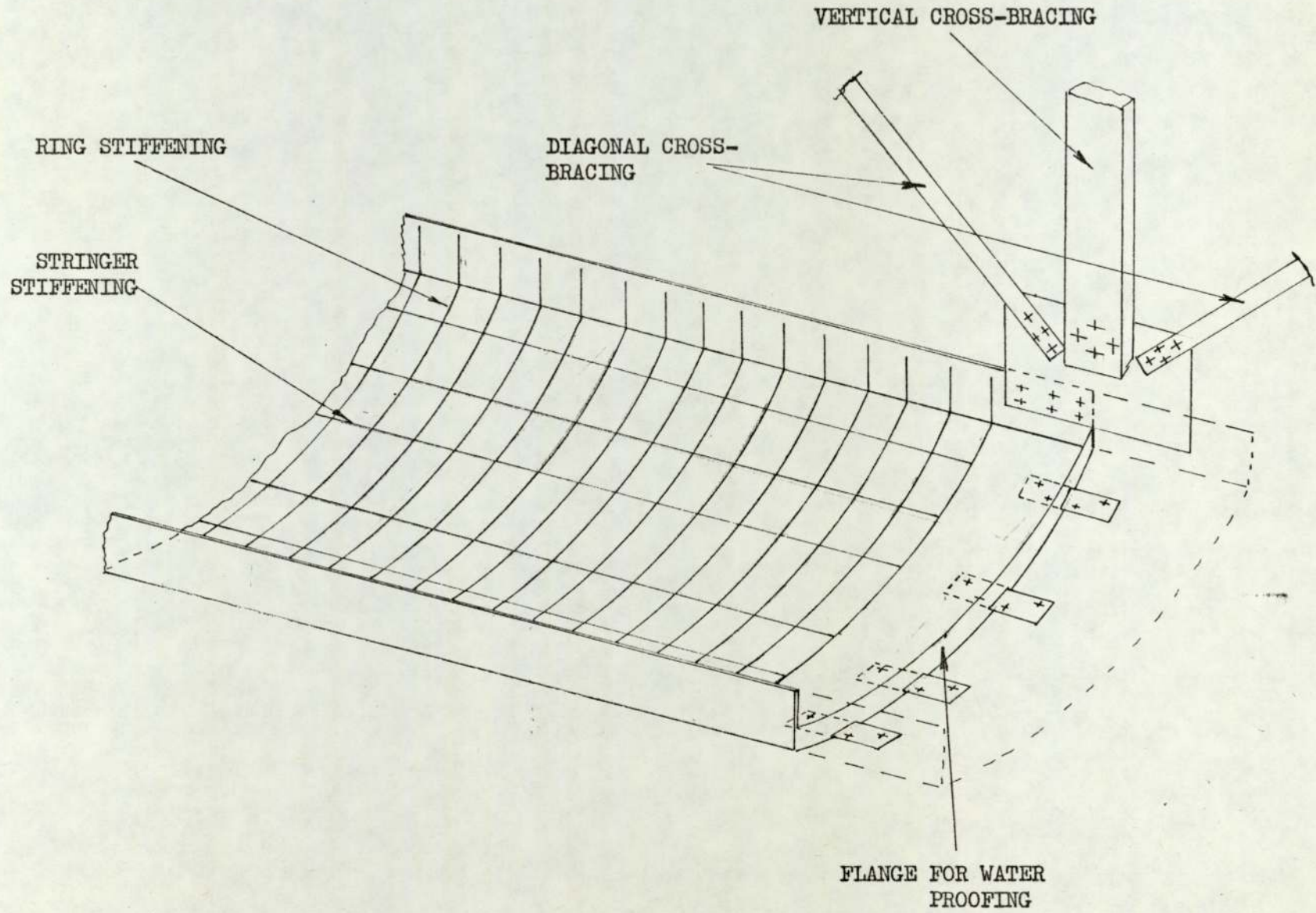


FIG. 5.2 VIEW OF LOWER SURFACE UNIT JOINT REGION

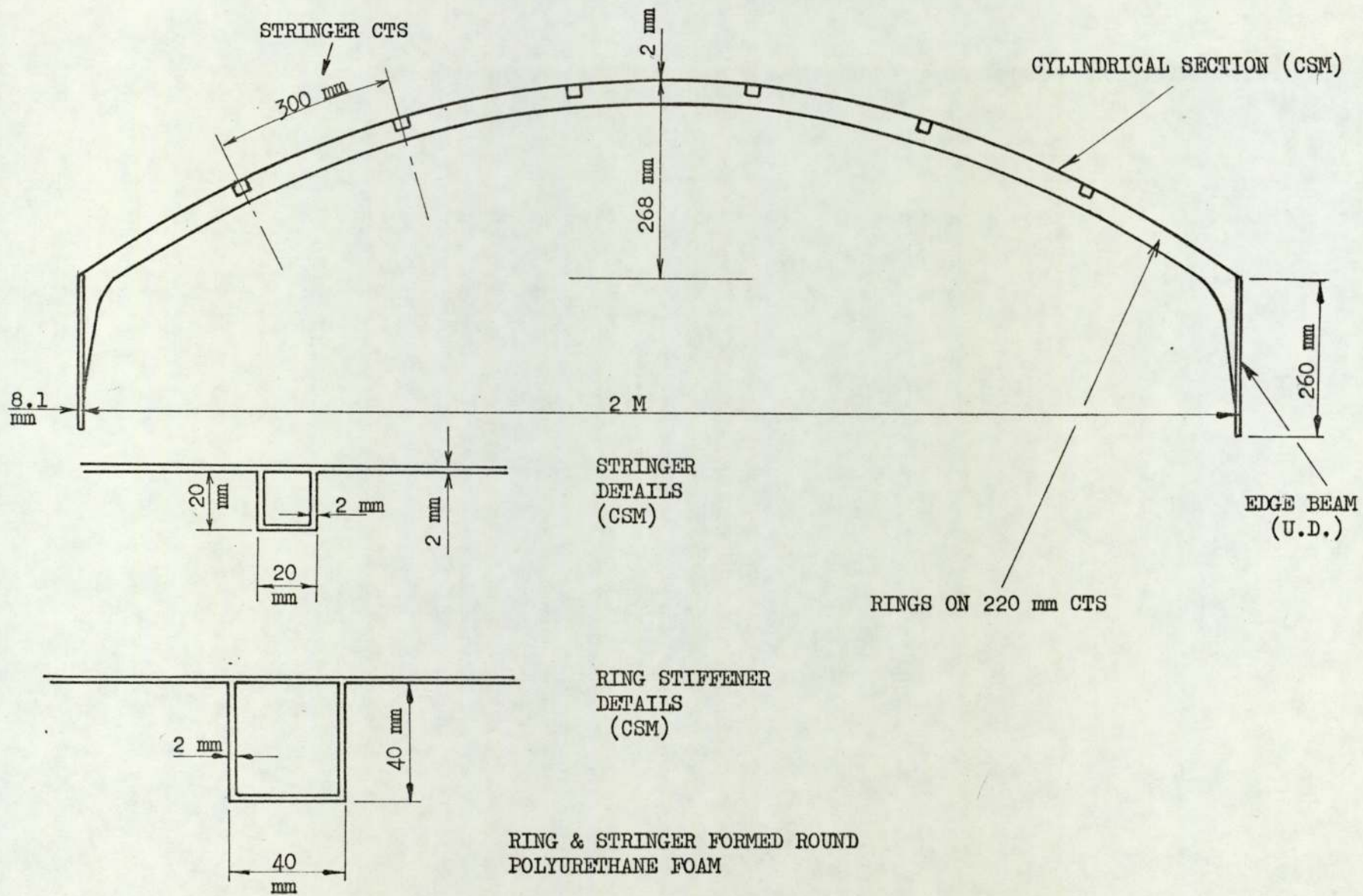
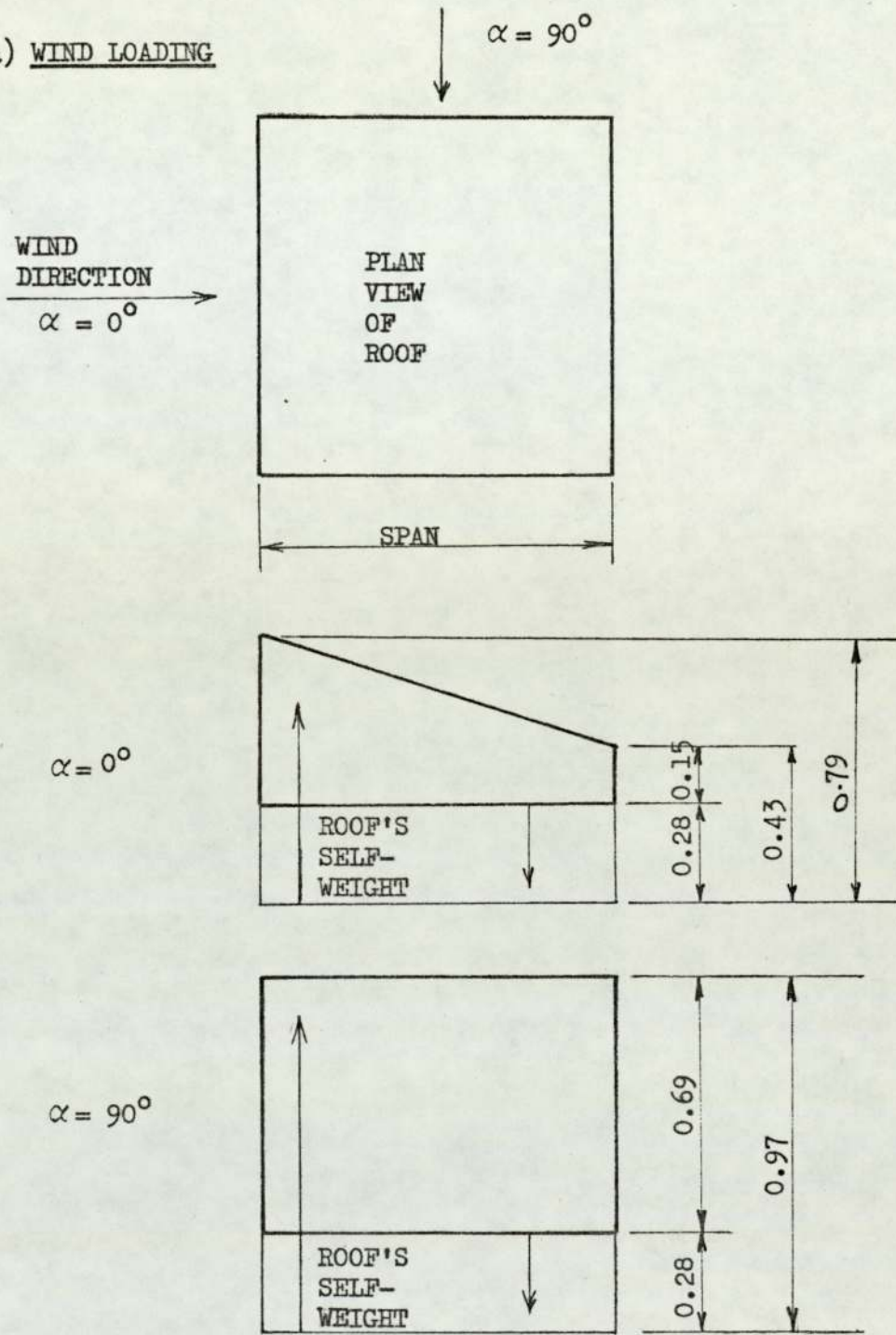


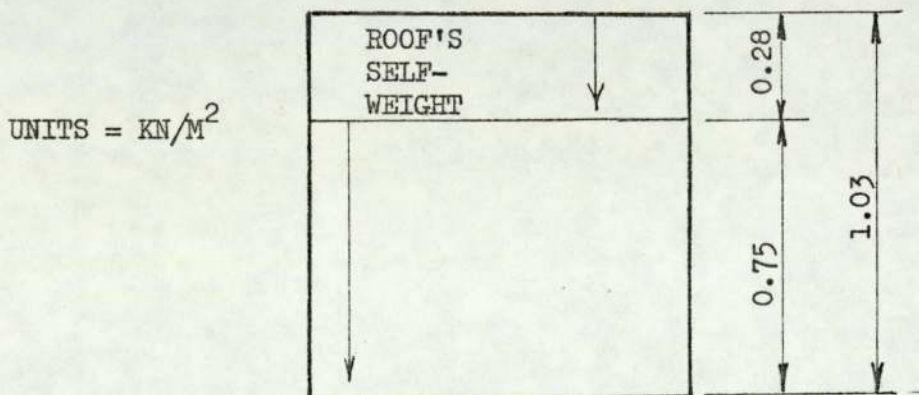
FIG. 5.3 ROOF SURFACE UNIT: CROSS-SECTIONAL DETAILS

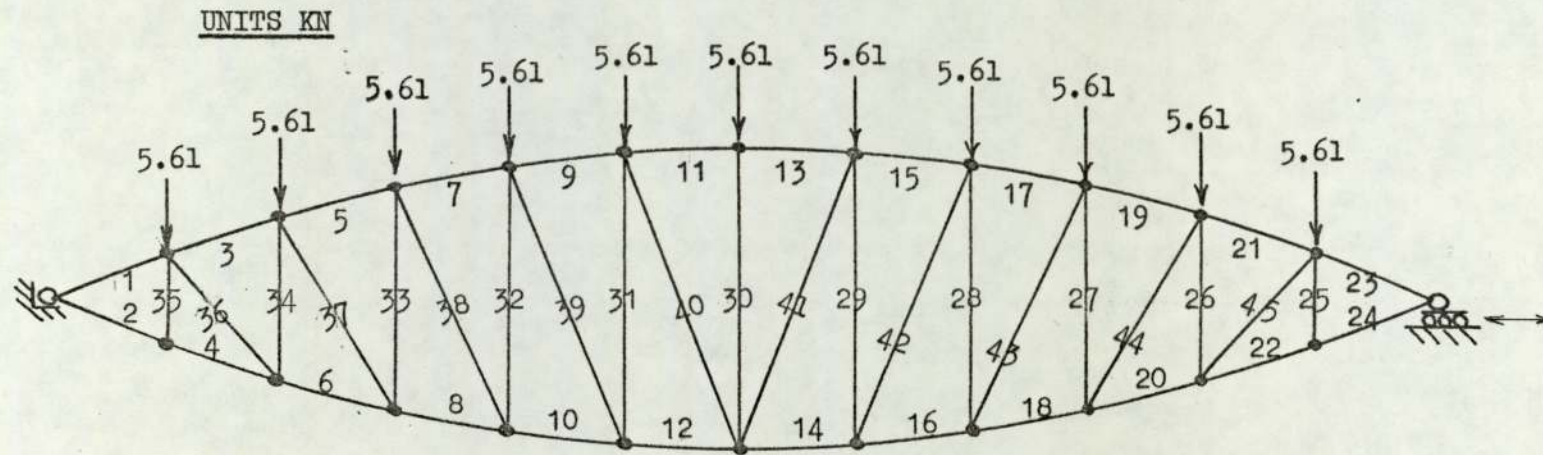
FIG. 5.4 **ROOF LOADING**

a) WIND LOADING



b) SNOW LOADING + SELF-WEIGHT





- PINNED JOINT
- RIGID JOINT

<u>MEMBER PROPERTIES</u>	<u>E</u>	<u>A_s</u>	<u>I_s</u>
GRP ROOF UNITS	1.97	22.9×10^{-3}	3.09×10^{-4}
VERTICAL CROSS-BRACING	203	1.58×10^{-3}	2.13×10^{-7}
DIAGONAL CROSS-BRACING	203	1.77×10^{-4}	1.0×10^{-8}
	$\times 10^6$ KN/M ²	M ²	M ⁴

FIG. 5.5 IDEALISED STRUCTURAL SYSTEM

FIG. 5.6 MEMBER LOADING

MEMBER NO.	AXIAL FORCE (KN)	SHEAR FORCE (KN)	B.MOMENT END 1 (KN M)	B.MOMENT END 2 (KN M)
1	- 98	0.64	0	-3.21
2	98	-0.64	0	3.21
3	-101.5	-0.56	3.12	-0.34
4	97.6	0.56	-3.12	0.34
5	-101.1	0.07	0.37	-0.71
6	101.3	-0.07	-0.37	0.70
7	-101	-0.05	0.71	-0.48
8	100.9	0.05	-0.71	0.48
9	-100.9	0	0.48	-0.47
10	100.9	0	-0.49	0.47
11	-100.8	0	0.47	-0.45
12	100.8	0	-0.47	0.45
30	-2.7	0	0	0
31	-2.7	0	0	0
32	-2.7	0	0	0
33	-2.7	0	0	0
34	-2.2	-0.02	-0.03	-0.03
35	-1.7	0.12	0.09	0.09
36	4.3	0	0	0
37	-0.21	0	0	00
38	0.22	0	0	0
39	0	0	0	0
40	0.05	0	0	0

SIGN CONVENTION : THE RIGHT HAND SCREW RULE IS ASSUMED. TRANSLATIONS AND ROTATIONS IN A POSITIVE SENSE WITH RESPECT TO THIS RULE ARE POSITIVE.

SCALE 1:250

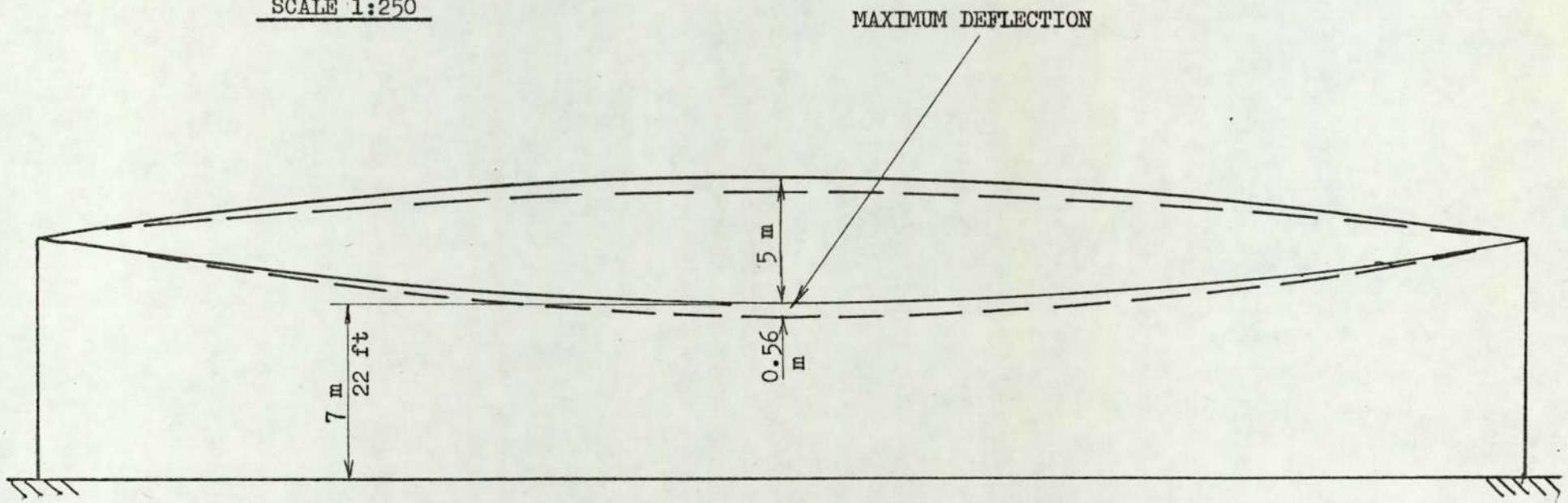
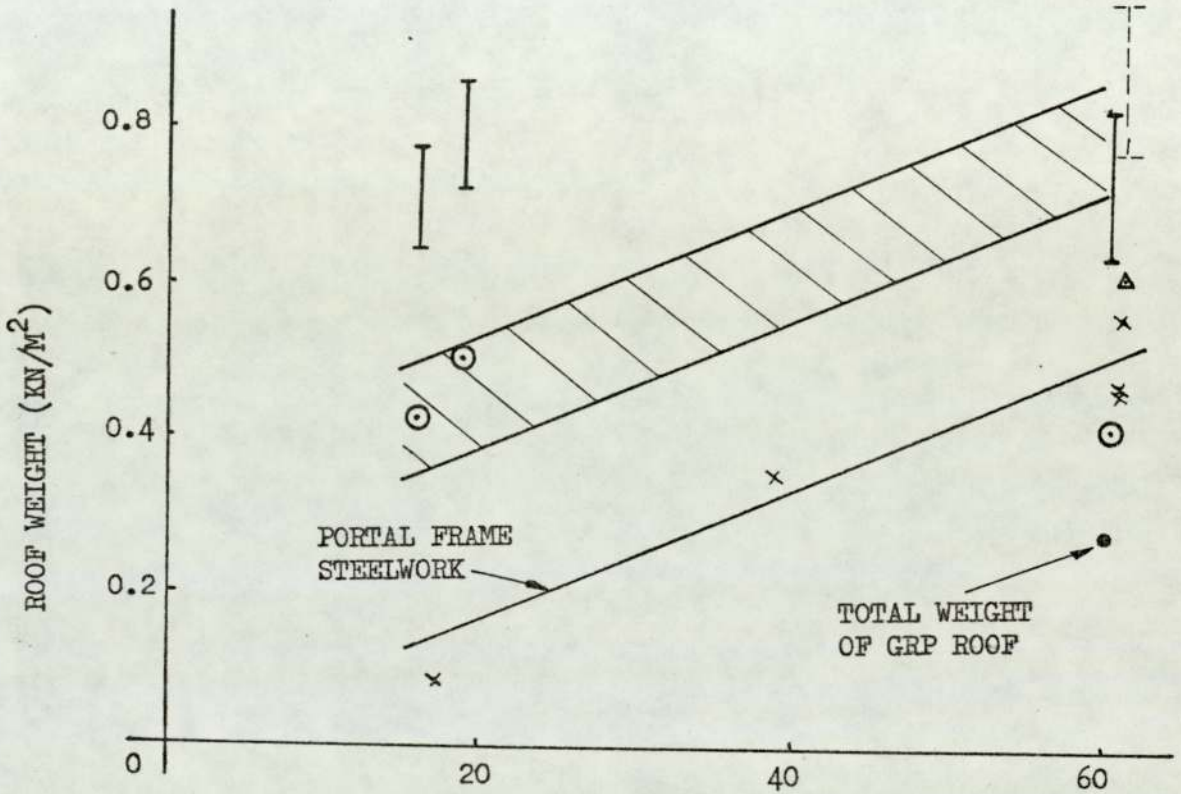





FIG. 5.7 ROOF DEFLECTION

FIG. 5.8 ROOF WEIGHT AGAINST SPAN



<u>STEEL WORK WEIGHTS</u>		<u>RANGE OF CLADDING WEIGHTS</u>	
x	PORTAL FRAME		PORTAL FRAME
⊙	LATTICE FRAMES (VARIOUS TYPES)		LATTICE FRAMES
△	POST-TENSIONED PRECAST CONCRETE ARCH		POST-TENSIONED PRECAST CONCRETE ARCH

CHAPTER 6

DESIGN, MANUFACTURE AND TESTING OF

A MODEL LONG SPAN ROOF

CHAPTER SIX

Design, Manufacture and Testing of a Model Long Span Roof

6.1

Introduction

In the previous chapter a preliminary design of a 60 m span grp roof was presented. In this chapter a model roof will be designed using similar principles. This will be followed by a brief description of the manufacture of the roof.

The purpose of the model roof is: a) to enable various tests to be applied so that the accuracy of the structural analysis may be examined, and b) to confirm the predicted structural behaviour of the roof as a whole and hence the suitability of grp as a structural material.

The model roof testing will be carried out in three stages: the roof will be tested under a uniformly distributed load simulating snow loading; secondly, under an unsymmetrical load to simulate behaviour under wind loading, and finally the roof will be left for an extended period under a simulated snow load so that the creep characteristics of the roof may be studied.

6.2

Scale of Model Roof

The size of the designed roof makes it impossible to build for testing within the resources of this project. Instead, a scaled down roof will be designed. A suitable scale for the model roof is 1/6th of the full size. This scale is large enough for the model to be reasonably realistic in shape and proportion, and small enough to be within the project's resources.

Although the major dimensions of the roof, such as span-to-depth ratio, will be designed to this scale, it will in some cases be impractical and in others imprudent to do so. For instance, the length of the surface units will be designed to a 1/5th scale so that the model surface unit's resistance to Euler buckling will be reduced to a level closer to that of the full scale roof. Also the manufacture of the model is simplified.

6.3.1 Surface Unit Design

The cross-section of the model surface unit is shown in Fig. 6.1. It will be noticed that orthotropic stiffening has not been included in the design. As it is not practical to reduce the skin thickness of the 60 m roof (2 mm) by a factor of 6, the model roof's skin is relatively thick at 1.49 mm, and stiffening is not required.

The distance between joints has been reduced by a factor of 5 to 1 M, making the length of each surface unit 2 m and the distance between cross-bracing joints 1 m.

The edge-beam stiffening shown in Fig. 6.1 is to be included on the outer edges of the compressive surface of the model. In this position there are no adjacent units to support the edge-beams against buckling. The diaphragm shown in the cross-sectional view is included in all the compressive surface units to prevent "flattening" of the cylindrical section.

6.3.2 Cross-bracing Design

The design of the cross-bracing is mainly influenced by the test loading technique. It is proposed to load the model using dead

weights slung below the roof. Thus all the cross-bracing may be designed for tensile forces only. This arrangement has the disadvantage that the vertical cross-bracing members are not used in precisely the same way as they would be under the snow load in the full size roof. However, this is not considered to be a serious disadvantage, since it does not affect greatly the grp members which are of most interest and concern. The arrangements considered to avoid this were either too complicated, expensive, inaccurate or required equipment which was not available. It should also be realised that the arrangement adopted is realistic in the case of wind loads, i.e. the vertical cross-bracing members would be expected to be in tension under this load.

The cross-sectional area, A_S , of the vertical cross-bracing is 600 mm^2 and the diagonals are 300 mm^2 and the second moment of areas, I_S , are 2290 mm^4 and 271 mm^4 respectively.

6.3.3 Joint Design

The joints between the grp surface units may be divided into two groups. Firstly, the joints in the cylindrically shaped part and secondly the edge-beam joints. The cylindrical section joints are shown in Fig. 6.2 and the edge-beam joints are shown together with a typical cross-bracing joint in Fig. 6.3.

6.3.4 End Fixing Design

The roof support and end joints are shown in Fig. 6.4. The knife edges employed effectively make the joints pinned, as was assumed in the analysis of the 60 m roof in Chapter 5 (Fig. 5.5). A small amount of horizontal movement was allowed for in the size of the "vee" support locating holes at one end.

6.3.5 Materials Summary

Fig. 6.5 shows the overall design of the model roof structure. The width of the roof, is 1 m, i.e. three beam-like elements. For two main reasons this width is considered to be the minimum required for testing. Firstly, a narrower roof would be susceptible to lateral buckling. The two outside beams are special cases since they have support only on one side. This is particularly important in the compressive surface which is subject to instability effects. Thus only the centre beam is a typical roof beam-like element.

The materials required for the roof structure as shown in Fig. 6.5 are as follows:

CSM 21 kg or 2.1 kg/m^2

Roving 12.6 kg or 1.26 kg/m^2

Polyester resin 65 kg or 6.5 kg/m^2

Total weight of grp in roof 98.6 kg or 9.9 kg/m^2

Total weight of steel 140 kg or 14 kg/m^2

Total self-weight of the roof is 0.23 KN/m^2 .

6.3.6 Analysis of Model

The analysis of the model roof will be carried out in three stages as follows:

- 1) Analysis based upon the theoretically determined elastic properties of grp.
- 2) Analysis based upon the experimentally determined elastic properties (Section 3.4).
- 3) Analysis based upon the visco-elastic properties of grp (Section 3.5) under prolonged loading.

6.3.6.1 Theoretical Elastic Analysis

The approach to the loading of the model roof will be similar to that adopted in the previous chapter. The uniformly distributed snow load will be idealised to nine discrete equal loads. The idealised system is shown in Fig. 6.6. The non-symmetrical wind loading is also idealised as shown in Fig. 6.6.

Based on the theories discussed in Sections 3.2 and 3.3 the following moduli may be calculated:

$$E_{\text{CSM}} (V_f = 0.16) = 7.74 \times 10^6 \text{ KN/M}^2 \text{ (See Fig. 3.10)}$$

$$E_{\text{UD}} (V_f = 0.32) = 25.58 \text{ KN/M}^2 \text{ (See Fig. 3.6)}$$

On the same basis it follows that:

$$\mu_{12, \text{CSM}} = \mu_{21, \text{CSM}} = 0.32 (V_f = 0.16)$$

By changing the unidirectional material of the edge-beams to an equivalent volume of CSM by the method of equivalent sections according to equation 5.9 it may be shown that:

$$A_S = 4.49 \times 10^{-3} \text{ m}^2$$

$$I_S = 3.27 \times 10^{-6} \text{ m}^4$$

On feeding these properties into the computer programme [5.6] the following were obtained:

Snow Loading

$$F_{\text{max}} = - 11.6 \text{ KN (Member 10 and 12)}$$

Max. bending moment applied to grp roof unit

$$= \pm 9.35 \times 10^{-2} \text{ KN M (Members 1, 2, 19 and 20)}$$

Max. deflection of roof = 12.7 mm (At centre line).

Wind Loading

$$F_{\text{max}} = - 5.73 \text{ KN (Member 4)}$$

Max. bending moment applied to grp roof unit

$$= - 5.0 \times 10^{-2} \text{ KN M (Member 2)}$$

Max. deflection of roof = 9.40 mm (At centre line).

6.3.6.2 Empirical Elastic Analysis

The applied loading for this analysis is identical to that used for the above computations.

From graph 3.6 and 3.10 it may be determined that the actual elastic moduli of the grp materials used are:

$$E_{\text{CSM}} = 7.05 \times 10^6 \text{ KN/M}^2$$

$$E_{\text{UD}} = 20.0 \times 10^6 \text{ KN/M}^2$$

Again using the method of equivalent sections, the following may be determined:

$$A_S = 4.13 \times 10^{-3} \text{ m}^2$$

$$I_S = 3.10 \times 10^{-6} \text{ m}^4$$

Computations based upon the modified data above lead to member loadings as tabulated in Figs. 6.7 and 6.8 for snow and wind loadings respectively. The tables show that the highest stresses are, as expected, due to the snow loading. The maximum deflection is shown to be 14.5 mm in table: Fig. 6.9.

The tabulated forces and moments and the equation below may be used to calculate the various stresses and strains.

$$\sigma = \frac{F}{A_S} \pm \frac{M y}{I_S} \quad 6.1$$

where σ = direct stress referred to CSM

F = member axial force

M = applied bending moment

y = distance from the neutral axis

y_{max} = 46 mm for the cylindrical section and

39 mm for the edge-beams.

Shear stresses have been neglected as insignificant and

will be less than 15 KN/M^2 .

From equation 6.1 it may be shown that the stress due to solely the snow load are:

1) For CSM: a) the maximum compressive stress, predicted in the cylindrical sections, is in members 10 and 12 and equal to $-2,800 \text{ KN/M}^2$.

b) the maximum compressive stress, predicted in the edge-beams, is in members 2 and 20:- $- 3500 \text{ KN/M}^2$.

c) the maximum tensile stress is in members 1 and 19:- $3,700 \text{ KN/M}^2$.

2) For unidirectional material:

a) the maximum compressive stress occurs in members 2 and 20:- $- 9,950 \text{ KN/M}^2$.

b) the maximum tensile stress occurs in members 9 and 11:- $7,800 \text{ KN/M}^2$.

To calculate stress in the unidirectional material, equation 6.1 is multiplied by a factor: $\frac{E_{UD}}{E_{CSM}}$

In cases 1b) and 2a) the maximum stresses occur at a cross-bracing node where there is some local reinforcement. The maximum stresses will, therefore, be very slightly lower.

If the self-weight of the model roof is allowed for, the stresses are increased by the following factor:

$$\frac{\text{model self-weight} + \text{snow load}}{\text{snow load}} = 1.31$$

6.2

The maximum stresses then become:

- 1) a) - 3,670 KN/M²
 b) - 4,590 KN/M²
 c) 4,850 KN/M²
- 2) a) - 13,000 KN/M²
 b) 10,200 KN/M²

The short term strength for CSM in tension, which is less than the compressive strength, is approximately 75×10^3 KN/M², giving a short-term safety factor of over 15. The corresponding strength of the unidirectional material is approximately 300×10^3 KN/M² giving a minimum safety factor of over 20.

Stability of cylindrical section

The critical stress for a cylinder subjected to an axial compressive load is given by Timoshenko 6.1 as:

$$\sigma_{cr} = \frac{E h}{a \left(\frac{3}{1 - \mu^2} \right)^{\frac{1}{2}}} \quad 6.3$$

However, cylinders are known to be very susceptible to imperfections of the cylinder wall so that the stress level predicted by equation 6.3 is never reached in practice. A more reliable equation is suggested by Little [6.2] as follows:

$$\sigma_{cr} = \frac{0.33 E h}{a \left(\frac{3}{1 - \mu^2} \right)^{\frac{1}{2}}} \quad 6.4$$

where h = cylinder wall thickness
 a = cylinder radius

Based upon equation 6.4 the critical stress of the cylindrical section is -6350 KN/M^2 giving a safety factor of 1.73 on the stress in the cylindrical section due to the snow load and self-weight. This, however, will be a slightly conservative estimate since the section is under combined bending and axial compression. Timoshenko [6.1] estimates an increase of about 30% in the critical stress for the pure bending case.

Euler buckling of surface unit

Treating the roof surface units as simply supported struts as in the previous chapter the buckling load is given by equation 5.10:

$$P_E = \frac{\pi^2 EI_s}{l^2} = 216 \text{ KN}$$

The maximum compressive axial force occurs in members 10 and 12, -11.6 KN, giving a factor of safety of 18.6.

Buckling of Steel Cross-bracing

Under wind loading steel work members 34 are under compression. There is a danger, therefore, of Euler buckling. As there is a large difference between the rigidities of the grp surface members and the cross-bracing, member 34 will be treated as a strut with rigid ends. Thus the buckling load (P_E) is given by:

$$P_E = \frac{4 \pi^2 EI}{l^2} = 1.27 \text{ KN/M width of roof}$$

The theoretical member load is given in Fig. 6.8 as 0.27 KN giving an adequate safety factor of 4.7.

6.3.6.3 Visco-elastic Analysis

It is intended to load the model roof simulating snow loading for a period of 4 weeks (672 hrs.). To calculate the approximate change in deflection over this period of time equations 5.2 to 5.5 will be used. In this case F equals the mean axial force in the grp members computed from table Fig. 6.7 and is equal to 10.95 KN.

$$\begin{aligned}\sigma_{\text{CSM}} &= 1266 \text{ KN/M}^2 \\ \sigma_{\text{UD}} &= 10,923 \text{ KN/M}^2 \\ \bar{E}_{\text{CSM}} &= 2.30 \times 10^6 \text{ KN/M}^2 \\ \bar{E}_{\text{UD}} &= 19.3 \times 10^6 \text{ KN/M}^2 \\ I_{\text{S}} &= 4.36 \times 10^{-6} \text{ m}^4 \\ A_{\text{S}} &= 8.50 \times 10^{-3} \text{ m}^2\end{aligned}$$

The deflection at the end of the loading period (δ_v) may be estimated in the following way:

$$\delta_v = \frac{\delta_{\text{EP}} \times (\bar{E}_{\text{CSM}} \times A_{\text{S}})_{\text{EP}}}{(\bar{E}_{\text{CSM}} \times A_{\text{S}})_v} \quad 6.4a$$

where suffix v refers to visco-elastic term suffix EP refers to an empirical elastic term.

$$\delta_v = 20.7 \text{ mm}$$

It is assumed here that the change in deflection is due to the change in axial stiffness of the grp members of the model roof structure. It is also assumed that the change in stiffness will not

lead to a large redistribution of load within the structure. This is supported by the fact that the difference in the loads in the grp members in the two elastic analyses was small. The axial force in members 10 and 12 remained unchanged and maximum bending moment in member 2 changed by only 10%.

The flexural rigidity (EI_g) of the grp members is reduced, i.e. from 21.9 KN M^2 to 10 KN M^2 , leading to a reduced but still adequate safety factor (≈ 7) against Euler buckling.

6.4

Preliminary Tests

6.4.1 Surface Unit Compression Test

6.4.1.1 Introduction

It is proposed to test the model roof upto a load equivalent to 1.75 times the snow load. Thus, at this maximum short term load, including the roof's self-weight, the safety factor of Section 6.3.6.2 will be reduced by a factor of 1.57. The safety factor for local buckling thus becomes 1.1. This may be inadequate to prevent local buckling due to the empirical nature of equation 6.4.

Local buckling of the cylindrical section will lead to a redistribution of stress in the surface unit. This, in turn, may lead to further buckling. In addition, thin-walled open sections have

been known to buckle in unexpected modes and thus it is considered necessary to carry out a preliminary compression test on a surface unit. Further, such a test provides an opportunity to examine:

- a) the compressive strength of joints similar to the surface unit joints, and b) the accuracy of the buckling formula, equation 6.4.

6.4.1.2 Description of Test

Fig. 6.13 shows a general view of the test specimen and equipment. The roof unit is shown as a column with its edges stiffened with special aluminium channel. The purpose of the edge stiffening is to simulate the support given to the edges, in the roof, by adjacent units. Fig. 6.14 shows a more detailed view of this arrangement. Of the several fixing screws in each stiffening section only one is tightened firmly. The others are "finger-tightened" only. This ensures that the aluminium does not take any axial load.

The column is mounted between two concrete blocks which are located in a large testing frame. The joints between the test specimen and the concrete blocks are equivalent to the inter-unit joints of the roof shown in Figs. 6.2 and 6.3. The steel joint plates are, however, set into the concrete blocks rather than in adjoining units.

The load was applied to the test specimen by use of a large calibrated hydraulic jack. The maximum load applied was built up in increments of 2.5 KN to 20 KN.

Electrical resistance strain gauges were used to detect the onset of local buckling (see Fig. 6.15). A dial test indicator was placed level with the web of the cylindrical section, where local buckling would not occur, to detect bending of the column. The electrical resistance strain gauges were used in conjunction with a computerised data logger. This enabled the time between load increments to be kept to a minimum and hence minimise the effect of creep.

6.4.1.3 Results of Test

Table, Fig. 6.16 shows strain gauge results and Fig. 6.17 shows a graph of lateral deflection against load as measured by the dial test indicator. These results indicate that the strain is approximately uniform throughout the section and that it is directly proportional to load up until the onset of local buckling. However, on close examination it can be determined that the strain and hence the axial load is greater in the edge-beams than in the cylindrical section. In fact, at a load of 12.5 KN the mean strain of all the edge-beam strain gauges is $- 1.374 \times 10^{-3}$ M/M, whereas in the cylindrical section the mean measured strain is $- 1.194 \times 10^{-3}$ M/M. The theoretical strain at this load is $- 1.290 \times 10^{-3}$ M/M. This compares well with the mean of all the strain gauge results, $- 1.284 \times 10^{-3}$ M/M. Fig. 6.18 shows the strain distribution at section A-A (Fig. 6.15) and the tendency for lower strain in the cylindrical section. This may be explained by the propensity of stress to be attracted to the stiffer elements of structures at the expense of the less stiff. Imperfections in the cylindrical part of the specimen will cause local

bending. This effectively reduces the axial stiffness of the material causing higher stresses to be taken by the relatively stiff edge-beams and the regions close to the corners between the cylindrical section and edge-beams.

The onset of buckling was observed visually (Fig. 6.19) at a load of 12.8 KN which corresponds to an overall mean strain of $- 1.330 \times 10^{-3}$ M/M. Allowing for the non-uniform strain distribution between the sections of the specimen the mean strain in the cylindrical section was $- 1.200 \times 10^{-3}$ M/M. The corresponding stress is $8,600 \text{ KN/M}^2$. From equation 6.4 the theoretical buckling stress is $6,350 \text{ KN/M}^2$ which is a factor of 1.35 lower.

Figs. 6.20 and 6.21 show the effect of buckling on the load-strain relationship is to cause sharp discontinuities. On further increases of load, buckling develops further until at 20 KN local buckling was general throughout the specimen including the short unsupported lengths of the edge-beams (see Fig. 6.22). However, no material failure occurred and on unloading, the specimen recovered its original geometry.

Fig. 6.17 shows a graph of lateral displacement of the specimen, as measured by the dial test indicator, against load. Again the graph is linear upto buckling, whereupon a sharp discontinuity occurs. The maximum deflection, however, was approximately 1.3 mm and occurred after buckling. This corresponds to a span to deflection ratio of 770:1 and indicates that little bending took place.

The joints showed no signs of damage as a result of the test. The maximum axial stress in the CSM material was $- 14,500 \text{ KN/M}^2$ and

the maximum compressive stress expected in the model roof is
- 7200 KN/M².

6.4.1.4 Conclusions

- 1) The local buckling stress of the cylindrical section was 8,600 KN/M². Equation 6.4 was shown to be conservative in this case. On the basis of this result the equation may be modified to:

$$\sigma_{cr} = \frac{0.45 E h}{a \left(3 (1 - \mu^2) \right)^{\frac{1}{2}}}$$

However, a wide range of values for buckling stress would be expected from a large number of test specimens, and would depend upon the irregularities of each specimen.

- 2) No indication of Euler buckling of the specimen was found before or after local buckling.
- 3) Grp is capable of complete recovery after buckling.
- 4) The joints are capable of sustaining greater loads than they are expected to encounter during tests of the model roof.
- 5) There is a tendency for the cylindrical section to take less load than expected theoretically.

- 6) The design is adequate for use in testing the model roof.

6.4.2 Tensile Joint Tests

6.4.2.1 Introduction

Insufficient theory or data is available to be able to design reliably the joints for the model roof. In the previous section a joint design was proved in compression; in this section the joints will be tested in tension. Other similar joints will be also tested for comparison.

6.4.2.2 Description of Tests

The grp lay-up for all the joints was as shown in Figs. 6.2 and 6.3; the details of the proposed model roof joints, which are denoted as Type A. The details of the other joints to be tested are shown in Figs. 6.23 and 24. In all cases the joints were tested in a Denison testing machine at a strain rate causing failure within 1.5 to 2.5 mins.

6.4.2.3 Results of Tests

Cylindrical Section Joints

The strongest joint was type B, Fig. 6.23, which failed at 11.6 KN. Fig. 6.25 shows the failed specimen. Joint type A Fig. 6.2 failed at a marginally lower load of 10.2 KN and is shown in Fig. 6.25. The weakest joint was type C, Fig. 6.26 with a failure load of $0.6 T_f$.

Edge-beam Joints

Of the two types of edge-beam joints tested, type A, Fig. 6.3 was the stronger with a failure load of 25.3 KN. Type B, Fig. 6.24 failed at 23.5 KN. The failed specimens are shown in Fig. 6.27.

6.4.2.4 Discussion of Results

The failed specimens in general show clear evidence of material crushing at the bolts, which is an indication that the edge and side distances, measured from the holes, are adequate (see Section 4.6.2). Modification of these distances would, therefore, not be expected to increase the strength of the joints for a given hole arrangement.

Although previous evidence suggests that several small bolts are preferable to a smaller number of large bolts (see Section 4.6.2) this was not found to be the case in this instance for the cylindrical section joints.

The strength of the cylindrical section joint, A, used in the model roof design is capable of producing a stress in the section of $63,400 \text{ KN/M}^2$, whereas the maximum tensile stress expected in the section under the design load is 4850 KN/M^2 giving a safety factor of about 13. The safety factor for the edge-beam joint is greater than this.

Although the cylindrical section joint B is stronger than the designed model joint A, it is not proposed to use the joint B as its large hole is more difficult to manufacture than the two smaller holes of joint A.

6.4.2.5 Conclusions

- 1) The strongest joints were found to be cylindrical section joint B and edge-beam joint A.
- 2) The joints used in the design of the model roof (types A) are adequate.

6.5

Model Roof Manufacture

The grp roof members were manufactured by the hand lay-up process described in Sections 2.10.1 and 4.4.1 using a female mould.

The steel work was manufactured from hot-rolled mild steel and required only cutting to size and drilling.

The roof was assembled on its side using a floor to mark out the roof shape. The roof, having been bolted together, was correctly orientated and lifted onto its supports with the aid of hydraulic fork lifts.

Typical inter-surface section joints are shown in Figs. 6.2 and 6.3 and a cross-bracing node where sections are not joined is shown in Fig. 6.10. The roof supports are shown in Fig. 6.4 and a general view of the roof can be seen in Fig. 6.11.

6.6

Model Roof Testing

6.6.1 Introduction

In this section the model roof testing technique will be described. To prove the roof design and to confirm its predicted behaviour, the testing will be carried out in three stages: firstly a uniform load, equivalent to the statutory snow load x 1.75, will be applied to the roof over a short period of time to examine the elastic behaviour; this will be followed by a test under non-uniform loading to examine the elastic response to wind loading; and finally the roof will be tested under prolonged snow loading and the creep behaviour of the roof observed.

6.6.2 Loading Details

The loading system of the model roof corresponds in principle to the system shown in Fig. 6.6. The dead-weights were supported by means of specially made trays and nylon ropes from the lower cross-bracing nodes as shown in Fig. 6.12. The dead-weights themselves consisted of rectangular buckets filled to various degrees with scrap iron so that the maximum load of 1.75 x the snow load could be applied in seven increments. Unfortunately, for practical reasons it was not possible to simply add additional buckets for each increment: it was necessary to replace buckets leading to an irregular loading cycle. Three groups of buckets, corresponding to $\frac{1}{4}$, $\frac{1}{2}$ and 1 x the snow load, were used in the following ways.

A) Snow Load:

Increment	Buckets (x snow load)
1	$\frac{1}{4}$
2	$\frac{1}{2}$
3	$\frac{1}{4} + \frac{1}{2}$
4	1
5	$1 + \frac{1}{4}$
6	$1 + \frac{1}{2}$
7	$1 + \frac{1}{4} + \frac{1}{2}$

B) Wind Load:

Increment	Joint Nos.	Joint Nos.	Joint Nos.
	16,18,14,12	10	8,6,4,2
1	$\frac{1}{2}$	$\frac{1}{4}$	0
2	$\frac{1}{4} + \frac{1}{2}$	$\frac{1}{2}$	$\frac{1}{4}$
3	1	$\frac{1}{4} + \frac{1}{2}$	$\frac{1}{2}$
4	$1 + \frac{1}{4}$	1	$\frac{1}{4} + \frac{1}{2}$
5	$1 + \frac{1}{2}$	$1 + \frac{1}{4}$	1
6	$1 + \frac{1}{4} + \frac{1}{2}$	$1 + \frac{1}{2}$	$1 + \frac{1}{4}$

C) Creep Test Loading:

Load intensity was constant as per increment 4 of the snow loading test.

For cases A) and B) 10 mins. were allowed inbetween increments of load.

6.6.3 Gauging

The behaviour of the roof was monitored by the use of electrical resistance strain gauges, in conjunction with a computerised data logger, and dial test indicators for the short term tests. The dial test indicators were used alone for the creep test.

176 strain gauges were used to detect the onset of buckling and to check the predicted member forces. All strain gauges were used in pairs: one on each side of the section to be gauged. By taking the mean reading of these pairs, the effect of local bending in the direction of the roof beams' axis could be eliminated. Three main roof sections were examined with the gauges: the central regions of members 19 and 20, 17 and 18 and members 11 and 12. Steel work members 21, 22, 36 and 37 between beams A and B and beams B and C were also gauged.

Four dial test indicators were used to measure the deflection of the lower surface of the roof as follows:

Dial Test Indicator	Joint No.	Beam No.
1	4	B
2	10	B
3	10	A
4	16	B

The location of indicator 1 may be seen in Fig. 6.12.

The temperature of the environment varied between 14' - 16°C during testing.

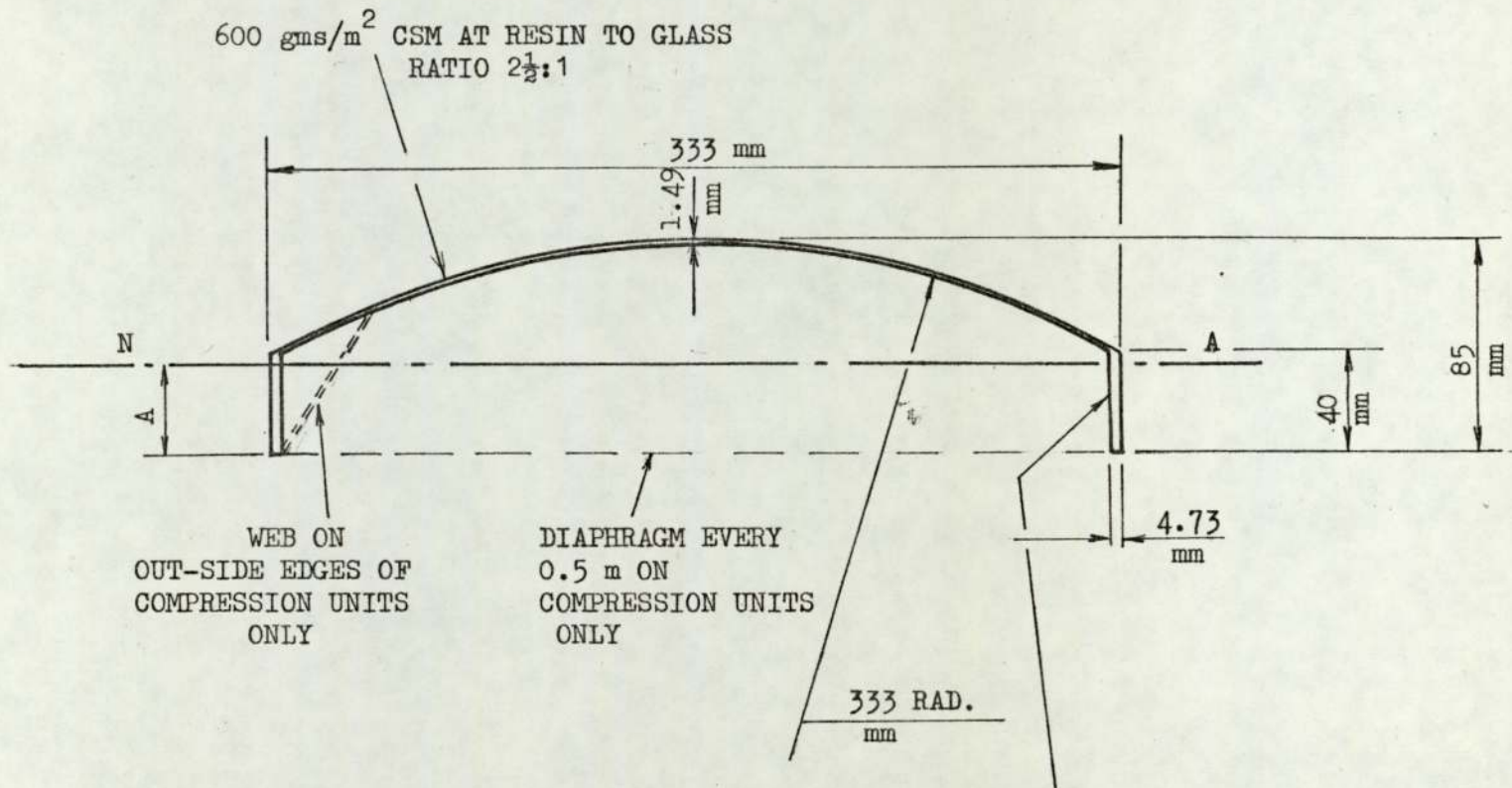


FIG. 6.1 CROSS-SECTION OF ROOF SURFACE UNIT

DIMENSION A

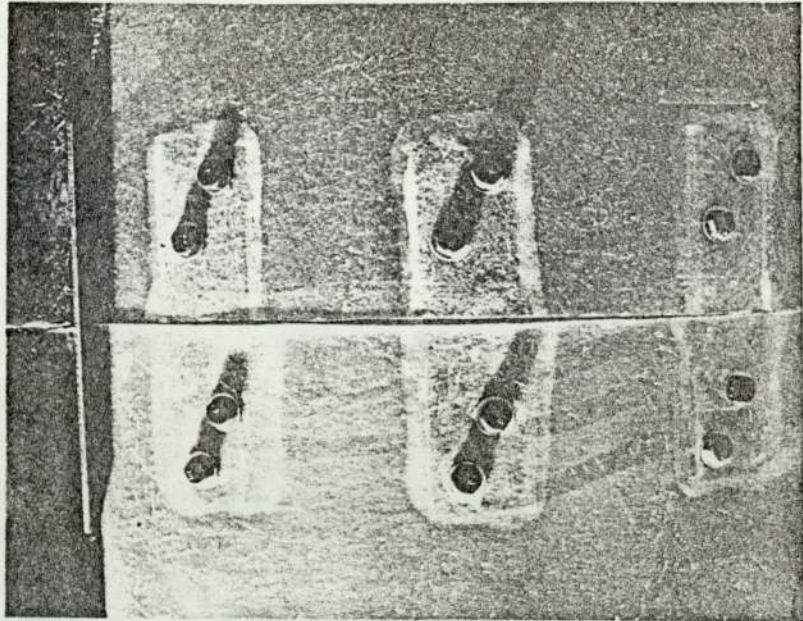
THEORETICAL MODULUS A = 37.5 mm

EMPIRICAL MODULUS A = 39 mm

600 gms/m² CSM AT 2½:1
 PLUS 2600 gms/m² ROVINGS
 AT 1:1 RESIN TO GLASS RATIO

FIG. 6.2 SURFACE UNIT CYLINDRICAL SECTION JOINT
(TYPE A)

GENERAL VIEW



PARTIAL VIEW AT CROSS-SECTION ON
CENTRE LINE

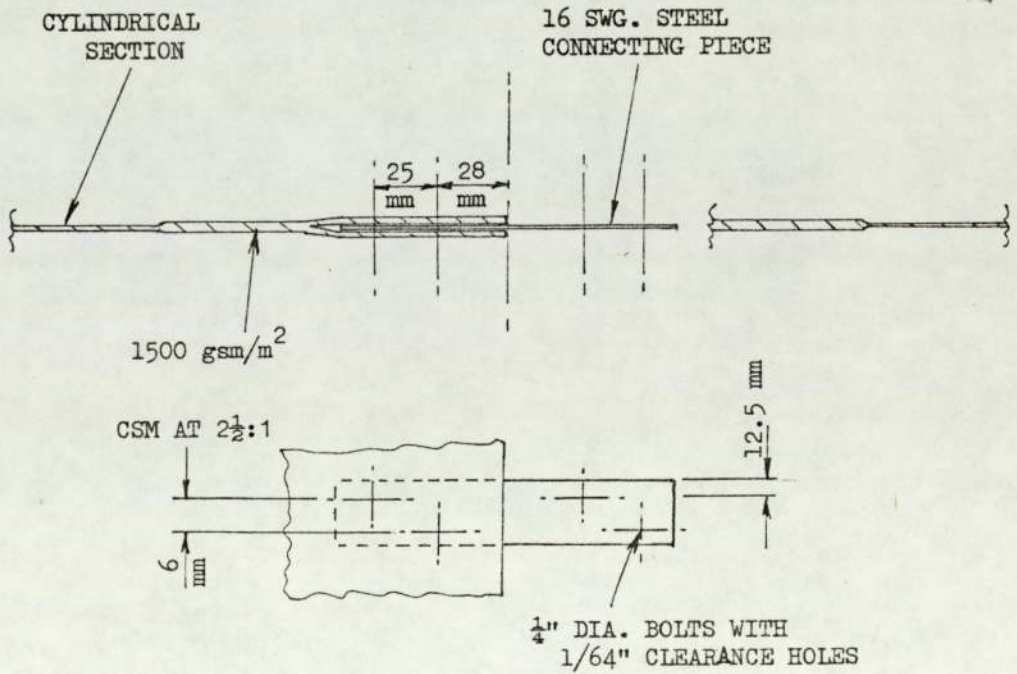
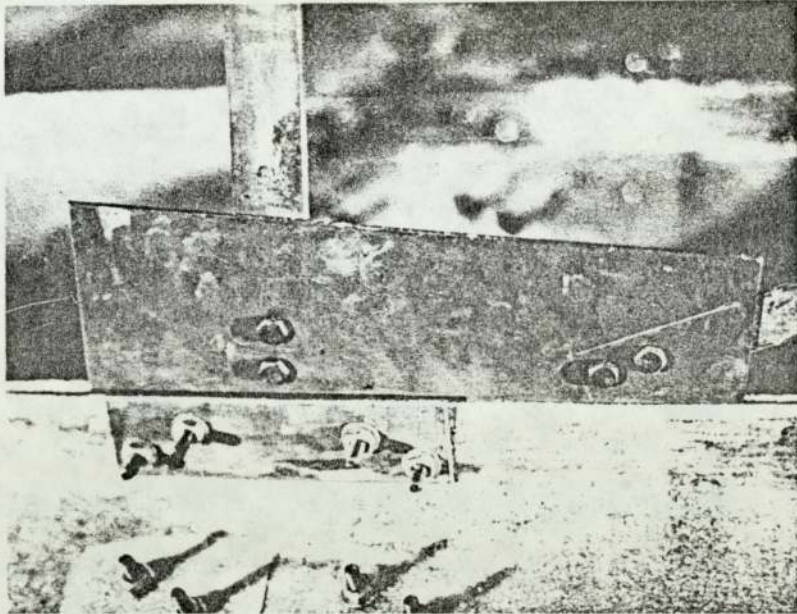


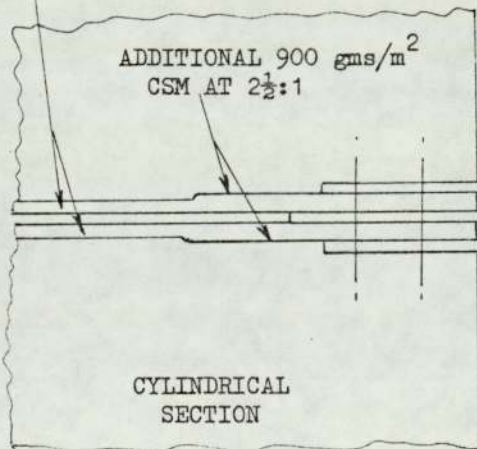
FIG. 6.3 EDGE-BEAM AND CROSS-BRACING JOINT
(TYPE A)

GENERAL VIEW



VIEW SHOWING LOCAL REINFORCEMENT
AND JOINT DETAILS

EDGE-BEAMS
SEE FIG. 6.1



JOINT FISH
PLATES

CROSS-BRACING
JOINT PLATE

¼" DIA. BOLTS WITH
1/64" CLEARANCE HOLES

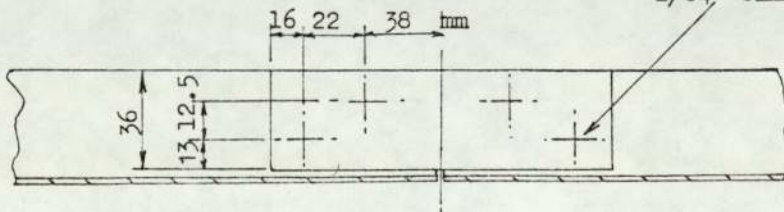
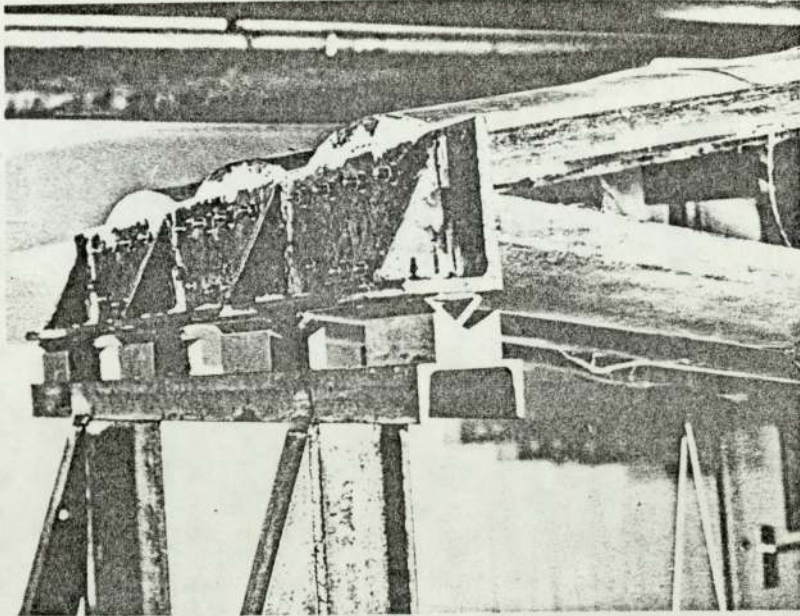
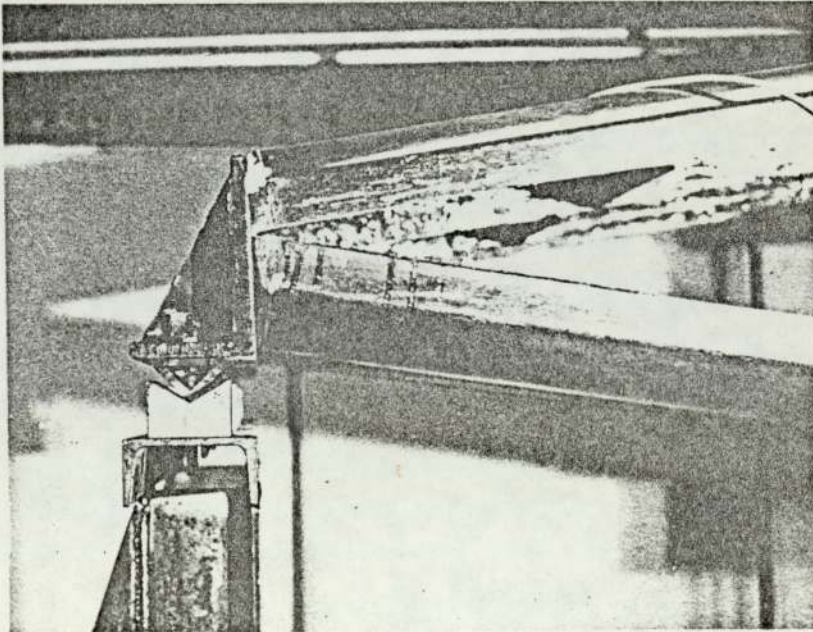


FIG. 6.4 ROOF SUPPORT AND END JOINTS

GENERAL VIEW



END ELEVATION



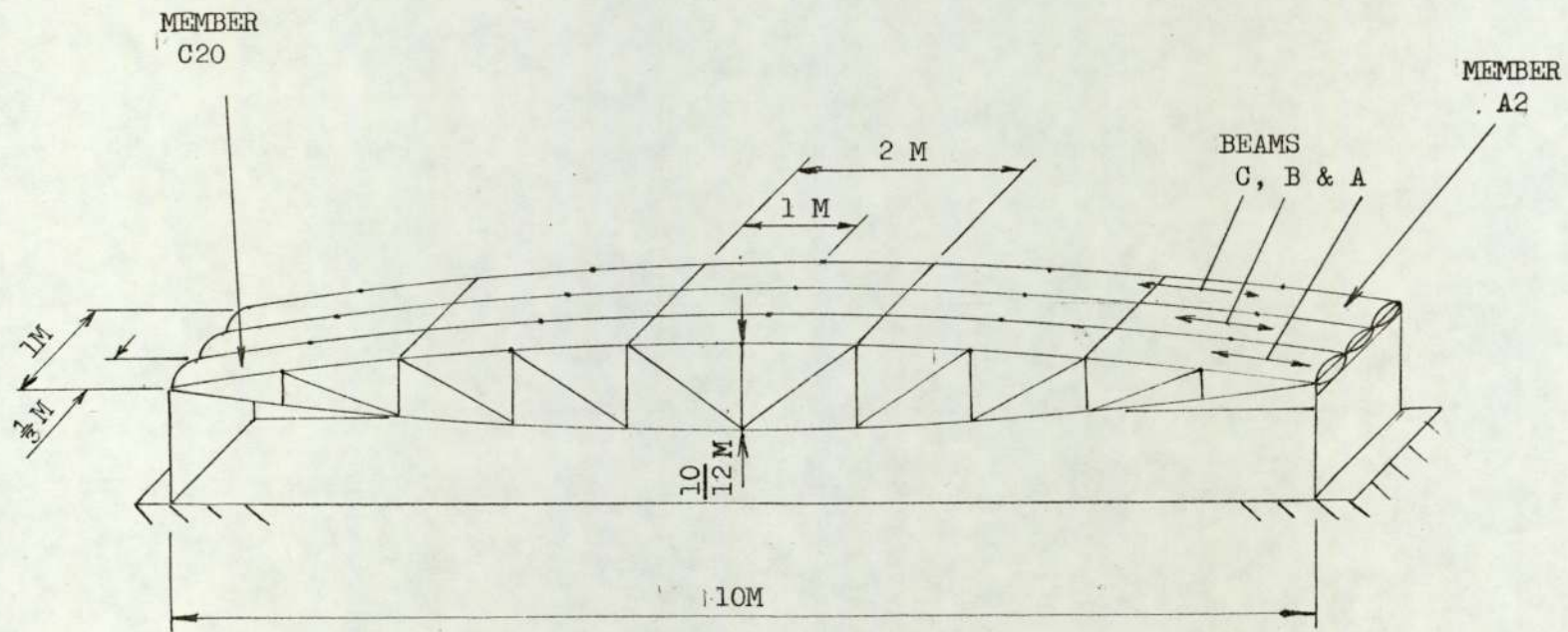


FIG. 6.5 DIAGRAM OF MODEL ROOF

- PINNED JOINTS
- RIGID JOINTS
- 3 MEMBER NO.
- 3 JOINT NO.

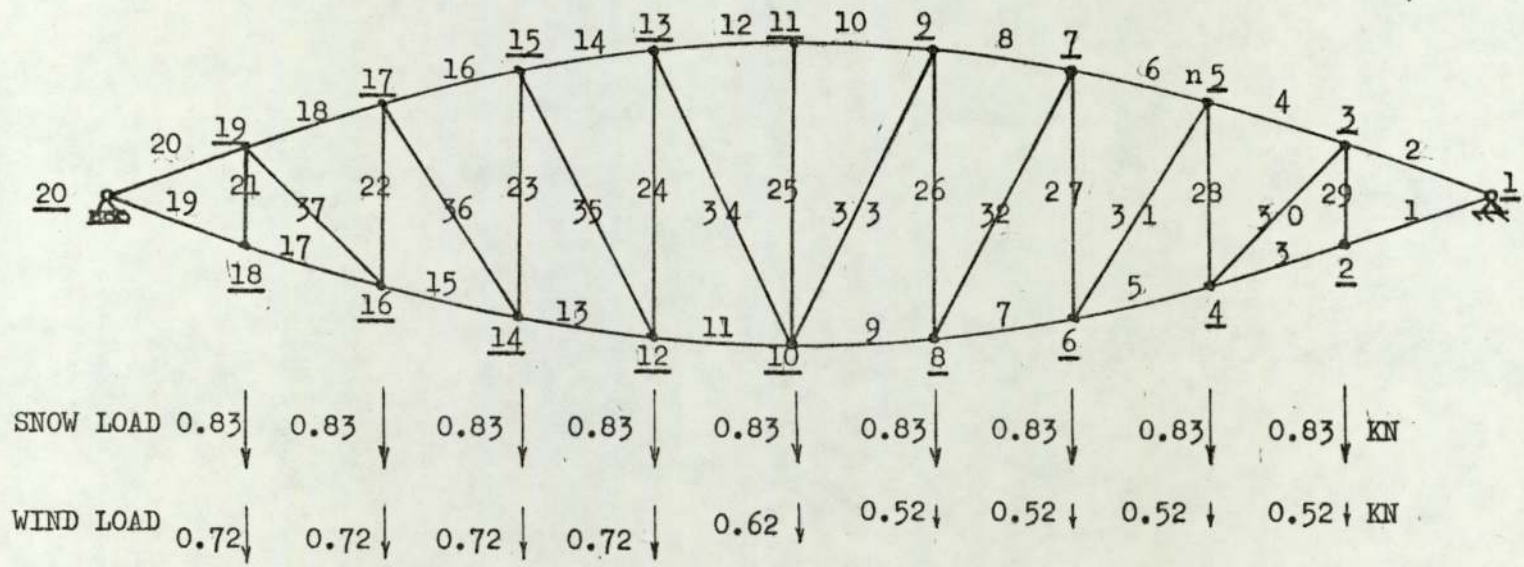


FIG. 6.6 LOADING OF MODEL ROOF

FIG. 6.7 ROOF MEMBER LOADING - SNOW LOAD

MEMBER NO.	AXIAL FORCE KN	SHEAR FORCE KN	MOMENT END 1 KN M	MOMENT END 2 KN M
1	9.88	-0.09	0	0.087
2	- 9.88	0.09	0	-0.087
3	9.93	0.05	-0.058	0.014
4	- 9.93	-0.04	0.053	-0.015
5	11.1	0	-0.022	0.018
6	-11.4	0	0.019	-0.019
7	11.4	0	-0.021	0.015
8	-11.5	0	0.019	-0.016
9	11.5	0	-0.017	0.017
10	-11.6	0	0.016	-0.017
25	0.37	0	0	0
26	0.34	0	0	0
27	0.25	0	0	0
28	0.06	-0.02	0.006	
29	0.06	0.15	-0.029	-0.028
30	1.32	0	-0.006	0.002
31	0.43	0	-0.002	0.002
32	0.17	0	-0.002	0.002
33	0.72	0	-0.001	0.002

FORCES AND MOMENTS ARE PER METRE WIDTH OF ROOF.

OTHER MEMBER FORCES AND MOMENTS MAY BE OBTAINED BY SYMMETRY.

POSITIVE ROTATIONS AND TRANSLATIONS CONFORM TO THE "RIGHT HAND SCREW RULE".

FIG. 6.8 ROOF MEMBER LOADING - WIND LOAD

MEMBER NO.	AXIAL FORCE KN	SHEAR FORCE KN	MOMENT END 1 KN M	MOMENT END 2 KN M
1	6.78	-0.067	0	0.068
2	-6.78	0.069	0	-0.070
3	6.81	0.035	-0.046	0.008
4	-7.77	0.032	0.045	-0.013
5	7.71	0	-0.018	0.015
6	-8.10	0	0.015	-0.016
7	8.07	0.005	-0.018	0.013
8	-8.34	-0.001	0.015	-0.014
9	8.34	-0.001	-0.015	0.014
10	-8.61	0.002	0.012	-0.014
11	8.79	- .001	-0.015	0.016
12	-8.61	0	0.015	-0.015
13	8.88	-0.007	-0.013	0.020
14	-8.82	0.004	0.014	-0.018
15	8.73	-0.003	-0.017	0.020
61	-8.91	0	0.018	-0.019
17	7.89	-0.033	-0.012	0.055
18	-8.79	0.039	0.014	-0.053
19	7.86	0.080	-0.080	0
20	-7.86	-0.081	0.081	0
21	0.10	-0.132	0.025	0.024
22	0.14	0.021	-0.061	-0.006
23	0.33	0	0	0
24	0.48	0	0	0
25	0.27	0	0	0
26	0.36	0	0	0
27	0.33	0	0	0
28	-0.05	-0.015	0.004	0.005
29	-0.02	0.118	-0.022	-0.021
30	1.03	0	0	0
31	0.45	0	0	0
32	0.34	0	0	0
33	0.36	0	0	0
34	-0.27	0	0	0
35	-0.08	0	0	0
36	0.19	0	0	0
37	0.99	0	0	0

FIG. 6.9 DEFLECTION OF MODEL ROOF - EMPIRICAL
ELASTIC ANALYSIS

JOINT NO.	DEFLECTION (mm)	
	SNOW LOAD	WIND LOAD
1	0	0
2	6.5	4.6
4	10.2	7.3
6	12.7	9.2
8	14.0	10.3
10	14.5	10.7
12	14.0	10.5
14	12.7	9.6
16	10.2	7.8
18	6.5	5.0
20	0	0

FIG. 6.10 ROOF CROSS-BRACING NODE

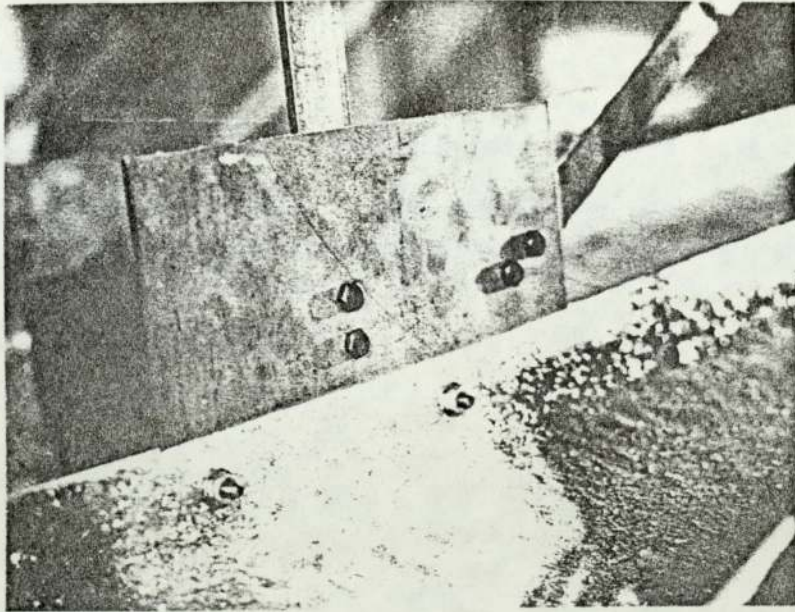


FIG. 6.11 GENERAL VIEW OF MODEL ROOF

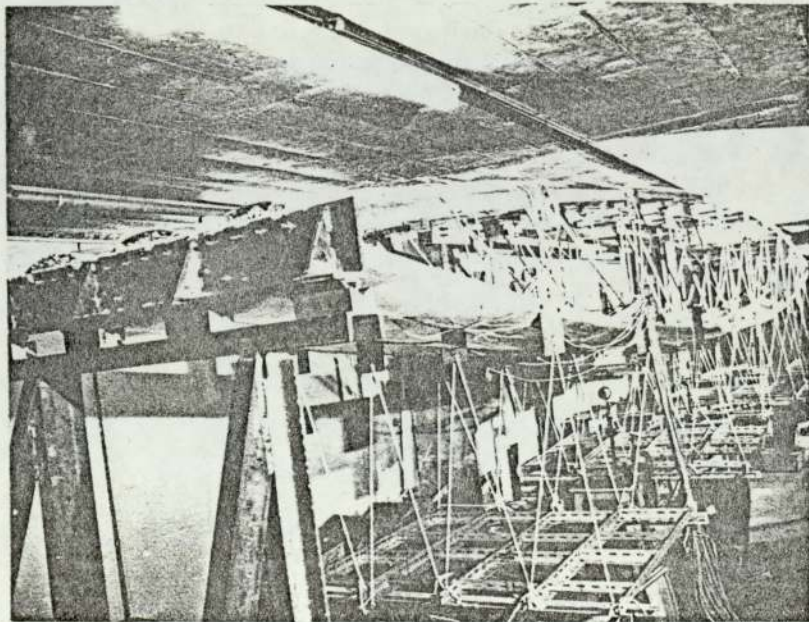


FIG. 6.12 LOAD SUPPORT ARRANGEMENTS

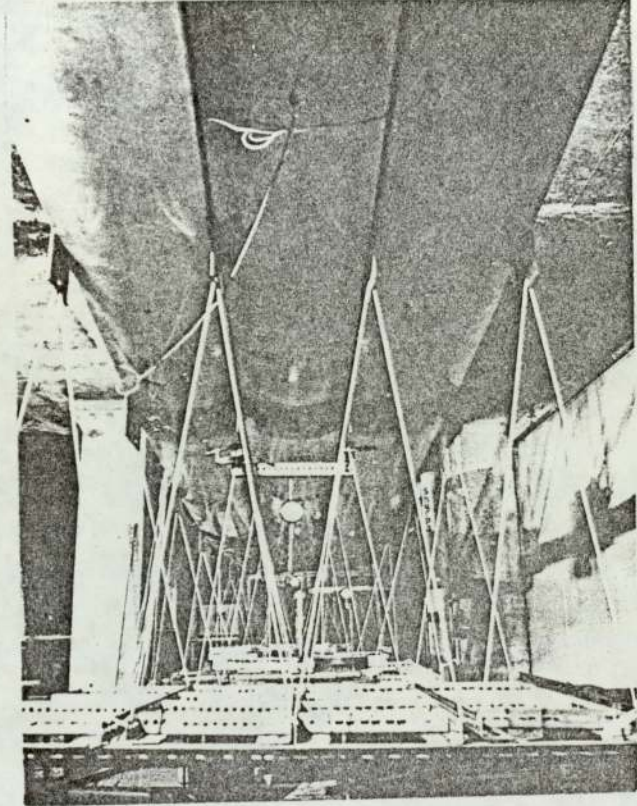


FIG. 6.13 GENERAL VIEW OF PRELIMINARY COMPRESSION TEST

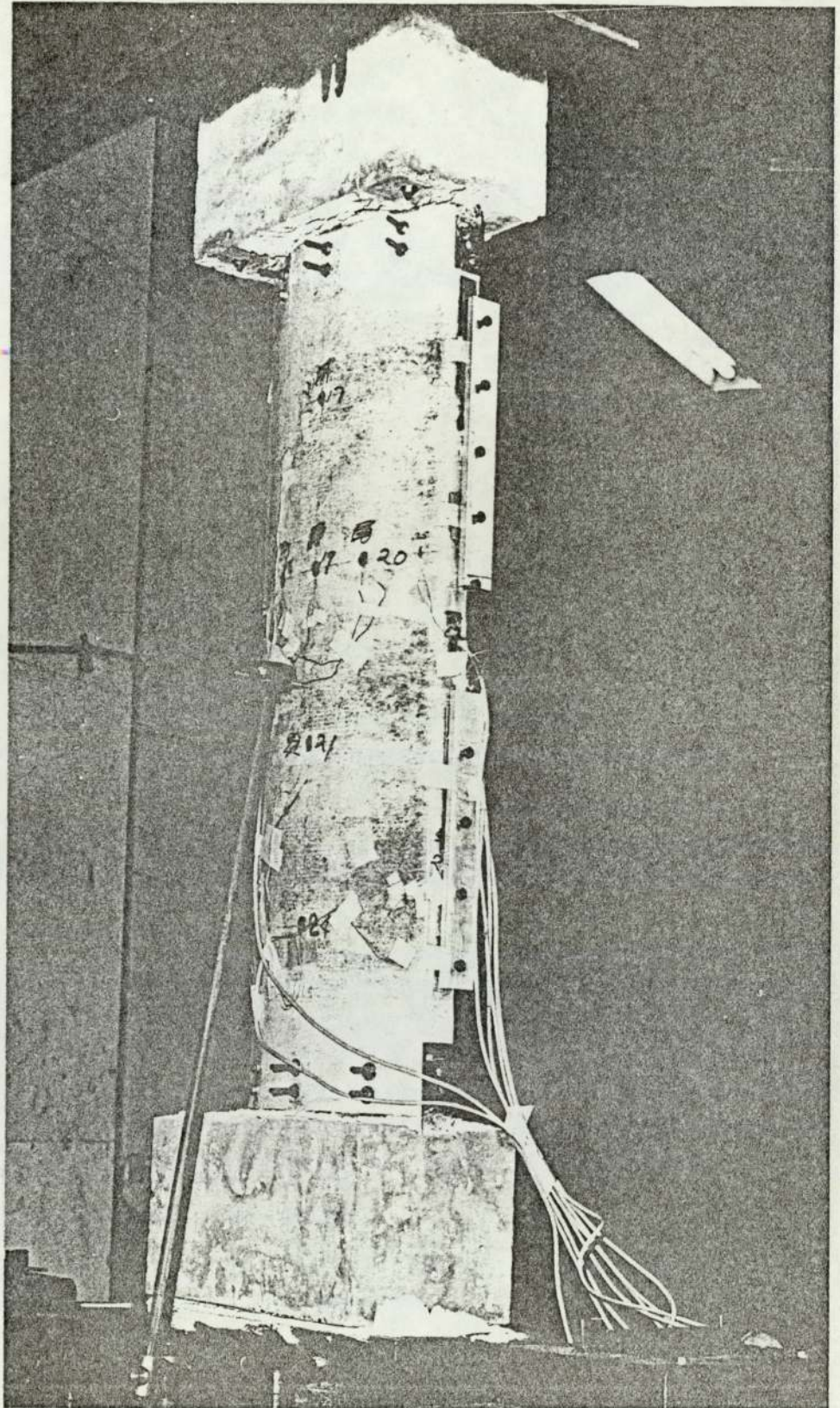
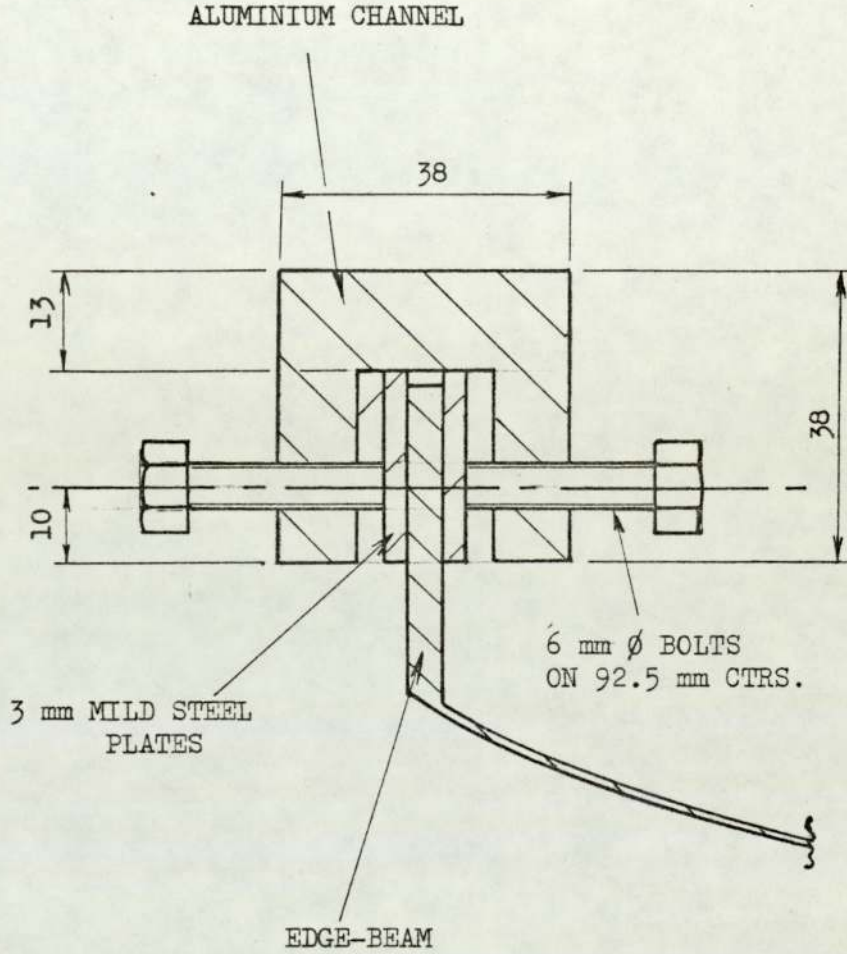


FIG. 6.14 COMPRESSION SPECIMEN EDGE-BEAM
SUPPORT



DIMENSIONS IN MILLIMETERS

FIG. 6.15 DEPLOYMENT OF STRAIN GAUGES

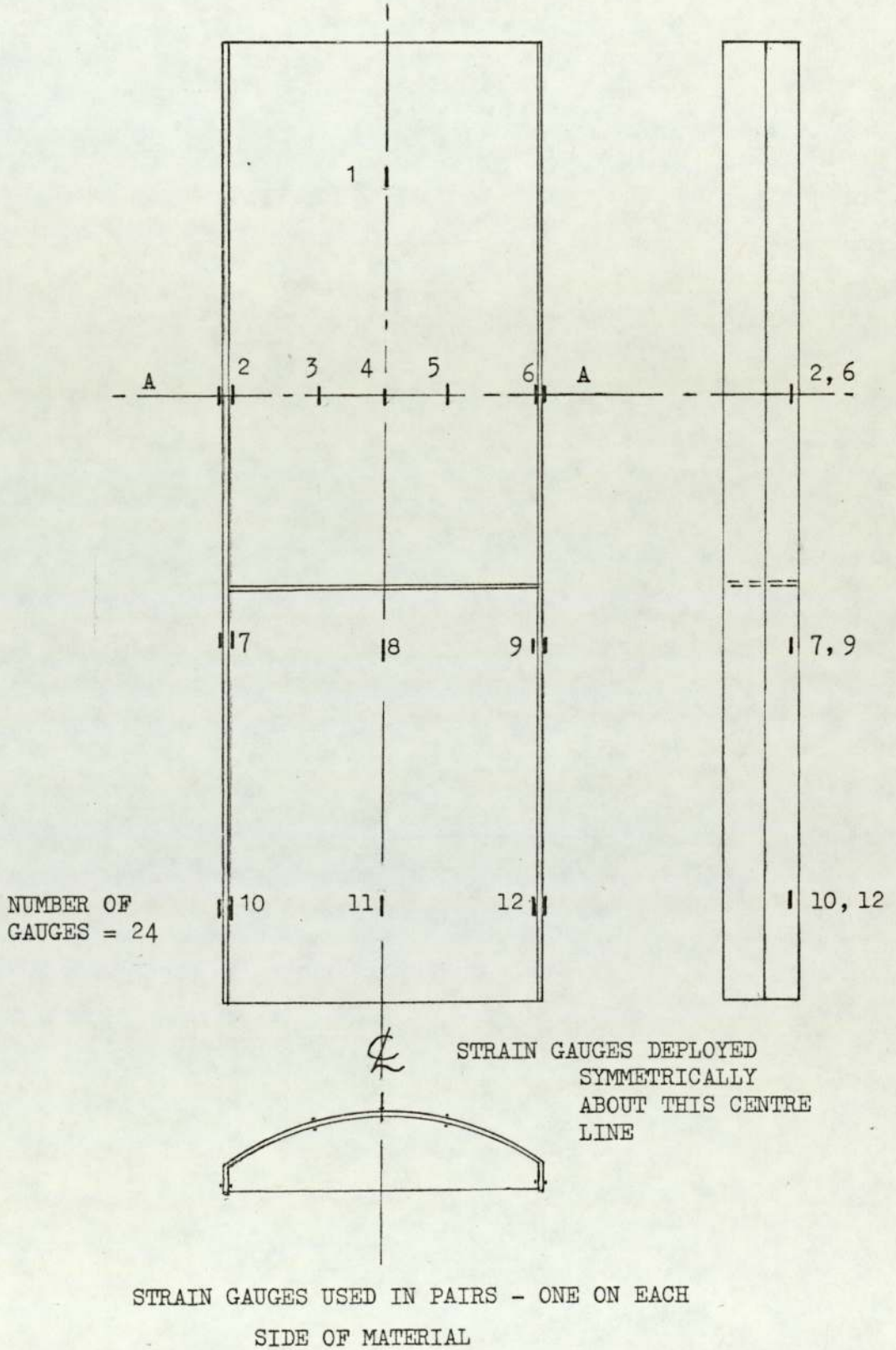


FIG. 6.16 STRAIN GAUGE RESULTS

LOAD (KN x 10)	MEAN OF STRAIN GAUGE PAIRS (SEE FIG. 6.15) (M/M x 10 ⁻³)					
	1	2	3	4	5	6
0	0	0	0	0	0	0
0.25	-0.409	-0.390	-0.271	-0.296	-0.322	-0.344
0.5	-0.643	-0.641	-0.450	-0.496	-0.558	-0.585
0.75	-0.892	-0.900	-0.637	-0.701	-0.816	-0.858
1.0	-1.117	-1.134	-0.805	-0.878	-1.049	-1.071
1.25	-1.376	-1.395	-1.001	-1.072	-1.355	-1.296
1.5	-1.279	-1.838	-0.466	-1.208	-0.304	-1.598
1.75	-1.339	-2.160	-0.369	-2.007	-0.220	-1.854
2.0	-0.689	-2.594	+0.024	-2.312	-0.242	-2.203
	7	8	9	10	11	12
0.25	-0.324	-0.304	-0.372	-0.365	-0.275	-0.319
0.5	-0.620	-0.520	-0.636	-0.619	-0.464	-0.552
0.75	-0.922	-0.754	-0.937	-0.904	-0.702	-0.828
1.0	-1.184	-0.964	-1.189	-1.142	-0.921	-1.028
1.25	-1.473	-1.205	-1.452	-1.418	-1.158	-1.210
1.5	-1.946	-0.866	-1.959	-2.008	-0.531	-1.527
1.75	-2.195	-0.546	-2.451	-2.300	-0.225	-1.710
2.0	-2.418	-0.114	-2.922	-2.515	-0.151	-1.650

FIG. 6.17 LATERAL DEFLECTION OF SPECIMEN IN
PRELIMINARY COMPRESSION TEST

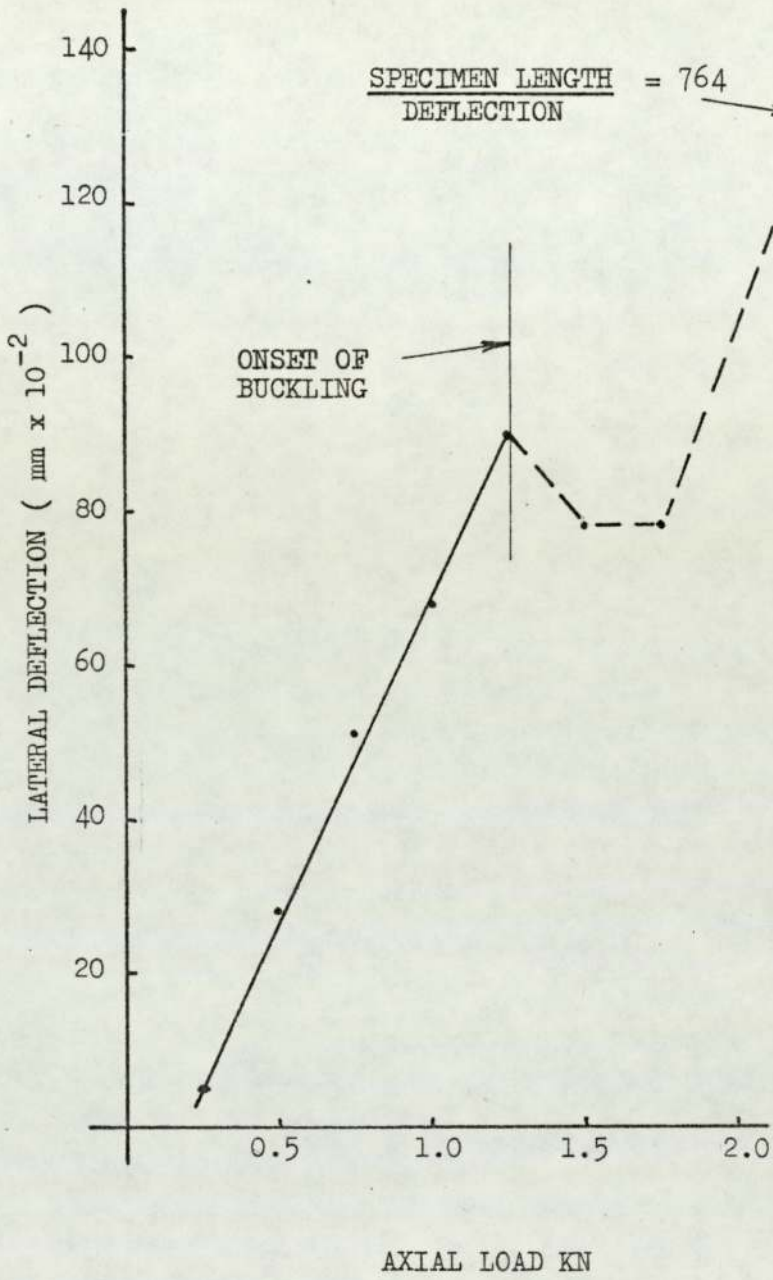


FIG. 6.18 STRAIN DISTRIBUTION ACROSS THE SPECIMEN

AT SECTION A-A AT LOAD 12.5 KN

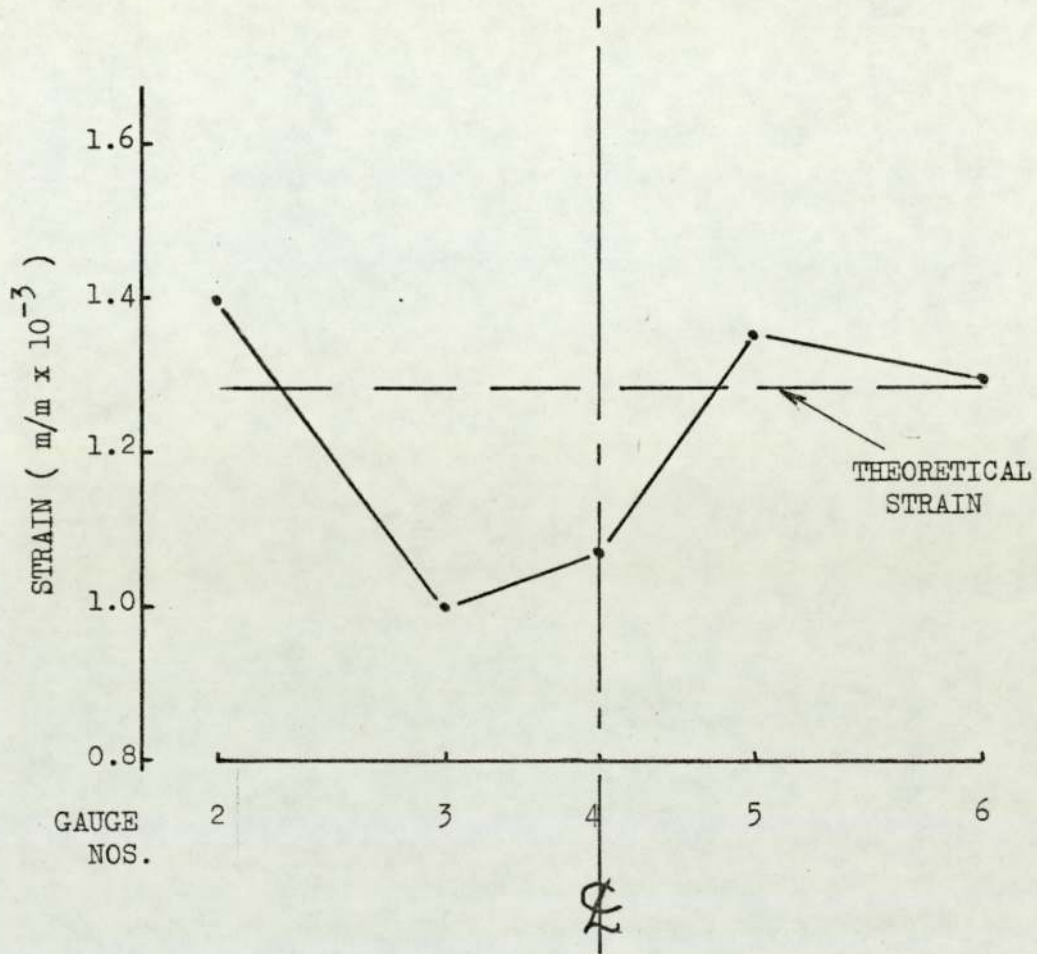


FIG. 6.19 LOCAL BUCKLING OF CYLINDRICAL SECTION

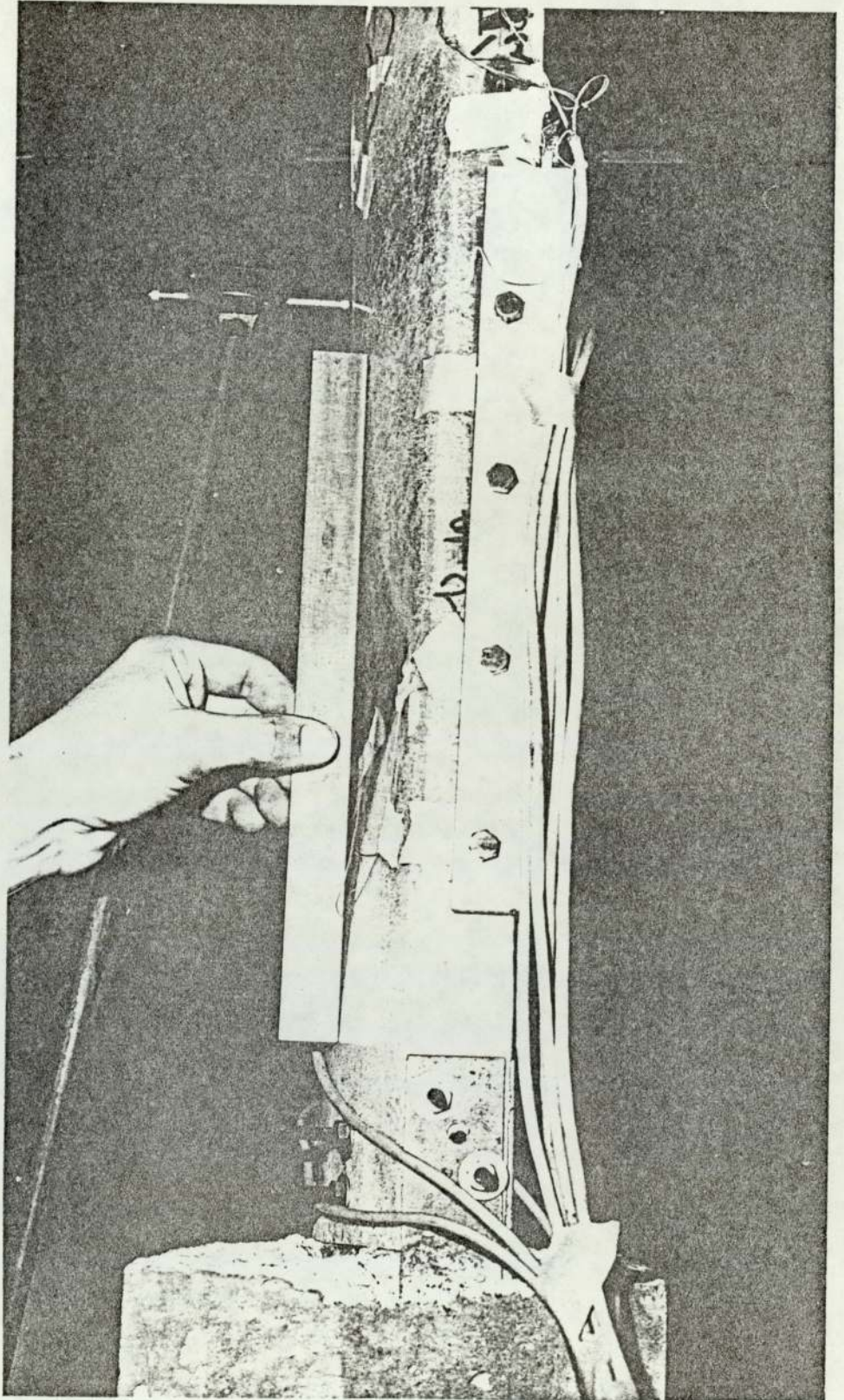


FIG. 6.20 GRAPH OF LOAD AGAINST STRAIN AT SECTION

A-A. (FIG. 6.15)

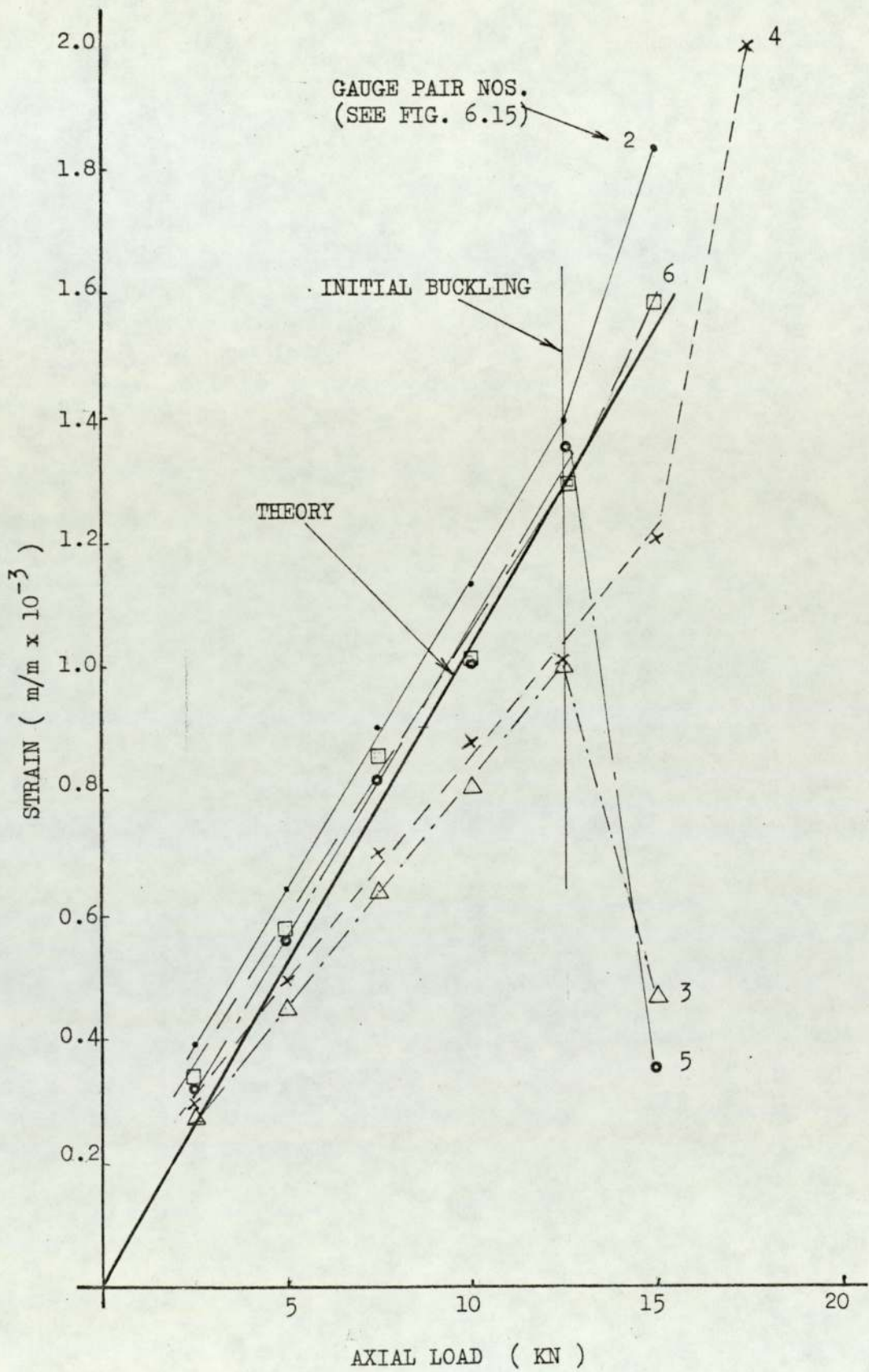


FIG. 6.21 GRAPH OF STRAIN AGAINST LOAD FOR
STRAIN GAUGE PAIR 11

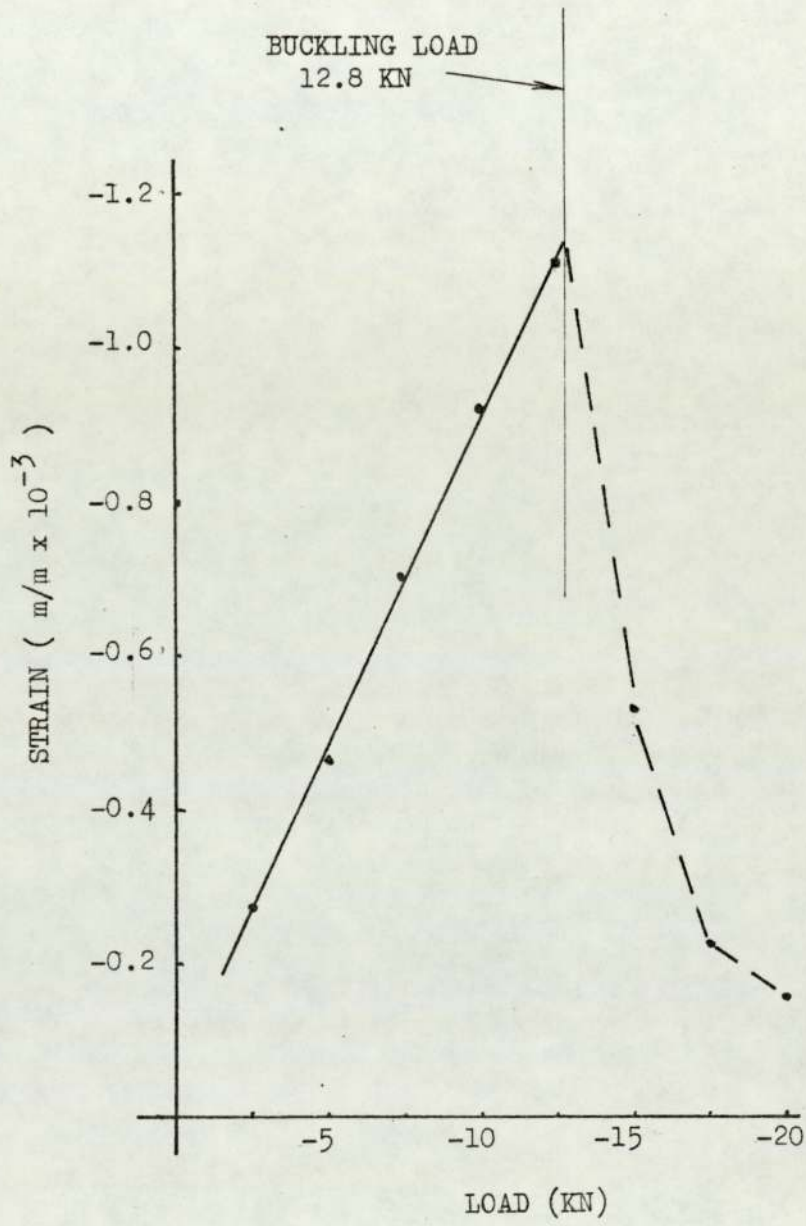


FIG. 6.22 COMBINED BUCKLING OF CYLINDRICAL SECTION

AND EDGE-BEAM

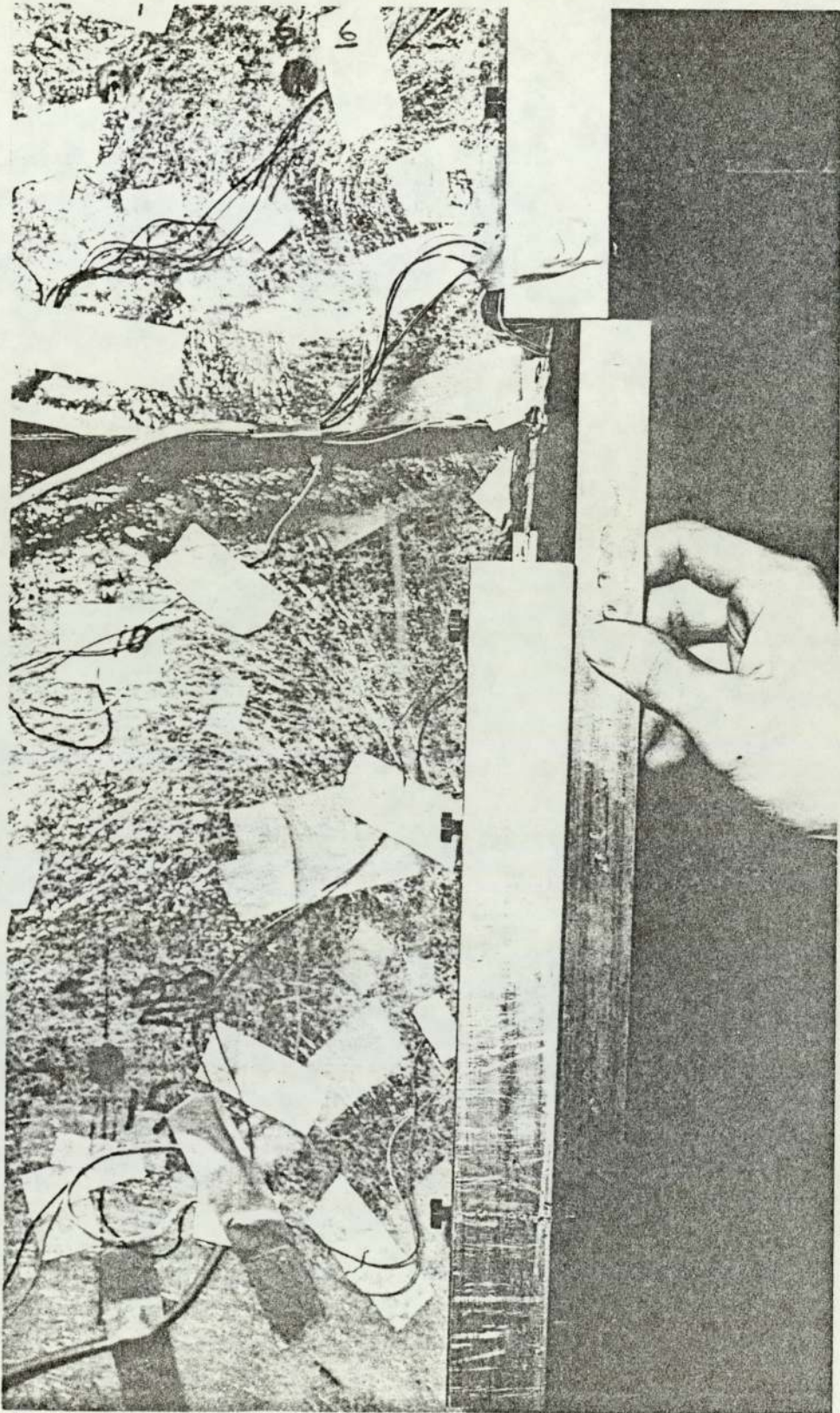


FIG. 6.23 CYLINDRICAL SECTION JOINTS

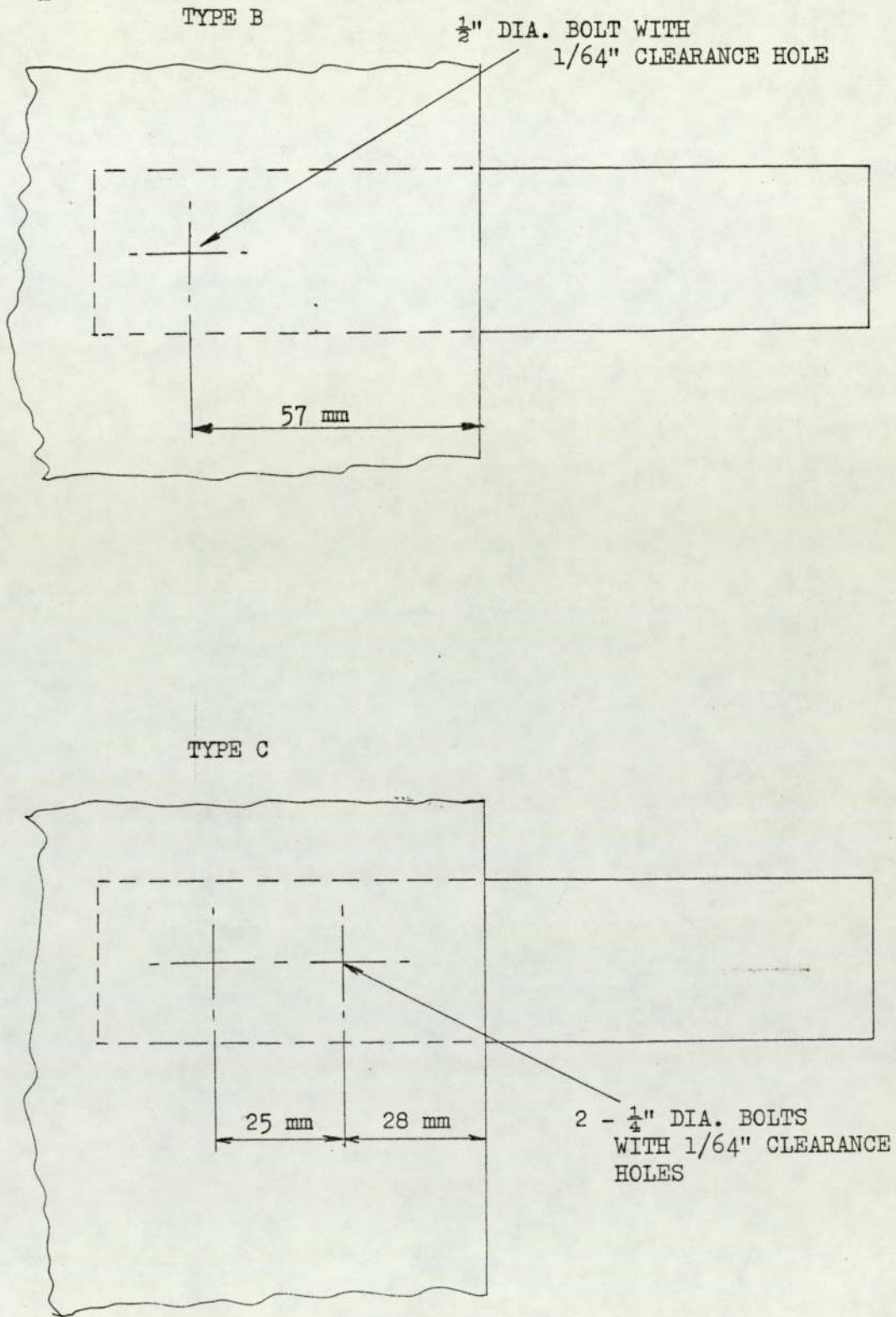
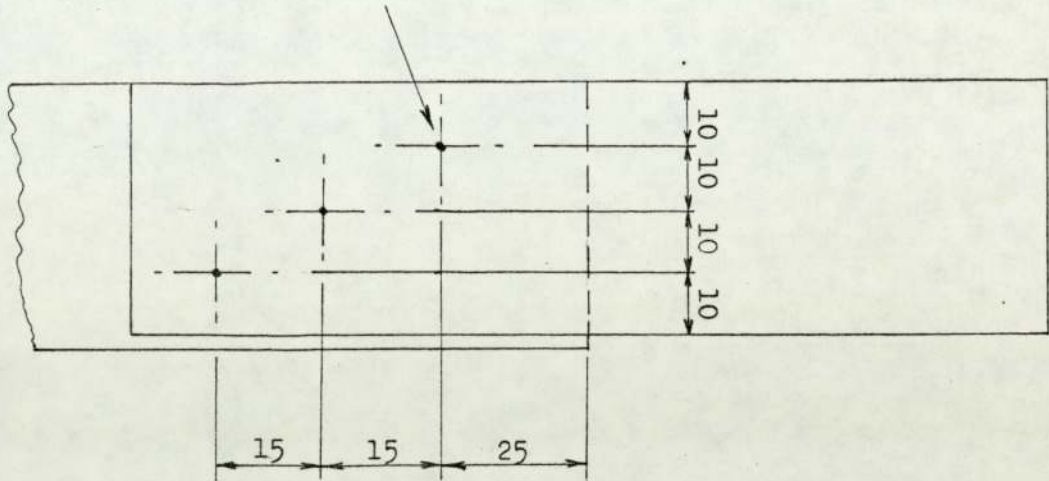


FIG. 6.24 EDGE-BEAM JOINT TYPE B

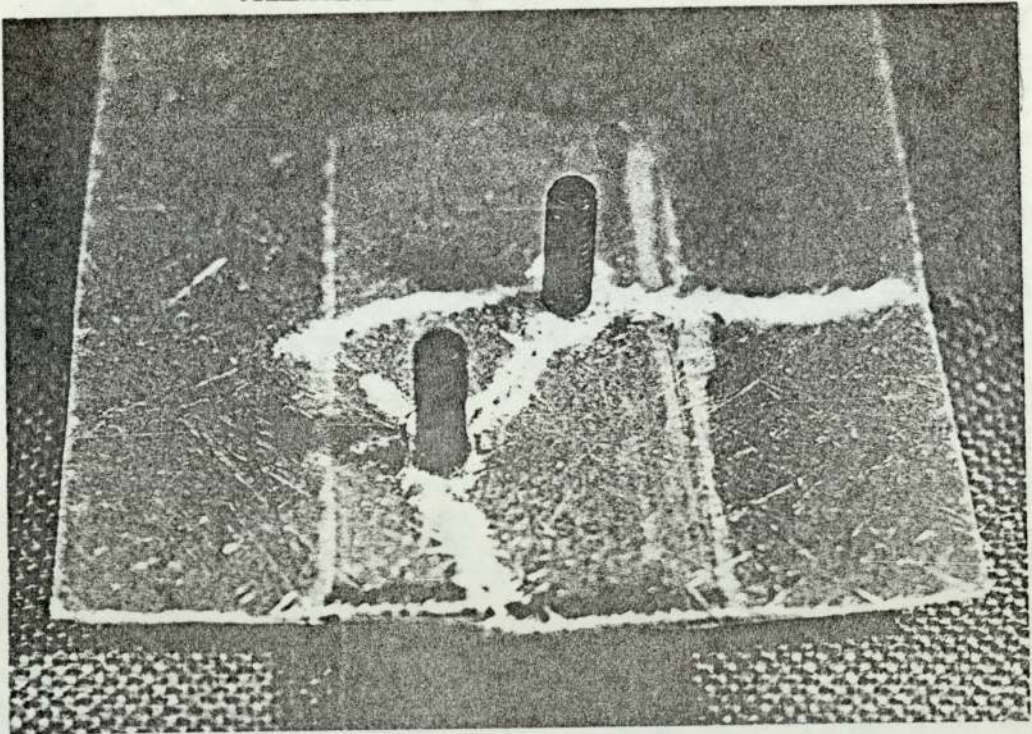
3 - BOLTS $\frac{1}{4}$ " DIA. WITH
1/64" CLEARANCE HOLES



DIMENSIONS IN MILLIMETERS

FIG. 6.25 JOINT FAILURE MODES

CYLINDRICAL SECTION JOINT TYPE A



CYLINDRICAL SECTION JOINT TYPE B

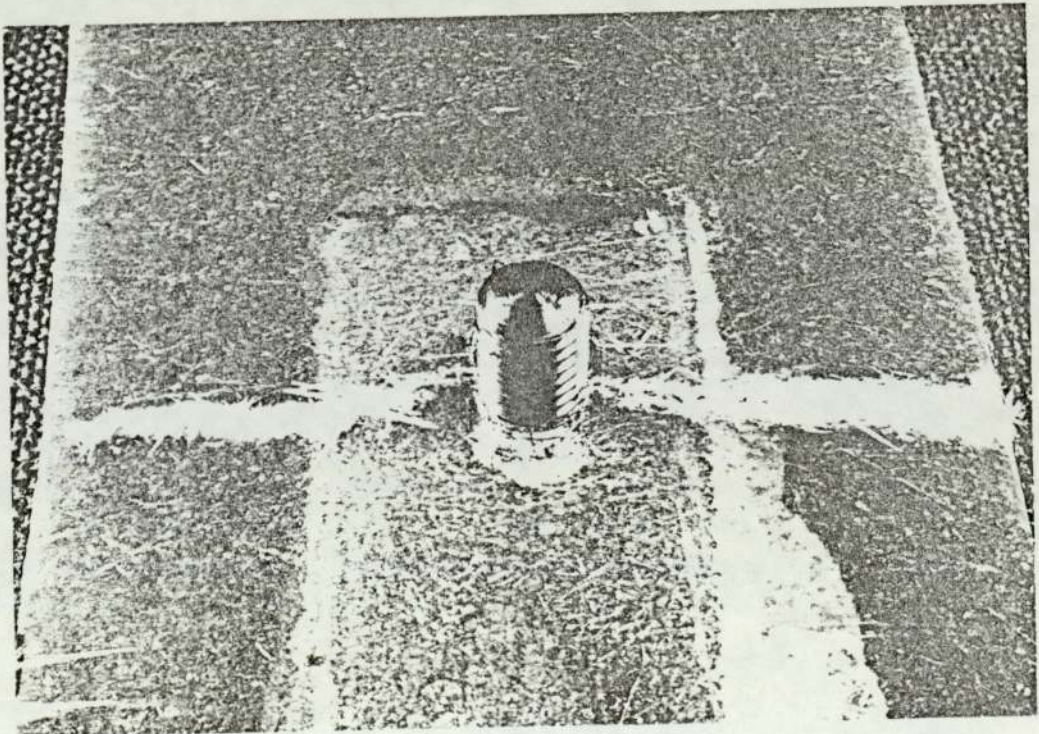
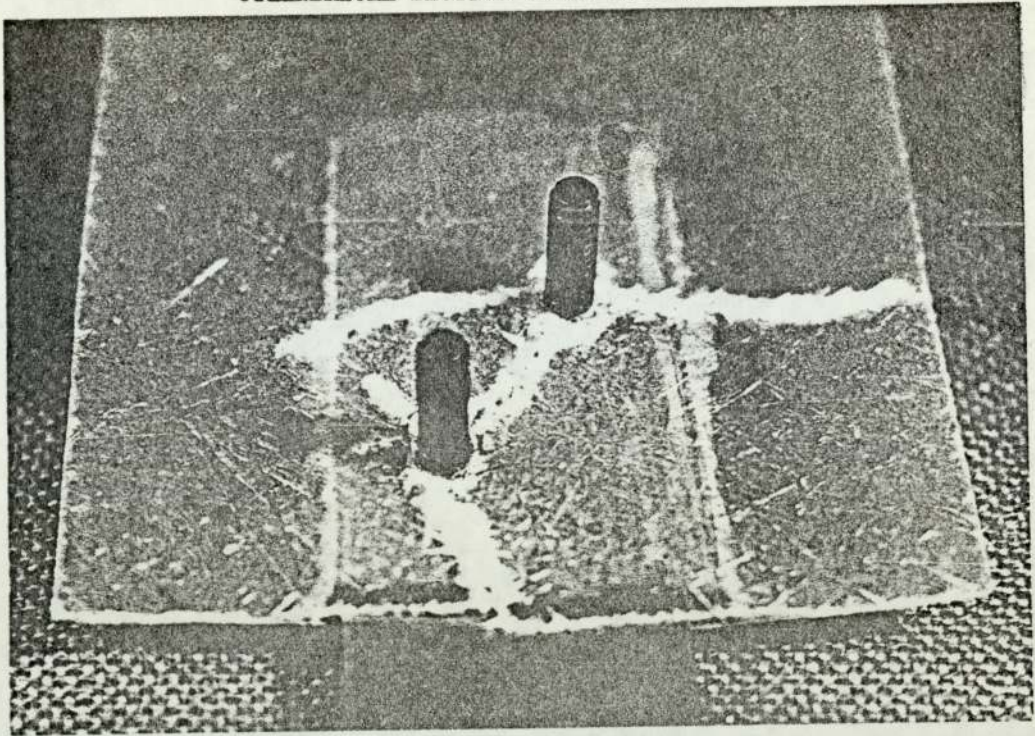


FIG. 6.25 JOINT FAILURE MODES

CYLINDRICAL SECTION JOINT TYPE A



CYLINDRICAL SECTION JOINT TYPE B

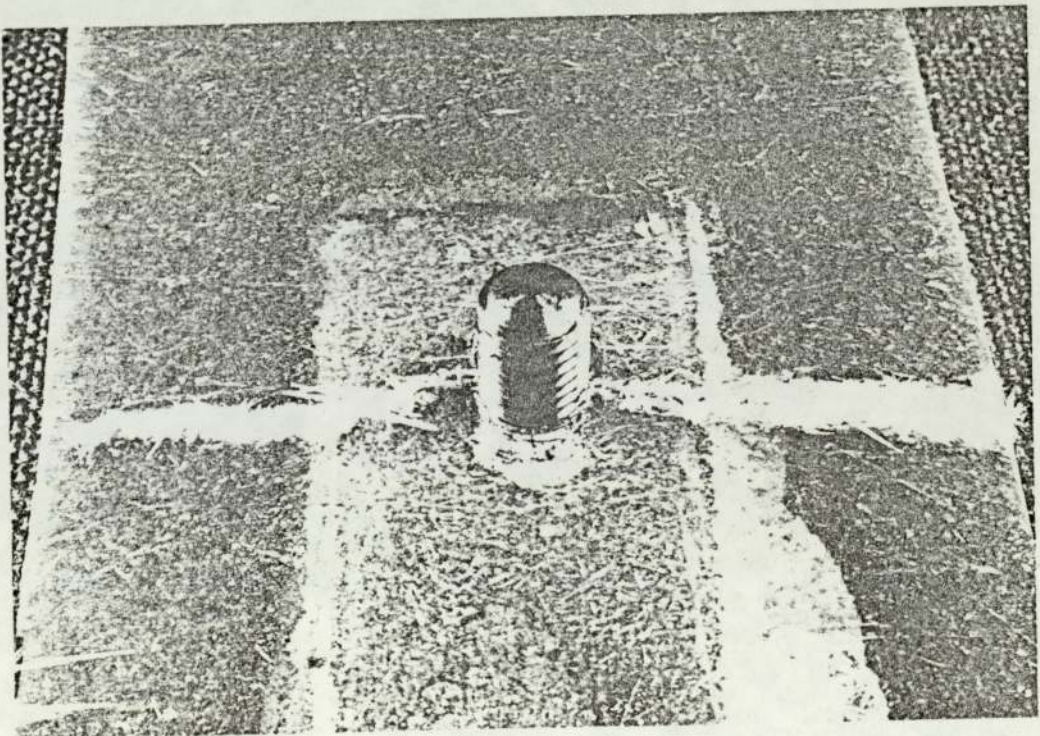


FIG. 6.26 JOINT FAILURE MODES

CYLINDRICAL SECTION JOINT TYPE C

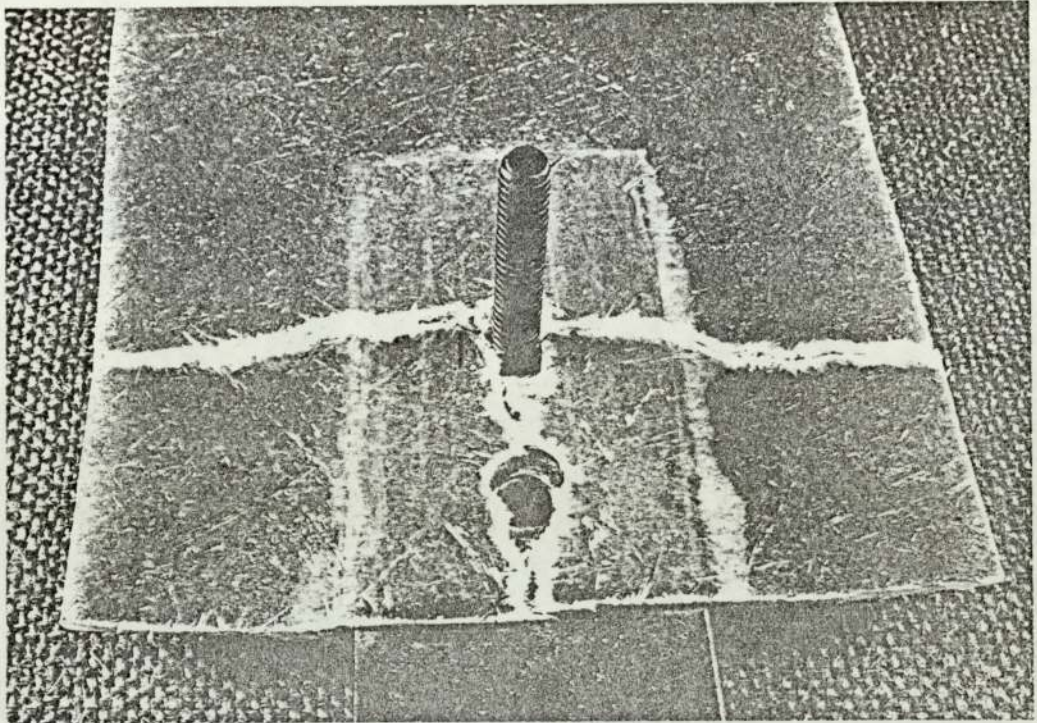
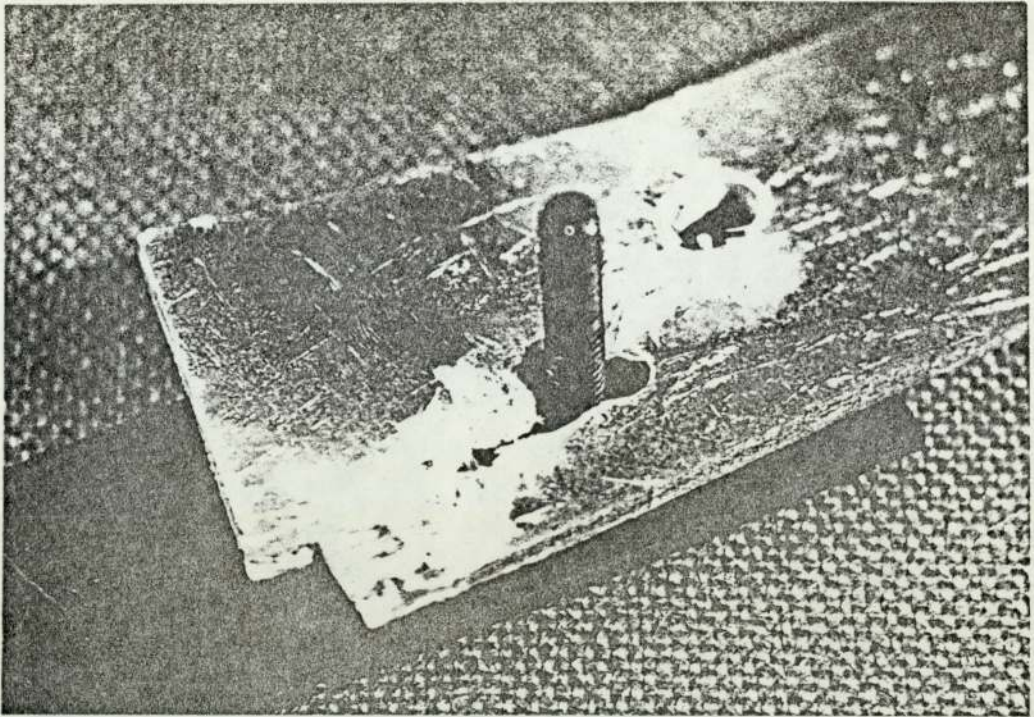
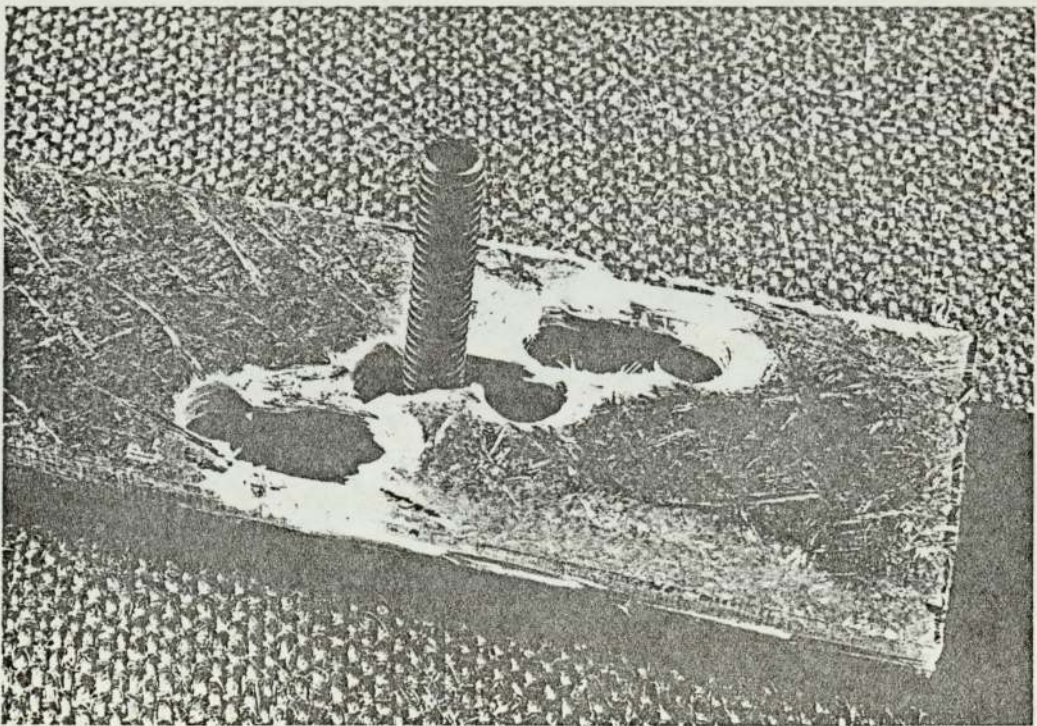


FIG. 6.27 JOINT FAILURE MODES

EDGE-BEAM JOINT TYPE A



EDGE-BEAM JOINT TYPE B



CHAPTER 7

DISCUSSION BETWEEN THEORY & EXPERIMENTAL

MODEL TEST RESULTS

CHAPTER SEVEN

Discussion Between Theory and Experimental Model Test Results

7.1

Introduction

This chapter is concerned with the comparison between the predicted behaviour of the model roof and that which was experienced under test. The test procedure has been described in Chapter 6. The comparison will enable conclusions to be drawn concerning the structural feasibility of the 60 m span roof designed in Chapter 5.

7.2.1 Deflection

Table Fig. 7.1 compares the theoretically (empirical modulus) determined deflections with those obtained experimentally. The latter were marginally greater than those predicted, with the exception of the deflection at point B (See Fig. 7.2). In both the snow and wind loading tests the deflection at point B was less than predicted.

Fig. 7.3 shows graphically the deflections of the model roof at mid-span plotted against load. Theoretical deflection was plotted on the basis of both theoretical modulus and empirical modulus. Experimental results are in close agreement with the empirically-determined modulus theory, particularly if the mean of the two central deflections is considered (points B & C). Although the experimental results also agree reasonably well with the theory based on the theoretical modulus, the discrepancy is greater. Consequently only the empirically based modulus theory will now be considered.

On unloading, the roof did not return to its original position, but maintained a 1.5 mm deflection. Thus the roof did not behave perfectly elastically.

The deflections of points A and D (Fig. 7.2) are presented in Fig. 7.4. In both cases the deflection was a linear function of load, and compared reasonably well with theory. Point D however, deflected more than point A, whereas in theory their deflection is

identical due to symmetry. The deflection of point A was 9% greater than theory, and point B 15% greater. Again, permanent deflection was experienced on unloading.

The central deflection under the action of wind loading is shown in Fig. 7.5. Point C again deflected more than point B, and again experimental results were in close agreement with theory. As was the case with the roof behaviour under snow loading, permanent deflection was observed after unloading.

Fig. 7.6 shows the deflections of point A and D. Point D deflected more than point A, as expected, but the error between observed and predicted deflection was 22% in the case of point D, and 7% in the case of point A.

The time-dependent nature of the deflection of the roof under snow load is shown in Fig. 7.7. The logarithm of the deflection is shown to vary approximately linearly with the logarithm of time according to the following equation:

$$\log \delta = 0.0316 \log t + 1.12 \quad 7.1$$

Equation 7.1 is analogous to the equation describing the creep behaviour of grp as discussed in Chapter 3, and may be written:

$$\delta = 13.18 t^{0.0316} \quad 7.2$$

Fig. 7.8 shows the creep behaviour on a linear scale and also the recovery of the roof on unloading. The observed deflection of the roof after 672 hrs. (4 weeks) is substantially less than the predicted deflection calculated in Section 6.3.6.3, which was based on grp's creep properties at 20°C and a relative humidity of 100%.

By analogy with the equation

$$\varepsilon = \frac{\sigma t^n}{E_1}$$

established in Chapter 3, equation 7.2 may be written:

$$\delta = \frac{W t^{0.0316}}{k} \quad 7.3$$

where k = a term representing the roof stiffness

W = the total applied load

$$\frac{W}{k} = 1.12$$

As the snow load (W) = $10 \times 0.75 \text{ KN/M}^2$

$$\therefore k = \frac{10 \times 0.75}{1.12} = 0.569 \text{ KN/M}$$

Applying the Boltzmann superposition principle to the deflection of the roof after unloading and neglecting the roof's self-weight and previous loading cycles:

$$\delta = \left(7.5 t_n^{0.0316} - 7.5 (t_n - t_{872})^{0.0316} \right) \quad 7.4$$

The recovery curve predicted by equation 7.4 is also plotted in Fig. 7.8 and is in reasonable agreement with the empirical results.

7.2.2 Member Loads, Strains and Buckling

The theoretical and experimental strains for the grp roof members are tabulated in Figs. 7.9 & 10. Each of the experimental strains tabulated is the mean of two strain gauge readings. Fig. 7.11 shows the deployment of the strain gauges on the members. In general the observed and predicted strains are not equal.

Figs. 7.12 - 7.17 show theoretical and typical experimental load-strain relationships for the grp members. In general the load-strain relationship is linear, but in Figs. 7.12, 13 and 15 sharp discontinuities were observed in the strain gauge results between the sixth and seventh load increments. These discontinuities coincided with the local buckling of the grp members 14C and 4B. Fig. 7.18 shows a photograph of a locally buckled member. The graphs (Fig. 7.12 - 17) confirm the lack of agreement between theoretical and experimental strain, and in general, the theory provides either an upper or lower bound to the observed results.

Figs. 7.19 to 7.21 show the strain distribution at snow load, across sections of the roof's upper and lower surfaces. Again the discrepancy between theory and experiment is shown.

Typical results of steelwork strain measurement are shown in Fig. 7.22, and it is apparent that the experimental results bear little relationship to the predicted strains. Unlike the grp experimental results, the steelwork measured strain is not a linear function of load intensity. Although, theoretically all the steelwork members were in tension, member 34 on the outside of beam C was observed to buckle at a load intensity of $1.25 \times$ snow load, illustrating a compressive load.

Figs. 7.23 - 26 illustrate that the experimentally determined strain in the grp members under wind loading compares with theory in a similar way to the strain under snow loading. That is:

- a) the load/strain relationship is approximately linear.
- and b) in general the theoretical strain curve provides an upper or lower bound to the experimental results.

Local buckling of the grp members was not observed under wind loading. However, two steelwork members were observed to buckle prematurely under the first increment of load; i.e. members 34 on the outside of beams A and C.

7.3

Discussion of Results

7.3.1 Deflection

In general the predicted and experimental elastic (short term) deflections correlated satisfactorily. There are discrepancies between the two however, which are considered to be the result of the following:

- 1) joint slippage; leading to non-rigid joints which behave in a manner between rigid and pin-jointed.
- 2) creep; the durations of the roof tests were 70 mins. for the snow loading test and 60 mins. for the wind loading test. Consequently, some creep is bound to have taken place even though the structure was not loaded continuously.
- 3) geometric inaccuracies of the structure as a whole and within the material, stemming from all stages of manufacture. On a microscopic scale the hand lay-up process used to manufacture the grp components will have led to areas of gross inhomogeneity and anisotropy. On a larger scale the mould used for laminating would not have been geometrically perfect, leading to an

imperfect moulding shape. On a macroscopic scale geometric inaccuracies will have been built into the roof during assembly.

The non-recovered deflections observed are considered to be best explained by 1) and 2) above. The lack of symmetry observed in the deflections may be explained by a combination of joint slippage and macroscopic geometric inaccuracies distributed within the roof unsymmetrically. These phenomena could lead to unpredicted bending and twisting of the surface units.

The large discrepancy between the predicted and experimental long term deflection of the roof (See Fig. 7.8) was due mainly to the environmental difference between the roof test and the material characterisation tests of Chapter 3. However, the same basic creep law was found to apply approximately as well to the structure as a whole as to the constituent materials (See Fig. 7.7). On unloading the roof, deflection recovery was found to follow, reasonably well, the recovery curve as predicted on the basis of the Boltzmann superposition principle. The small discrepancy between the two may be explained in part by the fact that neither the total roof loading history nor the self-weight was taken into account. However, the roof had been assembled and the short term tests completed approximately three months before the creep test was carried out, so that the effect of these factors is expected to have been small. In addition, any contribution to deflection which did not result in the storage of strain energy, such as joint slippage or debonding of the glass fibres and resin, would contribute to the discrepancy.

7.3.2 Member Forces, Strains and Buckling

The three main causes of the discrepancies between theoretical and experimental deflection are also considered to be the main causes of the differences between measured and predicted strain, and therefore stress, in the roof members.

Joint slippage would reduce the predicted bending strains in the members, and the difference between maximum and minimum strains would be reduced. The theoretical strains in the cylindrical section and the edge-beams will form upper and lower bounds to the experimental results. As pointed out in Section 7.2 this was generally the case as observed. However, the discrepancies were too large for this to totally explain the results. Not only can joint slippage cause the roof to behave more like a pin-jointed structure, but it can also cause unpredicted bending in the plane of the roof surface units and also out-of-plane twisting. These phenomena can cause principal stress and strains in directions other than the predicted axial stresses and strains. This can lead to incorrect interpretation of the strain gauge readings, since the results have been assumed to be principal strains resulting from uni-axial stresses. Although the strain gauge readings in general increase linearly with increasing load, if the results are closely examined it can be seen that in many cases strain increases spasmodically (see Fig. 7.13). This is considered to be due to a combination of joint slippage and the loading method where the load was occasionally removed before being increased (as described in Chapter 6); on reloading, different joints may slip.

Geometric inaccuracies can also lead to stresses and strains in non-principal axis directions. For example, there will be at least a two-dimensional stress field round a resin-rich or resin starved area. Also, small areas of anisotropy will cause local bending and twisting of the laminates. This is particularly likely to occur in the edge-beams where the unidirectional material may not be perfectly straight as a result of stippling during lamination.

Creep may also be a factor in the variance due to the non-homogeneous nature of grp. There is likely to be a time-dependent strain distribution between a resin-rich surface and the main body of the laminate. This effect however, is considered to be of little significance.

Since the measured deflections of the roof compare well with those predicted, the mean theoretical and experimental member strains would be expected to be similar. The mean of all the theoretical strains at snow load was 0.353×10^{-3} m/m and the mean of all the measured strains was 0.307×10^{-3} m/m. The discrepancy here is 13%. The maximum strain expected to be measured in the roof at snow load was -4.43×10^{-4} m/m in the edge-beams of members 18 A, B and C. The largest strain actually measured was -5.74×10^{-4} m/m in the cylindrical section of member 8c, which is 30% greater than the predicted maximum strain.

During the snow loading test, measured strain in the steel cross-bracing was grossly different from that predicted. Indeed, one member (member 34) was observed to buckle when it was theoretically a tensile member. During the wind loading test the same member

buckled again, plus one other member as described in Section 7.2.2. However, under wind loading these members were expected to be under compression. The theoretical buckling load for these members was 1.27 KN and the theoretical load at buckling was 0.09 KN. The buckling load is small compared with the forces in the grp surface units, and so bending or twisting of these units could cause buckling. There are four cross-bracing members at the particular section where the members buckled, but only two actually buckled. This would seem to support the above view. This cross-bracing buckling is undesirable but does not have any significant effect on the design of the 60 m roof, since its cross-bracing was designed on the cross-wire principle. Also the buckling apparently did not have any significant effect on the deflection of the model roof.

The strains, and therefore the stresses, in the cylindrical section of the grp compression members tended to be greater than predicted, occasionally by a factor of 2. It is, therefore, to be expected that local buckling would occur, as observed, since the safety factor at maximum load was only 1.73. The effect of local buckling, however, was small since the relationship between load and deflection remained sensibly linear after buckling. Further, on unloading, the buckled areas returned to their original shape without any apparent material damage.

Finally, it would appear that where there was a large variance between theory and experiment, joint slippage was a major cause. Bolted joints are known to frequently give problems in this respect. In this case, however, it is thought that the problem was exacerbated by the rough grp surfaces to which the fishplates were bolted. The rough surfaces were a result of the hand lay-up manufacturing process.

- 1) The short term elastic deflection of the model roof was predicted with adequate accuracy under uniform and unsymmetric loads using empirically determined material moduli.
- 2) The creep behaviour of the roof structure as a whole was similar to that of grp as a material.
- 3) The visco-elastic character of grp causes significant increases in the deflection (28%) over a period of one month in addition to the elastic deflection.
- 4) The environment has a considerable effect on the rate of creep.
- 5) Creep strain is largely recoverable after a period of unloading equal to the loading period. This may only be the case when the maximum strains do not approach the failure strains.
- 6) Locally, strains were not predicted accurately but the maximum and mean theoretical and experimental strains of the roof were in reasonable agreement.
- 7) Local buckling of the cylindrical section of the grp members did not have any immediate serious effect.

- 8) Bolted joints were a major source of variance between theoretical and experimental results.
- 9) The roof's structural design is efficient compared with conventional roof structures when measured in terms of weight per unit area.
- 10) The structural properties of grp adequately meet the requirements of roof structures, as tested in this project.
- 11) The 60 m span grp roof, designed in Chapter 5 is structurally feasible.

FIG. 7.1 COMPARISON BETWEEN THEORETICAL
ELASTIC ANALYSIS DEFLECTION AND
EXPERIMENTAL DEFLECTION

SNOW LOAD (0.75 KN/M)

MEASURING POINT (SEE FIG. 7.2)	THEORETICAL mm	EXPERIMENTAL mm
A	10.2	10.6
B	14.5	13.5
C	14.5	15.2
D	10.2	12.2

WIND LOAD (INCREMENT 3)

MEASURING POINT (SEE FIG. 7.2)	THEORETICAL mm	EXPERIMENTAL mm
A	7.3	7.4
B	10.7	9.7
C	10.7	11.4
D	7.8	9.4

FIG. 7.2 DEFLECTION MEASURING POINTS

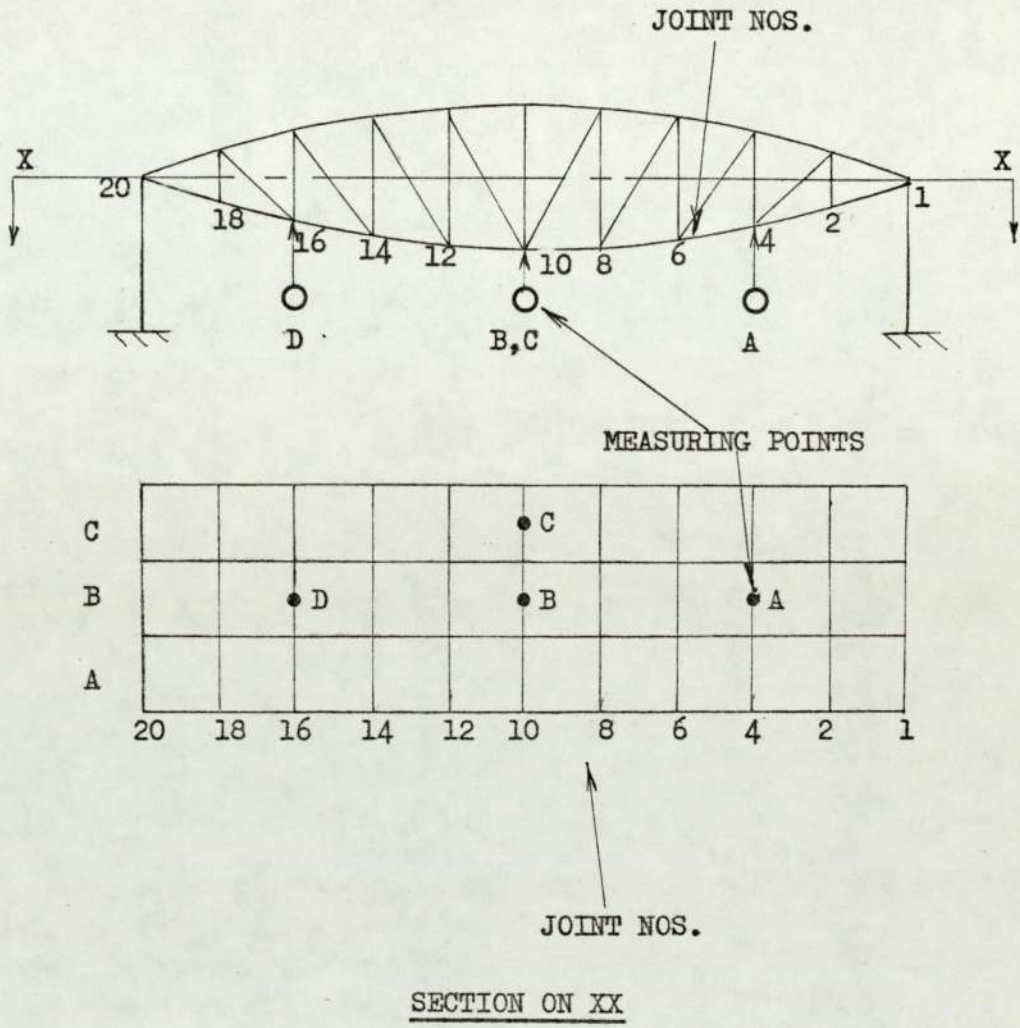


FIG. 7.3 COMPARISON BETWEEN THEORETICALLY DETERMINED
AND EMPIRICALLY DETERMINED MODEL ROOF
DEFLECTIONS
SNOW LOADING

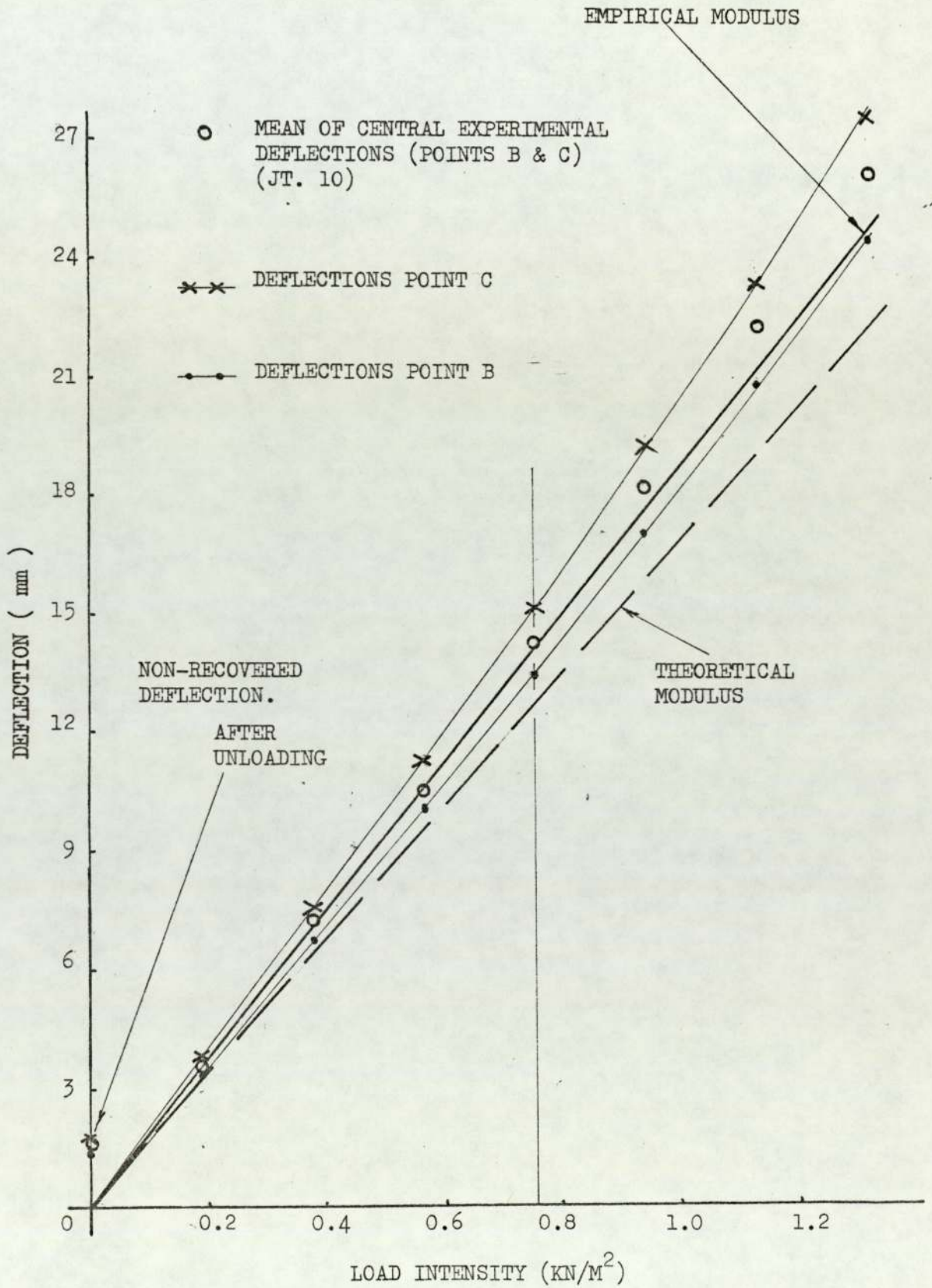


FIG. 7.4 DEFLECTION OF JOINTS 4 AND 16 (POINTS A & D)
SNOW LOADING

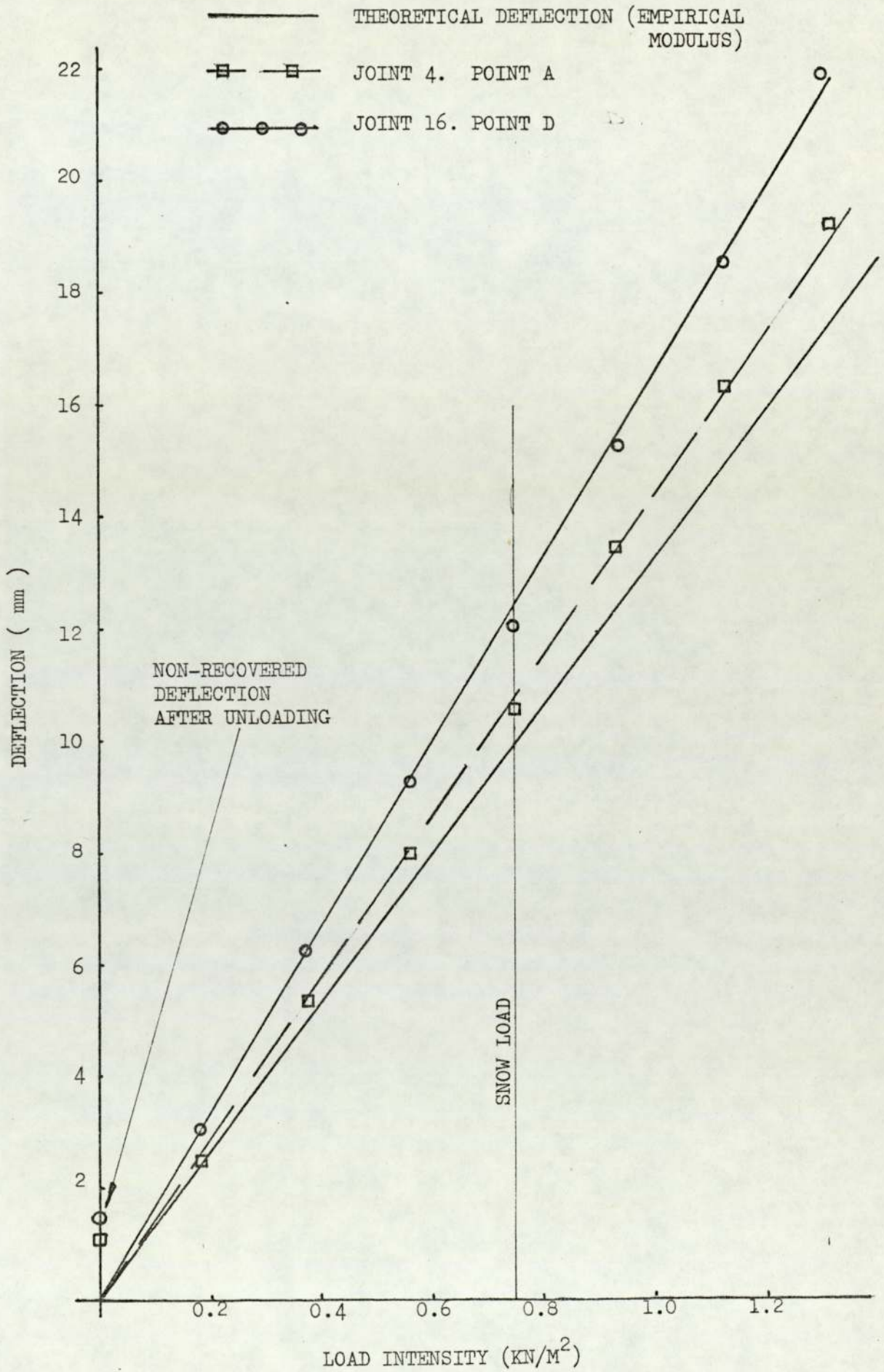


FIG. 7.5 COMPARISON BETWEEN THEORETICAL AND
EXPERIMENTAL CENTRAL ROOF
DEFLECTIONS. WIND LOAD

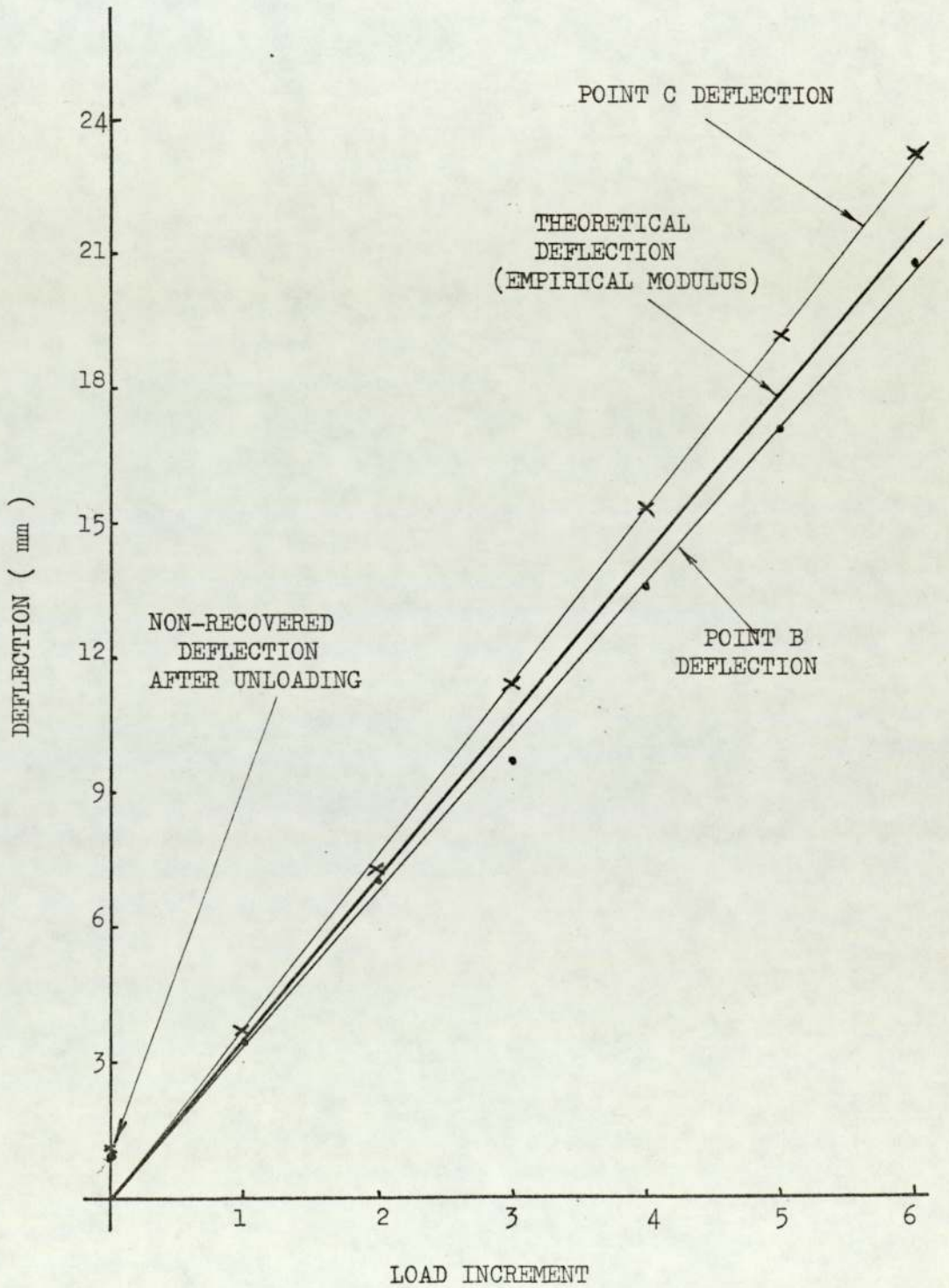
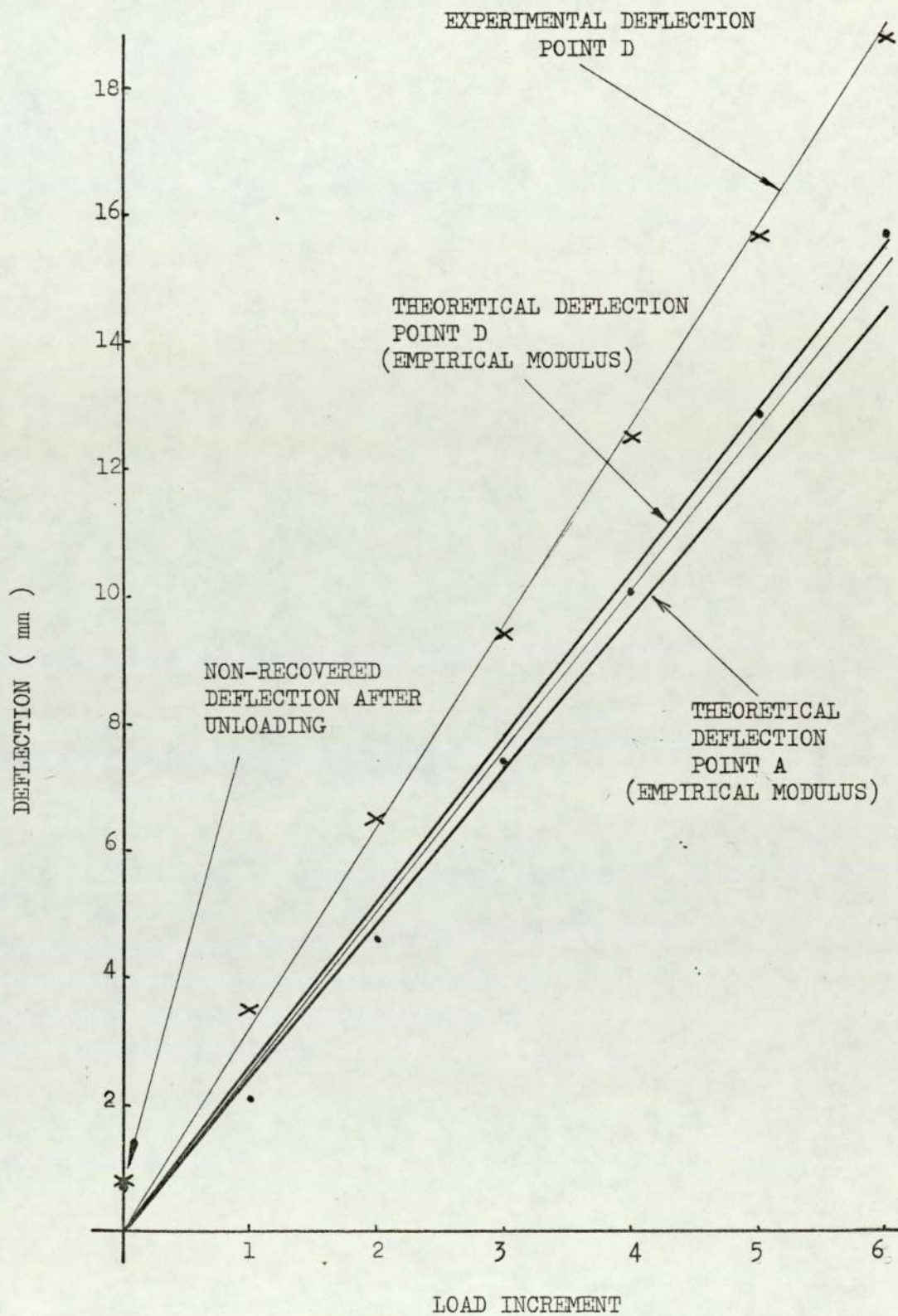


FIG. 7.6 DEFLECTION OF JOINTS 4 AND 16 (POINTS A & D)
WIND LOADING



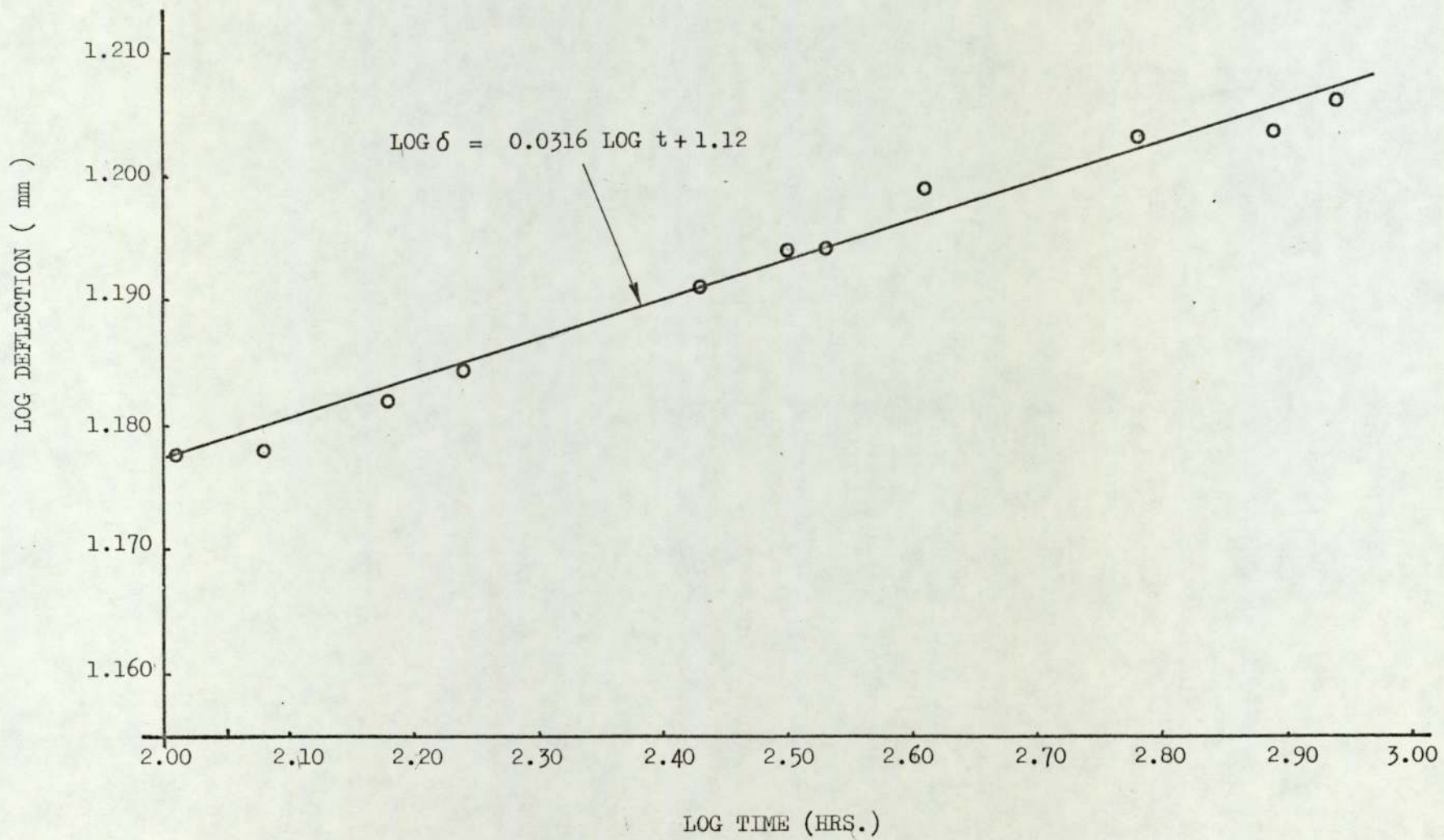


FIG. 7.7 ROOF CREEP: GRAPH OF LOG TIME
AGAINST LOG DEFLECTION

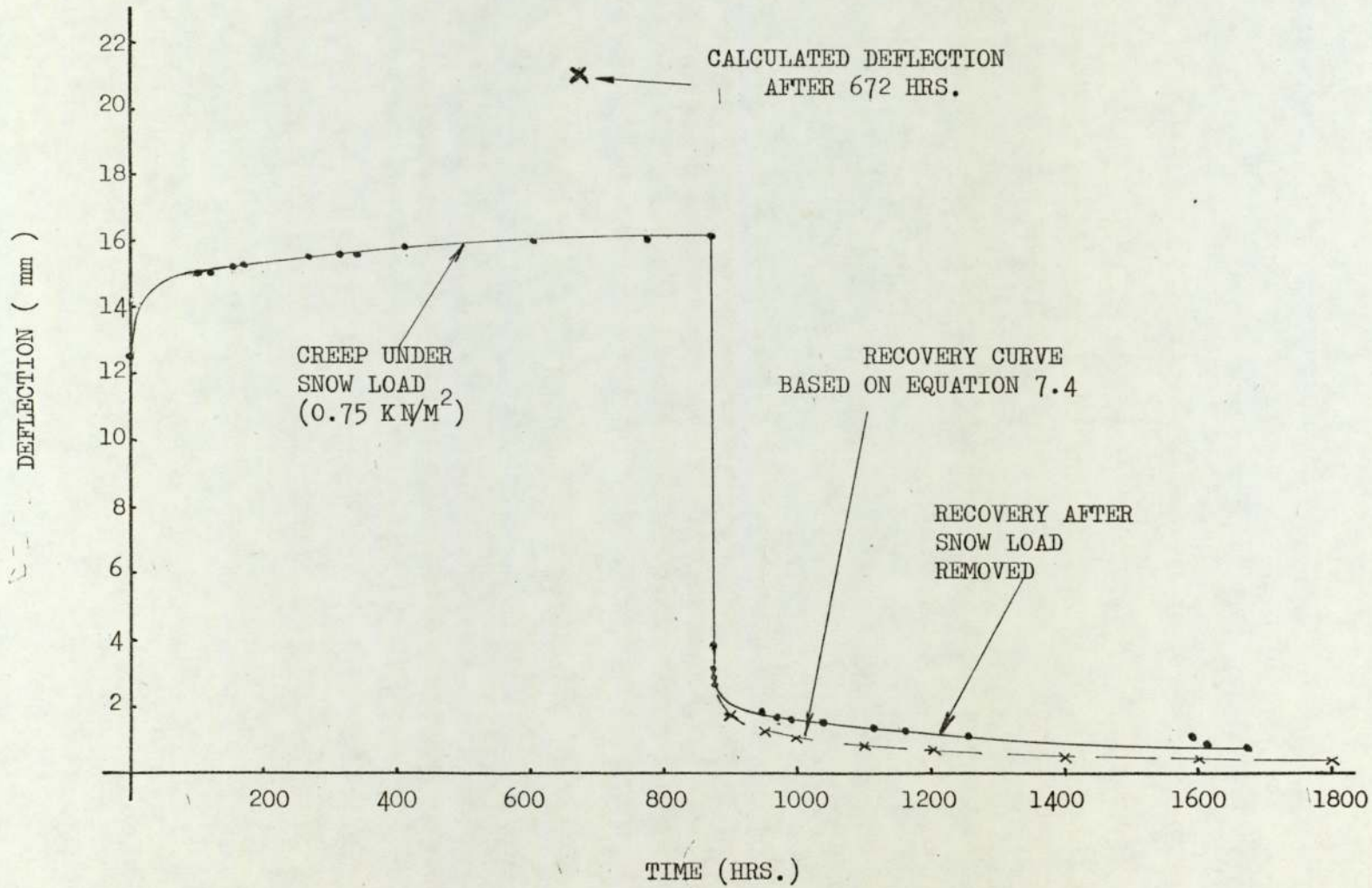


FIG. 7. 8 ROOF CREEP: GRAPH OF TIME AGAINST DEFLECTION

MEMBER	STRAIN GAUGE NOS. (SEE FIG. 7.9)	STRAIN ($M/M \times 10^{-4}$)															
		1		2		3		4		5		6		7		8	
		THRY	EXP	THRY	EXP	THRY	EXP	THRY	EXP	THRY	EXP	THRY	EXP	THRY	EXP	THRY	EXP
20A		-4.07	-2.18	-4.07	-0.94	-2.48	-2.47										
20B		-4.07	-3.40	-4.07	-1.82	-2.48	-1.98	-2.68	-2.51	-2.68	-2.76	-2.87	-1.69	-2.87	-1.04	-2.72	-0.80
20C		-4.07	-4.06	-4.07	-3.10	-2.48	-3.38										
19A		2.77	2.28	2.77	-0.73	4.30	0.56										
19B		2.77	1.89	2.77	1.86	4.30	3.22										
18A		-4.43	-1.68	-4.43	-2.86	-2.84	-4.50										
18B		-4.43	-3.43	-4.43	-2.74	-3.84	-4.16	-2.84	-4.33	-2.84	-4.14	-2.93	-4.03	-2.93	-3.52	-2.79	-4.67
18C		-4.43	-3.17	-4.43	-1.32	-2.84	-5.74										
17A		2.86	2.62	2.86	3.03	4.16	4.53										
17B		2.86	4.56	2.86	2.82	4.16	0.51										
17C		2.86	4.42	2.86	2.63	4.16	3.05										
12B		-4.24	-3.27	-4.24	-3.67	-3.63	-	-3.91	-4.12	-3.91	-3.59						
11B		3.64	3.20	3.64	3.12	4.31	2.70	3.98	2.29	3.98	3.18						

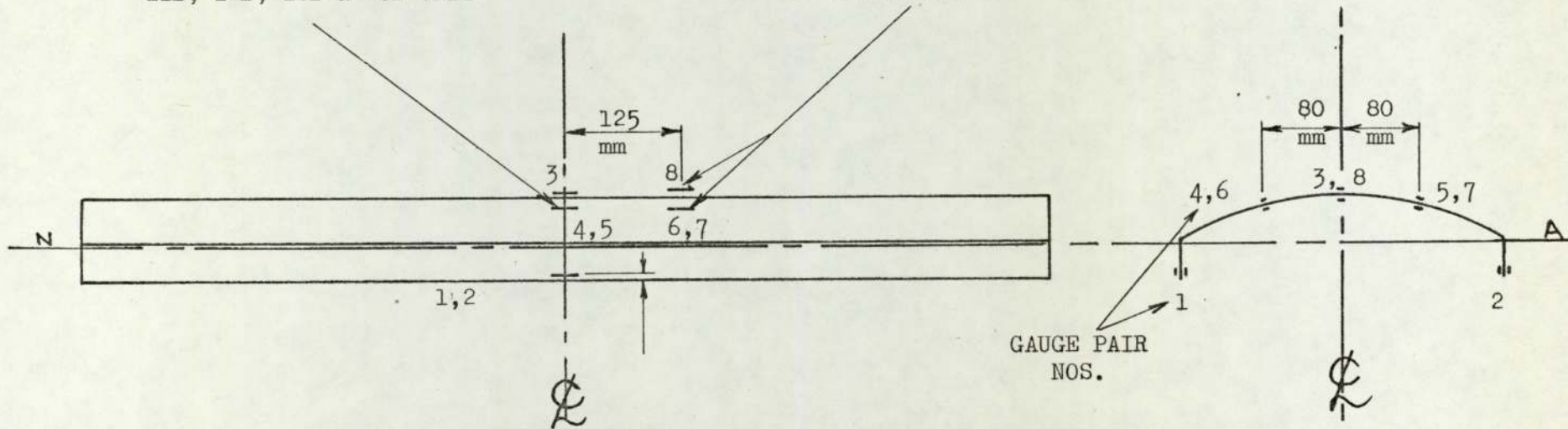
FIG. 7.9. TABLE OF THEORETICAL AND EXPERIMENTAL STRAINS AT SNOW LOAD ($0.75 \times KN/M^2$)

MEMBER	STRAIN GAUGE NOS. (SEE FIG. 7.11)	STRAIN ($M/M \times 10^{-4}$)					
		1		2		3	
		THYR	EXP	THYR	EXP	THYR	EXP
12A		-4.24	-3.68	-4.24	-4.20	-3.63	-4.59
11A		3.64	4.54	3.64	3.52	4.31	4.68
10B		-4.24	-3.48	-4.24	-2.96	-3.63	-3.97
9B		3.64	3.38	3.64	2.82	4.31	3.41
2B		-4.07	-4.58	-4.07	-3.16	-2.48	-2.36
1B		2.77	4.11	2.77	2.93	4.30	-

FIG. 7.10 TABLE OF THEORETICAL AND EXPERIMENTAL
STRAINS AT SNOW LOAD (0.75 KN/M²)

GAUGES IN THIS
POSITION ON MEMBERS:
11B, 12B, 18B & 20B ONLY

GAUGES IN THESE
POSITIONS ON MEMBERS:
18B & 20B ONLY



GAUGES USED IN PAIRS: ONE ON
EACH SIDE OF SECTION

FIG. 7.11 POSITION OF STRAIN GAUGES

FIG. 7.12 GRAPH OF EDGE-BEAM STRAIN AGAINST LOAD

FOR MEMBERS 20 A, B & C

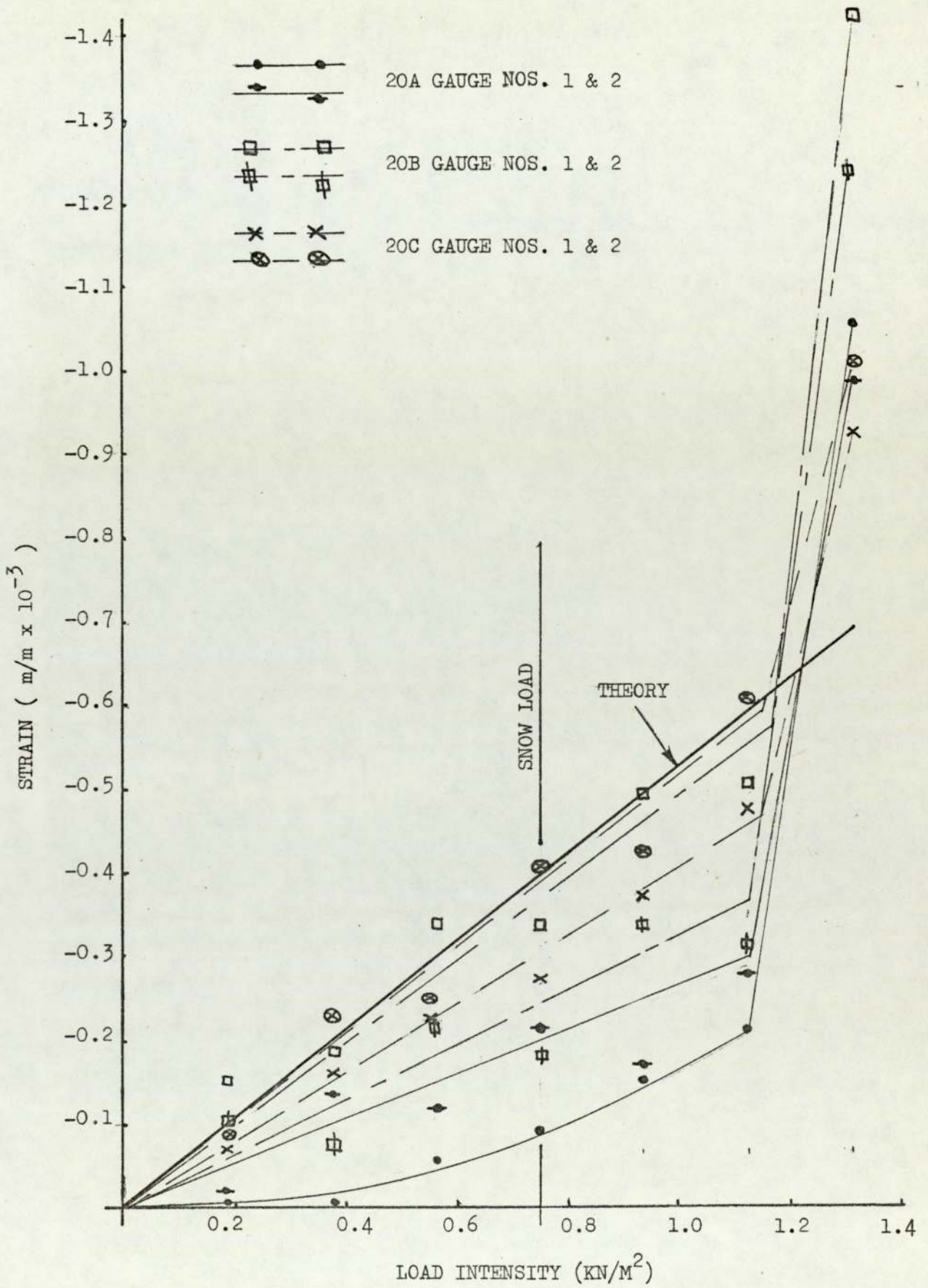


FIG. 7.13 GRAPH OF CYL. SECTION SUMMIT STRAIN

AGAINST LOAD FOR MEMBERS

20 A, B & C

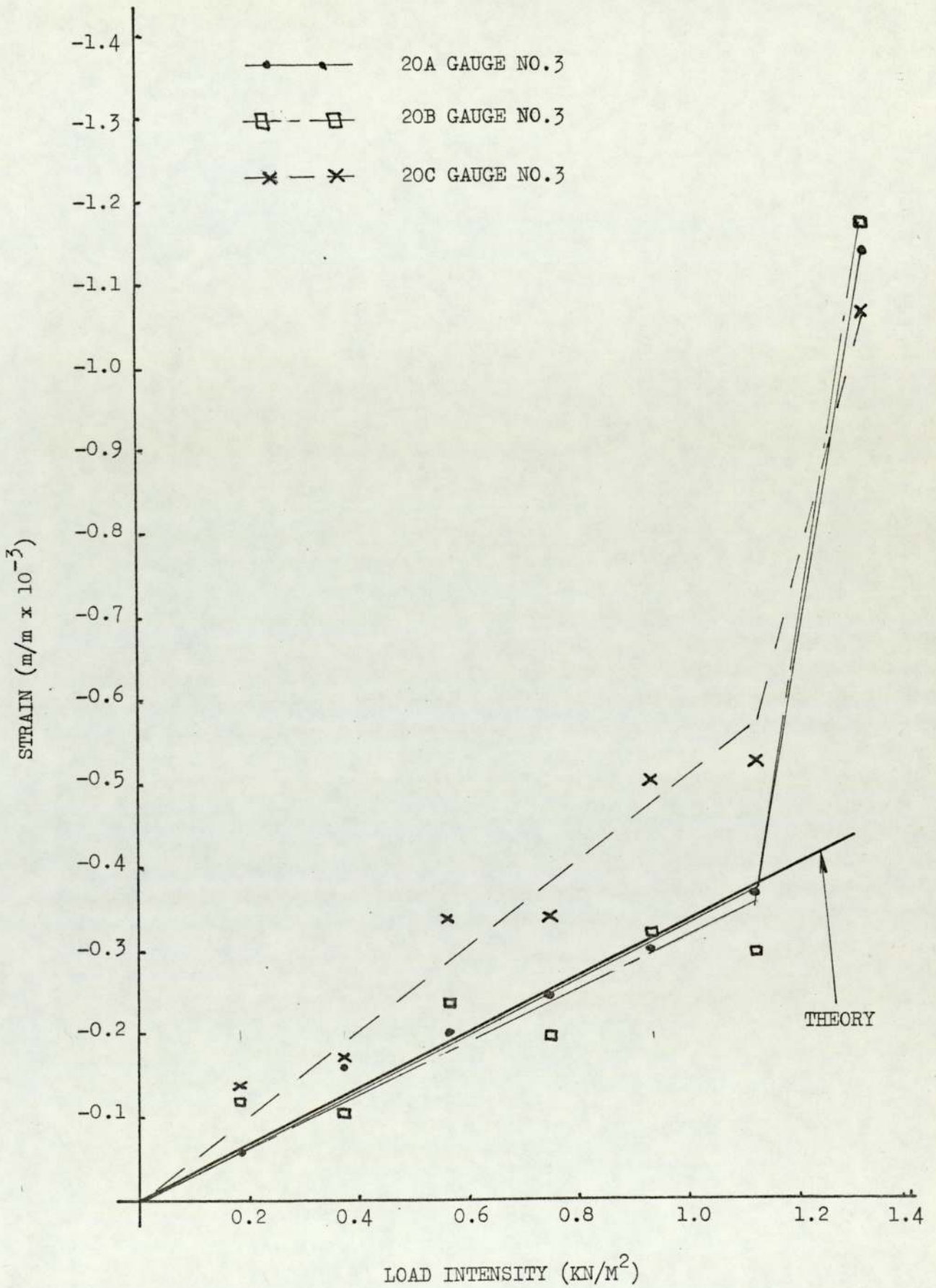


FIG. 7.14 GRAPH OF EDGE-BEAM STRAINS AGAINST LOAD
FOR MEMBERS 18 (STRAIN GAUGE NOS. 1 & 2)

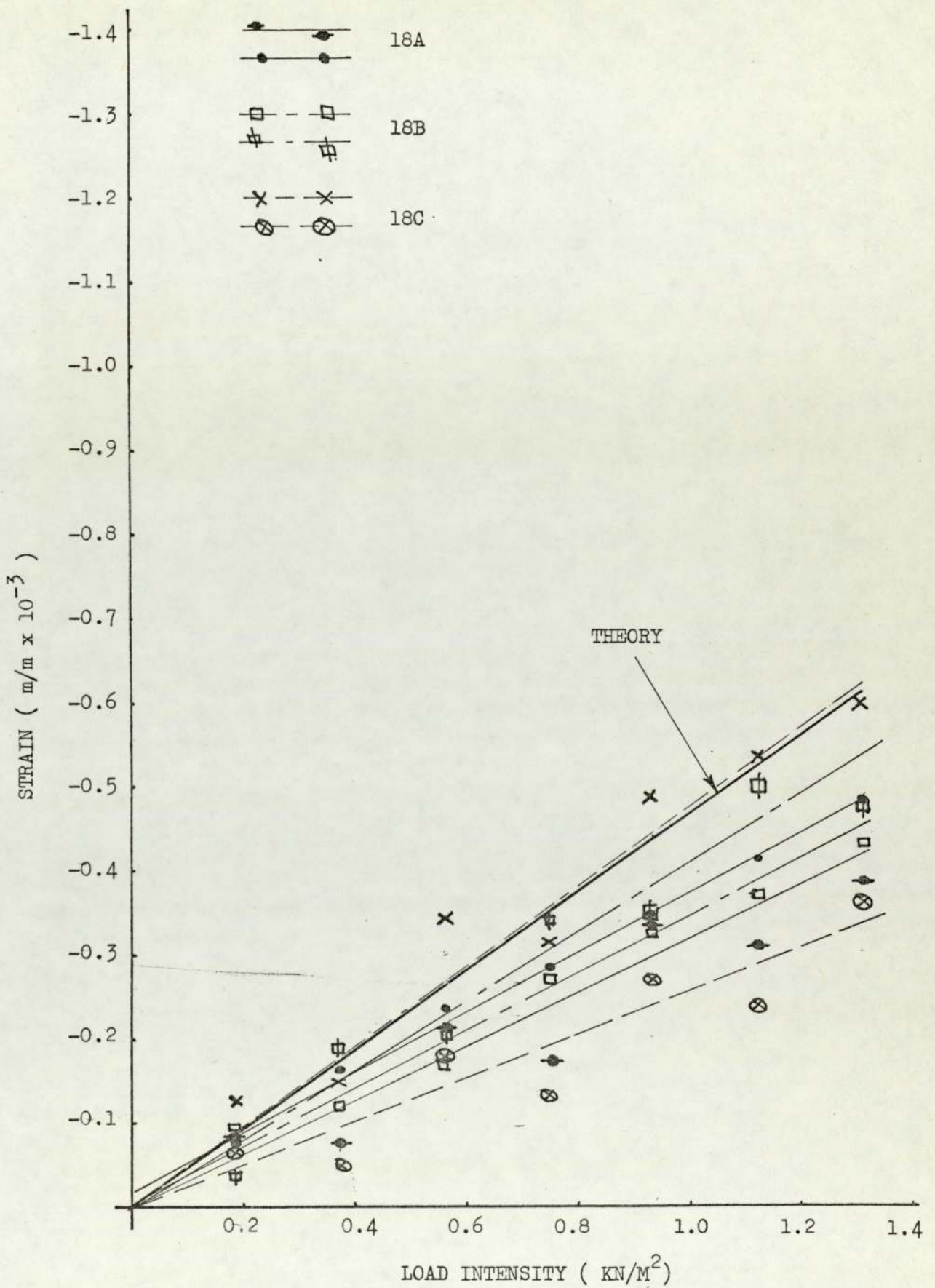


FIG. 7.15 GRAPH OF CYLINDRICAL SECTION SUMMIT

STRAIN AGAINST LOAD FOR MEMBERS

18 A, B & C (GAUGE NO. 3)

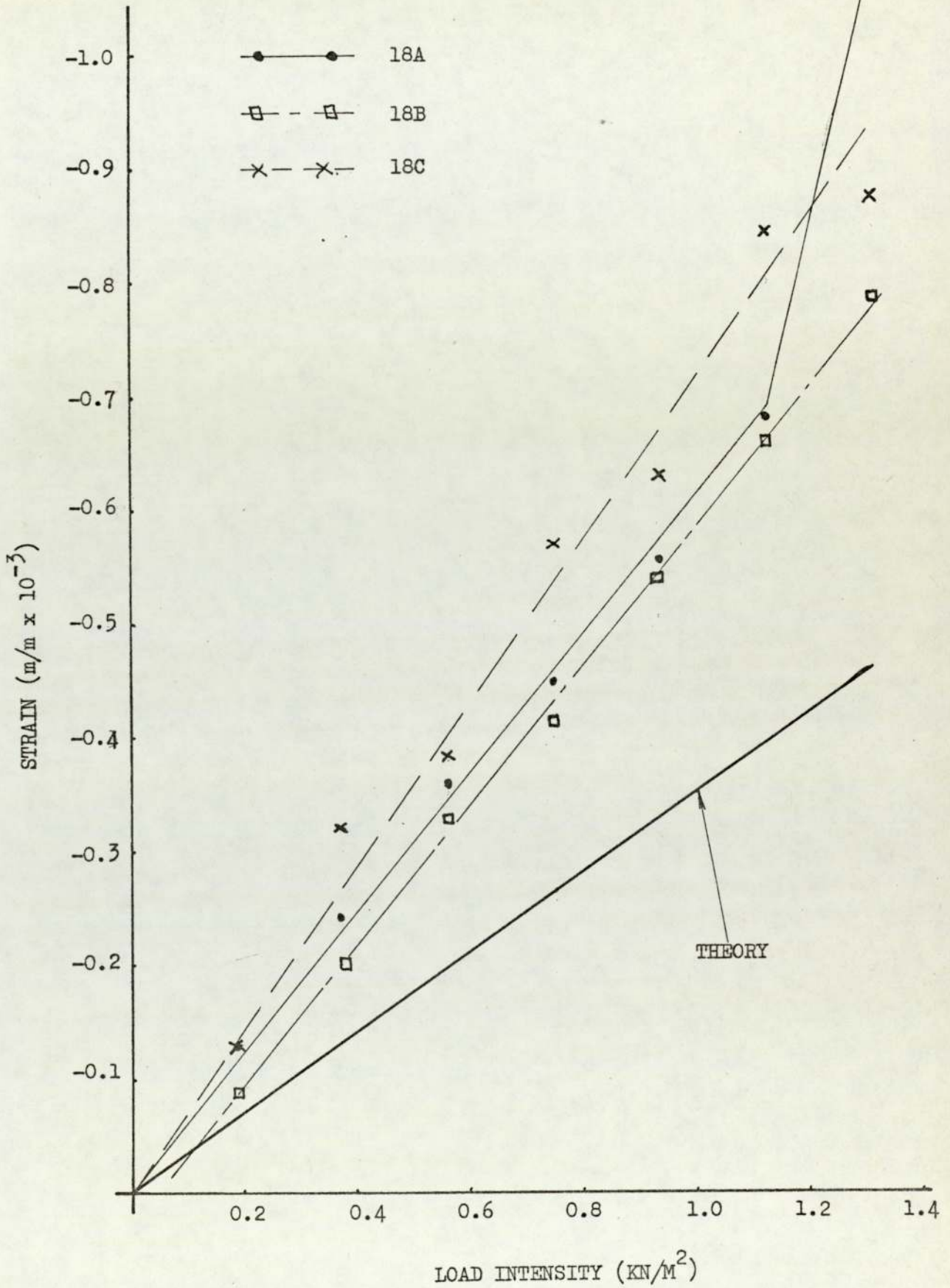


FIG. 7.16 GRAPH OF EDGE-BEAM STRAIN AGAINST

LOAD FOR MEMBERS 17 A, B & C

(GAUGE NOS. 1 & 2)

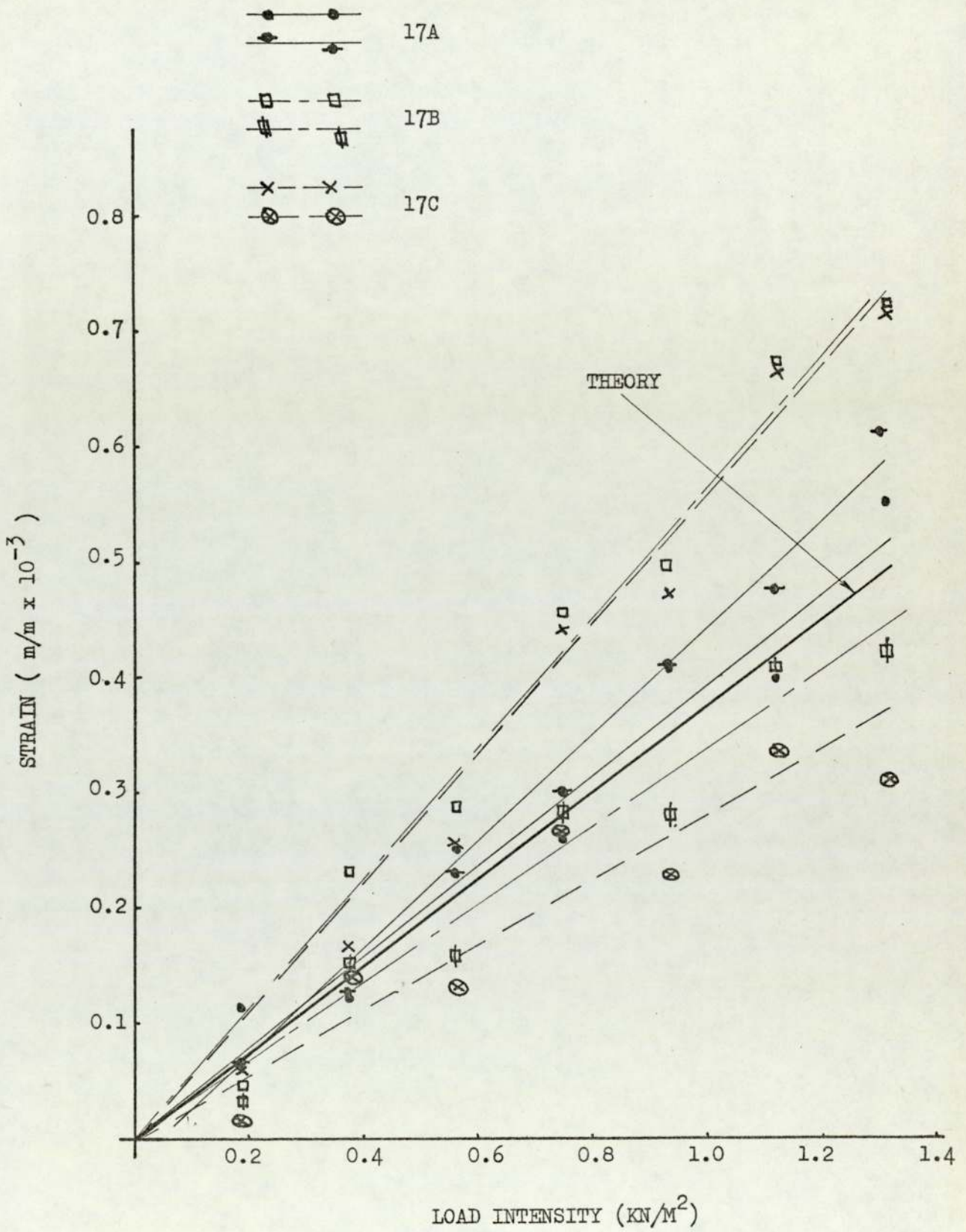


FIG. 7.1⁷
GRAPH OF CYLINDRICAL SECTION SUMMIT
STRAIN AGAINST LOAD FOR MEMBERS
17 A, B & C (GAUGE NO. 3)

- — ● 17A
- — □ 17B
- × — × 17C

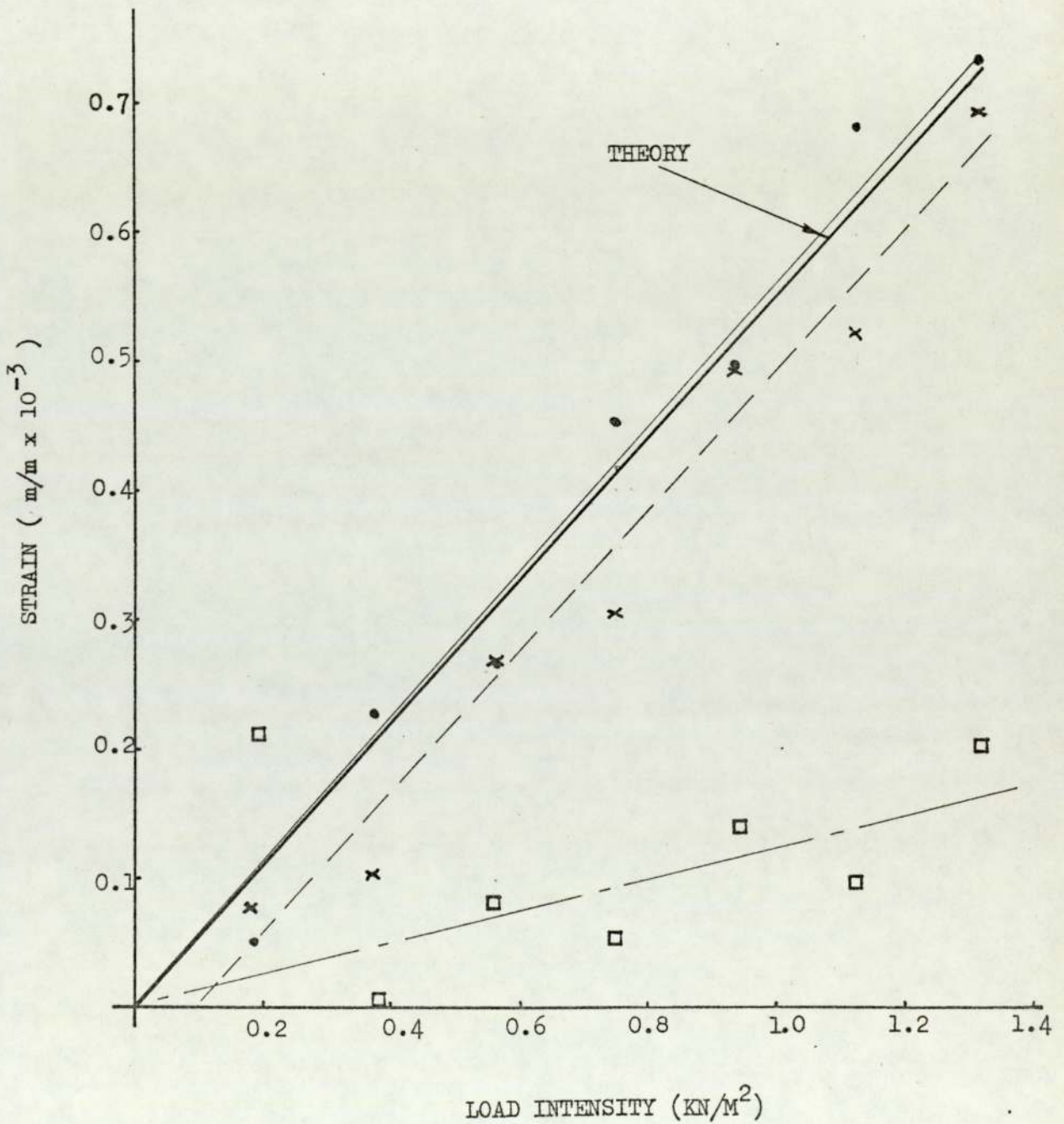


FIG. 7.18 ROOF MEMBER AFTER LOCAL BUCKLING

EXPERIMENTAL STRAIN IN MEMBERS 20
AT SNOW LOAD (0.75 KN/M²)

* * *

THICK

EXPERIMENTAL RESULTS

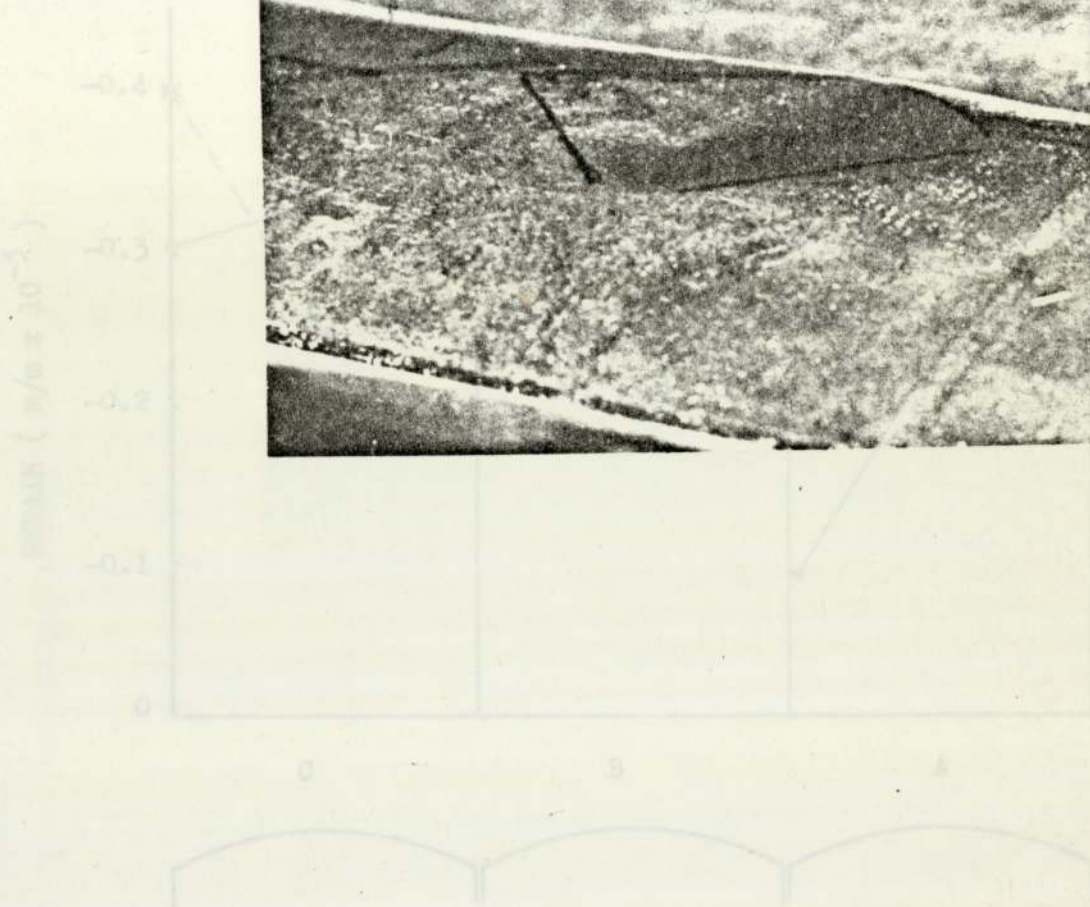
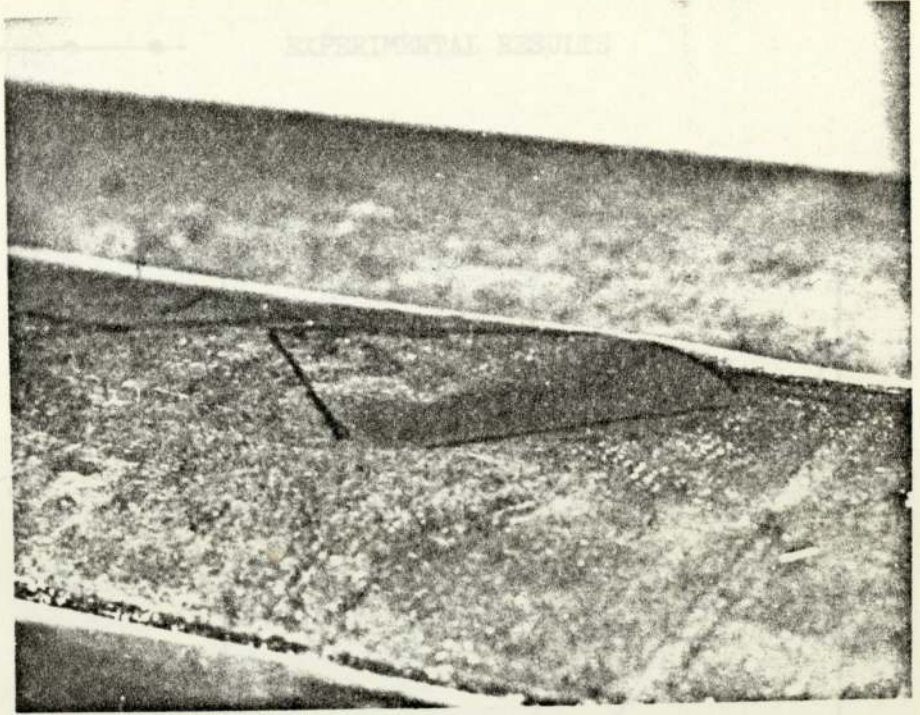


FIG. 7.20 COMPARISON BETWEEN THEORETICAL AND EXPERIMENTAL
STRAIN IN MEMBERS 19 A, B & C UNDER SNOW LOADING

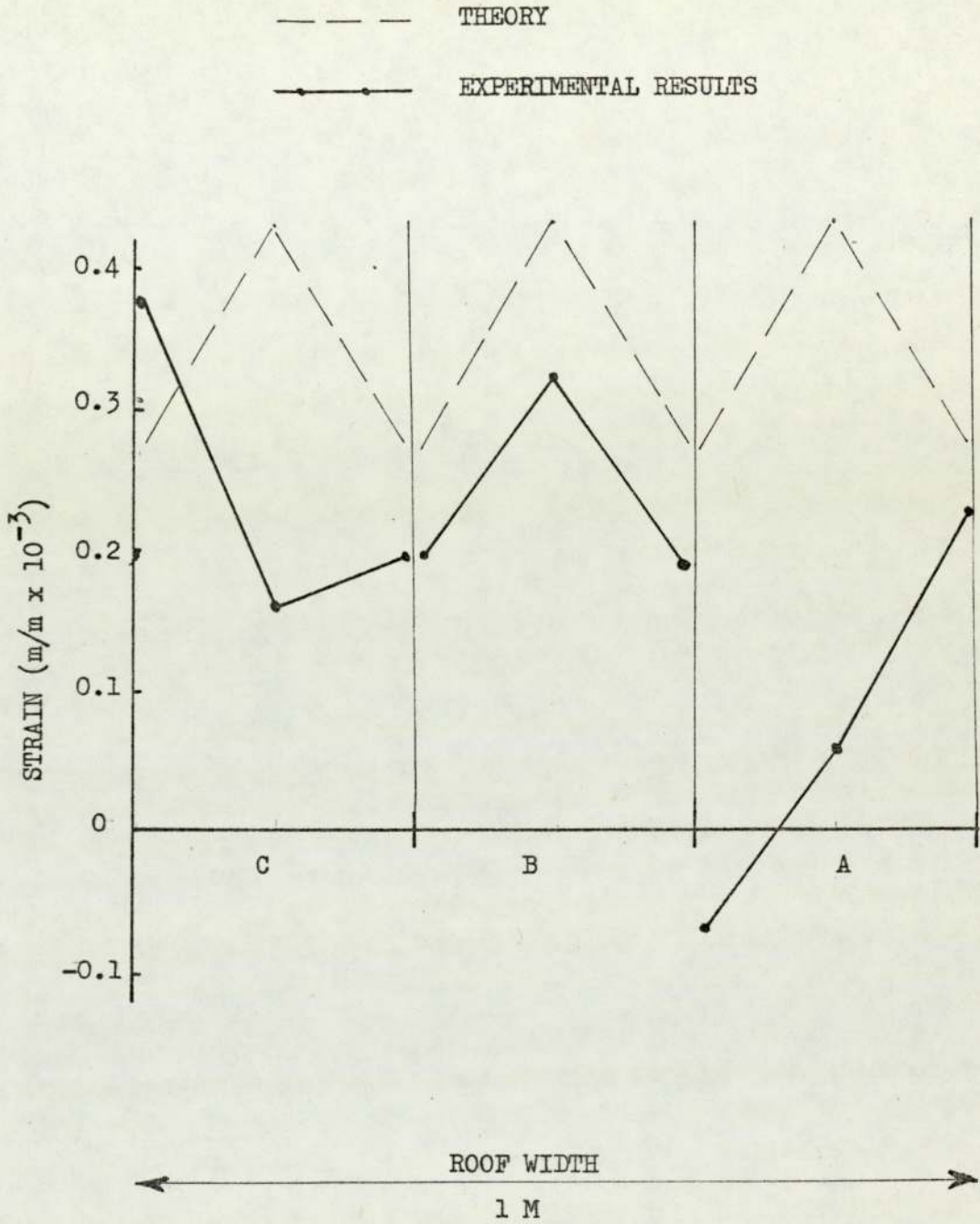


FIG. 7.22 GRAPH OF STEEL MEMBERS 21, 36 & 37

STRAIN AGAINST LOAD - SNOW LOADING

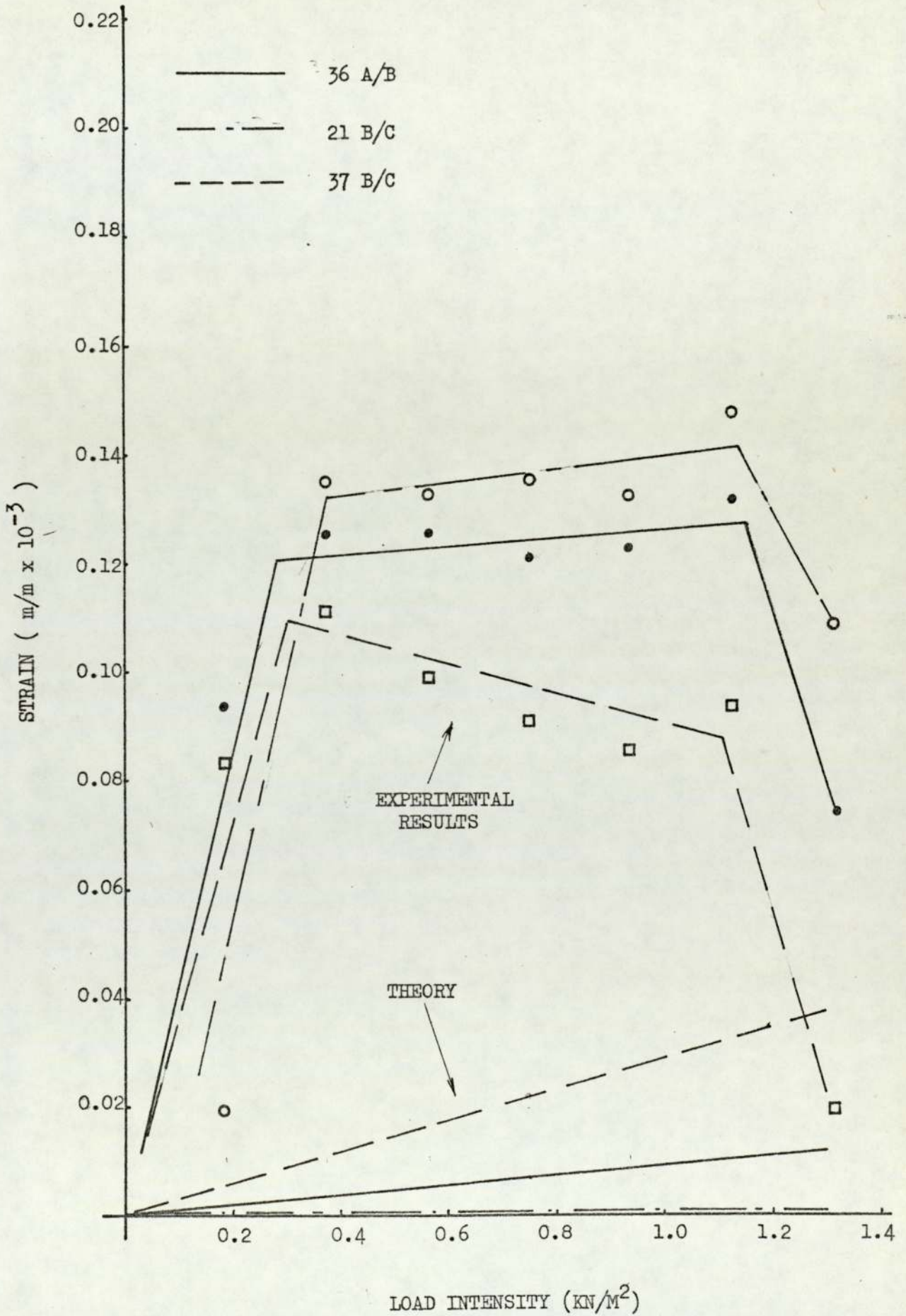


FIG. 7.23 GRAPH OF EDGE-BEAM STRAIN AGAINST LOAD FOR
MEMBERS 18 A, B & C - WIND LOADING (GAUGES 1 & 2)

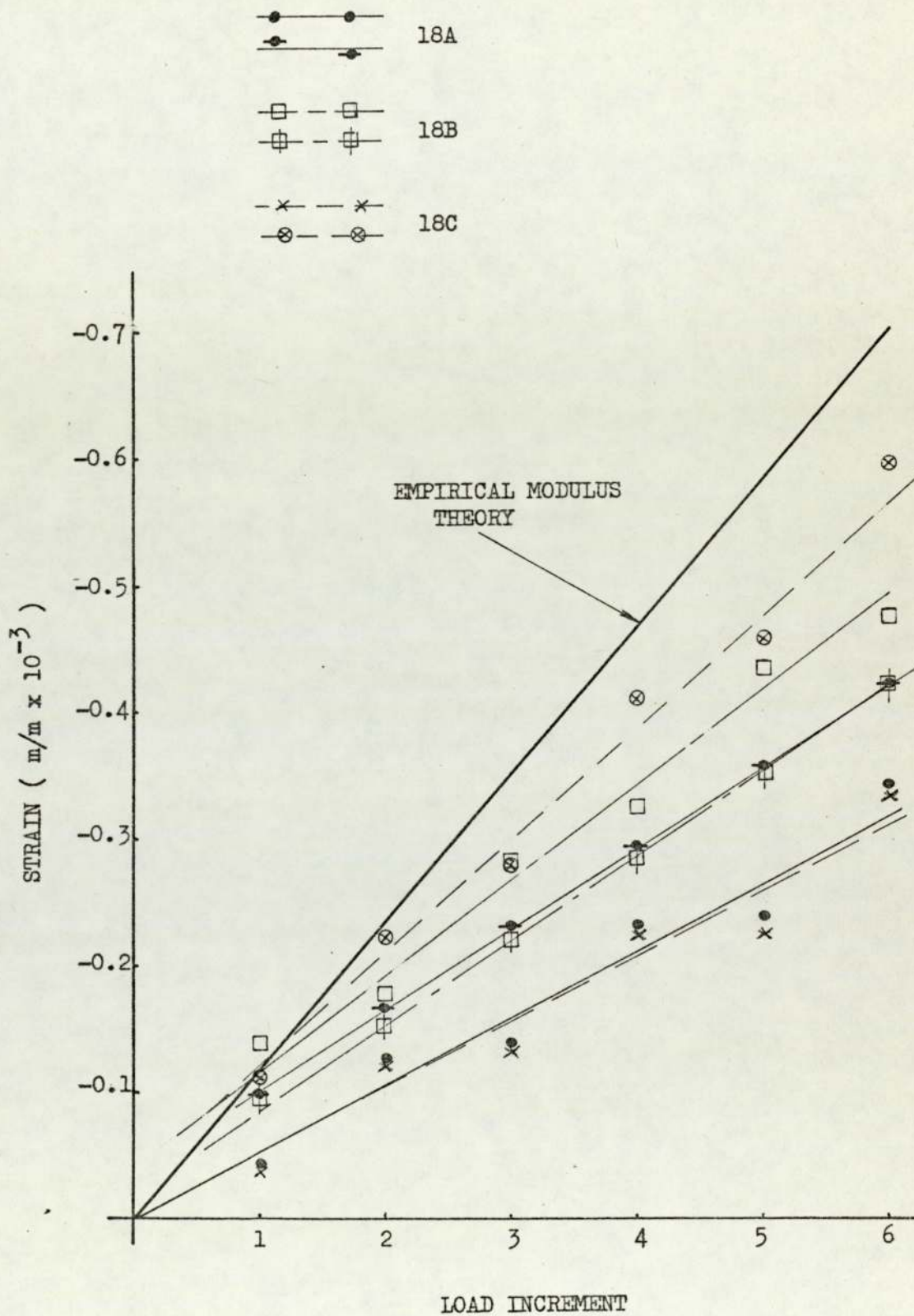


FIG. 7.24 GRAPH OF CYL. SECTION SUMMIT STRAIN AGAINST
LOAD FOR MEMBERS 18 A, B & C - WIND LOADING
STRAIN GAUGE NO. 3

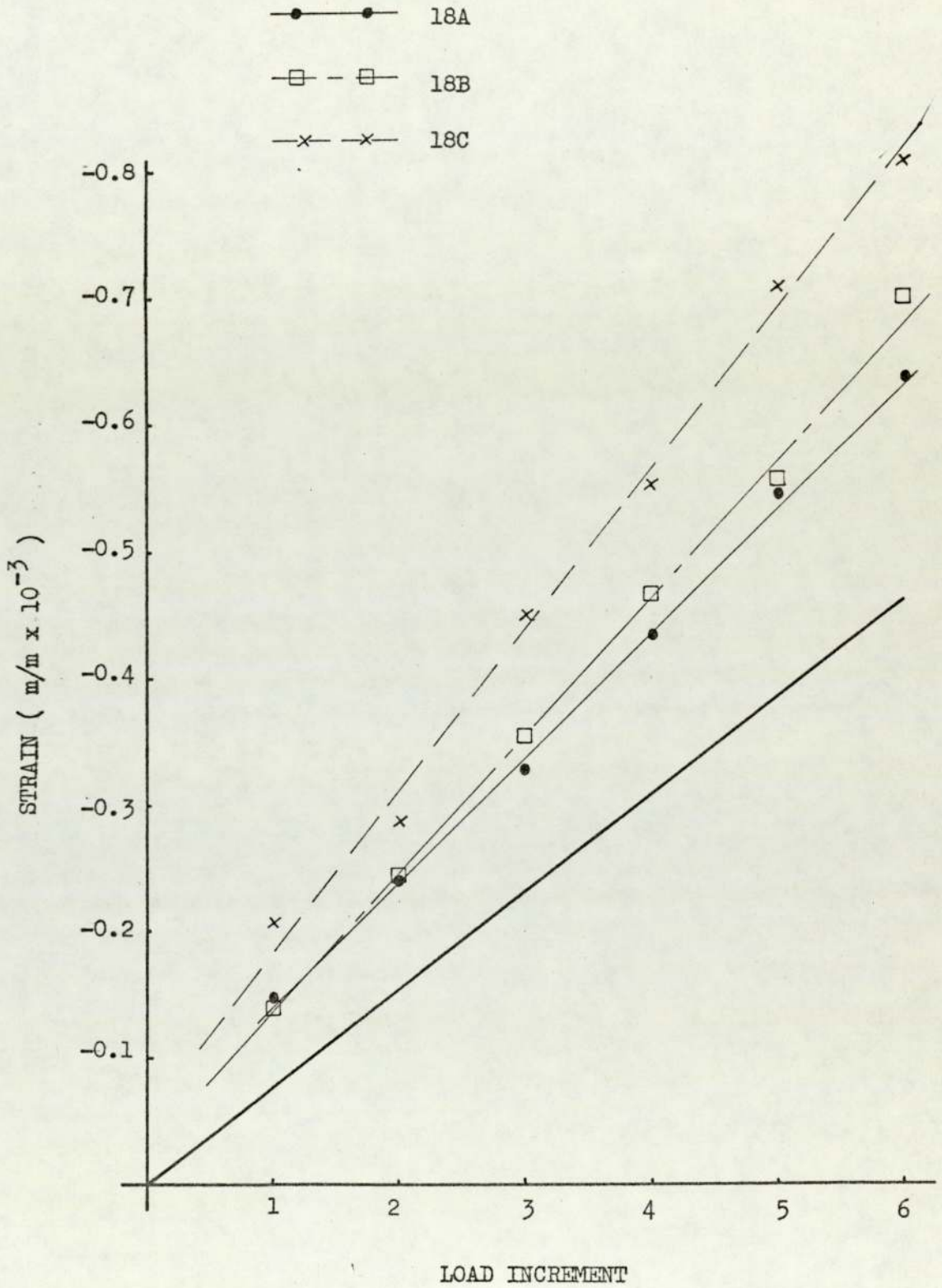


FIG. 7.25 GRAPH OF EDGE-BEAM STRAIN AGAINST LOAD FOR
MEMBERS 17 A, B & C - WIND LOADING
(GAUGE NOS. 1 & 2)

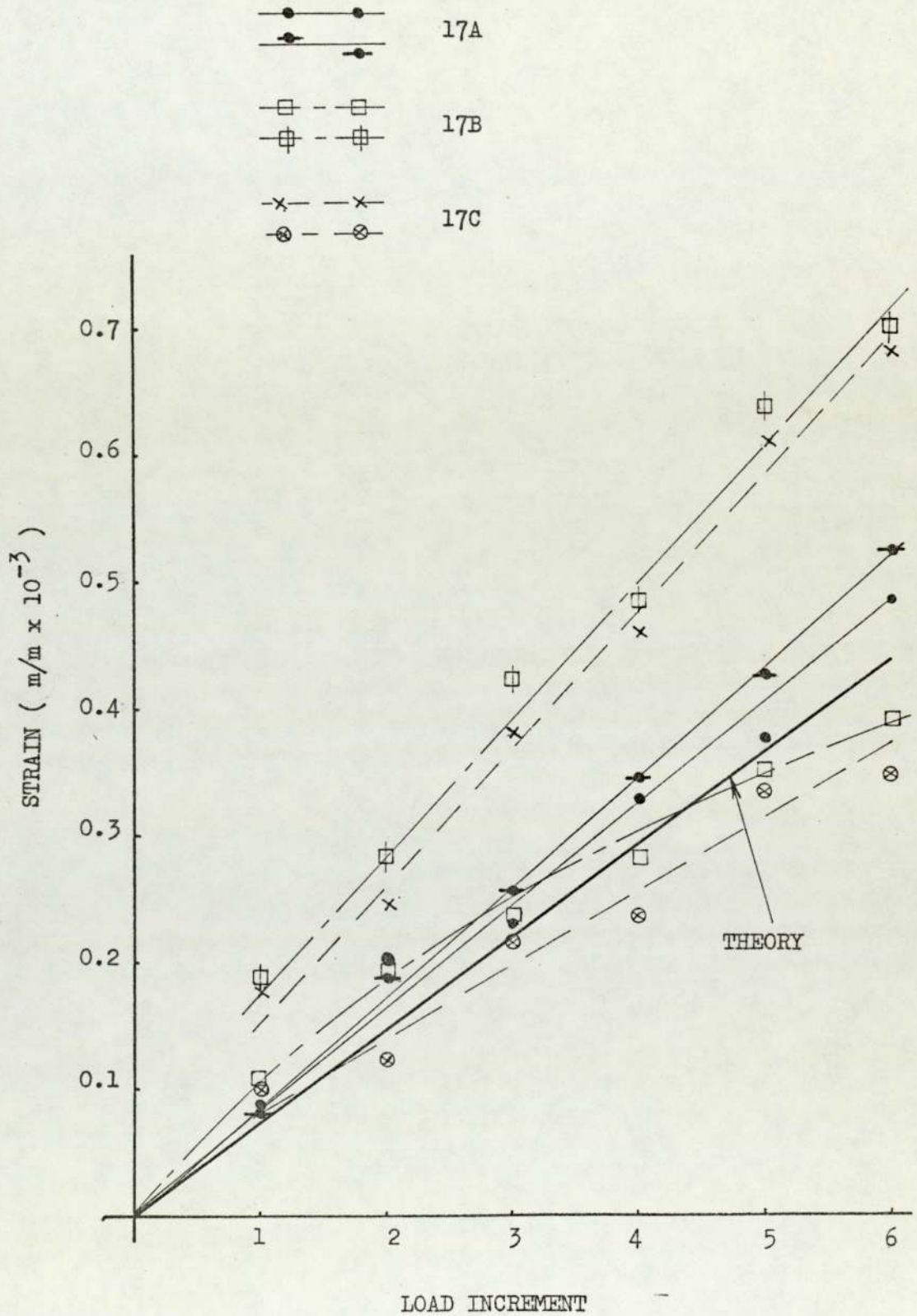
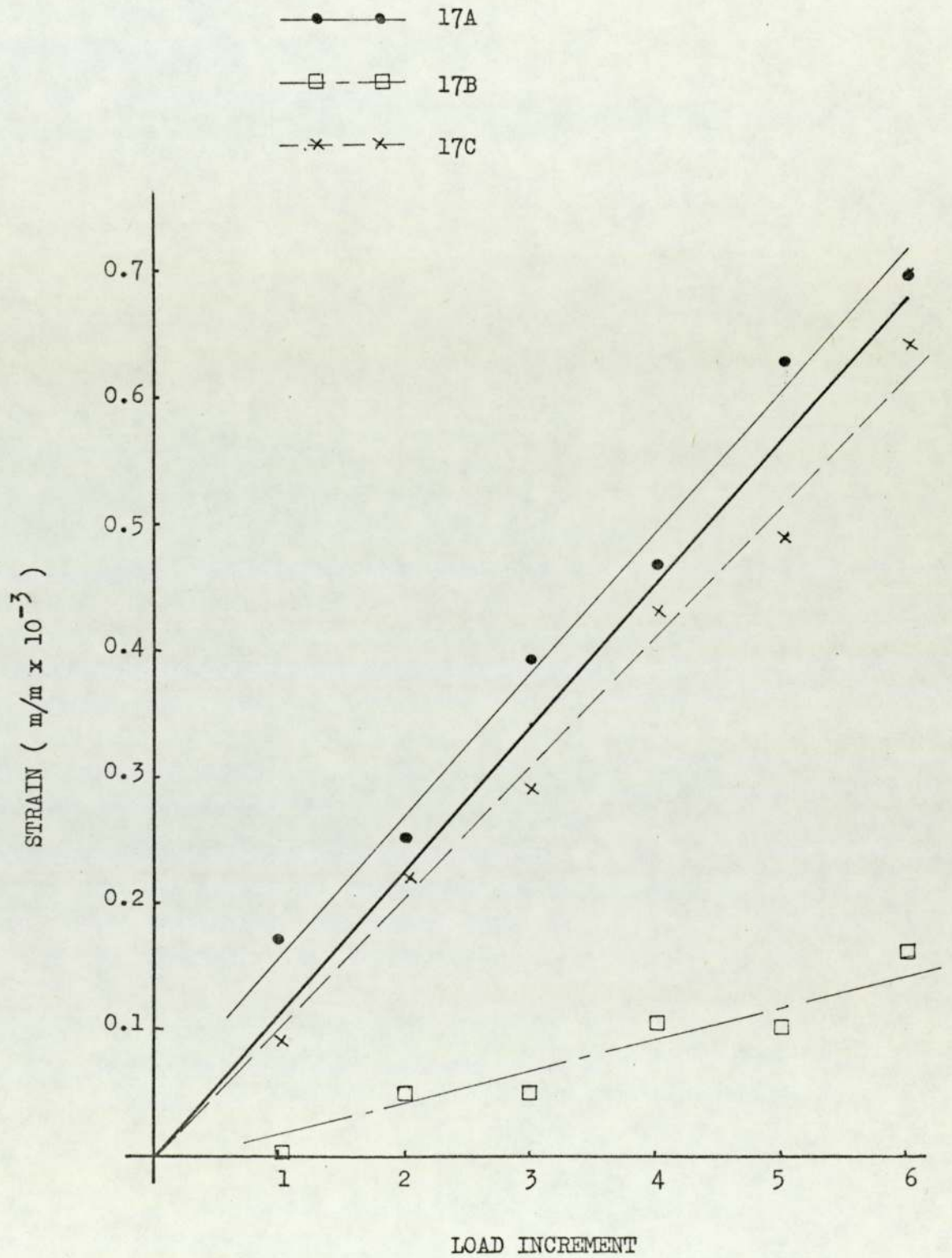


FIG. 7.26 GRAPH OF CYL. SECTION SUMMIT STRAIN AGAINST
LOAD FOR MEMBERS 17 A, B & C - WIND LOADING
(STRAIN GAUGE NO. 3)



CHAPTER 8

ECONOMIC ASPECTS

CHAPTER EIGHT

Economic Aspects

8.1

Introduction

In the previous chapters the structural feasibility of long-span lightly loaded structures has been investigated. In Chapter 4, the basis for an economic feasibility study was laid by analysing the production costs of grp components. The concern, therefore, of this chapter is to investigate the economics of long span roofs and in particular the 60 m roof designed in Chapter 5. The cost of the designed roof will be estimated and compared with conventional roof structures.

The costs of the conventional roof structures, the steel work for the grp roof and all erection costs are based on information supplied by I.D.C. Limited, Stratford. Grp raw material cost

figures were supplied by Fibreglass Limited. Profits have not been allowed for in the costings which are based on February 1975 figures. Many of the conventional roofs have actually been built for some years; accordingly their costs have been up-dated with the use of a "Building Costs Chart" published by "Building" [8.1].

8.2

The Cost of Long Span Grp Roofs

8.2.1 Selection of a Grp Production Process

In order to produce the grp roof surface units designed in Chapter 5 it is envisaged that two production processes would be utilised; i.e. the robot spray-up process for the unit as a whole, but with the unidirectional laminate in the edge-beams being produced using a crude "home-made" pultrusion process. In the latter process, rovings would be pulled firstly through a resin bath and then through a steel die. Finally, the laminate would be cured on a waxed flat surface at room temperature. The robot spray-up process has been chosen, in preference to the other processes considered in Chapter 4, for the following reasons:

- 1) Low cost glass reinforcement may be used.
- 2) Non-skilled labour used predominantly.
- 3) The laminate quality is more easily controlled and reproducible.
- 4) Efficient at reasonably low production rates.
- 5) Less initial capital investment required than for the hot press process.

8.2.2 Calculation of Roof Cost

For the purposes of calculating the grp surface units' production costs, a production rate of 5.3 units per day will be assumed. The significance of this assumption will be discussed in section 8.3. It will also be assumed that the production costs for product B, Chapter 4, expressed in terms of £/unit weight may be applied to the production of the surface unit including the pultruded edge-beams. The capital outlay required for the pultrusion process would be nominal, and the productivity of the process at least as high as the robot spray-up process. For the purposes of this study an additional allowance will be made for overheads based on 50% of the direct labour costs.

Costs of Product B

Direct Production Cost	£20.75 (See Fig. 4.17)
Overheads at 50% of labour	
Costs	<u>£ 7.97</u>
Total Production Cost	£28.72

Weight of Product B = 176 kg (1.8 KN)

Cost per unit weight = £0.163 kg (£16.6/KN)

The self-weight of grp in the 60 M roof = 0.172 KN/M^2

∴ Production cost of grp = $£2.86/\text{M}^2$ or the production cost of one surface unit = £28.6.